PO Box 2345, Beijing 100023, China
Fax: +86-10-85381893
E-mail: wjg@wjgnet.com www.wjgnet.com

World J Gastroenterol 2004;10(21):3081-3087
World Journal of Gastroenterology
 ISSN 1007-9327

• REVIEW •

Maintaining cholesterol homeostasis: Sterol regulatory element-binding proteins

Lutz W. Weber, Meinrad Boll, Andreas Stampfl

Lutz W. Weber, 554 Mariner Point Drive, Clinton, TN 37716, USA
Meinrad Boll, **Andreas Stampfl**, Institute for Toxicology, GSF - National Research Center for Environment and Health, Munich, D-85758 Neuherberg, Germany
Correspondence to: Lutz W. Weber, Institute of Toxicology, GSF - National Research Center for Environment and Health, Munich, D-85758 Neuherberg, Germany. stampfl@gsf.de
Telephone: +49-89-3187-2625 **Fax:** +49-89-3187-3449
Received: 2003-10-15 **Accepted:** 2004-04-13

Abstract

The molecular mechanism of how hepatocytes maintain cholesterol homeostasis has become much more transparent with the discovery of sterol regulatory element binding proteins (SREBPs) in recent years. These membrane proteins are members of the basic helix-loop-helix-leucine zipper (bHLH-Zip) family of transcription factors. They activate the expression of at least 30 genes involved in the synthesis of cholesterol and lipids. SREBPs are synthesized as precursor proteins in the endoplasmic reticulum (ER), where they form a complex with another protein, SREBP cleavage activating protein (SCAP). The SCAP molecule contains a sterol sensory domain. In the presence of high cellular sterol concentrations SCAP confines SREBP to the ER. With low cellular concentrations, SCAP escorts SREBP to activation in the Golgi. There, SREBP undergoes two proteolytic cleavage steps to release the mature, biologically active transcription factor, nuclear SREBP (nSREBP). nSREBP translocates to the nucleus and binds to sterol response elements (SRE) in the promoter/enhancer regions of target genes. Additional transcription factors are required to activate transcription of these genes. Three different SREBPs are known, SREBPs-1a, -1c and -2. SREBP-1a and -1c are isoforms produced from a single gene by alternate splicing. SREBP-2 is encoded by a different gene and does not display any isoforms. It appears that SREBPs alone, in the sequence described above, can exert complete control over cholesterol synthesis, whereas many additional factors (hormones, cytokines, *etc.*) are required for complete control of lipid metabolism. Medicinal manipulation of the SREBP/SCAP system is expected to prove highly beneficial in the management of cholesterol-related disease.

Weber LW, Boll M, Stampfl A. Maintaining cholesterol homeostasis: Sterol regulatory element-binding proteins. *World J Gastroenterol* 2004; 10(21): 3081-3087
http://www.wjgnet.com/1007-9327/10/3081.asp

INTRODUCTION

The view of cholesterol as a nasty substance which clogs arteries and causes heart disease is wide-spread, but it does not do the molecule justice. Not only is it a vital component of cell membranes without which the cell cannot function, but it is also the precursor to all steroid hormones, bile acids, and oxysterols, which by themselves are important regulatory molecules in many metabolic pathways.

Cholesterol and fatty acids as building blocks of cell membranes are synthesized via regulated pathways. All cells must control these pathways in order to maintain levels within physiological boundaries. Excessive amounts of cholesterol in cells can destroy membrane function, precipitate as crystals which will kill the cell or result in atherosclerotic damage if spread to blood[1]. However, the original view of random distribution of cholesterol and lipids in the cell membrane no longer holds: not only differs the lipid composition of the outer leaflet of the plasma membrane from the inner one, but the distribution of lipids and cholesterol in the outer leaflet is organized into domains, with so-called rafts[2] and caveolae[3] being rich in cholesterol and sphingomyelin. These structures play intricate roles in cholesterol trafficking to maintain cellular homeostasis, and they are also components of the cellular signalling system. The membranes of endoplasmic reticulum (ER) and Golgi, on the other hand, contain comparatively little cholesterol, a factor important in its own homeostasis, and one objective of this overview.

The understanding of cholesterol regulation has come a long way from the initial recognition of cholesterol feedback inhibition of its rate-limiting synthetic enzyme, 3-hydroxy-3-methylglutaryl coenzyme A (HMGCoA) reductase, through the role of lipoproteins in maintaining plasma cholesterol levels, to the recent discoveries of regulation of cholesterol synthesis via sterol-sensitive response elements (SREs), and degradation via liver X receptor (LXR) - or bile acid receptor (BAR) -regulated pathways.

Lipid homeostasis via SREs in animal cells is achieved by a family of transcription factors called SRE-binding proteins (SREBPs). SREBPs activate directly the expression of some 30-plus genes participating in the metabolism mostly of lipids, but also glucose. Activation of these originally membrane-bound transcription factors involves a proteolytic cascade through which the SREBP molecule is released from the membrane and obtains its mature form as a transcription factor. The active SREBP enters the nucleus and binds to those special DNA sequences, the SREs, in the promoter regions of many different genes.

In the health arena, SREBPs stand at a crucial point: they regulate expression of the LDL receptor, the molecule which enables the hepatocytes to remove cholesterol contained in LDL particles from the bloodstream. High (dietary) cholesterol prevents maturation of SREBPs and not only cuts off cholesterol synthesis, but also LDL receptor synthesis, resulting in high blood cholesterol and the imminent danger of atherosclerotic plaque formation. At this point in time the so-called statins, drugs which block HMGCoA reductase, another target of SREBP-mediated gene expression, are the most effective way to interrupt this vicious circle[4].

This brief overview is concerned with the SREBP-mediated control of cholesterol and lipid synthesis. Lipid synthesis is subject to many other regulatory influences which cannot be addressed here, nor can the degradation of cholesterol via hormone or bile acid synthesis be covered, which again commands its own set of regulatory substances. The focus of this minireview is to present the latest data on the SREBP-induced mechanism. Recent in-depth reviews have been available[5-9].

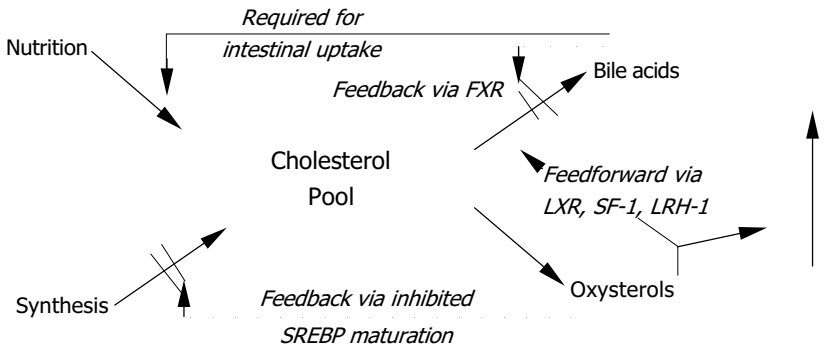

Figure 1 Feedforward and feedback effects of oxysterols FXR = farnesoid×receptor; LRH-1 = liver receptor homologue-1; LXR = liver×receptor; SF-1 = steroidogenic factor-1; SREBP = sterol responsive element binding protein.

OXYSTEROLS AS NEGATIVE AND POSITIVE REGULATORY MOLECULES

Cholesterol is not the only sterol inside the cell to act as a regulatory substance, many of its hydroxylated derivatives, the oxysterols, share these important functions. Oxysterols exert a feed-back effect and down-regulate cholesterol synthesis, to be detailed in the following sections of this overview, but they also up-regulate their own metabolism and elimination via a feed-forward effect which will be briefly described in this section.

Cholesterol directly affects two enzymes which are vital in its own removal. It activates acyl-CoA: cholesterol acyl transferase (ACAT), the enzyme required to synthesize cholesteryl esters, its major storage form, and it also activates cholesterol 7α-hydroxylase (CYP7A1), the initial and rate-limiting enzyme of bile acid synthesis, the leading pathway of cholesterol elimination[10].

The side chain-hydroxylated 27-hydroxycholesterol is presumed to function in cholesterol homeostasis by sustaining HDL-mediated reverse cholesterol transport, the process by which cholesterol is brought back to the liver from peripheral tissues[11]. The most important action of oxysterols, however, is to serve as ligands for nuclear orphan receptors. This family of proteins has been recognized as nuclear hormone receptors based on their molecular properties, but since ligands were initially not known, they were named orphan receptors. Most important among these is liver X receptor (LXR), which controls expression of CYP7A1[12] as the rate-limiting step of bile acid synthesis[13,14], reverse cholesterol transport[15], trafficking of cholesteryl esters, and aids in lipid metabolism[16] and the intestinal absorption of cholesterol. This receptor displays specific requirements for the position of additional hydroxy group (s) on the cholesterol molecule, the most potent ligands being 20 (S) -OH-, 22 (R) -OH-, 20, 22-di-OH-, and 24-OH-cholesterol[17,18]. An overview of oxysterol actions is shown in Figure 1.

Furthermore, oxysterols are ligands for steroidogenic factor-1 (SF-1) and liver receptor-homologue 1 (LRH-1), in which they regulate steroid hormone synthesis and sexual differentiation during prenatal development. SF-1 is limited to steroidogenic tissues, whereas LRH-1 occurs in liver and other tissues derived from the gut endoderm[7]. Oxysterols also play a role in meiosis[19]. Finally, these bile acids activate the farnesol X receptor (FXR) /retinoid X receptor (RXR)/receptor-interacting protein 14 (Rip14) system, FXR is also known as bile acid receptor (BAR). Binding of bile acids to FXR inhibits bile acids synthesis.

SREBPS, MEMBRANE-DERIVED TRANSCRIPTION FACTORS

SREBPs belong to the large family of basic helix-loop-helix-leucine zipper (bHLH-Zip) transcription factors. Three members of the SREBP family, SREBPs-1a, -1c, and -2, have been identified[20,21]. They are synthesized as inactive precursors. Isoforms -1a and -1c are produced from a single gene on human chromosome 17p11.2 by use of alternate promoters and splicing, resulting in different forms of exon-1[21-23]. SREBP-2 is encoded by a separate gene on human chromosome 22q13[20,24]. It has about 50% sequence identity with SREBP-1. Adipocyte determination differentiation factor (ADD)-1, a transcription factor which binds to E-boxes and promotes adipocyte differentiation in rats[25] is the homologue of human SREBP-1c[23].

Each nascent SREBP protein has a molecular size of about 125 ku and consists of about 1 150 amino acids (aa) in 3 functional domains. The first, NH_2-terminal domain of SREBP contains the bHLH-Zip and an acidic domain, located at the very NH_2 terminus. The acidic domain has to bind a transcription coactivator for function, it is shorter in SREBP-1c than in SREBP-1a, making SREBP-1c a weaker transcription activator[26]. The acidic domain is essential for function. When removed, the bHLH-Zip portion of SREBP still binds to DNA, but no longer activates transcription, thus acting as an inhibitor[27].

A djacent to the acidic DNA-binding domain is a variable area rich in serine, proline, glutamine, and glycine. Next follows the bHLH-Zip sequence, whose basic region mediates DNA binding. The rest of the bHLH-Zip motif imparts the ability to dimerize. Other bHLH-Zips tend to homo-dimerize, whereas SREBP needs other transcription factors such as SP-1 or NF-Y for full function. The remainder of the SREBP molecule has no analogy with other bHLH-Zip transcription factors[5].

SREBPs are embedded in membranes of the endoplasmic reticulum (ER) and the nuclear envelope, forming what has been called a hairpin shape[28,29]. The NH_2-terminal portion of the SREBP molecule through the bHLH-Zip region protrudes into the cytosol. The following central portion of SREBP, the membrane anchoring region, is about 90 aa in length. It consists of two hydrophobic, membrane-spanning segments separated by a hydrophilic loop which extends into the lumen of the ER. The COOH terminal segment of about 590 aa again extends into the cytosol and serves as the regulatory domain for transformation into the mature, a transcriptionally active form also known as nuclear SREBP (nSREBP). Neither the membrane-spanning, nor the regulatory regions, are found in other bHLH-Zip transcription factors.

The NH_2-terminal domain of SREBP binds to a sterol binding element (SRE) which must contain a direct, or tandem, repeat of the recognition sequence[30]. This is another evident difference to bHLH-Zip transcription factors, which will bind only to palindromic (i.e., tail-to-tail connected) repeats. SREBPs display no *in vivo* activity with palindromic sequences[5,19].

SREBP CLEAVAGE ACTIVATION PROTEIN (SCAP), AN ESCORT AND STEROL SENSOR PROTEIN

SREBPs attain biological activity only after being transferred to the membrane of the Golgi complex, where they are cleaved at the lumenal loop and the NH_2-end is released from the membrane. They are confined to the membranes of the ER unless they are

paired up with another protein which serves two functions: to sense the levels of sterols in the cell, and in response to low sterol levels, to escort SREBP to its place of activation. This is achieved by SREBP cleavage activating protein (SCAP), a protein originally cloned from a mutant cell line of Chinese hamster ovary cells which will not suppress SREBP cleavage even with very high sterol levels[31]. The mutation affects one specific codon, 443, where a C (ytosine) to G (uanine) transition on the DNA side replaces an aspartic acid by an asparagine in the amino acid sequence, rendering SCAP unresponsive to sterols[32].

SCAP has 1 276 amino acids[31] in two domains[33]: a membrane-spanning NH_2 terminal domain of 730 aa, and a COOH terminal domain of 546 aa, which extends into the cytosol. The NH_2-terminus contains eight hydrophobic sequences separated by short hydrophilic loops[31], the hydrophobic sequences are thought to span the membrane with the hydrophilic loops protruding at either side. SCAP shares this feature with HMGCoA reductase[34,35]. The membrane-spanning stretches comprise the sterol-sensing area, whereas the COOH-terminus contains all of the remaining biological activity[31]. The COOH-terminus is organized in five repeat sequences characteristic of the WD family. Wherever this sequence occurs, it mediates protein-protein interactions[36].

Newly synthesized SREBP forms a tight complex with the WD repeat domains of SCAP[37], but in the presence of oxysterols this complex is confined to the ER, establishing a feedback loop to control cholesterol synthesis. With oxysterol depletion, the SCAP/SREBP complex appears in vesicles budding from ER membranes[38] and translocates to another subcellular compartment, the Golgi[39-43]. Transfer of SREBP and proteolytic cleavage to release nSREBP cannot occur unless this complex has formed[42]. Oxysterols induce a change of the conformation of SCAP, and an additional protein has been postulated to retain SCAP in the ER once in its sterol-induced conformation[44]. Not only cholesterol, but also several other oxysterols display full activity in suppressing SCAP translocation into vesicles, but it has been suggested that cholesterol alone exerts the effect, while high levels of oxysterols simply force translocation of cholesterol from the plasma membrane to the ER[44]. Complete understanding could be of immense benefit in the management of hyperlipidemias.

SREBP ACTIVATION VIA TWO-STEP PROTEOLYTIC CLEAVAGE

The SREBP/SCAP-containing vesicles from the ER also contain a membrane-anchored serine protease of the subtilisin family, Site-1 protease (S1P), in an inactive form which becomes activated only during its transport to the Golgi[45]. The SREBP/SCAP complex and S1P now incorporate into the Golgi membrane. As the next step, the activated S1P attaches to the SCAP/SREBP complex and cuts the SREBP molecule right in the middle of its lumenal hydrophilic loop[29]. When active S1P is inserted into the ER, it will cleave SREBP without a need for SCAP[43].

To release active SREBP, another enzyme is required, Site-2 protease (S2P, a trans-membrane zinc metalloprotease). The cellular location of this enzyme is as yet unclear, but likely resides in the Golgi. S2P cuts the still membrane-anchored SREBP in a rather unusual place, viz., three amino acids into the membrane-spanning portion on the cytoplasmic side[46,47]. This process is known to regulate intra-membrane proteolysis (Rip)[48], and typically produces proteins which are transcriptionally active and participate in the control of various cellular processes[6]. S2P action is not directly affected by cellular oxysterol levels, since this enzyme cannot act unless S1P has separated the bHLH-Zip portion of SREBP from the regulatory COOH terminus[49]. S2P action results in the release of a mature, 68 kDa nSREBP, consisting of the bHLH-zipper domain with the first three membrane-spanning amino acids attached, which now can migrate to the nucleus and bind to a sterol-responsive element (SRE). SCAP is recycled back to the ER to chaperone another 125 kDa SREBP molecule to the Golgi[50], whereas the 68 kDa SREBP is degraded. Interestingly, the nuclear

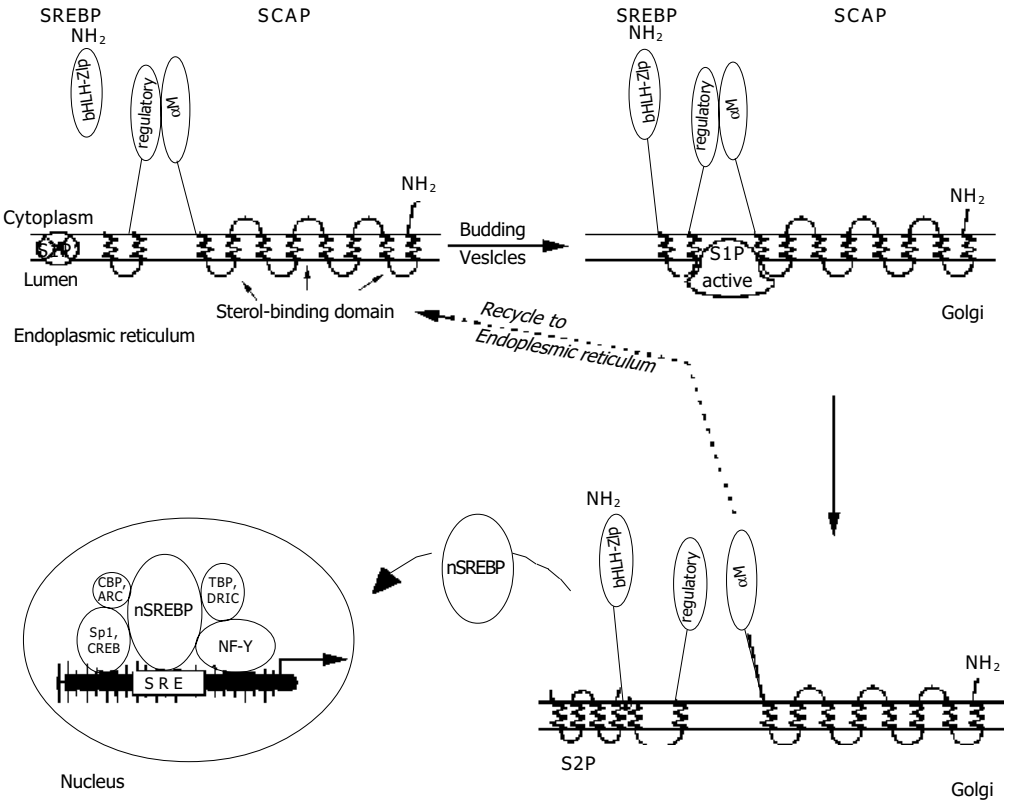

Figure 2 Maturation of SREBPs -NH_2 = amino-terminal ends of SREBP or SCAP. S1P = Site-1 protease (crossed-out = inactive); S2P = Site-2 protease. SRE = sterol-responsive element; nSREBP = nuclear SREBP. Arrangement of the additional transcription factors NF-Y, Sp1, CREB, ARC, CBP, TBP, and DRIC (see text) is tentative as their requirements are not exactly known.

action of nSREBP induces new SREBP mRNA synthesis by way of SREs located in the promoter regions of their own genes[51]. A synopsis is shown in Figure 2.

The process of SREBP cleavage and activation thus comprises 4 components which, upon mutation, can result in loss of oxysterol-sensitive regulation of cholesterol homeostasis. As a matter of fact, much of the knowledge of the SREBP regulatory system stems from experimentally mutated cell lines and subsequent selection for oxysterol resistance or cholesterol auxotrophy[8]. Oxysterol resistance has aided in cloning the genes for SREBP and SCAP, respectively. One type, class 1 mutation, produces an NH_2-terminal bHLH-Zip portion of SREBP which is truncated even before the S2P cleavage site[52,53]. This molecule is therefore not membrane bound and can access the nucleus immediately after its synthesis, turning on the complete SREBP gene battery regardless of cellular oxysterol levels. Class 2 mutants contain a mutated SCAP molecule[54] which holds the SREBP/SCAP/S1P complex in a permanently active configuration, no matter how high the oxysterol level in the cell, resulting in permanent release of nSREBP with concomitant overproduction of cholesterol[31].

Cholesterol auxotrophy has been used as a selection criterion to clone the genes for S1P and S2P. With S1P[55], S2P[41,46,56] or SCAP[57] rendered non-functional, cells become dependent on exogenous cholesterol because they cannot produce the enzymes necessary for its biosynthesis.

It is interesting to know that the proteolytic activation of SREBP-1 and SREBP-2, respectively, can be regulated individually. In rodents, treatment with cholesterol suppressing drugs (statins) or with cholesterol-sequestering agents results in up-regulation and increased activation of SREBP-2 while reducing activation of SREBP-1[58]. Another interesting feature is that polyunsaturated fatty acids inhibit the proteolytic activation of SREBP-1, but contrary to the action of oxysterols, they have no effect on SREBP-2 maturation[59]. In addition, glucose metabolites such as glucose-6-phosphate may serve to accelerate maturation of SREBP-1c only[60], but mechanistic details have not been elucidated.

GENE ACTIVATION BY SREBPs, TARGET GENES

Immediately after the second cleavage of the SREBPs the now mature protein enters the nucleus where it binds to SREs in the promoters of the target genes and activates transcription. The SRE nucleotide sequence displays considerable variation among the promoters of the many genes activated by an SRE, a commonly found sequence is represented by 5'-nTCACnCCA Cn-3' (cf.[6]). However, SREBP alone cannot activate transcription, but must act co-ordinately with additional transcription factors to obtain full activation of target genes.

Transcription factors known to activate SREs in conjunction with SREBP are Sp1, nuclear factor (NF)-Y, and cAMP response element binding protein (CREB)[10,61-64]. NF-Y interacts directly with SREBP[62], and Sp1 can stabilize the complex[61]. It appears that the promoters of different SRE-activated genes respond to different combinations of these transcription factors. Once a stable complex has formed in a promoter region, additional factors such as CREB binding protein (CBP)[65,66], activated recruited cofactor (ARC)[67], vitamin D receptor interacting protein (DRIC)[67], or TATA box-binding protein (TBP)-associated factors may be recruited to initiate transcription. Histone acetylation is also required for full transcriptional activity[68]. Such complexes have been shown to exist with SREBP-1a and -2, but not with SREBP-1c. This may explain its rather weak potency to activate the SRE gene battery.

SREBP-activated genes predominantly belong to lipid metabolism pathways, viz, cholesterogenesis, fatty acid synthesis, lipogenesis, triglyceride and phospholipid synthesis, but also glucose metabolism. Yet, the three SREBPs do not activate identical gene batteries. Using transgenic mice over-expressing just one type of nSREBP it has been discovered that SREBPs-1a and -1c actions favour fatty acid synthesis, whereas SREBP-2 action favours cholesterol synthesis[5,69-71], but *in vitro* both SREBPs-1a and -2 can trigger expression of the complete set of enzymes required for cholesterol synthesis with similar potency[72]. While SREBPs-1a and -2 predominate in cultured cells, intact liver and most other tissues primarily express SREBP-1c and -2[9]. An overview of SREBP pathways is given in Figure 3.

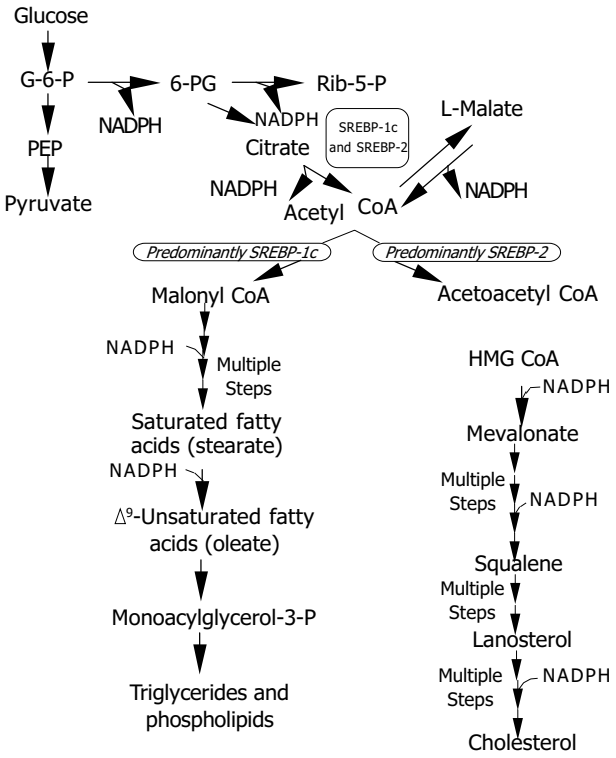

Figure 3 Metabolic pathways regulated by SREBPs G-6-P = glucose-6-phosphate; 6-PG = 6-phosphogluconate; Rib-5-P = ribulose-5-phosphate; PEP = phosphoenol pyruvate; CoA = coenzyme A; HMGCoA = 3-hydroxy-3-methylglutaryl coenzyme A. SREBP-1c and SREBP-2 activate genes for the generation of NADPH (ATP citrate lyase, malic enzyme, G-6-P dehydrogenase, 6-PG dehydrogenase) required in various steps of lipid synthesis.

SREBP-2 over-expression induces all 12 enzymes of the cholesterol biosynthetic pathway[72], most notably the mRNA for HMGCoA reductase, which may increase as many as 75-fold[73]. Overall cholesterol synthesis in such animals is up 28-fold, whereas fatty acid synthesis is increased only 4-fold. In contrast, expression of enzymes does not involve cholesterol synthesis but is related to cholesterol metabolism. Cholesterol 7α-hydroxylase (rate-limiting enzyme for bile acid synthesis) and acyl-CoA:cholesterol acyltransferase (ACAT, catalyses cholesterol ester formation), are not activated[72].

SREBP-1a appears to be constitutively expressed in most tissues, with as yet no known factor to stimulate its low expression[26]. Over-expression in adult rats also resulted in over-stimulation of lipid synthesis, but in this case fatty acid synthesis was increased 26-fold, and cholesterol synthesis 5-fold. Since SREBP-1a and -1c (see below) also induce enzymes for fatty acid elongation and desaturation[73,74], SREBP-1a over-expression resulted in elevated hepatic levels of oleate[75].

SREBP-1c is predominantly involved in the regulation of adipogenesis and also in the regulation of insulin-responsive genes which control lipogenesis and glucose metabolism[76,77], but *in vitro* it does not stimulate cholesterol synthesis[75]. SREBP-1c mRNA synthesis responds to nutritional changes in

parallel to insulin levels[78]. Insulin heightens the expression of SREBP-1c and its battery of genes involved in the synthesis of saturated and unsaturated fatty acids[75,79] as well as glucose metabolism genes[77,78]. The effect is opposed by glucagon and cyclic AMP. In short, available experimental data indicate that SREBP-1c mediates all effects of insulin on lipogenesis. In response to nutritional stimuli SREBP-1c also triggers expression of genes of enzymes required for fatty acid elongation[74], and of glycerol 3-phosphate acyltransferase required for triglyceride and phospholipid synthesis[6]. Last but not least SREBPs activate 3 genes necessary for the generation of NADPH, which is needed in fatty acid and cholesterol synthesis.

The promoter of the SREBP-1c gene contains response elements for insulin, glucagon, as well as liver X-activated receptors (LXR) α and LXRβ, the latter is activated by sterols[17,43]. This regulatory pathway, among others, results in increased synthesis of oleate[75], the major fatty acid used for cholesterol esterification, to ensure its removal from the liver.

KNOCK-OUT ANIMALS AND HEALTH IMPLICATIONS OF SREBPS

Knock-out mice which lack all SREBPs, or S1P to activate them, die at an early stage of embryonic development[80,81]. Specific knock-out of SREBP-2 also results in embryonic lethality. Deletion of SREBP-1a allows some foetuses to survive, whereas lack of SREBP-1c appears to be of no consequence. The survivors are found to compensate by higher SREBP-2 levels, and consequently, these animals have elevated hepatic cholesterol, but lower fatty acid levels[9].

In order to study SREBP knock-outs in adulthood, a gene manipulation was used in Brown and Goldstein's laboratory which allows to turn specific genes off at will by stimulating interferon production. Disruption of the SCAP or S1P gene, respectively, almost abolished nSREBPs-1 and -2 in liver and diminished expression of all target genes of cholesterol and fatty acid synthesis. The result was a reduction in cholesterol and fatty acid levels in livers by 70-80%[9].

The SREBP-related links between fatty acid and glucose metabolism draw immediate attention to the wide-spread disease, diabetes. It would appear that the fatty liver frequently observed in insulin-resistant diabetics is a result of high SREBP-1c levels caused by high insulin levels. Leptin, the organism's response to fat accumulation in adipocytes, opposes SREBP-1c action[82], and consequently can heal the derailment of fat metabolism in diabetic animals[83].

One of the genes activated by nSREBP-1c is that for the hepatic LDL receptor, an effect clearly targeting at maintaining plasma lipid homeostasis. At first sight this would appear beneficial for arteriosclerosis since it should reduce elevated LDL-cholesterol levels in blood. However, since nSREBP-1c also induces lipogenesis, its effect is ambiguous, and other factors will decide whether the net result fights arteriosclerosis, or rather exacerbates it[7]. It is at this point where the HMGCoA reductase inhibitors or statins work, but they are effective only in one third of cases[84].

It must be understood that fatty acid synthesis is not only subject to SREBP regulation, but a host of other factors, whereas cholesterol synthesis appears to be exclusively controlled by SREPBs. Additional unknowns are the exact regulation of system by which HDL via the scavenger receptor B-1 mediates efflux of cholesterol from the liver, and the ATP-binding cassette-1 (ABC-1) system which mediates transfer of cholesterol to HDL[84]. Profound knowledge of these pathways will open a perspective beyond the statin drugs to specifically lower cholesterol levels in disease conditions.

REFERENCES

1 **Small DM,** Shipley GG. Physical-chemical basis of lipid deposition in atherosclerosis. *Science* 1974; **185**: 222-229
2 **Simons K,** Ikonen E. Functional rafts in cell membranes. *Nature* 1997; **387**: 569-572
3 **Anderson RG.** The caveolae membrane system. *Annu Rev Biochem* 1998; **67**: 199-225
4 **Goldstein JL,** Brown MS. Regulation of the mevalonate pathway. *Nature* 1990; **343**: 425-430
5 **Brown MS,** Goldstein JL. The SREBP pathway: Regulation of cholesterol metabolism by proteolysis of a membrane-bound transcription factor. *Cell* 1997; **89**: 331-340
6 **Edwards PA,** Tabor D, Kast HR, Venkateswaran A. Regulation of gene expression by SREBP and SCAP. *Biochim Biophys Acta* 2000; **1529**: 103-113
7 **Schoonjans K,** Brendel C, Mangelsdorf D, Auwerx J. Sterols and gene expression: control of affluence. *Biochim Biophys Acta* 2000; **1529**: 114-125
8 **Goldstein JL,** Rawson RB, Brown MS. Mutant mammalian cells as tools to delineate the sterol regulatory element-binding protein pathway for feedback regulation of lipid synthesis. *Arch Biochem Biophys* 2002; **329**: 139-148
9 **Horton JD,** Goldstein JL, Brown MS. SREBPs: activators of the complete program of cholesterol and fatty acid synthesis in the liver. *J Clin Invest* 2002; **109**: 1125-1131
10 **Jackson MS,** Ericsson J, Edwards PA. Signaling molecules derived from the cholesterol biosynthetic pathway. *Subcell Biochem* 1997; **28**: 1-21
11 **Björkhem I,** Andersson O, Diczfalusy U, Sevastik B, Xin RJ, Duan C, Lund E. Atherosclerosis and sterol 27-hydroxylase: Evidence for a role of this enzyme in elimination of cholesterol from human macrophages. *Proc Natl Acad Sci U S A* 1994; **91**: 8592-8596
12 **Lehmann JM,** Kliewer ST, Moore LB, Smith-Oliver TA, Oliver BB, Su JL, Sundseth SS, Winegar DA, Blanchard DE, Spencer TA, Willson TM. Activation of nuclear receptor LXR by oxysterols defines a new hormone pathway. *J Biol Chem* 1997; **272**: 3137-3140
13 **Schwarz M,** Lund EG, Russell DW. Two 7 alpha-hydroxylase enzymes in bile acid biosynthesis. *Curr Opin Lipidol* 1998; **9**: 113-118
14 **Russell DW.** The enzymes, regulation, and genetics of bile acid synthesis. *Annu Rev Biochem* 2003; **73**: 137-174
15 **Babiker A,** Anderson O, Lund E, Xiu RJ, Deeb S, Reshef A, Leitersdorf E, Diczfalusy U, Björkhem I. Elimination of cholesterol in macrophage and endothelial cells by the sterol 27-hydroxylase mechanism. Comparison with high density lipoprotein-mediated reverse cholesterol transport. *J Biol Chem* 1997; **272**: 26253-26261
16 **Ishibashi S,** Schwarz M, Frykman PK, Herz J, Russell DW. Disruption of cholesterol 7a-hydroxylase gene in mice. I. Postnatal lethality reversed by bile acids and vitamin supplementation. *J Biol Chem* 1996; **271**: 18017-18023
17 **Janowski BA,** Willy PJ, Devi TR, Falck JR, Mangelsdorf DJ. An oxysterol signalling pathway mediated by the nuclear receptor LXRa. *Nature* 1996; **383**: 728-731
18 **Ventakeswaran A,** Lefitte BA, Josyl SB, Mak PA, Wilpitz DC, Edwards PA, Tontonoz P. Control of cellular cholesterol efflux by the nuclear oxysterol receptor LXRa. *Proc Natl Acad Sci U S A* 2000; **97**: 12097-12102
19 **Edwards PA,** Ericsson J. Sterols and isoprenoids: Signaling molecules derived from the cholesterol biosynthetic pathway. *Annu Rev Biochem* 1999; **68**: 157-185
20 **Hua X,** Yokoyama C, Wu J, Briggs MR, Brown MS, Goldstein JL, Wang X. SREBP-2, a second basic-helix-loop-helix-leucine zipper protein that stimulates transcription by binding to sterol regulatory elements. *Proc Natl Acad Sci U S A* 1993; **90**: 11603-11607
21 **Yokoyama C,** Wang X, Briggs MR, Admon A, Wu J, Hua X, Goldstein JL, Brown MS. SREBP-1, a basic helix-loop-helix-leucine zipper protein that controls transcription of the LDL receptor gene. *Cell* 1993; **75**: 187-197
22 **Hua X,** Wu J, Goldstein JL, Brown MS, Hobbs HH. Structure of human gene encoding sterol regulatory element binding protein-1 (SREBF1) and localization of SREBF1 and SREBF2 to chromosomes 17p11.2 and 22q13. *Genomics* 1995; **25**: 667-673
23 **Shimomura I,** Shimano H, Horton JD, Goldstein JL, Brown

MS. Differential expression of exons 1a and 1c in the mRNAs of sterol regulatory element binding protein-1 in human and mouse organs and cultured cells. *J Clin Invest* 1997; **99**: 838-845

24 **Miserez, AR**, Cao G, Probst L, Hobbs HH. Structure of the human gene encoding sterol regulatory element binding protein-2 (SREBP-2). *Genomics* 1997; **40**: 31-40

25 **Tontonoz P,** Kim JB, Graves RA, Spiegelman BM. ADD 1: a novel helix-loop- helix transcription factor associated with adipocyte determination and differentiation. *Mol Cell Biol* 1993; **13**: 4752-4759

26 **Shimano H,** Horton JD, Shimomura I, Hammer RE, Brown MS, Goldstein JL. Isoform-1c of sterol regulatory element-binding protein is less active than isoform 1a in livers of transgenic mice and in cultured cells. *J Clin Invest* 1997; **99**: 846-854

27 **Sato R,** Yang J, Wang X, Evans MJ, Ho YK, Goldstein JL, Brown MS. Assignment of the membrane attachment, DNA binding, and transcriptional activation domains of sterol regulatory element-binding protein-1 (SREBP-1). *J Biol Chem* 1994; **269**: 17267-17273

28 **Hua X,** Sakai J, Ho YK, Brown JL, Goldstein MS. Hairpin orientation of sterol regulatory element binding protein 2 in cell membranes as determined by protease protection. *J Biol Chem* 1995; **270**: 29422-29427

29 **Duncan EA,** Brown MS, Goldstein JL, Sakai J. Cleavage site for sterol regulatory protease localized to a Leu-Ser bond in lumenal loop of sterol regulatory element binding protein-2. *J Biol Chem* 1997; **272**: 12778-12785

30 **Magaña MM,** Osborne TF. Two tandem binding sites for sterol regulatory element binding proteins are required for sterol regulation of fatty acid synthase promoter. *J Biol Chem* 1996; **271**: 32689-32694

31 **Hua X,** Nohturfft A, Goldstein JL, Brown MS. Sterol resistance in CHO cells traced to point mutations in SREBP cleavage activating protein (SCAP). *Cell* 1996; **87**: 415-426

32 **Nohturfft A,** Hua X, Brown MS, Goldstein JL. Recurrent G-to-A substitution in a single codon of SREBP cleavage-activating protein causes sterol resistance in three mutant CHO cell lines. *Proc Natl Acad Sci U S A* 1996; **93**: 13709-13714

33 **Nohturfft A,** Brown MS, Goldstein JL. Topology of SREBP cleavage activating protein, a polytopic membrane protein with a sterol sensing domain. *J Biol Chem* 1998; **273**: 17243-17250

34 **Liscum L,** Finer-Moore J, Stroud RM, Luskey KL, Brown MS, Goldstein JL. Domain structure of 3-hydroxy-3-methylglutaryl coenzyme A reductase, a glycoprotein of the endoplasmic reticulum. *J Biol Chem* 1985; **260**: 522-530

35 **Olender EH,** Simoni RD. The intracellular targeting and membrane topology of 3-hydroxy-3-methylglutaryl coenzyme A reductase. *J Biol Chem* 1992; **267**: 4223-4235

36 **Neer EJ,** Schmidt CJ, Nambudripad R, Smith TF. The ancient regulatory protein family of WD-repeat proteins. *Nature* 1994; **371**: 297-300

37 **Sakai J,** Nohturfft A, Cheng D, Ho YK, Brown MS, Goldstein JL. Identification of complexes between the COOH-terminal domain of sterol regulatory element binding protein (SREBPs) and SREBP cleavage-activating protein (SCAP). *J Biol Chem* 1997; **272**: 20213-20221

38 **Nohturfft A,** Jabe D, Goldstein JL, Brown MS, Espenshade PJ. Regulated step in cholesterol feed back localized to budding of SCAP from ER membranes. *Cell* 2000; **102**: 315-323

39 **Wang X,** Sato R, Brown MS, Hua X, Goldstein JL. SREBP-1, a membrane-bound transcription factor released by sterol-regulated proteolysis. *Cell* 1994; **77**: 53-62

40 **Hua X,** Sakai J, Brown MS, Goldstein JL. Regulated cleavage of sterol regulatory element binding proteins (SREBPs) requires sequences on both sides of the endoplasmic reticulum membrane. *J Biol Chem* 1996; **271**: 10379-10384

41 **Sakai J,** Duncan EA, Rawson RB, Hua X, Brown MS, Goldstein JL. Sterol regulated release of SREBP-2 from cell membranes require two sequential cleavages, one within a transmembrane segment. *Cell* 1996; **85**: 1037-1046

42 **Sakai J,** Nohturfft A, Goldstein JL, Brown MS. Cleavage of sterol regulatory element-binding proteins (SREBPs) at site-1 requires interaction with SREBP cleavage-activating protein. Evidence from *in vivo* competition studies. *J Biol Chem* 1998; **273**: 5785-5793

43 **DeBose-Boyd RA,** Brown MS, Li WP, Nohturfft A, Goldstein JL, Espenshade PJ. Transport dependent proteolysis of SREBP: relocation of site-1 protease protein from Golgi to ER. *Cell* 1999; **99**: 703-712

44 **Brown AJ,** Sun L, Feramisco JD, Brown MS, Goldstein JL. Cholesterol addition to ER membranes alters conformation of SCAP, the SREBP escort protein that regulates cholesterol metabolism. *Mol Cell* 2002; **10**: 237-245

45 **Espenshade PJ,** Cheng D, Goldstein JL, Brown MS. Autocatalytic processing of site-1 protease removes propeptide and permits cleavage of sterol regulatory element-binding proteins. *J Biol Chem* 1999; **274**: 22795-22804

46 **Rawson RB,** Zelenski NG, Nijhawan D, Ye J, Sakai J, Hasan MT, Chang TY, Brown MS, Goldstein JL. Complementation cloning of S2P, a gene encoding a putative metalloprotease required for intramembrane cleavage of SREBPs. *Mol Cell* 1997; **1**: 47-57

47 **Duncan EA,** Dave UP, Sakai J, Goldstein JL, Brown MS. Second-site cleavage in sterol regulatory element-binding protein occurs at transmembrane junction as determined by cysteine panning. *J Biol Chem* 1998; **273**: 17801-17809

48 **Brown MS,** Ye J, Rawson RB, Goldstein JL. Regulated intramembrane proteo-lysis: a control mechanism conserved from bacteria to humans. *Cell* 2000; **100**: 391-398

49 **Brown MS,** Goldstein JL. A proteolytic pathway that controls the cholesterol content of membranes, cells and blood. *Proc Natl Acad Sci U S A* 1999; **96**: 11041-11048

50 **Nohturfft A,** DeBose-Boyd RA, Scheek S, Goldstein JL, Brown MS. Sterols regulate cycling of SREBP cleavage activating protein (SCAP) between endoplasmic reticulum and Golgi. *Proc Natl Acad Sci U S A* 1999; **96**: 11235-11240

51 **Sato R,** Inoue J, Kawabe Y, Kodama T, Takano T, Maeda M. Sterol-dependent transcriptional regulation of sterol regulatory element-binding protein-2. *J Biol Chem* 1996; **271**: 26461-26464

52 **Metherall JE,** Ridgway ND, Dawson PA, Goldstein JL, Brown MS. A 25-hydroxycholesterol-resistant cell line deficient in acyl-CoA: cholesterol acyltransferase. *J Biol Chem* 1991; **266**: 12734-12740

53 **Yang J,** Sato R, Goldstein JL, Brown MS. Sterol-resistant transcription in CHO cells caused by gene rearrangement that truncates SREBP-2. *Genes Dev* 1994; **8**: 1910-1919

54 **Korn BS,** Shimomura I, Bashmakov Y, Hammer RE, Horton JD, Goldstein JL, Brown MS. Blunted feedback suppression of SREBP processing by dietary cholesterol in transgenic mice expressing sterol-resistant SCAP / D443N. *J Clin Invest* 1998; **102**: 2050-2060

55 **Rawson RB,** Cheng D, Brown MS, Goldstein JL. Isolation of cholesterol-requiring mutant Chinese hamster ovary cells with defects in cleavage of sterol regulatory element-binding proteins at site 1. *J Biol Chem* 1998; **273**: 28261-28269

56 **Hasan MT,** Chang CC, Chang TY. Somatic cell genetic and biochemical characterization of cell lines resulting from human genomic DNA transfections of Chinese hamster ovary cell mutants defective in sterol-dependent activation of sterol synthesis and LDL receptor expression. *Somat Cell Mol Genet* 1994; **20**: 183-194

57 **Rawson RB,** DeBose-Boyd R, Goldstein JL, Brown MS. Failure to cleave sterol regulatory element-binding proteins (SREBPs) causes cholesterol auxotrophy in Chinese hamster ovary cells with genetic absence of SREBP cleavage-activating protein. *J Biol Chem* 1999; **274**: 28549-28556

58 **Sheng Z,** Otani H, Brown MS, Goldstein JL. Independent regulation of sterol regulatory element-binding proteins 1 and 2 in hamster liver. *Proc Natl Acad Sci U S A* 1995; **92**: 935-938

59 **Yahagi N,** Shimano H, Hasty AH, Amemiya-Kudo M, Okazaki H, Tamura Y, Iizuka Y, Shionoiri F, Ohashi K, Osuga J, Harada K, Gotoda T, Nagai R, Ishibashi S, Yamada N. A crucial role of sterol regulatory element-binding protein-1 in the regulation of lipogenic gene expression by polyunsaturated fatty acids. *J Biol Chem* 1999; **274**: 35840-35844

60 **Mourrieras F,** Foufelle F, Foretz M, Morin J, Bouche S, Ferre P. Induction of fatty acid synthase and S14 gene expression by glucose, xylitol and dihydroxyacetone in cultured rat hepatocytes is closely correlated with glucose 6-phosphate concentrations. *Biochem J* 1997; **326**: 345-349

61 **Sanchez HB,** Yieh L, Osborne TF. Cooperation by sterol regu-

latory element-binding protein and Sp1 in sterol regulation of low density lipoprotein receptor gene. *J Biol Chem* 1995; **270**: 1161-1169

62 **Dooley KA,** Millinder S, Osborne TF. Sterol regulation of 3-hydroxy-3-methylglutaryl-coenzyme A synthase gene through a direct interaction between sterol regulatory element binding protein and the trimeric CCAAT-binding factor/nuclear factor Y. *J Biol Chem* 1998; **273**: 1349-1356

63 **Dooley KA,** Benett MK, Osborne TF. A critical role for cAMP response element-binding protein (CREB) as a coactivator in sterol-regulated transcription of 3-hydroxy-3-methylglutaryl coenzymne A synthase promoter. *J Biol Chem* 1999; **274**: 5285-5291

64 **Magaña MM,** Koo SH, Towle HC, Osborne TF. Different sterol regulatory element-binding protein-1 isoforms utilize distinct co-regulatory factors to activate the promoter of fatty acid synthetase. *J Biol Chem* 2000; **275**: 4762-4733

65 **Oliner JD,** Andresen JM, Hansen SK, Zhou S, Tjian R. SREBP transcriptional activity is mediated through an interaction with the CREB-binding protein. *Genes Dev* 1996; **10**: 2903-2911

66 **Ericsson J,** Edwards PA. CBP is required for sterol-regulated and sterol regulatory element-binding protein-regulated transcription. *J Biol Chem* 1998; **273**: 17865-17870

67 **Näär AM,** Beaurang PA, Zhou S, Abraham S, Solomon W, Tjian R. Composite co-activator ARC mediates chromatin-directed transcriptional activation. *Nature* 1999; **389**: 828-832

68 **Näär AM,** Beaurang PA, Robinson KM, Oliner JD, Avizonis D, Scheek S, Zwicker J, Kadonaga JT, Tjian R. Chromatin, TAFs, and a novel multiprotein coactivator are required for synergistic activation by Sp1 and SREBP-1a *in vitro*. *Genes Dev* 1998; **12**: 3020-3031

69 **Ericsson J,** Jackson SM, Kim JB, Spiegelman BM, Edwards PA. Identification of glycerol-3-phosphate acyltransferase as an adipocyte determination and differentiation factor 1- and sterol regulatory element-binding protein-responsive gene. *J Biol Chem* 1997; **272**: 7298-7305

70 **Guan G,** Dai PH, Osborne TF, Kim JB, Shechter I. Multiple sequence elements are involved in the transcriptional regulation of the human squalene synthase gene. *J Biol Chem* 1997; **272**: 10295-10302

71 **Guan G,** Dai PH, Shechter I. Differential transcriptional regulation of the human squalene synthase gene by sterol regulatory element-binding proteins (SREBP) 1a and 2 and involvement of 5' DNA sequence elements in the regulation. *J Biol Chem* 1998; **273**: 12526-12535

72 **Sakakura Y,** Shimano H, Sone H, Takahashi A, Inoue K, Toyoshima H, Suzuki S, Yamada N. Sterol regulatory element –binding proteins induce an entire pathway of cholesterol synthesis. *Biochem Biophys Res Commun* 2001; **286**: 176-183

73 **Horton JD,** Shimomura I, Brown MS, Hammer RE, Goldstein JL, Shimano H. Acivation of cholesterol synthesis in preference to fatty acid synthesis in liver and adipose tissue of transgenic mice overproducing sterol regulatory element binding protein-2. *J Clin Invest* 1998; **101**: 2331-2339

74 **Moon YA,** Shah NA, Mohapatra S, Warrington JA, Horton JD. Identification of a mammalian long chain fatty acyl elongase regulated by sterol regulatory element-binding proteins. *J Biol Chem* 2001; **276**: 45358-45366

75 **Shimomura I,** Shimano H, Korn BS, Bashmakov Y, Horton JD. Nuclear sterol regulatory element-binding proteins activate genes responsible for the entire program of unsaturated fatty acid biosynthesis in transgenic mouse livers. *J Biol Chem* 1998; **273**: 35299-35306

76 **Flier JS,** Hollenberg AN. ADD-1 provides major new insight into the mechanism of insulin action. *Proc Natl Acad Sci U S A* 1999; **96**: 14191-14192

77 **Foretz M,** Guichard C, Ferre P, Foufelle F. Sterol regulatory element binding protein-1c is a major mediator of insulin action on the hepatic expression of gluco-kinase and lipogenesis-related genes. *Proc Natl Acad Sci U S A* 1999; **96**: 12737-12742

78 **Kim JB,** Sarraf P, Wright M, Yao KM, Mueller E, Solanes G, Lowell BB, Spiegelman BM. Nutritional and insulin regulation of fatty acid synthetase and leptin gene expression through ADD1/SREBP1. *J Clin Invest* 1998; **101**: 1-9

79 **Shimano H,** Yahagi N, Amemiya-Kudo M, Hasty AH, Osuga J, Tamura Y, Shionoiri F, Iizuka Y, Ohashi K, Harada K, Gotoda T, Ishibashi S, Yamada N. Sterol regulatory element-binding protein-1 as a key transcription factor for nutritional induction of lipogenic enzyme genes. *J Biol Chem* 1999; **274**: 35832-35839

80 **Mitchell KJ,** Pinson KI, Kelly OG, Brennan J, Zupicich J, Scherz P, Leighton PA, Goodrich LV, Lu X, Avery BJ, Tate P, Dill K, Pangilinan E, Wakenight P, Tessier-Lavigne M, Skarnes WC. Functional analysis of secreted and transmembrane proteins critical to mouse development. *Nat Genet* 2001; **28**: 241-249

81 **Yang J,** Goldstein JL, Hammer RE, Moon YA, Brown MS, Horton JD. Decreased lipid synthesis in livers of mice with disrupted site-1 protease gene. *Proc Natl Acad Sci U S A* 2001; **98**: 13607-13612

82 **Soukas A,** Cohen P, Socci ND, Friedman JM. Leptin-specific patterns of gene expression in white adipose tissue. *Genes Dev* 2000; **14**: 963-980

83 **Shimomura I,** Hammer RE, Ikemoto S, Brown MS, Goldstein JL. Leptin reverses insulin resistance and diabetes mellitus in mice with congenital lipodystrophy. *Nature* 1999; **401**: 73-76

84 **Libby P**, Aikawa M, Schönbeck U. Cholesterol and atherosclerosis. *Biochim Biophys Acta* 2000; **1529**: 299-309

Edited by Wang XL **Proofread by** Xu FM

PO Box 2345, Beijing 100023, China
Fax: +86-10-85381893
E-mail: wjg@wjgnet.com www.wjgnet.com

World J Gastroenterol 2004;10(21):3088-3093
World Journal of Gastroenterology
 ISSN 1007-9327

• REVIEW •

CDH1 germline mutation in hereditary gastric carcinoma

Hai-Dan Wang, Jun Ren, Lian Zhang

Hai-Dan Wang, Center of Clinical Oncology and International Collaborative Group on Hereditary Gastric Carcinoma, Xijing Hospital, the Fourth Military Medical University, Xi'an 710032, Shaanxi Province, China
Jun Ren, Lian Zhang, Peking University School of Oncology, Beijing 100036, China
Supported by the Teaching and Research Award Program for Outstanding Young Teachers, Ministry of Education, P R China, No. TRAPOYT99-016
Correspondence to: Jun Ren, M.D.,Ph.D, Professor and Chairman, Department of Medical Oncology, Peking University School of Oncology, Beijing 100036, China. renjun@fmmu.edu.cn
Telephone: +86-10-88123125 **Fax:** +86-10-88122437
Received: 2003-11-17 **Accepted:** 2004-01-15

Abstract

This paper provides a bird's-eye view both in preclinical and clinical aspects of E-cadherin germline gene (CDH1) in gastric cancer patients and their families. E-cadherin, a product of CDH1 gene, belonging to the functionally related trans-membrane glycoprotein family, is responsible for the Ca^{2+}-dependent cell-cell adhesion mechanism and contributes to dissociation followed by acquisition of cell motility, which usually occurs in the first step of cancer invasion and metastasis. CDH1 gene germline mutation is common in many types of carcinoma, and occurs very frequent in hereditary gastric carcinoma (HGC) patients and their families. Recently, more and more researches support that E-cadherin plays an important role in the differentiation, growth and invasion of HGC. So it is of great value to clarify its mechanisms both for understanding HGC pathogenesis and for clinical therapy, especially in China, where there are a high risk population of gastric cancer and a high HGC incidence rate. In this paper, recent researches on CDH1 gene mutation, especially its role in tumor genesis and progress of HGC, are reviewed, and advances in evaluation of its mutation status for HGC diagnosis, therapy and prognosis, are also discussed briefly.

Wang HD, Ren J, Zhang L. CDH1 germline mutation in hereditary gastric carcinoma. *World J Gastroenterol* 2004; 10(21): 3088-3093
http://www.wjgnet.com/1007-9327/10/3088.asp

INTRODUCTION

CDH1 mutation in HGC

Gastric carcinoma is one of the leading causes of cancer mortality in many countries, especially in most Asian countries. It is also one of the leading malignant diseases in China. According to data, approximately one Chinese person died of gastric cancer every 2 to 3 min. In the past decades, the incidence tended to increase gradually. Some population based surveys revealed that about 10% gastric cancer patients demonstrated familial clustering. The identification of genes predisposing to HGC is an essential step towards understanding the molecular events underlying tumorigenesis and critical for the clinical management. In 1998, a germline mutation in the CDH1 gene, which located on chromosome locus 16q22.1, was first recognized in Maori kindred from New Zealand with diffuse gastric carcinoma. The product of CDH1 gene, E-cadherin protein, a 120 ku transmembranous glycoprotein, is involved in Ca^{2+}-dependent intercellular adhesion. More and more researches confirm that impaired expression of E-cadherin contributes to histogenesis, tumor growth, metastasis and poor survival of gastric cancer patients, especially HGC patients. So further analyses are needed to clarify the mechanism of gastric cancer and provide better strategies for treatment of HGC patients and prophylaxis of their families.

E-CADHERIN: STRUCTURE AND FUNCTION

The newly mutated gene discovered in HGC, CDH1, is composed of 16 exons and 15 introns encoding the E-cadherin protein. E-cadherin, also called epithelial cadherin or uvomorulin, is a member of the subclass of cadherins, which are Ca^{2+}-dependent cell-cell adhesion receptors identified in vertebrates. The 120 ku E-cadherin molecule is made up of a 27 amino acid signal peptide (exons 1-2), a 154 amino acid precursor peptide (exons2-4), and a 728 amino acid mature peptide. The mature protein consists of three major domains, five extracellular repeats (CAD repeats) (exons 4-13), a single membrane-spanning region (exons 13-14) and a cytoplasmic region (exons 14-16). The N-terminal CAD1 repeat is essential for the homophilic binding specificity that directs "like" E-cadherins with each other. The cytoplasmic domain is bound to the actin cytoskeleton *via* intracellular attachment proteins, the catenins, forming the E-cadherin/catenin complex (Figure 1).

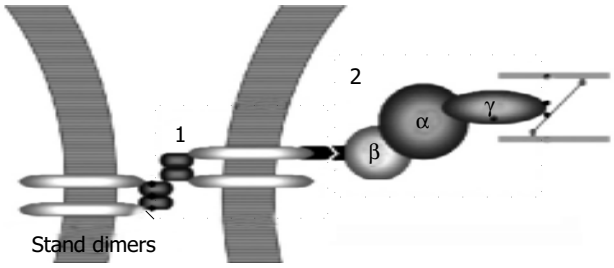

Figure 1 Formation of E-cadherin / catenin complex. Step1. E-cadherin stand dimers on the two adjacent cells' surface combine together and transfer the signals to catenin complex which is composed of β+α+γ subunits. Step2. The complex promotes actins to contract and enhance the intra-cellular adhesion.

Linkage between transmembranous cadherins and actin filament of the cytoskeleton is localized at the cell-cell adherent junction(AJ) and mediated by many associated undercoat proteins of the junction including catenins, vinculins, and actin[1]. Catenins are a series of cadherin-associated cytoplasmic proteins that are co-immunoprecipitated with cadherin by nonionic detergent, and classified by their molecular mass as α-(102 ku), β-(88 ku), γ-(80 ku)[2]. Furthermore, catenins connect cadherin to other integral membrane proteins, such as Na^+-K^+-ATPase, or to cytoplasmic structures, such as fodrin or ankyrin[3]. All these form a transcellular network, mediating structural integrity, cellular polarity and epithelial morphogenesis[4,5].

The CAD1 domain conformation of E-cadherin contains seven β strands (βA - βG) and two short α helices (αA, αB). The homophilic binding specificity appears to be governed by CAD1 domains through a surface including a HAV motif, which is found in or following βF. CAD1 also possesses the PEN (10-13), LDRE (66-69), DXND (100-104) motifs, while CAD2 possesses a DAD motif. These four Ca^{2+}-binding motifs can form a shared Ca^{2+}-binding pocket. The ligation of Ca^{2+} between tandem CAD domains explains the vulnerability of cadherins to proteolytic degradation when Ca^{2+} is depleted. Removal of Ca^{2+} would alter the junction between tandem CAD domains and likely expose the linkers to proteases. The binding of Ca^{2+} could provide the rigidity suggested by Ca^{2+}-induced changes of the entire extracellular region of E-cadherin from a globular to a rod-like structure observed by electronic microscopy[2,6].

Full length E-cadherin has a cleavage site near the transmembrane domain and soluble E-cadherin (s-E-cadherin), a soluble 80-84 ku amino-terminal fragment, can be produced artificially in the culture medium digested by trypsin, so E-cadherin is also named as cell CAM120/80[7]. s-E-cadherin can be detected in the protein extract of tissues, and in serum of peripheral blood or urine by means of immunoenzymometric assay (IEMA) and the volume did not depend on either age or sex[8]. Research also found it could be released from some human carcinoma cell lines (for instance MCF-7) into the culture medium[9].

E-CADHERIN ABNORMAL EXPRESSION IN CARCINOMA

E-cadherin is a crucial adhesion molecule which hampers tumor invasion and metastasis. Down-regulation of expression or impaired function would lead cells to poor intercellular adhesion through inhibiting homophilic binding. To normal epithelial tissues, it means poor differentiation, while to tumor, it means invasive growth pattern and easy to spread from the primary place. Disturbance of epithelial cell adhesion has been shown to be due to several mechanisms as shown in Figure1. The first is inefficiency of E-cadherin homophilic binding, the second is abnormality or deletion of catenins, the last is biochemical modification of catenins, such as tyrosine phosphorylation of β-catenin[10,11]. Among the factors that lead to inefficient homophilic binding of E-cadherin, the most important and widely recognized is E-cadherin down regulation or dysfunction due to CDH1 mutations.

Down-regulation of E-cadherin expression or CDH1 mutations could cause a change towards a less epithelial morphology and also interfered with initial adhesion of cells. Moreover, changed E-cadherins could sharply increase cell motility and change the organization of actin cytoskeleton. Nagafuchi *et al*.[12] showed that the enhanced expression of E-cadherin cDNA in fibroblastic cells could generate epithelial structures in their recent research. McNeill *et al*.[13] found that E-cadherin could cause polarized distribution of Na^+-K^+-ATPase, an important factor in the establishment of cell polarities. Mutations have been also found at very early non-invasive stages, thus associating E-cadherin mutations with loss of growth control and defining CDH1 as a real tumor suppressor[14,15]. All of these may contribute to the significant correlation between abnormal E-cadherin expression and degree of differentiation ($P = 0.0001$) or local tumor size ($P = 0.002$)[16].

Immunohistochemical studies have shown that expression of E-cadherin is reduced or lost in more than 15 different human carcinomas[17]. The frequency of reduced E-cadherin expression is higher in tumors with infiltrative growth than in those with expansive growth. These observations are supported by *in vitro* studies, which evaluated the influence of E-cadherin on cell behavior. Behrens *et al*.[18]found MDCK cells could invade into collagen gels when their E-cadherins were inactivated with antibodies. Frixen *et al*.[19] also observed the similar phenomenon that the invasiveness of several human carcinoma lines was suppressed by mouse E-cadherin cDNA transfection. Down regulation of E-cadherin or its functional defects could change the construction of actin cytoskeleton, which can weaken intracellular adhesion, increase the activity of epithelial cells and lead to more invasions.

Extensive immunohistopathologic studies, including those of squamous cell carcinomas of the head, neck and prostate also support the possibility that loss of E-cadherin expression may promote tumor metastasis to lymph nodes, Reduced E-cadherin expression of breast cancer was also found to have a higher frequency of blood-borne distant metastasis (*e.g.* bone or lung) than preserved E-cadherin expression of other tumors. There was a significant correlation between the degree of E-cadherin expression and the degree of tumor differentiation, as well as histological type according to the Lauren or the WHO classifications. Similarly, the correlation between E-cadherin expression and prognostic parameters (depth of invasion, lymph node involvement and vascular invasion) could be demonstrated according to some researches. These findings are consistent with the previous hypothesis that inhibition of E-cadherin function could enhance the release of cancer cells from their primary sites.

CDH1 MUTATION IN HGC PATIENTS AND FAMILIES

Lauren's classification of gastric cancer includes the intestinal (glandular) and diffuse type, as well as the mixed type. It has been reported that two histologic types have differences in epidemiology, clinicopathologic profile and molecular genetics, while both originate from *Helicobacter pylori* positive gastritis. The intestinal (glandular) type is especially predominant in high-risk population and elderly patients, and related with environmental factors, and their incident rates are decreasing in developed countries, suggesting that the pathogenesis of intestinal-type gastric carcinoma has an environmental component. Diffuse gastric cancer is determined significantly by heredity and the criteria for familial gastric cancer worked out by some investigators[20,21] are as follows. There should be at least 3 relatives with gastric cancer. One should be a first-degree relative of the other 2. At least 2 successive generations should be affected. At least 1 should be diagnosed before age 50. Other familial tumors should be excluded.

Several investigations outlined the role of lost or mutated junctional molecules (E-cadherin, catenins, integrins, *etc.*) in the pathogenesis of diffuse gastric cancer (DGC). In particular, more than 50% of advanced diffuse gastric cancer patients showed mutations of CDH1 gene[22-25]. Germline mutations of the CDH1 gene have been recently reported in gastric cancer families with diffuse-type tumors but not in those with intestinal-type tumors[26]. These families are characterized by a highly penetrant susceptibility to DGC with an autosomal dominant pattern of inheritance, predominantly in young persons. Familial aggregation of GC occurs in about 1% of gastric cancer patients. Although the genetic factors resulting in this aggregation have been unclear, the study indicates that germline mutations of CDH1 genes, do contribute to such a clustering. Mutations of the CDH1 gene has a high penetrance and confers a lifetime risk of gastric cancer of 75-80% for carriers[27-30].

The International Gastric Cancer Linkage Consortium (IGCLC) predicted that up to 25% of families fulfilling the criteria for hereditary DGC would harbour CDH1 germline mutations[29]. CDH1 is well known as a strong invasion suppressor in experimental tumor cell systems. Inactivated mutations have been identified for the CDH1 gene in HGC. To date, 69 somatic mutations have been reported comprising, in addition to few missense mutations, mainly splice site mutations and truncation mutations caused by insertions, deletions and nonsense mutations. Up to now,

27 germline mutations previously reported are distributed along with CDH1 gene in Table 1. While in sporadic gastric cancers, truncation mutations are uncommon and sequence changes usually result in either missense mutations (most commonly in exons 8 and 9) or exon skipping, especially in exons 6-9[30]. From the 27 CDH1 mutations described to date, 24 are inactivated ones (splice-site, frame shift and nonsense) and the remaining 4 are missense[31-37].

Table 1 CDH1 gene germline mutation patterns in HGC families

Ethnic background	Age at diagnosis	Mutation type	Mutation site
White	30-67	45insT	Exon 1
White	34-69	49-2A→G	Exon 2
-	-	53delC	Exon 2
White	27-50	59G→A	Exon 2
White	37-46	70G→T	Exon 2
Japanese	46-72	185G→T	Exon 3[1]
White	33-69	187C→T	Exon 3
Maori	22-28	190C→T	Exon 3
White	41-47	283C→T	Exon 3
White	15-58	372-377del1	Exon 3
White	31-55	586G→T	Exon 5
Korean	30-63	731A→G	Exon 6[1]
White	23-70	832 G→A	Exon 6
White	14-67	1008G→T	Exon 7
White	35-47	1018 A→G	Exon 8[1]
African-American	29-58	1137+1G→A	Intron 8
Korean	42-49	1460T→C	Exon 10[1]
White	32-40	1472insA	Exon 10
White	31	1487del7	Exon 10
-	-	1565+1 G→T	Intron 10
White	40-63	1588insC	Exon 11
-	-	1710delT	Exon 11
White	30-68	1711insG	Exon 11
White	23-43	1792C→T	Exon 12
Maori	30	2095C→T	Exon 13
-	-	2295+5 G→A	Intron 14
White	16-35	2381insC	Exon 15

[1]Missence mutation; -No information obtained from the published paper.

Mutant E-cadherins are not localized in the lateral regions of cell-to-cell contact sites of adherin junctions (AJs) and show apical and perinuclear localization. It is explained by an inability of the cells to complete polarization[38]. These may result in disassembly of AJs and consequently conversion to a spindled and more scattered cell morphology[39]. Impaired processing of mutant E-cadherin, loss of the putative calcium binding sites or essential amino acid motives, may cause a transition from a rigid to a more globular molecular structure of the extracellular domain. In response to extracellular signals, cells react by dissolving their cell-to-cell contacts and by changing their shape and the strength of their attachment to the substrate, thus resulting in significant reduction or loss of its ability to bind in a homophilic fashion to neighboring cells[40,41]. Cell motility is thought to be the result of the concerted action of all these individual events.

Mutant E-cadherin lacking the cytoplasmic domain or the β-catenin-binding site may tie up essential catenins, which influences its function to suppress cell motility. Actin filaments are drastically reduced[42]. The actin belt characteristics of epithelial cells are lost[43].Because proper anchorage to the cytoskeleton is necessary for E-cadherin function, suppression of E-cadherin expression or of its functional activity, or a defect in any of the molecules involved in this system, may account for the ability of cancer cells to detach from the primary tumor and invade locally. Cells with initial calcium-dependent cell aggregation exhibits decreased aggregation and remarkably increase cell motility when E-cadherin is not expressed (Figure 2).

We can conclude that these E-cadherin mutations may not only affect cell adhesion but also play an important role in a trans-dominant-active manner, thus leading to increased cell motility. They are the cause of multiple morphological and functional disorders and could induce scattered morphology and invasive behavior of diffuse gastric cancer.

Tissue specific gene expression has been explained by the interaction of promoter sequences with their specific transcription factors. *In vivo,* foot printing analysis revealed that positive regulatory elements of the E-cadherin promotor were specifically bound to transcription factors in E-cadherin-expressing cells. Mapping of DNase type I hypersensitive sites showed that the chromatin structure in the promotor region was loosened in expressing cells but condensed in non-expressing cells. Furthermore, endogenous E-cadherin promotor was methylated at CpG island sites in undifferentiated cells. All these suggested that silencing of the promotor during epithelial mesenchymal transition and tumor progression was due to a loss of factor-binding *in vivo* and chromatin rearrangement in

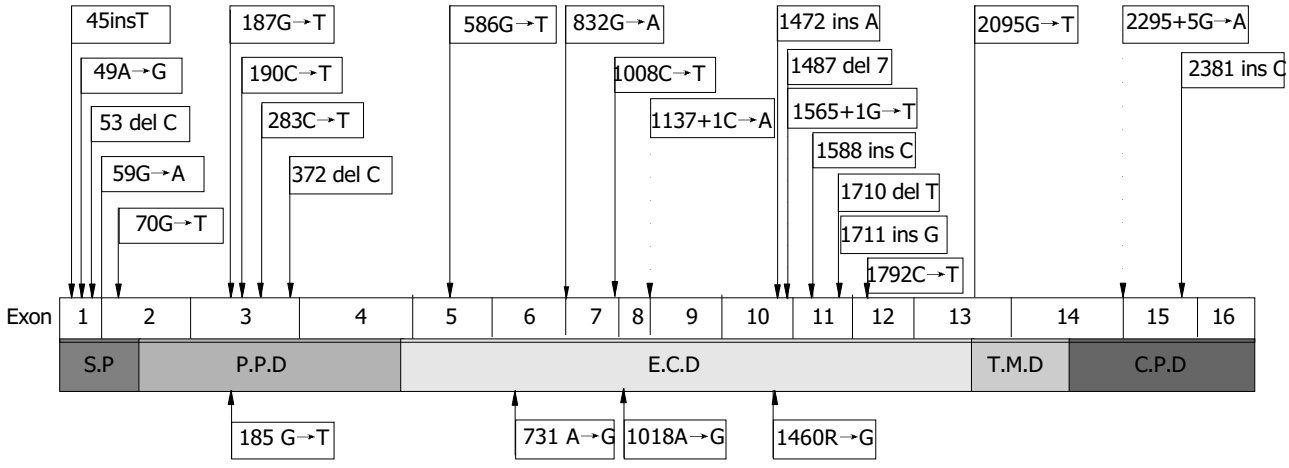

Figure 2 Schematic of CDH1 germline mutations in HGC. Truncating mutations are shown above the gene and missense mutations below. Arrowhead indicates the status in the dot frame refers to the alteration of intron pointed. S.P: signal peptide, P.P.D: protein precursor domain, E.C.D: extracellular domain, T.M.D: transmembrane domain and C.P.D: cytoplastic domain.

the regulatory region[10,44]. Comijn *et al*.[11] reported that multi-zinc finger protein, SIP1(ZEB-2) and snail showing specific DNA binding activity could bind to partly overlapping promotor sequences and had similar silencing effects.

CDH1 MUTATION FOR HCG DIAGNOSIS AND THERAPY

Indicator for prophylactic total gastrectomy

HGC was associated with E-cadherin. Penetrance of the gene ranged from 70% to 80%, and the average age of gastric cancer patients was 37 years[20,45,46]. These characteristics have led to the consideration of prophylactic total gastrectomy (PTG) in family members with CDH1 mutations. Lewis *et al*.[45] performed this operation on 6 asymptomatic members in 2 families based on family pedigree and genetic analysis. The gastric specimens appeared normal and the results of routine pathologic examination were negative for cancer, but all the patients had microscopic foci of cancer, often at multiple sites, with overlying normal gastric mucosa. These results indicate that CDH1 gene mutations in association with familial gastric cancer are a new disease for PTG. Huntsman *et al*.[28] also recommended genetic counseling and prophylactic gastrectomy in young people. The morbidity of this operation was much higher than that of other genetic diseases. The morbidity of prophylactic gastrectomy in the young, healthy population has been estimated as following: 1-2% mortality, 10-20% major acute morbidity, principally related to esophageal anastomotic proceduress, and 100% long term morbidity related to weight loss, rapid intestinal transit, dumping syndrome, and diarrhoea. The high surgical risk of the procedure should be minimised by operations at centers with experience rich in gastric surgery. The decision to perform prophylactic gastrectomy should be balanced with age based risk and based on age specific penetrance data. Other factors, for example, the decision to operate on children, may affect the decision regarding the timing of prophylactic gastrectomy, and it is essential that patients carrying the gene have the opportunity extensive counseling and discussion with clinicians, geneticists, and counsellors before making the decision. The risk of other cancers (breast, colon) should also be targets of screening, as they may also be increased in this population, and patients should be counselled regarding these. However, germline mutations of E-cadherin could be used to identify individuals with a high risk[47].

Target for radioimmunotherapy

Radiolabeled mAb used in radioimmunotherapy is limited because of lack of tumor specific antigens. In most cases reported thus far, tumor antigens serving as targets are not tumor-specific, being overexpressed in tumor cells and also at a lower level in normal cells. Only one tumor-specific mAb that recognizes a mutant form of the epidermal l growth factor receptor (EGFRv III) has been found in different tumor types[48]. Inframe deletions of exons 8 or 9 in the mRNA coding for E-cadherin are characteristic of DGC. So a rat mAb (d9mAb) was generated that specifically reacts with this mutation, and d9mAb was found to react with 13% of E-cadherin-expressing DGCs[49]. Senekowitsch-Schmidtke *et al*.[50] conjugated d9mAb with the α-emitting radionuclide ^{213}Bi, and tested for its binding specificity in sc and ip tumors expressing mutant E-cadherin. Seventy-eight percent of the total activity in ascites fluid was bound to free tumor cells, whereas in control cells expressing wild-type E-cadherin, the binding was only 18%. The selective binding of the ^{213}Bi-labeled, mutation-specific monoclonal antibody d9mAb raised its significant potential for the local radio-immunotherapy of disseminated, diffuse-type gastric carcinoma.

Markers for prognosis and evaluation

Gastric cancer remains a major cause of cancer mortality globally but no good prognostic tumor markers are available. The most frequently used tumor markers in gastric cancer are carcinoembryonic antigen (CEA) and CA19-9[51], Gastric cancer antigen MG-7 may be a good marker for GC[52], or even the detection of circulating DNA in serum reported recently[53], but only a modest proportion of patients had elevated levels of these markers. Under-expression of E-cadherin molecules has been found in various malignancies and has a potential value as a prognostic marker[54]. Serum soluble E-cadherin was found in the circulation of normal individuals but was particularly elevated in patients with malignancies. s-E-cadherin might derive from cancer tissues, though the expression of E-cadherin was decreased. With increased protease, the degradation products of tissue E-cadherin could accumulate and release into peripheral blood. However, its value in gastric cancer is controversial. Velikova *et al*.[55] were unable to show a significant difference in serum soluble E-cadherin between patients with gastric cancer and normal subjects, while Gofuku *et al*.[8] showed that concentrations were significantly elevated in 67% patients. Chan *et al*.[56] confirmed its potential value as a prognostic marker. A high concentration could predicte palliative/conservative treatment and T4 invasion. Gabbert *et al*.[57] studied 413 gastric cancer patients, including all histological tumor types and stages. As shown by univariate and multivariate Cox regression analyses, patients with E-cadherin-positive tumors had significantly better 3 and 5 year survival rates than patients with E-cadherin-negative tumors. This prognostic effect remained present in a multivariate Cox regression analysis, including the prognostic parameters pT category, pN category and vascular invasion, suggesting that it is an independent prognostic marker.

In short, hereditary gastric cancer is still a challenge, especially its diagnosis and treatment[58], although some progress has been achieved in recent years with the development of molecular biology and new methods.

ACKNOWLEDGEMENTS

We greatly thank Professor Bo-Rong Pan of the Fourth Military Medical University for his valuable comments on our study and Dr. Ying Lin, Department of Otolaryngology, Xijing Hospital, the Fourth Military Medical University for her helpful assistance on the manuscript.

REFERENCES

1 **Nagafuchi A**, Takeichi M, Tsukita S. The 102 kd cadherin-associated protein: similarity to vinculin and posttranscriptional regulation of expression. *Cell* 1991; **65**: 849-857
2 **Ozawa M**, Baribault H, Kemler R. The cytoplasmic domain of the cell adhesion molecule uvomorulin associates with three independent proteins structurally related in different species. *EMBO J* 1989; **8**: 1711-1717
3 **Nathke IS**, Hinck L, Swedlow JR, Papkoff J, Nelson WJ. Defining interactions and distributions of cadherin and catenin complexes in polarized epithelial cells. *J Cell Biol* 1994; **125**: 1341-1352
4 **Overduin M**, Harvey TS, Bagby S, Tong KI, Yau P, Takeichi M, Ikura M. Solution structure of the epithelial cadherin domain responsible for selective cell adhesion. *Science* 1995; **267**: 386-389
5 **Shapiro L**, Fannon AM, Kwong PD, Thompson A, Lehmann MS, Grubel G, Legrand JF, Als-Nielsen J, Colman DR, Hendrickson WA. Structural basis of cell-cell adhesion by cadherins. *Nature* 1995; **374:** 327-337
6 **Nagar B**, Overduin M, Ikura M, Rini JM. Structural basis of calcium-induced E-cadherin rigidification and dimerization. *Nature* 1996; **380**: 360-364
7 **Matsuyoshi N**, Tanaka T, Toda K, Okamoto H, Furukawa F, Imamura S. Soluble E-cadherin: a novel cutaneous disease marker. *Br J Dermatol* 1995; **132**: 745-749

8 **Gofuku J**, Shiozaki H, Doki Y, Inoue M, Hirao M, Fukuchi N, Monden M. Characterization of soluble E-cadherin as a disease marker in gastric cancer patients. *Br J Cancer* 1998; **78**: 1095-1101

9 **Damsky CH**, Richa J, Solter D, Knudsen K, Buck CA. Identification and purification of a cell surface glycoprotein mediating intercellular adhesion in embryonic and adult tissue. *Cell* 1983; **34**: 455-466

10 **Hennig G**, Behrens J, Truss M, Frisch S, Reichmann E, Birchmeier W. Progression of carcinoma cells is associated with alterations in chromatin structure and factor binding at the E-cadherin promoter *in vivo*. *Oncogene* 1995; **11**: 475-484

11 **Comijn J**, Berx G, Vermassen P, Verschueren K, van Grunsven L, Bruyneel E, Mareel M, Huylebroeck D, van Roy F. The two-handed E box binding zinc finger protein SIP1 downregulates E-cadherin and induces invasion. *Mol Cell* 2001; **7**: 1267-1278

12 **Nagafuchi A**, Shirayoshi Y, Okazaki K, Yasuda K, Takeichi M. Transformation of cell adhesion properties by exogenously introduced E-cadherin cDNA. *Nature* 1987; **329**: 341-343

13 **McNeill H**, Ozawa M, Kemler R, Nelson WJ. Novel function of the cell adhesion molecule uvomorulin as an inducer of cell surface polarity. *Cell* 1990; **62**: 309-316

14 **Blok P**, Craanen ME, Dekker W, Tytgat GN. Loss of E-cadherin expression in early gastric cancer. *Histopathology* 1999; **34**: 410-415

15 **Li YJ**, Ji XR. Relationship between expression of E-cadherin-catenin complex and clinicopathologic characteristics of pancreatic cancer. *World J Gastroenterol* 2003; **9**: 368-372

16 **Karayiannakis AJ**, Syrigos KN, Chatzigianni E, Papanikolaou S, Karatzas G. E-cadherin expression as a differentiation marker in gastric cancer. *Hepatogastroenterology* 1998; **45**: 2437-2442

17 **Potter E**, Bergwitz C, Brabant G. The cadherin-catenin system: implications for growth and differentiation of endocrine tissues. *Endocr Rev* 1999; **20**: 207-239

18 **Behrens J,** Vakaet L, Friis R, Winterhager E, Van Roy F, Mareel MM, Birchmeier W. Loss of epithelial differentiation and gain of invasiveness correlates with tyrosine phosphorylation of the E-cadherin/beta-catenin complex in cells transformed with a temperature-sensitive v-SRC gene. *J Cell Biol* 1993; **120**: 757-766

19 **Frixen UH,** Behrens J, Sachs M, Eberle G, Voss B, Warda A, Lochner D, Birchmeier W. E-cadherin-mediated cell-cell adhesion prevents invasiveness of human carcinoma cells. *J Cell Biol* 1991; **113**: 173-185

20 **Humar B**, Toro T, Graziano F, Muller H, Dobbie Z, Kwang-Yang H, Eng C, Hampel H, Gilbert D, Winship I, Parry S, Ward R, Findlay M, Christian A, Tucker M, Tucker K, Merriman T, Guilford P. Novel germline CDH1 mutations in hereditary diffuse gastric cancer families. *Hum Mutat* 2002; **19**: 518-525

21 **Caldas C**, Carneiro F, Lynch HT, Yokota J, Wiesner GL, Powell SM, Lewis FR, Huntsman DG, Pharoah PD, Jankowski JA, MacLeod P, Vogelsang H, Keller G, Park KG, Richards FM, Maher ER, Gayther SA, Oliveira C, Grehan N, Wight D, Seruca R, Roviello F, Ponder BA, Jackson CE. Familial gastric cancer: overview and guidelines for management. *J Med Genet* 1999; **36**: 873-880

22 **Becker KF**, Atkinson MJ, Reich U, Becker I, Nekarda H, Siewert JR, Hofler H. E-cadherin gene mutations provide clues to diffuse type gastric carcinomas. *Cancer Res* 1994; **54**: 3845-3852

23 **Mayer B**, Johnson JP, Leitl F, Jauch KW, Heiss MM, Schildberg FW, Birchmeier W, Funke I. E-cadherin expression in primary and metastatic gastric cancer: down-regulation correlates with cellular dedifferentiation and glandular disintegration. *Cancer Res* 1993; **53**: 1690-1695

24 **Graziano F,** Humar B, Guilford P. The role of the E-cadherin gene (CDH1) in diffuse gastric cancer susceptibility: from the laboratory to clinical practice. *Ann Oncol* 2003; **14**: 1705-1713

25 **Zhou YN**, Xu CP, Han B, Li M, Qiao L, Fang DC, Yang JM. Expression of E-cadherin and beta-catenin in gastric carcinoma and its correlation with the clinicopathological features and patient survival. *World J Gastroenterol* 2002; **8**: 987-993

26 **Zheng ZH**, Sun XJ, Qiu GR, Liu YH, Wang MX, Sun KL. E-cadherin gene mutation in precancerous condition' early and advanced stages of gastric cancer. *Shijie Huaren Xiaohua Zazhi* 2002; **10**: 153-156

27 **Giarelli E**. Prophylactic gastrectomy for CDH1 mutation carriers. *Clin J Oncol Nurs* 2002; **6**: 161-162

28 **Huntsman DG**, Carneiro F, Lewis FR, MacLeod PM, Hayashi A, Monaghan KG, Maung R, Seruca R, Jackson CE, Caldas C. Early gastric cancer in young, asymptomatic carriers of germ-line E-cadherin mutations. *N Engl J Med* 2001; **344**: 1904-1909

29 **Oliveira C**, Bordin MC, Grehan N, Huntsman D, Suriano G, Machado JC, Kiviluoto T, Aaltonen L, Jackson CE, Seruca R, Caldas C. Screening E-cadherin in gastric cancer families reveals germline mutations only in hereditary diffuse gastric cancer kindred. *Hum Mutat* 2002; **19**: 510-517

30 **Berx G**, Becker KF, Hofler H, van Roy F. Mutations of the human E-cadherin (CDH1) gene. *Hum Mutat* 1998; **12**: 226-237

31 **Richards FM**, McKee SA, Rajpar MH, Cole TR, Evans DG, Jankowski JA, McKeown C, Sanders DS, Maher ER. Germline E-cadherin gene (CDH1) mutations predispose to familial gastric cancer and colorectal cancer. *Hum Mol Genet* 1999; **8**: 607-610

32 **Guilford PJ**, Hopkins JB, Grady WM, Markowitz SD, Willis J, Lynch H, Rajput A, Wiesner GL, Lindor NM, Burgart LJ, Toro TT, Lee D, Limacher JM, Shaw DW, Findlay MP, Reeve AE. E-cadherin germline mutations define an inherited cancer syndrome dominated by diffuse gastric cancer. *Hum Mutat* 1999; **14**: 249-255

33 **Shinmura K**, Kohno T, Takahashi M, Sasaki A, Ochiai A, Guilford P, Hunter A, Reeve AE, Sugimura H, Yamaguchi N, Yokota J. Familial gastric cancer: clinicopathological characteristics, RER phenotype and germline p53 and E-cadherin mutations. *Carcinogenesis* 1999; **20**: 1127-1131

34 **Gayther SA**, Gorringe KL, Ramus SJ, Huntsman D, Roviello F, Grehan N, Machado JC, Pinto E, Seruca R, Halling K, MacLeod P, Powell SM, Jackson CE, Ponder BA, Caldas C. Identification of germ-line E-cadherin mutations in gastric cancer families of European origin. *Cancer Res* 1998; **58**: 4086-4089

35 **Dussaulx-Garin L**, Blayau M, Pagenault M, Le Berre-Heresbach N, Raoul JL, Campion JP, David V, Bretagne JF. A new mutation of E-cadherin gene in familial gastric linitis plastica cancer with extra-digestive dissemination. *Eur J Gastroenterol Hepatol* 2001; **13**: 711-715

36 **Keller G**, Vogelsang H, Becker I, Hutter J, Ott K, Candidus S, Grundei T, Becker KF, Mueller J, Siewert JR, Hofler H. Diffuse type gastric and lobular breast carcinoma in a familial gastric cancer patient with an E-cadherin germline mutation. *Am J Pathol* 1999; **155**: 337-342

37 **Yoon KA**, Ku JL, Yang HK, Kim WH, Park SY, Park JG. Germline mutations of E-cadherin gene in Korean familial gastric cancer patients. *J Hum Genet* 1999; **44**: 177-180

38 **Handschuh G**, Candidus S, Luber B, Reich U, Schott C, Oswald S, Becke H, Hutzler P, Birchmeier W, Hofler H, Becker KF. Tumour-associated E-cadherin mutations alter cellular morphology, decrease cellular adhesion and increase cellular motility. *Oncogene* 1999; **18**: 4301-4312

39 **Birchmeier W**, Hulsken J, Behrens J. Adherens junction proteins in tumour progression. *Cancer Surv* 1995; **24**: 129-140

40 **Lauffenburger DA**, Horwitz AF. Cell migration: a physically integrated molecular process. *Cell* 1996; **84**: 359-369

41 **Fukudome Y**, Yanagihara K, Takeichi M, Ito F, Shibamoto S. Characterization of a mutant E-cadherin protein encoded by a mutant gene frequently seen in diffuse-type human gastric carcinoma. *Int J Cancer* 2000; **88**: 579-583

42 **Mitchison TJ**, Cramer LP. Actin-based cell motility and cell locomotion. *Cell* 1996; **84**: 371-379

43 **Zhu AJ**, Watt FM. Expression of a dominant negative cadherin mutant inhibits proliferation and stimulates terminal differentiation of human epidermal keratinocytes. *J Cell Sci* 1996; **109** (Pt 13): 3013-3023

44 **Leung WK**, Yu J, Ng EK, To KF, Ma PK, Lee TL, Go MY, Chung SC, Sung JJ. Concurrent hypermethylation of multiple tumor-related genes in gastric carcinoma and adjacent normal tissues. *Cancer* 2001; **91**: 2294-2301

45 **Lewis FR**, Mellinger JD, Hayashi A, Lorelli D, Monaghan KG, Carneiro F, Huntsman DG, Jackson CE, Caldas C. Prophylac-

tic total gastrectomy for familial gastric cancer. *Surgery* 2001; **130**: 612-617

46 **Chun YS**, Lindor NM, Smyrk TC, Petersen BT, Burgart LJ, Guilford PJ, Donohue JH. Germline E-cadherin gene mutations: is prophylactic total gastrectomy indicated? *Cancer* 2001; **92**: 181-187

47 **Becker KF**, Keller G, Hoefler H. The use of molecular biology in diagnosis and prognosis of gastric cancer. *Surg Oncol* 2000; **9**: 5-11

48 **Wikstrand CJ**, McLendon RE, Friedman AH, Bigner DD. Cell surface localization and density of the tumor-associated variant of the epidermal growth factor receptor, EGFRvIII. *Cancer Res* 1997; **57**: 4130-4140

49 **Becker KF**, Kremmer E, Eulitz M, Becker I, Handschuh G, Schuhmacher C, Muller W, Gabbert HE, Ochiai A, Hirohashi S, Hofler H. Analysis of E-cadherin in diffuse-type gastric cancer using a mutation-specific monoclonal antibody. *Am J Pathol* 1999; **155**: 1803-1809

50 **Senekowitsch-Schmidtke R**, Schuhmacher C, Becker KF, Nikula TK, Seidl C, Becker I, Miederer M, Apostolidis C, Adam C, Huber R, Kremmer E, Fischer K, Schwaiger M. Highly specific tumor binding of a 213Bi-labeled monoclonal antibody against mutant E-cadherin suggests its usefulness for locoregional alpha-radioimmunotherapy of diffuse-type gastric cancer. *Cancer Res* 2001; **61**: 2804-2808

51 **Ren J,** Ge L, Li Y, Bai J, Liu WC, Si XM. Detection of circulating CEA molecules in human sera and leukopheresis of peripheral blood stem cells with *E. coli* expressed bispecific CEAScFv-streptavidin fusion protein-based immuno-PCR technique. *Ann N Y Acad Sci* 2001; **945**: 116-118

52 **Ren J**, Chen Z, Juan SJ, Yong XY, Pan BR, Fan DM. Detection of circulating gastric carcinoma-associated antigen MG7-Ag in human sera using an established single determinant immuno-polymerase chain reaction technique. *Cancer* 2000; **88**: 280-285

53 **Wang HD,** Ren J, Si XM, Zhang YJ, You XH, Liu WC, Fan L. Detection of circulating p53 gene mutation in HCC patients by DHPLC. *Int J Cancer* 2002; **13**: s112

54 **Takeichi M**. Cadherins in cancer: implications for invasion and metastasis. *Curr Opin Cell Biol* 1993; **5**: 806-811

55 **Velikova G**, Banks RE, Gearing A, Hemingway I, Forbes MA, Preston SR, Jones M, Wyatt J, Miller K, Ward U, Al-Maskatti J, Singh SM, Ambrose NS, Primrose JN, Selby PJ. Circulating soluble adhesion molecules E-cadherin, E-selectin, intercellular adhesion molecule-1 (ICAM-1) and vascular cell adhesion molecule-1 (VCAM-1) in patients with gastric cancer. *Br J Cancer* 1997; **76**: 1398-1404

56 **Chan AO**, Lam SK, Chu KM, Lam CM, Kwok E, Leung SY, Yuen ST, Law SY, Hui WM, Lai KC, Wong CY, Hu HC, Lai CL, Wong J. Soluble E-cadherin is a valid prognostic marker in gastric carcinoma. *Gut* 2001; **48**: 808-811

57 **Gabbert HE**, Mueller W, Schneiders A, Meier S, Moll R, Birchmeier W, Hommel G. Prognostic value of E-cadherin expression in 413 gastric carcinomas. *Int J Cancer* 1996; **69**: 184-189

58 **Medina-Franco H.** Hereditary gastric cancer. Genetics and clinical management. *Rev Gastroenterol Mex* 2003; **68**: 51-54

Edited by Zhu LH and Wang XL **Proofread by** Xu FM

PO Box 2345, Beijing 100023, China
Fax: +86-10-85381893
E-mail: wjg@wjgnet.com www.wjgnet.com

World J Gastroenterol 2004;10(21):3094-3098
World Journal of Gastroenterology
 ISSN 1007-9327

• GASTRIC CANCER •

Expression of survivin in primary and metastatic gastric cancer cells obtained by laser capture microdissection

Zhen-Ning Wang, Hui-Mian Xu, Li Jiang, Xin Zhou, Chong Lu, Xue Zhang

Zhen-Ning Wang, Li Jiang, Xue Zhang, The Research Center for Medical Genomics and MOH Key Laboratory of Cell Biology, China Medical University, Shenyang 110001, Liaoning Province, China
Zhen-Ning Wang, Hui-Mian Xu, Xin Zhou, Chong Lu, Department of Surgical Oncology, the First Affiliated Hospital of China Medical University, Shenyang 110001**,** Liaoning Province, China
Xue Zhang, Department of Medical Genetics and National Key Laboratory of Medical Molecular Biology, Chinese Academy of Medical Sciences and Peking Union Medical College, Beijing 100005, China
Supported by the Nationa l 973 Program of China, No. G1998051203, the National Science Fund for Distinguished Young Scholars of China, No. 30125017, and the MOE TRAPOYT Program of China, No. 1999-96
Correspondence to: Dr. Xue Zhang, The Research Center for Medical Genomics, China Medical University, Shenyang 110001, Liaoning Province, China. xuezhang@pumc.edu.cn
Telephone: +86-10-86319731 **Fax:** +86-10-65124876
Received: 2003-09-06 **Accepted:** 2003-10-22

Abstract

AIM: Survivin, a recently identified member of the inhibitor of apoptosis protein family, is expressed during development and in various human cancers. However, its expression in normal tissues and clinical relevance in cancers are still debated. In the present study, we analyzed the expression of the survivin gene in human primary and metastatic gastric cancer cells as well as in paired epithelial cells from normal gastric mucosa by means of a novel laser capture microdissection (LCM) technique coupled with reverse transcription - polymerase chain reaction (RT-PCR).

METHODS: Thirty patients who had undergone gastrectomy with lymph node dissection for gastric cancer without preoperative treatments were included. Neoplastic tissue, metastatic lymph nodes, and apparently uninvolved normal tissue were collected from each patient. LCM-captured "pure" cell groups were respectively subjected to RT-PCR analysis with primers specific for the survivin gene.

RESULTS: Of the paired samples from 30 gastric cancer patients studied, 24 (80%) primary gastric cancer cell groups and 7 (23%) adjacent morphologically "normal" gastric epithelial cell groups were shown to have a detectable survivin expression. There was a statistically significant difference in suvivin expression between these two groups ($P<0.01$). Meanwhile, 95% (19/20) of the metastatic gastric cancer cell groups from lymph nodes had a clear expression of the survivin gene. However, no significant correlation between survivin expression and clinicopathological features of gastric cancer was observed in the present study.

CONCLUSION: Survivin expression is present in the majority of gastric cancer cell groups obtained by LCM techniques. The high expression rate in metastatic lesions suggests a possible role of survivin in cancer invasiveness and metastasis. It may contribute to the detection of gastric cancer micrometastasis as a potential molecular marker. In addition, the high expression percentage renders survivin a potential target in the therapy for gastric cancer.

Wang ZN, Xu HM, Jiang L, Zhou X, Lu C, Zhang X. Expression of survivin in primary and metastatic gastric cancer cells obtained by laser capture microdissection. *World J Gastroenterol* 2004; 10(21): 3094-3098
http://www.wjgnet.com/1007-9327/10/3094.asp

INTRODUCTION

Alteration of the balance between apoptosis and cell proliferation could result in a disturbance of tissue homeostasis, and dysregulation of apoptosis is associated with various cancers[1]. Considerable interest has focused on the identification of regulators of apoptosis, which may potentially contribute to the development of cancer. Recently, a novel member of the inhibitor of apoptosis (IAP) protein family, designated as survivin, has been identified. The surviving gene is located on chromosome 17 and spans 14.7 kb, encoding a protein of 142 amino acids. Unlike other IAP proteins, survivin contains a single baculovirus IAP repeat and lacks a C-terminal RING finger[2]. Another significant feature of survivin is its unique expression pattern as one of the most tumor-specific human gene products[3]. While embryonic and fetal organs contain abundant survivin mRNA and protein, most terminally differentiated normal tissues do not. By contrast, dramatically strong expression of survivin is detected in the vast majority of tumors[4]. Moreover, the overexpression of survivin has been shown to be correlated with aggressive and histologically unfavorable neuroblastoma[5], and associated with the poor prognostic outcome in colorectal cancer[6], non-small-cell lung cancer[7], breast cancer[8], soft tissue sarcoma[9] and B-cell lymphoma[10].

However, since its identification five years ago, there have been some contradictory reports about the clinical relevance of survivin expression in cancer. Gianani *et al*.[11] found the expression of survivin was not a specific marker of adenocarcinoma of the colon but showed characteristic patterns of expression in normal colonic mucosa. In gastric carcinoma which is the second most frequent cause of cancer death according to a worldwide estimation, Lu *et al*.[12] showed that survivin could promote aberrantly tumor cell viability, whereas Okada *et al*.[13] indicated that survivin expression in nuclei of tumor cells was predictive of favorable prognosis in patients. In the present study, we used laser capture microdissection (LCM), a novel technique that allows rapid, reliable and accurate procurement of cells from specific regions of tissue sections under direct visualization, to obtain the primary and metastatic gastric cancer cells as well as the matched normal epithelial cells from the same patient and analyzed mRNA expression of the survivin gene.

MATERIALS AND METHODS

Patients

Thirty patients (25 males and 5 females) underwent gastrectomy

with lymph node dissection for gastric carcinoma at China Medical University between March and September of 2 000 were included in the study. None of the patients received preoperative chemotherapy. The patients ranged in age from 33 to 78 years (median, 57 years). Routinely, the resected specimens were histologically examined by H&E staining according to the general rules of the classification of gastric carcinoma suggested by the Japanese Research Society of Gastric Cancer[14]. Details of the Borrmann gross type, the Lauren histological classification, the Ming classification of growth patterns, grade of differentiation, and levels of lymph node metastasis were obtained from the operative records and the pathology reports. The pT classification representing the depth of wall invasion and the pN classification representing the extent of regional lymph node metastasis were performed using standard criteria of the 5th TNM staging system[15]. The total lymph node number collected from the tissue was 15 or more for a reliable pN classification.

Tissue samples

Tumor tissues, lymph nodes, and apparently uninvolved normal tissues were collected from each patient immediately after surgical removal and snap-frozen in liquid nitrogen and kept at -80 ℃ until use. The tissues were then embedded in OCT for subsequent LCM harvest. Sections were cut at 8 μm with a cryostat and mounted on uncoated glass slides. The slides could be immediately stored at -80 ℃ for a few weeks. In order to exclude the areas of necrosis, tumor tissues from all patients were selected from the most viable areas of tumors. The lymph nodes were obtained according to the standard protocol. The number of removed and positive lymph nodes for various stations was documented by the pathologists. For the selection of matched uninvolved gastric mucosa, specimens were obtained from tissues at a distance of more than 10 cm from the tumor edge and confirmed histologically.

LCM

OCT embedded blocks of frozen tissue were serially cut. For each case, the first section was stained with H&E routinely for histological analysis and digitalized. The following serial sections stained with H&E according to the standard protocol recommended by NIH[16] were subjected to LCM using a LM200 system (Olympus, Japan/Arcturus Engineering Inc, US). Areas of interest were selected under microscopic guidance, and covered with ethylene vinyl thermoplastic (EVA) film mounted on optically transparent cap. The infrared laser was activated by the push of a button, which melts the film directly above the target cells. This melt caused a binding to form between the cells and the transfer film that was stronger than the binding between the cells and the slide[17]. The parameters used for LCM included a laser diameter of 7.5 μm, laser power of 50-60 mW. Five thousand laser pulse discharges per specimen were used to "capture" approximately 10 000 morphologically normal gastric epithelial cells, malignant primary gastric cancer cells and malignant metastatic (to a perigastric lymph node) gastric cancer cells from each case. Each population was estimated to be >95% "homogeneous" as determined by microscopic visualization of the captured cells. The caps with captured cells were then fitted onto 0.5 mL microcentrifuge tubes containing 200 μL TRIZOL Reagent. Caps briefly placed onto the section without laser activation were used as negative control.

RNA extraction from LCM-captured cells

Total RNA from each population of laser-captured cells was independently extracted using TRIZOL Reagent (Life Technologies, Inc) by means of a modification of the RNA microisolation protocol recommended by the manufacturer. Briefly, tubes containing collected cells and TRIZOL Reagent were inverted and allowed to sit at room temperature for 30 min, then 0.5 μL glycogen (20 μg/μL) carrier and 40 μL chloroform were added to each tube. The tubes were vigorously shaken by hand for 15 s and incubated at room temperature for 2 min. The samples were centrifuged at 11 000 *g* for 15 min at 4 ℃. The aqueous layer was transferred to a fresh 0.5 mL tube, 100 μL isopropanol was added and precipitated at -70 ℃ for 1 h. After centrifuged at 11 000 *g* for 10 min at 4 ℃, the pellet was then washed in 200 μL of 750 mL/L ethanol and resuspended in 7 μL diethylpyrocarbonate-treated RNase free water.

Reverse transcription-polymerase chain reaction (RT-PCR)

For RT-PCR analysis of the LCM-captured cells, first strand cDNA was prepared from total RNA by using a first-strand synthesis kit (Life Technologies, Inc). Seven microliters of total RNA isolated from approximate 10 000 cells was mixed with 1 μL of oligo-$(dT)_{12\text{-}18}$ primer, 1 μL of random hexamers primer (N_6) and 1 μL of 10 mmol/L dNTPs in a total volume of 10 μL. They were heat denaturated at 65 ℃ for 5 min, then chilled in ice. Four microliters of 5×first-strand reaction buffer, 2 μL of 0.1 mol/L DTT, 2 μL of 25 mmol/L $MgCl_2$, 1 μL of RNasin (40 U/μL) (Promega, Madison, WI, USA), and 1 μL of SUPERSCRIPT II RTase (200 U/μL) (Life Technologies, Inc) were added and incubated at 25 ℃ for 10 min, followed by incubation at 42 ℃ for 50 min for first-strand synthesis. The reverse transcriptase was inactivated at 70 ℃ for 15 min. PCR amplification with specific primers was performed in a final reaction volume of 50 μL containing 1×PCR buffer, 200 μmol/L each dNTP, 0.5 μmol/L each primer, 1.25 unit of Taq polymerase (TaKaRa Biotech, Dalian, China) and 2 μL of RT product. Programmable temperature cycling (UNO II, Biometra, Germany) was performed using the following profiles: an initial hot start at 95 ℃ for 2 min, followed by 38 cycles at 95 ℃ for 30 s, at 58 ℃ for 20 s and at 72 ℃ for 30 s. After the last cycle, an elongation step was extended at 72 ℃ for 5 min. For each set of PCR, parallel reactions with human genomic DNA from peripheral blood were performed to test for genomic DNA contamination, and double distilled water instead of cDNA template was also included as negative control to assure the quality of PCR. An 8 μL aliquot of the PCR product underwent electrophoresis on 15 g/L agarose gel stained with ethidium bromide and was visualized under UV trans-illuminator. The following primers were used: (A) survivin gene, forward primer 5'-CCCTGCCTGGCAGCCCTTTC- 3', and reverse primer 5'-CTGGCTCCCAGCCTTCCA-3' (PCR product, 188 bp); (B) glyceraldehyde-3-phosphate dehydrogenase (G3PDH), forward primer 5'-AGGGGTCTACATGGCAACTG-3', and reverse primer 5'- CGACCACTTTGTCAAGCTCA-3' (PCR product, 227 bp).

Statistical analysis

Statistical comparisons for significance between nominal variables were evaluated by the chi-square test and the Fisher's exact probability test. All the statistical analyses were performed using SPSS10.0 computer software and *P* of 0.05 was used as significance criterion.

RESULTS

Survivin expression in microdissected gastric epithelial and cancer cells

As shown in Figure 1, LCM allowed us to precisely sample the targeted cells. In this manner, gastric normal epithelial or cancer cells were homogenously obtained and bonded to the transfer film. When the cap together with the film was lifted from the tissue section, surrounding tissues remained attached to the glass slide. As a result, the morphology of the captured cells was well preserved and could be readily visualized under a microscope. To detect survivin gene mRNA expression by RT-PCR, a pair of specific primers located at 2 flanking exons was

designed and synthesized. The expected specific transcript of survivin gene represented by an 188 bp fragment was amplified (Figure 2). Of the paired samples from 30 gastric cancer patients studied, 24 (80%) primary gastric cancer cell groups and 7 (23%) adjacent morphologically "normal" gastric epithelial cell groups were shown to have a detectable survivin expression. There was a statistically significant difference in suvivin expression between these two groups ($P<0.01$). Furthermore, survivin mRNA was never detected in morphologically non-tumorous gastric epithelial cell groups when the paired cancer cell group was negative for survivin mRNA.

Strikingly, 95% (19/20) of the metastatic gastric cancer cell groups from lymph nodes had a clear expression of the survivin gene. Three cases showed positive results for the surviving-specific RT-PCR assay in metastatic cancer cells while none of their paired primary cancer cells had a detectable expression of the survivin mRNA.

Relationship between survivin expression and clinicopathological characteristics in gastric cancer patients

We examined the relationship between survivin expression in microdissected primary cancer tissues and the clinicopathological features of gastric cancer (Table 1). There was no significant correlation between survivin expression and Borrmann gross type, depth of wall invasion, Lauren histological classification, Ming's classification of growth patterns, grade of differentiation, the presence and extent of lymph node metastasis.

We also analyzed the survivin gene expression pattern in

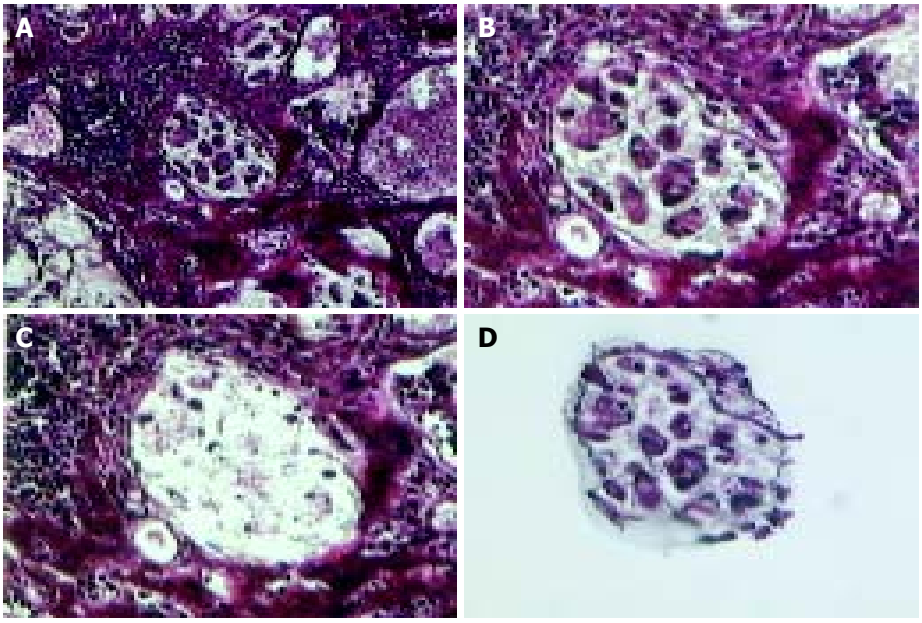

Figure 1 Laser capture microdissection of cells from gastric carcinoma. A: Morphology map view for pathological diagnosis (×100). B: Group of gastric carcinoma cells were selected for LCM (×200). C: The same section revealed where carcinoma cells were lifted from the section (×200). D: The carcinoma cells were removed on the plastic film to provide a template for PCR.

Table 1 Relationship between survivin expression and different histopathological features

Variant	Survivin expression in primary cancer			Survivin expression pattern in cancer and normal tissues			
	Positive	Negative	[1]*P*	N(-)T(-)	N(-)T(+)	N(+)T(+)	*P*
Gross type							
Borrmann I + II	7	1	[2]NS	1	4	3	NS
Borrmann III+IV	17	5		5	13	4	
Depth of invasion							
pT_1+pT_2	9	1	NS	1	5	4	NS
pT_3+pT_4	15	5		5	2	3	
Differentiation							
Well and medorate	7	1	NS	1	4	3	NS
Poor and undifferentiate	17	5		5	13	4	
Lauren classification							
Intestinal type	21	4	NS	4	16	5	NS
Diffuse type	3	2		2	1	2	
Ming growth pattern							
Expanding	9	3	NS	3	6	3	NS
Infiltrative	15	3		3	11	4	
Lymph node metastasis							
pN0	8	2	NS	2	5	3	NS
pN1	5	1		1	3	2	
pN2+pN3	11	3		3	9	2	

[1]*P* was estimated by the fFsher's exact test [2]NS, not significant.

both paired normal and primary cancer cells and its relationship with clinicopathological features. Thirty patients were divided into N (-) T (-), N (-) T (+) and N (+) T (+) groups. Still, no significant correlation between survivin expression pattern and the factors mentioned above was observed.

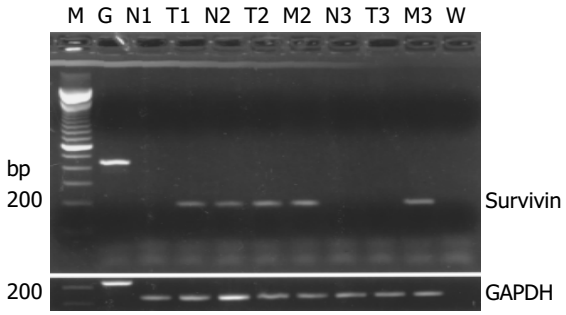

Figure 2 Representative RT-PCR results of survivin expression in normal (N), tumor (T) and metastatic carcinoma (M) cells obtained by LCM from 3 patients suffering gastric cancer. Case 1 was a patient without lymphatic metastasis, cases 2 and 3 were patients with lymphatic metastasis. G: Genomic DNA from human peripheral blood. W: Water as negative control.

DISCUSSION

Apoptosis plays an important role in organ homeostasis, by eliminating senescent or damaged cells. The suppression of apoptosis has been considered to contribute to carcinogenesis and cancer progression by aberrantly prolonging cell viability with accumulation of mutations[18,19]. Survivin is a newly identified bifunctional protein that suppresses apoptosis and regulates cell division. Based on the previously published studies, its mRNA is abundantly expressed in fetal tissues, but not in normal adult tissues except placenta and thymus. Meanwhile, reactivation of survivin expression has been demonstrated in tumors of lung[7], stomach[20], breast[8], colon[21], esophagus[22], liver[23], pancreas[24], bladder[25], uterus[26], ovary[27], *etc*. This specific distribution pattern has aroused great interest in making the survivin gene as a potential cancer therapeutic target. However, the expression of the survivin gene in normal tissues is currently debated. Several recent studies have shown survivin expression in normal tissues including skin[28], endometrium[29], endothelial cells[30], colonic mucosa[11] and muscle[9]. In the present studies, we sought to investigate whether survivin expression could be a specific marker during the development of gastric cancer.

It has been generally accepted that molecular analysis of neoplastic tissues *in vivo* is challenged by the heterogeneity of samples. Genetic alternations can be masked by contaminating bystander cells. Survivin mRNA was detected in normal tissue adjacent to soft tissue sarcoma cells[9]. Therefore, it is necessary to obtain a pure population of cells to evaluate the possible role of the survivin gene in tumor progression. The recent development in LCM, a highly sophisticated technique for the transfer of isolated pure cells from the histological slide into a reaction tube, could afford the opportunity to overcome this obstacle[31]. A few published studies and our previous data (unpublished data) have shown that LCM coupled with RT-PCR technique is a reliable method for the molecular analysis of gene profiles in specific tissues. We combined RT-PCR with LCM to determine the survivin expression in primary cancer cells, metastatic cancer cells, and paired normal epithelial cells.

Our results demonstrated that 23% of morphologically normal epithelial cells had a detectable survivin mRNA expression. By contrast, Lu *et al*.[12] reported that no survivin expression was found in normal gastric mucosa neighboring the cancer cells in an immunohistochemical analysis. Meanwhile, the rate of survivin expression was relatively lower in normal tissue we examined than in previous studies reporting 47.1% in normal esophageal epithelial tissues[22] and 29.1% or 100% in normal colorectal tissues[6,11]. One possible explanation for these results could be the different sensitivity of methods and the varied criteria for positivity determination. Further studies may be required to check out whether the expression of the survivin gene in normal tissues is caused by a high proportion of mitotically active cells.

In accordance with the recently published reports showing 88% positive survivin expression in gastric cancer tissues, we found a detectable expression of the survivin gene in 24 of 30 primary gastric cancer cell groups. The percentage was significantly higher than that in normal gastric epithelial cells. These results suggested that survivin expression in gastric cancer was a quite common event and might play an important role in the carcinogenesis of stomach. Several studies have consistently shown that survivin expression could inhibit cell death induced by various apoptotic stimuli[4]. A role for survivin in blocking apoptosis has also been found *in vivo*[32]. Like other proteins in the IAP family, survivin might bind specifically to caspase-3 or caspase-9, which are the effectors of apoptosis[33]. On the other hand, survivin was expressed in the G2-M phase of the cell cycle and its overexpression might contribute to overcoming the G2-M phase checkpoint to enforce progression of cells through mitosis[34]. Therefore, not surprisingly, survivin was shown to be present in the majority of gastric cancer cells.

Even though no significant correlation was observed between survivin expression in primary cancer or its distribution pattern in normal and cancer tissues and tumor invasiveness or the presence of lymph node metastasis, it is still striking to find that 95% of the metastatic cancer cells from lymph nodes had a clear expression of the survivin mRNA. In three cases, survivin expression was detected in metastatic lesions, but not in primary cancer cell groups. One possible explanation might be that survivin expression was upregulated in some metastatic cancer cells. By sensitive quantitative RT-PCR assay, significantly increased survivin expression levels were found in soft tissue sarcomas with more aggressive biological behavior[9]. Alternatively, more survivin expressions detected in metastatic lesions could result from the presence of a higher proportion of survivn-expressing cells compared with that in primary sites. Immunohistochemical analysis revealed that the percentage of survivin-positive cells in primary gastric cancer was quite variable, ranging from 20-100%[12]. It has been shown that failures in normal apoptosis pathways could contribute to cancer progression by supporting anchorage-independent survival during metastasis. Considering the anti-apoptotic function of survivin, it seems reasonable to deduce that survivin expression might facilitate the survival of cancer cells at distant sites[35]. Also, survivin played a crucial role in angiogenesis[30,36], which is considered as one of the critical steps for cancer cell spread and metastasis. Moreover, when analyzed retrospectively, cancer patients expressing survivin exhibited a shorter survival, correlated with unfavorable prognosis and accelerated rates of recurrences[5-10]. These results together with ours suggested a possible role of survivin in cancer invasiveness and metastasis. Further analysis is necessary to assess the expression levels in metastatic lesions by accurately quantitative methods.

Furthermore, the extremely high survivin expression rate in metastatic lesions indicated a possible approach using survivin as a molecular diagnostic marker for micrometastasis in gastric cancer. Our parallel studies have shown that the detection of survivin expression in peritoneal lavaged fluid is a specific and sensitive assay for prediction of peritoneal micrometastasis in gastric cancer. Also, survivin was detected in the urine of all patients tested with new or recurrent bladder cancer, whereas normal volunteers and patients with non-neoplastic diseases were tested negative for urine survivin[4]. However, a large scale

and long follow-up should be carried out to validate these results.

Recently, expression of a phosphorylation-defective survivin mutant (Thr34→Ala), which acted as a dominant-negative antagonist of survivin pathway and prevented phosphorylation of endogenous protein, has been reported to trigger apoptosis in several human melanoma cell lines *in vitro* and to prevent tumor formation or suppress the growth of existing tumors by 60-70% *in vivo*[37]. Therefore, the role of survivin in cancer progression has made it an attractive therapeutic target against cancer development.

In summary, our data indicate survivin expression is present in the majority of gastric cancer cell groups obtained by LCM techniques. The high expression rate in metastatic lesions suggests a possible role of survivin in cancer invasiveness and metastasis. It might contribute to the detection of micrometastasis in gastric cancer as a potential molecular marker. In addition, the high expression percentage renders survivin a candidate target in the therapy for gastric cancer.

REFERENCES

1 **Hetts SW**. To die or not to die: an overview of apoptosis and its role in disease. *JAMA* 1998; **279**: 300-307
2 **Ambrosini G,** Adida C, Altieri DC. A novel anti-apoptosis gene, survivin, expressed in cancer and lymphoma. *Nat Med* 1997; **3**: 917-921
3 **Velculescu VE,** Madden SL, Zhang L, Lash AE, Yu J, Rago C, Lal A, Wang CJ, Beaudry GA, Ciriello KM, Cook BP, Dufault MR, Ferguson AT, Gao Y, He TC, Hermeking H, Hiraldo SK, Hwang PM, Lopez MA, Luderer HF, Mathews B, Petroziello JM, Polyak K, Zawel L, Kinzler KW, Zhang W, Zhang X, Zhou W, Haluska FG, Jen J, Sukumar S, Landes GM, Riggins GJ, Vogelstein B, Kinzler KW. Analysis of human transcriptomes. *Nat Genet* 1999; **23**: 387-388
4 **Altieri DC.** The molecular basis and potential role of survivin in cancer diagnosis and therapy. *Trends Mol Med* 2001; **7**: 542-547
5 **Adida C,** Berrebi D, Peuchmaur M, Reyes-Mugica M, Altieri DC. Anti-apoptosis gene, survivin, and prognosis of neuroblastoma. *Lancet* 1998; **351**: 882-883
6 **Sarela AI,** Macadam RC, Farmery SM, Markham AF, Guillou PJ. Expression of the antiapoptosis gene, survivin, predicts death from recurrent colorectal carcinoma. *Gut* 2000; **46**: 645–650
7 **Monzo M,** Rosell R, Felip E, Astudillo J, Sanchez JJ, Maestre J, Martin C, Font A, Barnadas A, Abad A. A novel anti-apoptosis gene: re-expression of survivin messenger RNA as a prognosis marker in non-small-cell lung cancers. *J Clin Oncol* 1999; **17**: 2100–2104
8 **Tanaka K,** Iwamoto S, Gon G, Nohara T, Iwamoto M, Tanigawa N. Expression of survivin and its relationship to loss of apoptosis in breast carcinomas. *Clin Cancer Res* 2000; **6**: 127–134
9 **Kappler M,** Kohler T, Kampf C, Diestelkotter P, Wurl P, Schmitz M, Bartel F, Lautenschlager C, Rieber EP, Schmidt H, Bache M, Taubert H, Meye A. Increased survivin transcript levels: an independent negative predictor of survival in soft tissue sarcoma patients. *Int J Cancer* 2001; **95**: 360-363
10 **Adida C,** Haioun C, Gaulard P, Lepage E, Morel P, Briere J, Dombret H, Reyes F, Diebold J, Gisselbrecht C, Salles G, Altieri DC, Molina TJ. Prognostic significance of survivin expression in diffuse large B-cell lymphomas. *Blood* 2000; **96**: 1921-1925
11 **Gianani R,** Jarboe E, Orlicky D, Frost M, Bobak J, Lehner R, Shroyer KR. Expression of survivin in normal, hyperplastic, and neoplastic colonic mucosa. *Hum Pathol* 2001; **32**: 119-125
12 **Lu CD,** Altieri DC, Tanigawa N. Expression of a novel antiapoptosis gene, survivin, correlated with tumor cell apoptosis and p53 accumulation in gastric carcinomas. *Cancer Res* 1998; **58**: 1808–1812
13 **Okada E,** Murai Y, Matsui K, Isizawa S, Cheng C, Masuda M, Takano Y. Survivin expression in tumor cell nuclei is predictive of a favorable prognosis in gastric cancer patients. *Cancer Lett* 2001; **163**: 109-116
14 **Hermanek P.** The second English edition of the Japanese Classification of Gastric Carcinoma. A Western commentary. *Gastric Cancer* 1999; **2**: 79-82
15 **Wang Z,** Xu H, Wang S, Chen J. Relationship between new TNM classification and the prognosis and biological behavior of gastric cancer. *Zhonghua Waike Zazhi* 2000; **38**: 493-495
16 http://dir.niehs.nih.gov/dirlep/lcm/protocols.html
17 **Bonner RF,** Emmert-Buck M, Cole K, Pohida T, Chuaqui R, Goldstein S, Liotta LA. Laser capture microdissection: molecular analysis of tissue. *Science* 1997; **278**: 1481-1483
18 **Ogawa N,** Dang H, Talal N. Apoptosis and autoimmunity. *J Autoimmun* 1995; **8**: 1-19
19 **Wyllie AH**. Apoptosis and carcinogenesis. *Eur J Cell Biol* 1997; **73**: 189-197
20 **Zhu XD,** Lin GJ, Qian LP, Chen ZQ. Expression of survivin in human gastric carcinoma and gastric carcinoma model of rats. *World J Gastroenterol* 2003; **9**: 1435-1438
21 **Lin LJ,** Zheng CQ, Jin Y, Ma Y, Jiang WG, Ma T. Expression of survivin protein in human colorectal carcinogenesis. *World J Gastroenterol* 2003; **9**: 974-977
22 **Kato J,** Kuwabara Y, Mitani M, Shinoda N, Sato A, Toyama T, Mitsui A, Nishiwaki T, Moriyama S, Kudo J, Fujii Y. Expression of survivin in esophageal cancer: correlation with the prognosis and response to chemotherapy. *Int J Cancer* 2001; **95**: 92–95
23 **Ikeguchi M,** Ueda T, Sakatani T, Hirooka Y, Kaibara N. Expression of survivin messenger RNA correlates with poor prognosis in patients with hepatocellular carcinoma. *Diagn Mol Pathol* 2002; **11**: 33-40
24 **Satoh K,** Kaneko K, Hirota M, Masamune A, Satoh A, Shimosegawa T. Expression of survivin is correlated with cancer cell apoptosis and is involved in the development of human pancreatic duct cell tumors. *Cancer* 2001; **92**: 271–278
25 **Swana HS,** Grossman D, Anthony JN, Weiss RM, Altieri DC. Tumor content of the antiapoptosis molecule survivin and recurrence of bladder cancer. *N Engl J Med* 1999; **341**: 452–453
26 **Saitoh Y,** Yaginuma Y, Ishikawa M . Analysis of Bcl-2, Bax and Survivin genes in uterine cancer. *Int J Oncol* 1999; **15**: 137–141
27 **Yoshida H,** Ishiko O, Sumi T, Matsumoto Y, Ogita S. Survivin, bcl-2 and matrix metalloproteinase-2 enhance progression of clear cell- and serous-type ovarian carcinomas. *Int J Oncol* 2001; **19**: 537–542
28 **Chiodino C,** Cesinaro AM, Ottani D, Fantini F, Giannetti A, Trentini GP, Pincelli C. Communication: expression of the novel inhibitor of apoptosis survivin in normal and neoplastic skin. *J Invest Dermatol* 1999; **113**: 415–418
29 **Konno R,** Yamakawa H, Utsunomiya H, Ito K, Sato S, Yajima A. Expression of survivin and Bcl-2 in the normal human endometrium. *Mol Hum Reprod* 2000; **6**: 529–534
30 **O'Connor DS,** Schechner JS, Adida C, Mesri M, Rothermel AL, Li F, Nath AK, Pober JS, Altieri DC. Control of apoptosis during angiogenesis by survivin expression in endothelial cells. *Am J Pathol* 2000; **156**: 393–398
31 **Simone NL,** Bonner RF, Gillespie JW, Emmert-Buck MR, Liotta LA. Laser-capture microdissection: opening the microscopic frontier to molecular analysis. *Trends Genet* 1998; **14**: 272-276
32 **Grossman D,** Kim PJ, Blanc-Brude OP, Brash DE, Tognin S, Marchisio PC, Altieri DC. Transgenic expression of survivin in keratinocytes counteracts UVB-induced apoptosis and cooperates with loss of p53. *J Clin Invest* 2001; **108**: 991–999
33 **Tamm I,** Wang Y, Sausville E, Scudiero DA, Vigna N, Oltersdorf T, Reed JC. IAP-family protein survivin inhibits caspase activity and apoptosis induced by Fas (CD95), Bax, caspases, and anticancer drugs. *Cancer Res* 1998; **58**: 5315–5320
34 **Li F,** Ambrosini G, Chu EY, Plescia J, Tognin S, Marchisio PC, Altieri DC. Control of apoptosis and mitotic spindle checkpoint by survivin. *Nature* 1998; **396**: 580–584
35 **Reed JC**. Dysregulation of apoptosis in cancer. *J Clin Oncol* 1999; **17**: 2941–2953
36 **Tran J,** Rak J, Sheehan C, Saibil SD, LaCasse E, Korneluk RG, Kerbel RS. Marked induction of the IAP family antiapoptotic proteins survivin and XIAP by VEGF in vascular endothelial cells. *Biochem Biophys Res Commun* 1999; **264**: 781–788
37 **Grossman D,** Kim PJ, Schechner JS, Altieri DC. Inhibition of melanoma tumor growth *in vivo* by survivin targeting. *Proc Natl Acad Sci U S A* 2001; **98**: 635–640

Edited by Zhang JZ and Wang XL **Proofread by** Xu FM

PO Box 2345, Beijing 100023, China
Fax: +86-10-85381893
E-mail: wjg@wjgnet.com www.wjgnet.com

World J Gastroenterol 2004;10(21):3099-3102
World Journal of Gastroenterology
 ISSN 1007-9327

• LIVER CANCER •

Interferon plus ribavirin and interferon alone in preventing hepatocellular carcinoma: A prospective study on patients with HCV related cirrhosis

Azzaroli Francesco, Accogli Esterita, Nigro Giovanni, Trerè Davide, Giovanelli Silvia, Miracolo Anna, Lodato Francesca, Montagnani Marco, Tamé Mariarosa, Colecchia Antonio, Mwangemi Constance, Festi Davide, Roda Enrico, Derenzini Massimo, Mazzella Giuseppe

Francesco Azzaroli, Accogli Esterita, Nigro Giovanni, Giovanelli Silvia, Miracolo Anna, Lodato Francesca, Montagnani Marco, Tamé Mariarosa, Colecchia Antonio, Mwangemi Constance, Festi Davide, Roda Enrico, Mazzella Giuseppe, Department of Internal Medicine and Gastroenterology, University of Bologna
Trerè Davide, Derenzini Massimo, Department of Experimental Pathology, University of Bologna
Correspondence to: Azzaroli Francesco, M.D., Department of Internal Medicine and Gastroenterology, S.Orsola Hospital (Pad. 5), University of Bologna Via Massarenti 9, 40138 Bologna. azzaroli@med.unibo.it
Telephone: +39-338-5316190 **Fax:** +39-51-6363316
Received: 2003-11-04 **Accepted:** 2004-04-06

Abstract

AIM: To determine the role of interferon (IFN) with or without ribavirin in preventing or delaying hepatocellular carcinoma (HCC) development in patients with hepatitis C virus (HCV) related cirrhosis. Data on the preventive effect of IFN plus ribavirin treatment are lacking.

METHODS: A total of 101 patients (62 males and 39 females, mean age 55.1±1.4 years) with histologically proven HCV related liver cirrhosis plus compatible biochemistry and ultrasonography were enrolled in the study. Biochemistry and ultrasonography were performed every 6 mo. Ultrasound guided liver biopsy was performed on all detected focal lesions. Follow-up lasted for 5 years. Cellular proliferation, evaluated by measuring Ag-NOR proteins in hepatocytes nuclei, was expressed as AgNOR-Proliferative index (AgNOR-PI) (cut-off = 2.5). Forty-one patients (27 males, 14 females) were only followed up after the end of an yearly treatment with IFN-alpha2b (old treatment control group = OTCG). Sixty naive patients were stratified according to sex and AgNOR-PI and then randomized in two groups: 30 were treated with IFN-alpha2b + ribavirin (treatment group = TG), the remaining were not treated (control group = CG). Nonresponders (NR) or relapsers in the TG received further IFN/ribavirin treatments after a 6 mo of withdrawal.

RESULTS: AgNOR-PI was significantly lowered by IFN ($P<0.001$). HCC incidence was higher in patients with AgNOR-PI>2.5 (26% *vs* 3%, $P<0.01$). Two NR in the OTCG, none in the TG and 9 patients in the CG developed HCC during follow-up. The Kaplan-Mayer survival curves showed statistically significant differences both between OTCG and CG ($P<0.004$) and between TG and CG ($P<0.003$).

CONCLUSION: IFN/ribavirin treatment associated with re-treatment courses of NR seems to produce the best results in terms of HCC prevention. AgNOR-PI is a useful marker of possible HCC development.

Francesco A, Esterita A, Giovanni N, Davide T, Silvia G, Anna M, Francesca L, Marco M, Mariarosa T, Antonio C, Constance M, Davide F, Enrico R, Massimo D, Giuseppe M. Interferon plus ribavirin and interferon alone in preventing hepatocellular carcinoma: A prospective study on patients with HCV related cirrhosis. *World J Gastroenterol* 2004; 10(21): 3099-3102
http://www.wjgnet.com/1007-9327/10/3099.asp

INTRODUCTION

A number of studies have reported that treatment of HCV related cirrhosis might have a preventive effect on hepatocellular carcinoma development[1-15]. This has been recently confirmed by a meta-analysis concluding that "Interferon (IFN) prevents or delays the development of hepatocellular carcinoma (HCC) in patients with HCV-related cirrhosis, the magnitude of the overall effect is low and the benefit may be partly due to spurious associations. The preventive effect seems more evident among sustained responders to IFN[16]". However, with old interferon schedules, sustained responders did not exceed 10-15% of treated patients[1-15].

The response rate to IFN has changed since the introduction of ribavirin[17], the induction protocols[18] and, finally, the pegylated interferons[19]. Data on the preventive effect on HCC of more powerful therapeutic schemes are lacking.

Our study was started in 1997 with the purpose of assessing the efficacy of interferon (given with an induction protocol) plus ribavirin (the gold standard treatment at that time) in the prevention of HCC development.

MATERIALS AND METHODS

Patients

A total of one hundred and one consecutive patients (62 males and 39 females, mean age 55.1±1.4 years) with HCV related liver cirrhosis diagnosed by liver biopsy plus compatible biochemical parameters and ultrasonographic signs of portal hypertension were enrolled in the study. The baseline histologic activity of all patients was moderate to severe.

Study design (Figure 1)

Forty one subjects (27 males and 14 females, mean age 55.0±1.1 years), who were ending a 12-mo IFN course were followed-up without any other treatment (old treatment control group = OTCG). All patients of OTCG underwent liver biopsy at the end of treatment, while still on IFN.

The other 60 untreated patients (35 males and 25 females, mean age 55.7±1.7 years) were randomized in two groups of 30 subjects stratified according to sex and silver stained nucleolar organizer region - proliferative index (AgNOR-PI). Thirty were treated with IFN+ribavirin (treatment group = TG) and the remaining received no drugs (control group = CG). Nonresponders or relapsers to IFN/ribavirin received further courses of treatment after a 6 mo withdrawal. All patients were followed up for five years.

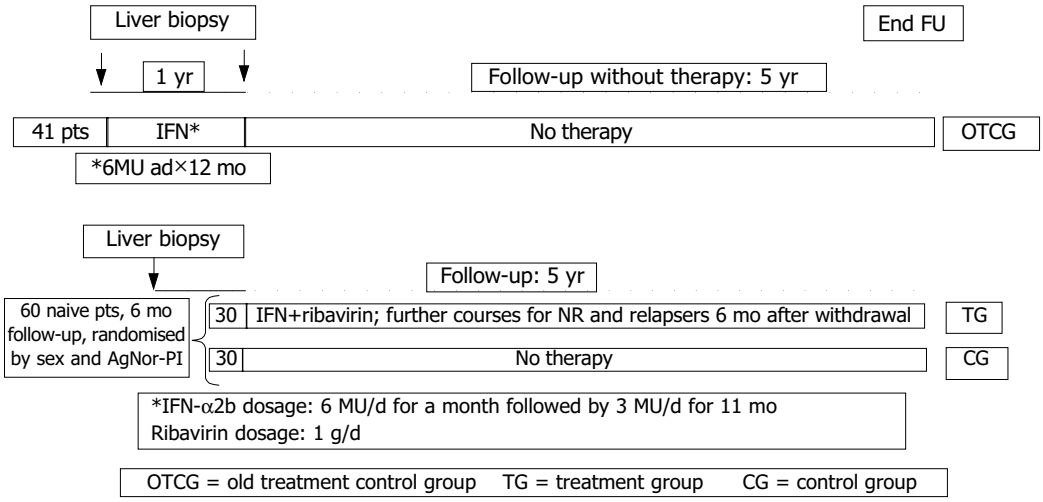

Figure 1 Study design.

The study was carried out according to the Helsinki protocol and all patients gave their written informed consent.

Ultrasonographies, blood cell count, α1-fetoprotein, γGT, transaminases, PT, total protein and their fractions were performed every 3 mo in all patients. Additional tests were performed in patients under active treatment: blood cell count every 10 d for two months and then monthly; transaminases, urea, creatinine and uric acid were tested monthly. When focal lesions were detected by ultrasound (US), US-guided liver biopsy was performed.

Protocol treatments

The 41 patients in OTCG were treated with IFNα-2b 6 MU/d for a month followed by 3 MU/d for 11 mo. The 30 patients in TG received the following α-2b schedule: 6 MU/d for a mo then 3 MU/d for 11 mo plus ribavirin 1 g/d for 12 mo. IFN and ribavirin dose reductions were made according to the biochemistry and tolerance of each patient. However, a total dose equal to or greater than 540 MU and 400 mg of ribavirin per day were considered suitable. Nonresponders and/or relapsers received further IFN treatment courses after a 6-mo withdrawal.

Liver histology and AgNOR-PI determination

Ultrasound guided liver biopsies were fixed in 40 g/L formaldehyde solution for 6 h and embedded in paraffin wax. Four 4 μm thick sections were cut from routinely processed paraffin blocks. Hematoxylin-eosin, silver impregnation, Pearl's staining were performed to define the severity of parenchymal, portal and periportal inflammation and the stage of disease by evaluating fibrosis and the presence of stainable iron into the liver. Histology was evaluated by two blinded independent observers according to Scheuer score.

The AgNOR staining was performed on routine sections of liver tissue on poly-lysine pretreated slides after immersion in xylene and ethanol. After progressive re-hydration sections were covered with plastic resistant to high temperature, put in a sodium citrate (100 g/L, pH 6.0) solution and boiled in pressured ovens (120 ℃ for 20 min). Then, sections were stained by silver impregnation in a gelatine solution (formic acid 10 mL/L and silver nitrate 500 g/L, 100:2 v/v) according to Ploton[20], for 10 min, at 37 ℃. Quantitative analysis of Ag-NOR proteins was made by measuring silver-stained areas (μm^2) within nuclei present in 50 consecutive microscopic fields (40× magnification) using a specific computer-assisted imaging software on biopsy specimen sections (VIDAS, Kontron Elecktronic, Germany). The percentage of hepatocytes with an AgNOR area >7 μm^2 (indicative of a proliferative state) was expressed as proliferative index (AgNOR-PI) (cut-off = 2.5%).

Statistical analysis

Results were expressed as mean±SE. The statistical analysis was carried out according to the intention to treat analysis. Wilcoxon test was used when appropriate and the Kaplan-Mayer model was applied to the evaluation of survival probability.

RESULTS

Biochemistry

Demographic and biochemical characteristics of the patients at enrollment are shown in Table 1. The three groups were comparable for age, sex, biochemical parameters, genotype distribution and AgNOR-PI.

Table 1 Baseline patient characteristics

	OTCG	TG	CG	*P*<
M:F ratio	27:14	17:13	18:12	NS
Age (yr)	55.3±1.8	54.6±2.1	57.2±2.0	NS
AST (U/L)	67.1±6.6	61.9±7.2	79.4±8.4	NS
ALT (U/L)	92.5±10.8	79.8±8.7	91.8±9.1	NS
γGT (U/L)	56.5±7.2	52.1±7.3	65.2±9.4	NS
Albumin (g/dL)	4.2±0.07	4.2±0.07	4.1±0.06	NS
α1feto (ng/mL)	6.8±1.25	8.4±2.36	6.3±1.0	NS
HCV1b	63%	67%	65%	NS
AgNOR-PI (%)	20.1±2.35	19.6±2.84	18.2±2.6	NS

OTCG = old treatment control group; TG = treatment group, CG = control group.

AgNOR PI

A significant reduction in AgNOR-PI was observed after IFN-treatment (Figure 2).

A significant difference in HCC development was observed according to AgNOR-PI: 9 out of 35 (26%) with basal AgNOR-PI >2.5% *vs* 2 out of 66 (3%) with basal AgNOR-PI <2.5% (P<0.01) (Figure 3).

Virological response

Six months after IFN withdrawal 8 out of 19 responders (24.5%) achieved sustained response (6 with genotype 2 or 3 and 2 with genotype 1) in the OTCG. Twenty one out of 30 patients in TG (70%) achieved a virological response that was sustained in 13 (43%) (9 genotype 2 and 4 genotype 1). None of the re-treated patients showed a sustained response.

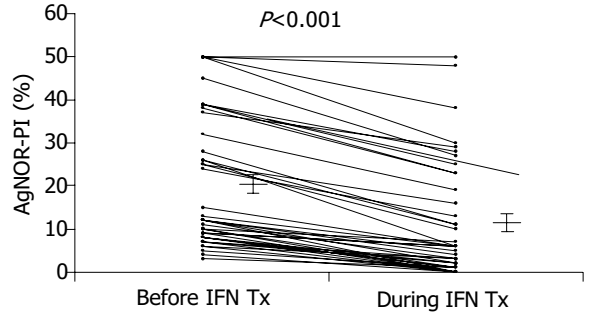

Figure 2 AgNOR-PI in OTCG before and after 1 year of IFN treatment.

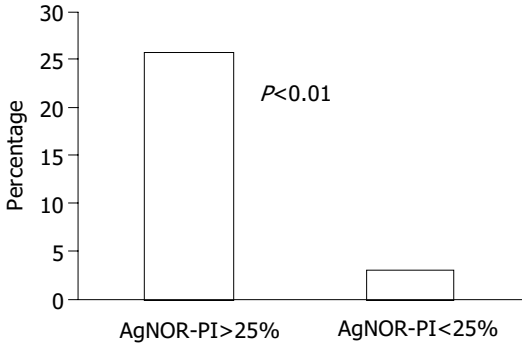

Figure 3 Incidence of HCC according to AgNOR-PI.

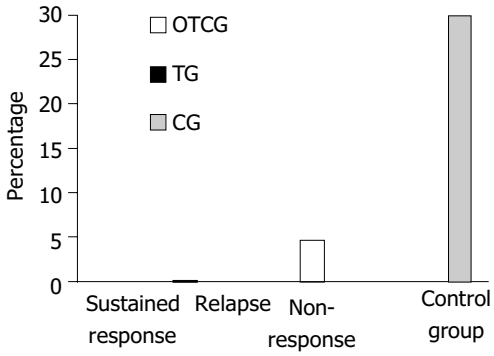

Figure 4 Percentage of HCC according to response to IFN.

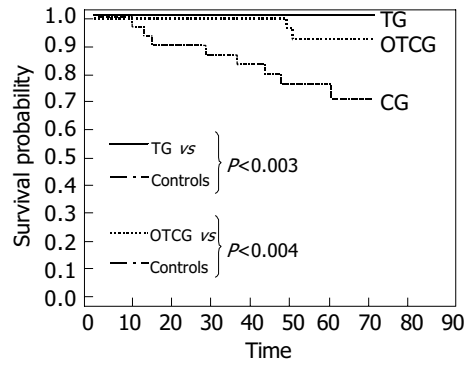

Figure 5 Survival probability evaluated by Kaplan-Mayer model.

HCC appearance

Two nonresponders in OTCG developed HCC during 5 years of follow-up after about 50 mo from interferon withdrawal. No subject in TG while 9 (30%) patients in CG developed HCC (Figure 4). The Kaplan-Mayer survival model showed statistically significant differences both between OTCG and CG (P<0.004) and between TG and CG (P<0.003) (Figure 5). The HCC annual rate of incidence in the CG was 5%.

DISCUSSION

The present data add new evidence on the clinical efficacy of IFN re-treatment of cirrhotic patients and show the usefulness of AgNOR-PI. The ability of IFN to prevent HCC development is evident both alone and in combination with ribavirin.

Previous observations in patients with chronic hepatitis C[21-24], with or without cirrhosis, reported that re-treatment with IFN was more effective than single courses in preventing HCC appearance. However, in these studies[21-24], the vast majority of patients had chronic hepatitis and no conclusions could be drawn on cirrhotic patients. We extended those observations to patients with HCV related cirrhosis. In accordance with a previous study[1], a single course of IFN did not seem to be protective toward HCC appearance in a long term follow-up. In fact, in the two nonresponder patients of OTCG, HCC developed after about 50 mo, suggesting that the protective effect of IFN may vanish over time. This hypothesis is strengthened by the observation that re-treatment of nonresponders in the TG prevented HCC development during the 5 years of follow-up.

It is interesting to note that no statistically significant difference was observed in survival between TG and OTCG. This may suggest that the addition of ribavirin to IFN did not add any significant benefit in cirrhotics. However, the number of patients was probably not sufficient to appreciate any possible difference coming from the higher rate of sustained response obtained with the combination treatment. However, it remains that the key to HCC prevention is treatment with interferon that might be helpful even after a curative resection of HCC[25].

Our study also showed that AgNOR-PI was a useful marker of hepatocyte regeneration which is able to predict a possible evolution to HCC. Furthermore, the two patients who developed HCC in the OTCG were those with the highest AgNOR-PI without improvement after treatment. This underlines the relevance of the index in the clinical setting, particularly in nonresponders to IFN. In fact, it may restrict the need of a strict surveillance only to those patients with a higher risk of developing HCC.

Previous observations with different techniques[26-29] have shown that high hepatocyte proliferation is associated with HCC development. A recent paper evaluating nucleolar hypertrophy in patients with HBV and HCV related cirrhosis reported the index was significantly predictive of HCC development only in patients with HBV related cirrhosis[30]. In patients with HCV related cirrhosis the index was not significantly related with HCC development, although a trend could be appreciated. A much larger and more homogeneous population of patients with HCV related cirrhosis (only Child A) in our study could account for the different results between the two studies.

In conclusion, the preventive effect of IFN on HCC development in HCV related cirrhosis is confirmed. Furthermore, a more efficacious treatment associated with re - treatment courses of nonresponders seems to produce the best results in term of HCC prevention. AgNOR-PI is a useful marker of hepatocyte proliferation that identifies patients at higher risk of developing HCC.

REFERENCES

1 **Nishiguchi S,** Kuroki T, Nakatani S, Morimoto H, Takeda T, Nakajima S, Shiomi S, Seki S, Kobayashi K, Otani S. Randomised trial of effects of interferon-alpha on incidence of hepatocellular carcinoma in chronic active hepatitis C with cirrhosis. *Lancet* 1995; **346**: 1051-1055

2 **Mazzella G,** Accogli E, Sottili S, Festi D, Orsini M, Salzetta A, Novelli V, Cipolla A, Fabbri C, Pezzoli A, Roda E. Alpha inter-

feron treatment may prevent hepatocellular carcinoma in HCV-related liver cirrhosis. *J Hepatol* 1996; **24**: 141-147

3 **Bruno S,** Silini E, Crosignani A, Borzio F, Leandro G, Bono F, Asti M, Rossi S, Larghi A, Cerino A, Podda M, Mondelli MU. Hepatitis C virus genotypes and risk of hepatocellular carcinoma in cirrhosis: a prospective study. *Hepatology* 1997; **25**: 754-758

4 **Fattovich G**, Giustina G, Degos F, Tremolada F, Diodati G, Almasio P, Nevens F, Solinas A, Mura D, Brouwer JT, Thomas H, Njapoum C, Casarin C, Bonetti P, Fuschi P, Basho J, Tocco A, Bhalla A, Galassini R, Noventa F, Schalm SW, Realdi G. Morbidity and mortality in compensated cirrhosis type C: a retrospective follow-up study of 384 patients. *Gastroenterology* 1997; **112**: 463-472

5 International Interferon-alpha Hepatocellular Carcinoma Study Group. Effect of interferon-alpha on progression of cirrhosis to hepatocellular carcinoma: a retrospective cohort study. *Lancet* 1998; **351**: 1535-1539

6 **Imai Y**, Kawata S, Tamura S, Yabuuchi I, Noda S, Inada M, Maeda Y, Shirai Y, Fukuzaki T, Kaji I, Ishikawa H, Matsuda Y, Nishikawa M, Seki K, Matsuzawa Y. Relation of interferon therapy and hepatocellular carcinoma in patients with chronic hepatitis C. *Ann Intern Med* 1998; **129**: 94-99

7 **Gramenzi A**, Andreone P, Fiorino S, Camma C, Giunta M, Magalotti D, Cursaro C, Calabrese C, Arienti V, Rossi C, Di Febo G, Zoli M, Craxi A, Gasbarrini G, Bernardi M. Impact of interferon therapy on the natural history of hepatitis C virus related cirrhosis. *Gut* 2001; **48**: 843-848

8 **Serfaty L,** Aumaitre H, Chazouilleres O, Bonnand AM, Rosmorduc O, Poupon RE, Poupon R. Determinants of outcome of compensated hepatitis C virus-related cirrhosis. *Hepatology* 1998; **27**: 1435-1440

9 **Sofia S,** Casali A, Buscarini E, Castagnetti E, Rapaccini GL, Levantesi L, Salmi A, Boccia S, Miglio F, Ricca Rossellini S, Bolondi L. Effect of lymphoblastoid IFN in the treatment of liver cirrhosis and prevention of HCC. *Ital J Gastroenterol Hepatol* 1998; **30**: A67

10 **Benvegnu L,** Chemello L, Noventa F, Fattovich G, Pontisso P, Alberti A. Retrospective analysis of the effect of interferon therapy on the clinical outcome of patients with viral cirrhosis. *Cancer* 1998; **83**: 901-909

11 **Shioda A**, Moriyama M, Kaneko M, Shimizu T, Gotou I, Tanaka N, Ookubo H, Arakawa Y. Long term prognosis of hepatocellular carcinoma developing after treatment of interferon in patients with chronic hepatitis C and liver cirrhosis. *Hepatology* 1999; **30**: A268

12 **Yoshida H**, Shiratori Y, Moriyama M, Arakawa Y, Ide T, Sata M, Inoue O, Yano M, Tanaka M, Fujiyama S, Nishiguchi S, Kuroki T, Imazeki F, Yokosuka O, Kinoyama S, Yamada G, Omata M. Interferon therapy reduces the risk for hepatocellular carcinoma: national surveillance program of cirrhotic and noncirrhotic patients with chronic hepatitis C in Japan. IHIT Study Group. Inhibition of Hepatocarcinogenesis by Interferon Therapy. *Ann Intern Med* 1999; **131**: 174-181

13 **Mura D**, Delliperi R, Fastame L, Carlini A, Cussu PA, Pisanu G, Dore MP, Realdi G. Five years follow-up after interferon therapy in HCV positive compensated cirrhosis. *Ital J Gastroenterol Hepatol* 1998; **30**: A114

14 **Valla DC**, Chevallier M, Marcellin P, Payen JL, Trepo C, Fonck M, Bourliere M, Boucher E, Miguet JP, Parlier D, Lemonnier C, Opolon P. Treatment of hepatitis C virus-related cirrhosis: a randomized, controlled trial of interferon alfa-2b versus no treatment. *Hepatology* 1999; **29**: 1870-1875

15 **Ikeda K**, Saitoh S, Arase Y, Chayama K, Suzuki Y, Kobayashi M, Tsubota A, Nakamura I, Murashima N, Kumada H, Kawanishi M. Effect of interferon therapy on hepatocellular carcinogenesis in patients with chronic hepatitis type C: A long-term observation study of 1,643 patients using statistical bias correction with proportional hazard analysis. *Hepatology* 1999; **29**: 1124-1130

16 **Camma C,** Giunta M, Andreone P, Craxi A. Interferon and prevention of hepatocellular carcinoma in viral cirrhosis: an evidence-based approach. *J Hepatol* 2001; **34**: 593-602

17 **Davis GL.** Combination treatment with interferon and ribavirin for chronic hepatitis C. *Clin Liver Dis* 1999; **3**: 811-826

18 **Vrolijk JM,** Bekkering FC, Brouwer JT, Hansen BE, Schalm SW. High sustained virological response in chronic hepatitis C by combining induction and prolonged maintenance therapy. *J Viral Hepat* 2003; **10**: 205-209

19 **McHutchison JG**, Fried MW. Current therapy for hepatitis C: pegylated interferon and ribavirin. *Clin Liver Dis* 2003; **7**: 149-161

20 **Ploton D**, Menager M, Jeannesson P, Himber G, Pigeon F, Adnet JJ. Improvement in the staining and in the visualization of the argyrophilic proteins of the nucleolar organizer region at the optical level. *Histochem J* 1986; **18**: 5-14

21 **Hino K,** Kitase A, Satoh Y, Fujiwara D, Yamaguchi Y, Korenaga M, Shingai Y, Konishi T, Yamashita S, Uchida K, Mori K, Hanada H, Kodama T, Nukui K, Okita K. Interferon retreatment reduces or delays the incidence of hepatocellular carcinoma in patients with chronic hepatitis C. *J Viral Hepat* 2002; **9**: 370-376

22 **Tanaka H**, Tsukuma H, Kasahara A, Hayashi N, Yoshihara H, Masuzawa M, Kanda T, Kashiwagi T, Inoue A, Kato M, Oshima A, Kinoshita Y, Kamada T. Effect of interferon therapy on the incidence of hepatocellular carcinoma and mortality of patients with chronic hepatitis C: a retrospective cohort study of 738 patients. *Int J Cancer* 2000; **87**: 741-749

23 **Toyoda H,** Kumada T, Nakano S, Takeda I, Sugiyama K, Kiriyama S, Sone Y, Hisanaga Y. The effect of retreatment with interferon-alpha on the incidence of hepatocellular carcinoma in patients with chronic hepatitis C. *Cancer* 2000; **88**: 58-65

24 **Takimoto M**, Ohkoshi S, Ichida T, Takeda Y, Nomoto M, Asakura H, Naito A, Mori S, Hata K, Igarashi K, Hara H, Ohta H, Soga K, Watanabe T, Kamimura T. Interferon inhibits progression of liver fibrosis and reduces the risk of hepatocarcinogenesis in patients with chronic hepatitis C: a retrospective multicenter analysis of 652 patients. *Dig Dis Sci* 2002; **47**: 170-176

25 **Sun HC**, Tang ZY. Preventive treatments for recurrence after curative resection of hepatocellular carcinoma-A literature review of randomized control trials. *World J Gastroenterol* 2003; **9**: 635-640

26 **Tarao K,** Ohkawa S, Shimizu A, Harada M, Nakamura Y, Ito Y, Tamai S, Hoshino H, Inoue T, Kanisawa M. Significance of hepatocellular proliferation in the development of hepatocellular carcinoma from anti-hepatitis C virus-positive cirrhotic patients. *Cancer* 1994; **73**: 1149-1154

27 **Ballardini G,** Groff P, Zoli M, Bianchi G, Giostra F, Francesconi R, Lenzi M, Zauli D, Cassani F, Bianchi F. Increased risk of hepatocellular carcinoma development in patients with cirrhosis and with high hepatocellular proliferation. *J Hepatol* 1994; **20**: 218-222

28 **Sangiovanni A,** Colombo E, Radaelli F, Bortoli A, Bovo G, Casiraghi MA, Ceriani R, Roffi L, Redaelli A, Rossini A, Spinzi G, Minoli G. Hepatocyte proliferation and risk of hepatocellular carcinoma in cirrhotic patients. *Am J Gastroenterol* 2001; **96**: 1575-1580

29 **Donato MF,** Arosio E, Del Ninno E, Ronchi G, Lampertico P, Morabito A, Balestrieri MR, Colombo M. High rates of hepatocellular carcinoma in cirrhotic patients with high liver cell proliferative activity. *Hepatology* 2001; **34**: 523-528

30 **Trerè D,** Borzio M, Morabito A, Borzio F, Roncalli M, Derenzini M. Nucleolar hypertrophy correlates with hepatocellular carcinoma development in cirrhosis due to HBV infection. *Hepatology* 2003; **37**: 72-78

Edited by Wang XL and Xu FM

PO Box 2345, Beijing 100023, China
Fax: +86-10-85381893
E-mail: wjg@wjgnet.com www.wjgnet.com

World J Gastroenterol 2004;10(21):3103-3106
World Journal of Gastroenterology
 ISSN 1007-9327

• LIVER CANCER •

Transfection of p27 ^{kip1} enhances radiosensitivity induced by ^{60}Co γ-irradiation in hepatocellular carcinoma HepG$_2$ cell line

Xiao-Xiang Guan, Long-Bang Chen, Gui-Xia Ding, Wei De, Ai-Hua Zhang

Xiao-Xiang Guan, Long-Bang Chen, Department of Oncology, Jinling Hospital, Nanjing University School of Medicine, Nanjing 210002, Jiangsu Province, China
Gui-Xia Ding, Ai-Hua Zhang, Center of Pediatric Nephrology, Nanjing Medical University, Nanjing 210029, Jiangsu Province, China
Wei De, Institute of Molecular and Cellular Biology, Nanjing Medical University, Nanjing 210029, Jiangsu Province, China
Supported by the National Postdoctor Research Foundation of China, No. 2003034383
Co-correspondents: Ai-Hua Zhang
Correspondence to: Dr. Long-Bang Chen, Department of Oncology, Jinling Hospital, Nanjing University School of Medicine, Nanjing 210002, Jiangsu Province, China. xxguan@hotmail.com
Telephone: +86-25-86062033 **Fax:** +86-25-84801861
Received: 2004-03-27 **Accepted:** 2004-04-13

Abstract

AIM: To study the cell cycle alterations of human hepatoma cell line HepG$_2$ *in vitro* after ^{60}Co γ-irradiation and further to examine the mechanisms underlying the enhancement of radiosensitivity to γ-irradiation in HepG$_2$ transiently transfected with wild type p27^{kip1}.

METHODS: The proliferation of HepG$_2$ cells was evaluated with MTT assay, and the cell cycle profile and apoptosis were assessed by cell morphology, DNA fragmentation analysis and flow cytometry. HepG$_2$ cells were transfected with p27^{kip1} wild type by using Lipofectamine (LF2000), and the expression and subcellular localization of p27^{kip1} in HepG$_2$ were detected by immunocytochemistry.

RESULTS: ^{60}Co γ-irradiation inhibited the growth of HepG$_2$ cells in a dose-dependent manner. Apoptosis of HepG$_2$ cells was induced 48 h after γ ray exposure. Furthermore research was carried out to induce exogenous expression of p27^{kip1} in HepG$_2$. The expression of p27^{kip1} induced G_0/G_1 phase arrest in HepG$_2$ cells. The overexpression of p27^{kip1} enhanced ^{60}Co γ-irradiation-induced radiosensitivity in HepG$_2$ cells.

CONCLUSION: Overexpression of p27^{kip1} is a rational approach to improve conventional radiotherapy outcomes, which may be a possible strategy for human hepatoma therapy.

Guan XX, Chen LB, Ding GX, De W, Zhang AH. Transfection of p27 ^{kip1} enhances radiosensitivity induced by ^{60}Co γ-irradiation in hepatocellular carcinoma HepG$_2$ cell line. *World J Gastroenterol* 2004; 10(21): 3103-3106
http://www.wjgnet.com/1007-9327/10/3103.asp

INTRODUCTION

Hepatocellular carcinoma (HCC) is a relatively common malignancy, ranking fifth in frequency on a worldwide basis and causing more than one million deaths annually[1,2] and there has been a progressive increase in the number of hepatoma cases over the past two decades[3]. Unfortunately, most of the cases of hepatoma are not curable because extensive resection is not possible. Though many approaches, such as transarterial chemoembolization (TACE), percutaneous ethanol injection (PEI), radiofrequency ablation (RFA), radiotherapy and liver transplantation have been developed to treat it, and the effective and survival rates are increased, a large number of patients would die from recurrence and metastasis[4-8]. It is well known that improving the overall therapeutic effects of liver cancer depends on the combined therapies. The purpose of combined interventional therapies for HCC is to increase their therapeutic efficiencies and to reduce the side effects and complications.

Radiotherapy presents another interesting option for the treatment of HCC amidst the wide array of non-surgical modalities available[11] and experimental and clinical studies have been reported that gene therapy is one of the more promising approaches for patients with advanced liver tumours[9-12].

It is unknown about the combination of radiotherapy and gene therapy, especially the relationship between p27^{kip1} and radiosensitivity, although p27^{kip1} is a target for cancer therapeutics[13]. p27^{kip1} is a key molecule in cell cycle control because of their specific and periodic expression during cell cycle progression. Knowledge of the function of cell cycle checkpoints in tumour cells may be important to develop treatment strategies for human cancers. Recent studies indicate that mutations in the p27^{kip1} gene have not been seen in many tumors including human hepatoma[14]. Down-regulation and mislocalization expression of p27^{kip1} have recently been found to be associated with a poor prognosis in patients with hepatoma[15]. However, the role of p27^{kip1} expression and gamma irradiation-induced apoptosis in human hepatoma cells has not been examined previously.

The purpose of this study was to investigate the function of p27^{kip1} and ^{60}Co γ-irradiation in the HepG$_2$ cell cycle progress and apoptosis, and then to examine the molecular mechanisms of radiosensitivity induced by p27^{kip1} and gamma irradiation in human hepatoma cells, focusing on the possibility that it might act, at least in part, by increasing the expression of p27^{kip1} in human hepatoma cells. This study may help us to understand radiosensitivity and develop a new treatment strategy.

MATERIALS AND METHODS

Reagents

RPMI-1640 medium and Lipofectamine (LF2000) were purchased from GIBCO. Anti-Flag (M2) was purchased from Sigma. FITC conjugated-IgG was purchased from Santa Cruz Biotechnology. The plasmid containing p27^{kip1} was kindly provided by Dr. Keiichi Nakayama at Kyushu University, Japan.

Cells and treatment with gamma-irradiation radiation treatment

Human hepatoma cell line, HepG$_2$, was routinely maintained in RPMI-1640 medium supplemented with 100 mL/L heat-inactivated fetal bovine serum at the 100 mL/L concentration and incubated in 100 U/mL penicillin-streptomycin in 50 mL/L CO_2 in air at 37 ℃ with 50 mL/L CO_2. Hepatoma cells were plated into 6-well culture plates (5×10^4 cells/well) and exposed to 0, 1.0, 2.0, 3.0, 4.0, 5.0 and 6.0 Gy of γ-irradiation from a telecobalt therapy source at a dose rate of 5.0 cGy/minute.

Transient transfection of p27^{Kip1}

Transfection of the cells with wild type p27^{kip1} cDNA constructs was performed using Lipofectamine (LF2000) reagent according to the manufacturer's instructions. Briefly, cells were plated in a 6-well plate at a density of 5×10^4 /well and incubated overnight in RPMI-1640 supplemented with 100 mL/L FCS. The cDNA constructs encoding p27^{kip1} were diluted in RPMI-1640 (100 μL) and then mixed with the transfection solution for 15 min. After washed twice with phosphate-buffered saline (PBS) to remove serum, the cells were incubated with the transfection mixture at 37 ℃ for 4 h and then refreshed with RPMI-1640 medium.

Proliferation assays

Cell proliferation was measured by MTT assay. After $HepG_2$ cells were treated with different dose gamma-irradation for indicated time and dose, then 10 μL MTT (5 mg/mL) was added to each well and incubated for an additional 4 h, and then the liquid in the wells was evaporated. To dissolve the formazam, 200 μL of DMSO was added. Control wells were treated with 1 g/L DMSO alone. The absorbance was detected in the microplate reader 550 model at 570 nm wavelength. Growth inhibition was equal to (1-absorbance of the treated wells)/(absorbance of the control wells) ×100%.

Immunohistochemistry

Immunohistochemical staining was performed to determine the expression of Flag-P27^{kip1} fusion protein. $HepG_2$ cells transiently expressing p27^{kip1} were grown on a glass coverslip in a 6-well plate for 24 h after transfetion. The cells on the coverslips were fixed in 20 g/L paraformaldehye at room temperature for 5 min on the next day of transfection, and sequentially incubated for 60 min with anti-mouse Flag (M2) and then FITC-conjugated second antibody. The slides were lightly counterstained with Hoechst 33258, washed with water and then mounted. Finally coverslips were mounted with other glass slides, the cells were examined by immunofluorescence microscopy at the excitation/emission wavelengths of 488 nm and 520 nm alternatively.

Flow cytometry analysis

$HepG_2$ cells were plated onto a 6-well plate (5×10^4 cells/well) in RPMI-1640 containing 100 mL/L FBS and grown overnight to allow cell attachment. They were then treated with irradiation, harvested, fixed with 700 mL/L ethanol, centrifuged, resuspended in 400 μL of PBS, and 2 mg/mL RNase was added to avoid double-stranded RNA staining, then stained with 400 μL of 0.1 mg/mL propidium iodide (PI). The cell suspension was filtered through a 60-μm Specrta/Mesh nylon filter. Samples of 20 000 cells were then analyzed for DNA histograms and cell cycle phase distributions by flow cytometer using a FACSCalibur instrument (Becton Dickinson), and the data were analyzed by a CELLQuest computer program.

DNA fragmentation assay

The integrity of DNA was assessed by agarose gel electrophoresis. Cells (1×10^6) were centrifuged for 5 min at 3 000 r/min, washed once with PBS, and cell pellets were resuspended in 100 μL of lysis buffer (50 mmol/L Tris-HCl, pH 8.0, 10 mmol/L tetraacetic acid, 4 g/L SDS, 0.5 g/L proteinase K) and incubated for 8 h at 50 ℃, then 10 μL of 0.5 g/L RNase A was added. The samples were incubated for 1 h at 50 ℃ and heated to 70 ℃ for 5 min, then 100 μL of phenol: chloroform:isopropanol (25:24:1) was added. After centrifugation, the supernatants were transferred to new tubes, and twice volume ethanol (ice cold) was added. After centrifugation, the pellets were solubilized in TE buffer and loaded on 18 g/L agarose gel for electrophoresis. The gel was stained with ethidium bromide, and photographed with UV illumination.

Hoechst 33258-propidium iodide counterstaining

Apoptosis and death cells were identified by Hoechst 33258-PI counterstaining[16]. Briefly, cell pellets (1×10^9) were suspended by 100 μL PBS containing Hoechst33258 at the concentration of 1 μL/mL. The cells were incubated at 37 ℃ for 7 min, and then centrifuged. The cell pellets were resuspended in 100 μL staining solution containing PI at the concentration of 5 μg/mL. The stained cells were analyzed using a fluorescence microscope. Samples of 200 cells were then analysed.

Statistical analysis

Data were represented as mean±SD. Differences were evaluated by SPSS10.0 software. $P\leqslant0.05$ was considered statistically significant.

RESULTS

Growth inhibition of $HepG_2$ cells by ^{60}Co γ-irradiation

The irradiation of $HepG_2$ cells caused a dose-dependent cell growth inhibition, and a maximum inhibitory effect was observed at 6 Gy. MTT assay showed that irradiation had anti-proliferative effects on $HepG_2$ cells in a dose-dependant manner. At the dose of 0, 1.0, 2.0, 3.0, 4.0, 5.0 and 6.0 Gy, the inhibitory rate was 2.62±0.18%, 26.85±0.21%, 54.11±0.47%, 57.19±0.54%, 60.26±0.53% and 67.12±0.65% respectively (Figure 1). The cell growth inhibitory effect was due to apoptosis or necrosis induced by excessively high dose irradiation. The counterstaining of PI and Hoechst 33258 proved to be an excellent probe to distinguish apoptotic cells from necrotic cells. Live and apoptotic cells were only probed by Hoechst 33258 (blue in color) and exclusion of propidium iodide due to plasma membrane integrity. The morphological features of apoptotic cells were cell shrinkage, nuclear condensation and genomic fragmentation down to the size of individual nucleosome units. On the contrary, necrotic cells were probed by PI (red in colors) (Figure 2). The apoptotic rate reached the top at the dose of 4.0 Gy, when irradiated by 6.0 Gy, most of $HepG_2$ cells were in necrotic state (Figure 3).

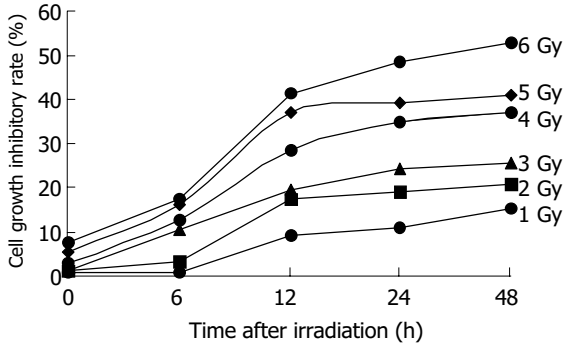

Figure 1 Effect of irradiation on proliferation of $HepG_2$ cells.

p27^{kip1} expression enhanced radiosensitivity induced by ^{60}Co γ-irradiation in $HepG_2$ cells

Overexpression of p27^{kip1} protein was observed in transfected cells (Figure 4). As a result, the proliferation of $HepG_2$ cells was greatly inhibited and cell cycle was arrested in G_1 phase after exogenous p27^{kip1} expression (Figure 5). Further results showed that overexpression of p27^{kip1} enhanced radiosensitivity in $HepG_2$ cells induced by ^{60}Co γ-irradiation, and 2.0 Gy irradiation induced maximum apoptotic rate by 40.6% in $HepG_2$ cells transfected with p27^{Kip1}, whereas $HepG_2$ cells transfected empty vector, only 4.0 Gy reached the maximum apoptotic rate of 35.3% (Figure 6). Apoptosis of $HepG_2$ cells indicated by flow cytometry and Hoechest33258 staining was then confirmed by DNA fragmentation, which was visualized as the characteristic oligonucleosome-sized fragmentation in ethidium bromide after DNA agarose gel electrophoresis (date not shown).

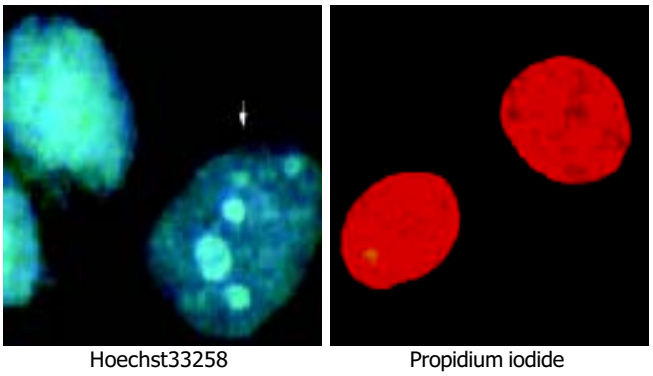

Figure 2 Counterstaining of Hoechst 33258 and propidium iodide to distinguish apoptotic from necrotic cells.

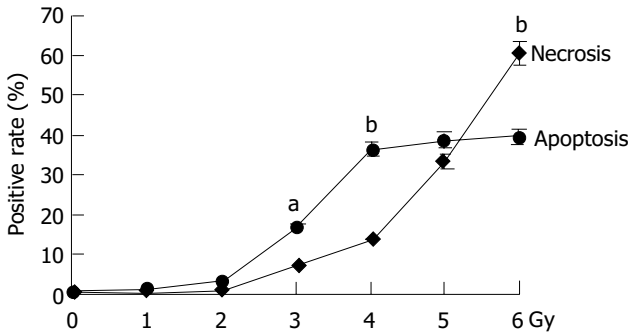

Figure 3 Comparsion of apoptosis and necrosis rate of HepG$_2$ treated by ^{60}Co γ-irradiation. $^aP<0.05$, $^bP<0.01$ *vs* necrosis.

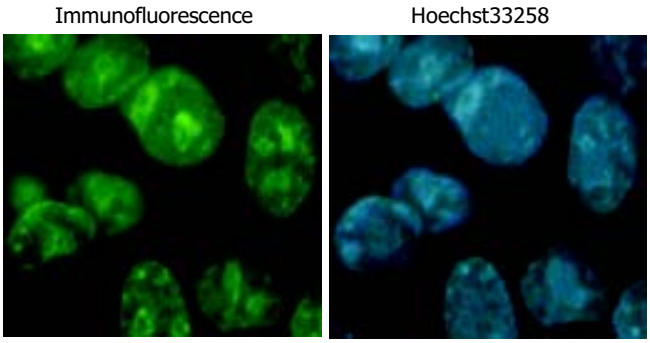

Figure 4 Subcellular localization and expression of p27^{kip1} in tranfected HepG$_2$ cells.

DISCUSSION

HCC remains one of the most difficult tumors to treat. Primary HCC is the second most common cancer and the leading cause of cancer deaths behind gastric cancer in China. Surgical resection has been accepted as the only curative therapy for primary liver cancer. Unfortunately, most patients are surgically unresectable, and are sometimes recommended to receive non-surgical therapies, including radiotherapy, radiofrequency hyperthermia, genetherapy or combination of the above methods. Radiation therapy has been commonly used in the treatment of unamenable human hepatoma. Unfortunately, the cause of this radiosensitization has not met expectations fully. New approches that may reduce side-effects and provide good quality of life are required. Thus, it is imperative to develop new and effective treatments, such as gene therapy, in order to treat this disease.

Gene therapy is one of the more promising approaches for patients with advanced liver tumour. Experimental and clinical studies have reported that gene therapy and molecular prevention are becoming a part of patient management and

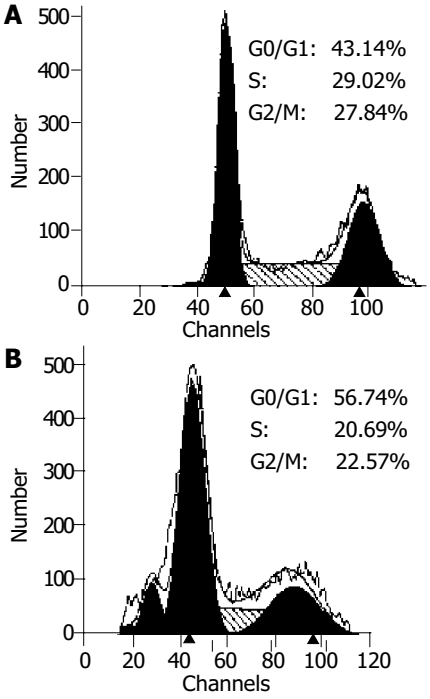

Figure 5 Flow cytometry analysis of cell cycle of nontransfected and transiently transfected HepG$_2$ cells. A: nontransfected HepG$_2$ cells. B: p27^{kip1} transiently transfected HepG$_2$ cells.

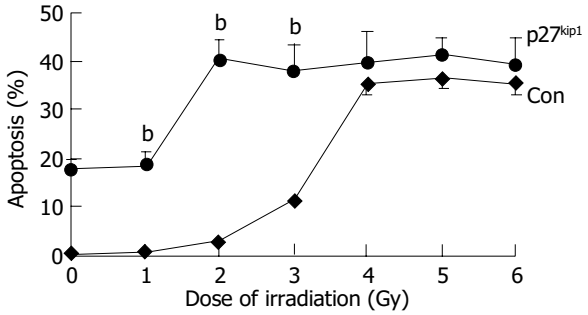

Figure 6 Apoptotic rates induced by γ-irradiation in nontransfected and transfected HepG$_2$ cells. $^bP<0.01$ *vs* control.

would eventually complement or in part replace the existing therapeutic and preventive strategies[17]. Recent researches have indicated that p27^{kip} is a new target for gene therapy and p27^{kip1} is a new suitable candidate for gene therapy[9,18]. The protein p27^{kip1} is an important factor that regulates cell cycle progression and apoptosis. Mutations in p27^{kip1} gene have not been seen in many tumors including human hepatoma. Down-regulation and mislocalized expression have recently been found to be associated with poor prognosis in patients with hepatoma. Therefore, regulation of p27^{kip1} activity is a new strategy for hepatoma therapy.

Pretreatment of hepatocellular carcinoma cells with overexpression of p27^{kip1} protein before irradiation enhanced the cell-killing effect of irradiation. Interaction with moderate doses of radiation caused a substantial increase in tumor cell killing. The beneficial effect of this interaction was further evidenced by the significant increase in the number of apoptic cells. The HepG$_2$ cells treated with p27^{kip1} and exposed to 6.0 Gy showed a maximum apoptosis percentage when compared to the other irradiation doses or p27^{kip1} transfection. Our results showed that overexpression of p27^{kip1} could enhance the radiosensitivity in HepG$_2$ cells. Overexpression of p27^{kip1} in HepG$_2$ cells cound sensitize cells to ionizing radiation. Recent advances have been made in the understanding of molecular

events following cell exposure to ionizing radiation. Our results suggest that $p27^{kip1}$ protein could be used to modulate radio-induced cellular responses.

However, the molecular machanism of $p27^{kip1}$ in radiosensitivity induced by ^{60}Co γ-irradiation is still unclear, and further studies are needed to identify the molecular mechanisms for the radiosensitizing activity, with emphasis on the study of $p27^{kip1}$ in cell cycle progress and radiosensitivity.

Our results here provide some experimental evidences that overexpression of $p27^{kip1}$ increases the radiosensitivity of gamma irradiation. It may help us understand radiosensitivity and develop strategies for liver cancer.

REFERENCES

1 **Hao XS**, Chen KX, Wang PP, Rohan T. Changes in survival patterns in urban Chinese patients with liver cancer. *World J Gastroenterol* 2003; **9**: 1212-1215

2 **Bosch FX**, Ribes J, Borras J. Epidemiology of primary liver cancer. *Semin Liver Dis* 1999; **19**: 271-285

3 **el-Serag HB**. Epidemiology of hepatocellular carcinoma. *Clin Liver Dis* 2001; **5**: 87-107

4 **Hanazaki K**, Kajikawa S, Shimozawa N, Mihara M, Shimada K, Hiraguri M, Koide N, Adachi W, Amano J. Survival and recurrence after hepatic resection of 386 consecutive patients with hepatocellular carcinoma. *J Am Coll Surg* 2000; **191**: 381-388

5 **Takayama T**, Sekine T, Makuuchi M, Yamasaki S, Kosuge T, Yamamoto J, Shimada K, Sakamoto M, Hirohashi S, Ohashi Y, Kakizoe T. Adoptive immunotherapy to lower postsurgical recurrence rates of hepatocellular carcinoma: a randomised trial. *Lancet* 2000; **356**: 802-807

6 **Huang YH**, Wu JC, Lui WY, Chau GY, Tsay SH, Chiang JH, King KL, Huo TI, Chang FY, Lee SD. Prospective case-controlled trial of adjuvant chemotherapy after resection of hepatocellular carcinoma. *World J Surg* 2000; **24**: 551-555

7 **Tung-Ping Poon R**, Fan ST, Wong J. Risk factors, prevention, and management of postoperative recurrence after resection of hepatocellular carcinoma. *Ann Surg* 2000; **232**: 10-24

8 **Keng GH**, Sundram FX. Radionuclide therapy of hepatocellular carcinoma. *Ann Acad Med Singapore* 2003; **32**: 518-524

9 **Schmitz V**, Wang L, Barajas M, Gomar C, Prieto J, Qian C. Treatment of colorectal and hepatocellular carcinomas by adenoviral mediated gene transfer of endostatin and angiostatin-like molecule in mice. *Gut* 2004; **53**: 561-567

10 **Shiba H**, Okamoto T, Futagawa Y, Ohashi T, Eto Y. Efficient and cancer-selective gene transfer to hepatocellular carcinoma in a rat using adenovirus vector with iodized oil esters. *Cancer Gene Ther* 2001; **8**: 713-718

11 **Iwazawa T**, Chau GY, Mori T, Dookeran KA, Rubin JT, Watkins S, Robbins PD, Lotze MT, Tahara H. Potent antitumor effects of intra-arterial injection of fibroblasts genetically engineered to express IL-12 in liver metastasis model of rat: no additional benefit of using retroviral producer cell. *Cancer Gene Ther* 2001; **8**: 17-22

12 **Humphreys MJ**, Ghaneh P, Greenhalf W, Campbell F, Clayton TM, Everett P, Huber BE, Richards CA, Ford MJ, Neoptolemos JP. Hepatic intra-arterial delivery of a retroviral vector expressing the cytosine deaminase gene, controlled by the CEA promoter and intraperitoneal treatment with 5-fluorocytosine suppresses growth of colorectal liver metastases. *Gene Ther* 2001; **8**: 1241-1247

13 **Sasaki T**, Katayose Y, Suzuki M, Yamamoto K, Shiraso S, Mizuma M, Unno M, Takeuchi H, Lee CT, Matsuno S. Adenovirus expressing mutant p27kip1 enhanced apoptosis against cholangiocarcinoma than adenovirus-p27kip1 wild type. *Hepatogastroenterology* 2004; **51**: 68-75

14 **Ponce-Castaneda MV**, Lee MH, Latres E, Polyak K, Lacombe L, Montgomery K, Mathew S, Krauter K, Sheinfeld J, Massague J. p27Kip1: chromosomal mapping to 12p12-12p13.1 and absence of mutations in human tumors. *Cancer Res* 1995; **55**: 1211-1214

15 **Fiorentino M**, Altimari A, Ravaioli M, Gruppioni E, Gabusi E, Corti B, Vivarelli M, Bringuier PP, Scoazec JY, Grigioni WF, D'Errico-Grigioni A. Predictive value of biological markers for hepatocellular carcinoma patients treated with orthotopic liver transplantation. *Clin Cancer Res* 2004; **10**: 1789-1795

16 **Darzynkiewicz Z**, Bruno S, Del Bino G, Gorczyca W, Hotz MA, Lassota P, Traganos F. Features of apoptotic cells measured by flow cytometry. *Cytometry* 1992; **13**: 795-808

17 **Blum HE**. Molecular therapy and prevention of hepatocellular carcinoma. *Hepatobiliary Pancreat Dis Int* 2003; **2**: 11-22

18 **Katner AL**, Gootam P, Hoang QB, Gnarra JR, Rayford W. A recombinant adenovirus expressing p7(Kip1) induces cell cycle arrest and apoptosis in human 786-0 renal carcinoma cells. *J Urol* 2002; **168**: 766-773

Edited by Zhang JZ and Wang XL **Proofread by** Xu FM

PO Box 2345, Beijing 100023, China
Fax: +86-10-85381893
E-mail: wjg@wjgnet.com www.wjgnet.com

World J Gastroenterol 2004;10(21):3107-3111
World Journal of Gastroenterology
 ISSN 1007-9327

• LIVER CANCER •

Nude mice model of human hepatocellular carcinoma via orthotopic implantation of histologically intact tissue

Yong-Shun Gao, Xiao-Ping Chen, Kai-Yan Li, Zai-De Wu

Yong-Shun Gao, Xiao-Ping Chen, Zai-De Wu, Hepatic Surgery Center, Tongji Hospital, Tongji Medical College, Huazhong University of Science and Technology, Wuhan 430030, Hubei Province, China
Kai-Yan Li, Department of Ultrasonography, Tongji Hospital, Tongji Medical College, Huazhong University of Science and Technology, Wuhan 430030, Hubei Province, China
Supported by the Science and Technology Special Fund of Ministry of Public Health, No. WKZ-2000-1-15; the Key Clinic Programs of Ministry of Public Health, No. 2001-2003
Correspondence to: Xiao-Ping Chen, M.D., Professor and Chairman, Department of Surgery, Tongji Hospital, Tongji Medical College, Huazhong University of Science and Technology, Wuhan 430030, Hubei Province, China. chenxp-53@sina.com
Telephone: +86-27-83662599 **Fax:** +86-27-83662851
Received: 2003-11-13 **Accepted:** 2003-12-16

Abstract

AIM: To establish a nude mice model of human hepatocellular carcinoma (HCC) via orthotopic implantation of histologically intact tissue, in order to study biologic features of HCC *in vivo* and to direct clinical treatment respectively.

METHODS: Histologically intact fresh specimens of HCC were orthotopically implanted in nude mice (BALB/c, nu/nu). Survival rate and growth curve were investigated with B-ultrasound. Morphological characteristics of pathology and spontaneous metastatic rates were detected with microscopy. Expression of multidrug resistance genes studied with immunohistochemical method and RT-PCR, and other biologic features of implanted tumor were observed and compared with human HCC specimens.

RESULTS: Out of the specimens from two patients with HCC, only one specimen survived in nude mice. The orthotopic implantation tumor survival rate, spontaneous intrahepatic metastatic rate, pulmonary metastatic rate and bone metastases rate were 100%, 75.0%, 37.5% and 37.5% respectively in the first passage. AFP was kept on secreting and increasing with the size of the tumor. The morphological characteristics and biologic features were similar to the donor's, the protein and mRNA of MDR1 and LRP were expressed in tumors of the model and the donor, and there was no significant difference between them (P>0.05).

CONCLUTION: The model of nude mice with orthotopic implantation of histologically intact HCC tissue is an ideal model to study biologic features of HCC *in vivo* and to direct clinical treatment.

Gao YS, Chen XP, Li KY, Wu ZD. Nude mice model of human hepatocellular carcinoma via orthotopic implantation of histologically intact tissue. *World J Gastroenterol* 2004; 10 (21): 3107-3111
http://www.wjgnet.com/1007-9327/10/3107.asp

INTRODUCTION

Liver cancer is one of the most common carcinomas, the highest age-standardised mortality rate in China, and accounts for 53% of all liver cancer deaths worldwide[1,2]. Surgical resection has been accepted as the best treatment for hepatocellular carcinoma (HCC). However, recurrence and metastases and non-sensitivity to chemotherapy remain the major obstacles for further prolonging survival after resection[3]. Study of HCC, therefore, has become an important issue. But the experiments can not be done on patients with HCC. So human HCC model in nude mice is needed for the study of HCC and its mechanism, chemotherapy, multidrug resistance (MDR), *etc*.

Shimosato *et al*.[4,5] established a series of human tumors in nude mice including the human HCC nude mice model for study of alpha-fetoprotein (AFP) in relation to tumor growth in 1976. Liu *et al*.[6] established a nude mice xenograft model from human HCC in 1995. Leveille-Webster *et al*.[7] established an intrahepatic xenograft of human HCC in severe combined immunodeficiency mice for the study of multidrug resistance in 1996. Sun *et al*.[8,9] reported a metastatic human HCC model in nude mice with 100% of spontaneous metastases to lung, lymph node and liver. Peng *et al*.[10] established a human HCC model in nude mice using orthotopic implantation and observed malignant behavior. Tao *et al*.[11] established a human HCC in nude mice model using SMMC-LTNM tumor transplanted into abdominal cavity and liver, the lung metastatic rate was 59%. Genda *et al*.[12] reported the construction of metastatic models using orthotopic implantation of human HCC cell lines into livers of SCID mice, two of the 5 cell lines injected showed vascular tumor thrombi and intrahepatic metastases. Zheng *et al*.[13] established an orthotopic implantation tumor model from the subcutaneous model of human HCC in nude mice, the spontaneous metastatic rate was 57.8%. Shi *et al*.[14] established a human HCC model in nude mice with a high metastatic rate in lymph node.

Metastatic models constructed in nude mice by orthotopic implantation of histologically intact patient specimens have been used in Hoffman's group, and several such models including cancers of the lung, pancreas and ovarium, have been reported[15-17]. However, patient-like human HCC model in nude mice with metastatic behaviors was not found. After the study on HCC cell lines and subcutaneous HCC model in nude mice, we established a patient-like human HCC model with spontaneous metastases in liver, lung and bones.

MATERIALS AND METHODS

Mice

There to four weeks BALB/ c, nu/nu, nude mice (Experimental Animal Center, Tongji Medical College, Huazhong University of Science and Technology, Wuhan), weighting 10.1-16.0 g, were used in this study.

Surgical specimens of human HCC

Fresh surgical specimens were obtained from 2 patients with HCC who underwent surgery at the Hepatic Surgery Center, Tongji Hospital, Tongji Medical College, Huazhong University of Science and Technology. The specimens were rinsed and preserved in saline at 4-8 ℃ and sent to the Experimental Animal Center as soon as possible. After necrotic tissue and non-

cancerous tissue of the specimens were removed, the remaining cancerous tissues were cut into small pieces of about 1 mm^3 in size.

Implantation procedure

Tumor pieces were implanted into the livers of nude mice. A left subcostal incision was made under anaesthesia with 200 g/L urethane. The left lobe of the liver was exposed and the liver capsule was mechanically injured with needle. Then one or two pieces of tumor tissue were filled into the liver tissue with forceps which could be seen as a white spot and abdominal wall was finally closed. Mice were kept in laminar-flow cabinets under specific-pathogen-free conditions.

Evaluation of growth and metastases

Nude mice were weighted and the size of tumors was weekly measured with B-ultrasound from 2 to 9 wk after orthotopic implantation. Tumor size (mm^3) was evaluated by measurement of two diameters with B-ultrasound and using the formula $1/2\ LW^2$, where L is the longest diameter and W is the shortest diameter. Bone metastases was detected with SPECT 8 wk after implantation and then other organ metastases was detected with autopsy and microscopy when the mice were killed. The liver, lymph node, lungs, and bone suspected of metastases were collected and processed for routine gross and microscopic examination. Metastases was diagnosed if at least one microscopic metastatic lesion was found in any resected organ.

Serum detection

AFP in serum from tail vein was detected every two weeks, and hepatitis virus-B surface antigen (HBsAg), antibody to hepatitis virus-B surface (HBsAb), hepatitis virus-B e antigen (HBeAg), antibody to hepatitis virus-B e (HBeAb) and antibody to hepatitis virus-B core (HBcAb) of serum from heart blood were detected after mice were killed (ELISA assay).

Immunohistochemical studies

Expression of MDR1 and LRP was studied by using mouse anti-human MDR1 C219 and LRP monoclonal antibodies (neomarkers) respectively. Tumor tissues from patients with HCC and mice carrying human HCC were fixed in formalin and embedded in paraffin. Sections of 5 μm were assayed for MDR1 and LRP expression by immunoperoxidase staining with the SP method (SP kit, Zhongshan Biocompany, China).

Table 1 Primers for MDR1 and LRP

Gene	Size (bp)	Quantification method	Sequence (5'-3')
B-actin	530	Forward primer	GTGCGTGACATTAAGGAG
		Reverse primer	CTAAGTCATAGTCCGCCT
MDR1	174	Forward primer	CATTGGTGTGGTGAGTCAGG
		Reverse primer	CTCTCTCTCCAACCAGGGTG
LRP	237	Forward primer	TAAGGGCTTCCAGCACCAAC
		Reverse primer	GGAGTTCTCGCTTCTCGTCC

Detection of MDR1 and LRP expression by RT-PCR

Total RNA was extracted from tumors of nude mice and patients using Trizol (Promega) according to the manufacturer's instructions. Reverse transcription (RT) was performed with random primers using a complementary DNA (cDNA) synthesis kit (promega). Following RT-reaction reagents were added: 2 μL $MgCL_2$ (50 mmol/L), 2 μL RT buffer (Tris-HCL pH 8.3), 2 μL deoxynucleotide mixture (100 mmol/L), 0.5 μL RNase (20 units), 1 μL M-MLV reverse transcriptase, 1 μL of random primers (500 μg/mL) and 5 μg substrate RNA. The final volume of RT-reaction (25 μL) was completed with RNase free water. First strand cDNA synthesis was carried out at 37 ℃ for 60 min in a DNA thermal cycler. Afterwards, the tubes were incubated at 95 ℃ for 5 min to terminate the reaction. Then each tube was kept at -20 ℃ until PCR was performed. Primers of the target gene MDR1, LRP and endogenous reference GAPDH were designed using the Primer Express software (Applied Biosystems) (Table 1). The final volume of PCR reaction (50 μL) was completed including an initial phase at 94 ℃ for 4 min, and followed by 30 cycles at 94 ℃ for1 min, and at 56 ℃ for 45 s, at 72 ℃ for 45 s, and finally at 72 ℃ for 10 min.

Statistical analysis

Data were presented as mean±SD and analyzed with SPSS11.0. $P<0.05$ was considered statistically significant.

RUSULTS

Establishment of patient-like metastatic HCC model

Human HCC model of orthotopic implantation was successfully established in nude mice with histologically intact tissues. Out of the 2 specimens from 2 patients with HCC, only one specimen from a 39-year-old man with HCC was at Edmonson grade II-III, whose serum AFP (1 746 ng/mL), HBsAg, HBeAg, HBcAb were all positive, and he had extensive intrahepatic metastases but no hilus hepatis lymph node metastases during operation. Bone metastases were found in the patient one month after operation. Two weeks after implantation, all the livers of 8 nude mice gave rise to tumors and the size of tumors was observed every week with B-ultrasound or by autopsy after they were killed. (Figures 1-3).

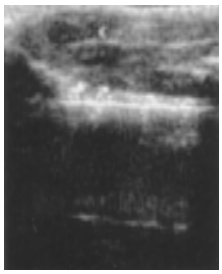

Figure 1 Ultrasonic image of implanted tumors in nude mice liver.

Figure 2 Implanted tumors in nude mice liver by autopsy.

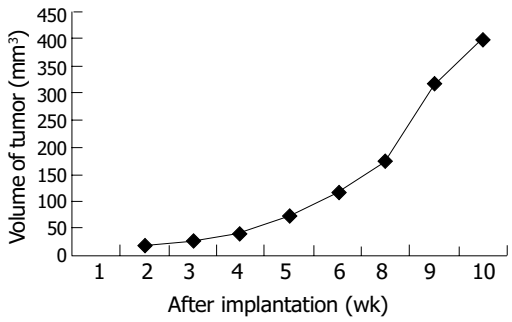

Figure 3 Relation between volume of implanted tumor and time after implantation.

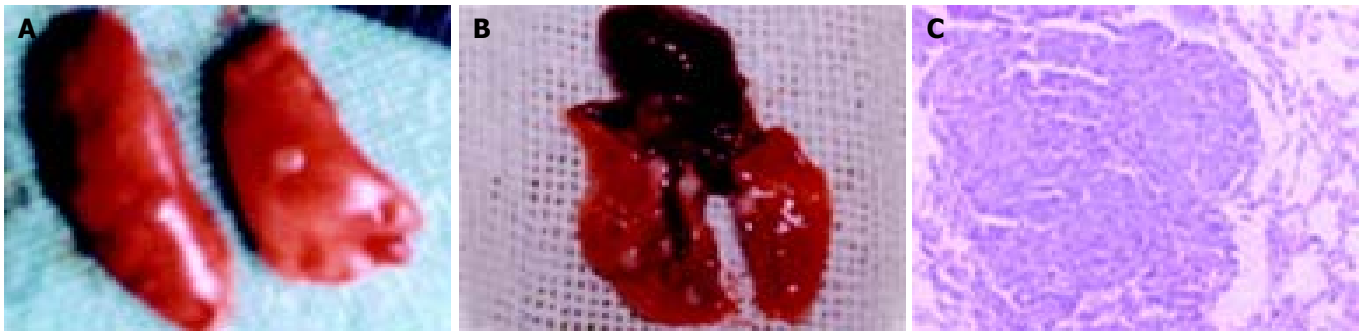

Figure 4 Implanted tumor in nude mice liver metastases to lungs. The first passage just formed a few metastatic lesions A; The 4th passage formed multiple metastatic lesions B; and metastatic lesions in lungs were found under microscope C.

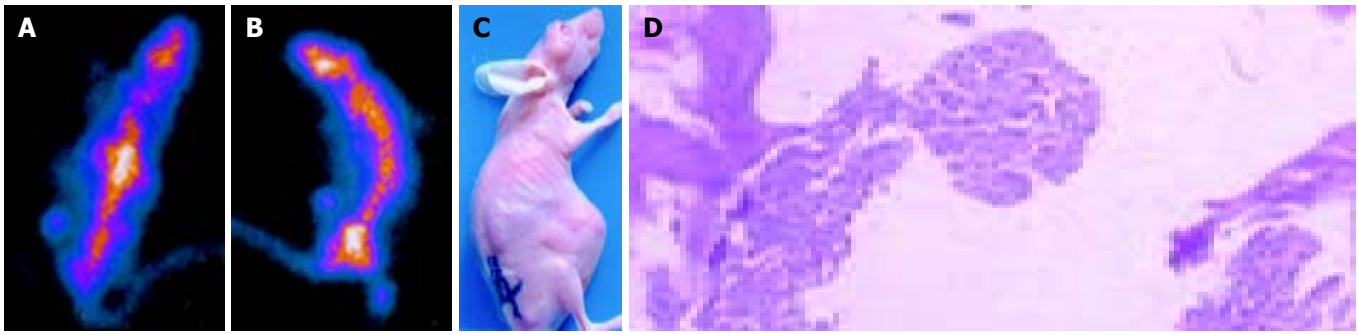

Figure 5 Implanted tumor in nude mice liver spontaneously metastasized to bone. The first passage metastasized to vertebra thoracica just as the donor A, and the 4th passage showed multiple bone metastases B, C. Metastatic lesions were shown in bones under microscope D.

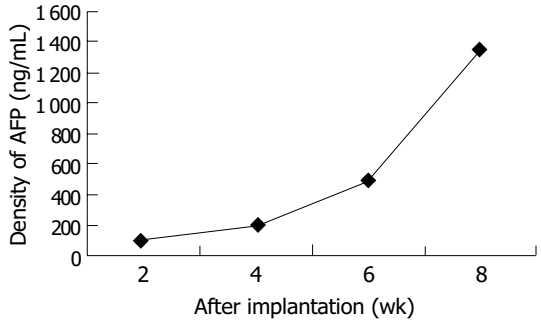

Figure 6 Relation between density of AFP in serum and time of tumor after implantation.

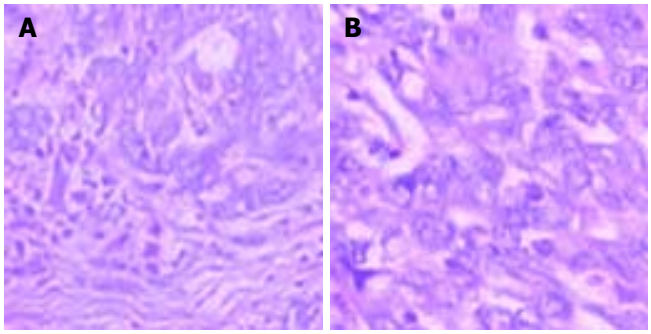

Figure 7 Edmonson grade II-III HCC specimen from patients A and in tumor tissue from nude mice model B.

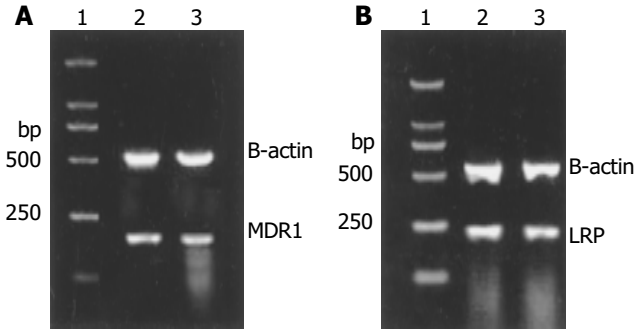

Figure 8 MDR1 and LRP expressed in tumors of the donor (2) and the mude mice model (3), and the expression had no significant difference between both. A: MDR1 expressed in tumors. B: LRP expressed in tumors.

The tumor behavior of this model was the same as the tumor in the patient who donated the specimen. Nine weeks after implantation, the 8 nude mice with normal weight were killed by drawing blood from heart. According to autopsy and microscopic examination, implanted tumor survived in all nude mice (8/8), intrahepatic invasion was seen in all nude mice (8/8), intrahepatic metastases was seen 75% (6/8) (Figure 2), lung metastases was seen in 3 nude mice (35.5%) (Figure 4), the wound seeding was seen in all mice (8/8), and bone metastases occurred in 35.5%(3/8) (Figure 5), but lymph node metastases was not found.

Findings in serum

Serum AFP was detected from tail blood of nude mice (Figure 6), but all markers of hepatitis were negative.

Histological findings

Histological characteristics of the model tumor were similar to those of the donor's tumor (Figure 7).

Immunohistochemistry and RT-PCR results (Figure 8, Table 2)

Table 2 Expression of MDR1 and LRP in HCC from donor and nude mice

	Immunohistochemistry (%)		mRNA of RT-PCR (%)	
	MDR1	LRP	Mdr1	LRP
Donor	31.26	27.18	61.47	56.71
Nude mice	29.20±2.81	25.44±2.43	65.42±13.59	58.63±9.37
t	2.077	2.030	0.823	2.288
P	0.076	0.080	0.438	0.056

DISCUSSION

Subcutaneous tumor implantation has been used as a standard method to establish animal models of human cancer[18,19]. Although such models help to understand the nature of human cancers and their therapeutic approaches, but many problems still remain unsolved. One major problem is that the tumor which was derived from a patient and implanted subcutaneous into an immunodeficient animal no longer behaves as it did in the patient. Although the tumor could sometimes grow subcutaneously, it was encapsulated and usually failed to metastasize either regionally or at distant site[19].

Recently, a new strategy of "orthotopic implantation" has been used to develop rodent models of metastatic human cancer[19,20]. In the first generation of these models, cell lines or disaggregated cells were injected into the organ of mice that corresponded to the organ from which human tumor was derived. This method allowed metastases to occur at least in certain cases[19,21-23]. The cell line and disaggregated cells used for orthotopic implantation were obtained by disrupting the original structure of human tumor tissue, which might lead to a change in nature and biological behavior and could be the basis of the greatly reduced metastases rate[24]. Holfman[25] developed an orthotopic implantation model utilizing intact tissues obtained directly from surgery. This approach has yielded a high survive rate and frequent metastases in cancers of the colon[26], bladder[24], lung[27], pancreas[28], prostate[29] and stomach[30]. These models of human cancer in nude mice could show various manifestations similar to tumor behavior in patients.

However, it remains difficult to obtain satisfactory models for human cancers in nude mice, particularly with regard to spontaneous metastases and reduction of the latent period when cell suspension or histologically intact tissues were used for orthotopic implantation, which could not really reflect the nature of HCC of patients and preclude *in vivo* effective study of important events including spontaneous metastases and mutidrug resistance. Therefore, our approach includes the selection of highly invasive and intrahepatic metastases of human HCC samples and orthotopic transplantation of histologically intact tissues into 3-4 wk old nude mice. In the first generation, the result demonstrated that the specimen from the 39-year-old patient with HCC gave rise to growth of tumor at the implantation site in all the 8 nude mice 2 wk after implantation. In the course of the study, lung and bone metastases were found in the patient donating specimens 1 mo after operation. So we began to pay attention to nude mice in terms of metastases. Fortunately, metastases occurred in all the mice 7-8 wk after implantation, 3 (3/8) had lung metastases, and 3 (3/8) had spontaneous bone metastases, and all had wound seeding and intrahepatic invasion. Lymph node metastases, however, was not found. Spontaneous metastases of human cancer xenografts in nude mice was rare[9,11]. We believe the reasons of cancer growth and metastases in nude mice were that the specimen selected was highly metastatic and that the nude mice were younger (3-4 wk) than those used in other studies[13,31]. But metastases was not found in all the mice. We believe the reasons might be that the time after implantation was not so long that the metastases could not occur in each one, and that it was related to the methods detecting the metastases. So in the 2-4 passages, the nude mice carrying implantation tumor were not killed until they developed signs of distress so as to give full time to metastases and to observe the nature of the tumor. As a result, intrahepatic, lung and bone metastases and wound seeding and multiple metastatic sites in those organs were surprisingly observed in all nude mice over a period ranging 5-16 wk after implantation. Besides selection of the highly invasive and metastatic samples and age of the nude mice, we think there were two key factors, one was that we selected and isolated more higher metastatic subpopulation from the parent tumor, and the other was that a long time could give chance to implanted tumor to metastasize.

As shown in the results, the expression of AFP, MDR1, and LRP was well maintained in locally growing tumor tissues as well as in metastases. These results indicated that this nude mice model represented the majority of biological natures including local invasion, spontaneous lung, bone and intrahepatic metastases, MDR and secreted AFP, suggesting that our model indeed has some features resembling the natural biological behaviors of human HCC.

Although spontaneous metastases models of HCC have been established in nude mice, but bone metastases and MDR studies are not available. Our model well maintained the native structure of HCC and exhibited spontaneous lung metastases, especially spontaneous bone metastases and expression of MDR just as the patient donating the specimen. Thus, this model represents the features of patients with HCC, and could be an interesting tool for studying human HCC.

REFERENCES

1 **Zhang S,** Li L, Lu F. Mortality of primary liver cancer in China from 1990 through 1992. *Zhonghua Zhongliu Zazhi* 1999; **21**: 245-249

2 **Pisani P,** Parkin DM, Bray F, Ferlay J. Estimates of the world-wide mortality from 25 cancers in 1990. *Int J Cancer* 1999; **83**: 18-29

3 **Chen XP,** Wu ZD, Qiu FZ. The history, present and prospect of the surgical treatment of primary liver cancer in China. *Zhongguo Puwai Jichu Yu Linchuang Zazhi* 2000; **4**: 257-258

4 **Shimosato Y,** Kameya T, Nagai K, Hirohashi S, Koide T, Hayashi H, Nomura T. Transplantation of human tumors in nude mice. *J Natl Cancer Inst* 1976; **56**: 1251-1260

5 **Hirohashi S,** Shimosato Y, Kameya T, Koide T, Mukojima T, Taguchi Y, Kageyama K. Production of alpha-fetoprotein and normal serum proteins by xenotransplanted human hepatomas in relation to their growth and morphology. *Cancer Res* 1979; **39**: 1819-1828

6 **Liu X,** Hu J, Cui H, Yang X, Li S. Establishment and biological characteristics of the nude mice xenograft model from human hepatocellular carcinoma. *Zhongguo Yixue Kexueyuan Xuebao* 1995; **17**: 98-103

7 **Leveille-Webster CR,** Arias IA. Establishment and serial quantification of intrahepatic xenografts of human hepatocellular carcinoma in severe combined immunodeficiency mice, and development of therapeutic strategies to overcome multidrug resistance. *Clin Cancer Res* 1996; **2**: 695-706

8 **Sun FU,** Tang Z, Liu K. Growth pattern and metastatic behavior of orthotopically metastatic model of human hepatocellular carcinoma in nude mice. *Zhonghua Yixue Zazhi* 1995; **75**: 673-675

9 **Sun FX,** Tang ZY, Lui KD, Ye SL, Xue Q, Gao DM, Ma ZC. Establishment of a metastatic model of human hepatocellular carcinoma in nude mice via orthotopic implantation of histologically intact tissues. *Int J Cancer* 1996; **66**: 239-243

10 **Peng BG,** Ding J, Lü MD, Cheng LJ, Huang JF, Lu LJ. A model of transplantation of human hepatocellular carcinoma in mouse: its establishment and characterization. *Zhongshan Yike Daxue Xuebao* 1996; **17**(Suppl): 7-10

11 **Tao WZ,** Zheng WQ, Gong ZJ. The tumor invasion and metastasis in the transplantation of transplanted human hepatocellular carcinoma into nude mice abdominal cavity and orthotopic hepatic tissue. *Dier Junyi Daxue Xuebao* 1998; **19**: 54-56

12 **Genda T,** Sakamoto M, Ichida T, Asakura H, Kojiro M, Narumiya S, Hirohashi S. Cell motility mediated by rho and Rho-associated protein kinase plays a critical role in intrahepatic metastasis of human hepatocellular carcinoma. *Hepatology* 1999; **30**: 1027-1036

13 **Zheng JM,** Tao WZ, Zheng WQ, Bao JZ, Wang YL, Zhu MH. Establishment of the orthotopic transplantation tumor model from the subcutaneous model of human hepatocellular carcinoma in nude mice. *Dier Junyi Daxue Xuebao* 2000; **21**: 456-459

14 **Shi CH**, Wang XW, Wang WY, Shi XY, Zhu DS. Experimental study on a human hepatocellular carcinoma model using orthotopic transplantation. *Zhongguo Shiyan Dongwu Xuebao* 2001; **9**: 57-61

15 **Fu X,** Guadagni F, Hoffman RM. A metastatic nude-mouse model of human pancreatic cancer constructed orthotopically with histologically intact patient specimens. *Proc Natl Acad Sci U S A* 1992; **89**: 5645-5649

16 **Wang X,** Fu X, Hoffman RM. A patient-like metastasizing model of human lung adenocarcinoma constructed via thoracotomy in nude mice. *Anticancer Res* 1992; **12**: 1399-1401

17 **Fu X,** Hoffman RM. Human ovarian carcinoma metastatic models constructed in nude mice by orthotopic transplantation of histologically-intact patient specimens. *Anticancer Res* 1993; **13**: 283-286

18 **Fidler IJ.** Rationale and methods for the use of nude mice to study the biology and therapy of human cancer metastasis. *Cancer Metastasis Rev* 1986; **5**: 29-49

19 **Fidler IJ.** Critical factors in the biology of human cancer metastasis: twenty-eighth G.H.A. Clowes memorial award lecture. *Cancer Res* 1990; **50**: 6130-6138

20 **Manzotti C,** Audisio RA, Pratesi G. Importance of orthotopic implantation for human tumors as model systems: relevance to metastasis and invasion. *Clin Exp Metastasis* 1993; **11**: 5-14

21 **Giavazzi R,** Jessup JM, Campbell DE, Walker SM, Fidler IJ. Experimental nude mouse model of human colorectal cancer liver metastases. *J Natl Cancer Inst* 1986; **77**: 1303-1308

22 **Bresalier RS,** Raper SE, Hujanen ES, Kim YS. A new animal model for human colon cancer metastasis. *Int J Cancer* 1987; **39**: 625-630

23 **Morikawa K,** Walker SM, Nakajima M, Pathak S, Jessup JM, Fidler IJ. Influence of organ environment on the growth, selection, and metastasis of human colon carcinoma cells in nude mice. *Cancer Res* 1988; **48**: 6863-6871

24 **Fu XY,** Theodorescu D, Kerbel RS, Hoffman RM**.** Extensive multi-organ metastasis following orthotopic onplantation of histologically-intact human bladder carcinoma tissue in nude mice. *Int J Cancer* 1991; **49**: 938-939

25 **Hoffman RM.** Orthotopic is orthodox: why are orthotopic-transplant metastatic models different from all other models? *J Cell Biochem* 1994; **56**: 1-3

26 **Fu XY,** Besterman JM, Monosov A, Hoffman RM. Models of human metastatic colon cancer in nude mice orthotopically constructed by using histologically intact patient specimens. *Proc Natl Acad Sci U S A* 1991; **88**: 9345-9349

27 **Wang X,** Fu X, Hoffman RM. A new patient-like metastatic model of human lung cancer constructed orthotopically with intact tissue via thoracotomy in immunodeficient mice. *Int J Cancer* 1992; **51**: 992-995

28 **Fu X,** Guadagni F, Hoffman RM. A metastatic nude-mouse model of human pancreatic cancer constructed orthotopically with histologically intact patient specimens. *Proc Natl Acad Sci U S A* 1992; **89**: 5645-5649

29 **Fu X,** Herrera H, Hoffman RM. Orthotopic growth and metastasis of human prostate carcinoma in nude mice after transplantation of histologically intact tissue. *Int J Cancer* 1992; **52**:987-990

30 **Furukawa T,** Fu X, Kubota T, Watanabe M, Kitajima M, Hoffman RM. Nude mouse metastatic models of human stomach cancer constructed using orthotopic implantation of histologically intact tissue. *Cancer Res* 1993; **53**: 1204-1208

31 **Tang ZY,** Sun FX, Tian J, Ye SL, Liu YK, Liu KD, Xue Q, Chen J, Xia JL, Qin LX, Sun HC, Wang L, Zhou J, Li Y, Ma ZC, Zhou XD, Wu ZQ, Lin ZY, Yang BH. Metastatic human hepatocellular carcinoma models in nude mice and cell line with metastatic potential. *World J Gastroenterol* 2001; **7**: 597-601

Edited by Wang XL and Zhang JZ **Proofread by** Xu FM

PO Box 2345, Beijing 100023, China
Fax: +86-10-85381893
E-mail: wjg@wjgnet.com www.wjgnet.com

World J Gastroenterol 2004;10(21):3112-3117
World Journal of Gastroenterology
 ISSN 1007-9327

• LIVER CANCER •

Experimental and clinical assessment of percutaneous hepatic quantified ethanol injection in treatment of hepatic carcinoma

Li-Wu Lin, Xue-Ying Lin, Yi-Mi He, Shang-Da Gao, En-Sheng Xue, Xiao-Dong Lin, Li-Yun Yu

Li-Wu Lin, Xue-Ying Lin, Yi-Mi He, Shang-Da Gao, En-Sheng Xue, Xiao-Dong Lin, Li-Yun Yu, Fujian Provincial Ultrasonic Medicine Institute, Ultrasound Department, Union Hospital of Fujian Medical University, Fuzhou 350001, Fujian Province, China
Correspondence to: Li-Wu Lin, Ultrasound Department, Union Hospital of Fujian Medical University, Fuzhou 350001, Fujian Province, China. lxdghl@163.net
Telephone: +86-591-3357896 Ext. 8352 **Fax:** +86-591-3339732
Received: 2003-09-15 **Accepted:** 2003-10-22

Abstract

AIM: To detect the relationship between absolute ethanol injection quantity, the interval and formation of fibreboard, the curative effect in treatment of hepatocarcinoma and to evaluate the clinical application of percutaneous hepatic quantified ethanol injection (PHQEI) in treatment of hepatic carcinoma (HCC).

METHODS: (1) Experimental study: Twenty-four human hepatic carcinoma SMMC-7721 xenografted nude mice were randomly divided into three groups: group A injected with quantified ethanol at short intervals (QESI), group B with quantified ethanol at long intervals (QELI) and group C with a small quantity of ethanol at long intervals (SQLI). The tumor tissues were sent for patho-histology and electron microscopic examinations. The diameters of tumors were measured with high frequency ultrasound before and after therapies and tumor growth index (TGI) was calculated. (2) Clinical study: Tumors of 122 cases of pathologically proved HCC were injected with quantified ethanol guided by ultrasound every 3-5 d 4-10 times per period of treatment. The quantity of ethanol was calculated according to the regressive equations where Y = 2.885X when the mass was ≤5 cm in diameter and Y = 1.805X when the mass was >5 cm in diameter (X is the maximal diameter of the mass with the unit cm, Y is the ethanol quantity with the unit mL). The survival rates of 1, 2, 3 and 4 years and recurrent rates *in situ* as well as dystopia in the liver were calculated.

RESULTS: (1) Experimental study: TGI of QESI group (0.072±0.018) and QELI group (0.094±0.028) was apparently lower than that of SQLI group (1.982±0.482) (P<0.01). TGI of QESI group seemed to be lower than that of QELI group, but it was not markedly different (P>0.05) between two groups. Severe degeneration and necrosis could be seen in QESI group by patho-histology examination. Coagulative necrosis could be seen in most tumors of QESI group and there were no residual cancer cells under electronic microscope, while the residual cancer and inflammatory cells and fibre tissues could be seen around the tumors of QELI group. Infiltration of inflammatory cells could be seen and fibre tissues were formed. (2) Clinical study: B mode ultrasound showed that 62.5% of tumors shrank after PHQEI. The survival rates of 1, 2, 3 and 4 years of the group with tumors ≤3 cm in diameter were higher than those of the group with tumors >3 cm in diameter. The recurrent rates of tumors *in situ* of the former group were apparently lower than those of the latter group. The recurrent rates of tumors in dystopia in the liver of the former group were markedly lower than those of the latter group. The 122 cases underwent a total of 1221 PEI. There were no complications such as hemorrhage and severe heart, liver and kidney functional injuries except for 1 case of melena and 4 cases of jaundice who recovered after 1-2 wk under common therapies.

CONCLUSION: The experimental study shows quantified ethanol at intervals of 3-5 d could improve the curative effect of hepatocarcinoma. The clinical study shows PHQEI is an effective therapeutic method for HCC with few side-effects, and a low-cost. The treatment efficacy is more remarkable for tumors ≤3 cm in diameter.

Lin LW, Lin XY, He YM, Gao SD, Xue ES, Lin XD, Yu LY. Experimental and clinical assessment of percutaneous hepatic quantified ethanol injection in treatment of hepatic carcinoma. *World J Gastroenterol* 2004; 10(21): 3112-3117
http://www.wjgnet.com/1007-9327/10/3112.asp

INTRODUCTION

Because ultrasound-guided percutaneous ethanol injection (PEI) has the advantages of easy operation, definite curative effect, little damage and few side-effects, it has been widely used in clinical practice in recent years since the report by Japanese scholars in 1983[1-10]. Though more ultrasound-guided methods have been applied since then[11-20], PEI is still one of the most widely used non-operative methods in the treatment of hepatic carcinoma. Because there is no common standard for ethanol injection quantity and interval, the efficacy is affected apparently. In order to improve the efficacy, according to the pathological biological characteristics of HCC that there are capsula and tiny satellitic foci of cancer cells in the periphery of HCC, we once conducted the study of percutanous hepatic quantified ethanol injection (PHQEI) in treatment of HCC (Ethanol was injected until the diffusing area was 1-2 cm more than the maximal diameter of tumor ≤5 cm in diameter. According to the endurance of patients the ethanol was injected from several directions and diffused throughout the nodules >5 cm in diameter as fully as possible.) and we put forward the regressive equations[21]: Y = 2.885X (X≤5 cm), Y = 1.805X (X>5 cm) (X is the maximal diameter of the tumor with the unit cm, Y is the ethanol quantity with the unit mL). Recently, some scholars have reported that it could cause cancer cells to remain as the fibreboard in tumors affected the wide infiltration of ethanol[22]. So we carried out experimental studies to prove the relationship between absolute ethanol injection quantity and the formation of fibreboard. We have followed up 122 cases of hepatocarcinoma treated by PHQEI for 1-4 years to assess its clinical application.

MATERIALS AND METHODS

Experimental studies

Experimental animals For the experiment, we used 24 BALB/CA nude mice, which were 5-8 wk old, provided by the Medical Experiment Animal Unit of Anti-cancer Center of Xiamen University, China. The average weight was 18±2.1 grams. They were raised in the layer drift shelves under aseptic conditions. The cages, cushion, drinking water and standard forage provided by Shanghai Bikai Company were changed periodically.

Experimental methods Twenty-four nude mice with human HCC-transplanted hypodermically were randomly divided into three groups: group A injected with quantified ethanol (the ethanol diffused throughout the tumor) at short intervals (5 d) (QESI), group B with quantified ethanol at long intervals (10 d) (QELI) and group C with a small quantity of ethanol (half quantity of ethanol as used in QESI) at long intervals (SQLI). Each group contained 8 nude mice.

Three dimensional diameters of the tumors were measured by high frequency ultrasound (Aloka-5500 with 10 MHz probe) after 10 d of transplantation of HCC and the volume was calculated. Then ethanol was injected into the center of the tumor with No.5 needles. All the mice were injected twice. The three dimensional diameters of the tumors were measured again 5 d after the last injection and then the mice were killed. The center and peripheral tissues of tumors were sent for pathologic histology and electron microscopic examination. The experiment was carried out with double blind method.

Observation indexes Tumor growth index (TGI) was calculated by the formula: volume of the tumor (after treatment-before treatment)/volume of the tumor (before treatment). The degree of degeneration and necrosis, inflammatory response of tissues and fibre tissue were observed by pathologic histology examination. The microstructure of tumor tissues, inflammatory cells and fibre cells, fibreboard were observed under electron microscope.

Statistical methods

The data of each group were exporessed as mean±SD. Necrosis area of each group was calculated and analyzed with ANOVA. $P<0.05$ was considered statistically significant. All statistical analyses were performed using SPSS for windows version 8.0 software package.

Clinical studies

Patients One hundred and twenty-two cases of HCC, including 96 cases recurring after operation, consisted of 105 males and 17 females were enrolled in the study. The mean age was 54.8 years (range, 28-81). The diagnosis was established by pathocytology and/or histology. One hundred and twenty-two cases had 168 nodules including 62 cases with single nodules. The mean diameter of tumor was 3.8 cm (1.2-7.2 cm) and 122 cases comprised 64 cases with tumors <3 cm in diameter and 58 cases with tumors >3 cm in diameter (27 cases with tumor >5 cm in diameter). Seventy-eight cases had AFP >20 ng/mL.

Instruments Real-time ultrasonography (Aloka-650, 1700, Japan) was performed with a 3.5 MHz probe. The puncture needles were 22G PTC fine-needles and 15-20 cm in length. The platelet count of the patients was $>50\times10^9$/L.

Injection methods The point of puncture was determined by ultrasonography. Under local anesthesia, the fine needle punctured from the point into the posterior of the axis of nodules. Then ethanol was injected into the nodule gradually and the needle was withdrawn slowly. The injection quantity was calculated according to the regressive equations: Y = 2.885X (X<5 cm), Y = 1.805X (X>5 cm) (X is the maximal diameter of the tumor with the unit cm, Y is the ethanol quantity with the unit mL). All the cases were injected every 3-5 d 4-10 times per period of treatment. The tumor>5 cm in diameter could also be injected 10-20 times per period of treatment.

Follow-up time The follow-up period lasted for 12-48 mo (mean period 34 mo). The survival rates of 1, 2, 3 and 4 years and recurrent rates *in situ* as well as dystopia in the liver of each group were calculated and compared using ANOVA. The 14 nodules of 9 cases were resected after quantified ethanol injection 2-4 times and sent for pathologic examination.

RESULTS

Experimental studies

Tumor growth index Table 1 shows that TGI of QESI and QELI groups was apparently smaller than that of SQLI group ($P<0.01$). TGI of QESI group seemed to be smaller than that of QELI group, but not different markedly ($P>0.05$).

Table 1 Comparison of TGI between groups (mean±SD)

Groups	Cases (*n*)	TGI	*P*
A: QESI	8	0.072±0.018	>0.05[1]
B: QELI	8	0.094±0.028	<0.01[b]
C: SELI	8	1.982±0.482	<0.01[d]

[1]$P>0.05$ *vs* group B, [b]$P<0.01$ *vs* group C, [d]$P<0.01$ *vs* group A.

Table 2 Comparison of the percentage of tumor necrosis between groups

Necrosis area	QESI (A)	QELI (B)	SELI (C)	*P*
80%-	87.5 (7/8)	50 (4/8)	0	<0.01[b] <0.01[d]
30%-	12.6 (1/8)	50 (4/8)	100 (8/8)	<0.01[f]

[b]$P<0.01$ between groups A and C, [d]$P<0.01$ between groups A and B, [f]$P<0.01$ between groups B and C.

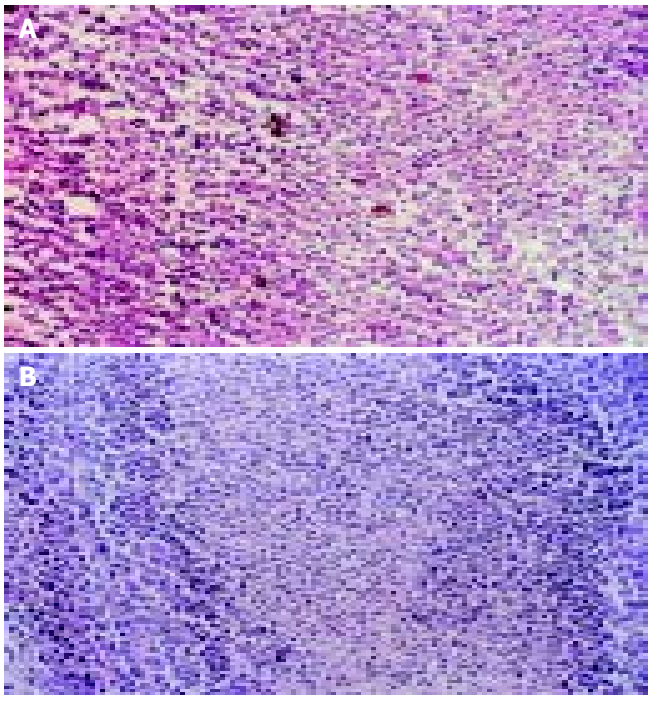

Figure 1 Coagulation necrosis in the center to periphery of the tumors of QESI after injection. (A, HE×10). The center of the tumor of SELI appeared coagulation necrosis, but in the periphery cancer cells grew luxuriantly after injection (B, HE×10).

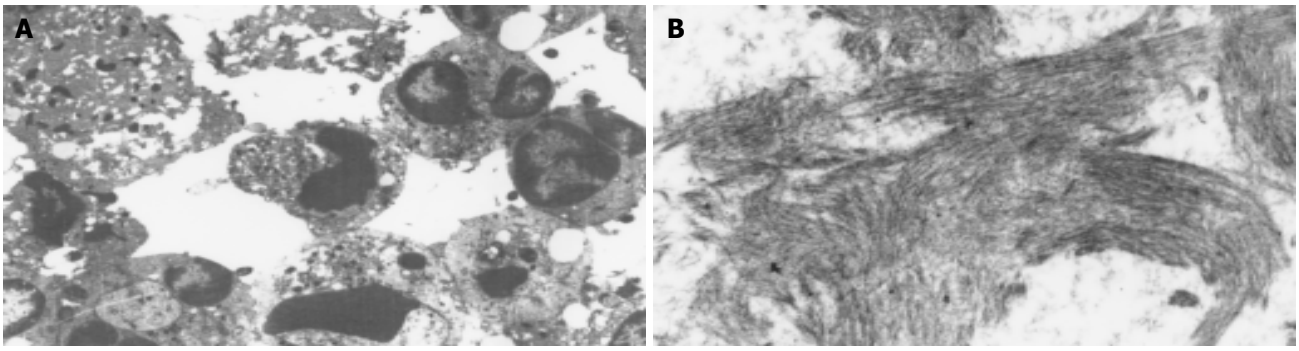

Figure 2 Inflammation cell infiltration (A) and faciculus (B) in the periphery of tumors of SQLI group. electron microscope examination.

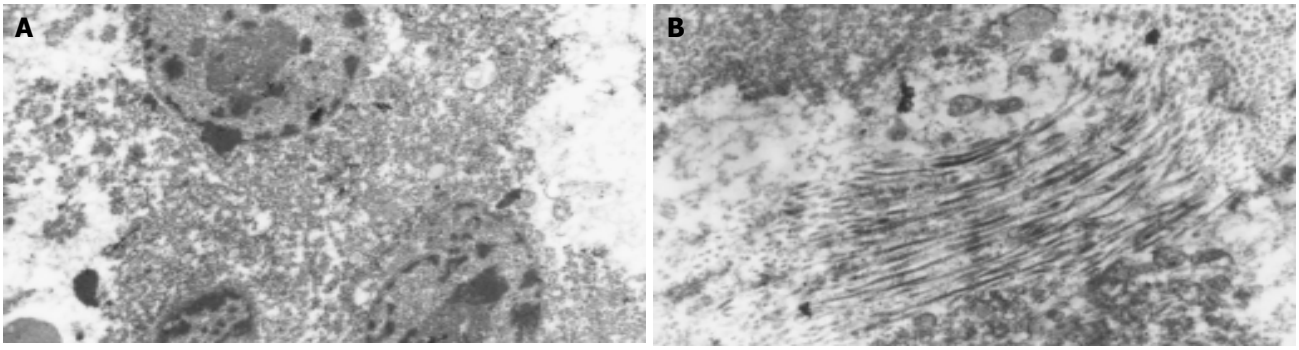

Figure 3 Degeneration cancer cells (A) and fasciculus (B) in the periphery of the tumors of QELI. Shown in electron microscope examination after injection.

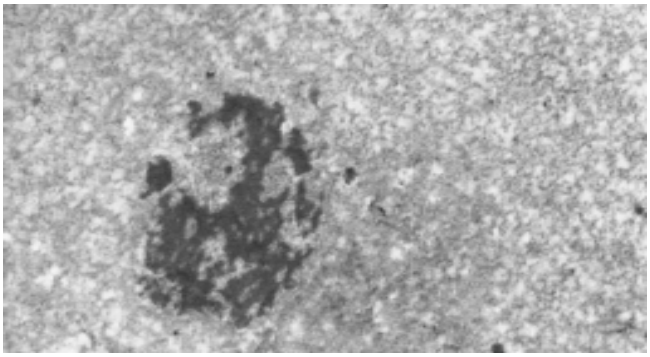

Figure 4 Necrosis changes such as karyalysis, karyorrhexis and cell membrane disappearance in the tumors of QESI after injection under election microscope.

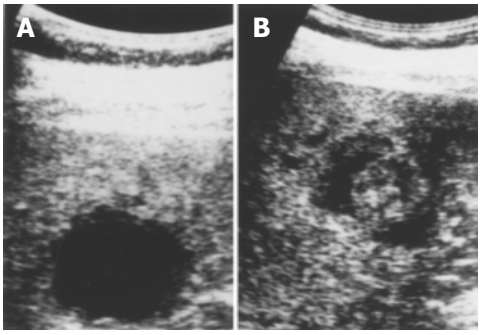

Figure 5 Reduction of the average diameter of HCC nodules from 3.6 cm (before injection, A) to 2.6 cm (two years after injection, B) and hyperechogenic rings in the periphery with haloes surrounding them after injection.

Patho-histology examination Table 2 shows the percentage of tumor necrosis of each group. Necrosis of QESI group was most severe. Coagulative necrosis could be seen from center to periphery of the tumor of QESI group. Eighty-seven point five percent of QESI group showed necrosis area >80%, markedly higher than those of QELI and SELI groups. None of SELI group showed necrosis area >80%. The center of the tumor of SELI group showed necrosis but in the periphery cancer cells grew actively (Figure 1).

Electron microscopic observation (1) SELI group: Cancer cells showed coagulation necrosis in the center only and most cancer cells grew luxuriantly, especially in the periphery. Most cancer cells only showed orbicular karyotheca, nuclei in different size, abundant euchromatin, orbicular cytomembrane, many inflammatory cells, fibrocytes and fasciculus (Figure 2).

(2) QELI group: Coagulation necrosis was comparably severe, but in the periphery orbicular cancer cells, some degenerative cancer cells, inflammatory cells and fasciculus could be seen (Figure 3).

(3) QESI group: Necrotic changes, such as karyalysis, karyorrhexis and cell membrane disappearance could be seen in most cancer cells (6/8) (Figure 4). There were severe degenerative cancer cells in which heterochromatin agglutinated under the nuclear membrane. No fasciculus formed.

Clinical studies

Ultrasonography, CT or MRI showed that 168 nodules in 122 cases of HCC shrank 2-8 wk after the last PHQEI. The average diameter reduced from 3.8 cm to 2.9 cm. Ultrasound showed the echoes of tumor nodules enhanced after PEI therapy. Hyperechogenic rings could be seen in the periphery of 25% (42/168) cases of haloes surrounding them (Figure 5). The diameters of 62.5% (105/168) tumors shrank and the internal echo enhanced and facula or light dot formed (Figure 6). Tumor nodules disappeared in 12.5% cases. CT showed that the nodules showed homogeneous hypodensity or/and non-enhanced changes in 62 cases after PHQEI. MRI showed that 38 nodules of 26 cases showed low T1 and T2 signals. fine-needle or/and

thick-needle biopsies were taken 1-3 times in all the cases and no cancer cells appeared in 88.5% (108/122) cases and degenerative cancer cells appeared in 11.5% (14/122) cases with nodules >5 cm in diameter. After therapy AFP reduced in 78 cases with high AFP before therapy and 82.1% (64/78) cases turned negative.

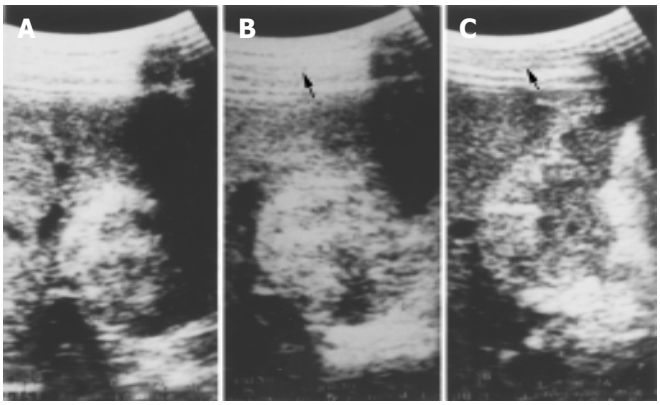

Figure 6 A: Average diameter of HCC nodule was 4.4 cm. B: It was 4.8 cm after 10 injections of absolute ethanol and the echogenic enhanced. C:After 42 mo of therapy the tumor shrank to 2.9 cm in diameter and formed facula.

Table 3 Efficacy of PEI reported in literature

Scholar	Time	Cases	Diameters of nodules (cm)	Survival rate (%)				
				1 yr	2 yr	3 yr	4 yr	5 yr
Ebara	1992	112	≤3	94	84	63	49	39
Castells	1992	162	<5	90	80	63		
Li Po	1996	188	4.6	85	44	19		
This article	2002	58	>3	84	64	58	52	
This article	2002	64	≤3	94	85	72	63	

Table 3 shows the survival rates of 1, 2, 3 and 4 years of each group with tumors <3 cm (64 cases) and >3cm in diameter (58 cases) and the treatment efficacy reported by different scholars.

Table 4 shows that the recurrent rate of tumors *in situ* and dystopia of the group with tumor ≤3 cm in diameter was apparently lower than that of the group with tumor >3 cm in diameter.

None of 9 cases with 14 nodules but 1 case showed cancer cells in pathologic examination of the resected specimens after 2-4 PHQEIs.

The 122 cases underwent a total of 1 221 PHQEIs. There were no complications such as hemorrhage and severe heart, liver and kidney functional injuries except that 1 case of melona after the injection of 8 mL ethanol and 4 cases of jaundice after 2-3 PHQEIs recovered after 1-2 wk under common therapies. Different degrees of pains occurred in 33.6% (41/122) cases after 1-2 PHQEIs and disappeared in 30 min without any therapy. Low-fever appeared in 56.6% (69/122) cases and disappeared after 2-4 d. GPT increased in 16.4% (20/122) cases and reduced to normal in 1 mo. There were no apparent changes of kidney function and ECG examination in all cases before and after therapy.

DISCUSSION

HCC is one of the most common cancers throughout the world. In order to surmount the obstinate disease scholars at home and abroad have conducted a great number of studies from many aspects, such as causa moli, pathology, diagnosis and therapy, and have acquired some accomplishments, especially in therapy[23-35]. Operation is the most common method in early stage, while HCC has the biologic characteristics of early invasion to blood vessels and multiple origins, which cause low resection rate and high recurrent rate (90%) of 5 years. With the advantages of definite efficacy, low complication and easy operation, PEI is still one of the most appropriate non-operative methods for small HCC which is unsuitable for resection and recurrent hepatic carcinoma. The mechanism of PEI is to make cancer cells incur dehydration and coagulative necrosis by injecting ethanol into tumors. But there is not a unified standard for total injection quantity, quantity per time and injection interval. At present, some scholars have adopted the formula[36]: $V = 4/3 \pi (r+0.5)^3$ (V is the total quantity, r is the radius of focus.) and others used the calculation[37]: Injection quantity (mL) = diameter (cm) or quantity (mL) = diameter (cm) +1 (tumor ≤5 cm in diameter) and quantity (mL) = diameter (cm) + 2 (tumor >5 cm in diameter). Liu *et al*.[38] reported that 238 cases of HCC were given PEI with 1-20 mL ethanol per injection and 1-2 times per week. The injection area involved the center as well as periphery of tumor and the part adhering closely to the capsule. Excessive ethanol increases side-effects and unnecessary liver injury, while too little ethanol could not kill cancer thoroughly and cause tumors to recur and metastasize. We once conducted the study of percutaneous hepatic quantified ethanol injection in treatment of HCC and put forward the regressive equation based on tumor diameter and injection quantity of ethanol[21]. The initial clinical application and following observation showed PHQEI had apparent efficacy. This experimental study was to further probe the pathologic basis of ethanol injection quantity, interval and the formation of fibreboard and to assess the clinical application value of PHQEI by follow-up observations.

Experimental study showed that tumor growth of QESI group (The ethanol diffused throughout the tumor and was injected every 5 d) was markedly inhibited after 2 injections. Extensive coagulative necrosis could be seen from the center to periphery of tumors and the necrosis area of 87.5% (7/8) cases reached more than 80% by pathologic histology. Electron microscopy showed the majority had coagulative necrosis and some had severe degenerative tumor cells. Though the growth of tumor of QELI group (The injection quantity was the same as that of QESI, but the interval was prolonged twice.) was also inhibited, the necrosis area of only 50% (4/8) cases was >80%. There were more residual cancer cells in the periphery of tumors and fibre tissue and inflammatory cells could be seen under electron microscope. Because ethanol injection was only half of that of QESI group and the injection interval was prolonged twice, growth inhibition and necrosis degree of tumors of SQLI group

Table 4 Comparison of the recurrent rates between groups

Group	Total Cases	Recurrent rate *in situ* (%)				Recurrent rate in dystopia (%)			
		1 yr	2 yr	3 yr	4 yr	1 yr	2 yr	3 yr	4 yr
>3 cm (A)	58	6.9 (4/58)	7.1 (3/42)	24.2 (8/33)	28.6 (6/21)	15.5 (9/58)	21.4 (9/42)	36.4 (12/33)	52.4 (11/21)
≤3 cm (B)	64	0 (0/64)[a]	2.1 (1/48)	5.1 (2/39)[a]	4.2 (1/24)[a]	9.0 (6/64)	10.4 (5/48)	12.8 (5/39)[a]	20.8 (5/24)[a]

[a]$P<0.05$ *vs* group A.

were apparently slighter than those of the former two groups. Except for necrosis in the center, cancer cells grew luxuriantly, inflammatory response appeared and fasciculus formed in the periphery of the tumor.

Tumors in 122 cases of pathologically proved HCC, including 58 cases with tumors >3 cm in diameter and 64 cases with tumors ≤3 cm in diameter, were given PHQEL. We followed up the cases for 12-48 mo and proved that PHQEI had good efficacy, especially for tumors ≤3 cm in diameter. The 1-4 year survival rates of the group with tumors ≤3 cm in diameter were markedly higher than those of the group with tumors >3 cm in diameter and *in situ* tumor as well as dystopia recurrent rates were lower than those of the latter group. The reason might be that the ethanol quantity was not enough to meet the therapy standard for tumors >5 cm in diameter of 27/58 cases for the patients were weak and their liver function was bad. Giorgio *et al*.[39] reported that 112 cases were given single-session percutanous large dosage ethanol infection therapy with 16-120 mL ethanol per injection in panplegia. Five patients died after 7-10 h, and the 1, 2 and 3 year survival rates of the remaining 107 cases were 88%, 76% and 76%, respectively. The result showed that large amount ethanol injection could improve the treatment efficacy, while the side-effect also increased. So patients with advanced HCC of large tumors should be closely observed and an appropriate injection quantity should be chosen[40].

Recently, some scholars have proposed that fibreboard also appeared in HCC of 3 cm in diameter and the infiltration capacity of absolute ethanol was bad. In order to improve the treatment efficacy, ethanol should be injected from different points repeatedly[22]. Some scholars used drugs with a stronger infiltration capacity, for example, 50% acetic acid injection (PAAI)[41]. Ohnishi *et al*.[42] reported that the 1 and 2 year survival rates of PAAI were 100% and 92%, markedly higher than those of PEI which were 63% and 53%, respectively. The recurrent rate was 8%, lower than that of PEI which was 37%. But our study showed that the survival rate of HCC ≤3 cm in diameter was not lower and the recurrent rate was not higher than those of PAAI. The 4 year recurrent rate *in situ* was only 4.2% (1/24). Except for 1 case with a tumor of 5.1 cm in diameter none of the 9 cases with 14 nodules showed cancer cells in pathologic examination of resected specimens after 2-4 PHQEIs. Okuda *et al.* reported that about 90% of small HCCs had different degree of gross fibre pseudo-capsule and tumors <1 cm in diameter seldom had fibre capsule due to the gradually enhanced immune response of the body during the growth of tumor[22]. Our experimental study showed that SQLI injection could stimulate strong immune response of organisms and cause inflammatory cell infiltration and fibreboard formation even if the tumor was less than 1 cm in diameter.

In conclusion, the experimental study shows that, in order to improve the efficacy of PEI adequate quantity must be adopted to maintain a strong diffusing capacity of ethanol in tumor and the interval must be short (The appropriate interval is 3-5 d) because small dosage and long interval will cause incomplete coagulated necrosis and formation of fibreboard and/or fasciculus which will influence the infiltration of ethanol and cause cancer cells to remain and metastasize.

The clinical study also shows that PHQEI has a high application value. So PEI is still the method with advantages of convenience, few side-effects and effectiveness. To further improve the treatment efficacy, studies on the quantity per injection and injection interval are needed.

REFERENCES

1 **Kuriyama H,** Okada S, Okusaka T, Ueno H, Ikeda M. Prognostic factors in patients with small hepatocellular carcinoma treated by percutaneous ethanol injection. *J Gastroenterol Hepatol* 2002; **17:** 1205-1210

2 **Huo TI**, Huang YH, Wu JC, Lee PC, Chang FY, Lee SD. Survival benefit of cirrhotic patients with hepatocellular carcinoma treated by percutaneous ethanol injection as a salvage therapy. *Scand J Gastroenterol* 2002; **37:** 350-355

3 **Yamamoto J**, Okada S, Shimada K, Okusaka T, Yamasaki S, Ueno H, Kosuge T. Treatment strategy for small hepatocellular carcinoma: comparison of long-term results after percutaneous ethanol injection therapy and surgical resection. *Hepatology* 2001; **34**(4 Pt 1)**:** 707-713

4 **Casella G,** Cacopardo E, Rovere G, Buda CA, Cascinu S, Baldini V. Cutaneous seeding after ultrasound-guided percutaneous ethanol injection for treatment of hepatocellular carcinoma. *J Clin Ultrasound* 2001; **29:** 354-358

5 **Giorgio A,** Tarantino L, de Stefano G, Perrotta A, Aloisio V, del Viscovo L, Alaia A, Lettieri G. Ultrasound-guided percutaneous ethanol injection under general anesthesia for the treatment of hepatocellular carcinoma on cirrhosis: long-term results in 268 patients. *Eur J Ultrasound* 2000; **12:** 145-154

6 **Fiore F**, Vallone P, Ricchi P, Tambaro R, Daniele B, Sandomenico F, De Vivo R, Civiletti C, Izzo F, Pignata S, Ziviello M. Levovist-enhanced Doppler sonography versus spiral computed tomography to evaluate response to percutaneous ethanol injection in hepatocellular carcinoma. *J Clin Gastroenterol* 2000; **31:** 164-168

7 **Caselitz M**, Gebel M, Wagner S, Ockenga J, Lange P, Bleck JS, Ostertag H, Manns MP. Treatment of multilocular hepatocellular carcinoma (HCC) of 4.5 cm and 3.5 cm diameter using percutaneous ethanol injection in a patient with advanced liver cirrhosis. *Z Gastroenterol* 1999; **37**: 1175-1178

8 **Lin SM,** Lin DY, Lin CJ. Percutaneous ethanol injection therapy in 47 cirrhotic patients with hepatocellular carcinoma 5 cm or less: a long-term result. *Int J Clin Pract* 1999; **53:** 257-262

9 **Hasegawa S**, Yamasaki N, Hiwaki T, Sako K, Komorizono Y, Baba Y, Imamura Y, Kubozono O, Yoshida A, Arima T. Factors that predict intrahepatic recurrence of hepatocellular carcinoma in 81 patients initially treated by percutaneous ethanol injection. *Cancer* 1999; **86:** 1682-1690

10 **Lin LW,** He MY, Gao SD, Yu LY, Ye Z, Xue ES, Lin XD. Value of DNA analysis of ultrasound-guided fine-needle aspiration biopsy in assessment of therapeutic efficacy for hepatic carcinoma. *Zhongguo Chaosheng Yingxiangxue Zazhi* 2000; **10:** 538-541

11 **Ahrar K,** Gupta S. Hepatic artery embolization for hepatocellular carcinoma: technique, patient selection, and outcomes. *Surg Oncol Clin N Am* 2003; **12**: 105-126

12 **Livraghi T,** Lazzaroni S, Meloni F. Radiofrequency thermal ablation of hepatocellular carcinoma. *Eur J Ultrasound* 2001; **13:** 159-166

13 **Llovet JM,** Vilana R, Bru C, Bianchi L, Salmeron JM, Boix L, Ganau S, Sala M, Pages M, Ayuso C, Sole M, Rodes J, Bruix J. Increased risk of tumor seeding after percutaneous radiofrequency ablation for single hepatocellular carcinoma. *Hepatology* 2001; **33:** 1124-1129

14 **Crucinio N,** Palieri AP, Nacchiero MC, Cela EM, Muscatiello N, Sgarro C, Faleo D. Radiofrequency ablation: a new approach in the treatment of hepatocellular carcinoma. *G Chir* 2001; **22:** 89-92

15 **Cioni D,** Lencioni R, Bartolozzi C. Therapeutic effect of transcatheter arterial chemoembolization on hepatocellular carcinoma: evaluation with contrast-enhanced harmonic power Doppler ultrasound. *Eur Radiol* 2000; **10**: 1570-1575

16 **Levy I,** Verstandig A, Sasson T, Wolf D, Krichon I, Libson E, Levensart P, Papo O, Yurim O, Id A, Shouval D. Transarterial oil chemoembolization for hepatocellular carcinoma, in 100 cases. *Harefuah* 2000; **138:** 89-93

17 **Acunas B**, Rozanes I. Hepatocellular carcinoma: treatment with transcatheter arterial chemoembolization. *Eur J Radiol* 1999; **32:** 86-89

18 **Yamasaki T,** Kurokawa F, Shirahashi H, Kusano N, Hironaka K, Okita K. Percutaneous radiofrequency ablation therapy for patients with hepatocellular carcinoma during occlusion of hepatic blood flow. Comparison with standard percutaneous radiofrequency ablation therapy. *Cancer* 2002; **95:** 2353-2360

19 **Rui JA**, Wang SB, Chen SG, Zhou L. Right trisectionectomy for

primary liver cancer. *World J Gastroenterol* 2003; **9**: 706-709
20 **Lin LW,** Lin XY, He YM, Gao SD, Lin XD. Biological characteristics of HCC by ultrasound-guided aspiration biopsy and its clinical application. *World J Gastroenterol* 2003**; 9**: 941-945
21 **Lin LW,** Ye Z, Xue ES, Gao SD, He YM. A study of percutaneous hepatic quantified ethanol injection in treatment of hepatocarcinoma. *Zhongguo Chaosheng Yixue Zazhi* 2000; **16:** 514-516
22 **Torimura T,** Ueno T, Inuzuka S, Tanaka M, Abe H, Tanikawa K. Mechanism of fibrous capsule fromation surrounding hepatocellular carcinoma. Immunohistochemical study. *Arch Pathol Lab Med* 1991; **115:** 365-371
23 **Liao CS,** Yang KC, Yen MF, Teng LL, Duffy SW, Chen TH. Prognosis of small hepatocellular carcinoma treated by percutaneous ethanol injection and transcatheter arterial chemoembolization. *J Clin Epidemiol* 2002; **55:** 1095-1104
24 **Daniele B,** De Sio I, Izzo F, Capuano G, Andreana A, Mazzanti R, Aiello A, Vallone P, Fiore F, Gaeta GB, Perrone F, Pignata S, Gallo C. Hepatic resection and percutaneous ethanol injection as treatments of small hepatocellular carcinoma: a Cancer of the Liver Italian Program (CLIP 08) retrospective case-control study. *J Clin Gastroenterol* 2003; **36:** 63-67
25 **Chen X,** Luo P, Lin H, Shao P, Zhou Z, Fu L. Optimum mode of interventional treatment for hepatocellular carcinoma. *Zhonghua Zhongliu Zazhi* 2002; **24:** 501-503
26 **Kamada K**, Kitamoto M, Aikata H, Kawakami Y, Kono H, Imamura M, Nakanishi T, Chayama K. Combination of transcatheter arterial chemoembolization using cisplatin-lipiodol suspension and percutaneous ethanol injection for treatment of advanced small hepatocellular carcinoma. *Am J Surg* 2002; **184:** 284-290
27 **Kurokohchi K,** Watanabe S, Masaki T, Hosomi N, Funaki T, Arima K, Yoshida S, Miyauchi Y, Kuriyama S. Combined use of percutaneous ethanol injection and radiofrequency ablation for the effective treatment of hepatocelluar carcinoma. *Int J Oncol* 2002; **21:** 841-846
28 **Kurokohchi K,** Watanabe S, Masaki T, Hosomi N, Funaki T, Arima K, Yoshida S, Nakai S, Murota M, Miyauchi Y, Kuriyama S. Combination therapy of percutaneous ethanol injection and radiofrequency ablation against hepatocellular carcinomas difficult to treat. *Int J Oncol* 2002; **21:** 611-615
29 **Arata S,** Tanaka K, Okazaki H, Kondo M, Morimoto M, Saito S, Numata K, Nakamura S, Sekihara H. Risk factors for recurrence of large HCC in patients treated by combined TAE and PEI. *Hepatogastroenterology* 2001; **48:** 480-485
30 **Liu Y,** Wu M, Qian G, Zhang B, Chen H, Fu J, Huang C. Changes and significance of circulating hepatocellular carcinoma cells in recurrent hepatocellular carcinoma patients after combined treatment. *Zhonghua Ganzangbing Zazhi* 2001; **9**: 40-41
31 **Rust C,** Gores GJ. Locoregional management of hepatocellular carcinoma. Surgical and ablation therapies. *Clin Liver Dis* 2001; **5:** 161-173
32 **Puleo S,** Lombardo R, Li Destri G, Azzarello G, Rinzivillo C, Di Carlo I. Multimodal therapy of hepatocarcinoma: personal experience on 90 cases. *Hepatogastroenterology* 2000; **47:** 1379-1381
33 **Wu GX,** Lin YM, Zhou TH, Gao H, Pei G. Significant down-regulation of alpha-albumin in human hepatoma and its implication. *Cancer Lett* 2000; **160:** 229-236
34 **Allgaier HP,** Rossi S, Deibert P, Zuber I, Hering M, Blum HE. Hepatocellular carcinoma: percutaneous ethanol injection / transarterial chemoembolization / radiofrequency thermoablation. *Schweiz Rundsch Med Prax* 2000; **89:** 1056-1060
35 **Lin LW,** He YM, Gao SD, Yang FD, Ye Z, Xue ES, Yu LY, Lin XD. Value of ultrasound-guided fine-needle aspiration biopsy and ejection heavy needle biopsy in diagnosis and assessment of therapeutic effect for hepatic carcinoma. *Zhonghua Chaosheng Yingxiangxue Zazhi* 2001; **10**: 608-610
36 **Livraghi T,** Salmi A, Bolondi L, Marin G, Arienti V, Monti F, Vettori C. Small hepatocellular carcinoma: percutaneous alcohol injection-results in 23 patients. *Radiology* 1988; **168:** 313-317
37 **Li B**, Chen H, Wu MC, Guo XH. Chao sheng yin dao gan zang chuan ci liu nei zhu she wu shui jiu jing zhi liao gan ai. *Zhongguo Shiyong Waike Zazhi* 1996; **16**: 84-85
38 **Liu LM,** Xu ZZ, Wang WP, Ding H. Percutaneous ethanol injection therapy for liver carcinoma. *Linchuang Yixue Yingxiang Zazhi* 1997; **8**: 101-104
39 **Giorgio A,** Tarantino L, Mariniello N, de Stefano G, Perrotta A, Aloisio V, Voza A, Finizia L, Alaia A, Del Viscovo L. Percutaneous ethanol injection under general anesthesia for hepatocellular carcinoma: 3 year survival in 112 patients. *Eur J Ultrasound* 1998; **8:** 201-206
40 **Meloni F,** Lazzaroni S, Livraghi T. Percutaneous ethanol injection: single session treatment. *Eur J Ultrasound* 2001; **13:** 107-115
41 **Ohnishi K,** Ohyama N, Ito S, Fujiwara K. Small hepatocellular carcinoma: treatment with US-guided intratumoral injection of acetic acid. *Radiology* 1994; **193**: 747-752
42 **Ohnishi k,** Ohyama N, Ito S, Fujiwara K. Comparison of percutaneous acetic acid injection and percutanous ethanol injection for small hepatocellular carcinoma. *Hepatogastroenterology* 1998; **45**(Suppl 3): 1254-1258

Edited by Zhu LH and Wang XL **Proofread by** Xu FM

PO Box 2345, Beijing 100023, China
Fax: +86-10-85381893
E-mail: wjg@wjgnet.com www.wjgnet.com

World J Gastroenterol 2004;10(21):3118-3121
World Journal of Gastroenterology
 ISSN 1007-9327

• LIVER CANCER •

Multi-phasic CT arterial portography and CT hepatic arteriography improving the accuracy of liver cancer detection

Li Li, Li-Zhi Liu, Zhuan-Miao Xie, Yun-Xian Mo, Lie Zheng, Chao-Mei Ruan, Lin Chen, Pei-Hong Wu

Li Li, Li-Zhi Liu, Zhuan-Miao Xie, Yun-Xian Mo, Lie Zheng, Chao-Mei Ruan, Lin Chen, Pei-Hong Wu, Imaging Diagnosis & Interventional Center, Cancer Center, Sun Yat-sen University, 651 Dongfeng Road East, Guangzhou 510060, Guangdong Province, China
Correspondence to: Dr. Pei-Hong Wu, Imaging Diagnosis & Interventional Center, Cancer Center, Sun Yat-sen University, 651 Dongfeng Road East, Guangzhou 510060, Guangdong Province, China. wupeihong@yahoo.com
Telephone: +86-20-87343270 **Fax:** +86-20-87343392
Received: 2004-02-23 **Accepted:** 2004-04-13

Abstract

AIM: To evaluate the value of multi-phasic CT arterial portography (CTAP) and CT hepatic arteriography (CTHA) in differential diagnosis of liver diseases, and to improve the specificity of CTAP and CTHA for liver cancer detection.

METHODS: From January 1999 to December 2002, multi-phasic CTAP and CTHA were performed in 20 patients with suspected liver disease. CT scanning was begun 25 s, 60 s and 120 s for the early-, late- and delayed-phase CTAP examinations, and 6sec, 40 s and 120 s for the early-, late- and delayed-phase CTHA examinations respectively, after a transcatheter arterial injection of non-ionic contrast material. If a lesion was diagnosed as a liver cancer, transcatheter hepatic arterial chemoembolization (TACE) treatment was performed, and the follow-up CT was performed three or four weeks later.

RESULTS: All eighteen HCCs in 12 cases were shown as nodular enhancement on early-phasic CTHA. The density of the whole tumor decreased rapidly on late and delayed phases, and the edge of 12 tumors (12/18) remained relatively hyperdense compared with the surrounding liver tissue, and demonstrated as rim enhancement. All HCCs were shown as perfusion defect nodules on multi-phasic CTAP. Five tumors (5/18) were shown as rim enhancement on delayed-phasic CTAP. Rim enhancement was shown as 1 to 2-mm-wide irregular, uneven and discontinuous circumferential enhancement at late-, and delayed-phase of CTHA or CTAP. Five pseudolesions and 4 hemoangiomas were found in multi-phasic CTAP and CTHA. No pseudolesions and hemoangiomas were shown as rim enhancement on late- or delayed-phasic CTHA and CTAP.

CONCLUSION: Multi-phasic CTAP and CTHA could help to recognize the false-positive findings in CTAP and CTHA images, and improve the accuracy of CTAP and CTHA of liver cancer detection.

Li L, Liu LZ, Xie ZM, Mo YX, Zheng L, Ruan CM, Chen L, Wu PH. Multi-phasic CT arterial portography and CT hepatic arteriography improving the accuracy of liver cancer detection. *World J Gastroenterol* 2004; 10(21): 3118-3121
http://www.wjgnet.com/1007-9327/10/3118.asp

INTRODUCTION

CT arterial portography (CTAP) and CT hepatic arteriography (CTHA) are considered as the most sensitive imaging methods of detecting small liver cancers[1,2]. Micro liver cancer as small as 0.2 cm in diameter could be detected by CTAP and CTHA[3]. However, the prevalence of tumor-mimicking benign perfusion abnormalities decreases the specificity of these examinations and the accuracy of tumor detection[4,5]. In order to improve the specificity of CTAP and CTHA for liver cancer detection, multi-phasic helical CT arterial portography (CTAP) and multi-phasic helical CT hepatic arteriography (CTHA) are recommended[6-8]. From January 1999 to December 2002, multi-phasic CTAP and multi-phasic CTHA examinations were performed for more accurate evaluation in 20 patients with suspected liver malignancy.

MATERIALS AND METHODS

Materials

From January 1999 to December 2002, 20 patients (10 men, 5 women) with suspected liver diseases underwent multi-phasic CTAP and CTHA including 12 cases of hepatocellular carcinomas (HCCs), 3 of cavernous hemangiomas, and 5 of pseudolesions. They aged from 25 to 64 years (mean age, 42.5 years). The serum level of α-fetoprotein (AFP) was elevated in all patients with small HCC, ranged from 410 ng/mL to 2 540 ng/mL. Cirrhosis occurred in all 12 cases with HCC. Five patients with HCC were histologically proven by needle biopsy, and 7 were clinically diagnosed when tumors were demonstrated as lipiodol deposit foci on follow-up CT (lipiodol-CT, Lp-CT) images after transcatheter hepatic arterial chemoembolization (TACE), and the elevated AFP level returned to normal in all patients with HCC.

In this work, we decided a lesion was a pseudolesion when it was proved as normal hepatic tissue by needle liver biopsy, and did not change for at least 1 year. The diagnosis of a cavernous hemangioma was basic on typical findings on dynamic enhanced CT and MRI (very long T2) images, and when it did not enlarge for at least 1 year.

Methods

Multi-phasic CTAP examinations were performed with incremental scanning of liver in cranial-to-caudal direction with 2.7-mm to 5-mm collimation on an CT Twin Flash scanner (Philips Corp.). Data acquisition was started 25 s, 60 s and 120 s for the early-, late- and delayed-phase CTAP respectively, after a transcatheter superior mesenteric arterial injection of 40 mL of non-ionic contrast material at 3.0 mL/s, using an automatic power injector (Medrad, Pittsburgh). During the catheterization, contrast material administered before CT scanning was limited to 10 mL injected by hand to visualize aberrant vessels and to facilitate proper catheter placement.

Multi-phasic CTHA examinations were done 20 min after CTAP. Data acquisition was started 6 s, 40 s and 120 s for the early-, late- and delayed-phase CTHA respectively, after the initiation of a transcatheter common hepatic arterial injection of 15 mL of contrast material at 3.0 mL/s.

If serum AFP level exceeded 400 ng/mL, and a lesion was

highly suspected as an HCC on CTAP and CTHA images, TACE treatment was recommended to this patient, and plain CT scanning was performed 3 or 4 wk later (Lipiodol CT, Lp-CT).

RESULTS

The images of multi-phasic CTAP and CTHA in 20 cases were carefully interpreted by two experienced radiologist. On early-phasic CTHA, all eighteen HCCs were shown as nodular enhancement. The density of the whole tumor decreased rapidly and became hypodense or isodense compared with the surrounding liver tissue on late and delayed phases. However, the edge of tumors (12/18) remained relatively hyperdensity compared with the surrounding liver tissue, and demonstrated as rim enhancement. Rim enhancement was demonstrated as

Figure 1 Images of multi-phasic CTAP and CTHA. A: A nodular perfusion defect of HCC on CTAP image. B: A small round enhancement nodule of HCC on early-phasic CTHA image. C: Rim enhancement of HCC on delayed-phasic CTHA image obtained 2 min later.

Figure 2 HCC on early-phasic CTAP and late-phasic CTHA. A: HCC shown as a well-fined hypodense nodule on early-phasic CTAP image. B: HCC demonstrated as rim enhancement on late-phasic CTHA image. C: HCC demonstrated as irregular enhancement on CTHA image.

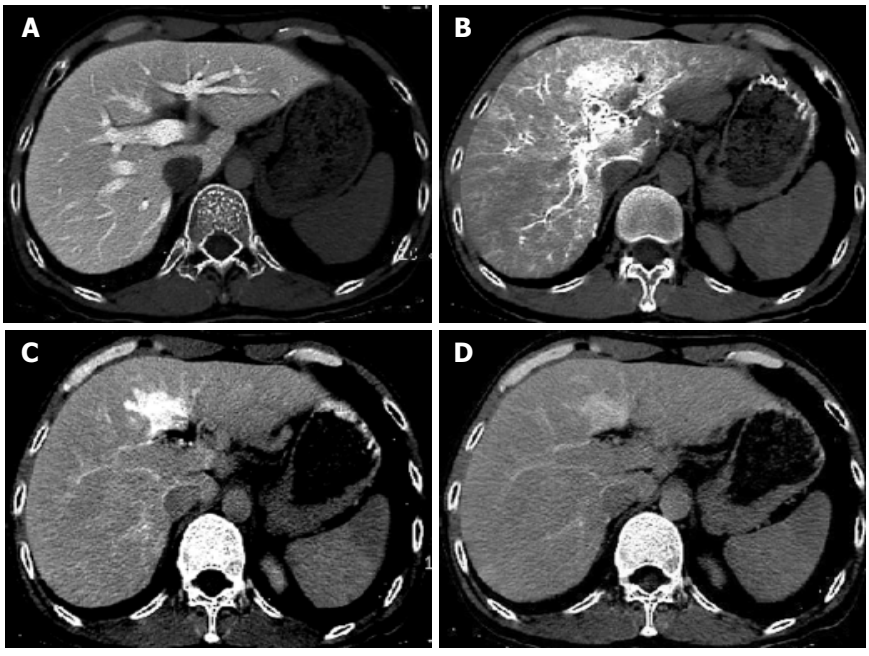

Figure 3 Pseudolesions on CTAP and CTHA. A: No lesion demonstrated on CTAP. B: Pseudolesion shown as an irregular enhancement focus on early-phasic CTHA. C: Change in shape and size of pseudolesion on late-phasic CTAP. D: Pseudolesion demonstrated as isodensity to liver tissue on delayed-CTHA.

Figure 4 Hemangiomas on CTAP and CTHA. A: A small hemangioma in segment II of left lobe as a perfusion defect nodule on CTAP. B: Lesion demonstrated as a punctulate, peripheral enhancement focus on early-phasic CTHA. C: Hemangioma demonstrated as hyperdensity to liver tissue on delayed-CTHA.

distinct 1 to 2-mm-wide circumferential enhancement at late-, and delayed-phase of multi-phasic CTHA (Figure 1). The shape of enhancement might be irregular, uneven and discontinuous.

All HCCs were shown as perfusion defect nodules on multi-phasic CTAP. The edge of five HCCs (5/18) became relatively hyperdense compared with the surrounding liver tissue and demonstrated as rim enhancement during delayed CT scanning (Figure 2).

Four of 5 pseudolesions were found in the segment IV of left lobe, and one in the segment VI of right lobe. All pseudolesions were shown as isodense or hypodense compared with the surrounding liver tissue on CTAP images. On CTHA images, pseudolesions were demonstrated as oval, wedge or irregular enhancement. The shape and size of pseudolesions were changed during delayed CT scanning. All pseudolesions gradually became isodense compared with the surrounding liver tissue on delayed phase. No pseudolesions were demonstrated as rim enhancement on late- or delayed-phasic CTHA and CTAP (Figure 3).

Four hemangiomas of 3 cases were shown as well-defined nodular perfusion defects on multi-phasic CTAP images. On early-phasic CTHA, hemangiomas were demonstrated as peripheral enhancement or nodular enhancement foci. On delayed CT scanning, all hemangiomas became isodense compared with the surrounding liver tissue. There was no hemangioma demonstrated as rim enhancement on late- or delayed-phasic CTHA and CTAP images in our study (Figure 4).

DISCUSSION

CTAP and CTHA have a high sensitivity for detection of liver diseases[3,9]. Especially, the use of helical CT technique has greatly improved the quality of images and accelerated the scanning[1]. However, the false-positive findings on CTAP and CTHA images have greatly limited its further clinical application[5,10]. Many methods were performed to improve the specificities of CTAP and CTHA for the detection of liver cancer, and combined CTHA and CTHA was recommended to interpret a malignant lesion[9]. Inoue *et al*.[8] and Matsuo *et al*.[6] performed combined CTAP and biphasic CTHA in the pre-operative detection of liver neoplasms. Their results suggested that late-phasic CTHA was useful in differentiating a malignant hepatic tumor from a pseudolesion. Ueda *et al*. performed single-level dynamic CTHA in differentiating hypervascular pseudolesion from hypervascular HCC. They found that the stain of pseudolesion on CTHA was transient and could be divided into three phases: (1) inflow of contrast material into the portal vein within the lesion, (2) lesion staining, and (3) fading out of the staining. However, the staining of HCC might have four phases: (1) inflow of contrast material into tumor, (2) tumor staining, (3) inflow of contrast material into adjacent liver, and (4) "coronal staining" of adjacent liver[7,11].

Rim enhancement was demonstrated as distinct 1 to 2-mm-wide irregular coronal or circumferential enhancement at late-, and delayed-phase of multi-phasic CTHA or CTAP[12,13]. According to our experience, the indistinct circumferential enhancement was only transiently demonstrated during multi-phase of CTHA and CTAP. Delayed CT scanning 120 s after a transcatheter arterial injection of material might increase the detection of rim enhancement of liver malignancy.

Inoue *et al*. reported that 84% of hepatocellular carcinomas and 73% of hepatic metastases showed rim enhancement on late-phase CTHA, and all non-tumourous perfusions on CTHA images did not show rim enhancement[8]. They concluded that biphasic CTHA was useful in differentiating hepatic malignancy from benign perfusion abnormalities. Similar findings were confirmed by Matsuo *et al*.[6] and Ueda *et al*.[7].

The reason why the malignant tumors showed delayed rim enhancement and pseudolesions did not at late-, or delayed-phase CTHA or CTAP is unclear[14,13]. Ueda *et al*.[7] suggested that rim enhancement in hepatocellular carcinoma was caused by inflow of contrast material from tumor into the adjacent liver. They studied the haemodynamics of hepatocellular carcinoma using single level dynamic CTHA, and demonstrated that arterial blood flowed into the tumor via the hepatic artery, filled the inner part of the tumor, penetrated the capsule, ran through the surrounding hepatic parenchyma and entered the portal branches. The haemodynamics can explain the change of homogeneous enhancement pattern on early-phasic CTHA to rim enhancement on late- or delayed-phasic CTHA. However, the contrast material inside pseudolesions faded out after lesion staining, just like liver tissue.

In our study, rim enhancement usually demonstrated on late-phasic CTHA images could be shown on late- and delayed-phase of CTAP in some cases. The reason of similar findings on CTAP might be that some HCCs could obtain blood supply from portal vein branches surrounding the tumor, especially, in the edge of tumor. This "double" blood supply usually occurred in liver tumors with less vascularity[15]. The border of tumor could be enhanced as a rim of relatively high density during late- and delayed-phase CTAP.

There is a controversy that rim enhancement originates from the normal hepatic tissue surrounding the tumor or from the border of tumor (such as capsule or pseudo-capsule of tumor). Irie *et al*. had performed an CT-pathologic study of metastatic liver tumors, and suggested that rim enhancement of tumor on delayed-phasic CTAP or CTHA images was perilesional enhancement, and it could mainly be caused by an increased supply of arterial flow, a draining of tumorous blood, or an increased interstitial space in the hepatic parenchyma due to fibrotic and desmoplastic changes[12]. However, Semelka *et al*. suggested that rim enhancement might be the enhancement of

histological tumor border that was defined as the histologically altered liver parenchyma surrounding the tumor, rather than the outer portion of the tumor[14].

To our knowledge, it is difficult to distinguish tumor border from perilesional area on CT images. During growth, the tumor infiltrates and compresses surrounding hepatic tissue. The capsule or false-capsule of tumor is formed and contains rich blood flow. It might be difficult to distinguish perilesional enhancement of normal tissue from circumferential enhancement of tumor border on CT and MR images. Rim enhancement demonstrated on late- or delayed-phasic CTHA and CTAP might not be confined to the tumor border because it could extend into the surrounding normal liver tissue.

One of the commonest pseudolesions on CTAP and CTHA images was seen in the liver adjacent to gallbladder or in dorsum of segment IV[4,16]. In our study, four of 5 pseudolesions were found in the left lobe, and one in segment VI of the right lobe. All five pseudolesions demonstrated as isodense lesions or perfusion defects on CTAP images. The shape of enhancement on early-phasic CTHA images might be oval, wedge or irregular. Pseudolesions were changed in shape and size on multi-phasic CTHA images, and gradually became isodense to normal on delayed phase. No pseudolesions were demonstrated as rim enhancement on late- or delayed-phasic CTHA.

Yamagami *et al*.[4] investigated the haemodynamics of pseudolesions using a biphasic CTHA examination, and suggested that pseudolesions on segment IV were caused by direct blood inflow from cholecystic vein to the liver parenchyma, and concluded that later phase CTHA could clearly differentiate pseudolesions from tumors.

Multi-phasic CTAP and CTHA were valuable for differentiating benign lesions from malignancy[10,17]. Hemangiomas were found on multi-phasic CTAP and CTHA images. Four hemangiomas of 3 cases were shown as well-defined perfusion defect nodules on CTAP images, and as nodular enhancement on early-phasic CTHA. On delayed CT scanning, all hemangiomas became isodense to the normal. No hemangioma was demonstrated as rim enhancement on late- or delayed-phasic CTHA images in our study. According to our experience, rim enhancement on multi-phasic CTHA could also be used as a characteristic finding to differentiate malignancy from benign lesions, such as hemangiomas.

In conclusion, multi-phasic CTAP and CTHA could raise the specificity for malignant hepatic tumor detection. Rim enhancement demonstrated on late- and delayed-phasic CTAP and CTHA images might help to differentiate a HCC from benign lesions.

REFERENCES

1 **Murakami T**, Oi H, Hori M, Kim T, Takahashi S, Tomoda K, Narumi Y, Nakamura H. Helical CT during arterial portography and hepatic arteriography for detecting hypervascular hepatocellular carcinoma. *Am J Roentgenol* 1997; **169**: 131-135

2 **Hori M**, Murakami T, Kim T, Takahashi S, Oi H, Tomoda K, Narumi Y, Nakamura H. Sensitivity of double-phase helical CT during arterial portography for detection of hypervascular hepatocellular carcinoma. *J Comput Assist Tomogr* 1998; **22**: 861-867

3 **Li L**, Wu PH, Mo YX, Lin HG, Zheng L, Li JQ, Lu LX, Ruan CM, Chen L. CT arterial portography and CT hepatic arteriography in detection of micro liver cancer. *World J Gastroenterol* 1999; **5**: 225-227

4 **Yamagami T**, Nakamura T, Kin Y, Nishimura T. Non-tumorous enhancement caused by cholecystic venous inflow shown on biphasic CT hepatic arteriography: comparison with hepatocellular carcinoma. *Br J Radiol* 2000; **73**: 1275-1281

5 **Li L**, Wu PH, Lin HG, Li JQ, Mo YX, Zheng L, Lu LX, Ruan CM, Chen L. Findings of non-pathologic perfusion defects by CT arterial portography and non-pathologic enhancement of CT hepatic arteriography. *World J Gastroenterol* 1998; **4**: 513-515

6 **Matsuo M**, Kanematsu M, Inaba Y, Matsueda K, Yamagami T, Kondo H, Arai Y, Hoshi H. Pre-operative detection of malignant hepatic tumours: value of combined helical CT during arterial portography and biphasic CT during hepatic arteriography. *Clin Radiol* 2001; **56**: 138-145

7 **Ueda K**, Matsui O, Kawamori Y, Nakanuma Y, Kadoya M, Yoshikawa J, Gabata T, Nonomura A, Takashima T. Hypervascular hepatocellular carcinoma: evaluation of hemodynamics with dynamic CT during hepatic arteriography. *Radiology* 1998; **206**: 161-166

8 **Inoue E**, Fujita M, Hosomi N, Sawai Y, Hashimoto T, Kuroda C, Nakano H, Sasaki Y, Ishiguro S. Double phase CT arteriography of the whole liver in the evaluation of hepatic tumors. *J Comput Assist Tomogr* 1998; **22**: 64-68

9 **Kim HC**, Kim TK, Sung KB, Yoon HK, Kim PN, Ha HK, Kim AY, Kim HJ, Lee MG. Preoperative evaluation of hepatocellular carcinoma: combined use of CT with arterial portography and hepatic arteriography. *Am J Roentgenol* 2003; **180**: 1593-1599

10 **Lim JH,** Kim EY, Lee WJ, Lim HK, Do YS, Choo IW, Park CK. Regenerative nodules in liver cirrhosis: findings at CT during arterial portography and CT hepatic arteriography with histopathologic correlation. *Radiology* 1999; **210**: 451-458

11 **Ueda K**, Matsui O, Kawamori Y, Kadoya M, Yoshikawa J, Gabata T, Nonomura A, Takashima T. Differentiation of hypervascular hepatic pseudolesions from hepatocellular carcinoma: value of single-level dynamic CT during hepatic arteriography. *J Comput Assist Tomogr* 1998; **22**: 703-708

12 **Irie T**, Tsushima Y, Terahata S, Hatsuse K, Kusano S. Rim enhancement in colorectal metastases at CT during infusion hepatic arteriography. Does it represent liver parenchyma or live tumor cell zone? *Acta Radiol* 1997; **38**: 416-421

13 **Terayama N**, Matsui O, Ueda K, Kobayashi S, Sanada J, Gabata T, Kawamori Y, Kadoya M. Peritumoral rim enhancement of liver metastasis: hemodynamics observed on single-level dynamic CT during hepatic arteriography and histopathologic correlation. *J Comput Assist Tomogr* 2002; **26**: 975-980

14 **Semelka RC**, Hussain SM, Marcos HB, Woosley JT. Perilesional enhancement of hepatic metastases: correlation between MR imaging and histopathologic findings-initial observations. *Radiology* 2000; **215**: 89-94

15 **Hayashi M**, Matsui O, Ueda K, Kawamori Y, Gabata T, Kadoya M. Progression to hypervascular hepatocellular carcinoma: correlation with intranodular blood supply evaluated with CT during intraarterial injection of contrast material. *Radiology* 2002; **225**: 143-149

16 **Yamagami T,** Takeuchi Y, Inaba Y, Matsueda K, Arai Y, Maeda T. Correlation of a defect of portal perfusion in the dorsal part of segment IV of the liver on CT arterial portography with inflow of the aberrant pancreaticoduodenal vein. *Br J Radiol* 1999; **72**: 552-555

17 **Onaya H**, Itai Y, Satake M, Luo T, Saida Y, Haruno M, Hasebe T, Moriyama N. Highly enhanced hepatic masses seen on CT during arterial portography: early hepatocellular carcinoma and adenomatous hyperplasia. *Jpn J Clin Oncol* 2000; **30**: 440-445

Edited by Zhu LH and Wang XL **Proofread by** Xu FM

PO Box 2345, Beijing 100023, China
Fax: +86-10-85381893
E-mail: wjg@wjgnet.com www.wjgnet.com

World J Gastroenterol 2004;10(21):3122-3126
World Journal of Gastroenterology
 ISSN 1007-9327

• COLORECTAL CANCER •

Induction of HSF1 expression is associated with sporadic colorectal cancer

Hui Cen, Shu Zheng, Yong-Ming Fang, Xiao-Ping Tang, Qi Dong

Cen Hui, Shu Zheng, Yong-Ming Fang, Qi Dong, Cancer Institute, The Second Affiliated Hospital of Medical School, Zhejiang University, Hangzhou 310009, Zhejiang Province, China
Hui Cen, Xiao-Ping Tang, Institute of Optic and Electronic Technologies, Chinese Academy of Sciences, Chengdu 610209, Sichuan Province, China
Supported by 100 Scholars Plan of Chinese Academy of Sciences
Correspondence to: Shu Zheng, Cancer Institute, The Second Affiliated Hospital of Medical School, Zhejiang University, Hanzhou 310009, Zhejiang Province, China. zhengshu@zju.edu.cn
Telephone: +86-571-87784501 **Fax:** +86-571-87214404
Received: 2003-06-21 **Accepted:** 2003-07-31

Abstract

AIM: To explore the activation of signal transduction pathways related with the carcinogenesis of sporadic colon cancers.

METHODS: A gene array monitoring the activation of 8 signal transduction pathways (PathwayFinder GEArray) was used to screen the differentially expressed genes between colorectal cancer and normal colon tissues. The differentially expressed genes were further analyzed by RT-PCR, using RNA derived from colorectal cancer and normal colon tissue of 35 patients.

RESULTS: The expression of HSF1, HSF27, HSP90 and iNOS was increased in colon cancer tissues compared to normal colon tissue using PathwayFinder GEArray. The RT-PCR results showed that the expression of HSF1 was increased in 86% (30/35) patients and the expression of iNOS was increased in 63% (22/35) patients.

CONCLUSION: The induction of HSF1 gene expression is associated with sporadic colon cancer. HSF1 induces heat shock stress signaling pathway, which might play a role in the carcinogenesis of sporadic colorectal cancer.

Cen H, Zheng S, Fang YM, Tang XP, Dong Q. Induction of HSF1 expression is associated with sporadic colorectal cancer. *World J Gastroenterol* 2004; 10(21): 3122-3126
http://www.wjgnet.com/1007-9327/10/3122.asp

INTRODUCTION

Colorectal cancer (CRC) is one of the most common cancers in China. The incidence of CRC has increased over the last years and the fourth or fifth most prevalent cancers in China. The incidence of CRC increases 3.7% in Chinese cities annually[1] while the five-year survival rate has not improved significantly. Early detection and treatment remain a major factor for good survival rate of CRC. Therefore, exploration of early diagnostic markers and the mechanism study on CRC oncogenesis are in imminent need for early diagnostic and better treatments. Recently, mutation of APC tumor suppressor gene has been found to be responsible for initiating neoplastic process of familial adenomatous polyposis (FAP)[2]. APC is a major regulator in the Wnt signal pathway that is activated due to APC mutation in FAP. The Wnt signal pathway is the oncogenic pathway for FAP. Although APC mutation was found in 60% sporadic CRC, Wnt signal pathway has not been proved to be an oncogenic pathway for sporadic CRC or any specific type of CRC. The oncogenic pathway for sporadic CRC remains to be determined.

Potter[3] has once summarized four signal pathways attributing to oncogenesis of hereditary CRC: APC-catenin-TCF-c-myc pathway (Wnt signal pathway) in FAP; microsatellite unstable pathway with mutation in hMLH1, hMSH2, hMSH6, hPMS1 or hPMS2 in HNPCC; p53 signal pathway with p53 mutation for CRC associated with chronic colon inflammation; estrogen receptor hypermethylation pathway for CRC associated with menopause. FAP and HNPCC are two hereditary CRCs. Other hereditary CRC also includes Peutz-Jeghers syndrome and juvenile polyposis whose genetic predisposition is currently under investigation. The hereditary CRCs makes up less than 1/3 of CRCs while more than 2/3 of CRCs are sporadic. Therefore, it is important to identify oncogenic pathways for sporadic CRC. As an open system, colon receives various chemical, physical and biological stimuli constantly. These stimuli vary among individuals according to their occupations, living environments and life styles. Some signal pathways that are activated by certain stimuli associated with particular occupations, environments and life styles may induce sporadic CRC. To explore the association between sporadic CRC and activation of signal pathways, we used PathwayFinder GEArray from SuperArray, a gene array capable of monitoring activation of 8 common signal transduction pathways to screen differential gene expression between colorectal cancer tissue and normal colon tissue. We found expressions of HSF1, HSF27, HSP90 and iNOS were increased in CRC tissue in comparison with normal colon tissue. RT-PCR was used for further confirmation. Our results suggest activation of heat shock stress signal pathway may attribute to oncogenesis of sporadic CRC.

MATERIALS AND METHODS

GEArray

PathwayFinder GEArray kit was obtained from SuperArray Bioscience Corp. (Frederick, MD, USA). It included reagents for probe generation and hybridization, and two identical gene arrays containing 23 marker genes for each array. The marker genes were used to the monitor the activation of their associated pathways. The induction of marker genes suggested the activation of their associated pathways. The marker genes were transcriptional target genes of their associated pathways. These 8 signal transduction pathways and their associated marker genes are listed bellow.

Signal transduction pathways	Marker genes
Mitogenic signaling pathway	*egr-1, c-fos*
Stress signaling pathway	*c-myc, ATF-2, c-fos, p53, hsf1, hsp90, hsp27*
NFκB signaling pathway	*iNOS, NFκB, iκB, c-myc*
NFAT signaling pathway	*IL-2, FasL, CD5*
Anti-proliferation/TGFβ signaling pathway	*p19, $p21^{waf1}$, $p57^{kip2}$*
Wnt signaling pathway	*c-myc*
P53 signaling pathway	*$p21^{waf1}$, pig7, pig8, mdm2, bax*
CREB signaling pathway	*cyp19, egr-1, c-fos*

Tissue and RNA preparation

Specimens of colorectal cancer and normal colon tissues were obtained from 36 patients (age: 32-89 years) at the Second Affiliated Hospital of Zhejiang University. The membranes of cancer and normal tissues of each patient were separated and placed into liquid nitrogen immediately after the removal of cancer mass from the patients. Total RNA was prepared from each specimen using Trizol kit from GIBCO (San Diego, CA, USA) to derive total RNA from cancer tissue and normal tissue. One pair of specimens from a patient (patient 1) was used to perform gene array analysis and the rest of 35 pairs of specimens were used for RT-PCR analysis.

Probe preparation

Anneal Five μg total RNA was used to mix with 2 μL buffer A containing gene specific primers GEAprimers (SuperArray, Frederick, MD, USA) and water to bring up a volume to 20 μL. The annealing of GEAprimers to RNA was achieved at 72 ℃ for 2 min at 42 ℃ for 2 min in water bath.

Reverse transcription for probe labeling A cocktail containing the following components was assembled in a 0.5 mL centrifuge tube containing 16 μL of 5× GEAlabeling buffer, buffer B (SuperArray, Frederick, MD, USA), 10 μL of [α-^{32}P]-dCTP (370 GBq/L), 2 μL of RNAse inhibitor, 4 μL of MMLV reverse transcriptase (50 MU/L), 8 μL of RNAse-free H_2O. The cocktail was placed in 42 ℃ water bath for 2 min followed by aliquoting 20 μL of the cocktail into the above primer annealed RNA from cancer tissue and 20 μL of the cocktail into above primer annealed RNA from normal tissue. After mixed, the mixture was placed in 42 ℃ water bath for 25 min for reverse transcription and labeling cDNA with α-^{32}P.

Labeling termination A 5 μLof 10× stop solution, buffer C (SuperArray, Frederick, MD, USA) was added to each reaction mixture to stop reverse transcription.

Probe denaturation: The labeled probe was placed in 94 ℃ heat block for 5 min, then immediately placed on ice until use.

Hybridization

Two PathwayFinder GEArrays were prehybridized with 10 mL GEAhyb solution (SuperArray, Frederick, MD, USA) for 2 h at 68 ℃. The denatured probes obtained from cancer and normal tissues of patient 1 were then added separately to two 5 mL GEAhyb solution preheated to 68 ℃. Each of the probe-containing GEAhyb solution was then used to hybridize with one PathwayFinder GEArray at 68 ℃ overnight. The GEArray was washed twice with 2×SSC, 10 g/L SDS for 20 min at 68 ℃ and twice with 0.1×SSC, 5 g/L SDS at 68 ℃. X-ray films were placed on GEArrays to capture array images at -70 ℃ overnight.

Density scan and analysis

The hybridization signals on the X-ray film were scanned by IS1000 system to obtain digital number for its density. The average signal was obtained from duplicates of each gene. The normalized value for each gene was calculated by the ratio of averaged value of each gene divided by the average value of β-actin or GAPDH.

RT-PCR

A 1 μg of total RNA obtained from each specimen was mixed with oligo $(dT)_{15}$ for reverse transcription using MMLV (Promega, Madison, WI, USA) to derive the first strand cDNA. A pair of gene specific PCR primers was designed for HSF1, iNOS, MDR1 and β-action genes. HSF1: CCATCCTGCGGGAGA GTG AA for 5'end of the gene and GGCTCCGAGCCTGTCAG CA for 3'end of the gene. iNOS: CACCATCCTGGTGGAACTCT for 5'end of the gene and TCTTGGGGCTTCAGGCT GTT for 3'end of the gene. MDR1: GCTCAAGTTAAAGGGGCTATA for 5'end of the gene and GCTCAAGTTAAAGGGGCTATA for 3' end of the gene. β-actin: GGCA TCCTCACCCTGAAGTA for 5' end of the gene and GTCCAGACGCAGGATGGCA for 3' end of the gene. PCR reaction was carried out at 95 ℃ for 3 min for denaturing followed multiple cycles at 95 ℃ for 15 s, at 56 ℃ for 10 s, at 72 ℃ for 45 s. For HSF1, iNOS and MDR1, the cycle number was 35 and for β-actin, the cycle number was 25. The PCR products were separated by electrophoresis and their quantity was determined by Kodak 1D image analysis software.

RESULTS

Identification of differential gene expression between cancer and normal colorectal tissues

Two identical PathwayFinder gene arrays from SuperArray (Frederick, MD, USA), each of which contained 23 marker genes monitoring the activation of 8 signal transduction pathways, were used to hybridize with labeled probes obtained from total RNA of cancer and normal colorectal tissues of a patient separately. The hybridized signal detected for each gene was normalized to the signal obtained for β-actin or GAPDH on the same gene array to derive gene expression value for each gene. After comparing gene expression value of each gene between two gene arrays, we found increased expressions of HSF1, HSF27, HSF90 genes of stress signaling pathway and iNOS gene of NFκB pathway in cancer tissue in comparison with normal tissue (Figure 1, Table 1).

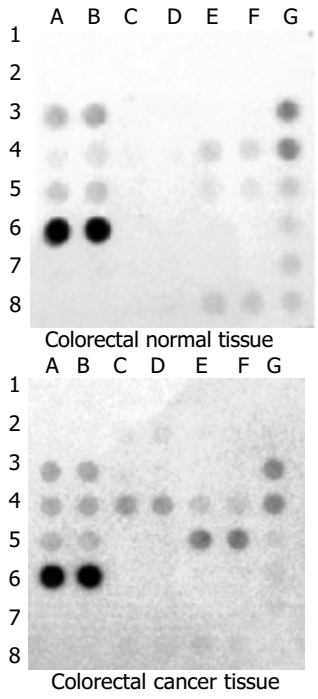

Figure 1 Comparison of hybridization results of gene arrays. Genes and their corresponding positions on gene arrays were as follows: ATF-2: 1A and 1B; Bax: 1C and 1D; CD5: 1E and 1F; c-fos: 2A and 2B; c-myc: 2C and 2D; Cypl9: 2E and 2F; egr-1: 3A and 3B; fas ligand: 3C and 3D; gadd45: 3E and 3F; hsp1: 4A and 4B; hsf27: 4C and 4D; hsp90: 4E and 4F; ikBa: 5A and 5B; Il-2 5C and 5D; iNOS: 5E and 5F; mdm2: 6A and 6B; NFκB: 6C and 6D; pl9: 6E and 6F; p21^{waf1}: 7A and 7B; p53: 7C and 7D; p57^{kip2}: 7E and 7F; Pig7: 8A and 8B; Pig8: 8C and 8D; β-actin: 3G and 4G; GAPDH: 5G, 6G, 7G, 8E, 8F and 8G; PUC18: 1G and 2G.

HSF1, HSF27 and HSP90 are marker genes for the stress signaling pathway. The induction of these genes in colorectal cancer tissue compared to its normal tissue indicated the activation of stress signaling pathway in cancer tissue. iNOS is a marker gene for NFκB signaling pathway and its activation suggested that NFκB might be activated. Since we did not detect

activation of other NFκB pathways associated marker genes, the induction of iNOS expression might be due to the activation of other signal pathways other than NFκB signal pathways.

Table 1 Analysis of scanned density on gene arrays

Gene	Ratio of cancer tissue *vs* normal tissue (β-actin)[1]	Ratio of cancer tissue *vs* normal tissue (GAPDH)[2]
Egr-1	1.16	0.94
Hsf1	1.43	1.17
i κB	1.23	1.00
Mdm2	0.98	0.80
Hsp27	1.58	1.28
Hsp90	1.31	1.06
iNOS	1.49	1.22

[1]Ratio of cancer tissue versus normal tissue (β-actin): "Ratio to β-actin" from cancer / "Ratio to β-actin"from normal tissue; [2]Ratio of cancer tissue versus normal tissue (GAPDH): "Ratio to GAPDH" from cancer / "Ratio to GAPDH"from normal tissue.

Table 2 Comparison of gene expression between normal and cancer tissue by RT-PCR

Patient	Dukes'	Ratio of cancer *vs* normal[1]		
		HSF1[2]	iNOS[2]	MDR1[2]
1	C	0.87	0.78	2.71
2	B	2.13	2.57	0.64
15	B	1.34	1.17	0.23
21	A	1.68	0.81	1.71
29	A	1.96	1.32	1.02
33	C	1.71	0.72	0.64
34	B	3.44	1.04	2.08
38	B	1.78	1.17	0.87
40	B	2.25	0.35	0.25
45	B	2.07	0.44	1.50
48	A	1.96	0.60	0.81
52	B	1.75	1.83	0.35
71	D	0.91	3.55	1.31
79	C	1.11	0.39	0.99
82	C	0.79	2.33	0.29
84	C	1.53	1.07	1.04
85	C	2.25	6.49	0.70
95	C	1.64	0.88	0.40
99	C	1.28	3.79	0.61
100	A	1.70	0.62	0.16
104	A	57.47	2.77	0.47
105	B	1.54	4.53	0.55
106	C	4.52	4.97	0.25
113	C	2.08	0.17	0.97
117	C	1.84	2.49	0.87
118	B	1.43	4.45	2.08
122	C	1.78	0.57	0.25
125	C	4.14	12.24	1.73
128	B	0.79	1.31	0.08
130	C	1.07	0.73	0.73
131	B	2.11	2.66	1.61
132	C	0.73	1.55	1.20
142	C	2.44	6.00	0.52
151	B	2.16	1.06	4.31
153	C	1.20	0.62	0.37

[1]Ratio of HSF1, iNOS or MDR1 to β-actin; [2][(HSF1, iNOS or MDR1) / β-actin, Cancer)] / [(HSF1, iNOS or MDR1) / β-actin, Normal)].

RT-PCR analysis for association of with sporadic colon cancer

A pair of gene specific PCR primers was designed for HSF1 and iNOS. RT-PCR was used to analyze the gene expression level of HSF1 and iNOS in both colon cancer and normal tissues of 35 patients. We confirmed increased HSF1 expression in 30 out of 35 patients in their cancer tissue in comparison to their normal tissue (Table 2). The average HSF1 expression value was 1.116±0.849 for normal tissue and 1.823±1.337 for cancer tissue. Using pair-wise *t* test analysis, the *t* value was 4.433 and *P* value was <0.001 (<0.05). Thus, it was statistically significant. The induction of HSF1 expression in tumor tissue was confirmed to be strongly associated with sporadic colorectal cancer. We also confirmed increased iNOS expression in 22 out of 35 patients in their cancer tissue in comparison to their normal tissue (Table 2). The average iNOS expression value was 0.867±0.761 for normal tissue and 1.133±0.843 for cancer tissue. Using pair-wise *t* test analysis, the *t* value was 1.803 and *P* value was 0.08 (>0.05). Thus, it was not statistically significant.

HSF1 was found to induce expression of MDR1. To explore whether HSF1 induction could increase expression of MDR1, we performed RT-PCR analysis on the same specimens from 35 patients. To our surprise, we found reduction of MDR1 expression in most (23/35) cancer tissues in comparison to normal tissues. The average MDR1 expression value was 1.099±0.885 for normal tissue and 1.443±1.096 for cancer tissue. Using pair-wise *t* test analysis, the *t* value was -2.329 and *P* value was 0.026 (<0.05). Thus, it was statistically significant.

Among sporadic CRCs from these 35 patients, 5 cases were at stage A, 12 at stage B, 17 at stage C and 1 at stage D. Five cases whose HSF1 expression did not increase in cancer tissue mainly belonged to late-stage patients (3 cases at stage C, 1 at stage D and 1 at stage B). However, statistical analysis could not be performed due to the limited number of cases.

DISCUSSION

Cellular signal transduction regulates almost all biological and physiological functions within cells. It is executed by a complex system where multiple signal transduction pathways interact together and are tightly controlled at different levels. The abnormality in cellular signal transduction can affect various cellular functions such as cell growth and proliferation, differentiation and metabolism and eventually lead to various diseases. Cancer is a typical disease resulting from abnormality in cellular signal transduction. Mutations of multiple genes in somatic cells are involved in the process of neoplastic formation. These mutations result in activation of oncogenes and inactivation of tumor suppressor genes, which lead to uncontrolled cell growth due to the loss of cellular differentiation and/or apoptosis ability. Further mutations in genes controlling cellular adherence and movement lead to tumor metastasis. Therefore, multiple signal transduction pathways in cell growth and proliferation, differentiation, apoptosis, adherence and movement are involved in initiation and progression of cancer.

There are four signal transduction pathways described by Potter[3,4] to be involved in the oncogenesis of hereditary CRC: APC-β-catenin-TCF-myc (Wnt) pathway[5], microsatellite unstable pathway[6], p53 pathway and estrogen receptor hypermethylation pathway. However, the signal transduction pathways involved in sporadic CRC remain unclear. APC mutation responsible for FAP's oncogenesis was also found in 60-70% sporadic CRCs[7, 8]. Similarly, microsatellite instability was found in over 30% sporadic CRCs[9] and p53 mutation was found in 50% sporadic CRCs[10]. In addition, non-steroidal anti-inflammatory drugs (NSAIDs) were found to efficiently suppress tumorigenesis of CRC by inhibiting Cox-2 activity[11-14]. It indicates Cox-2 pathway is involved in CRC oncogenesis as well. These results suggest multiple signal pathways are involved in the oncogenesis of

sporadic CRC. To efficiently identify signal pathways involved in sporadic CRC, we employed PathwayFinder gene arrays that utilize pathway target genes to monitor the activation of 8 important pathways related to cell growth, proliferation, survival, stress, apoptosis and inflammation. Monitoring induction of target genes by PT-PCR was found to be an effective way to identify the activation of Wnt signal pathway in adenomas of FAP compared to matched normal mucosa[15,16]. The utilization of gene array to identify induction of target genes greatly increased its efficiency.

We found HSF1 gene expression was significantly increased (30/35) in cancer tissue compared to its normal tissue in 35 patients. HSF1 stands for heat shock transcription factor 1 and is a transcription factor with a molecular weight of 82KD. HSF1 could be induced by heat, chemicals and hypoxia[17-19] and usually exists as a monomer in the cytoplasm. After heat stimulation, it became a trimer and could be translocated into nucleus[20]. Its transcriptional activity was greatly increased by the phosphorylation of serine induced by stimuli. HSF1 could activate transcription of its target genes by binding to a heat shock element[7]. The heat shock element was present in the promoter region of many genes such as HSP90, HSP27, HSP70 and drug resistant gene MDR1[21]. Hoang[22] recently reported HSF1 expression was increased in a prostate cancer cell line. Our study not only provided the first evidence to demonstrate the association of HSF1 gene expression and CRC, but also suggested that the induction of HSF1 gene expression might be associated with a broad range of cancer. The reduced HSF1 expression in the remaining 5 cancer tissues might be due to different oncogenic mechanisms occurring in these CRCs from HSF1 induction related sporadic CRCs.

In this study, the induction of HSF1 gene expression was accompanied with the induction of HSP27 and HSP90 which were two target genes of HSF1, suggesting that the induction of HSF1 gene expression could activate HSF1 heat shock stress signal pathway in sporadic CRC. Heat shock stress signal pathway is highly involved in carcinogenesis since heat shock proteins (HSP90, HSP70, *etc*.) are responsible for maintaining the conformation, stability and function of key oncogenic client proteins involved in signal transduction pathways leading to proliferation, cell cycle progression and apoptosis, as well as other features of the malignant phenotype such as invasion, angiogenesis and metastasis[23-26]. HSP90 has currently served as an anti-cancer drug target for various drug development[27-29]. Also, HSP70 was found to inhibit apoptosis[30]. Our result suggested heat shock stress pathway contributed to carcinogenesis actively instead of passively as a bystander. Our hypothesis of heat shock stress pathway contributing to carcinogenesis of sporadic CRCs coincides with the fact that colon is an open system where it could retain and receive various kinds of "stress" substances for a long period of time. The "stress" substances might come from meat, alcohol, inflammatory tissue and others[31]. The prolonged exposure of these "stress" substances could lead to activation of heat shock stress pathway, thus leading to carcinogenesis through enhancing function of oncogenic proteins occurring in cells. The heat shock stress pathway could be further activated by hypoxia occurring in the tumor which was found to increase HSF1 expression as well[18,19]. Vegetables, nonsteroidal anti-inflammatory drugs (NSAIDs), hormone replacement therapy, and physical activity[31] could reverse the activation of heat shock stress pathway and therefore suppress carcinogenesis.

Hoang *et al*.[22] found HSF1 expression was increased in a prostate cancer cell line PC-3 derived PC-3M clone with metastatic ability compared to its parent cell line. By Western-blot and immunohistochemistry analysis of 18 prostate cancer and 4 normal prostate tissues, they confirmed the induction of HSF1 expression in prostate cancer tissues. However, since Western-blot and immunohisto- chemistry analyses detect protein expression instead of gene expression, it remains to be confirmed that the induction of HSF1 is at gene expression level. Our gene array analysis and RT-PCR directly measured mRNA level. We clearly demonstrated the induction of HSF1 was on the gene expression level and its strong association with sporadic CRCs. Nevertheless, in our study, each cancer tissue was paired with its matched normal tissue from the same patient for comparison of gene expression eliminating differential gene expression caused by individual genetic background.

PathwayFinder gene array from SuperArray provided two spots for each gene. The variation between the two spots was below 5%. According to Table 1, if β-actin expression level was used for normalization, genes whose expression was increased in cancer tissue included HSP27 (1.58 fold), iNOS (1.49 fold), HSF1 (1.43 fold), HSP90 (1.31 fold), iκB (1.25 fold), egr-1 (1.16 fold). However, if GAPDH expression level was used for normalization, genes whose expression was increased in cancer tissue only include HSP27 (1.28 fold), iNOS (1.22 fold), HSF1 (1.17 fold), HSP90 (1.06 fold). Therefore, it is important to use multiple housekeeping genes for normalization since expression of house keeping genes such as β-actin and GAPDH may fluctuate sometimes.

Vilaboa[31] found HSF1 could bind to the promoter region of MDR1 to increase its expression transcriptionally. However, MDR1 was also a target gene for Wnt signal pathway and the expression of MDR1 was increased in precancerous lesion of FAP patients[32]. We found reduced MDR1 gene expression in most (23/35) cancer tissues. Our result suggested MDR1 gene expression was not regulated under heat shock stress signal pathway in colon tissue, more likely under Wnt signal pathway. The reverse association of MDR1 expression with HSF1 and β-catenin (Wnt pathway) indicated that different signal pathways contributed to the carcinogenesis of FAP and sporadic CRC. The reduced MDR1 gene expression was also found in other cancers such as kidney cancer[33] and brain cancer[34].

Recently, a large number of studies have revealed the association of iNOS expression with various cancers[35-39]. Yagihashi[40] studied 22 cases of colorectal cancer tissues by immunohistochemistry and RT-PCR and found increased iNOS expression was associated with colorectal cancer. Bing *et al*.[37] found increased expression of iNOS and production of prostanoids in colorectal cancer paralleled to the increase in COX-2, confirming the importance of this emzyme in colon cancer. Ropponen[39] found iNOS expression in colorectal cancer might be used as a prognosis marker as well. Our study also confirmed induced iNOS expression in 22 out of 35 cancer tissues, indicating that the biological significance of MDR1 and iNOS expression in CRC needs to be further studied.

REFERENCES

1 **Li LD**, Rao KQ, Zhang SW, Lu FZ, Zhou XN. Statistical analysis of data from l2 cancer registries in China, 1993-1997. *Zhongguo Zhongliu* 2002; **11**: 497-507

2 **Fearnhead NS**, Britton MP, Bodmer WF. The ABC of APC. *Hum Mol Genet* 2001; **10**: 721-733

3 **Potter JD**. Colorectal cancer: molecules and populations. *J Natl Cancer Inst* 1999; **91**: 916-932

4 **Tejpar S**, Cassiman JJ, Van Cutsem E. The molecular basis of colorectal cancer. *Acta Gastroenterol Belg* 2001; **64**: 249-254

5 **Wang HL**, Wang J, Xiao SY, Haydon R, Stoiber D, He TC, Bissonnette M, Hart J. Elevated protein expression of cyclin D1 and Fra-1 but decreased expression of c-Myc in human colorectal adenocarcinomas overexpressing beta-catenin. *Int J Cancer* 2002; **101**: 301-310

6 **Wijnen J**, de Leeuw W, Vasen H, van der Klift H, Moller P, Stormorken A, Meijers-Heijboer H, Lindhout D, Menko F, Vossen S, Moslein G, Tops C, Brocker-Vriends A, Wu Y, Hofstra R, Sijmons R, Cornelisse C, Morreau H, Fodde R. Familial en-

dometrial cancer in female carriers of MSH6 germline mutations. *Nat Genet* 1999; **23**: 142-144
7 **Chung DC**. The genetic basis of colorectal cancer: insights into critical pathways of tumorigenesis. *Gastroenterology* 2000; **119**: 854-865
8 **Bright-Thomas RM**, Hargest R. APC, beta-Catenin and hTCF-4; an unholy trinity in the genesis of colorectal cancer. *Eur J Surg Oncol* 2003; **29**: 107-117
9 **Goel A**, Arnold CN, Niedzwiecki D, Chang DK, Ricciardiello L, Carethers JM, Dowell JM, Wasserman L, Compton C, Mayer RJ, Bertagnolli MM, Boland CR. Characterization of sporadic colon cancer by patterns of genomic instability. *Cancer Res* 2003; **63**: 1608-1614
10 **Goh HS**, Elnatan J, Low CH, Smith DR. p53 point mutation and survival in colorectal cancer patients: effect of disease dissemination and tumour location. *Int J Oncol* 1999; **15**: 491-498
11 **Hasegawa K**, Ichikawa W, Fujita T, Ohno R, Okusa T, Yoshinaga K, Sugihara K. Expression of cyclooxygenase-2 (COX-2) mRNA in human colorectal adenomas. *Eur J Cancer* 2001; **37**: 1469-1474
12 **Ricchi P**, Zarrilli R, Di Palma A, Acquaviva AM. Nonsteroidal anti-inflammatory drugs in colorectal cancer: from prevention to therapy. *Br J Cancer* 2003; **88**: 803-807
13 **Nasir A**, Fernandez PM, Chughtai OR, Kaiser HE. COX-2, NSAIDs and human neoplasia. Part I: Colorectal neoplasms. *In Vivo* 2002; **16**: 501-509
14 **Reddy BS**, Rao CV. Novel approaches for colon cancer prevention by cyclooxygenase-2 inhibitors. *J Environ Pathol Toxicol Oncol* 2002; **21**: 155-164
15 **D'Orazio D**, Muller PY, Heinimann K, Albrecht C, Bendik I, Herzog U, Tondelli P, Bauerfeind P, Muller H, Dobbie Z. Overexpression of Wnt target genes in adenomas of familial adenomatous polyposis patients. *Anticancer Res* 2002; **22**: 3409-3414
16 **Kolligs FT**, Bommer G, Goke B. Wnt/beta-catenin/tcf signaling: a critical pathway in gastrointestinal tumorigenesis. *Digestion* 2002; **66**: 131-144
17 **Wu C**. Heat shock transcription factors: structure and regulation. *Annu Rev Cell Dev Biol* 1995; **11**: 441-469
18 **Eickelberg O**, Seebach F, Riordan M, Thulin G, Mann A, Reidy KH, Van Why SK, Kashgarian M, Siegel N. Functional activation of heat shock factor and hypoxia-inducible factor in the kidney. *J Am Soc Nephrol* 2002; **13**: 2094-2101
19 **Baek SH**, Lee UY, Park EM, Han MY, Lee YS, Park YM. Role of protein kinase Cdelta in transmitting hypoxia signal to HSF and HIF-1. *J Cell Physiol* 2001; **188**: 223-235
20 **Newton EM**, Knauf U, Green M, Kingston RE. The regulatory domain of human heat shock factor 1 is sufficient to sense heat stress. *Mol Cell Biol* 1996; **16**: 839-846
21 **Cotto JJ**, Kline M, Morimoto RI. Activation of heat shock factor 1 DNA binding precedes stress-induced serine phosphorylation. Evidence for a multistep pathway of regulation. *J Biol Chem* 1996; **271**: 3355-3358
22 **Hoang AT**, Huang J, Rudra-Ganguly N, Zheng J, Powell WC, Rabindran SK, Wu C, Roy-Burman P. A novel association between the human heat shock transcription factor 1 (HSF1) and prostate adenocarcinoma. *Am J Pathol* 2000; **156**: 857-864
23 **Ochel HJ**, Gademann G. Heat-shock protein 90: potential involvement in the pathogenesis of malignancy and pharmacological intervention. *Onkologie* 2002; **25**: 466-473
24 **Blagosklonny MV**. Hsp-90-associated oncoproteins: multiple targets of geldanamycin and its analogs. *Leukemia* 2002; **16**: 455-462
25 **Witkin SS**. Heat shock protein expression and immunity: relevance to gynecologic oncology. *Eur J Gynaecol Oncol* 2001; **22**: 249-256
26 **Sarto C**, Binz PA, Mocarelli P. Heat shock proteins in human cancer. *Electrophoresis* 2000; **21**: 1218-1226
27 **Neckers L**. Hsp90 inhibitors as novel cancer chemotherapeutic agents. *Trends Mol Med* 2002; **8**(4 Suppl): S55-61
28 **Manjili MH**, Wang XY, Park J, Facciponte JG, Repasky EA, Subjeck JR. Immunotherapy of cancer using heat shock proteins. *Front Biosci* 2002; **7**: d43-52
29 **Maloney A**, Workman P. HSP90 as a new therapeutic target for cancer therapy: the story unfolds. *Expert Opin Biol Ther* 2002; **2**: 3-24
30 **Beere HM**, Green DR. Stress management - heat shock protein-70 and the regulation of apoptosis. *Trends Cell Biol* 2001; **11**: 6-10
31 **Vilaboa NE**, Galan A, Troyano A, de Blas E, Aller P. Regulation of multidrug resistance 1 (MDR1)/P-glycoprotein gene expression and activity by heat-shock transcription factor 1 (HSF1). *J Biol Chem* 2000; **275**: 24970-24976
32 **Yamada T**, Takaoka AS, Naishiro Y, Hayashi R, Maruyama K, Maesawa C, Ochiai A, Hirohashi S. Transactivation of the multidrug resistance 1 gene by T-cell factor 4/beta-catenin complex in early colorectal carcinogenesis. *Cancer Res* 2000; **60**: 4761-4766
33 **Yan C**, Luo B, Chen WG. Expression of multidrug resistance genes and multidrug resistance-associated protein genes in renal cell carcinomas. *Qingdao Daxue Yixueyuan Xuebao* 2001; **37**: 103-105
34 **Demeule M**, Shedid D, Beaulieu E, Del Maestro RF, Moghrabi A, Ghosn PB, Moumdjian R, Berthelet F, Beliveau R. Expression of multidrug-resistance P-glycoprotein (MDR1) in human brain tumors. *Int J Cancer* 2001; **93**: 62-66
35 **Zhang SZ**, Peng JP, Ye F, Zheng S. Expression of inducible nitric oxide synthase in breast cancer and its relation to carcinoargiogenesis. *Zhongguo Aizheng Zazhi* 2001; **20**: 762-765
36 **Wolf H**, Haeckel C, Roessner A. Inducible nitric oxide synthase expression in human urinary bladder cancer. *Virchows Arch* 2000; **437**: 662-666
37 **Bing RJ**, Miyataka M, Rich KA, Hanson N, Wang X, Slosser HD, Shi SR. Nitric oxide, prostanoids, cyclooxygenase, and angiogenesis in colon and breast cancer. *Clin Cancer Res* 2001; **7**: 3385-3392
38 **Brandao MM**, Soares E, Salles TS, Saad ST. Expression of inducible nitric oxide synthase is increased in acute myeloid leukaemia. *Acta Haematol* 2001; **106**: 95-99
39 **Ropponen KM**, Kellokoski JK, Lipponen PK, Eskelinen MJ, Alanne L, Alhava EM, Kosma VM. Expression of inducible nitric oxide synthase in colorectal cancer and its association with prognosis. *Scand J Gastroenterol* 2000; **35**: 1204-1211
40 **Yagihashi N**, Kasajima H, Sugai S, Matsumoto K, Ebina Y, Morita T, Murakami T, Yagihashi S. Increased in situ expression of nitric oxide synthase in human colorectal cancer. *Virchows Arch* 2000; **436**: 109-114

Edited by Wang XL **Proofread by** Xu FM

PO Box 2345, Beijing 100023, China
Fax: +86-10-85381893
E-mail: wjg@wjgnet.com www.wjgnet.com

World J Gastroenterol 2004;10(21):3127-3131
World Journal of Gastroenterology
 ISSN 1007-9327

• COLORECTAL CANCER •

An integrated approach to the detection of colorectal cancer utilizing proteomics and bioinformatics

Jie-Kai Yu, Yi-Ding Chen, Shu Zheng

Jie-Kai Yu, Cancer Institute, the Second Affiliated Hospital of Zhejiang University Medical College, Hangzhou 310009, Zhejiang Province, China
Jie-Kai Yu, College of Life Science of Zhejiang University, Hangzhou 310029, Zhejiang Province, China
Jie-Kai Yu, Hangzhou Genomics Institute, Hangzhou 310008, Zhejiang Province, China
Yi-Ding Chen, Department of Oncology, the Second Affiliated Hospital of Zhejiang University Medical College, Hangzhou 310009, Zhejiang Province, China
Shu Zheng, Cancer Institute, Zhejiang University, Hangzhou 310009, Zhejiang Province, China
Supported by the Major State Basic Research Development Program of China 973 program, No. G1998051200
Correspondence to: Shu Zheng, Cancer Institute, Zhejiang University, Hangzhou 310009, Zhejiang Province, China. zhengshu@mail.hz.zj.cn
Telephone: +86-571-87783868 **Fax:** +86-571-87214404
Received: 2004-04-09 **Accepted:** 2004-05-09

Abstract

AIM: To find new potential biomarkers and to establish patterns for early detection of colorectal cancer.

METHODS: One hundred and eighty-two serum samples including 55 from colorectal cancer (CRC) patients, 35 from colorectal adenoma (CRA) patients and 92 from healthy persons (HP) were detected by surface-enhanced laser desorption/ionization mass spectrometry (SELDI-MS). The data of spectra were analyzed by bioinformatics tools like artificial neural network (ANN) and support vector machine (SVM).

RESULTS: The diagnostic pattern combined with 7 potential biomarkers could differentiate CRC patients from CRA patients with a specificity of 83%, sensitivity of 89% and positive predictive value of 89%. The diagnostic pattern combined with 4 potential biomarkers could differentiate CRC patients from HP with a specificity of 92%, sensitivity of 89% and positive predictive value of 86%.

CONCLUSION: The combination of SELDI with bioinformatics tools could help find new biomarkers and establish patterns with high sensitivity and specificity for the detection of CRC.

Yu JK, Chen YD, Zheng S. An integrated approach to the detection of colorectal cancer utilizing proteomics and bioinformatics. *World J Gastroenterol* 2004; 10(21): 3127-3131
http://www.wjgnet.com/1007-9327/10/3127.asp

INTRODUCTION

Colorectal cancer (CRC) is one of the most common malignant tumors that threaten people's health[1-5]. At present, CRC is one of the three leading causes of worldwide cancer mortality and the second leading cause of cancer-related deaths in the Western world[6,7]. The prognosis of CRC is strongly related to early diagnosis. CRC patients diagnosed in early stage have a five-year survival post-operation of over 80%, but in the advanced stage the five-year survival is lower than 40%. So, early diagnosis is very important to improve the prognosis of CRC[8].

Recently serum tumor markers, such as carcinoembryonic antigen (CEA), are commonly used to detect CRC for the advantages of less pain and accessibility. However all the existing biomarkers have a low diagnostic sensitivity in CRC (sensitivity of 23% with CEA[9]). New biomarkers with a high sensitivity and specificity to detect CRC in early stage are urgently needed. A novel proteomic approach for the detection of cancer which is called surface enhanced laser desorption/ionization time-of-flight mass spectrometry (SELDI-TOF MS), and ProteinChip technology, have been developed. SELDI-TOF MS coupled with bioinformatics approach has successfully found new biomarkers and achieved high sensitivity and specificity for the diagnosis of cancers of bladder[10], prostate[11-14], ovary[15,16], breast[17,18], liver[19], neck[20], lung[21,22] , pancreas[23].

The aim of this study was to find the potential biomarkers in CRC and to establish the patterns to diagnose CRC.

MATERIALS AND METHODS

Samples

A total of 182 serum samples were obtained from the serum banks of the Cancer Institute of the Second Affiliated Hospital of Zhejiang University Medical College. The cancer group consisted of 55 serum samples from CRC patients at different clinical stages: Dukes' A (n = 8), Dukes' B (n = 22), Dukes' C (n = 13), Dukes' D (n = 12). The median age of CRC patients was 57 years (range, 31-84 years). The two non-cancer control groups included 35 serum samples from patients with colorectal adenoma (CRA) and 92 serum samples from healthy persons (HP). They were age and sex matched with cancer group. Diagnoses were pathologically confirmed, and specimens were obtained before treatment. All samples were stored at -80 ℃.

Proteinchip array analysis

Serum samples were thawed in ice and centrifuged at 3 000 r/m for 5 min at 4 ℃, supernatants were retained. We added 90 μL of 5 g/L CHAPS (Sigma) (pH 7.4) in PBS to 10 μL of each serum sample, and vortex-mixed them. The diluted samples were added to 100 μL Cibacron Blue 3GA (Sigma) (previously equilibrated with 5 g/L CHAPS three times) in a 96-well cell culture plate and agitated on a platform shaker at 4 ℃ for 60 min. After centrifuged at 1 000 r/m, 50 μL supernatant was sampled and further diluted by 150 μL 20 mmol/L HEPES (pH 7.4) and applied to each well of a bioprocessor (Ciphergen Biosystems) containing hydrophobic surface (H4) chips previously activated with 20 mmol/L HEPES. The bioprocessor was then sealed and agitated on a platform shaker for 60 min at 4 ℃. The excess serum mixtures were discarded, and the chips were washed three times with 20 mmol/L HEPES and 2 times with deionized water. The chips were then removed from the bioprocessor, air-dried. Before SELDI analysis, 0.5 μL of a saturated solution of α-cyano-4-hydroxycinnamic acid (CHCA) in 0.5 L/L acetonitrile and 5 mL/L trifluoroacetic acid was applied onto each chip twice, air-dried.

Chips were detected on the protein biological system II

(PBS-II) plus a mass spectrometer reader (Ciphergen Biosystems). Data were collected by averaging 65 laser shots with an intensity of 135, a detector sensitivity of 7, a highest mass of 30 000 Da and an optimized range of 2 000-20 000 Da. Mass accuracy was calibrated to less than 0.1% using the all-in-one peptide molecular mass standard (Ciphergen Biosystems).

Bioinformatics analysis

The spectra intensities of all samples were normalized to the total ion current of m/z between 2 000 and 30 000 Da. The noise of spectra was filtrated and peaks were detected with an automatic peak detection pass using signal-to-noise ratio. Peak clusters were completed to cluster the peaks in different samples that had similar masses (defined by a mass window in 0.3% mass error). All these were performed using ProteinChip Software 3.1 (Ciphergen). The peak intensities were preprocessed by scaling all the data to the range[-1, 1].

The pattern recognition techniques were applied to diverse areas including prediction of cancer[24], gene microarray[25] and mass spectrometry[26]. We utilized a multi-layer perception (MLP) ANN with a scaled conjugate gradient (SCG) optimized back propagation algorithm for discriminating CRC from HP, and a linear support vector machine (SVM) for discriminating CRC from CRA. They were powerful tools for analysis of the complex data[14] derived from SELDI-MS.

Feature selection

We estimated the power of each peak in discriminating different group samples by integrating approaches such as *t*-test, receive option curve (ROC) and mean square error (MSE) of ANN.

The ANN used to calculate the MSE of each peak had 3 layers, with 1 node in input and output layer, 2 nodes in hidden. For each peak the ANN was trained with all the samples, performed 1 000 epochs to get the MSE respectively. The MSE was calculated as the difference between the target output and the ANN predictive value. The lower MSE value of the peak showed a higher relative importance value for their ability to accurately discriminate the different groups.

Integrated ANN classifier

The ANN established for discriminating different groups had 4 layers. Except output layer and input layer ANN also had 2 hidden layers each with 100 nodes. We randomly selected 1/3 of all the samples to be the blinded test set, and the remaining 2/3 samples for training, the procedure was repeated 10 times.

In the procedure of training ANN we used a cross-validation approach to reduce the risk of "over fit"[27]. The samples for training were randomly divided into 2 sets: 2/3 samples for training set and 1/3 samples for validation set. The random shuffling was redone 100 times. Thus 100 different ANNs were established to predict the blinded test set samples. The predictive values of the blinded test set samples were the average of all the predicted outputs of 100 ANNs.

SVM classifier

SVM is a new machine learning approach originally proposed and developed by Vladimir Vapnik. SVM applications were actively pursued in various areas recently, from genomics to face recognition[28,29]. SVM is powerful for small sample data. We used the linear SVM classifier and set the cost of the constrain violation (C) to 1. The 3-fold cross-validation approach was applied to estimate the accuracy of the classifier.

RESULTS

Bioinformatics analysis of CRC and HP data

After noise was filtrated by Ciphergen ProteinChip Software 3.1, there were 61 peaks detected for discriminating CRC from HP and 235 peaks for discriminating CRC from CRA. The peaks were between 2 k and 30 kDa. Peaks with an m/z <2 kDa were mainly ion noise from the matrix and therefore excluded[10].

The 61 qualified peaks detected from the two groups were ranked by the MSE values of ANN. We input the 61 peaks respectively. For each peak we trained the ANN with all the 147 healthy and CRC samples to give an MSE value. The top 15 peaks with lower MSE values were selected for further analysis (Figure 1). The *t*-test and ROC method confirmed the results with the same 15 peaks.

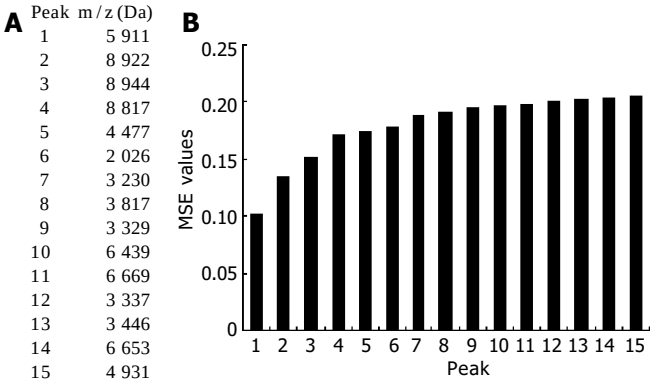

Figure 1 MSE values of the top 15 peaks. A: m/z of peaks. B: MSE values of peaks.

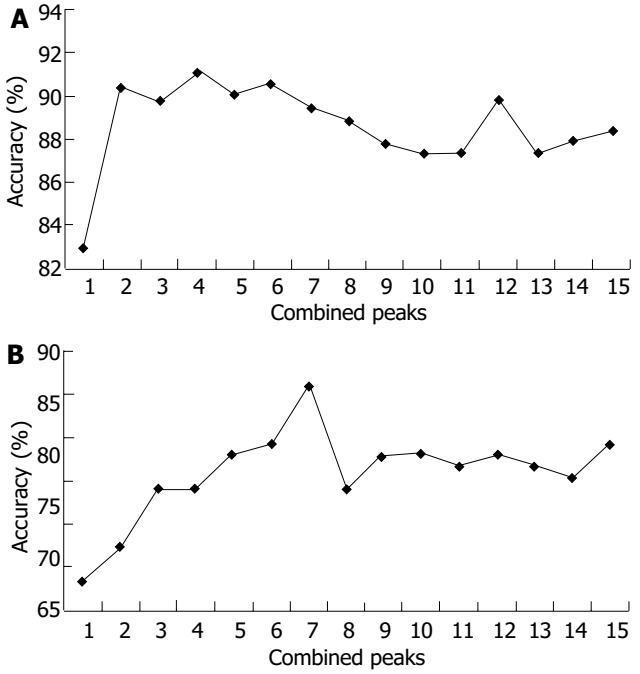

Figure 2 Accuracies of different combinations of peaks. A: Accuracies of different combinations of peaks in the pattern discriminating CRC patients from HP. B: Accuracies of different combinations of peaks in the pattern discriminating CRC patients from CRA patients.

To further select the set of candidate biomarkers, we used a stepwise approach in which many integrated ANNs were trained. The top 1 peak with the highest ability to predict the two groups (had the lowest MSE value) was selected as a single input to build the integrated ANN. We estimated the discriminating ability of this integrated ANN by the accuracy of blind test set. Next, the top 2 peaks were input to integrated ANN and the accuracy was calculated. The following peaks were added as

input stepwise to train integrated ANN and the accuracy was calculated. In this way, the 15 models combining different peaks were built. The peaks input to the model with the highest accuracy were selected as the set of potential biomarkers. The top 4 peaks were finally selected as potential biomarkers, an accuracy of 92% was achieved. The accuracies of these 15 models are plotted in Figure 2 (A).

The m/z of the 4 candidate biomarkers were 5 911, 8 922, 8 944, 8 817 Da. These 4 peaks all appeared to highly express in CRC and lowly express in healthy persons, as shown in Figure 3 (A, B). Between the two groups, the *P* value of *t*-test ($<10^{-9}$) and the area under the ROC curve (>8.0) showed statistical significance of all the 4 peaks. Table 1 shows the descriptive statistics of the 4 peaks.

Table 1 Descriptive data for the 4 potential biomarkers in the pattern discriminating CRC patients from HP (mean±SD)

M/Z (Da)	AUC	HP	CRC patients
5 911	0.908	0.824±0.504	2.763±1.720
8 922	0.872	1.254±0.724	2.767±1.445
8 944	0.828	0.999±0.626	2.651±1.851
8 817	0.811	0.878±0.607	1.744±0.940

AUC: area under the carve.

The 4 peaks were combined and evaluated by integrated ANN. We trained the integrated ANN with 89 samples and tested 49 samples. We randomly selected the test set 10 times, and each time 100 ANNs were built to predict the test set. So 1 000 ANNs were built up. Table 3 shows the results of this classifier. For the integrated ANN classifier, the estimated specificity in the blind test set was 92% with a 95% confidence interval of 89-95%, the estimated sensitivity was 89% (85-93%), the estimated positive predictive value was 86% (82-90%).

Table 2 Descriptive statistics for the 7 potential biomarkers in the pattern discriminating CRC patients from CRA patients (mean±SD)

M/Z (Da)	*P* value ($\times10^{-5}$)	CRA patients	CRC patients
17 247	0.71	0.211±0.130	0.113±0.100
18 420	1.27	0.039±0.036	0.076±0.040
5 911	1.71	1.459±0.977	2.763±1.720
9 294	2.76	0.617±0.385	1.105±0.563
4 654	6.74	0.503±0.493	1.164±0.943
21 694	7.48	0.489±0.145	0.698±0.267
21 742	12.10	0.536±0.161	0.744±0.282

Table 3 Predicted results of classifier for discriminating CRC patients from HP

	Test set (49×10)		Training set (98×10)	
	HP	CRC	HP	CRC
HP (92×10)	287	25	599	9
CRC (55×10)	19	159	29	343
Specificity (%)	92(287/(287+25))		99(599/(599+9))	
Sensitivity (%)	89(159/(159+19))		92(343/(343+29))	
Positive value (%)	86(159/(159+25))		97(343/(343+9))	

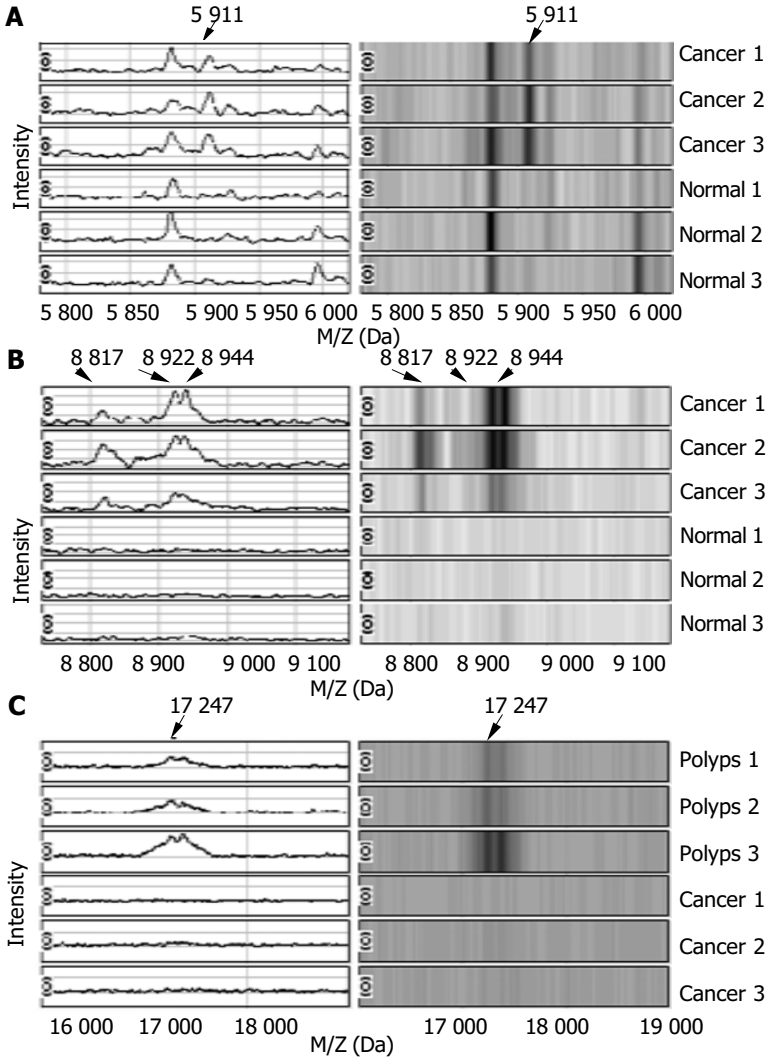

Figure 3 Spectra and gel maps of potential biomarkers. A: Spectra and gel maps of the peak with the m/z of 5 911 Da. B: Spectra and gel maps of the peak with the m/z of 8 922, 8 944, 8 817 Da. C: Spectra and gel maps of the peak with the m/z of 17 247 Da.

Bioinformatics analysis of CRC and CRA data

The 235 qualified peaks detected from the two groups were ranked by the *P* values of *t*-test. The top 15 peaks were selected for further analysis. For these data we utilized the 3-fold cross-validation SVM classifier to select the potential biomarkers to build the model to predict the test sets. This approach randomly selected 1/3 of samples to be the blinded test set, and the remaining 2/3 samples to be the training set and the procedure was repeated 3 times. We still used stepwise method to add the peaks in the rank of *P* value one by one to be the input of 3-cross-validation SVM. The top 7 peaks with the highest accuracy (86.7%) were selected as final potential biomarkers to separate the two groups. Table 2 shows the descriptive data of the 7 peaks. Between the two groups, the *P* values of *t*-test ($<10^{-4}$) and the area under the ROC curve (>7.0) showed the statistical significance of the 7 peaks. In the 7 peaks only the peak of 17 247 Da appeared to lowly express in CRC and highly express in CRA as shown in Figure 3C, others were highly expressed in CRC.

We used 3-fold cross-validation SVM to combine the 7 peaks, and trained it with 60 samples. For the 3-fold cross-validation SVM, the estimated specificity in the blind test set (30 samples) was 83% with a 95% confidence interval of 79-87%, the estimated sensitivity was 89% (86-92%), the estimated positive predictive value was 89% (86-92%). Table 4 shows our results for this classifier.

Table 4 Predicted results of classifier for discriminating CRC patients from CRA

	Test set (30×3)		Training set (60×3)	
	CRA	CRC	CRA	CRC
CRA (35×3)	29	6	56	14
CRC (55×3)	6	49	16	94
Specificity (%)	83(29/(29+6))		80(56/(56+14))	
Sensitivity (%)	89(49/(49+6))		85(94/(94+16))	
Positive value (%)	89(49/(49+6))		87(94/(94+14))	

DISCUSSION

CRC screening includes fecal occult blood test (FOBT), sigmoidoscopy, air-contrast barium enema examination, colonoscopy[30]. But they have not been commonly accepted due to costs, bowel preparation, sedation and perforation risks. Detection of serum tumor markers (such as CEA) is an inexpensive and facile screening method compared to others. However, all the existing biomarkers in serum lack sufficient sensitivity for screening and diagnosis of CRC[31-35]. In this study, we detected CEA values (cut-off value of CEA level of 5 ng/mL) of 182 serum samples (including 55 from CRC patients, 35 from CRA and 92 from HP which were also detected by SELDI), and a sensitivity of 47% was achieved in screening for CRC. The results also showed that CEA lacked sufficient sensitivity for screening and diagnosis of CRC.

Because of the multi-factorial nature of CRC, it is very clear that a combination of several markers would be necessary to effectively detect and diagnose CRC. SELDI-MS and the ProteinChip technology could provide the high-throughput proteomic profiling[36]. Coupled with sophisticated bioinformatics tools for complex data analysis they could find the "fingerprints" of CRC and build the diagnosis model.

One hundred and forty-seven CRC patients and HP were detected by SELDI-TOF-MS and the complex data were analyzed by integrated ANN, we found 4 potential biomarkers and achieved a specificity of 92% (89-95%), sensitivity of 89% (85-93%), positive predictive value of 86% (82-90%). Ninety CRC and CRA patients were detected by SELDI-MS and analyzed by an SVM classifier. We found 7 potential biomarkers and achieved a specificity of 83% (79-87%), sensitivity of 89% (86-92%), positive predictive value of 89% (86-92%).

Early detection remains one of the most urgent issues in CRC research[37]. Our two patterns could recognize early Dukes samples as efficiently as other Dukes samples. The biomarkers used in the final selection were not sensitive to different Dukes, stages of cancer patients. In almost all the patients with CRC, preceding lesions were asymptomatic adenomas[38]. So it is very important to discriminate the noncancer CRA patients from early CRC. We also achieved a high sensitivity and specificity model to recognize CRC and CRA patients.

We developed an integrated approach using bioinformatics and biostatics tools to analyze the large data of spectra. The ROC curve, *t*-test and MSE values were used to rank and select the peaks according to their contribution to the separation of two groups. To accurately estimate the sensitivity and specificity of the classifiers established by potential biomarkers, the test sets were randomly selected many times, independent of training sets each time.

The peak of 4 645 Da was identified as doubly charged forms of 9 294 Da by Ciphergen ProteinChip Software 3.1. The recognition of both the doubly charged and the singly charged forms of these peaks suggested their importance in discriminating the two diagnostic groups. The peak of 5 911 Da was selected as a potential biomarker in both the pattern discriminating CRC patients from HP and the pattern discriminating CRC from CRA patients. The expression of this biomarker increased step by step in HP, CRA and CRC patients as shown in Figure 3A. Therefore the peak of 5 911 Da may play an important role in the formation and progression of CRC.

In conclusion, SELDI-TOF-MS in combination with sophisticated bioinformatics tools could facilitate the discovery of new biomarkers and establish patterns with a high sensitivity and specificity for the detection of CRC.

REFERENCES

1 **Zhang YL,** Zhang ZS, Wu BP, Zhou DY. Early diagnosis for colorectal cancer in China. *World J Gastroenterol* 2002; **8**: 21-25

2 **Thiis-Evensen E,** Hoff GS, Sauar J, Majak BM, Vatn MH. Flexible sigmoidoscopy or colonoscopy as a screening modality for colorectal adenomas in older age groups? Findings in a cohort of the normal population aged 63-72 years. *Gut* 1999; **45**: 834-839

3 **Li S,** Nie Z, Li N, Li J, Zhang P, Yang Z, Mu S, Du Y, Hu J, Yuan S, Qu H, Zhang T, Wang S, Dong E, Qi D. Colorectal cancer screening for the natural population of Beijing with sequential fecal occult blood test: a multicenter study. *Chin Med J* 2003; **116**: 200-202

4 **Repetto L,** Venturino A, Fratino L, Serraino D, Troisi G, Gianni W, Pietropaolo M. Geriatric oncology: a clinical approach to the older patient with cancer. *Eur J Cancer* 2003; **39**: 870-880

5 **Gatta G,** Faivre J, Capocaccia R, Ponz de Leon M. Survival of colorectal cancer patients in Europe during the period 1978-1989. *Eur J Cancer* 1998; **34**: 2176-2183

6 **Ries LA,** Wingo PA, Miller DS, Howe HL, Weir HK, Rosenberg HM, Vernon SW, Cronin K, Edwards BK. The annual report to the nation on the status of cancer, 1973-1997, with a special section on colorectal cancer. *Cancer* 2000; **88**: 2398-2424

7 **Jemal A,** Murray T, Samuels A, Ghafoor A, Ward E, Thun MJ. Cancer statistics, 2003. *CA Cancer J Clin* 2003; **53**: 5-26

8 **Dashwood RH.** Early detection and prevention of colorectal cancer (review). *Oncol Rep* 1999; **6**: 277-281

9 **Mishaeli M,** Klein B, Sadikov E, Bayer I, Koren R, Gal R, Rakowsky E, Levin I, Kfir B, Schachter J, Klein T. Initial TPS serum level as an indicator of relapse and survival in colorectal cancer. *Anticancer Res* 1998; **18**: 2101-2105

10 **Vlahou A,** Schellhammer PF, Mendrinos S, Patel K, Kondylis FI, Gong L, Nasim S, Wright GL Jr. Development of a novel proteomic approach for the detection of transitional cell carcinoma of the bladder in urine. *Am J Pathol* 2001; **158**: 1491-1501

11 **Adam BL,** Qu Y, Davis JW, Ward MD, Clements MA, Cazares

LH, Semmes OJ, Schellhammer PF, Yasui Y, Feng Z, Wright GL Jr. Serum protein fingerprinting coupled with a pattern-matching algorithm distinguishes prostate cancer from benign prostate hyperplasia and healthy men. *Cancer Res* 2002; **62**: 3609-3614

12 **Qu YS,** Adam BL, Yasui Y, Ward MD, Cazares LH, Schellhammer PF, Feng Z, Semmes OJ, Wright GL Jr. Boosted decision tree analysis of surface-enhanced laser desorption/ionization mass spectral serum profiles discriminates prostate cancer from noncancer patients. *Clin Chem* 2002; **48**: 1835-1843

13 **Wagner M,** Naik DN, Pothen A, Kasukurti S, Devineni RR, Adam BL, Semmes OJ, Wright GL Jr. Computational protein biomarker prediction: a case study for prostate cancer. *BMC Bioinformatics* 2004; **5**: 26

14 **Jr GW,** Cazares LH, Leung SM, Nasim S, Adam BL, Yip TT, Schellhammer PF, Gong L, Vlahou A. Proteinchip (R) surface enhanced laser desorption/ionization (SELDI) mass spectrometry: a novel protein biochip technology for detection of prostate cancer biomarkers in complex protein mixtures. *Prostate Cancer Prostatic Dis* 1999; **2**: 264-276

15 **Petricoin EF,** Ardekani AM, Hitt BA, Levine PJ, Fusaro VA, Steinberg SM, Mills GB, Simone C, Fishman DA, Kohn EC, Liotta LA. Use of proteomic patterns in serum to identify ovarian cancer. *Lancet* 2002; **359**: 572-577

16 **Vlahou A,** Schorge JO, Gregory BW, Coleman RL. Diagnosis of ovarian cancer using decision tree classification of mass spectral data. *J Biomed Biotechnol* 2003; **2003**: 308-314

17 **Li J,** Zhang Z, Rosenzweig J, Wang YY, Chan DW. Proteomics and bioinformatics approachs for identification of serum biomarkers to detect breast cancer. *Clin Chem* 2002; **48**: 1296-1304

18 **Vlahou A,** Laronga C, Wilson L, Gregory B, Fournier K, McGaughey D, Perry RR, Wright GL Jr, Semmes OJ. A novel approach toward development of a rapid blood test for breast cancer. *Clin Breast Cancer* 2003; **4**: 203-209

19 **Poon TC,** Yip TT, Chan AT, Yip C, Yip V, Mok TS, Lee CC, Leung TW, Ho SK, Johnson PJ. Comprehensive proteomic profiling identifies serum proteomic signatures for detection of hepatocellular carcinoma and its subtypes. *Clin Chem* 2003; **49**: 752-760

20 **Wadsworth JT,** Somers KD, Stack BC Jr, Cazares L, Malik G, Adam BL, Wright GL Jr, Semmes OJ. Identification of patients with head and neck cancer using serum protein profiles. *Arch Otolaryngol Head Neck Surg* 2004; **130**: 98-104

21 **Xiao X,** Liu D, Tang Y, Guo F, Xia L, Liu J, He D. Development of proteomic patterns for detecting lung cancer. *Dis Markers* 2003; **19**: 33-39

22 **Zhukov TA,** Johanson RA, Cantor AB, Clark RA, Tockman MS. Discovery of distinct protein profiles specific for lung tumors and pre-malignant lung lesions by SELDI mass spectrometry. *Lung Cancer* 2003; **40**: 267-279

23 **Koopmann J,** Zhang Z, White N, Rosenzweig J, Fedarko N, Jagannath S, Canto MI, Yeo CJ, Chan DW, Goggins M. Serum diagnosis of pancreatic adenocarcinoma using surface-enhanced laser desorption and ionization mass spectrometry. *Clin Cancer Res* 2004; **10**: 860-868

24 **Bottaci L,** Drew PJ, Hartley JE, Hadfield MB, Farouk R, Lee PW, Macintyre IM, Duthie GS, Monson JR. Artificial neural networks applied to outcome prediction for colorectal cancer patients in separate institutions. *Lancet* 1997; **350**: 469-472

25 **Romualdi C,** Campanaro S, Campagna D, Celegato B, Cannata N, Toppo S, Valle G, Lanfranchi G. Pattern recognition in gene expression profiling using DNA array: a comparative study of different statistical methods applied to cancer classification. *Hum Mol Genet* 2003; **12**: 823-836

26 **Ball G,** Mian S, Holding F, Allibone RO, Lowe J, Ali S, Li G, McCardle S, Ellis IO, Creaser C, Rees RC. An integrated approach utilizing artificial neural networks and SELDI mass spectrometry for the classification of human tumours and rapid identification of potential biomarkers. *Bioinformatics* 2002; **18**: 395-404

27 **Khan J,** Wei JS, Ringner M, Saal LH, Ladanyi M, Westermann F, Berthold F, Schwab M, Antonescu CR, Peterson C, Meltzer PS. Classification and diagnostic prediction of cancers using gene expression profiling and artificial neural networks. *Nature* 2001; **7**: 658-659

28 **Peng S,** Xu Q, Ling XB, Peng X, Du W, Chen L. Molecular classification of cancer types from microarray data using the combination of genetic algorithms and support vector machines. *FEBS Lett* 2003; **555**: 358-362

29 **Koike A,** Takagi T. Prediction of protein-protein interaction sites using support vector machines. *Protein Eng Des Sel* 2004; **17**: 165-173

30 **Church TR,** Yeazel MW, Jones RM, Kochevar LK, Watt GD, Mongin SJ, Cordes JE, Engelhard D. A randomized trial of direct mailing of fecal occult blood tests to increase colorectal cancer screening. *J Natl Cancer Inst* 2004; **96**: 770-780

31 **Kornek GV,** Depisch D, Rosen HR, Temsch EM, Scheithauer W. Comparative analysis of CA72-4, CA195 and carcinoembryonic antigen in patients with gastrointestinal malignancies. *J Cancer Res Clin Oncol* 1992; **118**: 318-320

32 **Posner MR,** Mayer RJ. The use of serologic tumor markers in gastrointestinal malignancies. *Hematol Oncol Clin North Am* 1994; **8**: 533-553

33 **Ohuchi N,** Takahashi K, Matoba N, Sato T, Taira Y, Sakai N, Masuda M, Mori S. Comparison of serum assays for TAG-72, CA19-9 and CEA in gastrointestinal carcinoma patients. *Jpn J Clin Oncol* 1989; **19**: 242-250

34 **Ueda T,** Shimada E, Urakawa T. The clinicopathologic features of serum CA 19-9-positive colorectal cancers. *Surg Today* 1994; **24**: 518-525

35 **Nakagoe T,** Sawai T, Tsuji T, Jibiki MA, Nanashima A, Yamaguchi H, Yasutake T, Ayabe H, Arisawa K. Preoperative serum level of CA19-9 predicts recurrence after curative surgery in node-negative colorectal cancer patients. *Hepatogastroenterology* 2003; **50**: 696-699

36 **Srinivas PR,** Srivastava S, Hanash S, Wright GL Jr. Proteomics in early detection of cancer. *Clin Chem* 2001; **47**: 1901-1912

37 **Hurlstone DP,** Fujii T, Lobo AJ. Early detection of colorectal cancer using high-magnification chromoscopic colonoscopy. *Br J Surg* 2002; **89**: 272-282

38 **Vogelstein B,** Fearon ER, Hamilton SR, Kern SE, Preisinger AC, Leppert M, Nakamura Y, White R, Smits AM, Bos JL. Genetic alterations during colorectal-tumor development. *N Engl J Med* 1988; **319**: 525-532

Edited by Wang XL and Zhu LH **Proofread by** Xu FM

PO Box 2345, Beijing 100023, China
Fax: +86-10-85381893
E-mail: wjg@wjgnet.com www.wjgnet.com

World J Gastroenterol 2004;10(21):3132-3136
World Journal of Gastroenterology
 ISSN 1007-9327

• VIRAL HEPATITIS •

A novel hepatitis B virus genotyping system by using restriction fragment length polymorphism patterns of S gene amplicons

Guo-Bing Zeng, Shu-Juan Wen, Zhan-Hui Wang, Li Yan, Jian Sun, Jin-Lin Hou

Guo-Bing Zeng, Zhan-Hui Wang, Li Yan, Jian Sun, Jin-Lin Hou, Department of Infectious Diseases, Nanfang Hospital, Southern Medical University, Guangzhou 510515, Guangdong Province, China
Guo-Bing Zeng, Department of Infectious Diseases, 458 Hospital of PLA, Guangzhou 510602, Guangdong Province, China
Shu-Juan Wen, Genetic Laboratory, Nanfang Hospital, Southern Medical University, Guangzhou 510515, Guangdong Province, China
Supported by the Major State Basic Research Development Program of China. 973 Program, No.G1999054106; and the National Science Fund for Distinguished Young Scholars, No.30225042
Correspondence to: Dr. Jin-Lin Hou, Hepatology Unit and Department of Infectious Diseases, Nanfang Hospital, Southern Medical University, Guangzhou 510515, Guangdong Province, China. jlhou@fimmu.edu.cn
Telephone: +86-20-85141941 **Fax:** +86-20-87714940
Received: 2003-08-03 **Accepted:** 2003-12-22

Abstract

AIM: Traditional hepatitis B virus (HBV) genotyping methods using restriction fragment length polymorphism (RFLP) can reliably identify genotypes A to F. As HBV genotypes G and H have been recently identified, this study was to establish an accurate and simple genotyping method for all eight HBV genotypes (A to H).

METHODS: Two hundred and forty HBV small S sequences obtained from GeneBank were analysed for restriction enzyme sites that would be genotype-specific. Restriction patterns following digestion with restriction enzymes BsrI, StyI, DpnI, HpaII, and EaeI, were determined to identify all eight HBV genotypes. Mixed genotype infections were confirmed by cloning and further RFLP analysis.

RESULTS: The new genotyping method could identify HBV genotypes A to H. Genotypes B and C could be determined by a single step digestion with BsrI and StyI in parallel. This was particularly useful in the Far East where genotypes B and C are predominant. Serum samples from 187 Chinese HBV carriers were analysed with this genotyping system, and the genotype distribution was 1.1% (2), 51.9% (97), 40.6% (76) and 4.8% (9) for genotypes A, B, C, and D, respectively. Mixed genotypes were found in only 3 patients (1.6%). Sequence data analysis confirmed the validity of this new method.

CONCLUSION: This HBV genotyping system can identify all eight HBV genotypes. It is accurate and simple, and can be widely used for studies on HBV genotyping.

Zeng GB, Wen SJ, Wang ZH, Yan L, Sun J, Hou JL. A novel hepatitis B virus genotyping system by using restriction fragment length polymorphism patterns of S gene amplicons. *World J Gastroenterol* 2004; 10(21): 3132-3136
http://www.wjgnet.com/1007-9327/10/3132.asp

INTRODUCTION

Hepatitis B virus (HBV) exhibits genetic variability which gives rise to the well recognized subtypes and genotypes of the virus. In addition, virus variants arise during replication as a result of nucleotide misincorporations, in the absence of any proof-reading capacity by the viral polymerase. Based on an inter-group divergence of 8% or more in the complete genome nucleotide sequence, HBV has been classified into at least 8 different genotypes[1-4]. Genotyping could also be accomplished based on partial sequences from the pre-S or S genes of the HBV genome[5-7].

HBV genotypes have distinct geographical distributions. Genotypes A and D occur frequently in Africa and Europe[5,8], while genotypes B and C are prevalent in Asia[1]. Genotype E is almost entirely restricted to Africa, and F is found preferentially in Central and South America[9]. Genotype G was reported in France and the United States[3]. Recently, the eighth genotype H has been described in Central America[4].

An increasing number of studies showed that HBV genotypes might influence HBeAg seroconversion rates[10], mutation patterns in precore and core promoter regions[11,12], severity of liver disease[13-15] and response to antiviral treatment[11,16]. In order to confirm and extend these observations, further studies are needed to be carried out, using reliable and simple methods for HBV genotyping. Though several HBV genotyping methods have been reported so far[5-7,17,18], these could identify genotypes A to F, but not G or H.

The aim of this study was therefore to establish a simple and accurate HBV genotyping system using restriction fragment length polymorphism (RFLP) of the small S gene region, which could identify HBV genotypes A to H and would be applicable to large-scale studies.

MATERIALS AND METHODS

HBV sequences and computerized analyses

Two hundred and thirty-two complete and 8 S sequences of HBV were obtained from the DNA database (GenBank), comprising 24 sequences of genotype A, 35 of B, 97 of C, 38 of D, 5 of E, 30 of F, 8 of G and 3 of H. The small S gene regions of all these sequences were aligned and analysed to identify conserved regions and restriction enzyme sites that were genotype-specific. Five restriction enzymes were deemed to be appropriate for this purpose, and restriction patterns were determined by computerized analysis of each of the above mentioned sequences. The DNASIS software package (Hitachi Software Engineering, 1991) was used in this study.

Patient sera and HBV genotypes

Serum samples from 190 Chinese patients with chronic hepatitis B were collected from 2 liver units in mainland of China, and stored at -70 ℃. All subjects (male/female = 161/29, mean age = 29.5± 9.16 years) were HBsAg-positive by commercially available immunoassays (Abbort Laboratories). Of them, 116 (61%) were HBeAg positive, and the mean alanine transaminase value (ALT) was 248.5±342.8 IU/L. These samples were initially genotyped by RFLP analysis of pre-S amplicons as previously described[6].

Genotyping PCR and restriction enzyme treatment

The S gene sequences were amplified by nested PCR. Based

on the most conserved regions, we designed PCR primers to amplify the sequence between nt 203 to nt 787, yielding an amplicon of 585 bp. The outer primers were PrsS2 (sense, nt 2820-2837, 5'-GGGACACCATATTCTTGG) and S1R (antisense, nt 842-821, 5'- TTAGGGTTTAAATGTATACCCA). The inner primers were YS1 (sense, nt 203-221, 5'-GCGGGGTTTTTCTTGT TGA) and YS2 (antisense, nt 787-767, 5'-GGGACTCAAGATG TTGTACAG). DNA was extracted from the serum as previously described[19]. A 5 μL of the resuspended DNA was added to an amplification mixture containing 5 μL of 10× Taq polymerase buffer, 5 μL of 25 mmol/L deoxyribonucleotide triphosphates, 1 μL (2U) of Taq polymerase (Promega, Beijing, China) and 10 pmoL each of primers PrsS2 and S1R (total volume of 50 μL). The PCR profile was an initial 3 min denaturation at 94 ℃, followed by 35 cycles of amplification including denaturation for 45 s at 94 ℃, annealing for 60 s at 53 ℃, and extension for 90 s at 72 ℃. Strand synthesis was completed at 72 ℃ for 6 min. A 1 μL of the first-round PCR products was then used for the second-round PCR under the same conditions but with the primers YS1 and YS2.

A 10 μL of the second-round PCR products was mixed with 0.5 μL (5U) of the chosen restriction enzyme (New England Biolabs, Hong Kong, China), 1.5 μL of 10× buffer and 3.0 μL of water. After incubation at 37 ℃ for 4 h, the samples were electophoresed on a 30 g/L agarose gel. A 10 μL of undigested second-round PCR products was run in parallel with the enzyme-digested samples. The restriction patterns were read visually under ultraviolet light.

Identification of mixed genotypes

When non-specific, atypical or mixed RFLP patterns were found, and the small S gene region was amplified with primers BS1 (sense, nt 56-76, 5'-CCTGCTGGTGGCGCCAGTTCC) and S1R, yielding an amplicon of 797-bp in length. These PCR products were purified and ligated into the pGEM-T vector using a commercial kit (Promega, Beijing, China). Ten positive clones were selected for further analysis. Extracted plasmid DNA was amplified with primers YS1 and YS2. PCR products were digested with restriction enzymes and analysed by electrophoresis. Samples that did not give clear results were then sequenced directly.

Sequencing and sequence data analysis

Three serum samples each of genotypes B, C and D, and 2 serum samples of genotype A by our method were randomly selected for sequencing. The small S gene region was amplified with primers BS1 and S1R and ligated into the pGEM-T vector as described above. Plasmid DNA was extracted from positive clones and sequenced using an ABI automatic DNA sequencer. Sequences were then edited, aligned and compared with reference sequences using the DNASIS software.

RESULTS

Predicted RFLP patterns

Following alignment of S gene sequences, five restriction enzymes, StyI, BsrI, DpnI, HpaII and EaeI were deemed to be suitable for yielding restriction patterns that would identify all eight HBV genotypes.

Genotype C had a StyI site at nt position 455, cutting the S gene into two fragments of 253- and 332-bp in length. This restriction pattern was found in 95 of 97 genotype C sequences examined. This restriction site was absent in all other genotypes. All genotype B sequences could be distinguished by the fact that the S gene had a unique BsrI site at nt position 328, which gave two characteristic bands of 126- and 459-bp in length. A BsrI site at nt position 502 was observed in 22 of 24 genotype A and all genotype E and G sequences. Moreover, genotype E PCR products could be digested at position 706 by HpaII, while genotype G had no EaeI site, which was present in all other genotypes. The BsrI site at nt position 502 was also found in 1 of 38 genotype D sequences, which could be mistaken as genotype A. Thus the sequences which still left unresolved were those of genotypes D, F and H. For genotype F, a DpnI site was found at nt positions 491 and 747, while genotypes D and H were cut at nt position 491 but not at 747. Finally, a HpaII site at nt position 292 in genotype H could be differentiated from genotype D. The sequences recognized by these enzymes are shown in Figure 1. The patterns created by these enzymes from the small S gene region are shown in Table 1.

Strategy for HBV genotyping using the new method

The optimal strategy, using the new method, which could be applied to a particular geographical region according to the most prevalent HBV genotype in that region, is summarized in Figure 2. For example, genotypes B and C were the most prevalent in the Far East. After parallel digestion by BsrI and

Table 1 Restriction digestion patterns that could identify HBV genotypes

Genotypes	Pattern	No. of sequences	Fragments obtained with				
			BsrI	StyI	DpnI	HpaII	EaeI
A	A1	12	300 285	585	85 204 296	585	100 485
	A2	10	300 285	585	289 296	585	100 485
	A3	1	585	585	85 204 296	585	100 485
	A4	1	585	585	289 296	585	100 485
B	B1	33	126 459	585	289 296	585	100 485
	B2	2	126 184 275	585	289 296	585	100 485
C	C1	95	585	253 332	585	585	100 485
	C2	2	585	585	585	585	100 485
D	D1	36	585	585	289 296	585	100 485
	D2	1	585	585	585	585	100 485
	D3	1	300 285	585	585	585	100 485
E	E1	4	300 285	585	289 296	504 81	100 485
	E2	1	126 174 285	585	289 296	504 81	100 485
F	F1	29	585	585	289 256 40	90 495	100 485
	F2	1	585	585	289 296	90 495	100 485
G	G1	8	300 285	585	289 296	585	585
H	H1	3	585	585	289 296	90 495	100 485

StyI, more than 90% of the serum samples from Chinese patients could be genotyped.

Comparison with genotyping by RFLP of PreS1 regions

Of the 190 serum samples, 3 were HBV DNA negative by nested PCR. Thus, 187 serum samples were analysed in this study, and compared to the results obtained by RFLP analysis of the pre-S1region. One hundred and eight-one of the 187 serum samples were classified as genotypes A (2), B (95), C (75) and D (9). These results were in full agreement with those obtained with our new method. Because of nonspecific amplification and atypical restriction patterns, 6 samples could not be classified by RFLP analysis of pre-S1 amplicons. However, these were resolved into either genotypes B (2), C (1) or mixed B+C (3) by

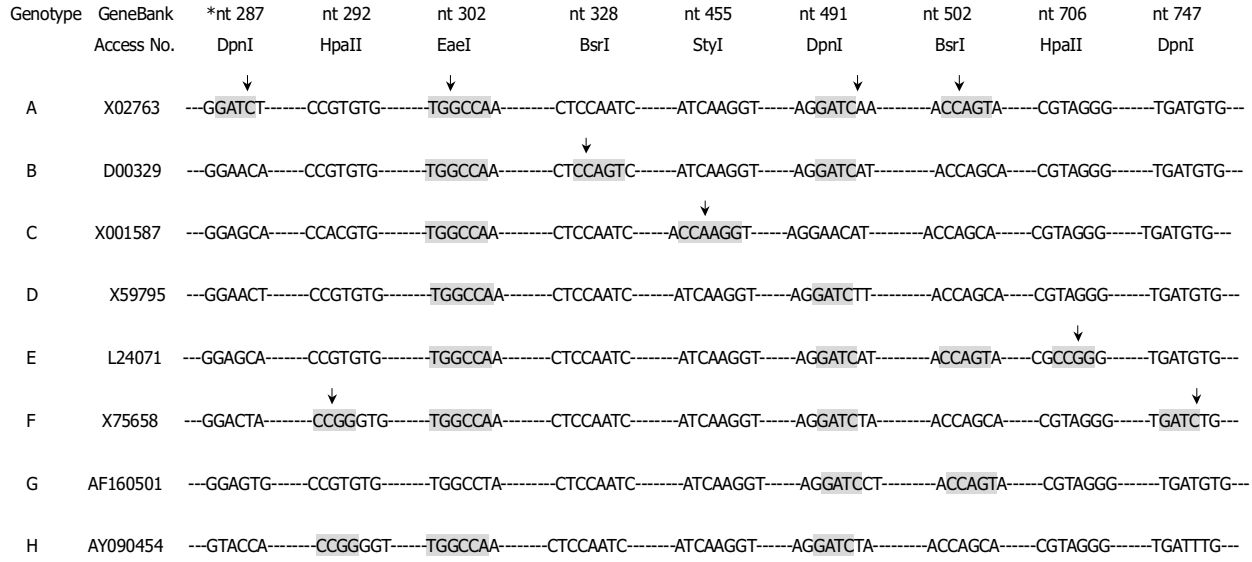

Figure 1 Genotype-specific sites recognized by restriction enzymes. GeneBank accession numbers and consensus sequences from HBV genotypes A to H are listed. The shaded letters indicate the sequences recognized by the relevant enzyme. StyI recognizes sequence C | C (A / T) (A / T) GG; BsrI, C | CAGT; DpnI, GA | TC; HpaII, C | CGG; EaeI, (C / T) | GGCC (A / G). *nt position number is from the unique *Eco*RI site according to the reference sequence ×001587 (genotype C).

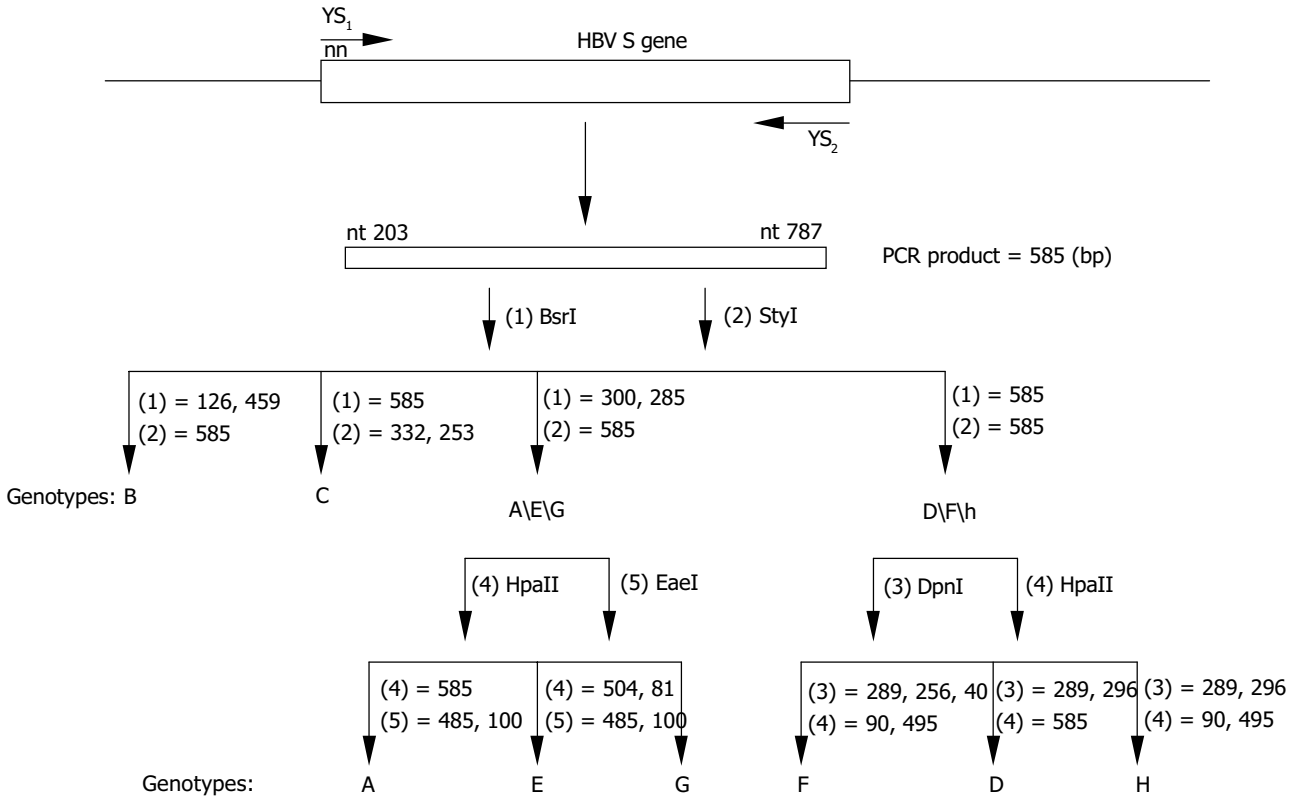

Figure 2 Diagrammatic representation of the position of PCR primers and RFLP analyses for HBV genotyping. The second round PCR products, which were 585 bp, were digested by (1) BsrI, (2) StyI, (3) DpnI, (4) HpaII and (5) EaeI. Genotypes B and C could be typed in one step using parallel digestion with BsrI and StyI.

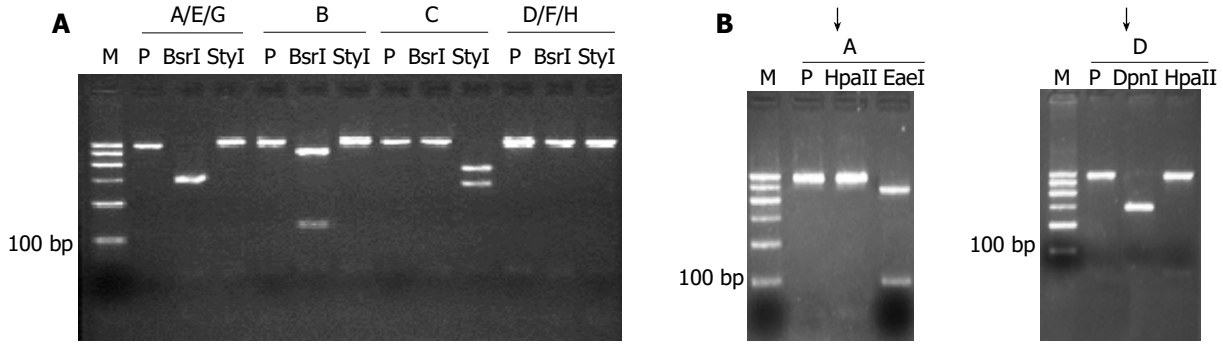

Figure 3 RFLP of S amplicon of HBV from 187 nested PCR-positive serum samples from Chinese carriers. Lane M: 100 bp ladder from 100-600 bp fragments, P: undigested PCR product. A: After the first step of parallel digestion with BsrI and StyI, the samples were divided into four groups: genotypes B, C, A/E/G and D/F/H; B: Groups A/E/G and D/F/H could be further resolved by the second parallel digestion. In this study, genotypes E, F, G and H were not observed, while genotypes B and C were the major ones.

our method after cloning and repeat RFLP analysis. These results were verified subsequently by direct sequencing of the S gene. Thus the final genotype distribution of the samples was A, 2 (1.1%); B, 97 (51.9%); C, 76 (40.6%); D, 9 (4.8%) and mixed (genotypes B and C), 3 (1.6%). Examples of RFLP analysis using the new method are shown in Figure 3.

Verification of reliability of the new method

Nucleotide sequences of 11 samples randomly selected were determined and then compared to reference sequences for genotypes A (X02763), B (D00329), C (X01587) and D (X59795). The homologies of the S gene region under investigation were 97.9-98.3%, 99.3-99.9%, 97.5-98.8% and 98.2-98.5%, respectively, which confirmed the validity of the new RFLP technique.

DISCUSSION

Great importance has been attached to the differences between HBV genotypes. In earlier studies[20,21], a higher frequency of liver dysfunction was observed in patients with subtype adr (most often genotype C) compared to those with subtype adw (mainly genotype B). These findings concurred with those reported by Lindh *et al*.[13] and Orito *et al*.[15]. Mayerat *et al*.[14] found that genotype A was more frequent in chronic hepatitis B patients than genotype D, while the opposite situation was true in acute hepatitis B patients. A study from Taiwan reported that genotype C was associated with more active liver disease compared to genotype B[22], and this was supported by a more recent study[23]. A retrospective study of 332 cases[10] showed that patients with HBV genotype B had a lower prevalence and earlier seroconversion to anti-HBe than those with genotype C, which could explain the less active liver disease seen in patients with genotype B. Another study[24] suggested that HBV genotype might influence HBV recurrence after liver transplantation as patients with genotype D appeared to have a higher risk for HBV recurrence and mortality. The correlation between HBV genotype and response to interferon therapy has also been reported. HBV genotype C was associated with a higher frequency of core promoter mutation and a lower response rate to interferon alfa therapy[16]. Hou *et al*.[11] studied 103 chronic hepatitis B patients from 16 European centers and found that HBV genotype A responded better to standard interferon treatment than other genotypes. This appeared to be related to its molecular characteristics, having a greater tendency to develop core promoter mutations and less variation in the nucleocapsid protein. A study reported that patients carrying the adw subtype were associated with a higher risk of lamivudine resistance than those with ayw subtype[25], although Chan *et al*. found that HBeAg seroconversion after treatment by lamivudine was not influenced by the HBV genotype[26]. To interpret these differences between HBV genotypes, larger-scale investigations are needed. So, development of accurate, simple and inexpensive HBV genotyping methods would be very useful in this respect.

Several methods have been used for HBV genotyping including direct sequencing, RFLP, PCR with genotype-specific primers[17], line probe assay[18] and enzyme-linked immunoassay[27]. Genotyping based on complete genome sequences is an ideal method, but sequencing is costly and cannot be easily carried out in clinical diagnostic laboratories for large-scale studies. Currently, PCR-RFLP is the most widely used method for HBV genotyping because it is simple and inexpensive. Norder *et al*.[2] found that HBV genotyping could be accomplished based on the sequence of the S gene. After analyzing 73 HBV sequences from GeneBank, Lindh *et al*.[5] developed a genotyping method based on RFLP patterns of a S gene amplicon, which first identified HBV genotypes A-F. They also reported another genotyping technique based on RFLP analysis of the pre-S region[6]. However, pre-S gene was less suitable for genotyping than S gene because it was not so conserved as S gene[28]. Mizokami *et al*.[7] compared 68 complete and 106 small S HBV sequences and confirmed that S gene could be used to accurately identify the six HBV genotypes A to F. They also described a RFLP genotyping system using five enzymes, HphI, NciI, AlwI, EarI, and NlaIV. Because genotypes G and H were not discovered then, they could not be assessed by these methods.

Compared with previous methods, our new method has several relative advantages. Firstly, it can identify all eight HBV genotypes. Secondly, it is more accurate because it was based on analysing many of the sequences deposited in GeneBank. Thirdly, a simple and inexpensive strategy can be adopted according to the most prevalent HBV genotypes in a particular geographical region. For example, the strategy shown in Figure 2 was especially suitable for the Far East where genotypes B and C are mostly found (85-98.6%)[21,29,30]. The RFLP patterns are simple, with one or two bands, and therefore easy to be recognized.

In this study, a new method for HBV genotyping based on RFLP analysis of S gene amplicons was established, and could identify all eight HBV genotypes. This HBV genotyping system is accurate, simple and can be expected to be widely used in studies of HBV genotyping.

REFERENCES

1 **Okamoto H,** Tsuda F, Sakugawa H, Sastrosoewignjo RI, Imai M, Miyakawa Y, Mayumi M. Typing hepatitis B virus by homology in nucleotide sequence: comparison of surface antigen subtype. *J Gen Virol* 1988; **69**(Pt 10): 2575-2583

2 **Norder H,** Courouce AM, Magnius LO. Complete genomes, phylogenetic relatedness, and structural proteins of six strains of the hepatitis B virus, four of which represent two new

genotypes. *Virology* 1994; **198**: 489-503
3 **Stuyver L,** De Gendt S, Van Geyt C, Zoulim F, Fried M, Schinazi RF, Rossau R. A new genotype of hepatitis B virus: complete genome and phylogenetic relatedness. *J Gen Virol* 2000; **81**(Pt 1): 67-74
4 **Arauz-Ruiz P,** Norder H, Robertson BH, Magnius LO. Genotype H: a new Amerindian genotype of hepatitis B virus revealed in Central America. *J Gen Virol* 2002; **83**(Pt 8): 2059-2073
5 **Lindh M,** Andersson AS, Gusdal A. Genotypes, nt 1858 variants, and geographic origin of hepatitis B virus-large-scale analysis using a new genotyping method. *J Infect Dis* 1997; **175**: 1285-1293
6 **Lindh M,** Gonzalez JE, Norkrans G, Horal P. Genotyping of hepatitis B virus by restriction pattern analysis of a pre-S amplicon. *J Virol Methods* 1998; **72**: 163-174
7 **Mizokami M,** Nakano T, Orito E, Tanaka Y, Sakugawa H, Mukaide M, Robertson BH. Hepatitis B virus genotype assignment using restriction fragment length polymorphism patterns. *FEBS Lett* 1999; **450**: 66-71
8 **Baptista M,** Kramvis A, Jammeh S, Naicker J, Galpin JS, Kew MC. Follow up of infection of chacma baboons with inoculum containing a and non-a genotypes of hepatitis B virus. *World J Gastroenterol* 2003; **9**: 731-735
9 **Norder H,** Hammas B, Lee SD, Bile K, Courouce AM, Mushahwar IK, Magnius LO. Genetic relatedness of hepatitis B viral strains of diverse geographical origin and natural variations in the primary structure of the surface antigen. *J Gen Virol* 1993; **74**(Pt 7): 1341-1348
10 **Chu CJ,** Hussain M, Lok AS. Hepatitis B virus genotype B is associated with earlier HBeAg seroconversion compared with hepatitis B virus genotype C. *Gastroenterology* 2002; **122**: 1756-1762
11 **Hou J,** Schilling R, Janssen HLA, Heijtink RA, Williams R, Schalm SW, Naoumov NV. Molecular characteristics of hepatitis B virus genotype A confer a higher response rate to interferon treatment. *J Hepatol* 2001; **34**(Suppl 1): 15-16
12 **Hou J,** Lin Y, Waters J, Wang Z, Min J, Liao H, Jiang J, Chen J, Luo K, Karayiannis P. Detection and significance of a G1862T variant of hepatitis B virus in Chinese patients with fulminant hepatitis. *J Gen Virol* 2002; **83**(Pt 9): 2291-2298
13 **Lindh M,** Hannoun C, Dhillon AP, Norkrans G, Horal P. Core promoter mutations and genotypes in relation to viral replication and liver damage in East Asian hepatitis B virus carriers. *J Infect Dis* 1999; **179**: 775-782
14 **Mayerat C,** Mantegani A, Frei PC. Does hepatitis B virus (HBV) genotype influence the clinical outcome of HBV infection? *J Viral Hepat* 1999; **6**: 299-304
15 **Orito E,** Mizokami M, Sakugawa H, Michitaka K, Ishikawa K, Ichida T, Okanoue T, Yotsuyanagi H, Iino S. A case-control study for clinical and molecular biological differences between hepatitis B viruses of genotypes B and C. Japan HBV genotype research group. *Hepatology* 2001; **33**: 218-223
16 **Kao JH,** Wu NH, Chen PJ, Lai MY, Chen DS. Hepatitis B genotypes and the response to interferon therapy. *J Hepatol* 2000; **33**: 998-1002
17 **Naito H,** Hayashi S, Abe K. Rapid and specific genotyping system for hepatitis B virus corresponding to six major genotypes by PCR using type-specific primers. *J Clin Microbiol* 2001; **39**: 362-364
18 **Grandjacques C,** Pradat P, Stuyver L, Chevallier M, Chevallier P, Pichoud C, Maisonnas M, Trepo C, Zoulim F. Rapid detection of genotypes and mutations in the pre-core promoter and the pre-core region of hepatitis B virus genome: correlation with viral persistence and disease severity. *J Hepatol* 2000; **33**: 430-439
19 **Hou J,** Karayiannis P, Waters J, Luo K, Liang C, Thomas HC. A unique insertion in the S gene of surface antigen-negative hepatitis B virus Chinese carriers. *Hepatology* 1995; **21**: 273-278
20 **Shiina S,** Fujino H, Kawabe T, Tagawa K, Unuma T, Yoneyama M, Ohmori T, Suzuki S, Kurita M, Ohashi Y. Relationship of HBsAg subtypes with HBeAg/anti-HBe status and chronic liver disease. Part II: Evaluation of epidemiological factors and suspected risk factors of liver dysfunction. *Am J Gastroenterol* 1991; **86**: 872-875
21 **Shiina S,** Fujino H, Uta Y, Tagawa K, Unuma T, Yoneyama M, Ohmori T, Suzuki S, Kurita M, Ohashi Y. Relationship of HBsAg subtypes with HBeAg/anti-HBe status and chronic liver disease. Part I: Analysis of 1744 HBsAg carriers. *Am J Gastroenterol* 1991; **86**: 866-871
22 **Kao JH,** Chen PJ, Lai MY, Chen DS. Hepatitis B genotypes correlate with clinical outcomes in patients with chronic hepatitis B. *Gastroenterology* 2000; **118**: 554-559
23 **Fang ZL,** Yang J, Ge X, Zhuang H, Gong J, Li R, Ling R, Harrison TJ. Core promoter mutations (A 1762 T and G 1764 A) and viral genotype in chronic hepatitis B and hepatocellular carcinoma in Guangxi, China. *J Med Virol* 2002; **68**: 33-40
24 **Devarbhavi HC,** Cohen AJ, Patel R, Wiesner RH, Dickson RC, Ishitani MB. Preliminary results: outcome of liver transplantation for hepatitis B virus varies by hepatitis B virus genotype. *Liver Transpl* 2002; **8**: 550-555
25 **Zollner B,** Petersen J, Schroter M, Laufs R, Schoder V, Feucht HH. 20-fold increase in risk of lamivudine resistance in hepatitis B virus subtype adw. *Lancet* 2001; **357**: 934-935
26 **Chan HLY,** Wong ML, Hui AY, Chim AML, Tse AML, Hung LCT, Chan FKL, Sung JJY. Hepatitis B virus genotype has no impact on hepatitis B e antigen seroconversion after lamivudine treatment. *World J Gastroenterol* 2003; **9**: 2695-2697
27 **Usuda S,** Okamoto H, Iwanari H, Baba K, Tsuda F, Miyakawa Y, Mayumi M. Serological detection of hepatitis B virus genotypes by ELISA with monoclonal antibodies to type-specific epitopes in the preS2-region product. *J Virol Methods* 1999; **80**: 97-112
28 **Mizokami M,** Orito E, Ohba K, Ikeo K, Lau JY, Gojobori T. Constrained evolution with respect to gene overlap of hepatitis B virus. *J Mol Evol* 1997; **44**(Suppl 1): S83-S90
29 **Ding X,** Mizokami M, Yao G, Xu B, Orito E, Ueda R, Nakanishi M. Hepatitis B virus genotype distribution among chronic hepatitis B virus carriers in Shanghai, China. *Intervirology* 2001; **44**: 43-47
30 **Orito E,** Ichida T, Sakugawa H, Sata M, Horiike N, Hino K, Okita K, Okanoue T, Iino S, Tanaka E, Suzuki K, Watanabe H, Hige S, Mizokami M. Geographic distribution of hepatitis B virus (HBV) genotype in patients with chronic HBV infection in Japan. *Hepatology* 2001; **34**: 590-594

Edited by Zhang JZ and Wang XL **Proofread by** Xu FM

PO Box 2345, Beijing 100023, China
Fax: +86-10-85381893
E-mail: wjg@wjgnet.com www.wjgnet.com

World J Gastroenterol 2004;10(21):3137-3140
World Journal of Gastroenterology
 ISSN 1007-9327

• VIRAL HEPATITIS •

Antigenic and immunogenic changes due to mutation of *s* gene of HBV

Jun-Hui Ge, Hui-Min Liu, Jing Sun, Le-Zhi Zhang, Jin He, Yu-Li Li, Hong Liu, Yi Xu, Hong-Yu Yu, Yi-Ping Hu

Jun-Hui Ge, Hui-Min Liu, Jing Sun, Jin He, Yu-Li Li, Yi Xu, Hong-Yu Yu, Department of Pathology, Changzheng Hospital, Second Military Medical University, Shanghai 200003, China
Le-Zhi Zhang, Department of Experimental Diagnosis, Changhai Hospital, Second Military Medical University, Shanghai 200433, China
Hong Liu, Yi-Ping Hu, Department of Cell Biology, Second Military Medical University, Shanghai 200433, China
Supported by National Science Foundation of China, No. 396670669 and No.39970676; Keystone basic research program of STCM, No. 03DZ14023
Co-correspondents: Le-Zhi Zhang and Yi-Ping Hu
Correspondence to: Hong-Yu Yu, Department of Pathology, Changzheng Hospital, Second Military Medical University, Shanghai, 200003, China. yuhongyu795@hotmail.com
Telephone: +86-21-63610109-73703 **Fax:** +86-21-25070291
Received: 2004-01-09 **Accepted:** 2004-03-12

Abstract

AIM: To investigate the change of immunological characteristics of HBsAg caused by the mutation at codon 145 of HBsAg using DNA-based immunization.

METHODS: Plasmids expressing mutant and wild type envelope antigens were transfected into human hepatocellular carcinoma cells via electrotransformation. The antigenicity of HBsAg was studied with EIA and immunocytochemical staining. Then plasmids were used to immunize 5 C57BL/6 mice. Sera of mice were detected for anti-HBs and anti-preS2 with ELISA.

RESULTS: The mutant HBsAg could be detected by native antibody in EIA and immunocytochemical study. But the $A_{(450\ nm)}$ value of the mutant HBsAg in the supernatant was apparently lower than that of the wild-type. Both mutant and native HBsAg expression plasmid could stimulate a strong humoral immune response to HBsAg and preS2 antigen in mice. Protective antibodies against HBsAg elicited by the native HBsAg occurred earlier than that elicited by the mutant HBsAg about one to two weeks. The occurrence of protective antibodies against preS2 antigen was one to two weeks earlier than that of anti-HBs.

CONCLUSION: The amino acid substitution causes changes of the antigenicity and immunogenicity of HBsAg, but mutant HBsAg can still induce a protective humoral immune response in mice.

Ge JH, Liu HM, Sun J, Zhang LZ, He J, Li YL, Liu H, Xu Y, Yu HY, Hu YP. Antigenic and immunogenic changes due to mutation of *s* gene of HBV. *World J Gastroenterol* 2004; 10(21): 3137-3140
http://www.wjgnet.com/1007-9327/10/3137.asp

INTRODUCTION

Hepatitis B infection is a serious problem worldwide. HBV vaccine is effective in preventing HBV infection. Antibody responses to the common epitope of HBsAg, the "a" determinant, are considered to confer protection against HBV infection regardless of viral subtypes. HBV infection still occurs in spite of the presence of anti-HBs[1-3]. Some cases were infected with a variant of HBV. This variant has a point mutation from guanosine to adenosine at nucleotide position 587 of the *s* gene that results in an amino acid substitution of arginine for glycine at codon 145 of HBsAg[4,5]. This mutation would greatly destroy the antigenicity of HBsAg, which directly impacts on the diagnosis and therapy of HBV[6]. Also, this variant was found in patients who had liver transplantations for end-stage liver diseases associated with HBV infection and received human monoclonal anti-HBs antibody or HBIG in an attempt to prevent recurrent hepatitis B[7-9]. This study was undertaken to determine whether the change from glycine to arginine at amino acid 145 of HBsAg could cause a loss of antigenicity and immunogenicity of HBsAg, thus allowing the mutant HBV to evade the humoral immune response.

MATERIALS AND METHODS

Reagents, plasmid, antibodies and animals

Restriction endonucleases and *T4* DNA ligase were obtained from Sangon Co. (Canada). Plasmid P II containing overlength HBV genomes was endowed by Dr. Jian-Wen He. Plasmid P II had a point mutation from guanosine to adenosine at the nucleotide position 587 of *s* gene and resulted in an aminoacid substitution of arginine for glycine at codon 145 of HBsAg. Plasmid pCMV-S2.S was a generous gift of Dr. Heather Davis (Loeb Research Institute, Ottawa, Canada). This vector contained a cytomegalovirus promoter and respiratory syncytial virus enhancer element and encoded HBsAg and MHBs proteins. Plasmid SEAP expressing alkaline phosphatase was a generous gift of Dr. Jian-Wen He. HBsAg and HBsAb ELISA reagents were purchased from Abbott Laboratories and Sino-American Biotechnology Co., respectively. PreS2 antigen and preS2-specific antibodies were measured using ELISA kits from Hepatic Disease Institute of Beijing Medical University. The mouse monoclonal antibody against HBsAg was purchased from DAKO (USA). Sheep anti-mouse IgG-HRP was obtained from CALBIOCHEM (Germany). QIA quick gene gel kit and plasmid extraction kit were purchased from QIA gene. C57BL/6 mouse strain bought from Animal Center of Shanghai Birth Control Research Institute was kept under standard pathogen-free conditions in the animal facility and maintained on a 14:10 light-dark schedule (lights off at 10 pm, on at 8 am). Mice used were aged 6-8 wk.

Construction of DNA expression plasmid

Plasmid P II used as the source of mutant viral gene and plasmid pCMV-S2. S used as the source of the vector were digested with *Dra* III and *Xho* I, respectively. Then the segment of mutant *s* gene from plasmid P II was inserted into the vector from pCMV-S2.S by *T4* DNA ligase. Eukaryotic expression plasmid pCMV-S2.S+145R containing a point mutation from guanosine to adenosine was constructed. Plasmid pCMV-S2.S+145R was confirmed by restriction endonuclease digestion and HBV insert was sequenced by the dideoxy method using a commercial kit. The plasmid was grown in DH5 α and extracted by QIA quick gene kit. DNA was dissolved in double distilled water, adjusted to 1.6 mg/L, and then diluted to a final concentration of 1 mg/L

for *in vivo* studies. Concentration and purity of the DNA were confirmed by measuring the optical density at 260 nm and by agarose gel electrophoresis.

In vitro assays for HBV protein expression

Human hepatocellular carcinoma cell lines (Hep G2) were transfected with the eukaryotic expression vectors pCMV-S2.S+145R, pCMV-S2.S or pcDNA3.0 via electrotransformation. The change of binding power of mutant antigens to anti-HBs was studied by EIA and immunocytochemical staining. To control transfection efficiency, cells were cotransfected with an alkaline-phosphatase-containing vector SEAP. Cells were lysed by freeze-thawing three times in phosphate-buffered saline (PBS), and the supernatants were collected at various time points after transfection for viral protein studies.

Analysis of viral proteins by ELISA

Concentrations of HBsAg and preS2 envelope proteins derived from culture supernatant or cell lysates of transfected cells were measured by enzyme-linked immunosorbent assay reagents according to the manufacturer's instructions. One hundred μL of culture supernatant or cell lysates was incubated with 100 μL of 2×SEAP buffer at 37 ℃ for 10 min. Twenty μL substrate buffer was added to the assay. $A_{(450\ nm)}$ value was determined after incubated at 37 ℃ for 30 min. All results were corrected according to the transfection efficiency using the SEAP assays.

Expression of viral proteins

Transfected cells were collected by centrifugation and spread on sterile glass slides, and then fixed with acetone at 4 ℃ for immunochemical staining. Slides were blocked with normal goat serum for 30 min at room temperature, then incubated either with monoclonal mouse anti-HBs at a dilution of 1:200 for detection of HBsAg or with monoclonal mouse anti-preS2 (1:500) for detection of preS2 antigen for 12 h at 4 ℃. After washed with PBS, a secondary antiserum consisting of biotin-conjugated goat anti-mouse immunoglobulin G was applied at a 1:100 dilution for 30 min at 37 ℃. The slides coated with antibody were washed with PBS, treated with streptavidin-horseradish peroxidase conjugates at a 1:600 dilution for 30 min at 37 ℃, stained with nitroblue tetrazolium chloride and 5-bromo-4-chloro-3-indolyl-phosphate (NBT/BCIP, MAXIN Co.), and counter-stained with Mayer's hematoxylin before mounted.

DNA immunization

Mice were injected on a single occasion with 100 μg of recombinant plasmid DNA pCMV-S2.S, pCMV-S2.S+145R or pcDNA3.0 in 100 μL of 0.9 g/L NaCl distributed into the anterior tibialis muscle of C57BL/6 mice 5 d after the injection of 100 μL bupivacaine (0.2-0.4%). Immunization with the empty plasmid pcDNA3.0 vector (mock) was used as a negative control. Mice were anesthetized with pentobarbitone prior to phlebotomy from the retro-orbital plexus 200 microliter using heparinized glass pipettes every week. Serum was isolated by centrifugation. Anti-HBs and anti-preS2 concentrations were analyzed by using ELISA kits according to the manufacturer's instructions.

Detection of serum anti-HBs and anti-preS2 titers

Standard anti-HBs at titres 80, 40, 20, 10 or 0 mIU/L was detected by ELISA at the time when serum samples were detected. The $A_{(450\ nm)}$ value was 0.872, 0.442, 0.225, 0.107 and 0.046, respectively. The data were analyzed by linear regression, and the equation between the $A_{(450\ nm)}$ value and the antibody titers was y = 94.442x-1.959. According to the manufacturer's instructions, inhibition rate (%) = (*A* value of negative control - *A* value of sample) / (*A* value of negative control - *A* value of positive control) × 100%.

Statistical analysis

The data were analyzed by SAS software.

RESULTS

Construction of recombinant eukaryotic expression plasmid pCMV-S2.S+145R

The results of endonuclease digestion and electrophoresis were in accordance to the graphic map of plasmids. The result of sequencing was same as the sequence in the other report[10], except the point mutation from guanosine to adenosine at the nucleotide position 587 of *s* gene (Figure 1).

Secretion and expression of HBsAg and preS2 antigen

HepG2 cells were transfected with pCMV-S2.S+145R, pCMV-S2.S or pcDNA3.0 and culture supernatant was collected at various intervals of 3, 5, 7 d after transfection. pCMV-S2.S-transfected cells secreted a higher amount of HBsAg compared with the pCMV-S2.S+145R-transfected cells in the culture supernatant and the cell lysates of transfected cells (Figure 2). But preS2 antigen was not detected in the culture supernatant or in the cell lysates of pCMV-S2.S-transfected and pCMV-S2.S+145R-transfected cells. In contrast, immunocytochemical studies clearly showed a substantial cytoplasmic accumulation of HBsAg and preS2 antigen in both of the pCMV-S2.S-transfected and pCMV-S2.S+145R- transfected cells. Furthermore, there was no difference in the expression of HBsAg and preS2 antigen between the two plasmid transfected cells. No staining pattern was observed in mock-transfected cells (data not shown).

Humoral immune response to HBV proteins

Anti-HBs responses to pCMV-S2.S+145R were detectable 4 wk after the immunization in C57BL/6 mice. The titer of anti-HBs increased gradually by the end of observation. The highest titer was 95.60 mIU/L at the twelfth week after immunization. Most importantly, anti-HBs responses to pCMV-S2.S were detectable 2 wk after immunization in C57BL/6 mice. The titer of anti-HBs also increased gradually by the end of observation. The highest titer was 99.57 mIU/L at the twelfth week after immunization. The mice immunized with pCMV-S2.S+145R developed anti-HBs after a delay of approximately 2 wk compared with those injected with pCMV-S2.S (Figure 3). The occurrence of protective antibodies against HBsAg elicited by native HBsAg was one to two weeks earlier than that elicited by mutant HBsAg. Nevertheless, pCMV-S2.S+145R-immunized as well as pCMV-S2.S-immunized mice developed a strong humoral immune response against HBsAg at levels far above the known anti-HBs protection limit for humans (>10 mU/mL). Anti-HBs response was not detected in C57BL/6 mice immunized with pcDNA3.0.

Both pCMV-S2.S+145R-immunized and pCMV-S2.S-immunized mice developed a significant preS2-specific antibody response, whereas antibody responses to the preS2 antigen were detectable two weeks after immunization. There was a slight difference between the two groups with respect to the level of anti-preS2 antigen response (Figure 4A).

Standardization of anti-HBs titer

In order to analyze the difference in immune response induced by pCMV-S2.S+145R and pCMV-S2.S and the validity of immunization and the titer of Anti-HBs were corrected according to the inhibition rate of anti-preS2 which was little affected by the point mutation, because the structures of pCMV-S2.S+145R and pCMV-S2.S were exactly the same except for a point mutation from guanosine to adenosine at the nucleotide position 587 of *s* gene. Therefore, the ratio of HBsAg and preS2 antigen expressed by the two plasmids was similar. Then the difference between the two plasmids due to the mutation could be observed correctly (Figure 4B).

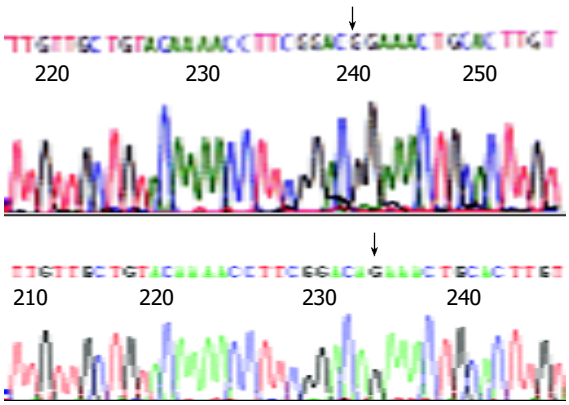

Figure 1 Partial sequences of plasmids pCMV-S.S2 and pCMV-S.S2+145R A: " ↓ "±stands for the "G" in gene sequences of pCMV-S.S2 B: " ↓ "± stands for the "A" in gene sequences of pCMV-S.S2+145R, namely mutant point.

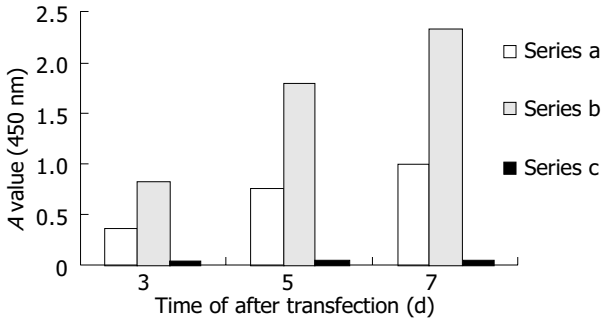

Figure 2 Secretion of HBsAg *in vitro*. Series A: HBsAg levels of supernatant collected from pCMV-S.S2+145R-transfected cells. Series B: HBsAg levels of supernatant collected from pCMV-S.S2-transfected cells. Series C: negative control.

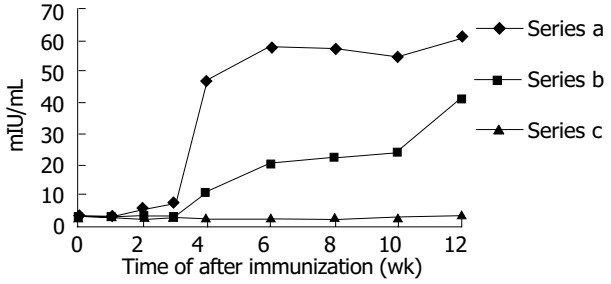

Figure 3 Humoral immune response induced by DNA-based immunization. Series A: anti-HBs level in pCMV-S.S2-immunized mice. Series B: anti-HBs level in pCMV-S.S2+145R-immunized mice. Series C: anit-HBs level in pcDNA3.0-immunized mice.

DISCUSSION

The antibody responses to the common "a" determinant of HBsAg confer protection against infection with HBV of all subtypes. Using monoclonal antibodies, this determinant is composed of a number of epitopes, and its tertiary structure is important for its antigenicity. The amino acid arginine, which is substituted for glycine, is a much larger residue and charged[11]. As a result the hydrophobicity profiles of this region of the two antigens are quite different and would be expected to affect the secondary and tertiary structures of the antigen. This amino acid substitution lies within the "a" determinant and so potentially alters the epitopes recognized by the protective immune response.

The secondary and tertiary structures of HBsAg expressed by the eukaryotic expression vector were most similar to those of viruses, which could exclude possible alterations of the antigenic properties by purification procedures of the recombinant vaccine. In transfection and *in vitro* expression study, HBsAg secreted by pCMV-S2.S-transfected cells had a higher affinity to the anti-HBs compared with that secreted by pCMV-S2.S+145R-transfected cells in the culture supernatant and the cell lysates of transfected cells, although the transfection efficiency was corrected. The antigenicity of HBsAg was altered by this single amino acid substitution. The mutant antigen could not be totally recognized by anti-HBs induced by naive antigens. The point mutation could influence the affinity, but mutant antigen could still be detected by anti-HBs.

The immunogenicity of HBsAg was also altered by this point mutation. The anti-HBs titer to the native HBsAg induced by mutant HBsAg was significantly lower than that induced by native HBsAg, while there was no significant difference between the titers of anti-preS2 induced by the two antigens. These results support the suggestion that this mutation was the result of immune pressure[12]. This variant could evade the immune response elicited after natural infection or after vaccination[13,14].

Both HBsAg and preS2 antigens, expressed by these two plasmids, were able to induce a strong humoral immune response. Indeed, anti-HBs titers induced by both plasmids were far above 10 mIU/L. The level of anti-HBs was sufficient to protect humans against HBV infection after exposure to the virus. This DNA vaccine could also confer the protection against infection with prototype HBV.

The preS2 antigen was not detected in the culture supernatant or cell lysates of transfected cells, but a substantial cytoplasmic accumulation was detected in plasmid transfected cells by immunocytochemical study, and the anti-preS2 was also detected in mice after DNA immunization. It is likely that the preS2 antigen was a nonsecreted protein expressed by this vector in HepG2 cells. It could be a nonsecreted protein *in vivo*, but it was possible that bupivacaine followed by plasmid DNA injections caused early activation of nonspecific inflammatory mediators by recruiting professional APCs[15,16], B cells, and T cells. In addition,

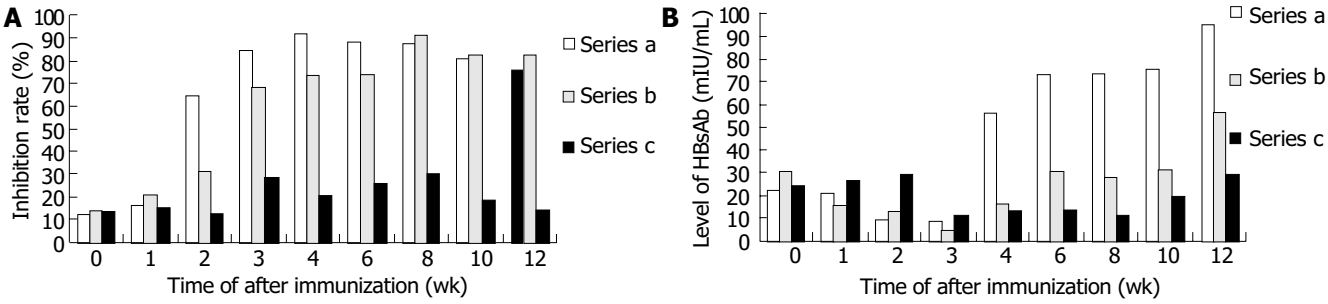

Figure 4 Comparison of humoral immune responses to preS2 anigen and HBsAg. A: Comparison of humoral immune responses to preS2 anigen. Series a: anti-preS2 level in pCMV-S.S2-immunized mice. Series b: anti-preS2 level in pCMV-S.S2+145R -immunized mice. Series c: negative control. B: Comparison of humoral immune responses to HBsAg. Series a: pCMV-S.S2 -immunized mice. Series b: pCMV-S.S2+145R-immunized mice. Series c: negative control.

a specific immune response against muscle cells expressing viral peptides or proteins might subsequently lead to damage of muscle fibers and release of sequestered antigens. Such antigens might eventually reach lymph nodes or alternatively taken up locally by APCs. The occurrence of protective antibodies of anti-HBs2 was one to two weeks earlier than that of anti-HBs in the same group. This result was similar to other reports[17,18]. There was little difference in occurrence, high titre and duration of anti-preS2 between the mutant and native viral protein expression plasmids. It indicated that this mutation had little impact on the antigenicity and immunogenicity of preS2 antigen. Therefore, the ingredient of preS2 antigen in hepatitis B vaccine would protect humans against this mutant HBV infection after exposure to the virus, and it also could shorten the occurrence of protective antibody and give an early stage protection. This would benefit the infants born by HBeAg positive mothers and persons exposed to HBV.

In conclusion, DNA immunization with the mutant HBsAg expression vector, produces a lower affinity than that elicited by the native HBsAg expression vector. The mutation changes the antigenicity and immunogenicity of HBsAg, and also induces a protective immune response.

REFERENCES

1 **Lee KM,** Kim YS, Ko YY, Yoo BM, Lee KJ, Kim JH, Hahm KB, Cho SW. Emergence of vaccine-induced escape mutant of hepatitis B virus with multiple surface gene mutations in a Korean child. *J Korean Med Sci* 2001; **16**: 359-362

2 **Kidd-Ljunggren K,** Miyakawa Y, Kidd AH. Genetic variability in hepatitis B viruses. *J Gen Virol* 2002; **83**(Pt 6): 1267-1280

3 **Nainan OV,** Khristova ML, Byun K, Xia G, Taylor PE, Stevens CE, Margolis HS. Genetic variation of hepatitis B surface antigen coding region among infants with chronic hepatitis B virus infection. *J Med Virol* 2002; **68**: 319-327

4 **Cooreman MP,** Leroux-Roels G, Paulij WP. Vaccine- and hepatitis B immune globulin-induced escape mutations of hepatitis B virus surface antigen. *J Biomed Sci* 2001; **8**: 237-247

5 **Osiowy C.** Sensitive detection of HBsAg mutants by a gap ligase chain reaction assay. *J Clin Microbiol* 2002; **40**: 2566-2571

6 **Fischer L,** Kalinina T, Rogiers X, Will H, Sterneck M. GLY145ARG mutation emerging under HBIG treatment in patients with recurrent HBV after liver transplantation strongly reduces viral secretion. *Transplant Proc* 2001; **33**: 3633-3636

7 **Kidd-Ljunggren K,** Miyakawa Y, Kidd AH. Genetic variability in hepatitis B viruses. *J Gen Virol* 2002; **83**(Pt 6): 1267-1280

8 **Rodriguez-Frias F,** Buti M, Jardi R, Vargas V, Quer J, Cotrina M, Martell M, Esteban R, Guardia J. Genetic alterations in the S gene of hepatitis B virus in patients with acute hepatitis B, chronic hepatitis B and hepatitis B liver cirrhosis before and after liver transplantation. *Liver* 1999; **19**: 177-182

9 **Grottola A,** Buttafoco P, Del Buono MG, Cremonini C, Colantoni A, Gelmini R, Morelli C, Masetti M, Jovine E, Fruet F, Pinna A, Manenti F, Villa E. Pretransplantation pre-S2 and S protein heterogeneity predisposes to hepatitis B virus recurrence after liver transplantation. *Liver Transpl* 2002; **8**: 443-448

10 **Gan RB,** Chu MJ, Shen LP, Qian SW, Li ZP. The complete nucleotide sequence of the cloned DNA of hepatitis B virus subtype adr in pADR-1. *Sci Sin* 1987; **30**: 507-521

11 **Waters JA,** Kennedy M, Voet P, Hauser P, Petre J, Carman W, Thomas HC. Loss of the common "A" determinant of hepatitis B surface antigen by a vaccine- induced escape mutant. *J Clin Invest* 1992; **90**: 2543-2547

12 **Oon CJ,** Chen WN, Goo KS, Goh KT. Intra-familial evidence of horizontal transmission of hepatitis B virus surface antigen mutant G145R. *J Infect* 2000; **41**: 260-264

13 **Hou J,** Wang Z, Cheng J, Lin Y, Lau GK, Sun J, Zhou F, Waters J, Karayiannis P, Luo K. Prevalence of naturally occurring surface gene variants of hepatitis B virus in nonimmunized surface antigen-negative Chinese carriers. *Hepatology* 2001; **34**: 1027-1034

14 **Chen WN,** Oon CJ. Hepatitis B virus surface antigen (HBsAg) mutants in Singapore adults and vaccinated children with high anti-hepatitis B virus antibody levels but negative for HBsAg. *J Clin Microbiol* 2000; **38**: 2793-2794

15 **Ulmer JB,** Donnelly JJ, Parker SE, Rhodes GH, Felgner PL, Dwarki VJ, Gromkowski SH, Deck RR, DeWitt CM, Friedman A. Heterologous protection against influenza by injection of DNA encoding a viral protein. *Science* 1993; **259**: 1745-1749

16 **Oka Y,** Akbar SM, Horiike N, Joko K, Onji M. Mechanism and therapeutic potential of DNA-based immunization against the envelope proteins of hepatitis B virus in normal and transgenic mice. *Immunology* 2001; **103**: 90-97

17 **Geissler M,** Tokushige K, Chante CC, Zurawski VR Jr, Wands JR. Cellular and humoral immune response to hepatitis B virus structural proteins in mice after DNA-based immunization. *Gastroenterology* 1997; **112**: 1307-1320

18 **Madalinski K,** Sylvan SP, Hellstrom U, Mikolajewicz J, Zembrzuska -Sadkowska E, Piontek E. Antibody responses to preS components after immunization of children with low doses of BioHepB. *Vaccine* 2001; **20**: 92-97

Edited by Wang XL and Ren SY **Proofread by** Xu FM

PO Box 2345, Beijing 100023, China
Fax: +86-10-85381893
E-mail: wjg@wjgnet.com www.wjgnet.com

World J Gastroenterol 2004;10(21):3141-3145
World Journal of Gastroenterology
 ISSN 1007-9327

• VIRAL HEPATITIS •

Replication and gene expression of mutant hepatitis B virus in a transgenic mouse containing the complete viral genome with mutant *s* gene

Jun-Hui Ge, Le-Zhi Zhang, Jian-Xiu Li, Hong Liu, Hui-Min Liu, Jin He, Yu-Cheng Yao, Yong-Ji Yang, Hong-Yu Yu, Yi-Ping Hu

Jun-Hui Ge, Hui-Min Liu, Jin He, Hong-Yu Yu, Department of Pathology, Changzheng Hospital, Second Military Medical University, Shanghai 200003, China
Le-Zhi Zhang, Department of Experimental Diagnosis, Changhai Hospital, Second Military Medical University, Shanghai 200433, China
Jian-Xiu Li, Hong Liu, Yu-Cheng Yao, Yong-Ji Yang, Yi-Ping Hu, Department of Cell Biology, Second Military Medical University, Shanghai 200433, China
Supported by National Science Foundation of China, No. 396670669 and No.39970676; Keystone basic research program of STCM, No. 03DZ14023
Co-correspondents: Le-Zhi Zhang and Yi-Ping Hu
Correspondence to: Hong-Yu Yu, Department of Pathology, Changzheng Hospital, Second Military Medical University, Shanghai, 200003, China. yuhongyu795@hotmail.com
Telephone: +86-21-63610109-73703 **Fax:** +86-21-25070291
Received: 2004-01-09 **Accepted:** 2004-03-12

Abstract

AIM: To establish the transgenic mouse line harbouring complete hepatitis B virus (HBV) genome with mutant *s* gene (*adr* subtype).

METHODS: Transgenic mice were generated by microinjecting HBV genome into fertilized eggs. Integration, expression, replication of HBV gene and histological changes in transgenic mice were estimated by genomic DNA PCR, serum DNA PCR, Southern blot, ELISA, HE staining, immunohistochemistry and transmission electron microscopy. Transgenic mice with HBsAg positive in serum were bred and analyzed.

RESULTS: A total of 288 eggs survived from microinjections were transplanted into the oviducts of 13 pseudopregnant mice and 49 pups were produced. Twenty-six mice were identified to have the integrated HBV gene. Serum HBsAg and HBeAg were detected in 2 of 43 mice. HBsAg and HBcAg in cytoplasm or nuclei of hepatocytes were detected in 10 mice. Founders with HBsAg in serum were named lineages G145R-15 and G145R-18. Of the 16 F1 offsprings generated by G145R-15 founder, 12 were positive for HBV genome with PCR, 10 were positive for HBsAg and HBcAg with immunohistochemistry and 7 were positive for HBsAg and HBeAg with ELISA. Only 1 of 8 F1 offsprings generated by G145R-18 founder was survived and it was detected positive for HBV genome, HBsAg, HBcAg and HBeAg. Both of the two lineages had some pathological characteristics of mild chronic hepatitis B in the liver, such as swelling of hepatocytes and focal hepatocellular necrosis and parenchymal lymphomononuclear cell infiltrate.

CONCLUSION: Transgenic mice harbouring HBV with mutant *s* gene can be generated. The HBV genes are integrated in the transgenic mice genome and can be expressed, replicated, packaged and excreted. HBV DNA can be stably transmitted in the transgenic mice.

Ge JH, Zhang LZ, Li JX, Liu H, Liu HM, He J, Yao YC, Yang YJ, Yu HY, Hu YP. Replication and gene expression of mutant hepatitis B virus in a transgenic mouse containing the complete viral genome with mutant *s* gene. *World J Gastroenterol* 2004; 10(21): 3141-3145
http://www.wjgnet.com/1007-9327/10/3141.asp

INTRODUCTION

Hepatitis B virus (HBV) is a major pathogen causing human acute and chronic hepatitis B[1] and has a very close association with cirrhosis and human hepatocellular carcinoma (HCC)[2-5]. Hepatitis B (HB) vaccine can protect human from infecting HBV. Many children born from HBeAg positive mothers would suffer from HBV after HB vaccination because of the mutation of HBV[6-7]. Genetic mutation in viruses is usually associated with escape of host immune responses, development of drug resistance, modification of virulence and patterns of epidemiology of diseases. In addition, HBV has a limited host range, which impedes much of the study on its biological characteristics and human hepatitis B. Over the past several years, many transgenic lineages harbouring intact HBV gene[8] or expressing the HBV envelope, core, precore and X proteins[9] under the control of HBV or cellular liver-specific promoters have been generated, thereafter, the transgenic mouse system was applied in HBV studies[10-12]. However, no reports of transgenic mouse harbouring mutant HBV are available.

HBV belongs to hepadnavirus family, containing a small (3.2-kb), circular, double-stranded DNA genome. The minus strand includes at least four open reading frames (ORF), of which, S-ORF is divided into pres1, pres2 and s gene. HBsAg encoded by the *s* gene is the major component of hepatitis B vaccine. It is also an important diagnostic evidence of HBV infection. Hepatitis B immunoglobulin could be used to protect the liver from reinfection after liver transplantation, but it depends on the interaction of HBsAg and anti-HBs. Therefore, the change of antigenicity of HBsAg has a direct impact on the diagnosis and therapy of HBV. It is most common to find the mutation at aa145 where glycine is substituted by arginine (G145R). This mutant could result in the failure of HB vaccination[13] and failing to protect the liver from reinfection after liver transplantation[14-16]. Recently, several lines of evidence of horizontal transmission have been found[17-18]. It brings about many new problems to prophylaxis and therapy of HB. It is necessary to study further on the change of biological characteristics related with this point mutation. Transgenic mice harbouring G145R mutant are a good animal model in study of changes of antigenicity and immunogenicity as well as pathogenicity of HBV. Therefore, we generated transgenic mice harboring complete genome of HBV (*adr* subtype) G145R mutant by microinjection method, in which HBsAg and HBeAg could be expressed, and genomic DNA of HBV could be replicated and packed into complete virus particles. This model makes it possible to examine many aspects of HBV and its associated biomedical issues *in vivo*, and is an animal model for drug screen and therapy involved in this mutant.

MATERIALS AND METHODS

Reagents, Plasmid, antibodies and animals

Restriction endonucleases and T4 DNA ligase were obtained from Sangon Co. Canada. Plasmid P II was endowed by Dr. Jian-Wen He and contained overlength HBV genomes, beginning at the middle of the X gene, terminating at nucleotides 1982, just downstream of the unique polyadenylation signal in the HBV genome at a unique *Bam*HI site. Plasmid P II contained a point mutation at the site of *s* gene nt 587(G→A). HBsAg and HBeAg ELISA reagents were purchased from Abbott Laboratories and Sino-American Biotechnology Co., respectively. Mouse monoclonal antibody against HBsAg and rabbit HBc/eAg primary anti-serum were purchased from DAKO, USA. Sheep anti mouse IgG-HRP was obtained from CALBIOCHEM, Germany. Serum DNA extraction kit was got from Sino-American Biotechnology. QIA quick gene gel kit and plasmid extraction kit were purchased from QIA-gene. C57BL/6 mice were SPF level and maintained on a 14:10 light-dark schedule (lights off at 10 pm, lights on at 8 am every day).

Microinjection and embryo manipulation of founder animals

HBV transgenic mice were produced by microinjection of the *Pvu* II fragment excised from plasmid P II into C57BL/6 embryos by conventional technology. In brief, the *Pvu* II fragment containing 1.2 copy HBV DNA was gel purified and dissolved in TE buffer (10 mmol/L Tris-HCl, 0.2 mmol/L EDTA, pH 7.5) at a final concentration of 1 mg/L (2000 copies/pL). After it was injected into male pronuclei obtained from C57BL/6 females, the eggs were implanted into oviducts of pseudopregnant recipients to enable further development before term. Founder animals were screened by analysis of serum for HBsAg and HBeAg. Animals positive for both antigens were expanded by repetitive backcrossing against the C57BL/6 strain and bred for analysis.

DNA isolation and PCR analysis of integrated transgenes

To isolate the total genomic DNA, approximately one third of the tail of 10-d-old mice was cut and placed into a 1.5 mL microcentrifuge tube containing 500 μL of TB buffer. The tubes containing the tail fragments were incubated overnight at 55 ℃. DNA was extracted once with 500 μL of 1:1 (v/v) equilibrated phenol-chloroform, and precipitated with 2 volumes of ethanol. After centrifugation, precipitates were resuspended in 500 μL water.

Total tail genomic DNA (1 mg) was analyzed by PCR using HBV-specific primers (5'-CCCAA CCTCC AATCA CTCAC CAACC-3' [sense, nt 2 139 to 2 153] and 5'-GGCCC CCAAT ACCAC ATCAT CCATA -3' [antisense, nt 2 583 to 2 556]). A 20 μL of samples of the products from direct PCR amplifications was analyzed by electrophoresis on a 10 g/L agarose gel in the presence of 0.5 μg of ethidium bromide per mL. DNA bands were visualized by UV fluorescence.

Southern blot analysis

Southern blot analysis was performed on the total genomic DNA by agarose gel electrophoresis of 20 μg of restricted genomic DNA as previously described. Before electrophoresis, all DNA samples were digested with *Eco*R I at 10 U/μg for 4 h at 37 ℃. Nylon filters were hybridized with HBV-specific digoxigeninlabeled DNA probes as previously described[19].

PCR analysis of HBV DNA in serum

Total serum genomic DNA from transgenic mice was extracted according to the manufacturer's instructions, and analyzed by PCR using HBV-specific primers as described above.

Immunohistochemical analysis of the expression of HBV

In selected experiments, liver tissue derived from transgenic mouse lineages was also studied. In some experiments, mice were anesthetized with pentobarbitone (Harvest Pharmaceutical Co. LTD) prior to phlebotomy from the retro-orbital plexus and before they were sacrificed by cervical dislocation. In the other experiments, mice were anesthetized with pentobarbitone prior to biopsy of the liver at the age of 3, 6, 9, 12, 15, 18 mo. Intracellular distributions of HBcAg and HBsAg were assessed by the labeled-avidin-biotin detection procedure[20]. Briefly, paraffin-embedded sections in PBS, pH 7.4, were treated for 15 min at 37 ℃ with 30 mL/L hydrogen peroxide and washed with PBS. After the sections were blocked with normal goat serum for 30 min at room temperature, rabbit anti-HBc/eAg primary antiserum or mouse anti-HBsAg monoclonal antibody was applied at a 1:100 (HBcAg) or 1:500 (HBsAg) dilution for 12 h at 4 ℃. After washed with PBS, a secondary antiserum consisting of biotin-conjugated goat anti-rabbit or goat anti-mouse immunoglobulin G was applied at a 1:100 dilution for 30 min at 37 ℃. The antibody coated slides were washed with PBS, treated with streptavidin-horseradish peroxidase conjugates at a 1:600 dilution for 30 min at 37 ℃, stained with nitroblue tetrazolium chloride and 5-bromo-4-chloro-3-indolyl-phosphate (NBT/BCIP, MAXIN Co.), and counterstained with Mayer's hematoxylin before mounted.

Serological analysis of the expression of HBV

Transgenic mice of lineages G145R-15 and G145R-18 were anesthetized with pentobarbitone prior to phlebotomy from the retro-orbital plexus 200 μL every week. Serum was isolated by centrifugation. HBsAg and HBeAg concentrations were analyzed every month by using commercially available enzyme-linked immunosorbent assay reagents according to the manufacturer's instructions.

Serum antibody analysis of transgenic mice

Serum from transgenic mice was also assayed for anti-HBsAg, anti-HBeAg and anti-HBcAg every month by using commercially available enzyme-linked immunosorbent assay reagents according to the manufacturer's instructions.

Electron microscopy

Intracellular nucleocapsid particles were analyzed exactly as described elsewhere. Briefly, thin liver sections were fixed overnight at 4 ℃ in 40 g/L paraformaldehyde-1 g/L glutaraldehyde in PBS. Sections were then postfixed in 10 g/L OsO_4 in cacodylate buffer (pH 7.4) for 1 h at room temperature, dehydrated in gradient ethanol, and embedded in epoxy resin (TAAB 812; Emmer Green, Reading, England). Sections were cut on a LKB Ultratome III, mounted on copper grids, stained in uranyl acetate and lead citrate, and viewed with a Hitachi H-800 electron microscope.

Serum-derived virus particles were analyzed as follows. Five hundred microliters of transgenic-mouse serum was centrifuged (300 000 *g*) for 12-16 h at 4 ℃ through 2.4 mL of 100 g/L sucrose into 0.8 mL of 600 g/L sucrose. Fractions (100 μL) were collected from the bottom, and the first fraction was incubated for 45 min at room temperature on MA18/ 7-coated (100 μg/mL) Parlodion-carbon-coated nickel grids that were subsequently drained with a piece of filter paper and washed twice in PBS. The grids were then fixed in 15 g/L glutaraldehyde for 2 to 5 min, washed twice in H_2O, negatively stained with uranyl acetate, and viewed with a Hitachi H-800 electron microscope.

Histological analysis

Tissue samples were fixed in 40 g/L neutral buffered formaldehyde, embedded in paraffin, sectioned (4 μm), and stained with hematoxylin and eosin as described[8].

Biochemical evidence of hepatocellular and renal injury

Serum alanine aminotransferase (sALT), serum aspartate

aminotransferase (sAST) , blood urea nitrogen (BUN), creatinine (Cr) and γ-glutamyl transpeptidase(γ-GT) were tested with an auto-biochemical analyzer.

RESULTS

Microinjection and production of transgenic mice

Hundreds of molecules of target fragments were microinjected into male pronuclei of fertilized eggs. A total of 288 eggs survived from microinjections were transplanted into the oviducts of 13 pseudopregnant mice and consequently, the mice were pregnant and gave birth to 49 pups. In addition, 43 were survived. HBsAg and HBcAg in cytoplasm or nuclei of hepatocytes were detected in 10 mice. Two of 43 founder animals whose sera were positive for both HBsAg and HBeAg were produced and named lineages G145R-15 and G145R-18. They were expanded by repetitive backcrossing against the C57BL/6 strain and studied in detail. Sixteen F1 offsprings of lineage G145R-15 founder mice were born. Twelve of them were identified as the integration of HBV gene by PCR and Southern blot hybridization analysis of tissues. HBsAg and HBcAg were detected in eight of them by immunohistochemistry. HBsAg and HBeAg were detected in seven of them by using ELISA. Only one of eight F1 offsprings generated by lineage G145R-18 founder was survived. In addition, all above methods detected it positive. F1 offsprings were positive for both HBsAg and HBeAg and expanded by repetitive backcrossing against the nontransgenic C57BL/6.

Analysis of integrated transgenes

Total DNA was isolated from tail tissues of lineages G145R-15 and G145R-18, digested with an enzyme (*Eco*R I) that was not cut within the transgene, and analyzed by Southern blot (Figure 1).

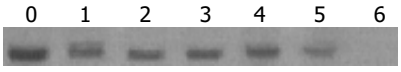

Figure 1 Southern blot analysis of 20 μg of total DNA extracted from transgenic mouse tail tissues of lineages G145R-15 and G145R-18. Lane 0: Positive control; Lane 1: lineage G145R-15; Lane 2: lineage G145R-15; Lane 3: F_1 transgenic mice of lineage G145R-15; Lane 4: F_1 transgenic mice of lineage G145R-18; Lane 5: lineage of transgenic mice harbouring prototype HBV genome; Lane 6: non-transgenic mice as negative control. All DNA samples were RNase treated before gel electrophoresis. The filters were hybridized with a digoxigeninlabeled HBV specific DNA probe.

Expression of viral proteins

At the protein level, HBsAg (a product of the 2.1-kb mRNA) and HBeAg (a product of the 3.5-kb mRNA) were easily detectable in the serum in both lineages (Table 1). As expected, HBcAg (also a product of the 3.5-kb mRNA) and HBsAg were easily detectable in the liver by immunohistochemical staining (Figures 2A, B).

Table 1 Serum HBV antigen levels

	4 wk	8 wk	12 wk	16 wk	72 wk
Normal mouse					
HBsAg[1]	0.056	0.052	0.056	0.055	0.053
HBe/cAg[2]	0.052	0.059	0.053	0.052	0.055
G145R-15					
HBsAg	0.126	0.153	0.151	0.132	0.158
HBe/cAg	0.236	0.272	0.228	0.265	0.243
G145R-18					
HBsAg	0.133	0.143	0.155	0.129	0.128
HBe/cAg	0.256	0.236	0.268	0.257	0.261

[1]Optical density (*A*) at 490 and 630 nm wavelength, cutoff value is 0.083. [2]Optical density (*A*) at 405 nm wavelength, cutoff value is 0.106.

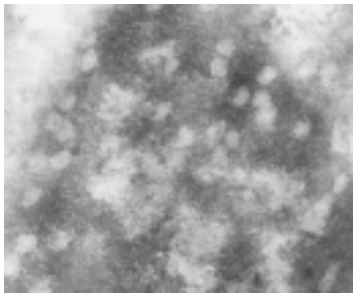

Figure 3 Ultrastructural analysis of HBcAg in the liver.

Distribution of HBcAg and HBsAg in liver

Both lineages displayed the same subcellular and architectural distribution of HBcAg in the liver. Figure 2A and 2B shows that HBcAg and HBsAg were present in the cytoplasm of almost all the hepatocytes distributed widely throughout the hepatic lobules from the centrilobular region around central veins to the periportal region around the portal tracts, but positive hepatocytes surrounding the central veins were much more than those around centrilobule. At the nucleic level, however, only HBcAg was detectable (Figure 2C). Typical 25-30 nm HBcAg particles (core particles and nucleocapsid particles) were detected in the nuclei (Figure 3). All indicated the existence of important host influences on viral gene expression in these animals.

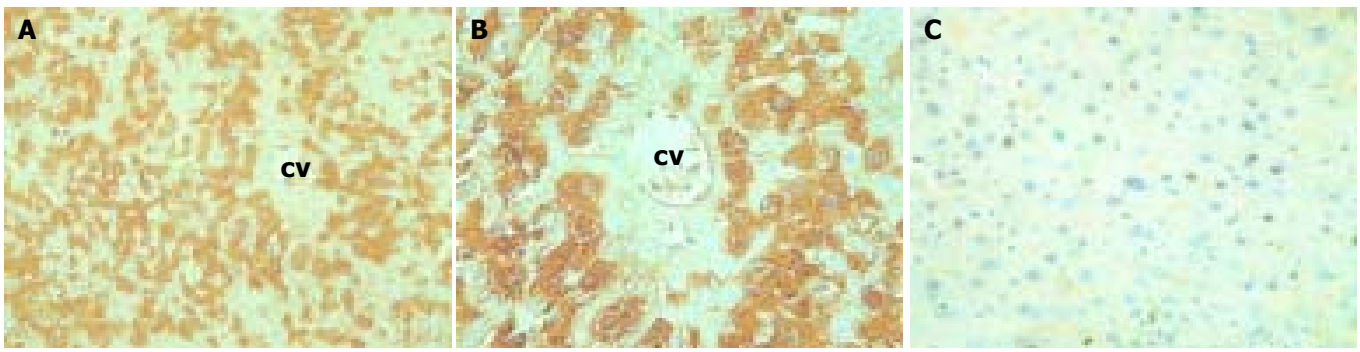

Figure 2 Immunohistochemical analysis of HBsAg and HBcAg in the liver. A: Presence of cytoplasmic HBsAg in almost all of hepatocytes in immunohistochemical analysis of the liver of an 6-week-old male mouse. Magnification, ×100. B: Cytoplasmic HBcAg in centrilobular region hepatocytes surrounding the central veins. Magnification, ×200. C: Nuclear HBcAg scattering widely throughout the hepatic lobule. Magnification, ×100.

Circulating viral particles

To determine whether potentially infectious viral particles were formed and secreted into the blood of these mice, serum was analyzed for the presence of HBV DNA and sedimentable particles displaying the ultrastructural characteristics of complete virions (Dane particles). HBV DNA was detectable in the serum of an HBV transgenic-mouse lineage that replicated the viral genome.

Histopathological findings

Animals from lineages G145R-15 and G145R-18 were monitored histologically for over eighteen months without evidence of pathological changes in the kidney, brain, spleen, lung, testis, ovaries, skin, and muscle except for the liver. In some region of the liver, swollen hepatocytes, hydropic degeneration or ballooning degeneration was observed in hepatic lobules that were distributed in the centrilobular region around central veins (Figure 4A, B). In the other, focal or unicellular necrosis, together with predominantly lymphocyte infiltrate was present (Figure 4D). In the portal or periportal tract, mild or moderate inflammation was also observed, as illustrated in Figure 4C. Interface inflammation could be observed in some cases. However, fibrosis was absent. Acidophilic body was scarce.

Serum antibody in transgenic mice

The ELISA test indicated that there was no significant positive result of HBV antibodies in HBV transgenic mouse serum.

Biochemical evidence of hepatocellular and renal injury

Animals from lineages G145R-15 and G145R-18 were monitored to have biochemical changes for over eighteen months without evidence of hepatocellular and renal injury, although there were histopathological changes in the liver.

DISCUSSION

In the study of vaccinated children whose mothers were positive for HBeAg, about 15% of them became anti-HBc positive. A proportion of these would be HBsAg positive and become the HBV carriers. About half of those were infected with variants of MHR, the most consistently observed to be G145R. Three population-based studies from Singapore, UK and USA had remarkably similar results. Mathematical modeling indicated it would be the dominant viral strain, although it could take a long time to emerge. Vaccination at birth is an ideal situation for selection of escape variants, being similar to liver transplantation, where high titer anti-HBs preparations are administered to prevent graft infection. Furthermore, naturally occurring G145R strains were reported.

To study the biological properties and pathologic conditions associated with this mutant, HBV transgenic mice whose hepatocytes expressed and replicated the virus and whose genome harbor HBV mutant G145R were produced with a terminally redundant, 1.2 genome length transgene that starts in the middle of the X gene and ends just downstream of the unique HBV polyadenylation site.

Only two of the forty-three founders were serum HBsAg-positive, and the expression level of the others was very low, which might be due to the different integrated sites of HBV DNA. In general, the exogenous gene would be integrated into multi-sites in transgenic mice. This is similar with other reports. Immunohistochemical assays of several tissues from transgenic mice revealed that HBV gene expressions were tissue-dependent, and the genes were only expressed in the liver and kidney, this is similar to HBV-infection in nature. The regulation of expression of a foreign gene in transgenic mice was subjected to different parameters, such as site of integration, influence of the mouse flanking sequences, cellular factors and structure of the integrated sequences. However, the general finding was that transgenes kept their developmental and tissue specific control of expression. Mouse genomic sequences might potentially have an influence on the level of transcription of tissue specificity. The important influence of cellular factors on expression was apparent since many hepatocytes, all the Kupffer cells, endothelial cells and bile duct epithelium in the tissue were antigen negative, although most cells in the liver probably contained integrated HBV DNA. It may be germane

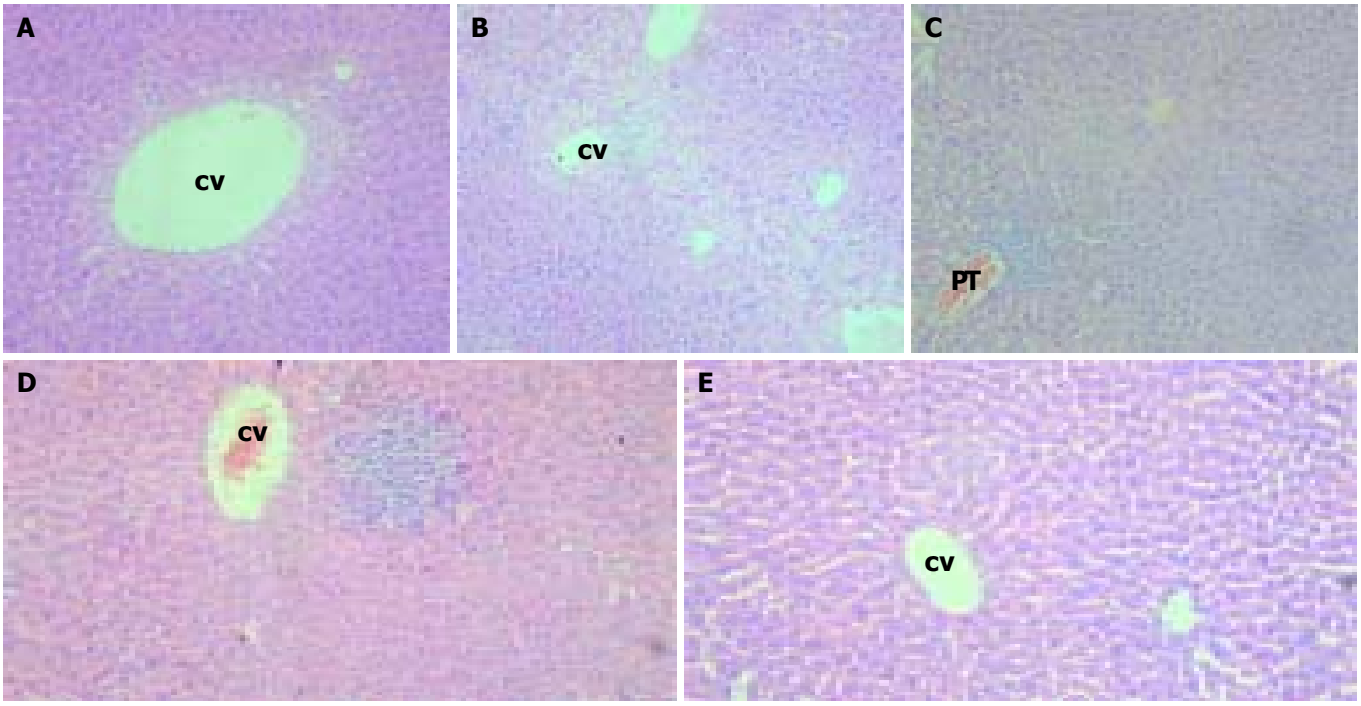

Figure 4 Analysis of pathological changes in the liver of transgenic mice by HE staining. Magnification ×100. A: Mild swollen hepatocytes around the central veins (CV) in the centrilobular region. B: "Ballooning degeneration" around the central veins or between the two central veins in the liver. C: Predominantly lymphocytic cell infiltrates in portal tract area and hepatic lobules. D: Focal necrosis and predominantly lymphocytic cell infiltrates in hepatic lobule. E: Liver of normal mice.

that hepatocyte nuclear factor 1 alpha (HNF 1 a) and retinoic acid are known to be preferentially expressed in hepatocytes. Interestingly, the positive cells were clustered like clones of cells. This was described in infected humans, and it was proposed that the synthesis of viral antigens depended on the metabolic state of cells.

HBcAg was detected both in the nuclei and in the cytoplasms of hepatocytes. The presence of HBcAg in the nuclei of hepatocytes was found in most of HBV-infected humans. Cytoplasmic location of HBcAg was also observed in some cases with active viral replication. Capsid antigens of ground squirrel hepatitis virus, duck hepatitis B virus and woodduck hepatitis virus were found almost exclusively in the cytoplasm. This may be the consequence of the constantly high level of replication of these viruses. Pre-core RNA is only used as a mRNA for the production of HBeAg that is secreted into the serum. This polypeptide can be aggregated into unstable particles but its location is in cytoplasm. Therefore, it is likely that it is responsible for the cytoplasm structure.

HBV transgenic mice showed replication of HBV in hepatocytes and had evidence of pathological lesions in the liver, which are different from other reports. Although there were some pathological characteristics of mild chronic hepatitis B in the transgenic mice, the change was obviously different from that of human chronic hepatitis B. Cellular pathological changes, such as swelling of hepatocytes and focal hepatocellular necrosis and parenchymal lymphomononuclear cell infiltrate were the main lesions. While the histological changes, such as the change or destruction of structure of hepatic lobules caused by hyperplasia of fibers, were not observed in all transgenic mice. Even fibrocytes and fibrous tissue were difficult to be observed in the portal tract, it was likely due to the difference of species. In normal mice, the borderline of hepatic lobules is not clear as that of human being's.

Serum anti-HBs, anti-HBc and anti-HBe detected by ELISA were negative in all of the transgenic mice, suggesting that these mice were tolerant to HBsAg, HBcAg and HBeAg. This result is consistent with that of another report.

What caused the pathological changes of the liver? We supposed the immune response of transgenic mice caused the pathological lesions. Some of transgenic mice were partially immunological tolerant to viral antigens. In our and another study, HBsAb could be induced by injection of HB vaccine into muscles of the HBV transgenic mice. This indicated that the immunological tolerance was not complete. We assume that although the gene of virus was integrated in the genome of mice, the time of expression of exogenous gene in thymus was a little later than the formation of immunological tolerance. Some children whose mothers were HBeAg positive did also have pathological changes in their liver, but without HBsAb in the serum.

In conclusion, HBV genome introduced by microinjection can be integrated into the mouse genome, and HBV genes can be expressed, replicated and packaged. Therefore, these lineage mutant HBV transgenic mice may be used as animal models for the study on mutant HBV and its associated biomedical issues. It can also be applied in the selection of anti-mutant HBV drugs and vaccine.

REFERENCES

1 **Merican I**, Guan R, Amarapuka D, Alexander MJ, Chutaputti A, Chien RN, Hasnian SS, Leung N, Lesmana L, Phiet PH, Sjalfoellah Noer HM, Sollano J, Sun HS, Xu DZ. Chronic hepatitis B virus infection in Asian countries. *J Gastroenterol Hepatol* 2000; **15**: 1356-1361

2 **Birrer RB**, Birrer D, Klavins JV. Hepatocellular carcinoma and hepatitis virus. *Ann Clin Lab Sci* 2003; **33**: 39-54

3 **Rabe C**, Cheng B, Caselmann WH. Molecular mechanisms of hepatitis B virus-associated liver cancer. *Dig Dis* 2001; **19**: 279-287

4 **Arbuthnot P**, Kew M. Hepatitis B virus and hepatocellular carcinoma. *Int J Exp Pathol* 2001; **82**: 77-100

5 **Brechot C**, Gozuacik D, Murakami Y, Paterlini-Brechot P. Molecular bases for the development of hepatitis B virus (HBV)-related hepatocellular carcinoma (HCC). *Semin Cancer Biol* 2000; **10**: 211-231

6 **Lee KM**, Kim YS, Ko YY, Yoo BM, Lee KJ, Kim JH, Hahm KB, Cho SW. Emergence of vaccine-induced escape mutant of hepatitis B virus with multiple surface gene mutations in a Korean child. *J Korean Med Sci* 2001; **16**: 359-362

7 **Kidd-Ljunggren K**, Miyakawa Y, Kidd AH. Genetic variability in hepatitis B viruses. *J Gen Virol* 2002; **83**(Pt 6): 1267-1280

8 **Hu YP**, Hu WJ, Zheng WC, Li JX, Dai DS, Wang XM, Zhang SZ, Yu HY, Sun W, Hao GR. Establishment of transgenic mouse harboring hepatitis B virus (adr subtype) genomes. *World J Gastroenterol* 2001; **7**: 111-114

9 **Singh M**, Kumar V. Transgenic mouse models of hepatitis B virus-associated hepatocellular carcinoma. *Rev Med Virol* 2003; **13**: 243-253

10 **Kimura K**, Kakimi K, Wieland S, Guidotti LG, Chisari FV. Activated intrahepatic antigen-presenting cells inhibit hepatitis B virus replication in the liver of transgenic mice. *J Immunol* 2002; **169**: 5188-5195

11 **Sitia G**, Isogawa M, Kakimi K, Wieland SF, Chisari FV, Guidotti LG. Depletion of neutrophils blocks the recruitment of antigen-nonspecific cells into the liver without affecting the antiviral activity of hepatitis B virus-specific cytotoxic T lymphocytes. *Proc Natl Acad Sci U S A* 2002; **99**: 13717-13722

12 **Baron JL**, Gardiner L, Nishimura S, Shinkai K, Locksley R, Ganem D. Activation of a nonclassical NKT cell subset in a transgenic mouse model of hepatitis B virus infection. *Immunity* 2002; **16**: 583-594

13 **Cooreman MP**, Leroux-Roels G, Paulij WP. Vaccine- and hepatitis B immune globulin-induced escape mutations of hepatitis B virus surface antigen. *J Biomed Sci* 2001; **8**: 237-247

14 **Fischer L**, Kalinina T, Rogiers X, Will H, Sterneck M. GLY145ARG mutation emerging under HBIG treatment in patients with recurrent HBV after liver transplantation strongly reduces viral secretion. *Transplant Proc* 2001; **33**: 3633-3636

15 **Rodriguez-Frias F,** Buti M, Jardi R, Vargas V, Quer J, Cotrina M, Martell M, Esteban R, Guardia J. Genetic alterations in the S gene of hepatitis B virus in patients with acute hepatitis B, chronic hepatitis B and hepatitis B liver cirrhosis before and after liver transplantation. *Liver* 1999; **19**: 177-182

16 **Grottola A**, Buttafoco P, Del Buono MG, Cremonini C, Colantoni A, Gelmini R, Morelli C, Masetti M, Jovine E, Fruet F, Pinna A, Manenti F, Villa E. Pretransplantation pre-S2 and S protein heterogeneity predisposes to hepatitis B virus recurrence after liver transplantation. *Liver Transpl* 2002; **8**: 443-448

17 **Oon CJ**, Chen WN, Goo KS, Goh KT. Intra-familial evidence of horizontal transmission of hepatitis B virus surface antigen mutant G145R. *J Infect* 2000; **41**: 260-264

18 **Chakravarty R**, Neogi M, Roychowdhury S, Panda CK. Pres ence of hepatitis B surface antigen mutant G145R DNA in the peripheral blood leukocytes of the family members of an asymptomatic carrier and evidence of its horizontal transmission. *Virus Res* 2002; **90**: 133-141

19 **Wang Y**, Wu MC, Sham JS, Tai LS, Fang Y, Wu WQ, Xie D, Guan XY. Different expression of hepatitis B surface antigen between hepatocellular carcinoma and its surrounding liver tissue, studied using a tissue microarray. *J Pathol* 2002; **197**: 610-616

20 **Jin YM**, Yun C, Park C, Wang HJ, Cho H. Expression of hepatitis B virus X protein is closely correlated with the high periportal inflammatory activity of liver diseases. *J Viral Hepat* 2001; **8**: 322-330

Edited by Wang XL and Ren SY **Proofread by** Xu FM

PO Box 2345, Beijing 100023, China
Fax: +86-10-85381893
E-mail: wjg@wjgnet.com www.wjgnet.com

World J Gastroenterol 2004;10(21):3146-3150
World Journal of Gastroenterology
 ISSN 1007-9327

Possibility of non-invasive diagnosis of gastric mucosal precancerous changes

Victor D. Pasechnikov, Sergey Z. Chukov, Sergey M. Kotelevets, Alexander N. Mostovov, Varvara P. Mernova, Maria B. Polyakova

Victor D. Pasechnikov, Sergey M. Kotelevets, Alexander N. Mostovov, Department of Therapy, Medical Academy, Stavropol, Russian Federation
Sergey Z. Chukov, Varvara P. Mernova, Maria B. Polyakova, Department of Pathology, Medical Academy, Stavropol, Russian Federation
Correspondence to: Professor Victor D. Pasechnikov, Aviatsionnaya street, 21, Stavropol, 355017, Russian Federation. passetchnikov@mail.ru
Telephone: +7-8652-354700
Received: 2004-03-11 **Accepted:** 2004-04-09

Abstract

AIM: To assess the possibility of non-invasive screening of atrophic chronic gastritis for preventing further development of gastric cancer.

METHODS: One hundred and seventy-eight consecutive *Helicobacter pylori* (*H pylori*)-positive dyspeptic patients after detection of serum levels of pepsinogen-1 (PG-1) and gastrin-17 (G-17) by enzyme immunoassay were proposed for endoscopy and histology. The serologic and morphologic results were compared with estimating the sensitivity, specificity and prognostic values of the tests.

RESULTS: There was statistically significant reverse dependence between the grade of stomach mucosal antral or corpus atrophy and the proper decreasing of serum G17 or PG1 levels. The serologic method was quite sensitive in the diagnosis of non-atrophic and severe antral and corpus gastritis. Also, it was characterized by the high positive and negative prognostic values.

CONCLUSION: Detection of serum G-17 and PG1 levels can be offered as the screening tool for atrophic gastritis. The positive serologic results require further chromoendoscopy with mucosal biopsy, for revealing probable progressing of atrophic process with development of intestinal metaplasia, dysplasia or gastric cancer.

Pasechnikov VD, Chukov SZ, Kotelevets SM, Mostovov AN, Mernova VP, Polyakova MB. Possibility of non-invasive diagnosis of gastric mucosal precancerous changes. *World J Gastroenterol* 2004; 10(21): 3146-3150
http://www.wjgnet.com/1007-9327/10/3146.asp

INTRODUCTION

According to the modern representations about stages of gastric carcinogenesis, it is supposed that chronic *Helicobacter pylori* (*H pylori*) infection is the trigger mechanism in 60-90% of gastric cancer cases[1,2]. In 1975, Correa proposed the consecutive line of events leading to gastric cancer development: normal mucosa - chronic active gastritis - chronic atrophic gastritis - intestinal metaplasia - dysplasia - carcinoma *in situ*. At present, this cascade of changes associates with a trigger role of *H pylori* and is called "Correa's gastric precancerous cascade"[2,3]. The early detection of gastric precancerous changes, mainly atrophic gastritis, may be helpful in prevention of gastric cancer or in diagnosis of cancer at curable stages. So, there is a critical need for valid diagnostic methods of stomach mucosal atrophy, that would be inexpensive and non-invasive, that is, suitable for screening of large groups of people.

Taking into account the known interrelations between the morphological status and functional activity of gastric corpus and antral mucosa and the secretion of, respectively, pepsinogen 1 and gastrin 17[4,5], we carried out a prospective study with the aim to detect *H pylori*-induced gastric precancerous changes, that were leading to cancer formation, and to evaluate the possibility of non-invasive screening of dyspeptic patients.

MATERIALS AND METHODS

Materials

The study was carried out in a group of dyspeptic *H pylori*-infected patients.

Methods

H pylori antibodies (Hp-Ab), serum levels of pepsinogen I (PGI) and gastrin-17 (G-17) were analyzed by enzyme immunoassay with Biohit GastroPanel® (Biohit Plc, Helsinki, Finland). According to the instructions of its manufacturer, serum levels of PG1 <25 μg/L were estimated as markers of gastric corpus atrophy, serum levels of G17 <5 pmol/L were estimated as markers of gastric antral atrophy, serum levels of G17 <10 pmol/L in a combination with serum levels of PG1 <50 μg/L were estimated as markers of mild gastric corpus atrophy. HPAb IgG titers were estimated as follows: < 32 enzyme immunoassay unit (EIU)- negative result, 32 - 44 EIU - doubtful result, >44 EIU - positive result. The numerical meanings of researched parameters were analyzed by the program GastroSoft® (Biohit Plc, Helsinki, Finland) enclosed to test-system Biohit GastroPanel®. On the basis of inserted data, the program composed the diagnosis in a view of the presence or absence of *H pylori*-infection and mucosal atrophy, with the estimation of gastric cancer or peptic ulcer risk and with recommendations on the treatment according to Maastricht-2 consensus.

After getting the GastroSoft® diagnosis, we randomized 178 patients for the following study. The patients underwent the upper gastrointestinal endoscopy with subsequent biopsy of the antral and corpus mucosa. To increase the accuracy of endoscopic diagnosis, we carried out an additional chromoendoscopy with methylene blue staining allowing the detection of foci of intestinal metaplasia (IM) of gastric mucosa which were unrecognized by routine endoscopy. Biopsy specimens were stained with hematoxylin-eosin and PAS reaction in combination with alcian blue at pH 2.5. The grade of stomach mucosal atrophy was estimated from 0 to 3 according to Houston visual analogous scale.

Statistical analysis was used to calculate the statistical significance of received data (Mann-Whitney criterion). Spearman's correlation coefficient (r_s), positive predictive value (PPV) and negative predictive value (NPV) of diagnosis by Biohit GastroPanel®.

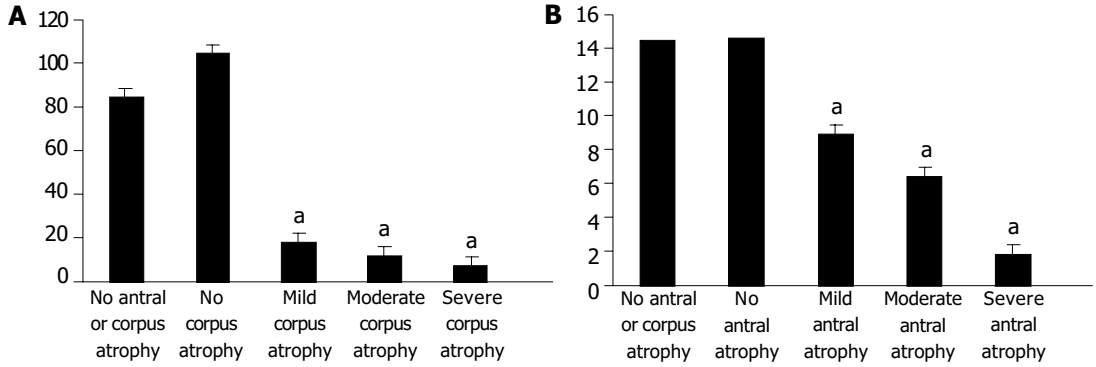

Figure 1 Comparison of serum PG1 (g/L) and G17 (pmol/L) levels and grade of gastric corpus and antral atrophy. A: Comparison of serum PG1 level and grade of gastric corpus atrophy. B: Comparison of serum G17 level and grade of gastric antral atrophy. [a]*P*<0.05 *vs* non-atrophic state.

RESULTS

Of the 178 patients, non-atrophic chronic gastritis (no antral atrophy and no corpus atrophy) was detected only in 5 patients. The mean of serum PG-1, G-17 and anti-*H pylori* IgG in this group was 85.28±35.07 μg/L, 14.44±1.90 pmol/L and 85.68±17.81 EIU, respectively. In all these cases there was no IM or dysplasia in stomach mucosal epithelium.

The morphological status of gastric corpus mucosa was compared with serum PG-1 levels (Figure 1A). The non-atrophic corpus mucosa was detected in 99 (55.62%) of 178 patients, mild atrophy of corpus mucosa was detected in 17 (9.55%) patients, moderate atrophy of corpus mucosa was detected in 36 (20.22%) patients, severe atrophy of corpus mucosa was detected in 26 (14.61%) patients.

The statistical analysis revealed that there were marked differences between the levels of PG1 in non-atrophic and atrophic corpus gastritis. The levels of PG1 in mild, moderate and severe corpus atrophy were significantly lower (P<0.0001) than those in non-atrophic state. In turn, the levels of PG1 in mild, moderate and severe corpus atrophy were significantly different from each other (P<0.0001).

The morphological status of gastric antral mucosa was compared with serum G-17 levels (Figure 1B). The non-atrophic antral mucosa was detected in 12 (6.74%) of 178 patients. Mild atrophy of antral mucosa was detected in 31 (17.42%) patients. Moderate antral mucosa atropy was detected in 69 (38.76%) patients. Severe antral mucosal atrophy was detected in 66 (37.08%) patients.

The statistical analysis revealed that there were marked differences between the levels of G17 in non-atrophic and atrophic antral gastritis. The latter was significantly lower (P<0.0001). Moreover, the levels of G17 in mild, moderate and severe antral atrophy were significantly different from each other (P<0.0001).

Table 1 Comparison of serum anti-*H pylori* IgG titers (mean±SD) and grade of mucosal atrophy

	Anti-*H pylori* IgG, EIU
No antral or corpus atrophy	85.68±17.81
No antral atrophy	62.29±12.02
Mild antral atrophy	78.25±5.86
Moderate antral atrophy	74.08±4.39
Severe antral atrophy	73.38±5.38
No corpus atrophy	68.76±8.35
Mild corpus atrophy	77.21±6.13
Moderate corpus atrophy	76.47±5.04
Severe corpus atrophy	72.61±4.72

Both antral and corpus stomach mucosal atrophy were not accompanied with statistically significant changes in anti-*H pylori* IgG serum titers (Table 1).

We detected intestinal metaplasia in 119 of 178 patients. The comparison of the grade of IM and the serum levels of PG-1 and G-17 showed the absence of invariables and statistically significant dependence between these parameters, except for the cases of moderate IM (Table 2).

Dysplasia of stomach mucosal epithelium was detected in 113 patients. We revealed the statistically significant dependence between the grade of dysplasia and the increased serum levels of PG-1, and the decreased levels of G-17 (Table 3), except the cases of severe dysplasia where the number of patients was not quite sufficient (6 subjects).

Table 2 Comparison of serum PG1 and G17 levels (mean±SD) and grade of IM

	No IM	Mild IM	Moderate IM	Severe IM
PG-1, μg/L	52.5±7.74	66.07±8.36	82.65±10.72[a]	53.08±12.24
G-17, pmol/L	6.79±0.55	5.48±0.50	4.73±0.67[a]	5.11±1.02

[a]*P*<0.05 *vs* non-metaplastic state.

Table 3 Comparison of serum PG1 and G17 levels (mean±SD) and the grade of dysplasia

	No dysplasia	Mild dysplasia	Moderate dysplasia	Severe dysplasia
PG-1, μg/L	33.6±5.41	79.98±7.92[a]	84.41±10.98[a]	71.88±27.25
G-17, pmol/L	7.37±0.46	5.28±0.50[a]	3.73±0.66[a]	4.53±1.95

[a]*P*<0.05 *vs* non-dysplastic state.

Among the 178 consecutive patients we detected 6 cases of gastric cancer: 2 early cancers and 4 progressed tumors. The mean of serum PG-1, G-17 and anti-*H pylori* IgG in these cases was 46.73±22.25 μg/L, 4.78±2.086 pmol/L and 89.5±11.7 EIU, respectively.

In general, our results showed that there was a statistically significant dependence between the presence and severity of stomach mucosal atrophy (antral or corpus) and the proper serologic markers (G17 or PG1) in *H pylori*-associated chronic gastritis. On the other hand, the presence and degree of IM did not correspond to the serum level of G17 or PG1. Thus, the serologic screening by means of Biohit GastroPanel® was useful for the selection of patients with stomach mucosal atrophy by subsequent thorough endoscopical and histological examination for the possible development of precancerous or malignant changes in stomach mucosa.

Table 4 Correlations between results of different methods in diagnosis of gastric mucosal changes

Parameters	r_s
Detection of IM by endoscopy and histology	0.41
Detection of IM by chromoendoscopy and histology	0.92
Detection of antral atrophy by histology and serum levels of G-17	-0.75
Detection of corpus atrophy by histology and serum levels of PG-1	-0.71
Degree of stomach mucosal atrophy and IM	0.21
Degree of stomach mucosal atrophy and dysplasia	0.23
Degree of IM and dysplasia	0.41

Table 5 Sensitivity (Se) and specificity (Sp), PPV and NPV of Biohit GastroPanel® in diagnosis of antral mucosal atrophy

Degree of antral atrophy (by histology)	Se (%)	Sp (%)	PPV (%)	NPV (%)
No	83	95	53	99
Mild	61	84	45	91
Moderate	67	90	81	81
Severe	89	99	98	94

Table 6 Sensitivity (Se) and specificity (Sp), PPV and NPV of Biohit GastroPanel® in diagnosis of corpus mucosal atrophy

Degree of corpus atrophy (by histology)	Se (%)	Sp (%)	PPV (%)	NPV (%)
No	92	97	98	91
Mild	71	92	48	97
Moderate	72	96	81	93
Severe	88	97	82	98

Table 7 Sensitivity (Se) and specificity (Sp), PPV and NPV of routine endoscopy and chromoendoscopy in diagnosis of intestinal metaplasia (IM)

	Routine endoscopy				Chromoendoscopy			
	Se (%)	Sp (%)	PPV (%)	NPV (%)	Se (%)	Sp (%)	PPV (%)	NPV (%)
No	98	6	35	86	94	99	98	97
Mild	4	98	50	68	88	88	79	94
Moderate	no data	no data	no data	no data	71	95	80	92
Severe	6	99	33	89	82	98	82	98

Furthermore, we compared the results of the serology, endoscopy and histology by Spearman's correlation coefficient. As shown in Table 4, the correlation between the results of routine endoscopy and histology was positive, but obviously weaker than the correlation between the results of chromoendoscopy and histology. As it was expected, there was a strong reverse correlation between the presence and degree of stomach mucosal atrophy and the serum levels of proper markers of its functional activity. The correlation between the degree of stomach mucosal atrophy and the subsequent morphological changes of mucosa - IM and dysplasia, was positive but quite weak.

The levels of sensitivity and specificity, PPV and NPV of Biohit GastroPanel® in diagnosis of stomach mucosal atrophy are presented in Tables 5 and 6.

Thus, the investigated non-invasive method was quite sensitive in the diagnosis of non-atrophic and severe antral and corpus gastritis. Also, this method was characterized by the high PPV and NPV (except the cases of mild stomach mucosal atrophy).

Finally, we carried out the comparison of sensitivity and specificity, PPV and NPV for routine endoscopy and chromoendoscopy in the diagnosis of IM (Table 7).

As a result, we established the obvious advantage of a method of chromoendoscopy in the diagnosis of IM, that had doubtless diagnostic importance in revealing precancerous changes of gastric mucosa.

DISCUSSION

Chronic *H pylori* gastritis eventually could lead in more than half of the affected subjects to a gradual loss of glandular structures with its specialized cells and a collapse of the reticulin skeleton of the mucosa, a condition of atrophic gastritis[8]. As a result, the glandular layer of the mucosa became thinner, and glands were replaced by fibrosis and intestinal metaplasia. The major clinical importance of this condition was that it could significantly increase the risk for the intestinal type of gastric cancer. This risk might be elevated up to 90- fold in subjects with severe atrophic gastritis throughout the complete stomach[9]. The annual incidence of gastric cancer among patients with atrophic gastritis varied in cohort studies between 0.3 and 1.0%[10]. This could explain the interest in the diagnosis of atrophic gastritis. At present, there is a wide circle of questions related to the diagnosis of critical stages of gastric carcinogenesis - gastric epithelial atrophy, intestinal metaplasia and dysplasia. Therefore, it is extremely important to recognize dyspeptic patients who have very high risk of gastric malignant changes and require dynamic surveillance with the purpose of early revealing of the preneoplastic changes in stomach mucosa. Atrophic gastritis is a serious disease, which often does not receive much attention. The relationship between gastritis, atrophic gastritis and other diseases of the stomach is based on the fact that infection and atrophy could alter the physiological functions of the stomach[11] and influence the growth and growth control of epithelial cells in the stomach. These consequences varied depending on whether the changes of the gastric mucosa caused by gastritis were located in the antrum or the corpus or both.

The most accurate diagnostic method of gastrointestinal tract diseases is endoscopy with subsequent biopsy, which should be made in all patients with the presence of clinical symptoms. However, because of patchy characteristics of atrophic changes in stomach mucosa, some histological researches could give false - negative results. Besides, biopsy was an expensive and labor-consuming method of research[12], so it could not be carried out for all patients in succession. Contrarily, due to invasiveness of biopsy, it is expedient to make only for monitoring precancerous changes in stomach mucosa. For the selection of patients recommended to biopsy, the presence of a screening method is necessary. Such a method should be capable of reflecting objectively the functional condition of stomach mucosa and its morphological status.

It has been known for over two decades that atrophic gastritis of the corpus and fundus of the stomach can be determined reliably by measuring the serum level of pepsinogen I (PGI) or the PGI/PGII ratio from a blood sample[13-15]. However, it has not been possible to determine from a blood sample the types of atrophic gastritis in which the atrophic changes are located solely in the antrum. The GastroPanel® serum test also enables the determination of atrophic gastritis of this antrum-limited subtype.

Group I pepsinogens are synthesized solely in the oxyntic glands and mucous neck cells of the gastric corpus. On the other hand, however, pepsinogens of group II are uniformly formed in the glands of the entire stomach and to some extent also in the Brunner glands in the first part of the duodenum.

The majority of pepsinogens are secreted into the lumen of the stomach where they are metabolized into an active pepsin. A small proportion of the pepsinogens leak for one reason or another into the blood circulation. In case of atrophic corpus gastritis, the level of serum pepsinogen I decreases whereas the level of pepsinogen II remains stable or decreases slightly. The level of serum pepsinogen I or the ratio of serum pepsinogen I to pepsinogen II could reflect with high reliability the number of cells and oxyntic glands in the corpus area of the stomach, i.e., they could reflect the degree of atrophy of the corpus mucosa[14-16]. As the severity of atrophic corpus gastritis corpus increases, the level of serum pepsinogen I or the PGI/PGII ratio decreases.

Gastrin is synthesized in G-cells, which are found in the gastric antrum. The gastrin secreted by the antrum is over 90% of type G-17 whereas the gastrin secreted by the duodenum is primarily type G-34. The fasting serum gastrin is primarily in the form of G-34 but the proportion of type G-17 increases after the dietary stimulus. The secretion of gastrin-17 can be studied with a simple protein stimulation test. First, a blood sample is taken after fasting, after which the patient eats a protein-rich meal. The maximum increase in the level of gastrin-17 can be seen in the serum within 20 min. If the serum gastrin does not increase as a result of protein or other physiological stimulation it is an indication of the loss of gastrin secreting G cells, i.e., an indication of the atrophy of the antrum mucosa. It is possible to make indirect conclusions of the status of the antrum mucosa by simultaneously assaying the serum gastrin and acid output[17]. In the cases with atrophic antral gastritis and loss of antral G cells, serum gastrin remains low although the stomach is achlorhydric or hypochlorhydric.

Several research groups have renewed the interest in serology for atrophic gastritis by combining gastrin and pepsinogens with *H pylori* serology. In this issue, Väänänen and colleagues presented a smart algorithm for the differentiation in both antrum and corpus between atrophic and non-atrophic gastritis[18]. The algorithm was tested in a cross-sectional study correlating gastric mucosal histology with *H pylori* IgG serum antibodies, serum PGI levels, and fasting and postprandial serum gastrin-17 levels. It appeared that in roughly 80% of the 404 cases tested, histology and serology matched a similar diagnosis. Sixty (15%) of the 404 subjects had atrophic gastritis, 6 (1%) had previously undergone antral resection, and 340 (84%) had a non-atrophic gastric mucosa either with or without inflammation. In this population with a rather low prevalence of atrophic gastritis, the negative predictive value of the serology panel was 93-97% and the positive predictive value was 64-75%. For these calculations, the authors combined all subjects with atrophic gastritis of the antrum, the corpus, or both. The data, however, showed that the serology panel performed much better in diagnosing atrophic gastritis in the corpus than in the antrum. Only 19 (50%) of the 38 patients diagnosed by serology as having antrum atrophic gastritis had this condition confirmed by histology. This revival of interest in the serological testing of the condition of the gastric mucosa is of importance, given the fact that *H pylori* eradication may cure gastritis and help to prevent further progression of gland loss. It is likely that this might also reduce the risk for gastric cancer[19], although many more data on this are needed. Screening and treatment of *H pylori* infection might in theory be cost-effective for the prevention of gastric cancer[12].

Sipponen *et al*.[20] have recently shown that simultaneous detection of serum concentrations of PG1 and G17 and HPAb titers is an effective method for non-invasive screening and diagnosis of atrophic gastritis using blood samples of the patients.

In our present research, the use of the test - system GastroPanel® allowed to receive statistically significant differences between the serum concentrations of PG1 and G17 depending on a degree of stomach mucosal atrophy. We obtained the very satisfactory means of the PPV and NPV of GastroPanel® test in revealing the atrophic state of stomach mucosa. Moreover, this test was sufficiently sensitive and specific as it was proven by chromoendoscopy and histology.

Thus, our study confirmed the usefulness of the test - system GastroPanel® as a "serologic biopsy" for authentic and non-invasive diagnosis of atrophic changes of stomach mucosa in patients with dyspepsia associated with *H pylori* - infection. Besides, we managed to show the advantage of a chromoendoscopy method prior to routine endoscopy in the diagnosis of intestinal metaplasia. Now is the time, almost a decade after the conclusion of the World Health Organization (WHO) about *H pylori* as a class I carcinogen[21], to use this serology for further studies in selected and general populations. This will allow evaluation of the feasibility of screening and treatment for gastritis and prevention of gastric cancer.

In conclusion, the noninvasive detection of gastric mucosal atrophy by means of enzyme immunoassay with assessment of G-17 and PG1 levels can be offered as the screening tool for gastric precancerous conditions. On the other hand, this method does not allow to diagnose intestinal metaplasia and cancer development in stomach mucosa. Therefore, the results of serological screening indicating the stomach mucosal atrophy require carrying out the chromoendoscopy with subsequent mucosal biopsy, for revealing probable progressing of atrophic process with development of intestinal metaplasia, dysplasia or gastric cancer.

REFERENCES

1 **Malfertheiner P**, Megraud F, O'Morain C, Hungin AP, Jones R, Axon A, Graham DY, Tytgat G. Current concepts in the management of *Helicobacter pylori* infection - The Maastricht 2 Concensus Report. *Aliment Pharmacol Ther* 2002; **16**: 167-180

2 **Correa P**. Human gastric carcinogenesis: a multistep and multifactorial process. First american cancer society award lecture on cancer epidemiology and prevention. *Cancer Res* 1992; **52**: 6735–6740

3 **Correa P**. A human model of gastric carcinogenesis. *Cancer Res* 1988; **48**: 3554–3560

4 **Kiyohira K**, Yoshihara M, Iio M, Haruma K, Tanaka S, Chayama K. Serum pepsinogen concentration as a marker of *Helicobacter pylori* infection and the histologic grade of gastritis; evaluation of gastric mucosa by serum pepsinogen levels. *J Gastroenterol* 2003; **38**: 332-338

5 **Sipponen P**, Ranta P, Helske T, Kääriäinen I, Mäki T, Linnala A, Suovaniemi O, Alanko A, Härkönen M. Serum levels of amidated gastrin-17 and pepsinogen I in atrophic gastritis. An observational case-control study. *Scand J Gastroenterol* 2002; **37**: 785-791

6 **Murray CJ**, Lopez AD. Mortality by cause for eight regions of the world: global burden of disease study. *Lancet* 1997; **349**: 1269–1276

7 **Correa P**, Haenszel W, Cuello C, Tannenbaum S, Archer M. A model for gastric cancer epidemiology. *Lancet* 1975; **2**: 58–60

8 **Kuipers EJ**, Uyterlinde AM, Pena AS, Roosendaal R, Pals G, Nelis GF. Long term sequelae of *Helicobacter pylori* gastritis. *Lancet* 1995; **345**: 1525–1528

9 **Sipponen P**, Kekki M, Haapakoski J, Ihamaki T, Siurala M. Gastric cancer risk in chronic atrophic gastritis: statistical calculations of cross-sectional data. *Int J Cancer* 1985; **35**: 173-177

10 **Kuipers EJ**. Review article: relationship between *Helicobacter pylori*, atrophic gastritis and gastric cancer. *Aliment Pharmacol Ther* 1998; **12**(Suppl 1): S25–36

11 **Varis K**, Ihamäki T, Härkönen M, Samloff IM, Siurala M. Gastric morphology, function, and immunology in first-degree relatives of probands with pernicious anemia and controls. *Scand J Gastroenterol* 1979; **14**: 129–139

12 **Parsonnet J**, Harris RA, Hack HM, Owens DK. Modelling cost-

effectiveness of *Helicobacter pylori* screening to prevent gastric cancer: a mandate for clinical trials. *Lancet* 1996; **348**: 150

13 **Miki K**, Ichinose M, Ishikawa KB. Clinical application of serum pepsinogen I and II levels for mass screening to detect gastric cancer. *Jpn J Cancer Res* 1993; **84**: 1086–1090

14 **Yoshihara M**, Sumii K, Haruma K, Kiyohira K, Hattori N, Kitadai Y, Komoto K, Tanaka S, Kajiyama G. Correlation of ratio of serum pepsinogen I and II with prevalence of gastric cancer and adenoma in Japanese subjects. *Am J Gastroenterol* 1998; **93**: 1090–1096

15 **Kekki M**, Samloff IM, Varis K, Ihamäki T. Serum pepsinogen serum and I gastrin in screening of severe atrophic corpus gastritis. *Scand J Gastroenterol* 1991; **186**: 109–116

16 **Varis K**, Sipponen P, Laxen F, Samloff IM, Huttunen JK, Taylor PR, Heinonen OP, Albanes D, Sande N, Virtamo J, Harkonen M. Implications of serum pepsinogen I in early endoscopic diagnosis of gastric cancer and dysplasia. Helsinki Gastritis Study Group. *Scand J Gastroenterol* 2000; **35**: 950–956

17 **Sipponen P**, Valle J, Varis K, Kekki M, Ihamäki T, Siurala M. Fasting levels of serum gastrin in different functional and morphological states of the antro-fundal mucosa. An analysis of 860 subjects. *Scand J Gastroenterol* 1990; **25**: 513–519

18 **Väänänen H**, Vauhkonen M, Helske T, Kääriäinen I, Rasmussen M, Tunturi-Hihnala H, Koskenpato J, Sotka M, Turunen M, Sandstrom R, Ristikankare M, Jussila A, Sipponen P. Non-endoscopic diagnosis of atrophic gastritis with a blood test. Correlation between gastric histology and serum levels of gastrin-17 and pepsinogen I: a multicentre study. *Eur J Gastroenterol Hepatol* 2003; **15**: 885–891

19 **Chun Y**, Wong B, Lam SK, Wong WM, Zheng T, Chen J, Chen B. Eradicating *Helicobacter pylori* infection in general population prevents gastric cancer: a 7-year prospective randomized placebo-controlled study. *Gastroenterology* 2002; **122** (Suppl 1): A588

20 **Suovaniemi O**, Harkonen M, Paloheimo L, Sipponen P. GastroPanel: diagnosing atrophic gastritis from serum – providing a tool for evidence-based medicine. Business Briefing: *Global Health Care* 2003: 1-4

21 International Agency for Research on Cancer. IARC monographs on the evaluation of carcinogenic risks to humans. Vol. 61: Schistosomes, liver flukes and *Helicobacter pylori*. *Lyon: IARC* 1994

Edited by Wang XL **Proofread by** Xu FM

PO Box 2345, Beijing 100023, China
Fax: +86-10-85381893
E-mail: wjg@wjgnet.com www.wjgnet.com

World J Gastroenterol 2004;10(21):3151-3156
World Journal of Gastroenterology
 ISSN 1007-9327

• BASIC RESEARCH •

Role of soluble Fas ligand in autoimmune diseases

Ning-Li Li, Hong Nie, Qi-Wen Yu, Ji-Ying Zhang, An-Lun Ma, Bai-Hua Shen, Li Wang, Jun Bai, Xue-Hua Chen, Tong Zhou, Dong-Qing Zhang

Ning-Li Li, Hong Nie, Qi-Wen Yu, Ji-Ying Zhang, An-Lun Ma, Bai-Hua Shen, Li Wang, Jun Bai, Dong-Qing Zhang, Department of Immunology, Shanghai Second Medical University, Shanghai Institute of Immunology, Shanghai 200025, China
Xue-Hua Chen, Department of Surgery, Shanghai Ruijin Hospital, Shanghai 200025, China
Tong Zhou, Department of Nephrology, Shanghai Ruijin Hospital, Shanghai 200025, China
Supported by Grant From Science and Technology Development Foundation of Shanghai High Education Committee, No. 98ZD35 (to Ning-Li Li), and No.S990202 (to Dong-Qing Zhang)
Correspondence to: Dong-Qing Zhang, Shanghai Second Medical University, Shanghai Institute of Immunology, Shanghai 200025, China. dqzhang13@sh163.net
Telephone: +86-21-64453149 **Fax:** +86-21-64453049
Received: 2003-12-23 **Accepted:** 2004-01-15

Abstract

AIM: To investigate the role of soluble Fas ligand in autoimmune diseases.

METHODS: RT-PCR was performed to amplify sFasL cDNA from the total RNA extracted from activated human peripheral blood lymphocytes. DNA fragments were cloned into PCR vector. After sequenced, sFasL gene fragments were inserted into pQE-31 vector and expressed in *E. Coli* M15 respectively. Proteins were purified through affinity chromatography column with ligand of 6×His tag and identified by SDS-PAGE and Western blot. Mice were immunized with sFasL protein and specific anti-serum was harvested 6 wk after immunization. Monoclonal anti-human FasL antibody was made from the immunized mice. Serum level of sFasL in different patients was detected using anti-FasL antibodies from the immunized mice.

RESULTS: The protein expressed was 24 ku by SDS-PAGE electrophrosis. The protein was specially bound to anti-human FasL antibody by Western blot analysis. The sFasL protein could induce Jurket cell apoptosis *in vitro*. The concentration of serum sFasL in patients with autoimmune diseases was higher than that in normal individuals. sFasL could reduce arthritis in collagen induced arthritis (CIA) mice model by subcutaneous injection.

CONCLUSION: sFasL may be involved in either induction of apoptosis or autoimmune diseases. Furthermore, sFasL may have potential application in treatment of autoimmune diseases.

Li NL, Nie H, Yu QW, Zhang JY, Ma AL, Shen BH, Wang L, Bai J, Chen XH, Zhou T, Zhang DQ. Role of soluble Fas ligand in autoimmune diseases. *World J Gastroenterol* 2004; 10 (21): 3151-3156
http://www.wjgnet.com/1007-9327/10/3151.asp

INTRODUCTION

Autoimmune diseases are a kind of diseases induced by auto-reactive T or B cells. Most common autoimmune diseases include rheumatoid arthritis (RA), insulin-dependent diabetes mellitus (IDDM), multiple sclerosis (MS) and systemic lupus erythematosus (SLE). Among these diseases, RA, IDDM and MS are believed to be autoimmune diseases induced by Th1 cells which can recognize auto-antigens on special tissues. For example, RA is a common disease characterized by the chronic lesion of polyarthritides. Autoimmunity to cartilage antigens may play a significant role in the pathogenesis of chronic inflammatory polyarthritis. It has been commonly accepted that cell mediated immune responses are involved in chronic inflammation since T and B lymphocytes and antigen presenting cells are observed to be enriched in the synovium fluid of RA patients. *In vivo* studies showed that T cells infiltrating into the synovium could express IL-2 receptors, IL-10, IFN-γ and activated CD4 T cells could be detected in the synovial fluid of RA patients[1,2]. It is believed that if auto-reactive T cells can be cleaned from circulation or RA can be located, the lesion induced by auto-reactive T cells may relieve. Actually, anti-TNF-α and anti-CD4 monoclonal antibodies have been used in treatment of RA patients.

In this study, we reported that sFasL proteins were expressed in *E. Coli* system. Anti-FasL antibodies were prepared in the mice using expressed FasL. Meanwhile, we set up a special ELISA method to identify sFasL molecules and its content in the serum of patients with RA, IDDM, MS and SLE. We also tried to use sFasL made in our lab oratory to treat collagen induced arthritis in this study.

MATERIALS AND METHODS

Blood samples and reagents

Fresh blood samples were supplied by healthy individuals. PHA was purchased from Sigma Com. San Diego, USA) IPTG and plasmid mini-prep Kit were products of Promega (Chicago, USA). DNA purification kit, Histidine resin, sequencing vector PCR2.1 and protein expression vector pQE-31 were purchased from QIAGEN (San Diego, USA). Rabbit anti-human FasL polyclonal antibody was purchased from Santa Cruz (Swedeen). Goat anti-rabbit IgG/HRP was purchased from Huamei (Shanghai, China). Nitofible membrane was purchased from Amersham (London, England). Trizol, dNTP, restricted enzymes were purchased from Gibco BRL (San Diego, USA) and MBI Fermentans (Philadophia, USA).

Activation of lymphocytes

Peripheral blood monocytes (PBMC) were isolated from blood from healthy individuals with Ficoll. PBMC were re-suspended in 100 mL/L fetal calf serum RPMI 1640 and incubated at 37 ℃ in bumidified atomosphere containing 5 mL/L CO_2 for 24 h. PHA (20 μg/mL) was added into the culture and incubated for another 8 h.

Identification of sFasL expression

sFasL expression on the cell surface was detected by direct influoroscense labeling with cytometry. Briefly, activated lymphocytes were collected and washed with PBS. FITC-labeled goat anti-human FasL (Oncogen Company, LA, USA) was added into the cells and incubated on ice for 30 min. The labeled

cells were washed with PBS and expression of FasL on the cell surface was detected by FACS. The percentage of expression of FasL was analyzed using system software II.

Amplification of gene fragments of sFasL

Total RNA was isolated from cells in which sFasL expression was enhanced and reversed into cDNA. sFasL gene fragments were amplified from cDNA template by special primers. sFasL: the sequence of forward primer was: 5'-ACG GAT CCG CAG CAG CCT TCA ATT A CC-3'; reverse primer: 5'-AAG CCG AAT ATA TTC GAG ATT AAG CTT CGC CG-3'. The size of sFasL fragments amplified from cDNA was 540 bp.

sFasL cloning and expression

PCR bands were cut and purified with gel extraction kit (QIAGEN). The purified PCR products were inserted into PCR 2.1 vector and DH 5α (*E. Coli*) was transfected with TA cloning kit (Invitrogen) according to the manufacturers introductions. White clones were picked up on selected LB plates containing ampcillin and X-gel and expensed in 3 mL of LB medium overnight. Plasmids were prepared from the culture with mini-prep Kit (Promega). The positive clones were identified by *Eco*R I digested and sequenced by Shanghai South Gene Tech Ltd. The identified sFasL fragments were digested by *Bam*HII and *Hin*d III and purified by gel extraction kit. The purified sFasL fragments were ligated into the expression vector pQE-31 and M15 (*E. Coli*) was transfected. White clones were picked up on selected LB plates containing Kanamycin and expensed in 3 mL of LB medium overnight and inoculated in 200 mL of selected LB medium containing Kanamycin until *A* reached to 0.7. A 1 mol/L of IPTG was added to culture and shaken for another 4 h. Bacteria were collected by spinning at 6 000 r/min for 10 min and lyzed in lysis buffer. Protein expressed was purified by His Tag resin.

Identification of expressed sFasL

sFasL expressed was identified by SDS-PAGE electrophrosis and Western blot. sFasL showed a single band with M_r 24 000 respectively after running from SDS-PAGE (120 g/L concentrated gel and 40 g/L separated gel). The sFasL bands were transferred onto membranes and blocked with 50 mL/L of free fat milk for 2 h at room temperature. The membranes were washed 3 times with PBS. The rabbit anti-human sFasL polyclonal antibody was added and incubated for 1 h at room temperature. Goat anti-rabbit IgG-HRP was added and incubated for another 1 h at room temperature after washed with PBS. DAB and H_2O_2 were added and the reaction was stopped by washing the membranes with water when brown color was visible.

Detection of apoptosis

sFasL (25, 50 and 100 μg/L) was added into 1×10^8/L of Jurket cell lines respectively and incubated for 8 h at 37 ℃ in humidified atomosphere containing 5 mL/L CO_2. The cells were collected and fixed by 700 mL/L ethanol for 45 min at 4 ℃. Ten μL of RNase was added to the fixed cells after washed with PBS and incubated for 30 min at 37 ℃. Then 10 μL of PI (50 mg/mL) was added to the cells and detected by cytometry. The percentage of apoptotic cells was calculated by apoptotic peak (A_0) area.

Preparation of mouse anti-human sFasL antibody

Two Balb/C mice were immunized with 80 μg of expressed sFasL mixed with complete Frund's adjuvent by injection with s.c on back. The mice were injected three times with sFasL, once every two weeks. Then blood was collected and anti-FasL titer was measured with ELISA.

Induction of collagen-induced arthritis in Wistar rats

Wistar rats were bred under pathogen-free conditions . Female mice were used at 2-3 mo of age and allowed free access to standard laboratory diet and water. Collagen II (CII) emulsion was prepared in an equel volume of IFA. A 100 μL (containing 300 μg of CII) of CII/IFA emulsion was intradermally injected, using the loose skin at the base of the tail. Seven days later, the primary immunization was administered, a booster intradermal injection containing 100 μg of CII in IFA. The rats were observed every day from the 4th wk after primary immunization. Arthritis was evaluated with standard 4 scores.

Administration of arthritis rats with sFasL

When arthritis occurred in rats immunized with CII/IFA, 1 μg of sFasL expressed in 100 μL of PBS was injected into one ankylosis side. Meanwhile 100 μL of PBS was injected into another ankylosis side of same arthritis rats as control. The injection was given three times, once every two days.

Detection of serum sFasL concentration using prepared mouse anti-human FasL antibody

Serum level of soluble FasL in different patients was detected with indirect ELISA. The ELISA plate was coated with 100 μL of serum and incubated overnight at 4 ℃. The coated plate was completely washed with PBS and prepared mouse anti-human FasL antibody was added. Rabbit anti-mouse IgG-HRP was then added and incubated for another 1 h at room temperature after washed with PBS. DAB and H_2O_2 were added and the reaction was stopped by washing the membranes with water when brown color was visible.

RESULTS

Enhanced expression of FasL on PMBC after PHA activation

PBMC was isolated from healthy individuals FasL was expressed on the cell surface after activated with PHA. The expression of FasL in PBMC was significantly higher after activated. The percentage of FasL detected on the non-activated PBMC was very low (2.15±1.7%), while FasL expressed on the activated PBMC reached 17.98±1.8% using cytometry detection after cells were labeled with specific fluorescence anti-human FasL antibody (Figuer 1).

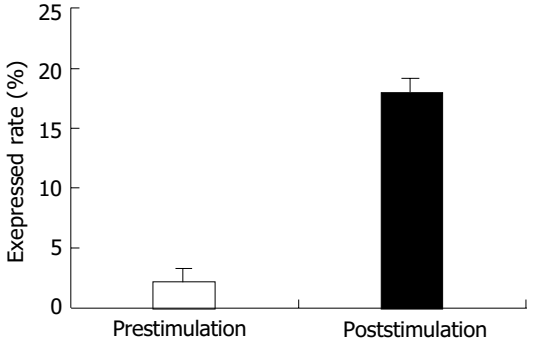

Figure 1 Peripheral blood mononuclear cells isolated from healthy individuals using Ficoll and co-cultured with PHA for 8 h at 37 ℃ in humidified atmosphere containing 50 mL/L CO_2. The expression of FasL on PBL before and after PHA stimulation was detected by special antibody using flow cytometer. Open bar indicates the percent of FasL on cells surface before PHA activation. Shadow bar shows the percent of FasL on cell surface after PHA stimulation.

Human sFasL cloning and expression

Human sFasL DNA fragments were amplified from activated PBMC using RT-PCR. The size of PCR product was 540 bp (Figure 2) which matched the size reported in the GenBank. The product was inserted into PCR2.1 vector and DH5α was

successfully transfected. The insert was confirmed by digestion with *Eco*R I after plasmid was miniprepared. The fragments were separated with a 3.9 kb vector. This result showed that sFasL (Figure 3) fragments were successfully inserted into the vector. The sequences of the inserted fragments were same as reported by GenBank after sequenced with 377 Sequencer. Identified fragments were digested by both *Bam*HI and *Hind* III and ligated into the expression vector pQE-31. The ligated products were put on selected LB plates after M15 was transfected and incubated for 18 h at 37 ℃. The expression was induced by IPTG for 4 h. The protein was purified by 6-histidine column. The molecular weight and purification of the protein were identified by SDS-PAGE. The result indicated that there was only one band in sFasL (24 000 dolton). Special mouse anti-human FasL antibody was used to confirm the bands transferred onto membranes with Western blotting. The result showed there was a sFasL positive band. This indicated that the protein expressed in M15 was human sFasL (Figure 4).

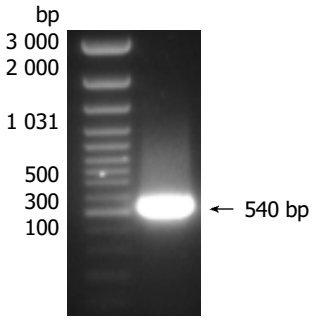

Figure 2 Reversion of total RNA isolated from PHA activated peripheral blood mononuclear cells to cDNA.

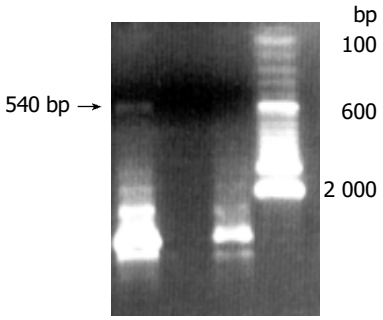

Figure 3 PCR bands and transfected DH 5a. Band1: inserted fragment of sFasL in pQE-31; Band 2: no inserted fragment.

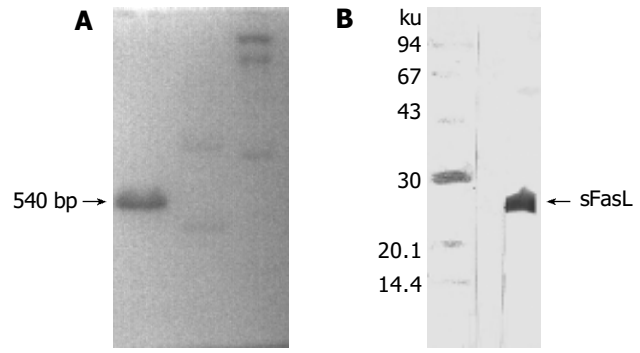

Figure 4 sFasL expression in SDS-gel (A) and hybridization with special anti-sFasL antibody (B).

Jurkat cell line apoptosis induced by sFasL expressed in M15

Different doses of expressed sFasL were added to log phase growing Jurkat cell line and cultured for another 18 h. The percentage of apoptosis of tested cell line was determined by cytometry after stained with PI dye. Figure 5 shows the apoptosis of Jurkat cells after co-cultured with expressed sFasL. The percentage of apoptotic Jurkat cells was similar to that of apoptotic cells co-incubated with commercial human sFasL. This result indicated that sFasL was able to induce cell apoptosis (Figure 5).

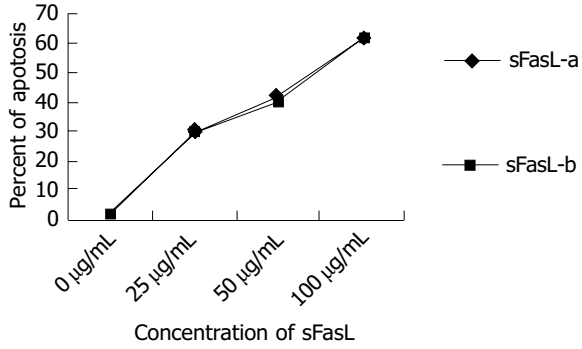

Figure 5 Cell apoptosis induced by different doses of sFasL (25, 50 and 100 μg/L).

Generation of anti-human sFasL antibody in mice immunized with expressed sFasL

Serum was isolated from two mice immunized wirh expressed human sFasL. We coated plates with this serum and detected anti-human FasL titer using special commercial standard sFasL protein by ELISA. The result showed that there was a high titer (>1:1 000) of anti-human sFasL special antibody in the serum of immunized mice. This indicated that expressed sFasL could specifically bind to standard human sFasL protein.

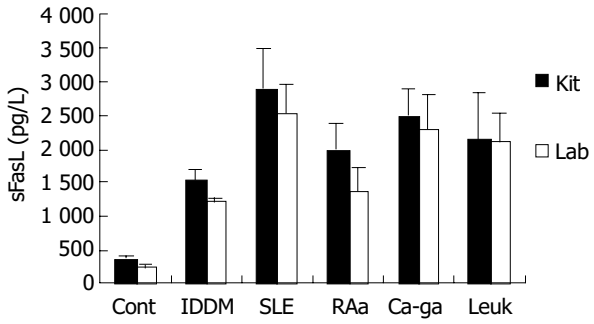

Figure 6 Levels of soluble FasL in serum from patients with different diseases. Cont: serum from healthy individuals; IDDM: serum from patients with IDDM; SLE: serum from IDDM; RAa: serum from RA patients with activated stage; Ca-ga: serum from patients with gastric cancer; Leuk: serum from patients with leukemia; Shadow bar: serum level detected by commercial sFasL kit. Open bar: serum level detected by anti-sFasL antibody.

Prepared special anti-humans sFasL antibody could be used to detect concentration of sFasL

We coated ELISA plates with special anti-human sFasL antibody generated from immunized mice to detect the concentration of sFasL in the serum of patients with tumor and autoimmune diseases. Twenty serum samples from healthy individuals, 95 serum samples from patients with different autoimmune diseases and 30 serum samples from patients with leukemia and cancer were detected by this way. As a parallel experiment, the concentration of sFasL in these serum samples was identified in duplicate using commercial Kit at the same time. The data showed that the concentration of sFasL was

significantly higher than that in healthy individuals ($P<0.05$). The result determined with prepared sFasL antibody in our lab oratory was same as that detected by commercial Kit (Figure 6).

Arthritis reduced by sFasL immunized rats

Arthritis occurred as early as 15 d after primary immunization with CII emulsified with IFA. The significant ankylosis was observed in rats. The joints of rats were red and swollen. The arthritis rats lost ability to move and showed difficult to reach food. The percentage of arthritis was 90% (Table 1). The mean score could reach the maximum 24 d after immunization began to decrease from d 30 (Figure 7).

Table 1 Incidence of chicken CII-induced arthritis in Wistar rats

Group	Immunized with	Incidence	Percentage of CIA (%)
Experimental	CII+CFA	18/20	90
Control	CII	0/5	0
	CFA	0/5	0

Wistar rats were intradermally injected with collagen II (CII) emulsion in an equel volume of IFA (100 μL (containing 300 μg of CII). Seven days later, a booster containing 100 μg of CII in IFA intradermally administered. The rats were observed every day from 4 wk and evaluated with standard 4 scores.

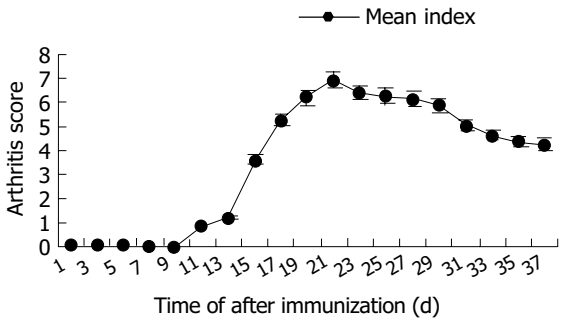

Figure 7 Mean arthritis score of rats with CIA.

When arthritis had a score of 7-8, 1 μg of sFasL in 100 μL of PBS was injected into one ankylosis side of rats. Meanwhile, 100 μL of PBS was injected into another ankylosis side of the same arthritis rats as control. After the arthritis rats were injected 3 times with sFasL, the rats showed reducible arthritis (Figure 8A) while control rats which received an equal volume PBS suffered from a more serious ankylosis (Figure 8B).

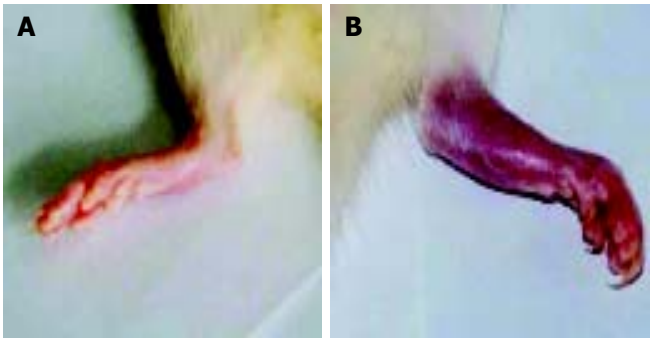

Figure 8 Ankylosis in arthritis rats. A: Ankylosis induced by sFasL in arthritis rats. B: Grade 4 inflammation in rat hind paw.

DISCUSSION

Human Fas ligand (CD95 ligand, FasL) was identified by Nagata's laboratory in 1993. Human FasL is consistented of 281 amino acids and a member of TNF family. The N terminal of FasL was located in the cytoplasm and C terminal is on cell surface. The region of the molecules in cytoplasm is consisted of 80 amino acids. The region though the cell membrane of FasL is consisted of 22 amino acids. The region of FasL exposed to outside of the cells is consisted of 179 amino acids[3]. Fas ligand molecules can be cut by matrix metalloproteinases (MMP) from membranes[15] and become a soluble form which is called soluble FasL (sFasL). FasL could induce apoptosis of cells when it binds to Fas which expresses on cell surface and acts as a special receptor of FasL.

Fas is ubiquitously expressed on a number of different cells including tumor cells. Likewise, as a ligand of Fas, FasL has many important functions. The expression of FasL is not only restricted to activated T cells and NK cells, but also on immune privileged sites such as eyes and testis. FasL can be up-regulated when cells are responsive to UV irradiation or treated by cytotoxic drugs. Over expression of FasL can inhibit some autoimmue diseases by deleting auto-immune memory cells[4,5]. Moreover, Fas-FasL interaction can protect allografts from immune attack and induce anti-tumor responses. Thus, myoblasts engineered to express FasL have been found to prolong the survival of co-transplanted islet allografts in diabetic mice. FasL expression on allogeneic fibroblasts was found to abolish tumor growth and induce specific protective immunity when mixed with neoplastic cells before implantation *in vivo*. Apoptosis induced by Fas-FasL interaction is believed to involve inflammation, anti-tumor and autoimmune reaction and aging[6-8]. Apoptosis has been found in almost all processes of the life. For example, activation induced cell death (AICD) may play a very important role in T cell activation and differentiation.

As the out-membrane region of FasL, sFasL involves the deletion of potentially hazardous peripheral memory cells[5]. Some studies suggested that change of sFasL in serum mignt be involved in many processes and progress of diseases. The serum level of sFasL was high in patients with large granule lymphocyte leukemia and NK like lymphoma, SLE, RA and EAE[9-11]. sFasL was upregulated on the tumor surface upon drug incubation in chemosensitive tumor cells. Tumor cells could mediate autocrine or paracrine to release soluble FasL (sFasL) and induce apoptosis of peripheral normal cells, CTL and NK which could express Fas and promote local tumor invasion or metastases[11-13]. Matsuno *et al*. reported that both sFas and sFasL were higher in the synovium fluid of RA patients compared with other arthritis[14]. Serve RA showed a higher level of sFasL than mild RA[13,21]. The concentration of Fas, receptors of FasL and sFasL, were changed in the process of diseases. Some investigators reported that sFas might block apoptosis by binding FasL or sFasL[5,6]. Membrane-bound FasL induced apoptosis in cultured synovial cells from RA and OA patients, but naturally processed human sFasL did not[23]. The role of sFasL still remains unclear.

T cells express both Fas and FasL on cell surface after stimulation. FasL existes in two forms: membrane-bound FasL and soluble FasL (sFasL). The out-membrane region of FasL is cleaved by a metalloproteinase (MP) and falls down from membrane to serum or body fluid[14]. Inhibition of metalloproteinase cleavage could enhance the cytotoxicity of FasL[15]. Activated T cells would die in a few minutes if no IL-2 was added after stimulation with antigens or mitogens. This process is called activated induced cell death (AICD). Because sFasL shows the same function of FasL but has smaller molecules. We expressed sFasL first in *E. Coli*. For preparing sFasL cDNA and stimulated T cells with PHA in this study. The expression of sFasL reached 20% after stimulation for 24 h compared with 3% expression on naïve T cells. We harvested sFasL expressed

T cells before they died and mRNA of sFasL was extracted. The fresh mRNA of sFasL was reversed into cDNA and successfully amplified. The sFasL was ligated into PCR2.1 vector. After the sFasL insert was confirmed by sequencing analysis, the fragment of sFasL was inserted into pQE-31 vector and expressed in M15 strain.

To identify whether sFasL expressed in this study had biological functions after purification, we chose Jucket cell line as a report cell because Fas molecules were expressed on Jucket cell line surface. When Fas expressed on cell surface bound to sFasL, the cells were activated and went to die after 48 h of binding. The results demonstrated that the expressed sFasL could induce Jucket cell line apoptosis. The percent of apotosis increased with the increased concentration in the culture. This result indicated that sFasL had the same function membrane FasL.

Recently, some reports demonstrated that FasL and sFasL played a different role in apoptosis. Generally, membrane-bound FasL, or FasL is fully competent in transducing Fas-mediated signals for apoptosis and NF-kappaB nuclear translocation because membrane FasL could possess both Fas-focusing and signal transducing functions. While sFasL is known to be deficient in transducing signals upon engagement with membrane Fas[4,14]. But in some cases, sFasL was found to be involved in the deletion of potentially hazardous peripheral memory cells[10]. A more study suggested that change of sFasL in serum was involved in the process and progress of diseases[9]. The report indicated there was a high serum level of sFasL in patients with large granular lymphocyte leukemia and NK-like lymphoma[12]. sFasL increased significantly in the serum of patients with activated systemic lupus erythematosus (SLE) and rheumatoid arthritis (RA). In some autoimmune diseases the serum level of sFasL was dramatically decreased after treatment in some patients[10,13]. We detected the serum level of sFasL in more than 90 samples from autoimmune disease in this study. Among these diseases, the serum levels were detected from 32 patients with IDDM, 31 patients with SLE, 16 RA patients in activative stage and 16 RA patients in resting stage. This result indicated that the circulation level of sFasL was higher in these autoimmune diseases. The role of sFasL in the pathogenesis of these autoimmune diseases is still under investigation.

It has been commonly accepted that activated CD4 T cell mediated immune responses are involved in the pathogenesis of RA. Both CD4 and CD8 T cells were observed to be enriched in the synovial fluid of RA patients. It is possible that if autoreactive T cells can be cleaned from circulation or RA can be located, the lesion caused by inflammation induced the autoreactive T cells may relieve. Similar with RA, it is believed that Th1 is involved in the pathogenesis of CIA. Collagen induced arthritis (CIA) has become a commonl animal model in studing the pathogenesis of rheumatoid arthritis[2,17]. Many potential factors involved in CIA[2,18-20], Th1 cells are mainly involved in the CIA. If Th1 cells are deleted from joints, the evolvement of joints in CIA may be lighter. Mattsson *et al*.[20] reported that the T cell marker O×40 was up-regulated in OVA-inhibited non-arthritic animals compared to control CIA animals. They found that the complete inhibition of CIA caused by addition of OVA to the collagen II inoculum was due to the presence of a TH2 environment resulting from an increased production of IL-4 mRNA and a parallel increase in O×40+ T cells[20]. In this report, we used sFasL to treat CIA mice. The anklynosis was reduced after 3 times of sFasL injection in arthritis rats. This result indicated that sFasL might induce apoptosis of activated autoimmune Th1 cells which infiltrated in joints and synovium so that the inflammation induced by autoimmune T cells decreased, or the above process increased the Th2 switch. But how sFasL induces these changes is still under investigation.

In this study, human sFas ligand was engineered in *E. Coli*. The expressed sFasL could induce apoptosis of Jurkat cell line. Anti-human sFasL antibody could be generated in the mice immunized with expressed sFasL. Anti-human sFasL antibody could be used in detection of sFasL in the serum of patients with autoimmune diseases. The results demonstrated that the level of sFasL in sera of patients with IDDM, SLE and RA was much higher than that in healthy individuals. Meanwhile, the result showed that sFasL antibody revealed the same sensitivity as commercial sFasL antibody. Injection of sFasL with sc in CIA rats could reduce inflammation, which may indicate that sFasL can be used in treatment of autoimmune diseases.

ACKNOWLEDGEMENTS

We thank professors Kang-Yan Zhou and Shan-Qing Tong for their critical review of this paper and Dr. Zuo-Qing Li for his assistance in preparation of this manuscript.

REFERENCES

1 **Li NL,** Zhang DQ, Zhou KY, Cartman A, Leroux JY, Pode AR, Zhang YP. Isolation and characteristics of autoreactive T cells specific to aggrecan G1 domain from rheumatoid arthritis patients. *Cell Res* 2000; **10:** 39-49

2 **Nandakumar KS,** Andren M, Martinsson P, Bajtner E, Hellstrom S, Holmdahl R, Kleinau S. Induction of arthritis by single monoclonal IgG anti-collagen type II antibodies and enhancement of arthritis in mice lacking inhibitory FcgammaRIIB. *Eur J Immunol* 2003; **33:** 2269-2277

3 **Takahashi T,** Tanaka M, Inazawa J, Abe T, Suda T, Nagata S. Human Fas ligand: gene structure, chromosomal location and species specificity. *Int Immunol* 1994; **6:** 1567-1574

4 **Ishimaru N,** Yanagi K, Ogawa K, Suda T, Saito I, Hayashi Y. Possible role of organ-specific autoantigen for Fas ligand-mediated activation-induced cell death in murine sjogren's syndrome. *J Immunol* 2001; **167:** 6031-6037

5 **Kim S,** Kim KA, Hwang DY, Lee TH, Kayagaki N, Yagita H, Lee MS. Inhibition of autoimmune diabetes by Fas ligand: the paradox is solved. *J Immunol* 2000; **164:** 2931-2936

6 **Hoffmann TK,** Dworacki G, Tsukihiro T, Meidenbauer N, Gooding W, Johnson JT, Whiteside TL. Spontaneous apoptosis of circulating T lymphocytes in patients with head and neck cancer and its clinical importance. *Clin Cancer Res* 2002; **8:** 2553-2562

7 **Suzuki N,** Ichino M, Mihara S, Kaneko S, Sakane T. Inhibition of Fas/Fas ligand-mediated apoptotic cell death of lymphocytes *in vitro* by circulating anti-Fas ligand autoantibodies in patients with systemic lupus erythematosus. *Arthritis Rheum* 1998; **41:** 344-353

8 **French LE,** Hahne M, Viard I, Radlgruber G, Zanone R, Becker K, Muller C, Tschopp J. Fas and Fas ligand in embryos and adult mice: ligand expression in several immune-privileged tissues and coexpression in adult tissues characterized by apoptotic cell turnover. *J Cell Biol* 1996; **133:** 335-343

9 **Zhu B**, Luo L, Chen Y, Paty DW, Cynader MS. Intrathecal Fas ligand infusion strengthens immunoprivilege of central nervous system and suppresses experimental autoimmune Encephalomyelitis. *J Immunol* 2002; **169:** 1561-1569

10 **Christensson M,** Pettersson E, Eneslatt K, Christensson B, Bratt J, Rantapaa-Dahlqvist S, Sundqvist KG. Serum sFAS levels are elevated in ANCA-positive vasculitis compared with other autoimmune diseases. *J Clin Immunol* 2002; **22:** 220-227

11 **Kayagaki N,** Kawasaki A, Ebata T, Ohmoto H, Ikeda S, Inoue S, Yoshino K, Okumura K, Yagita H. Metalloproteinase-mediated release of human Fas ligand. *J Exp Med* 1995; **182:** 1777-1783

12 **Nagao M,** Nakajima Y, Hisanaga M, Kayagaki N, Kanehiro H, Aomatsu Y, Ko S, Yagita H, Yamada T, Okumura K, Nakano H. The alteration of Fas receptor and ligand system in hepatocellular carcinomas: how do hepatoma cells escapem from the host immune surveillance *in vivo*? *Hepatology* 1999; **30:** 413-420

13 **Nozawa K,** Kayagaki N, Tokano Y, Yagita H, Okumura K, Hasimoto H. Soluble Fas (APO-1, CD95) and soluble Fas ligand in rheumatic diseases. *Arthritis Rheum* 1997; **40:** 1126-1129
14 **Matsuno H,** Yudoh K, Watanabe Y, Nakazawa F, Aono H, Kimura T. Stromelysin-1 (MMP-3) in synovial fluid of patients with rheumatoid arthritis has potential to cleave membrane bound Fas ligand. *J Rheumatol* 2001; **28:** 22-28
15 **Knox PG,** Milner AE, Green NK, Eliopoulos AG, Young LS. Inhibition of metalloproteinase cleavage enhances the cytotoxicity of Fas ligang. *J Immunol* 2003; **170:** 677-685
16 **Xiao S,** Jodo S, Sung SS, Marshak-Rothstein A, Ju ST. A novel signaling mechanism for soluble CD95 ligand. Synergy with anti-CD95 monoclonal antibodies for apoptosis and NF-kappaB nuclear translocation. *J Biol Chem* 2002; **277:** 50907-50913
17 **Vossenaar ER,** Nijenhuis S, Helsen MM, van der Heijden A, Senshu T, van den Berg WB, van Venrooij WJ, Joosten LA. Citrullination of synovial proteins in murine models of rheumatoid arthritis. *Arthritis Rheum* 2003; **48:** 2489-2500
18 **Banda NK,** Kraus DM, Muggli M, Bendele A, Holers VM, Arend WP. Prevention of collagen-induced arthritis in mice transgenic for the complement inhibitor complement receptor 1-related gene/proteiny. *J Immunol* 2003; **171:** 2109-2115
19 **Morgan ME,** Sutmuller RP, Witteveen HJ, van Duivenvoorde LM, Zanelli E, Melief CJ, Snijders A, Offringa R, de Vries RR, Toes RE. CD25+ cell depletion hastens the onset of severe disease in collagen-induced arthritis. *Arthritis Rheum* 2003; **48:** 1452-1460
20 **Mattsson L,** Lundberg K, Mussener E, Jansson A, Erlandsson Harris H, Larsson P. Antigen inhibition of collagen-induced arthritis is associated with up-regulation of IL-4 mRNA and induction of O×40 on T cells in draining lymph nodes. *Clin Exp Immunol* 2003; **131:** 241-247
21 **Hashimoto H,** Tanaka M, Suda T, Tomita T, Hayashida K, Takeuchi E, Kaneko M, Takano H, Nagata S, Ochi T. Soluble Fas ligand in the joints of patients with rheumatoid arthritis and osteoarthritis. *Arthritis Rheum* 1998; **41:** 657-662

Edited by Wang XL and Zhang JZ **Proofread by** Xu FM

PO Box 2345, Beijing 100023, China
Fax: +86-10-85381893
E-mail: wjg@wjgnet.com www.wjgnet.com

World J Gastroenterol 2004;10(21):3157-3160
World Journal of Gastroenterology
 ISSN 1007-9327

• BASIC RESEARCH •

Safe time to warm ischemia and posttransplant survival of liver graft from non-heart-beating donors

Xiao-Shun He, Yi Ma, Lin-Wei Wu, Wei-Qiang Ju, Jin-Lang Wu, Rui-De Hu, Gui-Hua Chen, Jie-Fu Huang

Xiao-Shun He, Yi Ma, Lin-Wei Wu, Wei-Qiang Ju, Gui-Hua Chen, Jie-Fu Huang, Organ Transplantation Center, First Hospital, Sun Yat-sen University, Guangzhou 510080, Guangdong Province, China
Jin-Lang Wu, Rui-De Hu, Department of Pathology, Sun Yat-Sen University, Guangzhou 510080, Guangdong Province, China
Supported by the Key Clinical Projects of Minister of Health, No 97040230 and the Scientific and Technological Committee of Guangdong Province, No. 99M4902G
Correspondence to: Xiao-Shun He, Organ Transplantation Center, First Hospital, Sun Yat-Sen University, Guangzhou 510080, Guangdong Province, China. xshe@gdvnet.com
Telephone: +86-20-87335101
Received: 2004-01-09 **Accepted:** 2004-02-24

Abstract

AIM: To explore the dynamical changes of histology, histochemistry, energy metabolism, liver microcirculation, liver function and posttransplant survival of liver graft in rats under different warm ischemia times (WIT) and predict the maximum limitation of liver graft to warm ischemia.

METHODS: According to WIT, the rats were randomized into 7 groups, with WIT of 0, 10, 15, 20, 30, 45, 60 min, respectively. The recovery changes of above-mentioned indices were observed or measured after liver transplantation. The graft survival and postoperative complications in each subgroup were analyzed.

RESULTS: Liver graft injury was reversible and gradually resumed normal structure and function after reperfusion when WIT was less than 30 min. In terms of graft survival, there was no significant difference between subgroups within 30 min WIT. When WIT was prolonged to 45 min, the recipients' long-term survival was severely insulted, and both function and histological structure of liver graft developed irreversible damage when WIT was prolonged to 60 min.

CONCLUSION: The present study indicates that rat liver graft can be safely subjected to warm ischemia within 30 min. The levels of ATP, energy charge, activities of glycogen, enzyme-histochemistry of liver graft and its recovery potency after reperfusion may serve as the important criteria to evaluate the quality of liver graft.

He XS, Ma Y, Wu LW, Ju WQ, Wu JL, Hu RD, Chen GH, Huang JF. Safe time to warm ischemia and posttransplant survival of liver graft from non-heart-beating donors. *World J Gastroenterol* 2004; 10(21): 3157-3160
http://www.wjgnet.com/1007-9327/10/3157.asp

INTRODUCTION

Attributed to the widespread applications of effective immunosuppressants and the prefect perioperative management, liver transplantation has achieved a great success during the past 40 years, but the shortage of liver donors has limited its clinical usage greatly. Quality of liver graft is a key factor for liver transplantation. Organs from NHBD (non-heart-beating donors) seem to be an option to alleviate the problem of liver donor shortage effectively[1]. However, warm ischemia to the liver related to cardiac arrest remained a main obstacle to the use of livers from NHBD[2-4]. Moreover, in liver transplantation, the allograft sustains inevitable cold ischemia in addition to rewarming injury during liver reperfusion[5]. Therefore, warm ischemia-reperfusion injury of liver grafts has become a hot topic with theoretical and clinical significance, and it has drawn more and more attention[1]. It is a main unfathomed problem of how to evaluate the quality of liver grafts and how to ascertain the safety time limit for warm ischemia of liver grafts. The outcomes of this research were rather different mainly because the previous researches focused on the relationship between warm ischemia time (WIT) and the short-time survival, neglecting the long-term survival and complications. We investigated the dynamical changes of histology, histochemistry, energy metabolism, microcirculation, especially focusing on liver function and posttransplant survival of liver graft, under different WIT to establish the predictive limitation of liver graft to warm ischemia injury, which might be helpful for the further research in similar clinical situation.

MATERIALS AND METHODS

Establishment of animal model

Adult healthy male Sprague-Dawley rats, weighing 250-300 g, supplied from Experimental Animal Center in Sun Yat-Sen University, were used for the models. Breeding conditions were in coincidence with SPF (specific pathogen free animal) standards. Mean weight of recipient rats was a little heavier than that of donor rats.

Animal model of warm ischemia A midline laparotomy was performed in supine position after an ether aspiration anesthesia, 0.2 mL of heparin sodium solution (1 250 U heparin sodium) was injected via dorsum of penis vein to heparinize the donor liver. Thereafter, we sheared diaphragm, clamped the basilar part of the heart and blocked the thoracic aorta. Thus, a donor liver warm ischemia model was established.

Animal model of liver transplantation After the predicted warm ischemia duration in each group, 20 mL of 0-4 ℃ lactic acid ringer's solution (50 U/mL heparin sodium) was infused into the abdominal aorta via a catheter. The liver graft turned fulvous when filling solution flowed out via the sheared right atria. All of the liver ligaments were dissected, the pyloric vein was ligated proximal to the portal vein after the hepatic proper artery and portal vein were freed, the infra-hepatic inferior vena cava was isolated and the right suprarenal vein and right renal vein were cut. The supra-hepatic inferior vena cava was cut in the position close to the diaphragm anulus, the hepatic artery was ligated and cut, the portal vein was cut in the confluence of portal vein and splenic vein, the infra-hepatic inferior vena cava was cut over the left renal vein. Specimens of donor liver were preserved in the 4 ℃ lactic acid ringer's solution. Anesthesia, position and incision were all the same in donors and recipients' operations. We modified the angio-anastomotic technique[6] on the basis of cuff technique suggested by Kamada *et al*.[7] and Sun *et al*.[8].

Cold ischemia time (CIT) was 50±3.5 min, anhepatic phase was 20±2.5 min.

Group and observation index

Three hundred and seventy eight SD rats were used in our study. Forty two (6 in each group with WIT of 0, 10, 15, 20, 30, 45 and 60 min) were used for the observation of histology, histochemistry, ultrastructure and metabolism change after only warm ischemia injury; other 336 rats were performed with orthotopic liver transplantation according to the "modified cuff method"[6]. Among the 336 rats, 168 were used for donors and 168 for receivers. The donor group was randomly divided into 2 subgroups: 84 for prolonged survival observation, including spirit, activity, complications, death diagnosis and mean survival; the other 84 rats for investigation of the dynamical changes of liver function, histology, histochemistry, microcirculation, energy metabolism and ultrastructure (transmission electron microscope and scanning electron microscope). Both groups were divided into 7 subgroups with WIT of 0, 10, 15, 20, 30, 45 and 60 min, each subgroup consisted of 12 rats. Liver transplantation and postoperative follow-up were performed respectively. Careful attention was paid to the fluid replacement after blood withdrawal.

Statistics analysis

Data were expressed as mean±SD. Analysis of variance (ANOVA including SNK-*q* test) was used to analyze the data. Enumeration data were analyzed by Chi-square test and Fisher test. The activity and distribution of succinic dehydrogenase (SDH), cytochrome oxidase (CO) and ATPase, were respectively observed under microscope in a semi-quantitative way. Kaplan-Meier analysis was applied for the relationship between WIT and survival, while correspondence analysis was applied for that between WIT and complication. All the statistical procedures were performed with SPSS package and $P<0.05$ was considered statistically significant.

RESULTS

Survival situation

In groups with WIT of 0, 10, 15, 20, 30, 45 and 60 min, the median survival time was 140.5, 132.5, 76, 109, 58, 13.5 and 3 d, respectively (Figure 1). One week, 1-mo and 3-mo postoperation survivals of each group are shown in Table 1. There was no significant difference between groups with WIT less than 30 min. One week survival in WIT of 0 min and 60 min group was significantly different ($P<0.05$). The difference was also significant between 45, 60 and 0 min in 1-mo and 3-mo survival ($P<0.05$)[9].

Dynamic histological and subcellular structure observation

The histological and subcellular structure change was a dynamic process[10]. Histological structure changed slightly when WIT was less than 30 min. Cytoplasm loosening, cells edema and focal vacuole degeneration were noted when WIT was over 30 min, especially in the lobule center area, leukocytes infiltration was noted in the portal area, acidophilus was obvious in some hepatocytes. The above pathologic changes aggravated when WIT elongated to 60 min, cell degeneration was diffuse or extended to a focal area, and even lipid degeneration could be seen. The degree of degeneration was depending on the duration of WIT, but necrosis could hardly be observed under light microscope. Six hours and 24 h after reperfusion, injury to liver graft became severer; in WIT 30 min group, hepatic cells presented obvious edema and some ballooning denegation; in WIT 45 min group, focal like necrosis could be noted, which was presented first in the lobule center area, the change aggravated with the elongation of WIT. Forty eight hours after reperfusion, hepatic injury resumed gradually in groups with WIT less than 45 min, while in WIT 60 min group, hepatic cells presented plaque or diffuse necrosis and the pathologic change was irreversible[11].

Electroscopically, swollen mitochondrion was noted and glycogen increased 24 h post liver transplantation in groups with WIT less than 30 min. When WIT was over 45 and 60 min, more swollen mitochondrion, vacuole degeneration, broken rough endoreticular, drop of nucleoprotein and hepatic apoptosis were observed, and cells necrosis could be noted with karyopyknosis, karyorrhexis and karyolysis. Thus, the subcellular structure then underwent irreversible injury. In addition, in WIT 45 min and 60 min groups, hepatic cells and endothelial cells presented apoptosis increasingly, and cells apoptosis and necrosis could be noted simultaneously[12,13].

Table 1 One week, 1-mo and 3-mo survival rate under different WIT (*n*,%)

Warm ischemia time (min)	1-wk survival rate	1-mo survival rate	3-mo survival rate
0	91.7 (11/12)	83.3 (10/12)	83.3 (10/12)
10	83.3 (10/12)	66.7 (8/12)	66.7 (8/12)
15	83.3 (10/12)	58.3 (7/12)	50.0 (6/12)
20	75.0 (9/12)	58.3 (7/12)	58.3 (7/12)
30	83.3 (10/12)	58.3 (7/12)	50.0 (6/12)
45	66.7 (8/12)	33.3 (4/12)[a,c]	8.3 (1/12)[a,c]
60	8.3 (1/12)[a,c]	0.0 (0/12)[a]	0.0 (0/12)[a]

[a]$P<0.05$ *vs* WIT 0 min group (*Fisher's* exact test); [c]$P<0.05$ *vs* groups WIT less than 45 min (*Fisher's* exact test).

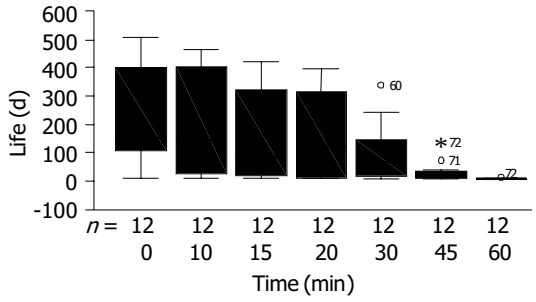

Figure 1 Statistical analysis of survival time.

Dynamic changes of histochemistry

The activities of SDH, CO, ATPase and content of glycogen decreased gradually after different WIT in a time-dependent manner, and especially significant over 30 min. The activities of SDH, CO, ATPase and content of glycogen of liver graft significantly decreased in 45 min and 60 min groups[14].

Hepatic glycogen and enzyme activities were positively related to warm ischemia time in a time-dependent manner during the reperfusion period. In WIT 15 and 30 min groups, periodic acid-Schiff reaction (PAS reaction) and enzyme histochemical activities showed a recovery potency. While in WIT 45 and 60 min groups, the liver graft underwent an irreversible injury; therefore, no evident recovery potency was found 24 h after implantation.

Microcirculation change patterns of liver graft

The microcirculation changes of liver graft were measured by serum hyaluronic acid (HA) and ultrastructural observation. The microcirculation of liver graft injury could be gradually resumed normal after reperfusion when WIT was less than 30 min. In the WIT 45 min group, part of blood sinusoids were full of the cytoplasmic blebs stemming from the microvilli of

hepatocytes and hemocytes accumulated there; the level of serum HA of each group within 45 min of WIT would almost recover after reperfusion[15].

Measurement of energy metabolism

ATP, TNA (Total adenine nucleotides) and EC in all groups were decreased dramatically after warm ischemia injury[16,17]. ATP in WIT 10, 15, 20, 30, 60 min groups was decreased to 58.7%, 34.7%, 30.1%, 20.5%, 15.3%, and 9.3% of that in WIT 0 min group, respectively. Twenty-four hours after transplantation, ATP, TNA and EC showed a tendency of recovery potency. ATP, TNA and EC had no significant difference between groups with WIT less than 30 min and WIT 0 min group. But when WIT was over 45 min the observation showed significant difference, which also could be seen between the WIT 45 min and 60 min groups. Forty-eight hours after transplantation, the above mentioned indexes recovered close to the normal level, there was no difference between groups with WIT less than 45 min and WIT 0 min group, while the indexes in group with WIT 60 min were still different from those in WIT 0 min group and WIT 45 min group[18].

Liver function

Twenty-four hours after transplantation, AST, ALT and LDH increased sharply with the elongation of WIT, the following recovering change showed a step-like pattern[19,20]. AST and ALT in groups with WIT less than 30 min decreased close to the normal level 3 d after transplantation, and the recovering course took 5 d in WIT 45 min group. LDH in groups with WIT less than 45 min recovered to the normal level 3 d after transplantation, while enzymes in WIT 60 min group could hardly recovered to the normal[21].

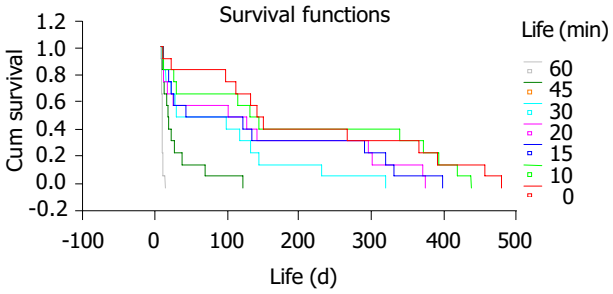

Figure 2 Survival curve (Kaplan-Meier method).

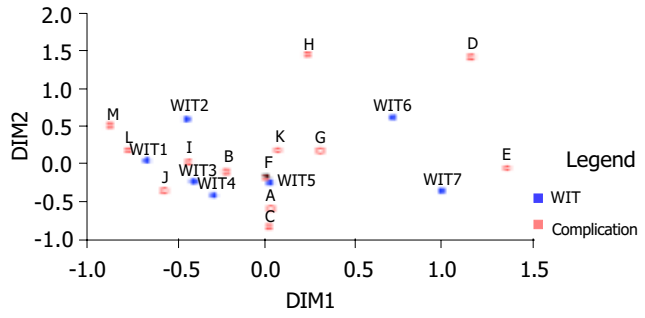

Figure 3 Relationship between WIT and complications (correspondence analysis). WIT 1, 2, 3, 4, 5, 6 and 7 represent WIT 0 min, 10 min, 15 min, 20 min, 30 min, 45 min and 60 min, respectively. A: Hemorrhage; B: SVC (superior vena cava) thrombosis; C: IVC (inferior vena cava) thrombosis; D: PV (portal vein) thrombosis; E: Liver dysfunction; F: Pulmonary infection; G: Abdominal infection; H: Bile leakage; I: Bile obstruction; J: Adhesive intestinal obstruction; K: Liver abscess; L: Unexplained; M: Natural death.

Relationship between WIT and survival

The survival curves are demonstrated in Figure 2. Survival time in groups with WIT less than 30 min had no statistical difference. Though short-term survival might be possible in WIT 45 min group, warm ischemia injury had insulted the long-term survival of liver graft. And in WIT 60 min group, the liver graft underwent irreversible injury.

Relationship between WIT and complication

The relationship between WIT and complications was illustrated by correspondence analysis (Figure 3). Complications in groups with WIT less than 30 min were similar, the incidence of liver graft dysfunction increased with the elongation of WIT and the incidence of biliary blockage was positively related to the survival time of recipient animals[22-24].

DISCUSSION

In the past 40 years, liver transplantation has achieved a great success and become the most effective method to treat end-stage hepatic diseases. Nowadays, liver transplantation is developing rapidly as a result of the perfect perioperative treatments and widespread applications of some immunosuppressants. However, there is an obvious problem that recipients are greatly more than donors. The disparity between the increasing demand for liver donors and the limited supply of donor organs has led to a reconsideration of the use of marginal pools, such as NHBD[25-27]. NHBD programs have been used successfully in kidney transplantation, and were able to increase donor pool of kidneys by 40%. In the field of liver transplantation the use of livers from NHBD shows a less favorable clinical results, because of the limited hepatic tolerance against warm ischemic damage compared with kidneys[28-30]. Although several clinical and experimental studies have shown that liver can compensate 60 min of WIT during liver resection[31,32], in transplantation settings, there were few studies about limit of the period of warm ischemia before transplantation. To evaluate the quality of liver grafts and to ascertain the safety time limit for warm ischemia of liver grafts, we should focus on the long-term survival of liver graft and the complications after transplantation[33].

In present study, we found that the pathologic changes of hepatic cells undergoing only warm ischemia injury was irreversible when WIT was less than 60 min, only part of hepatic cells underwent irreversible injury. But the damage to liver graft would aggravate in the cold preservation, operative ischemia stage and the reperfusion process. Histological and subcellular structure changes were reversible in groups with WIT less than 30 min, especially at 48 h after transplantation. In WIT 45 min and 60 min groups, hepatocellular degeneration became severer, necrotic cells spread from the center lobule area to a sheet or foci-like area involved several hepatic lobules, the liver graft then underwent irreversible injury[34].

The present study indicates that hepatic injury is reversible within 30 min of warm ischemia injury by cytochemical and histochemical dynamic observation. The glycogen and enzyme-histochemistry activities of liver graft and their recovery potency after reperfusion may serve as criteria to evaluate the quality of liver graft.

ATP, TAN and EC decreased after warm ischemia injury, especially in the first 30 min, the change was reversible within 30 min of warm ischemia injury. WIT and hepatic energy metabolism recovering potency were key factors to the postoperative survival. ATP, EC and their recovering potency of the liver graft may serve as criteria to evaluate the quality of liver graft.

Microcirculation of grafted liver could be gradually resumed normal after reperfusion when WIT was less than 30 min, which indicated that hepatic cells held the recovery potency and could regained normal microcirculatory structure after reperfusion if

the WIT was less than 30 min. After 45 min of warm ischemia, most hepatic sinus was unobstructed, but there were still some sinus filled with cytoplasm blebs, reticular fibrosis and hemocytes. So 45 min may be the deadline of hepatic warm ischemia. When WIT was more than 60 min, microcirculatory structure of liver graft presented irreversible injuries.

Besides the researches on the influence of warm ischemia time on energy metabolism, morphology and function, special attention was paid on the influence of warm ischemia on the postoperative long-term survival and complications. Correspondence analysis showed that complications in groups with WIT less than 30 min were similar; and the incidence of liver dysfunction increased gradually in a time-dependent manner; incidence of biliary obstruction increased with the elongation of survival time of the recipient rats. Kaplan-Meier analysis showed that survival time in groups with WIT less than 30 min had no significant difference. In WIT 45 min group, the animal might still survive early postoperative period, but the long-term survival was severely insulted, when WIT prolonged to 60 min, both function and histological structure of graft would develop irreversible damage and no recipients could survive.

REFERENCES

1 **Sato M**, Ohkohchi N, Tsukamoto S, Koyamada N, Asakura T, Enomoto Y, Usuda M, Miyagi S, Okada A, Satomi S. Successful liver transplantation from agonal non-heart-beating donors in pigs. *Transpl Int* 2003; **16**: 100-107

2 **Fondevila C**, Busuttil RW, Kupiec-Weglinski JW. Hepatic ischemia/reperfusion injury-a fresh look. *Exp Mol Pathol* 2003; **74**: 86-93

3 **Nowak G**, Ungerstedt J, Wernerson A, Ungerstedt U, Ericzon BG. Hepatic cell membrane damage during cold preservation sensitizes liver grafts to rewarming injury. *J Hepatobiliary Pancreat Surg* 2003; **10**: 200-205

4 **Hines IN**, Harada H, Wolf R, Grisham MB. Superoxide and post-ischemic liver injury: potential therapeutic target for liver transplantation. *Curr Med Chem* 2003; **10**: 2661-2667

5 **Totsuka E**, Fung JJ, Urakami A, Moras N, Ishii T, Takahashi K, Narumi S, Hakamada K, Sasaki M. Influence of donor cardiopulmonary arrest in human liver transplantation: possible role of ischemic preconditioning. *Hepatology* 2000; **31**: 577-580

6 **Ma Y**, He XS, Chen GH. Surgical technique of the model of orthotopic liver transplantation and prevention of operational complication in rat. *Zhonghua Xianwei Waike Zazhi* 2003; **26**: 45-47

7 **Kamada N**, Calne RY. A surgical experience with five hundred thirty liver transplants in the rat. *Surgery* 1993; **93**: 64-68

8 **Sun JH**, Zeng QH, Wu MC. Experience with orthotopic rat liver transplantation. *Chin Med J* 1990; **103**: 142-145

9 **He XS**, Ma Y, Chen GH, Zhang JX, Wu JL, Liang YJ, Lin GY, Zhu ZY, Hu RD, Huang JF. The influence of warm ischemia injury on viability and posttransplantative outcome of liver graft from non-heart-beating donor in rats. *Zhonghua Yixue Zazhi* 2003; **83**: 1236-1240

10 **He XS**, Ma Y, Chen GH, Wu JL, Hu RD, Liang YJ, Huang JF. Hepatic warm ischemia injury in rats: a dynamically histological and ultrastructural study. *Zhonghua Shiyan Waike Zazhi* 2002; **19**: 249-251

11 **Rudiger HA**, Graf R, Clavien PA. Liver ischemia: apoptosis as a central mechanism of injury. *J Invest Surg* 2003; **16**: 149-159

12 **Kurokawa T**, Takagi H. Mechanism and prevention of ischemia-reperfusion injury. *Transplant Proc* 1999; **31**: 1775-1776

13 **Belous A**, Knox C, Nicoud IB, Pierce J, Anderson C, Pinson CW, Chari RS. Reversed activity of mitochondrial adenine nucleotide translocator in ischemia-reperfusion. *Transplantation* 2003; **75**: 1717-1723

14 **Ma Y**, He XS, Chen GH, Liang YJ, Hu RD, Huang JF. Dynamical changes of glycogen and enzyme-histochemistry activities of liver graft following warm ischemia injury in rat. *Zhonghua Shiyan Waike Zazhi* 2003; **20**: 24-26

15 **Ma Y**, He XS, Chen GH, Wu JL, Liang YJ, Hu RD, Huang JF. Dynamical changes of microcirculation of liver graft from non-heart-beating donor in rat. *Zhonghua Shiyan Waike Zazhi* 2003; **20**: 895-896

16 **Astarcioglu H**, Karademir S, Unek T, Ozer E, Menekay S, Coker A, Astarcioglu I. Beneficial effects of pentoxifylline pretreatment in non-heart-beating donors in rats. *Transplantation* 2000; **69**: 93-98

17 **He X**, Ma Y, Chen G, Lin G, Wu J, Zhu Z, Huang J. Influence of warm ischemia injury on energy metabolism and survival of liver graft in rats. *Zhonghua Waike Zazhi* 2002; **40**: 936-939

18 **Peralta C**, Bartrons R, Serafin A, Blazquez C, Guzman M, Prats N, Xaus C, Cutillas B, Gelpi E, Rosello-Catafau J. Adenosine monophosphate-activated protein kinase mediates the protective effects of ischemic preconditioning on hepatic ischemia-reperfusion injury in the rat. *Hepatology* 2001; **34**: 1164-1173

19 **Ma Y**, He XS, Chen GH, Hu RD, Huang JF. Effect of warm ischemia injury on hepatic functional status and survival of liver graft in rats. *Zhonghua Shiyan Waike Zazhi* 2003; **20**: 322-324

20 **Matsumoto K**, Honda K, Kobayashi N. Protective effect of heat preconditioning of rat liver graft resulting in improved transplant survival. *Transplantation* 2001; **71**: 862-868

21 **He XS**, Ma Y, Wu LW, Ju WQ, Chen GH, Hu RD, Huang JF. Influence of warm ischemia injury on hepatic functional status and survival of liver graft in rats. *Hepatobiliary Pancreat Dis Int* 2003; **2**: 504-508

22 **Moench C**, Moench K, Lohse AW, Thies JC, Otto G. Arterial back table pressure perfusion prevents ischemic biliary lesions after orthotopic liver transplantation. *Chirurg* 2003; **74**: 570-574

23 **Steger U**, Sawitzki B, Gassel AM, Gassel HJ, Wood KJ. Impact of hepatic rearterialization on reperfusion injury and outcome after mouse liver transplantation. *Transplantation* 2003; **76**: 327-332

24 **Abt P**, Crawford M, Desai N, Markmann J, Olthoff K, Shaked A. Liver transplantation from controlled non-heart-beating donors: an increased incidence of biliary complications. *Transplantation* 2003; **75**: 1659-1663

25 **Takada Y**, Taniguchi H, Fukunaga K, Yuzawa K, Otsuka M, Todoroki T, Iijima T, Fukao K. Hepatic allograft procurement from non-heart-beating donors: Limits of warm ischemia in porcine liver transplantation. *Transplantation* 1997; **63**: 369-373

26 **D'Alessandro AM**, Hoffmann RM, Knechtle SJ, Eckhoff DE, Love RB, Kalayoglu M, Sollinger HW, Belzer FO. Controlled non-heart-beating donors: A potential source of extrarenal organs. *Transplant Proc* 1995; **27**: 707-709

27 **Imber CJ**, St Peter SD, Lopez de Cenarruzabeitia I, Pigott D, James T, Taylor R, McGuire J, Hughes D, Butler A, Rees M, Friend PJ. Advantages of normothermic perfusion over cold storage in liver preservation. *Transplantation* 2002; **73**: 701-709

28 **Koti RS**, Seifalian AM, Davidson BR. Protection of the liver by ischemic preconditioning: a review of mechanisms and clinical applications. *Dig Surg* 2003; **20**: 383-396

29 **Busuttil RW**, Tanaka K. The utility of marginal donors in liver transplantation. *Liver Transpl* 2003; **9**: 651-663

30 **Regueira FM**, Espi A, Nwose P, Diez-Caballero A, Baixauli J, Rotellar F, Olea J, Pardo F, Hernandez-Lizoain JL, Cienfuegos JA. Comparison between two warm ischemic models in experimental liver transplantation in pigs. *Transplant Proc* 2003; **35**: 1591-1593

31 **Schon MR**, Pegg DE. The possibility of resuscitation livers after warm ischemia injury. *Transplant Proc* 1991; **23**: 2456-2458

32 **Jiang Y**, Gu XP, Qiu YD, Sun XM, Chen LL, Zhang LH, Ding YT. Ischemic preconditioning decreases C-X-C chemokine expression and neutrophil accumulation early after liver transplantation in rats. *World J Gastroenterol* 2003; **9**: 2025-2029

33 **Selzner N**, Rudiger H, Graf R, Clavien PA. Protective strategies against ischemic injury of the liver. *Gastroenterology* 2003; **125**: 917-936

34 **Donckier V**, Loi P, Closset J, Nagy N, Quertinmont E, Le Moine O, Deviere J, Goldman M, Gelin M, Gianello P. Preconditioning of donors with interleukin-10 reduces hepatic ischemia-reperfusion injury after liver transplantation in pigs. *Transplantation* 2003; **75**: 902-904

Edited by Kumar M and Chen WW **Proofread by** Xu FM

PO Box 2345, Beijing 100023, China
Fax: +86-10-85381893
E-mail: wjg@wjgnet.com www.wjgnet.com

World J Gastroenterol 2004;10(21):3161-3164
World Journal of Gastroenterology
 ISSN 1007-9327

• BASIC RESEARCH •

Protective effects of tumor necrosis factor α antibody and ulinastatin on liver ischemic reperfusion in rats

Yan-Ling Yang, Ji-Peng Li, Xiao-Ping Xu, Ke-Feng Dou, Shu-Qiang Yue, Kai-Zong Li

Yan-Ling Yang, Ji-Peng Li, Ke-Feng Dou, Shu-Qiang Yue, Kai-Zong Li, Department of Hepatobiliary Surgery, Xijing Hospital, Fourth Military Medical University, Xi'an 710032, Shaanxi Province, China
Xiao-Ping Xu, Department of General Surgery, Zhujiang Hospital, First Military Medical University, Guangzhou 510282, Guangdong Province, China
Supported by the National Natural Science Foundation of China, No. 30070741
Correspondence to: Kai-Zong Li, Department of Hepatobiliary Surgery, Xijing Hospital, Fourth Military Medical University, Xi'an 710032, Shaanxi Province, China. gdwk@fmmu.edu.cn
Telephone: +86-29-83375259 **Fax:** +86-29-83375561
Received: 2003-08-26 **Accepted:** 2003-10-27

Abstract

AIM: To study the protective effects of tumor necrosis factor α (TNF α) antibody and ulinastatin on liver ischemic reperfusion in rats.

METHODS: One hundred and twenty male SD rats were randomly divided into four groups: normal control group, ischemic group, TNFα antibody group and TNFα antibody + ulinastatin group. The animals were killed at 0, 3, 6, 9, 12 h after ischemia for 60 min and followed by reperfusion. Serum alanine aminotransferase (ALT), malondialdehyde (MDA) and liver histopathology were observed.

RESULTS: After ischemic reperfusion, the serum ALT and MDA were remarkably increased, and the hepatic congestion was obvious. Treatment of TNFα antibody and ulinastatin could significantly decrease serum ALT and MDA levels, and relieve hepatic congestion.

CONCLUSION: Ulinastatin and TNFα antibody can suppress the inflammatory reaction induced by hepatic ischemic reperfusion, and have protective effects on rat hepatic ischemic reperfusion injury.

Yang YL, Li JP, Xu XP, Dou KF, Yue SQ, Li KZ. Protective effects of tumor necrosis factor α antibody and ulinastatin on liver ischemic reperfusion in rats. *World J Gastroenterol* 2004; 10(21): 3161-3164
http://www.wjgnet.com/1007-9327/10/3161.asp

INTRODUCTION

Liver ischemic reperfusion injury is induced when liver gets the retrieval of its blood perfusion or oxygen supply, and hepatic injury would aggravate due to ischemia and hypoxia injury[1-4]. Hepatic insufficiency or primary liver graft non-function can be caused by liver ischemic reperfusion injury after portal blockage, hemorrhagic shock or liver transplantation. As liver ischemic reperfusion is hard to be avoided in hepatic surgical practice and the existing prevention and cure methods are not satisfactory, research of the mechanisms and therapy on liver ischemic reperfusion becomes one of the hotspots in hepatic surgery[5,6].

Cytokines are polypeptides with extensive biological activities, and play important roles in the immunoloregulation. They prevent body from diseases and accelerate tissue rehabilitation. But on the other hand, too many cytokines can also lead to or aggravate tissue damages[7,8]. Recent researches have demonstrated that TNF α plays an important role in ischemic reperfusion injury of liver[9-12]. At the same time, ulinastatin has been applied in the clinical treatment of pancreatitis, shock and extracorporeal circulation because of its significant inhibitory effect on inflammation[13-15]. In the present study, we attempted to relieve ischemic reperfusion injury of liver by using TNF α antibody and ulinastatin, so as to provide experimental and theoretic bases for prevention and treatment of liver ischemic reperfusion injury.

MATERIALS AND METHODS

Animals

A total of 120 male Spargue-Dawfey (SD) rats weighing 230±20 g, were obtained from Animal Research Center of Shaanxi Chinese Medical Institute, and fed with standard rat chow.

Drugs

Ulinastatin (Tianpu Co. Ltd., Guangdong, China) was diluted to 50 U/L by saline prior to use. TNF α monoclonal antibody (Jingmei Co. Ltd., Guangdong, China) was diluted 100 times by saline prior to use.

Experimental grouping

The rats were randomly divided into four groups. Group I: the control group, sham operation was performed, hepatic lobes of the rats were exposed without any treatment. Group II: ischemic reperfusion injury group, in which blood stream of the rats' liver lobes were blocked and then recovered after 60 min. Group III: TNF α antibody treatment group, in which TNF α antibody (2.0 mg/kg) was injected into the rats through dorsum veins of penis 5 min prior to reperfusion. Group IV: TNF α antibody and ulinastatin treatment group, in which both TNF α antibody (2.0 mg/kg) and ulinastatin (500 000 U/L, 0.5 mL) were simultaneously injected into the rats through dorsum veins of penis 5 min prior to reperfusion. Blood samples (2 mL) of all animals in each group were taken from hepatic superior and inferior vena cava at 0, 3, 6, 9 and 12 h after reperfusion. Then the rats were killed and liver samples were obtained.

Operation

The animals were intraabdominally anesthetized by pentobarbital sodium (30 mg/kg, 0.1 mL/10 g), and incised through median incision of the abdomen. After the liver pedicel between left and middle lobes of liver was exposed, ligaments between liver and septum transversum and abdominal wall were cut. The scatheless vascular clamp was used to block blood stream of portal veins and hepatic arteries of left and middle lobes of liver. After 60 min, the vascular clamp was released and blood stream recovered. So approximately seventy percent of liver was hypoxia, thus severe congestion of the mesentery vein was prevented.

Table 1 Levels of serum ALT in rats (U/L)

Group	*n*	Time of after reperfusion (h)				
		0	3	6	9	12
I[d]	6	40.52±8.33	42.36±3.71	43.19±7.64	42.92±5.18	42.66±9.27
II	6	263.92±16.90	315.61±21.02	374.26±19.56	289.11±16.32	257.94±27.41
III	6	238.73±10.62	254.06±13.78	273.17±18.29	213.26±26.54	172.53±36.46
IV[b]	6	173.42±15.33	189.08±24.52	203.17±23.19	175.36±38.66	163.13±32.27

[b]P<0.01 *vs* other groups, [d]P<0.01 *vs* group II and III.

Table 2 Levels of serum MDA of rats (mmol/L)

Group	*n*	Time of after reperfusion (h)				
		0	3	6	9	12
I[d]	6	7.82±0.17	7.91±0.08	8.11±0.13	8.04±0.67	7.93±0.41
II	6	13.81±4.19	38.65±4.73	46.36±2.54	35.09±5.12	24.09±3.20
III	6	10.71±2.52	18.23±3.58	23.31±4.49	16.83±2.29	11.26±3.16
IV[b]	6	9.12±3.41	12.29±6.83	15.18±3.22	11.72±4.15	9.42±5.28

[b]P<0.01 *vs* group II and III, [d]P<0.01 *vs* other groups.

Determination of ALT and MDA in serum

The blood samples in each group were poured into centrifuge tubes and the placement lasted for 20 min without shaking. After centrifugation at 2 000 r/min for 10 min, the sample serum was extracted and stored at -80 ℃ for determination.

ALT levels of sample serum were determined by an automatic biochemistry analyzer. MDA levels of sample serum were determined by the method introduced by Mourek *et al.*[16], and the kit was purchased from Juli Biomedical Engineering Institute of Nanjing, China.

Pathological changes of liver

Fresh tissues of liver in each group were sampled. Haematoxylin-Eosin (HE) staining was performed on 100 g/L formaldehyde-fixed tissue sections. The histological patterns of the liver samples were observed under light microscope.

Statistical analysis

All the data were analyzed by Student's *t* test and expressed as mean±SD. P<0.05 was considered statistically significant and P<0.01 as very statistically significant.

RESULTS

ALT levels of sample serum

ALT levels of sample serum in each group were determined to assess the liver function of rats. The levels of ALT in ischemic reperfusion injury group at different time points were significantly higher than those in control (P<0.01). The levels of ALT increased gradually after reperfusion, reached the peak 6 h after reperfusion, and then decreased mildly. The levels of ALT in TNFα antibody treatment group were remarkably lower than those in ischemic reperfusion injury group (P<0.01). The levels of ALT in TNF α antibody and ulinastatin treatment group were lower than those in ischemic reperfusion injury group and TNFα antibody treatment group (P<0.01).

MDA levels of sample serum

The oxygen-derived free radidicals induced lipid peroxidation reaction of polyvalent unsaturated fatty acid at plasmalemma, which developed lipid peroxidation products, such as MDA. So the MDA levels of sample serum showed the degree of lipid peroxidation injury of liver. The levels of MDA in ischemic reperfusion injury group at different time points were significantly higher than those in control (P<0.01). The levels of MDA increased gradually after reperfusion, reached the peak 6 h after reperfusion, and then decreased. The levels of MDA in TNFα antibody treatment group were remarkably lower than those in ischemic reperfusion injury group (P<0.01). The levels of MDA in TNFα antibody and ulinastatin treatment group were lower than those in ischemic reperfusion injury group and TNFα antibody treatment group (P<0.01).

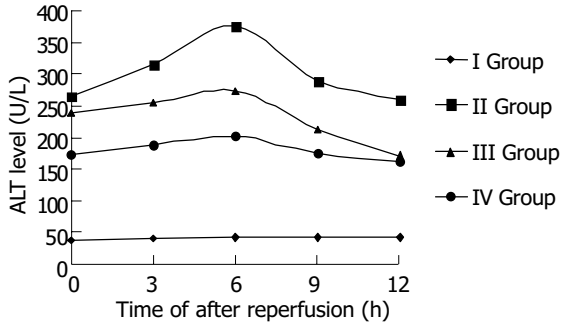

Figure 1 Serum ALT level after reperfusion in rats.

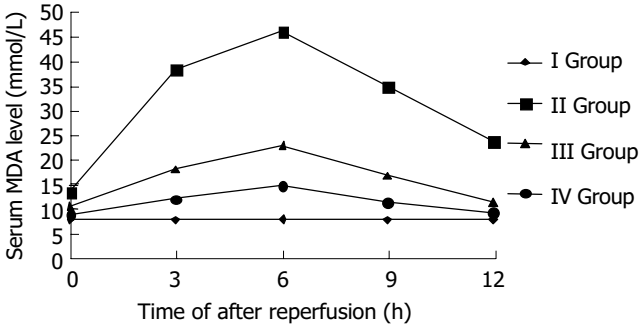

Figure 2 Serum MDA level after reperfusion in rats.

Histopathological observation

The blood stream in middle and left lobes of livers of rats was reperfused 1 h after blocked for 60 min. In ischemic reperfusion injury group, the middle and left lobes of livers were found to be swollen and faint. HE staining showed disorganized hepatic

lobules and extensive hepatocytic edema with various degrees of vacuolation and lamellar necrosis. The liver tissues in TNFα antibody treatment group and in TNFα antibody + ulinastatin treatment group were found to insignificantly swollen and faint in appearance. HE staining showed a sprinkle of hepatocytic edema without vacuolation and lamellar necrosis.

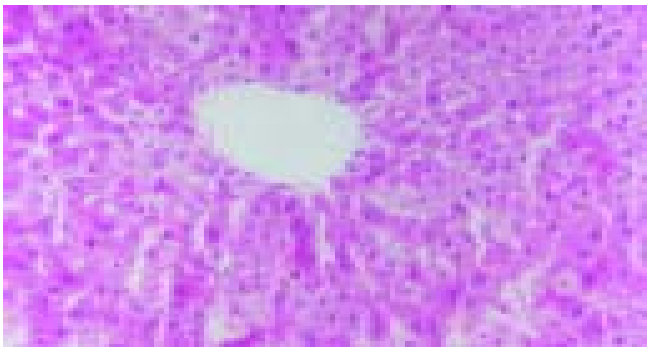

Figure 3 Disorganized hepatic lobules and extensive hepatocytic edema with various degrees of vacuolation and lamellar necrosis in ischemic reperfusion injury group.

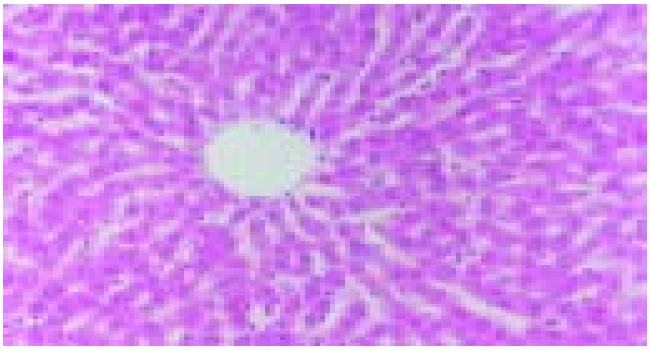

Figure 4 A sprinkle of hepatocytic edema without vacuolation and lamellar necrosis in TNFα antibody + ulinastatin treatment group.

DISCUSSION

Liver ischemic reperfusion injury can be frequently seen in surgical practice, and plays impotatnt roles in severe infection, trauma, shock, cardiorespiratory malfunction, organ transplantation, *etc*. Ischemic reperfusion can cause a series of injuries on metabolism, structure, and function in hepatic tissues and cells, and even liver function failure. So it is one of the major factors influencing the prognosis, operative success and survival of patients.

Cytokines, are the soluble polypeptides excreted by immunocytes, and play important roles in immunological activation and inflammatory reaction. The study of cytokine effects on ischemic reperfusion injury in liver has become highlights at present[17-22]. TNFα is the polypeptide excreted by activated macrophages, endothelial cells, neutrophilic granulocytes and B lymphocytes, and plays an important role in inflammatory reaction. Liver possesses tremendous Kupffer cells (KC) that have the great potency to produce TNFα in human body. At the time of liver ischemia, for the blockage of ATP production, calcium pump of liver is in dysfunction, which causes intracellular calcium overload. Aggravated calcium overload can activate Kupffer cells. On the other hand, Kupffer cells have complement receptors, intracellular protein was released during ischemic reperfusion, thus activating complements, which can also activate Kupffer cells. The activated Kupffer cells excrete TNFα. Liver has plenty of TNFα receptors, and also is the major target organ of TNFα[23-26]. Some mechanisms were used to explain the liver damage caused by TNFα[27-30]. Firstly, TNFα could directly injure hepatocytes. Secondly, TNFα could activate neutrophilic granulocytes and mononuclear macrophages to express IL-1 and IL-6, and phosphatidase A2 that can decompose arachidonic acids. Inflammatory media were produced such as platelet active factor, leukotriene, and thromboxane A2. So the inflammatory reaction was aggravated. Thirdly, the toxic effect of TNFα on endothelial cells could induce the circulatory disorder of hepatic sinusoid, and TNFα could activate complement system that aggravates tissue damage by cytotoxicity. Finally, the oxygen-derived free radidicals induced by TNFα could facilitate oxidation explosion of neutrophilic granulocytes, which could also result in liver damage. Therefore, the way to block the production of TNFα in liver can be used to prevent liver from injury by TNFα.

Ulinastatin is one kind of glycoproteins containing 143 amino acids with molecular weight of 67 ku. It is the typical urine protease inhibitor isolated and purified from human urine. Ulinastatin has two active function domains which have a wide restrained zymogram with no overlapped region each other. So ulinastatin can inhibit many hydrolytic enzymes in one time, including trypsin, phospholipase A_2, alidase and elastase. Moreover, the components of low molecular mass decomposed from ulinastatin can also inhibit hydrolytic enzymes strongly. On the other hand, ulinastatin could ameliorate the shock situation by blocking the production of myocardial depressant factors and stabilizing the membrane of lysosome[31-33]. Recent researches found that ulinastatin could block the release of inflammatory factors, prevent cascade reaction of cytokines, inhibit excessive activation of leukocytes and block vicious circles among cytokines, inflammatory factors and leukocytes. So when pancreatitis, shock or other severe infection occured, the action of multiple hydrolytic enzymes necessitated the use of ulinastatin, which can inhibit many hydrolytic enzymes at the same time and alleviate the vicious effects of multiple proteases on tissues and organs[34-36].

The present study was to verify the protective effect of TNFα antibody and ulinastatin on ischemic reperfusion injury of liver. The results showed that the levels of ALT and MDA in TNFα antibody and ulinastatin treatment group were remarkably decreased as compared with those in ischemic reperfusion injury group. Pathological changes of liver also demonstrated the significant protective effect of TNFα antibody and ulinastatin on ischemic reperfusion injury of liver. The present results suggest TNFα antibody and ulinastatin can effectively prevent ischemic reperfusion injury of liver. But further work is needed to make clear of their best concentrations, best ratio and their effect on immune system of the body.

REFERENCES

1 **Zhu X,** Qiu Y, Shi M, Ding Y. Matrine protects sinusoidal endothelial cells from cold ischemia and reperfusion injury in rat orthotopic liver transplantation. *Ann Clin Lab Sci* 2003; **33**: 216-225

2 **Zhou T,** Chen JL, Song W, Wang F, Zhang MJ, Ni PH, Geng JG. Effect of N-desulfated heparin on hepatic/renal ischemia reperfusion injury in rats. *World J Gastroenterol* 2002; **8**: 897-900

3 **Jawan B,** Goto S, Pan TL, Lai CY, Luk HN, Eng HL, Lin YC, Chen YS, Lan KM, Hsieh SW, Wang CC, Cheng YF, Chen CL. The protective mechanism of magnolol, a Chinese herb drug, against warm ischemia-reperfusion injury of rat liver. *J Surg Res* 2003; **110**: 378-382

4 **Teoh NC,** Farrell GC. Hepatic ischemia reperfusion injury: Pathogenic mechanisms and basis for hepatoprotection. *J Gastroenterol Hepatol* 2003; **18**: 891-902

5 **Fondevila C,** Busuttil RW, Kupiec-Weglinski JW. Hepatic ischemia/reperfusion injury-a fresh look. *Exp Mol Pathol* 2003; **74**: 86-93

6 **Donckier V,** Loi P, Closset J, Nagy N, Quertinmont E, Le Moine O, Deviere J, Goldman M, Gelin M, Gianello P. Precondi-

tioning of donors with interleukin-10 reduces hepatic ischemia-reperfusion injury after liver transplantation in pigs. *Transplantation* 2003; **75**: 902-904

7 **Banks WA,** Farr SA, Morley JE. Entry of blood-borne cytokines into the central nervous system: effects on cognitive processes. *Neuroimmunomodulation* 2003; **10**: 319-327

8 **Trefzer U,** Hofmann M, Sterry W, Asadullah K. Cytokine and anticytokine therapy in dermatology. *Expert Opin Biol Ther* 2003; **3**: 733-743

9 **Tsuchihashi S,** Tamaki T, Tanaka M, Kawamura A, Kaizu T, Ikeda A, Kakita A. Pyrrolidine dithiocarbamate provides protection against hypothermic preservation and transplantation injury in the rat liver: the role of heme oxygenase-1. *Surgery* 2003; **133**: 556-567

10 **Dutkowski P,** Wahl W, Winkelbach V, Watzka M, Krysiak M, Junginger T. Calcium prevents loss of glutathione and reduces oxidative stress upon reperfusion in the perfused liver. *Int J Surg Investig* 2000; **2**: 1-7

11 **Langdale LA,** Kajikawa O, Frevert C, Liggitt HD. Sustained tolerance to lipopolysaccharide after liver ischemia-reperfusion injury. *Shock* 2003; **19**: 553-558

12 **Chimalakonda AP,** Mehvar R. Attenuation of Kupffer cell activation in cold-preserved livers after pretreatment of rats with methylprednisolone or its macromolecular prodrug. *Pharm Res* 2003; **20**: 1001-1008

13 **Masuda T,** Sato K, Noda C, Ikeda KM, Matsunaga A, Ogura MN, Shimizu K, Nagasawa H, Matsuyama N, Izumi T. Protective effect of urinary trypsin inhibitor on myocardial mitochondria during hemorrhagic shock and reperfusion. *Crit Care Med* 2003; **31**: 1987-1992

14 **Yano T,** Anraku S, Nakayama R, Ushijima K. Neuroprotective effect of urinary trypsin inhibitor against focal cerebral ischemia-reperfusion injury in rats. *Anesthesiology* 2003; **98**: 465-473

15 **Sato N,** Endo S, Kimura Y, Ikeda K, Aoki K, Iwaya T, Akiyama Y, Noda Y, Saito K. Influence of a human protease inhibitor on surgical stress induced immunosuppression. *Dig Surg* 2002; **19**: 300-305

16 **Mourek J,** Koudelova J. Adrenergic tocolytics-their effects on lipoperoxidation in the brain. *Ceska Gynekol* 1997; **62**: 15-18

17 **Kato A,** Gabay C, Okaya T, Lentsch AB. Specific role of interleukin-1 in hepatic neutrophil recruitment after ischemia/reperfusion. *Am J Pathol* 2002; **161**: 1797-1803

18 **Shinoda M,** Shimazu M, Matsuda S, Wakabayashi G, Tanabe M, Hoshino K, Kamei S, Koyasu S, Kitajima M. c-Jun N-terminal kinase activation during warm hepatic ischemia/reperfusion injuries in a rat model. *Wound Repair Regen* 2002; **10**: 314-319

19 **Cutrn JC,** Perrelli MG, Cavalieri B, Peralta C, Rosell Catafau J, Poli G. Microvascular dysfunction induced by reperfusion injury and protective effect of ischemic preconditioning. *Free Radic Biol Med* 2002; **33**: 1200-1208

20 **Iwasaki Y,** Tagaya N, Hattori Y, Yamaguchi K, Kubota K. Protective effect of ischemic preconditioning against intermittent warm-ischemia-induced liver injury. *J Surg Res* 2002; **107**: 82-92

21 **Takahashi Y,** Ganster RW, Gambotto A, Shao L, Kaizu T, Wu T, Yagnik GP, Nakao A, Tsoulfas G, Ishikawa T, Okuda T, Geller DA, Murase N. Role of NF-kappaB on liver cold ischemia-reperfusion injury. *Am J Physiol Gastrointest Liver Physiol* 2002; **283**: G1175-1184

22 **Zamora R,** Vodovotz Y, Aulak KS, Kim PK, Kane JM 3rd, Alarcon L, Stuehr DJ, Billiar TR. A DNA microarray study of nitric oxide-induced genes in mouse hepatocytes: implications for hepatic heme oxygenase-1 expression in ischemia/reperfusion. *Nitric Oxide* 2002; **7**: 165-186

23 **Hines IN,** Kawachi S, Harada H, Pavlick KP, Hoffman JM, Bharwani S, Wolf RE, Grisham MB. Role of nitric oxide in liver ischemia and reperfusion injury. *Mol Cell Biochem* 2002; **234**: 229-237

24 **Kim YI,** Song KE, Ryeon HK, Hwang YJ, Yun YK, Lee JW, Chun BY. Enhanced inflammatory cytokine production at ischemia/reperfusion in human liver resection. *Hepatogastroenterology* 2002; **49**: 1077-1082

25 **Ben-Ari Z,** Hochhauser E, Burstein I, Papo O, Kaganovsky E, Krasnov T, Vamichkim A, Vidne BA. Role of anti-tumor necrosis factor-alpha in ischemia/reperfusion injury in isolated rat liver in a blood-free environment. *Transplantation* 2002; **73**: 1875-1880

26 **Kim YI,** Hwang YJ, Song KE, Yun YK, Lee JW, Chun BY. Hepatocyte protection by a protease inhibitor against ischemia/reperfusion injury of human liver. *J Am Coll Surg* 2002; **195**: 41-50

27 **Kataoka M,** Shimizu H, Mitsuhashi N, Ohtsuka M, Wakabayashi Y, Ito H, Kimura F, Nakagawa K, Yoshidome H, Shimizu Y, Miyazaki M. Effect of cold-ischemia time on C-X-C chemokine expression and neutrophil accumulation in the graft liver after orthotopic liver transplantation in rats. *Transplantation* 2002; **73**: 1730-1735

28 **Kato A,** Edwards MJ, Lentsch AB. Gene deletion of NF-kappa B p50 does not alter the hepatic inflammatory response to ischemia/reperfusion. *J Hepatol* 2002; **37**: 48-55

29 **Peralta C,** Perales JC, Bartrons R, Mitchell C, Gilgenkrantz H, Xaus C, Prats N, Fernandez L, Gelpi E, Panes J, Rosello-Catafau J. The combination of ischemic preconditioning and liver Bcl-2 overexpression is a suitable strategy to prevent liver and lung damage after hepatic ischemia-reperfusion. *Am J Pathol* 2002; **160**: 2111-2122

30 **Harada N,** Okajima K, Uchiba M, Katsuragi T. Ischemia/reperfusion-induced increase in the hepatic level of prostacyclin is mainly mediated by activation of capsaicin-sensitive sensory neurons in rats. *J Lab Clin Med* 2002; **139**: 218-226

31 **Itabashi K,** Ito Y, Takahashi T, Ishii K, Sato K, Kakita A. Protective effects of urinary trypsin inhibitor (UTI) on hepatic microvasculature in hypotensive brain-dead rats. *Eur Surg Res* 2002; **34**: 330-338

32 **Lin SD,** Endo R, Sato A, Takikawa Y, Shirakawa K, Suzuki K. Plasma and urine levels of urinary trypsin inhibitor in patients with acute and fulminant hepatitis. *J Gastroenterol Hepatol* 2002; **17**: 140-147

33 **Saitoh Y,** Kaneda K, Murakawa M. The effect of ulinastatin pre-treatment on vecuronium-induced neuromuscular block in patients with hepatic cirrhosis. *Anaesthesia* 2002; **57**: 218-222

34 **Pugia MJ,** Takemura T, Kuwajima S, Suzuki M, Cast TK, Profit JA, Schulman LS, Ohta Y, Lott JA. Clinical utility of a rapid test for uristatin. *Clin Biochem* 2002; **35**: 105-110

35 **Furukawa K,** Kamimura T, Mahune Y, Ohota H, Yoshida T, Ishihara N, Tazaki K, Suzuki Y, Honda S, Ito K, Miki I, Suzuki K, Honma A. Two patients with severe alcoholic hepatitis accompanied by hypercytokinemia and granulocytic hyperelastasemia, successfully treated by intravenous infusion of urinastarine Miradid. *J Gastroenterol Hepatol* 2001; **16**: 575-580

36 **Takada K,** Komori M, Notoya A, Tomizawa Y, Ozaki M. Effect of ulinastatin on microcirculation during excessive hemorrhage using fluid therapy. *In Vivo* 2003; **17**: 129-135

Edited by Zhang JZ and Wang XL **Proofread by** Xu FM

PO Box 2345, Beijing 100023, China
Fax: +86-10-85381893
E-mail: wjg@wjgnet.com www.wjgnet.com

World J Gastroenterol 2004;10(21):3165-3170
World Journal of Gastroenterology
 ISSN 1007-9327

• BASIC RESEARCH •

Oral and nasal administration of chicken type II collagen suppresses adjuvant arthritis in rats with intestinal lesions induced by meloxicam

Yong-Qiu Zheng, Wei Wei, Yu-Xian Shen, Min Dai, Li-Hua Liu

Yong-Qiu Zheng, Wei Wei, Yu-Xian Shen, Min Dai, Li-Hua Liu, Institute of Clinical Pharmacology, Anhui Medical University, Hefei 230032, Anhui Province, China
Correspondence to: Professor Wei Wei, Institute of Clinical Pharmacology, Anhui Medical University, Hefei 230032, Anhui Province, China. wwei@ahmu.edu.cn
Telephone: +86-551-5161208 **Fax:** +86-551-5161208
Received: 2004-03-23 **Accepted:** 2004-04-16

Abstract

AIM: To investigate the curative effects of oral and nasal administration of chicken type II collagen (CII) on adjuvant arthritis (AA) in rats with meloxicam-induced intestinal lesions.

METHODS: AA model in Sprague-Dawley (SD) rats with or without intestinal lesions induced by meloxicam was established and those rats were divided randomly into six groups which included AA model, AA model+meloxicam, AA model+oral CII, AA model+nasal CII, AA model+meloxicam+oral C II and AA model+meloxicam+nasal CII (n = 12). Rats was treated with meloxicam intragastrically for 7 d from d 14 after immunization with complete Freund's adjuvant (CFA), and then treated with chicken CII intragastrically or nasally for 7 d. Histological changes of right hind knees were examined. Hind paw secondary swelling and intestinal lesions were evaluated. Synoviocyte proliferation was measured by 3-(4,5-dimethylthiazol-2-thiazolyl)-2,5-diphenyl-2H tetrazolium bromide (MTT) method. Activities of myeloperoxidase (MPO) and diamine oxidase (DAO) from supernatants of intestinal homogenates were assayed by spectrophotometric analysis.

RESULTS: Intragastrical administration of meloxicam (1.5 mg/kg) induced multiple intestinal lesions in AA rats. There was a significant decrease of intestinal DAO activities in AA+meloxicam group (P<0.01) and AA model group (P<0.01) compared with normal group. DAO activities of intestinal homogenates in AA+meloxicam group were significantly less than those in AA rats (P<0.01). There was a significant increase of intestinal MPO activities in AA+meloxicam group compared with normal control (P<0.01). Oral or nasal administration of CII (20 μg/kg) could suppress the secondary hind paw swelling(P<0.05 for oral CII; P<0.01 for nasal CII), synoviocyte proliferation (P<0.01) and histopathological degradation in AA rats, but they had no significant effects on DAO and MPO changes. However, oral administration of CII (20 μg/kg) showed the limited efficacy on arthritis in AA+meloxicam model and the curative effects of nasal CII (20 μg/kg) were shown to be more efficient than that of oral CII (20 μg/kg) both in AA model and in AA+meloxicam model (P<0.05).

CONCLUSION: Oral administration of CII shows the limited efficacy on arthritis in AA rats with intestinal lesions, and nasal administration of CII is more efficient than oral administration of CII to induce mucosal tolerance in AA rats.

Zheng YQ, Wei W, Shen YX, Dai M, Liu LH. Oral and nasal administration of chicken type II collagen suppresses adjuvant arthritis in rats with intestinal lesions induced by meloxicam. *World J Gastroenterol* 2004; 10(21): 3165-3170
http://www.wjgnet.com/1007-9327/10/3165.asp

INTRODUCTION

Rheumatoid arthritis (RA) is a chronic autoimmune disease characterized by inflammation of the joints including proliferation of the synovium and progressive erosion of cartilages and bones[1]. The goals of treatment include reduction of pain and inflammation, maintenance of functional ability, slowing of disease progression, and prevention of adverse effects of drugs[2]. Administering antigens via a mucosal route has been recognized as a means to induce tolerance. The phenomenon of oral tolerance (OT) was first reported in 1911 by Wells[3]. Further studies demonstrated that CII could suppress arthritis induced by adjuvant[4], antigen[5], pristane[6] and collagen[7] in mice and rats. Moreover, several clinical trials based on the results from those experimental animal systems, have been conducted to test the feasibility of using oral tolerance in the treatment of RA[8,9]. However, it was reported that oral administration of CII in a low dose of 10 μg for 10 times demonstrated a doubtful effect on murine collagen-induced arthritis (CIA) model[10]. In clinical trials, oral administration of CII showed no efficacy in human arthritis given along with existing treatment[11] and moreover, the Peyer's patches (pp) in the gut-associated lymphoid tissue (GALT) were considered to mediate oral tolerance[12]. As we know, nonsteroidal anti-inflammatory drugs (NSAIDs) including meloxicam, which have been usually considered as the main drugs in the management of RA, could induce digestive lesions[13,14], and it might be an important reason for the invalidation of oral administration of CII. Therefore, nasal administration of CII should be considered as an alternative.

Adjuvant arthritis (AA) in rats is an experimental model that shares some features with human RA, such as swelling, cartilage degradation and loss of joint function[15]. In the present study, therefore, AA rats with or without intragastrically administration of meloxicam were used to compare the curative effects of oral and nasal administration of CII in rats with or without intestinal lesions. Based on the results of our report that oral administration of CII suppressed pro-inflammatory mediator production by synoviocytes in rats with adjuvant arthritis from 5 to 500 μg/kg[12], we chose the single dose of 20 μg/kg in the present study.

Diamine oxidase (DAO) is an intracellular enzyme with a high activity existing in intestinal villous cells and can catalyze the oxidation of diamines such as histamine, putrescine and cadaverine in both human beings and all other mammalians. The activity of DAO in intestinal mucosa decreases when its cells are injured. Thus the determination of the DAO activity of intestinal mucosa can reflect the changes in its cellular integrity[16]. Myeloperoxidase (MPO) plays a fundamental role in oxidant production by neutrophils and is considered to be a major effector in the tissue damage[17]. In our studies, MPO and DAO were used as markers of intestinal dysfunction.

The purpose of the present study was to compare the curative effects of oral and nasal administration of CII in AA rats with or without intestinal lesions induced by meloxicam.

MATERIALS AND METHODS

Animals

Male Sprague-Dawley (SD) rats weighting 147±25 g were purchased from Shanghai BK Experimental Animal Center (Grade II, Certificate No D-65). All rats were housed, five per cage and fed a standard laboratory chew and water and kept on a 12 h dark/12 h light cycle at a constant temperature of 20±5 ℃. All experimental protocols described in this study were approved by the Ethics Review Committee for Animal Experimentation of Institute of Clinical Pharmacology, Anhui Medical University.

Drugs and materials

Meloxicam (batch number 020401), nasal chicken CII (batch number 00031004) and oral chicken CII (batch number 00031002) were obtained from Shanghai Institute of Herb and Bio-medical Engineering and dissolved in sterile water containing 5 g/L carboxymethylcellulose (CMC-Na) solution. Dimethyl sulfoxide (batch number 000601) was obtained from Shanghai Vitriolic Factory. Bacillus Calmette Guerin (BCG) was obtained from Shanghai Biochemical Factory. Collagenase type II, trypsin, 3-(4,5-dimethylthiazol-2-thiazolyl)-2,5- diphenyl-2H tetrazolium bromide (MTT), RPMI 1640 medium, lipopolysaccharide (LPS), horseradish perozidase, cadaverine dihydrochloride, diamine oxidase (DAO) and *O*-dianisidine were purchased from Sigma Chemical Co. (St. Louis, MO, USA).

Induction and evaluation of AA

Complete Freund's adjuvant (CFA) was prepared by suspending heat-killed BCG in liquid paraffin at 10 mg/mL. AA was induced by a single intradermal injection of 100 μL of CFA into the left hind paw. On d 0, 14, 16, 20, 24 and 28 after immunization, the right hind paw volume was measured with a water replacement plethsmometer (Mukomachi Kiai CD, Japan). Paw swelling (mL) was calculated by taking away the paw volume on d 0 from the related one on d 14, 16, 20, 24 and 28.

Drug treatment

The rats with AA were divided randomly into six groups which included AA model, AA model+meloxicam, AA model+oral CII, AA model+nasal CII, AA model+meloxicam+oral C II and AA model+meloxicam+nasal C II. From d 14 after immunization, the rats were fasted for 12 h and then treated with meloxicam (1.5 mg/kg body weight) intragastrically for 7 d. The rats in normal group, AA group, AA model+oral CII group and AA+nasal CII group, were treated with an equal amount of vehicle. From d 21 after immunization, the rats were treated with oral or nasal administration of CII (20 μg/kg body mass) for 7 d. The rats in normal group, AA group and AA+meloxicam group, were treated with an equal amount of vehicle.

Evaluation of intestinal lesions

Rats were sacrificed on day 29 after immunization. The small intestines were removed, spread out on filter paper and opened by a longitudinal incision along the antimesenteric side. The length and width of each lesion were observed and the extent of haemorrhage was also observed according to scale scores 0-2: 0, absence; 1, slight haemorrhage; 2, severe haemorrhage.

Synoviocyte proliferation

Synovial tissue from rat knees was excised and dispersed with sequential incubation of 4 g/L collagenase type II and 2.5 g/L trypsin and then synoviocytes were suspended in RPMI-1640 medium with 200 mL/L fetal bovine serum (FBS) at a concentration of 1×10^6 cells/mL. In 96-well plates, 100 μL of synoviocyte suspension (1×10^5 cells/well) was cultured in triplicate with 100 μL of LPS (10 mg/L) in RPMI-1640 medium (pH7.0) containing 200 mL/L heat-inactivated FBS, 100 U/mL penicillin, 100 g/L streptomycin, 2 mmol/L *L*-glutamine , 5×10^{-5} moL/L 2-mercaptoethanol and 25 mmol/L HEPES. After cultured for 48 h at 37 ℃ in humidified atmosphere containing 50 mL/L CO_2 in air, proliferation of synoviocytes was measured by the MTT colorimetric method[18]. In brief, 48 h later, MTT was dissolved in phosphate buffered saline (PBS) at a dose of 5 mg/mL and added to all wells (10 μL/well), then the plates were incubated at 37 ℃ in humidified atmosphere containing 50 mL/L CO_2 for an additional 4 h. After incubation, the cells were centrifuged at 1000 r/min for 10 min and all the supernatants were discarded. Then 200 μL of dimethyl sulfoxide was added to each well, and the plates were read 30 sec later in an ELISA plate reader at a wavelength of 490 nm. The absorbance (*A*) of each well was regarded as the degree of synoviocyte proliferation.

Histological examination

The right legs and hind paws of rats were removed and fixed with 100 g/L paraformaldehyde in PBS, and then decalcified for 10 d with ethylene diamine tetraacetic acid (EDTA) and embedded in paraffin for histologic analysis. The paraffin sections were stained with hematoxylin and eosin. The slides were evaluated histologically by two independent observers, and the gradation of arthritis was scored from 0 to 4 according to the intensity of lining layer hyperplasia, mononuclear cell infiltration, and pannus formation, as described previously[19]: 0, normal ankle joint; 1, normal synovium with occasional mononuclear cells; 2, definite arthritis, a few layers of flat to rounded synovial lining cells and scattered mononuclear cells and dense infiltration with mononuclear cells; 3, clear hyperplasia of the synovium with three or more layers of loosely arranged lining cells and dense infiltration with mononuclear cells; 4, severe synovitis with pannus and erosions of articular cartilages and subchondral bones.

MPO bioassay

Animals were sacrificed and their small intestines were flushed with 10 mL of sterile saline, followed by separation from bodies. After dried with filter paper, 0.5 g of intestinal specimens was weighed and placed in 5 mL of ice-cold potassium phosphate buffer (pH 6.0) with 5 g/L hexadecyl- trimethylammonium bromide. The specimens were homogenized for 20 s (2×10 s) and sonicated for 30 s (3×10 s) and centrifuged at 12000 *g* for 15 min at 4 ℃. The supernatant was spectrophotometrically assayed for MPO activity by measuring the change in absorbance (at 460 nm) over time. The assay buffer consisted of 50 mmoL/L potassium phosphate, pH 6.0 (50 mL), 0.83 mL of H_2O_2 (3 mL/L solution), and 8.34 mg of *O*-dianisidine hydrochloride. The supernatant was mixed at 1:80 (supernatant: assay buffer). MPO units were expressed as $\Delta A/(min\cdot g)$.

DAO bioassay

Intestinal DAO activity was determined as follows. In brief, to 0.5 mL homogenate of intestinal specimens gained according to the above method or 0.5 mL dilated standard solution, 3 mL of PBS (0.2 mol/L, pH 7.2), 0.1 mL of horseradish peroxidase (4 μg), 0.1 mL of DAO (500 μg), and 0.1 mL of dianisidine were added. After mixed, the mixture was incubated in a water bath at 37 ℃ for 30 min, then the absorbance value at 436 nm (A_{436}) was recorded after rested for 5 min in the air. The DAO activities were calculated according to the standard curve. Protein activities of the tissue homogenates were determined with Lowry's method[20]. DAO units were expressed as A/mg pro.

Statistical analysis

Results were expressed as mean±SD, and *t*-test was used to make comparisons between the groups. $P<0.05$ was considered statistically significant.

RESULTS

Intestinal lesions induced by meloxicam

As shown in Figure. 1, intragastrical administration of meloxicam (1.5 mg/kg) for 7 d induced multiple intestinal lesions in AA rats. In normal control rats (Figure 1A), AA rats (Figure 1B), AA rats treated with oral CII (Figure 1D) and AA rats treated with nasal CII (Figure 1E), haemorrhage was not observed in antimesenteric side of small intestine (grade 0). In AA rats given meloxicam intragastrically (Figure 1C), AA+meloxicam rats treated with oral CII (Figure 1F) and AA+meloxicam rats treated with nasal CII (Figure 1G), severe haemorrhage was observed in antimesenteric side of small intestine (grade 2). After the animals were treated with oral or nasal administration of CII (20 μg/kg) for 7 d, development of these lesions was not prevented.

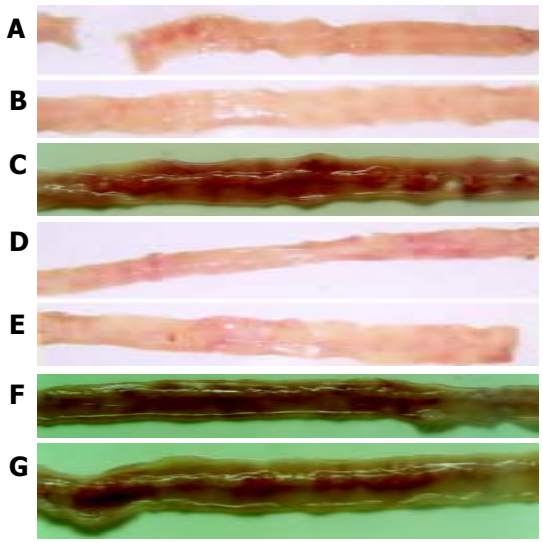

Figure 1 Intestinal lesions induced by meloxicam. A: Normal control rats; B: AA rats; C: AA rats given meloxicam intragastrically; D: AA rats treated with oral CII; E: AA rats treated with nasal CII; F: AA+meloxicam rats treated with oral CII; and G: AA+meloxicam rats treated with nasal CII.

DAO activities in intestinal homogenates

The levels of DAO in intestinal homogenates are shown in Table 1. There was a significant decrease of intestinal DAO activities in AA+meloxicam group ($P<0.01$) and AA model group ($P<0.01$) compared with normal group. DAO activities of intestinal homogenates in AA+meloxicam group were significantly less than those in AA rats ($P<0.01$). Oral or nasal administration of CII had no significant effects on DAO changes.

MPO activities in intestinal homogenates

The levels of MPO in intestinal homogenates are shown in Table 1. There was a significant increase of intestinal MPO activities in AA+meloxicam group compared with normal control ($P<0.01$). Oral or nasal administration of CII had no significant effects on MPO changes.

Table 1 Effects of oral and nasal administration of CII on activities of intestinal MPO and DAO in AA rats with or without intragastrical administration of meloxicam (n = 12, mean±SD)

Groups	DAO (A/mg pro)	MPO (ΔA/(min·g))
Nomal	0.37±0.065	99.47±22.54
AA model	0.26±0.031[b]	139.80±25.14
AA model+meloxicam	0.15±0.032[ab]	165.42±21.27[b]
AA model+oral CII	0.27±0.051	137.15±26.32
AA model+nasal CII	0.28±0.029	132.17±23.18
AA model+meloxicam +oral CII	0.15±0.052[ab]	159.25±33.36[b]
AA model+meloxicam +nasal CII	0.16±0.029[ab]	152.29±27.20[b]

[a]$P<0.05$ *vs* AA model; [b]$P<0.01$ *vs* normal control.

Effects of oral or nasal administration of CII on secondary arthritis in AA rats with or without intragastrical administration of meloxicam

As shown in Table 2, secondary arthritis appeared on d 14, and maintained to d 28 after immunization in AA rats ($P<0.01$). In AA+meloxicam rats, hind paw secondary swellings were suppressed on d 20 ($P<0.05$). The hind paw secondary swellings were suppressed on d 20 in AA model+meloxicam +oral C II group and AA model+meloxicam+nasal C II group ($P<0.05$). Oral treatment with CII (20 μg/kg body mass) significantly suppressed hind paw secondary swelling not only on d 24 and 28 in AA rats ($P<0.05$), but also on d 24 in AA rats with intestinal lesions induced by meloxicam ($P<0.05$). The effects of oral CII were more obvious in AA model than in AA model with intestinal lesions on d 28. While nasal treatment with CII at the same dose significantly suppressed hind paw secondary swelling on d 24 and 28 in both AA rats and AA rats with intestinal lesions ($P<0.01$). The effects of nasal CII in AA model were similar to those in AA+meloxicam model, and the effects of nasal CII were more efficient than those of oral CII both in AA model and in AA+meloxicam model ($P<0.05$).

Table 2 Effects of oral and nasal administration of CII on hind paw secondary swelling in AA rats with or without intragastrical administration of meloxicam (n = 12, mean±SD)

Groups	Dose (μg/kg)	d 14	d 16	d 20	d 24	d 28
Normal	---	0.07±0.05	0.12±0.04	0.19±0.04	0.23±0.03	0.26±0.03
AA model	---	0.41±0.31[d]	0.63±0.16[d]	0.99±0.21[d]	1.22±0.27[d]	1.16±0.21[d]
AA model+meloxicam	---	0.29±0.32[a]	0.45±0.27[a]	0.68±0.18[ad]	0.97±0.49[d]	0.99±0.32[d]
AA model+oral CII	20	0.39±0.12	0.59±0.27	0.97±0.15	0.81±0.17[a]	0.79±0.21[a]
AA model+nasal CII	20	0.38±0.12	0.63±0.13	1.03±0.10	0.69±0.07[b]	0.48±0.09[bc]
AA model l+meloxicam+oral CII	20	0.31±0.09	0.46±0.26	0.70±0.12[a]	0.79±0.31[a]	0.95±0.25
AA model+meloxicam+nasal CII	20	0.32±0.16	0.43±0.19	0.73±0.22[a]	0.61±0.21[b]	0.57±0.17[be]

[a]$P<0.05$ *vs* AA model; [b]$P<0.01$ *vs* AA model; [c]$P<0.05$ *vs* AA model + oral CII; [d]$P<0.01$ *vs* normal control; [e]$P<0.05$ *vs* AA model+ meloxicam+oral CII.

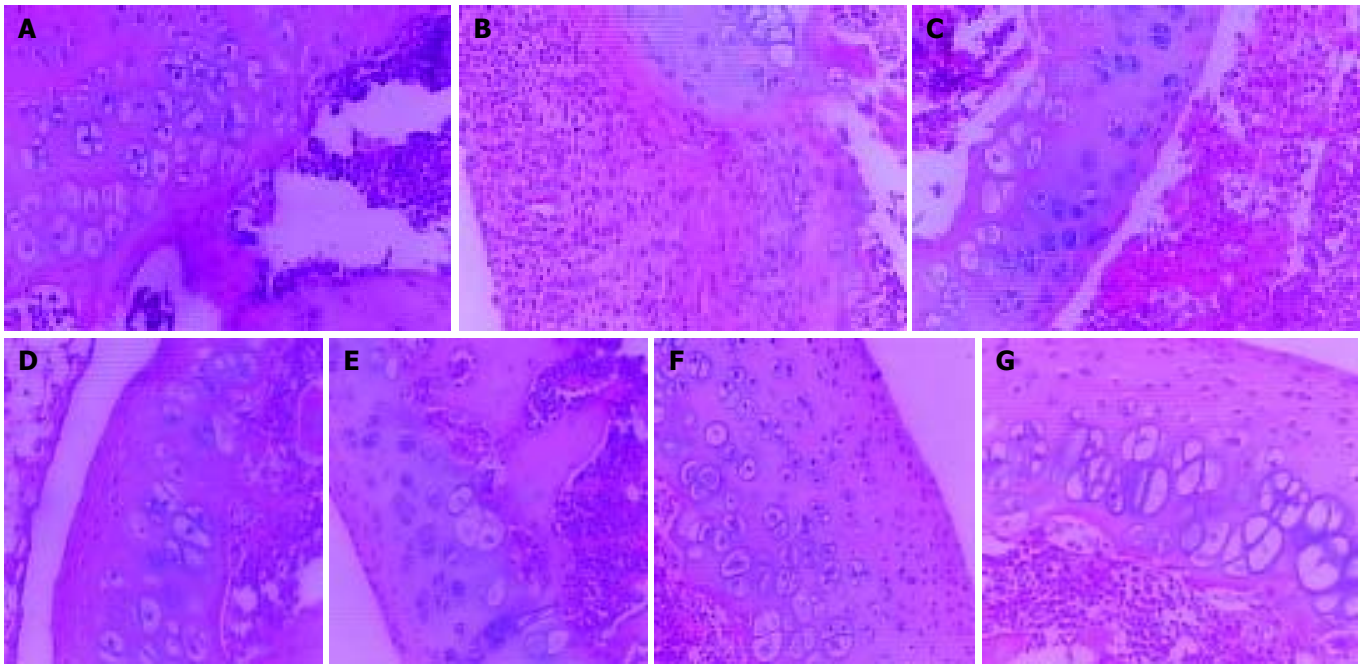

Figure 2 Effects of oral or nasal administration of CII on knee joint histopathology in AA rats with or without intragastrical administration of meloxicam (HE stain, ×100). A: Normal control rats (grade 0); B: AA rats (grade 4); C: AA rats given meloxicam intragastrically (grade 4); D: AA rats treated with oral CII (grade 3); E: AA rats treated with nasal CII (grade 2); F: AA+meloxicam rats treated with oral CII (grade 3); and G: AA+meloxicam rats treated with nasal CII (grade 2).

Effects of oral or nasal administration of CII on synoviocyte proliferation in AA rats with or without intragastrical administration of meloxicam

As shown in Table 3, synoviocyte proliferation in AA rats and AA+meloxicam rats was increased (P<0.01). Oral or nasal administration of CII (20 μg/kg) for 7 d significantly suppressed synoviocyte proliferation (P<0.01) in AA rats. In AA rats with intestinal lesions, nasal administration of CII (20 μg/kg) could also significantly suppress synoviocyte proliferation (P<0.01), while oral administration of CII at the same dosage suppressed synoviocyte proliferation at a lower degree (P<0.05). There was a significant difference between degrees of synoviocyte proliferation in AA rats with intestinal lesions treated by oral CII and those in the same model treated by nasal CII (P<0.05).

Table 3 Effects of oral and nasal administration of CII on synoviocytes proliferation in AA rats with or without intragastrical administration of meloxicam (n = 12, mean±SD)

Groups	Dose (μg/kg)	Synoviocytes proliferation (A_{490})
Nomal	-	0.27±0.024
AA model	-	0.32±0.045[d]
AA model+meloxicam	-	0.31±0.025[d]
AA model+oral CII	20	0.27±0.041[b]
AA model+nasal CII	20	0.24±0.048[b]
AA model l+meloxicam+oral CII	20	0.29±0.047[a]
AA model+meloxicam+nasal CII	20	0.25±0.041[bc]

[a]P<0.05 *vs* AA model; [b]P<0.01 *vs* AA model; [d]P<0.01 *vs* normal control; [c]P<0.05 *vs* AA model+meloxicam+oral CII.

Effects of oral or nasal administration of CII on knee joint histopathology in AA rats with or without intragastrical administration of meloxicam

In normal rats, synoviocytes were monolayer (Figure 2A). In AA rats, synoviocytes proliferated three to eight layers and became ovalis types, and articular cartilages were destructed and infiltrated with inflammatory cells. The hyperplastic synovial membranes in AA rats formed a large number of fibroblasts and new blood vessels. Proliferation of collagen fribrils was found under synovial membranes of AA rats (Figure 2B). In AA rats given meloxicam intragastrically, knee joint histopathology was similar to that in AA rats (Figure 2C). In AA rats treated with oral CII, hyperplastic synoviocytes decreased to two or three layers (Figure 2D). In AA rats treated with nasal CII, a few of hyperplastic fiber cells under synovial membranes could be found (Figure 2E). In AA+meloxicam rats treated with oral CII, synovial hyperplasia was observed and articular cartilages were destroyed and infiltrated with inflammatory cells (Figure 2F). In AA+meloxicam rats treated with nasal CII, a few of hyperplastic fiber cells under synovial membranes and partially reversed articular cartilage destrustion could be found (Figure 2G).

Oral or nasal administration of CII could ameliorate the pathologic changes in AA rats or AA+meloxicam rats, but oral administration of CII showed limited efficacy on suppressing the histopathological degradation in AA model with intestinal lesions.

DISCUSSION

In this study, it was found that intragastric administration of meloxicam (1.5 mg/kg) could induce multiple intestinal lesions in AA rats. The activities of DAO in intestinal homogenates were decreased and the activities of MPO were increased. Oral or nasal administration of CII at a dose of 20 μg/kg could suppress secondary hind paw swelling, synoviocyte proliferation and histopathological degradation in AA model and AA+meloxicam model. Moreover, oral administration of CII showed the limited efficacy on arthritis in AA+meloxicam model and curative effects of nasal CII were shown to be more efficient in comparison with oral CII both in AA model and AA+meloxicam model.

Just like RA, AA is a chronic disease and the ongoing disease can be blocked using antibodies to T cells. They are associated with major histocompatibility complex (MHC) and the primary inflammatory attack is directed to diarthriodial peripheral joints[21].

Thus, development of mucosal tolerance methods for treatment of RA is suitable and could be found successfully both in humans[22,23] and in animal models induced with various heterologous antigens[4-6,24]. Histopathological study showed that oral administration of CII resulted in reduction of synovial hyperplasia, mononuclear infiltration, pannus formation and cartilage erosions[6]. Results from the present study also showed that oral CII suppressed secondary paw swelling, synoviocyte proliferation and histopathological changes in AA rats. Furthermore, clinical studies with oral administration of heterologous CII in RA were carried out and had disputable results[8,22]. Barnett *et al*.[25] found that very low doses tended to give an overall ameliorative effect, whereas higher doses were negative. In addition, intranasal administration of CII could ameliorate ongoing arthritis in pristane-induced arthritis (PIA), collagen-induced arthritis (CIA) and AA[26]. The use of nasal instead of oral administration of the autoantigens has been shown to be more efficient and to require lower tolerogen doses, as demonstrated in several models including CIA in mice[27]. It was also demonstrated that nasal administration of CII in murine CIA model more efficiently inhibited the induction of CIA and CII-specific immune responses than oral adiministration[10]. Our present study indicated that nasal CII could suppress secondary paw swelling, synoviocyte proliferation and histopathological changes in AA rats and was superior to oral CII.

Meloxicam is a NSAID belonging to the enolic acid group of the oxicam family[28]. As a cyclooxygenase - 2 inhibitor, meloxicam has been considered with a good gastric tolerance[29,30]. But it was also reported that meloxicam could induce gastric lesions[31]. Neutrophils, which secrete MPO, appear to be the main effector cells in meloxicam-induced small intestinal damage[32]. On the other hand, there are two major mechanisms which have been put forward to explain the oral tolerance: active suppression or the antigen specfic induction of regulatory cells and T cell clonal anergy/deletion[33,34]. Cells from PP in GALT were reported to mediate the induction of active suppression[35]. PP cell dysfunction induced by NSAIDs might be the main mechanism of the limited therapeutic effects of oral CII in the suppression of RA in clinical trials. So far, there are few reports to determine it.

In our study, we found that meloxicam (1.5 mg/kg) could induce multiple intestinal lesions in AA rats, and in this model, the activities of DAO were decreased and the activities of MPO were increased. We also found that meloxicam had little effect on AA rats from d 24. These results also indicated that there was a functional turbulence in intestinal systems of AA rats. Furthermore, we found that the effects of oral CII were more obvious in AA model than in AA model with intestinal lesion induced by meloxicam. However, the effects of nasal CII were not influenced by meloxicam in AA rats with intestinal lesions. The results suggested that nasal CII was more efficient than oral CII both in AA rats and in AA rats with intestinal lesions.

In conclusion, at the dose of 20 μg/kg, oral administration of CII has a limited efficacy on arthritis in AA+meloxicam model and the effects of nasal administration of CII on AA are more efficient than that of oral administration of CII both in AA rats and in AA rats with intestinal lesions induced by meloxicam.

REFERENCES

1 **Strand V**, Kavanaugh AF. The role of interleukin-1 in bone resorption in rheumatoid arthritis. *Rheumatology* 2004; **43** (Suppl 3): III10-16

2 **Blake SM**, Swift BA. What next for rheumatoid arthritis therapy? *Curr Opin Pharmacol* 2004; **4**: 276-280

3 **Wells HG**. Studies on the chemistry of anaphylaxis (III). Experiments with isolated proteins, especially those of the hen's egg. *J Infect Dis* 1911; **9**: 147–171

4 **Hu Y**, Zhao W, Qian X, Zhang L. Effects of oral administration of type II collagen on adjuvant arthritis in rats and its mechanisms. *Chin Med J* 2003; **116**: 284-287

5 **Yoshino S**, Quattrocchi E, Weiner HL. Suppression of antigen-induced arthritis in Lewis rats by oral administration of type II collagen. *Arthritis Rheum* 1995; **38**: 1092-1096

6 **Thompson SJ**, Thompson HS, Harper N, Day MJ, Coad AJ, Elson CJ, Staines NA. Prevention of pristane-induced arthritis by the oral administration of type II collagen. *Immunology* 1993; **79**: 152-157

7 **Min SY**, Hwang SY, Park KS, Lee JS, Lee KE, Kim KW, Jung YO, Koh HJ, Do JH, Kim H, Kim HY. Induction of IL-10-producing CD4+CD25+T cells in animal model of collagen-induced arthritis by oral administration of type II collagen. *Arthritis Res Ther* 2004; **6**: R213-219

8 **Choy EH**, Scott DL, Kingsley GH, Thomas S, Murphy AG, Staines N, Panayi GS. Control of rheumatoid arthritis by oral tolerance. *Arthritis Rheum* 2001; **44**: 1993-1997

9 **Myers LK**, Higgins GC, Finkel TH, Reed AM, Thompson JW, Walton RC, Hendrickson J, Kerr NC, Pandya-Lipman RK, Shlopov BV, Stastny P, Postlethwaite AE, Kang AH. Juvenile arthritis and autoimmunity to type II collagen. *Arthritis Rheum* 2001; **44**: 1775-1781

10 **Higuchi K**, Kweon MN, Fujihashi K, McGhee JR, Kiyono H. Comparison of nasal and oral tolerance for the prevention of collagen induced murine arthritis. *J Rheumatol* 2000; **27**: 1038-1044

11 **Postlethwaite AE**. Can we induce tolerance in rheumatoid arthritis? *Curr Rheumatol Rep* 2001; **3**: 64-69

12 **Ding CH**, Li Q, Xiong ZY, Zhou AW, Jones G, Xu SY. Oral administration of type II collagen suppresses pro-inflammatory mediator production by synoviocytes in rats with adjuvant arthritis. *Clin Exp Immunol* 2003; **132**: 416-423

13 **Combe B**, Flipo RM. What treatments can reduce the digestive complications of NSAIDs. *Presse Med* 2003; (37 Pt 2)**32**: S33-37

14 **Hawkey CJ**, Wilson I, Naesdal J, Langstrom G, Swannell AJ, Yeomans ND. Influence of sex and *Helicobacter pylori* on development and healing of gastroduodenal lesions in non-steroidal anti-inflammatory drug users. *Gut* 2002; **51**: 344-350

15 **Jacobson PB**, Morgan SJ, Wilcox DM, Nguyen P, Ratajczak CA, Carlson RP, Harris RR, Nuss M. A new spin on an old model: *in vivo* evaluation of disease progression by magnetic resonance imaging with respect to standard inflammatory parameters and histopathology in the adjuvant arthritic rat. *Arthritis Rheum* 1999; **42**: 2060-2073

16 **Peng X**, Yan H, You Z, Wang P, Wang S. Effects of enteral supplementation with glutamine granules on intestinal mucosal barrier function in severe burned patients. *Burns* 2004; **30**: 135-139

17 **Takeuchi K**, Tanaka A, Ohno R, Yokota A. Role of COX inhibition in pathogenesis of NSAID-induced small intestinal damage. *J Physiol Pharmacol* 2003; **54**(Suppl 4): 165-182

18 **Russell CA**, Vindelov LL. Optimization and comparison of the MTT assay and the 3H-TdR assay for the detection of IL-2 in helper T cell precursor assays. *J Immunol Methods* 1998; **217**: 165-175

19 **Chen Q**, Wei W. Effects and mechanisms of glucosides of chaenomeles speciosa on collagen-induced arthritis in rats. *Int Immunopharmacol* 2003; **3**: 593-608

20 **Tomazic-Jezic VJ**, Truscott W. Identification of antigenic and allergenic natural rubber latex proteins by immunoblotting. *J Immunoassay Immunochem* 2002; **23**: 369-383

21 **Mimran A**, Mor F, Carmi P, Quintana FJ, Rotter V, Cohen IR. DNA vaccination with CD25 protects rats from adjuvant arthritis and induces an antiergotypic response. *J Clin Invest* 2004; **113**: 924-932

22 **Choy EH**, Scott DL, Kingsley GH, Thomas S, Murphy AG, Staines N, Panayi GS. Control of rheumatoid arthritis by oral tolerance. *Arthritis Rheum* 2001; **44**: 1993-1997

23 **Cazzola M**, Antivalle M, Sarzi-Puttini P, Dell'Acqua D, Panni B, Caruso I. Oral type II collagen in the treatment of rheumatoid arthritis. A six-month double blind placebo-controlled study. *Clin Exp Rheumatol* 2000; **18**: 571-577

24 **Bardos T**, Czipri M, Vermes C, Zhang J, Mikecz K, Glant TT. Continuous nasal administration of antigen is critical to main-

tain tolerance in adoptively transferred autoimmune arthritis in SCID mice. *Clin Exp Immunol* 2002; **29**: 224-231

25 **Barnett ML**, Kremer JM, St Clair EW, Clegg DO, Furst D, Weisman M, Fletcher MJ, Chasan-Taber S, Finger E, Morales A, Le CH, Trentham DE. Treatment of rheumatoid arthritis with oral type II collagen. Results of a multicenter, double-blind, placebo-controlled trial. *Arthritis Rheum* 1998; **41**: 290-297

26 **Lu S**, Holmdahl R. Different therapeutic and bystander effects by intranasal administration of homologous type II and type IX collagens on the collagen-induced arthritis and pristane-induced arthritis in rats. *Clin Immunol* 1999; **90**: 119-127

27 **Garcia G**, Komagata Y, Slavin AJ, Maron R, Weiner HL. Suppression of collagen-induced arthritis by oral or nasal administration of type II collagen. *J Autoimmun* 1999; **13**: 315-324

28 **Albengres E**, Urien S, Barre J, Nguyen P, Bree F, Jolliet P, Tillement JP, Tsai RS, Carrupt PA, Testa B. Clinical pharmacology of oxicams: new insights into the mechanisms of their dose-dependent toxicity. *Int J Tissue React* 1993; **15**: 125-134

29 **Cryer B**, Dubois A. The advent of highly selective inhibitors of cyclooxygenase-a review. *Prostaglandins Other Lipid Mediat* 1998; **56**: 341-361

30 **Layton D**, Harris S, Shakir S. Reply: Re: Layton et al. Comparison of the incidence rates of selected gastrointestinal events reported for patients prescribed rofecoxib and meloxicam in general practice in England using prescription-event monitoring data. *Rheumatology* 2004; **43**: 681-682

31 **Laporte JR**, Ibanez L, Vidal X, Vendrell L, Leone R. Upper gastrointestinal bleeding associated with the use of NSAIDs: newer versus older agents. *Drug Saf* 2004; **27**: 411-420

32 **Villegas I**, Martin MJ, La Casa C, Motilva V, De La Lastra CA. Effects of oxicam inhibitors of cyclooxygenase on oxidative stress generation in rat gastric mucosa. A comparative study. *Free Radic Res* 2002; **36**: 769-777

33 **Song F**, Whitacre CC. The role of the gut lymphoid tissue in induction of oral tolerance. *Curr Opin Investig Drugs* 2001; **2**: 1382-1386

34 **Wu HY**, Weiner HL. Oral tolerance. *Immunol Res* 2003; **28**: 265-284

35 **Toussirot EA.** Oral tolerance in the treatment of rheumatoid arthritis. *Curr Drug Targets Inflamm Allergy* 2002; **1**: 45-52

Edited by Kumar M and Wang XL **Proofread by** Xu FM

PO Box 2345, Beijing 100023, China
Fax: +86-10-85381893
E-mail: wjg@wjgnet.com www.wjgnet.com

World J Gastroenterol 2004;10(21):3171-3174
World Journal of Gastroenterology
 ISSN 1007-9327

• CLINICAL RESEARCH •

Expansion of endothelial surface by an increase of vessel diameter during tumor angiogenesis in experimental hepatocellular and pancreatic cancer

Eduard Ryschich, Eduard Schmidt, Sasa-Marcel Maksan, Ernst Klar, Jan Schmidt

Eduard Ryschich, Eduard Schmidt, Sasa-Marcel Maksan, Ernst Klar, Jan Schmidt, Department of Surgery, University of Heidelberg, Heidelberg, Germany
Correspondence to: Jan Schmidt, M.D., Department of Surgery, University of Heidelberg, Im Neuenheimer Feld 110, 69120 Heidelberg, Germany. jan_schmidt@med.uni-heidelberg.de
Telephone: +49-6221-562890 **Fax:** +49-6221-565331
Received: 2003-08-26 **Accepted:** 2004-01-20

Abstract

AIM: A low vessel density is a common feature of malignant tumors. We suggested that the expansion of vessel diameter might reconstitute the oxygen and nutritient's supply in this situation. The aim of the present study was to compare the number and diameter of blood vessels in pancreatic and liver carcinoma with normal tissue.

METHODS: Tumor induction of pancreatic (DSL6A) or hepatocellular (Morris-hepatoma) carcinoma was performed in male Lewis (pancreatic cancer) and ACI (hepatoma) rats by an orthotopic inoculation of solid tumor fragments (pancreatic cancer) or tumor cells (hepatoma). Six weeks (pancreatic cancer) or 12 d (hepatoma) after tumor implantation, the tumor microvasculature as well as normal pancreatic or liver blood vessels were investigated by intravital microscopy. The number of perfused blood vessels in tumor and healthy tissue was assessed by computer-assisted image analysis.

RESULTS: The vessel density in healthy pancreas (565±89 n/mm^2) was significantly higher compared to pancreatic cancer (116±36 n/mm^2) (P<0.001). Healthy liver showed also a significantly higher vessel density (689±36 n/mm^2) compared to liver carcinoma (286±32 n/mm^2) (P<0.01). The comparison of diameter frequency showed a significant increase of vessel diameter in both malignant tumors compared to normal tissue (P<0.05).

CONCLUSION: The expansion of endothelial cells during tumor angiogenesis is accompanied to a large extent by an increase of vessel diameter rather than by formation of new blood vessels. This may be a possible adaptive mechanism by which experimental pancreatic and hepatocellular cancers expand their endothelial diffusion surface of endothelium to compensate for inadequate neoangiogenesis.

Ryschich E, Schmidt E, Maksan SM, Klar E, Schmidt J. Expansion of endothelial surface by an increase of vessel diameter during tumor angiogenesis in experimental hepatocellular and pancreatic cancer. *World J Gastroenterol* 2004; 10(21): 3171-3174
http://www.wjgnet.com/1007-9327/10/3171.asp

INTRODUCTION

Angiogenesis, defined as proliferation of endothelial cells and subsequent formation of new blood vessels from pre-existing vessels, is a characteristic feature of numerous pathological processes, including cancer[1,2]. Tumor growth depends on a continuous blood supply to cover increasing requirements for nutrients and oxygen. During tumor neovascularization, new capillaries are recruited from the existing microvasculature, a process that is controlled by positive and negative regulators of blood vessel growth[3]. In contrast to the angiogenesis occurring in wound healing, the tumor angiogenesis is characterized by a discordance between pro- and anti-angiogenic factors. This discordant process of tumor angiogenesis leads to the formation of a microvascular system with a typically distorted vessel architecture[4,5], and consequently irregular flow patterns and heterogeneous oxygen supply[6,7] resulting in hypoxia[8,9]. These parameters contribute to a unique tumor microenvironment which in turn modulates the therapeutic responsiveness of solid tumors, e.g., towards chemotherapeutic agents or radiation therapy[10,11].

Our previous studies reported that the increased vessel diameter was an important feature of tumor microangioarchitecture in pancreatic[12] and hepatocellular[13] cancer of the rat. This feature was not only specific for transplantable tumor models and was found in spontaneous pancreatic tumors in transgenic mice[14]. We showed that the vessel dilation was the first detectable stage of ongoing angiogenesis during multistep tumorigenesis which preceded vessel sprouting[14]. These observations encouraged us to start a detailed investigation of tumor blood vessels by a combination of different techniques including intravital microscopy and immunohistochemistry. We hypothesized that the vessel dilation indicated a possible adaptive process, which may help the tumor to expand their diffusion surface of endothelium and to compensate for the inadequate supply with oxygen and nutritients. In the present study, we used intravital microscopy and immunohistochemistry to investigate this phenomenon in normal and malignant pancreatic tissues as well as in hepatic tissue of rats. The present study demonstrated that the decrease of vessel density in experimental pancreatic and liver carcinoma was accompanied with an increase of vessel diameter.

MATERIALS AND METHODS

Tumor inoculation

Established cell lines of pancreatic duct-like (DSL6A)[15] and hepatocellular carcinoma (Morris-hepatoma MH-3924A)[13] of rats were used. Since the expression profile of tumor cells was strongly dependent on the site of growth, e.g. implantation[16,17] we decided to inoculate the tumors orthotopically which ensured the appropriate microenvironment for tumor cell growth. Twelve male Lewis rats (160-180 g) were used for the inoculation of pancreatic carcinoma. Hepatocellular carcinomas were inoculated on 12 male ACI rats (220-250 g). Each animal was anaesthetized with intramuscular injection of xylazin (10 mg/kg, Rompun®, Bayer, Leverkusen, Germany) and ketamin (40 mg/kg, Ketanest®, Parke Davis, Berlin, FRG).

Tumor implantation was performed as previously described

for pancreatic[12] and hepatocellular[13] carcinoma. For the inoculation of pancreatic cancer, two sterile polymethylmethacrylat (PMMA)-plates (∅ 11 mm, Glasflex, Stirling, NJ, USA) were applied in "sandwich-technique" on both sides of the pancreatic head. The tumor of approximately 1 mm^3 was harvested from a subcutaneous parent tumor of a syngeneic rat and interposed intrapancreatically between the plates. Hepatocellular carcinomas were induced by a subcapsular injection of tumor cells (Morris hepatoma MH-3924A, 0.01 mL, 0.5×10^5 cells) into the left upper liver lobe. Major steps of both models are summarized in Table 1.

Table 1 Summary of tumor models used in present study

	Pancreatic cance	Hepatocellular cancer
Tumor cell line	DSL6A	Morris hepatoma 3924A
Syngeneic strain	Lewis	ACI
Tumor inoculation	Solid tumor fragment	Cell suspension
Time after inoculation	6 wk	12 d

Intravital microscopy

Intravital microscopy was performed 12 d after inoculation for hepatocellular carcinoma and 6 wk after inoculation for pancreatic cancer when tumors reached a diameter of 8-10 mm. All animals were re-anaesthetized as described above. A teflon catheter (I.D. 0.5 mm, B.Braun AG, Melsungen, FRG) was inserted into the right internal jugular vein for venous access. Another catheter was placed into the left carotid artery for blood sampling and monitoring of cardiovascular parameters. The abdomen was opened by midline incision. The animal was placed on a special stage automatically maintained at 37 ℃. The tumor was macroscopically identified. The tumor bearing pancreatic head was immobilized in a temperature-controlled (37 ℃) immersion chamber containing Ringer's solution. For the intravital microscopy of hepatocellular carcinoma, the tumor bearing liver lobe was placed on a rubber stage and superfused with Ringer's solution (37 ℃).

For intravital microscopy, the entire preparation was placed under a fluorescence microscope (Leica GmbH, Wetzlar, FRG). The fluorescence filter with excitation 450-490 nm and emission 520 nm was used. After the preparation was completed, all animals received an intravenous injection of 50 mg/kg of FITC-labeled albumin (Sigma Chemicals Co., St.Louis, MO, USA) dissolved in 1 mL saline. This fluorescent plasma marker ensured the maximal contrast of blood vessels and was utilized for the measurement of vessel diameter and vessel density. The microcirculatory images were transmitted by a video camera (CF 8/1, Kappa GmbH, Gleichen, FRG) to a monitor (PVM-1440 M, Sony, Tokyo, Japan) and recorded on a videorecorder (sVHS, AG-7 350-E, Panasonic, Osaka, Japan) for subsequent off-line analysis. After the experiment, the tumors and a fragment of normal tissue were harvested and frozen immediately in liquid nitrogen. The evaluation of vessel diameter and density in tumor microcirculation and in normal tissue was performed using special software (Capimage®, Zeintl GmbH, Heidelberg, FRG). The number of blood vessels was calculated on 3-4 randomly chosen fields and expressed as per 1 mm^2 of tumor surface.

Immunohistochemistry

After intravital microscopy, the tumors were removed for further histological analysis. The tissue was snap frozen in liquid nitrogen. Five μm thick sections were cut, air-dried and fixed in aceton. Immunohistochemical staining of endothelium was performed using monoclonal antibodies recognising RECA-1 rat endothelial antigen (Clone HIS52, Serotec, Germany) and the LSAB-kit (Dako, Hamburg, Germany). In addition, the slides were counterstained with Mayer's acid hemalum (Fluka, Steinheim, Germany). Quantitative analysis of immunohistochemical staining was performed by computer-assisted image analysis. For this aim, three microscopic fields of 3.18 mm^2 were randomly chosen by light microscope (Leica DMRB, Leica GmbH, Germany), digitalized by a colour video camera (CF 20/4DX, Kappa GmbH, Gleichen, Germany) to histological images and saved on a computer. The number of blood vessels was counted and expressed as per 1 mm^2 of surface.

Statistical analysis

All data were given as mean±SD. Mann-Whitney-U test was used to compare the differences between groups as appropriate. $P<0.05$ was considered statistically significant.

RESULTS

The intravital microscopy after injection of fluorescent plasma marker ensured the excellent contrast of all blood vessels in normal (Figure 1A, E) and in tumoral (Figure 1B, F) tissues. The microvascular system in healthy pancreas showed a capillary network of high density, the single afferent and efferent blood vessels were identified within normal pancreatic tissue (Figure 1A). Healthy liver showed a dense network of hepatic sinusoids which were drained by hepatic venules (Figure 1E). In contrast, the microangioarchtecture of both pancreatic and hepatocellular carcinomas was characterized by lost of normal vascular hierarchy "capillaries-arterioles (sinusoids) -venules", chaotic arrangement of blood vessels, irregular vessel diameters and formation of lacunar blood vessels (Figure 1B, F). In contrast to vascular systems of normal pancreatic and hepatic tissues, there were no specific features discriminating the microangioarchitecture of pancreatic cancer from that of hepatocellular carcinoma (Figure 1).

The measurement of vessel density either by intravital microscopy or by immunohistochemistry demonstrated different results (Tables 2, 3). The vessel density of all tissues measured by intravital microscopy was significantly higher than that measured by immunohistochemistry ($P<0.05$, Tables 2, 3). The vessel density in healthy pancreas was significantly higher compared to pancreatic cancer ($P<0.001$, Table 2). Healthy liver showed also a significantly higher vessel density compared to liver carcinoma ($P<0.01$, Table 3). The low vessel density of both pancreatic and hepatocellular carcinomas was accompanied with the development of tumor necrosis, which appeared frequently in the central area of the tumors and represented a characteristical feature of the tumors showing a cross-sectional diameter of more than 10 mm as opposed to smaller tumors.

Table 2 Vessel density in normal and malignant tissue

Vessel density (n/mm^2)	Healthy pancreas	Pancreatic cancer	P
Intravital microscopy	565±89	116±36	<0.001
Immunohistochemistry	91±22	35±10	<0.001

Table 3 Vessel density in normal and malignant liver tissue

Vessel density (n/mm^2)	Healthy liver	Liver carcinoma	P
Intravital microscopy	689±36	286±32	<0.01
Immunohistochemistry	196±30	49±13	<0.01

The frequency analysis of vessel diameters showed that the most frequent diameters in normal pancreas and liver were considerably smaller compared to the most frequent diameters in pancreatic and hepatocellular carcinomas (Figures 2, 3). Ninety-four percent of blood vessels in normal pancreas, 41% of blood vessels in pancreatic carcinoma and less than 9% of blood vessels in non-malignant and malignant hepatocellular tissues showed a diameter less than 10 μm. The most frequent diameter was between 10 and 20 μm (59%) in pancreatic carcinoma and more than 20 μm in hepatocellular carcinoma (59%).

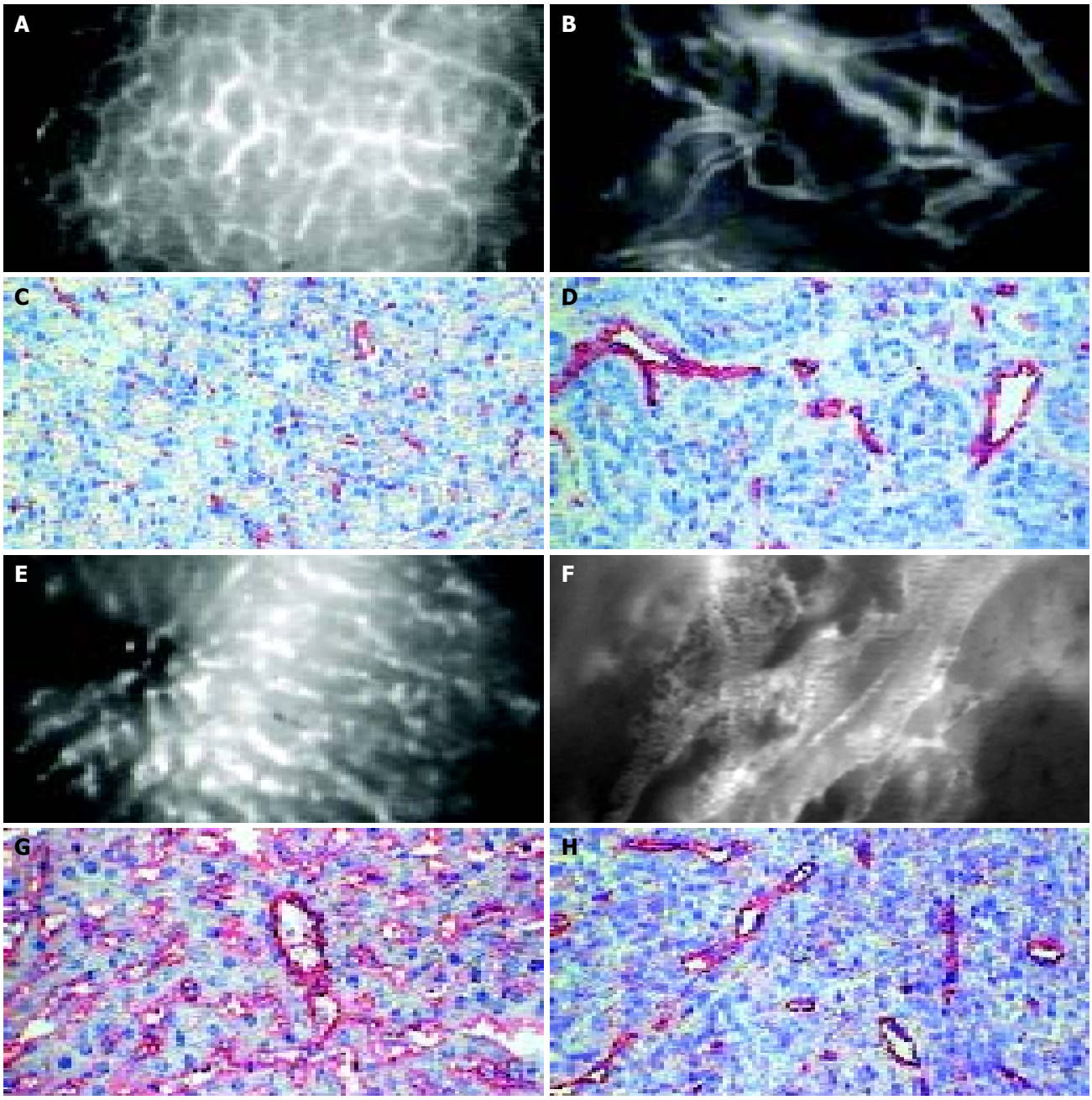

Figure 1 Microangioarchtecture investigated by intravital microscopy and immunohistochemical staining of endothelium of normal pancreas (A,B), liver (E,F), pancreatic (C,D) and hepatocellular (G,H) carcinoma: The microvascular system in healthy pancreas showed a dense network mainly consisting of capillaries in normal pancreas (A) and sinusoids in the liver (E). Both pancreatic (B) and hepatocellular (F) carcinomas showed a chaotic angioarchitecture with irregular diameter of blood vessels. Either intravital microscopy or immunohistochemical staining of endothelium turn up lower density and higher diameters of microvessels in both tumor types than in corresponding normal tissue (bar 50 μm).

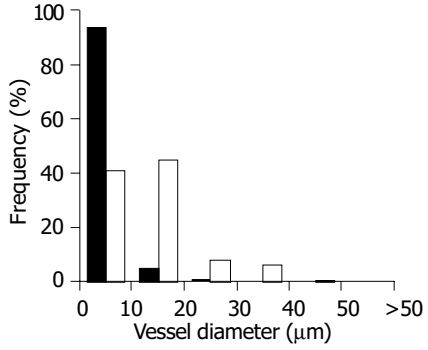

Figure 2 Frequency of vessel diameter in normal pancreas and experimental duct-like pancreatic carcinoma (DSL6A) ■-normal pancreas, □-pancreatic carcinoma.

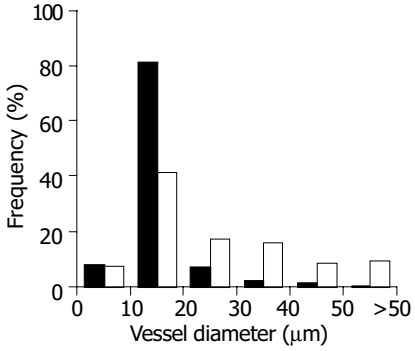

Figure 3 Frequency of vessel diameter in normal liver and experimental hepatocellular carcinoma (Morris-hepatoma) ■-normal liver, □-hepatocellular carcinoma.

DISCUSSION

Using intravital microscopy, we investigated the microvascular systems of pancreatic and liver carcinoma and performed a quantitative analysis of vessel density and vessel diameter. The present study demonstrated that the mean vessel density in both types of experimental malignant tumors was lower than that in the corresponding normal tissues. This hypovascularity was regarded as a main cause of hypoxia in tumor tissue which is responsible for the development of necrotic areas within solid tumors[8,11] as it has been observed in the present models of pancreatic and hepatocellular carcinoma once diameters exceeded 10 mm. However, as it was shown in the present study, tumor angiogenesis could compensate in part for this insufficient vascularisation by other mechanisms than growth of new blood vessels. Although vessel sprouting has been accepted as the main mechanism of angiogenesis, some pathological processes might display an angiogenic phenotype characterized by an extensive vessel dilatation[18,19]. Previous data demonstrated in a model of multistep tumorigenesis in mouse malignant insulinoma[14] and in the model of thyroid hyperplasia[18] that vessel dilatation was the first detectable stage of ongoing angiogenesis which preceded vessel sprouting and extended transformation of the cells. The results of the present study allowed to transfer these findings to solid murine tumors and demonstrated that the "non-sprouting" angiogenesis might accompany vessel sprouting during growth of solid pancreatic and hepatocellular cancer in rats. We suggested that the observed vessel dilatation during tumor development and growth could cause an increase of endothelial surface for the diffusion of oxygen and nutrition, representing a possible adaptive mechanism to compensate for the insufficient vascularisation.

In the present study, both tumor types were induced by an implantation of tumor cells and did not arise spontaneously. It is known that tumor blood vessels in transplantable tumor models develop from surrounding tissues[20,21], whereas the growth of autochtonous blood vessels forms the vascular system in spontaneous tumors[22,23]. However, the vessel dilatation as an initial step of the vascular transformation has been reported previously in spontaneous tumor model also and seems to be a feature which is likely to be a common feature in both transplanted and spontaneous tumors.

In a previous study we analysed the percentage of vascular surface of pancreatic cancer DSL6A which was performed on histological sections using intravascular perfusion with a fluorescent-labeled plasma marker[12]. In the present study, the number of blood vessels per mm^2 was investigated by intravital microscopy and immunohistochemistry. The values of vessel density obtained by these analyses corresponded well and both showed a significantly lower microvascularity of malignant tumors compared to normal tissues. The vessel density investigated by intravital microscopy was higher than that by immunohistochemistry. Since the optical depth of tissue accessable for the intravital microscopy (30-50 μm) is considerably higher than the thickness of histological sections (5 μm), the difference between the results of intravital microscopy and immunohistochemistry finds its logical explanation.

In summary, we compared the vessel density and vessel diameter of two experimental tumors by intravital microscopy. The present study demonstrates that the vessel dilatation is an integral part of the angiogenic activity which represents a possible mechanism by which the tumors expand their diffusion surface of endothelium to compensate for the inadequate neoangiogenesis.

REFERENCES

1 **Carmeliet P,** Jain RK. Angiogenesis in cancer and other diseases. *Nature* 2000; **407**: 249-257

2 **Folkman J.** Angiogenesis in cancer, vascular, rheumatoid and other disease. *Nat Med* 1995; **1**: 27-31

3 **Hanahan D,** Folkman J. Patterns and emerging mechanisms of the angiogenesis switch during tumorigenesis. *Cell* 1996; **86**: 353-364

4 **Konerding MA,** van Ackern C, Steinberg F, Streffer C. Combined morphological approaches in the study of network formation in tumor angiogenesis. Steiner R, Weisz PB, Langer R eds. Angiogenesis: key principles-science-technology-medicine. *Basel Birkhauser* 1992: 40-58

5 **Steinberg F,** Konerding MA, Sander A, Streffer C. Ultrastructural studies of tumour angiogenesis in human xenotransplanted tumours. *Int J Radiat Biol* 1991; **60**: 161-168

6 **Vaupel P,** Thews O, Kelleher DK, Hoeckel M. Oxygenation of human tumors: the Mainz experience. *Strahlenther Onkol* 1998; **174**(Suppl 4): 6-12

7 **Dewhirst MW,** Tso CY, Oliver R, Gustafson CS, Secomb TW, Gross JF. Morphologic and hemodynamic comparison of tumor and healing normal tissue microvasculature. *Int J Radiat Oncol Biol Phys* 1989; **17**: 91-99

8 **West CM,** Cooper RA, Loncaster JA, Wilks DP, Bromley M. Tumor vascularity: a histological measure of angiogenesis and hypoxia. *Cancer Res* 2001; **61**: 2907-2910

9 **Koong AC,** Mehta VK, Le QT, Fisher GA, Terris DJ, Brown JM, Bastidas AJ, Vierra M. Pancreatic tumors show high levels of hypoxia. *Int J Radiat Oncol Biol Phys* 2000; **48**: 919-922

10 **Kerbel RS.** Tumor angiogenesis: past, present and the near future. *Carcinogenesis* 2000; **21**: 505-515

11 **Brown JM,** Le QT. Tumor hypoxia is important in radiotherapy, but how should we measure it? *Int J Radiat Oncol Biol Phys* 2002; **54**: 1299-1301

12 **Schmidt J,** Ryschich E, Daniel V, Herzog L, Werner J, Herfarth CH, Longnecker DS, Gebhard MM, Klar E. Vascular structure and microcirculation of experimental pancreatic carcinoma in the rat. *Eur J Surg* 2000; **166**: 328-335

13 **Maksan SM,** Paulo H, Ryschich E, Kuntz C, Gebhard MM, Klar E, Schmidt J. *In vivo* assessment of angioarchitecture and microcirculation in experimental liver cancer: a new model in rats. *Dig Dis Sci* 2003; **48**: 279-290

14 **Ryschich E,** Schmidt J, Klar E, Haemmerling GJ, Ganss R. Transformation of the microvascular system during multistage tumorigenesis. *Int J Cancer* 2002; **97**: 719-725

15 **Pettengill OS,** Faris RA, Bell RHJ, Kuhlmann ET, Longnecker DS. Derivation of ductlike cell lines from a transplantable acinar cell carcinoma of the rat pancreas. *Am J Pathol* 1993; **143**: 292-303

16 **Gullino PM.** Microenvironment and angiogenic response. Steiner R, Weisz PB, Langer R eds. Angiogenesis: key principles-science-technology-medicine. *Basel Birkhauser* 1992: 125-128

17 **Fukumura D,** Yuan F, Monsky WL, Chen Y, Jain RK. Effect of host microenvironment on the microcirculation of human colon adenocarcinoma. *Am J Pathol* 1997; **151**: 679-688

18 **Many MC,** Denef JF, Haumont S. Precocity of the endothelial proliferation during a course of rapid goitrogenesis. *Acta Endocrinol Copenh* 1984; **105**: 487-491

19 **Bull RH,** Bates RO, Mortimer PS. Intravital capillaro-microscopy for the study of microcirculation in psoriasis. *Br J Dermatol* 1992; **126**: 436-445

20 **Sckell A,** Safabakhsh N, Dellian M, Jain RK. Primary tumor size-dependent inhibition of angiogenesis at a secondary site: an intravital microscopic study in mice. *Cancer Res* 1998; **58**: 5866-5869

21 **Vajkoczy P,** Thurnher A, Hirth KP, Schilling L, Schmiedek P, Ullrich A, Menger MD. Measuring VEGF-Flk-1 activity and consequences of VEGF-Flk-1 targeting *in vivo* using intravital microscopy: clinical applications. *Oncologist* 2000; **5**(Suppl 1): 16-19

22 **Folkman J,** Watson K, Ingber D, Hanahan D. Induction of angiogenesis during the transition from hyperplasia to neoplasia. *Nature* 1989; **339**: 58-61

23 **Bergers G,** Javaherian K, Lo KM, Folkman J, Hanahan D. Effects of angiogenesis inhibitors on multistage carcinogenesis in mice. *Science* 1999; **284**: 808-812

Edited by Wang XL **Proofread by** Xu FM

PO Box 2345, Beijing 100023, China
Fax: +86-10-85381893
E-mail: wjg@wjgnet.com www.wjgnet.com

World J Gastroenterol 2004;10(21):3175-3178
World Journal of Gastroenterology
 ISSN 1007-9327

• CLINICAL RESEARCH •

Biliary drainage after laparoscopic choledochotomy

Qi Wei, Hong-Jie Hu, Xiao-Yan Cai, Li-Bo Li, Guan-Yu Wang

Qi Wei, Xiao-Yan Cai, Li-Bo Li, Guan-Yu Wang, Department of General Surgery, Sir Run Run Shaw Hospital, Zhejiang University, Hangzhou 310016, Zhejiang Province, China
Hong-Jie Hu, Department of Radiology, Sir Run Run Shaw Hospital, Zhejiang University, Hangzhou 310016, Zhejiang Province, China
Correspondence to: Qi Wei, Department of General Surgery, Sir Run Run Shaw Hospital, Zhejiang University, Hangzhou 310016, Zhejiang Province, China. weiqi@hzcnc.com
Telephone: +86-571-86437761
Received: 2003-08-28 **Accepted:** 2003-09-25

Abstract

AIM: Transcystic biliary decompression (TCBD) has been proposed as an alternative to T-tube placement after laparoscopic choledochotomy (LCD). This permits safe primary closure of the choledochotomy and eliminates the complications associated with T-tubes. TCBD tube has been secured by Roeder knots and transfixation, and removed later than 3 wk after surgery. We presented a modified TCBD (mTCBD) method after LCD using the ureteral catheter and the Lapro-Clip (David and Geck, Danbury, Connecticut, USA), and compared it with T-tube drainage.

METHODS: Between October 2002 and June 2003, patients with choledocholithiasis undergoing LCD with mTCBD (mTCBD Group, n = 30) were retrospectively compared to those undergoing LCD with T-tube drainage (T-tube Group, n = 52) at a single institution.

RESULTS: There were no significant differences in operative time and retained stones between the two groups. Patients in mTCBD group had a significantly decreased average output of bile compared with those in T-tube group (306±141 *vs* 409±243 mL/24 h, P = 0.000). Removal of drain tubes in mTCBD group was done significantly earlier than that in T-tube group (median, 5 *vs* 29 d, P = 0.000). No complication related to drain tubes was found in mTCBD group, and morbidity rate with the T-tube was significantly higher (11.5%), and bile leakage following T-tube removal was 5.8%.

CONCLUSION: A modified TCBD after LCD is safe, effective and easy to perform. It may reduce postoperative complications, especially bile leakage.

Wei Q, Hu HJ, Cai XY, Li LB, Wang GY. Biliary drainage after laparoscopic choledochotomy. *World J Gastroenterol* 2004; 10(21): 3175-3178
http://www.wjgnet.com/1007-9327/10/3175.asp

INTRODUCTION

Laparoscopic choledochotomy (LCD) has been proposed as an efficacious, safe, and cost-effective method for the treatment of choledocholithiasis[1-6]. However, it is associated with a relatively higher morbidity rate, mainly related to T-tube insertion[7,8]. To eliminate the complications related to T-tubes, some authors have proposed transcystic biliary decompression (TCBD) after LCD, but the TCBD tube is still removed later than 3 wk after surgery[9,10], limiting the value of the procedure. We presented a modified TCBD (mTCBD) method using ureteral catheter and Lapro-Clip, and compared it with T-tube drainage.

MATERIALS AND METHODS

Patients

Eighty-two patients with choledocholithiasis undergoing LC plus laparoscopic choledochotomy were retrospectively reviewed at a single institution, between October 2002 and June 2003. mTCBD was performed for 30 patients (mTCBD group) and T-tube drainage for 52 patients (T-tube group). The clinical and demographic details are shown in Table 1. There were no significant differences between the groups. Preoperative investigations included liver function tests and external ultrasound. Six patients had ERCP or MRCP in the mTCBD group, and three in the T-tube group. The criteria for preoperative suspicion of CBD stones were serum alkaline phosphatase or bilirubin levels twice the upper normal limit, and an ultrasonic diameter of the CBD equal to or larger than 9 mm. Patients with acute cholecystitis underwent an operation within 48 h admission. Those with choledocholithiasis associated with acute pancreatitis were operated on after the acute bout of pancreatitis was subsided. The patients were restricted to the American Society of Anesthesiology class I and class II (ASA I and II). Cases were excluded if preoperative and intraoperative endoscopic sphincterotomy (ES) were performed. Two patients had previous biliary surgery in the mTCBD group, and three in the T-tube group.

Table 1 Clinical and demographic details of the patients

	mTCBD[1]	T-tube
n	30	52
Age range(yr)	28-77	26-82
Male:female	12:18	17:35
Jaundice	12	16
Acute cholecystitis	9	13
Acute pancreatitis	3	5
Known CBD stone (s)	16	37
Suspected CBD stone (s)	11	13
Dilated CBD (≥9 mm)	18	35
Biliary surgery	2	3

[1]Modified transcystic biliary decompression.

Operative techniques

Laparoscopic cholecystectomy was performed by a standardized technique. One 10 mm port was inserted into the left upper quadrant. Intraoperative cholangiography (IOC) was mandatory. Choledochotomy was performed by a vertical incision. CBD stones were retrieved by instrumental exploration with forceps, flushing of CBD with saline, and use of a Dormia basket with a 5 mm chledochoscopy.

***Modified transcystic biliary decompression* (mTCBD)** After complete clearance of the CBD, which was primarily closed with a running suture (3-0 vicryl). A 5Fr ureteral catheter was advanced into the CBD lumen 2 cm to 4 cm and a saline syringe was attached to the three-way stopcock external fitting of the catheter. If the position of the terminal segment of the ureteral

catheter inside CBD was correct, the catheter was fixed to the cystic duct by a 12 mm absorbable Lapro-Clip (Figure 1). Saline irrigation through the catheter was maintained during application of the Lapro-Clip to prevent overtightening the catheter. A loose loop of the catheter was left. A completion IOC was performed to confirm the correct position of the ureteral catheter, also to ensure the adequate closure of the CBD and free flow of contrast into the duodenal lumen. A postoperative cholangiogram was performed on d 3 to 7 after surgery. Under fluoroscopy, the catheter was removed.

T-tube drainage A latex rubber T-tube of appropriate size (12-16 Fr) was inserted completely into the abdomen. The T limbs were advanced with grasping forceps into the choledochotomy. After proper positioning, the choledochotomy was closed using interrupted sutures (3-0 vicryl). T-tube clamping was carried out 7-10 d postoperatively. A postoperative cholangiogram was performed 3 to 4 wk after surgery. If the examination was normal, the T-tube was removed. If retained stones were shown, the T-tube was left for another 3 to 4 wk. A No. 10 Jackson-Pratt drain was placed in the subhepatic space for all patients. The subhepatic drain tube was removed on the 3rd d for most of patients.

Five surgeons performed the 82 laparoscopic choledochotomies. In the mTCBD group, one senior author performed 25 of 30 procedures, whereas the remaining 5 procedures by one junior staff member. In the T-tube group, three senior staff performed 47 of 52 procedures, whereas 7 procedures by two junior members.

The output of bile was measured only during the hospital stay. The data recorded were insufficient in the case notes to compare the number and size of CBD stones, and postoperative liver function test.

A "drain complication" was defined as an event causing morbidity, requiring medical intervention, or resulting in a prolonged admission or requiring readmission. The complication had to be clearly related to the presence or removal of the drain.

Statistical analysis

Statistical analyses were performed using Student's *t* test, chi square test for likelihood ratio, and Mann-Whitney test for nonparametric data. Significance was set at the 5% level.

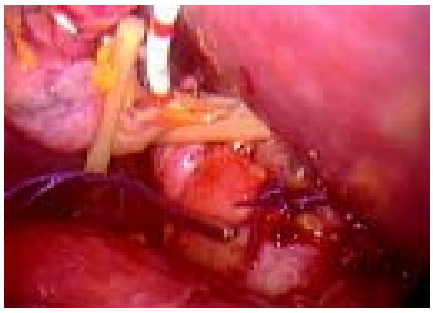

Figure 1 A 5 Fr ureteral catheter was placed for biliary decompression and secured with a 12 mm absorbable Lapro-Clip.

RESULTS

Outcome of mTCBD group

The average operative time was 178±34 min (Table 2). There were two conversions to open surgery (6.5%). One patient had large impacted stones, and the other had multiple stones. The modified transcystic biliary decompression (mTCBD) was also used in those patients. The average output of bile via the ureteral catheter was 306±141 mL/24 h. The median postoperative time of drain removal was 5 (range 4 to 5) d. Under fluoroscopy, the catheter could be pulled out easily from the cystic duct without any bile leakage or slippage of the Lapro-Clip (Figure 2). No patients developed complications from ureteral catheter occlusion. The median postoperative hospital stay was 5 (range 4 to 6) d.

Table 2 Comparison of clinical outcome between two groups

	mTCBD	T-tube	t or χ^2 (z)	P
Operative time (min)	178	173	-0.469	0.640[2]
Output of bile (mL/24 h)	306	409	2.118	0.037[2]
Postoperative stay(d)	5.4-6[1]	4.4-6[1]	(-2.060)	0.039[4]
Drain removal (d)	5.4-5[1]	29.22-32[1]	(-7.560)	0.000[4]
Complications (%)	0	11.5	5.736	0.017[3]
Retained stones (%)	3.3	13.5	2.574	0.109[3]
Convert to open (%)	6.5	3.8	0.315	0.575[3]

[1]Median, 25-75% quartile rang; [2]*t*-test; [3]Chi square test with Likelihood Ratio; [4]Mann-Whitney test.

One patient (3.3%) had unexpected retained stones, requiring endoscopic sphincterotomy (ES). Two patients had problems. The ureteral catheter was dislocated with the biliary tree not shown in the postoperative cholangiogram, but there was no bile leakage.

Outcome of T-tube group

The average operative time was 173±45 min (Table 2). There were two conversions to open surgery (6.5%). Two patients had large impacted stones. The average output of bile via T-tube was 409±243 mL/24 h. The median drain removal time was 29 (range 22 to 32) d. The median postoperative hospital stay was 4 (range 4 to 6) d.

Seven (13.5%) had retained stones (Table 4). There were intentionally retained stones in 5 patients (9.6%), 2 with intrahepatic duct stones, 1 with multiple common duct stones because of difficulty in removing them laparoscopically, and another 2 patients with temporary unavailability of the choledochoscope. There were unexpected residual stones in 2 patients (3.8%). All of the stones were successfully removed, 5 patients through the T-tube tract, using a choledochoscope, and a stone basket. The T-tube was taken out in two patients prior to planed removal, thereby requiring ES.

Table 3 Complications and problems of biliary drainage

	T-tube	mTCBD
Complications		
n	6 (11.5%)	0
Drain *in situ*		
Leak around drain	1	0
Stricture	1	0
Drain pulled out	1	0
Drain removed	3 (5.8%)	
Bile collection	2	0
Bile peritonitis	1	0
Problems		
n	3 (5.8%)	2 (6.7%)
Drain out	2	2
Dislocation	1	0

Table 4 Retained stones in T-tube group

	n(%)
Known stones	5 (9.6)
Instrument problems	2
Intrahepatic stones	2
Multiple stones	1
Unexpected stones	2 (3.8)
Total	7 (13.5)

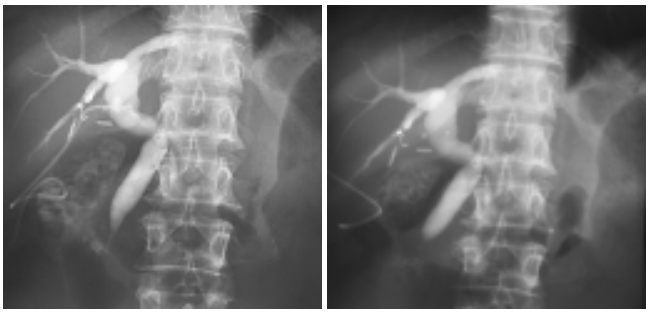

Figure 2 A ureteral catheter was pulled out without bile leakage. The cystic duct was closed with the Lapro-Clip.

Postoperative complications occurred in 6 patients (11.5%) (Table 3). Following T-tube removal, three patients had significant bile leakage (5.8%). Two patients developed severe abdominal pain, sweating and tachycardia and were diagnosed as localized bile collection. They were treated with antibiotics, parental fluids, analgesia, and the drain tube was reinserted through T-tube sinus tract. Recovery was achieved with this management. The third patient developed biliary peritonitis and required open drainage.

One patient had a CBD stricture and T-tube stenting was necessary for 3 mo. In the other patient the T-tube was pulled out on the second day after surgery and the subhepatic suction drain provided biliary drainage for two weeks postoperatively.

Other related morbidity was found in one patient with a bile leak around the T-tube. In addition, the tip of the T-tube in one patient was dislocated from the bile duct, but caused no problem.

Comparison of clinical outcome between two groups

The statistical analyses comparing the mTCBD group with the T-tube group are presented in Table 2. There were no significant differences in operative time and retained stones. Patients in mTCBD group had a significantly decreased average output of bile compared with those in T-tube group ($P = 0.000$). The biliary drainage tube in the mTCBD group was removed significantly earlier than that in the T-tube group ($P = 0.000$). No morbidity was directly related to drain tube in the mTCBD group, and the morbidity rate in the T-tube group was significantly higher (11.5%, $P = 0.017$). However, the postoperative hospital stay in the mTCBD group was significantly longer compared with that in the T-tube group ($P = 0.039$).

There was no postoperative mortality or recurrence of choledocholithiasis in this study. The length of follow-up was 4 to 30 wk.

DISCUSSION

Previous studies have documented a temporary obstruction at the lower end of the CBD due to sludge, fibrin debris, or edema following manipulations to extract duct calculi or retained stones in the first few days after surgery[9,11-16], thus temporary decompression is advisable in the prevention of postoperative bile leakage. A transcystic biliary decompression (TCBD) tube, like a T-tube, could achieve biliary decompression and has the advantage of avoiding the well-known complications of T-tubes. A TCBD tube was secured to the cystic duct with two Roeder knots or a transfixing suture. The biliary drainage tube must be kept in place for 2-4 wk[9,10]. This might not be easy to manipulate, and could reduce the benefits of the minimal access approach.

In October 2002, a modified TCBD (mTCBD) was placed followed by primary closure of the CBD. The ureteral catheter was inserted down into the CBD and once in the correct position, the cystic duct was clipped by a 12 mm Lapro-Clip. The Lapro-Clip has a two-part compression closure mechanism, the inner flexible track piece could close around the cystic duct, and rigid outer body could was then slide over the track piece to secure the cystic duct[17]. The ureteral catheter was pulled out easily with no bile leakage and the cystic duct was closed automatically with the Lapro-Clip even if drain displacement occurred.

In mTCBD group, no bile leakage was related to drain tube removal, and median time for ureteral catheter removal was 5 (range 4 to 5) d. The ureteral catheter in two patients was dislocated, this also caused no bile leakage.

Complications related to T-tubes were reported to occur between 5-15.3%[7,18,19]. Biliary leakage following removal was the most serious. Incidence of bile leak was 4.12-6.9%[19,20]. There was no difference when laparoscopic cases were compared to open and converted cases for overall complications (13.8% *vs* 15.5%) or for bile leakage after planned tube removal (6.9% *vs* 6.9%)[19].

In our study, postoperative complications in the T-tube group occurred in 6 patients (11.5%) (Table 3). Following T-tube removal, 3 patients developed bile leakage (5.8%). The T-tube was left in the three patients for three weeks postoperatively. Sinus tract formation of the T-tube might need a longer time because of the less reaction of laparoscopic approach[21-23]. Bile leakage was inevitable with accidental T-tube dislocation[7,18-20]. The median time for T-tube removed was 29 (range 22 to 32) d, even if cases of retained stones were excluded. The data suggest that placement of T-tube may require a longer time than 4 wk.

Biliary drainage with a TCBD tube and primary closure of the choledochotomy were indicated only for patients whose stones were completely extracted at the time of surgery. Routine intraoperative cholangiogram and chledochoscopy were used in the laparoscopic approach, and the occurrence of retained stones was decreased to accepted levels[7,24,25]. Endoscopic sphincterotomy could be a back up procedure for retained stones[25,26]. In the mTCBD group, one patient (3.3%) had unexpected retained stones retrieved by ES.

If there was any possibility of residual stones, T-tube placement was mandatory for postoperative choledochoscopy. Five patients (9.6%) in the T-tube group had intentionally retained stones (Table 4). T-tube placement may be needed for another 3-4 wk[21-23], in order to form a mature tract. It was worthwhile without any injury to the sphincter of Oddi, and complete removal could be expected.

Although patients in the mTCBD group had a significantly decreased average output of bile compared with those in the T-tube group (306±141 *vs* 409±243 mL/24 h, $P = 0.000$), it was shown that enough output of bile led to a decrease in the biliary pressure. Consequently, this finding suggested that the output of bile from mTCBD was sufficient to decompress the biliary tract as T-tube. On the other hand, the T-tube drain mostly was clamped on d 7 to 10, which means that many patients were discharged with an open drain.

The postoperative hospital stay in mTCBD group was significantly longer compared with that in T-tube group (median, 5 *vs* 4 d, $P = 0.039$). It may relate to the drain removal during hospitalization because of our initial trial for the mTCBD.

A modified TCBD is not suitable for patients with abnormal anatomy of cystic duct, intrahepatic duct stones and stricture of duodenal papillary.

The chief concern of the Lapro-Clip is the occlusion of the catheter. Maintaining saline irrigation through the ureteral catheter prevents occluding. We also feel that the diameter of the ureteral catheter is an important factor for avoiding occlusion or dislocation, so a 5Fr ureteral catheter is most suitable. We used a 5Fr ureteral catheter in all mTCBD cases.

A 12 mm Lapro-Clip holds the cystic duct tightly to a 5Fr ureteral catheter while the spring of the Lapro-Clip closes the cystic duct when the ureteral catheter is removed. In this study, no slippage of the clip occurred. The short period of TCBD could reduce the risk of ureteral catheter occlusion. No patients

in the present study developed catheter occlusion.

Our results were similar to the use of exclusive C-tube and elastic thread described by some authors[27-30]. Our initial experiences demonstrated that the modified transcystic biliary decompression (mTCBD) after laparoscopic choledochotomy (LCD) was useful for decreasing postoperative complications, especially bile leakage, and easy to perform. The patients were discharged without any drainage tube within a wk. If biliary drainage was used carefully with selected indications, patients with laparoscopic choledochotomy for CBD stones could achieve a better postoperative quality of life. We propose mTCBD as an option for patients with CBD stones.

ACKNOWLEDGMENTS

We thank Dr. C.Welch for editorial assistance and helpful suggestions.

REFERENCES

1 **Cuschieri A,** Lezoche E, Morino M, Croce E, Lacy A, Toouli J, Faggioni A, Ribeiro VM, Jakimowicz J, Visa J, Hanna GB. E.A.E.S. multicenter prospective randomized trial comparing two-stage *vs* single-stage management of patients with gallstone disease and ductal calculi. *Surg Endosc* 1999; **13**: 952-957

2 **Heili MJ,** Wintz NK, Fowler DL. Choledocholithiasis: endoscopic versus laparoscopic management. *Am Surg* 1999; **65**: 135-138

3 **Wei Q,** Wang JG, Li LB, Li JD. Management of choledocholithiasis: Comparison between laparoscopic common bile duct exploration and intraoperative endoscopic sphincterotomy. *World J Gastroenterol* 2003; **9**: 2856-2858

4 **Memon MA,** Hassaballa H, Memon MI. Laparoscopic common bile duct exploration: the past, the present, and the future. *Am J Surg* 2000; **179**: 309-315

5 **Patel AP,** Lokey JS, Harris JB, Sticca RP, McGill ES, Arrillaga A, Miller RS, Kopelman TR. Current management of common bile duct stones in a teaching community hospital. *Am Surg* 2003; **69**: 555-560

6 **Petelin JB.** Laparoscopic common bile duct exploration. *Surg Endosc* 2003; **17**: 1705-1715

7 **Martin IJ,** Bailey IS, Rhodes M, O'Rourke N, Nathanson L, Fielding G. Towards T-tube free laparoscopic bile duct exploration: A methologic evaluation during 300 consecutive procedures. *Ann Surg* 1998; **228**: 29-34

8 **Thompson MH,** Tranter SE. All-comers policy for laparoscopic exploration of the common bile duct. *Br J Surg* 2002; **89**: 1608-1612

9 **Hensman C,** Crosthwaite G, Cuschieri A. Transcystic biliary decompression after direct laparoscopic exploration of the common bile duct. *Surg Endosc* 1997; **11**: 1106-1110

10 **Paganini AM,** Feliciotti F, Guerrieri M, Tamburini A, DeSanctis A, Campagnacci R, Lezoche E. Laparoscopic common bile duct exploration. *J Laparoendosc Adv Surg Tech A* 2001; **11**: 391-400

11 **Holdsworth RJ,** Sadek SA, Ambikar S, Cuschieri A. Dynamics of bile flow through the choledochal sphincter following exploration of the common bile duct. *World J Surg* 1989; **13**: 300-304

12 **DePaula AL,** Hashiba K, Bafutto M, Machado C, Ferrari A, Machado MM. Results of the routine use of a modified endoprosthesis to drain the common bile duct after laparoscopic choledochotomy. *Surg Endosc* 1998; **12**: 933-935

13 **Gersin KS,** Fanelli RD. Laparoscopic endobiliary stenting as an adjunct to common bile duct exploration. *Surg Endosc* 1998; **12**: 301-304

14 **Isla AM,** Griniatsos J, Wan A. A technique for safe placement of a biliary endoprosthesis after laparoscopic choledochotomy. *J Laparoendosc Adv Surg Tech A* 2002; **12**: 207-211

15 **Chen XP,** Peng SY, Peng CH, Liu YB, Shi LB, Jiang XC, Shen HW, Xu YL, Fang SB, Rui J, Xia XH, Zhao GH. A ten-year study on non-surgical treatment of postoperative bile leakage. *World J Gastroenterol* 2002; **8**: 937-942

16 **Yamaner S,** Bilsel Y, Bulut T, Bugra D, Buyukuncu Y, Akyuz A, Sokucu N. Endoscopic diagnosis and management of complications following surgery for gallstones. *Surg Endosc* 2002; **16**: 1685-1690

17 **Darzi A,** Soin B, Coleman J, Lirici NM, Angelini L. Initial experience with an absorbable laparoscopic ligation clip. *Br J Surg* 1997; **84**: 974-976

18 **Moreaux J.** Traditional surgical management of common bile duct stones: a prospective study during a 20-year experience. *Am J Surg* 1995; **169**: 220-226

19 **Wills VL,** Gibson K, Karihaloot C, Jorgensen JO. Complications of biliary T-tube after choledochotomy. *ANZ J Surg* 2002; **72**: 177-180

20 **Gharaibeh KI,** Heiss HA. Biliary leakage following T-tube removal. *Int Surg* 2000; **85**: 57-63

21 **Schippers E,** Tittel A, Ottinger A, Schumpelick V. Laparoscopy versus laparotomy: comparison of adhesion-formation after bowel resection in a canine model. *Dig Surg* 1998; **15**: 145-147

22 **Tittel A,** Treutner KH, Titkova S, Ottinger A, Schumpelick V. Comparison of adhesion reformation after laparoscopic and conventional adhesiolysis in an animal model. *Langenbecks Arch Surg* 2001; **386**: 141-145

23 **Polymeneas G,** Theodosopoulos T, Stamatiadis A, Kourias E. A comparative study of postoperative adhesion formation after laparoscopic *vs* open cholecystectomy. *Surg Endosc* 2001; **15**: 41-43

24 **Riciardi R,** Islam S, Canete JJ, Arcand PL, Stoker ME. Effectiveness and long-term results of laparoscopic common bile duct. *Surg Endosc* 2003; **17**: 19-22

25 **Hawasli A,** Lloyd L, Cacucci B. Management of choledocholithiasis in the era of laparoscopic surgery. *Am Surg* 2000; **66**: 425-430

26 **Yamakawa T,** Sakai S, Mu ZB, Pineres G. Laparoscopic management of common bile duct stones. *J Hepatobiliary Pancreat Surg* 2000; **7**: 9-14

27 **Fujimura M,** Hirano M, Sato I, Kinoshita T, Yamamoto I, Nishimura K, Takahara H, Yamamoto A. The C tube in biliary surgery -its development and clinical application. *Nippon Geka Hokan* 2000; **68**: 85-122

28 **Shimizu S,** Yokohata K, Mizumoto K, Yamaguchi K, Chijiiwa K, Tanaka M. Laparoscopic choledochotomy for bile duct stones. *J Hepatobiliary Pancreat Surg* 2002; **9**: 201-205

29 **Tokumura H,** Umezawa A, Cao H, Sakamoto N, Imaoka Y, Ouchi A, Yamamoto K. Laparoscopic management of common bile duct stones: transcystic approach and choledochotomy. *J Hepatobiliary Pancreat Surg* 2002; **9**: 206-212

30 **Hotta T,** Taniguchi K, kobayashi Y, Johata K, Sahara M, Naka T, Maeda T, Tanimura H. Biliary drainage tube evaluation after common bile duct exploration for choledocholithiasis. *Hepatogastroenterology* 2003; **50**: 315-321

Edited by Zhang JZ and Wang XL **Proofread by** Xu FM

PO Box 2345, Beijing 100023, China
Fax: +86-10-85381893
E-mail: wjg@wjgnet.com www.wjgnet.com

World J Gastroenterol 2004;10(21):3179-3181
World Journal of Gastroenterology
 ISSN 1007-9327

• BRIEF REPORTS •

Lack of association between seroprevalence of *Helicobacter pylori* infection and primary biliary cirrhosis

Marilena Durazzo, Floriano Rosina, Alberto Premoli, Enrico Morello, Sharmila Fagoonee, Rosaria Innarella, Enrico Solerio, Rinaldo Pellicano, Mario Rizzetto

Marilena Durazzo, Alberto Premoli, Enrico Morello, Department of Internal Medicine, University of Turin, Turin, Italy
Floriano Rosina, Rosaria Innarella, Enrico Solerio, Department of Gastroenterology, Gradenigo Hospital, Turin, Italy
Sharmila Fagoonee, Department of Biology, Biochemistry and Genetics, University of Turin, Turin, Italy
Rinaldo Pellicano, Mario Rizzetto, Department of Gastroenterology, Molinette Hospital, Turin, Italy
Supported by Grant from CNR 1999
Correspondence to: Professor Marilena Durazzo, Department of Internal Medicine, Corso A.M.Dogliotti 14, 10126 Turin, Italy. marilena.durazzo@unito.it
Telephone: +39-11-6336040 **Fax:** +39-11-6634751
Received: 2004-02-02 **Accepted:** 2004-04-07

Abstract

AIM: To determine the association between seroprevalence of *Helicobacter pylori* (*H pylori*) infection and primary biliary cirrhosis (PBC).

METHODS: In this case-control study, 149 consecutive patients (10 males, 139 females, mean age 58.2±11 years, range 26-82 years) suffering from PBC and 619 consecutive healthy volunteer blood donors (523 males, 96 females, mean age 47±5.3 years, range 18-65 years) attending the Hospital Blood Bank and residing in the same area were recruited. A commercial enzyme linked immunosorbent assay was used to detect anti-*H pylori* (IgG) antibodies in serum.

RESULTS: Antibodies to *H pylori* were present in 78 (52.3%) out of 149 PBC-patients and in 291 (47%) out of 619 volunteers (P = 0.24, OR 1.24, 95% CI 0.85-1.80). In the subjects less than 60 years old, the prevalence of *H pylori* infection among PBC-patients (40/79) was slightly higher than in controls (50.6% *vs* 46.2%) P = 0.46, OR = 1.19, 95% CI: 0.72-1.95). In those over 60 years, the prevalence of *H pylori* infection was similar between PBC-patients and controls (54.2% *vs* 57.8%, P = 0.7, OR 0.86, 95% CI 0.36-2.07).

CONCLUSION: There is no association between seroprevalence of *H pylori* infection and primary biliary cirrhosis.

Durazzo M, Rosina F, Premoli A, Morello E, Fagoonee S, Innarella R, Solerio E, Pellicano R, Rizzetto M. Lack of association between seroprevalence of *Helicobacter pylori* infection and primary biliary cirrhosis. *World J Gastroenterol* 2004; 10(21): 3179-3181
http://www.wjgnet.com/1007-9327/10/3179.asp

INTRODUCTION

Helicobacter pylori (*H pylori*) infection is a chronic one. In most instances, it is acquired during childhood, and is often associated with low socio-economic class. The presence of the bacterium has been established as the main cause of several gastroduodenal diseases, including peptic ulcer disease[1,2], gastric carcinoma[3], and gastric MALT lymphoma[4].

Since the latest decade, several studies have reported on the link between chronic *H pylori* or *Helicobacter species* (*H species*) infections and a variety of extragastric manifestations. These include ischaemic heart disease (IHD), liver diseases, skin diseases, blood disorders and others[5]. However, the hypothesis of an etiological role has not yet been fully investigated.

Epidemiological studies have frequently involved control selection bias, population of small sizes, and presence of confounders, like age and socio-economic conditions.

Non randomised, long-period and large studies on the follow-up of *H pylori* eradication in extragastric diseases are lacking.

Several *H.species*, such as *H. bilis*, are capable of colonising different anatomical regions of the gastrointestinal tract in humans, including choledochus, gallbladder, intrahepatic bile ducts and liver[6].

Primary biliary cirrhosis (PBC) is a chronic cholestatic liver disease in which intra-hepatic bile ducts are progressively destroyed. The etiology of PBC is unknown, but immunological mechanisms may play a part in the pathogenesis. A causal role of infectious agents has been proposed but the data are inconclusive. Recently, Bogdanos and coworkers have shown that microbial mimics, comprising that of *H pylori*, are major targets of crossreactivity with human pyruvate dehydrogenase in PBC, strengthening the fact that microbial exposure may be instrumental to the appearance and/or maintenance of anti-mitochondrial antibody responses by a cross-reactive mechanism[7]. These data indicate that a relationship between *H. species* and the biliary tract of humans might exist, where the bacteria could be potentially involved in inflammatory changes or other pathologic manifestations. However, these findings have not been confirmed in other studies[8].

The prevalence of peptic ulcer is higher in cirrhotics than in control population and the risk is increased by the presence of *H pylori* infection[9]. However, in some groups of patients affected from liver disease, as in the case of PBC, the seroprevalence of *H pylori* infection is still undetermined.

The present study attempted to highlight on the seroprevalence of antibodies against *H pylori* in a cohort of patients suffering from PBC in comparison to a group of volunteers attending the Blood Bank of the San Giovanni Battista Hospital (Molinette) in Torino, Italy.

MATERIALS AND METHODS

The presence of anti-*H pylori* antibodies was evaluated in 149 consecutive subjects (10 males, 139 females, mean age 58.2±11 years, range 26-82 years) suffering from PBC.

Patients were considered to have PBC if they fulfilled at least 2 of the following criteria: positive anti-mitochondrial antibody (AMA) at a titer higher than 1/40, abnormal liver function tests (alkaline phosphatase, gamma glutamyl transpeptidase, bilirubin, transaminase level) or liver histology diagnostic or consistent with PBC[10].

AMA was evaluated by immunofluorescence using rat

stomach and kidney as substrate[10].

Other causes of liver disease, such as viral (hepatitis B virus, hepatitis C virus), autoimmune (anti-nuclear, anti- smooth muscle and anti-microsome antibodies) or metabolic (serum iron, percentage of transferrin saturation, ferritin, ceruloplasmin, alpha-1 antitripsin) hepatitis, were ruled out.

The controls were 619 consecutive volunteer blood donors (523 males, 96 females, mean age 47±5.3 years, range 18-65 years) attending the Hospital Blood Bank and residing in the same area[11].

A commercial enzyme linked immunosorbent assay (ELISA, Helori-test® Eurospital, Trieste Italy) was used to detect anti-*H pylori* (IgG) antibodies in serum. The assay sensitivity and specificity *versus* histology were 70.6% and 90.5% respectively, positive predictive value was 87.2% and negative predictive value 77.0%[12].

Briefly, calibrators, positive controls, negative controls and diluted (1:200) serum samples were added to wells coated with purified *H pylori* group-specific antigens. Plates were incubated for 60 min at 37 ℃. The plate was then washed thrice and anti-IgG conjugate was pipetted into each well and the plate was incubated again for 60 min at 37 ℃. The washing step was repeated, chromogenic substrate was added to each well, followed by incubation for 30 min at 37 ℃. The reaction was then stopped. Reading was performed at 405 nm and the mean optical density was expressed as a percentage of the optical density of the positive control serum assayed on the same plate.

A commercial enzyme immunoassay (Helori®-CTX Eurospital, Trieste, Italy) was used to detect serum IgG antibodies against more virulent strains of the bacterium, expressing cytotoxin-associated gene product A (CagA). The manufacturer's instructions were followed. The assay sensitivity and specificity given by the manufacturer were 94.1% and 97.9% respectively.

The seroprevalence of *H pylori* infection in cases and controls was compared using the chi-square test (χ^2) by means of 2×2 contingency table. Fisher's exact test was used for small sample size. Results were considered statistically significant when $P<0.05$.

RESULTS

Mean age between patients and controls was not statistically different.

The prevalence of antibodies to *H pylori* was 52.3% (78/149) in the patients with PBC compared to 47% (291/619) in the controls ($P = 0.24$, OR 1.24, 95% CI 0.85-1.80).

When the patients were subdivided into age-groups (<60 and ⩾60 years), the difference was as follows. In the youngest age group (less than 60 years old), the prevalence of *H pylori* infection among CBP-patients (50.6%, 40/79) was higher than in controls (46.2%, 269/581), but this was not significant ($P = 0.46$, OR 1.19, 95% CI 0.72-1.95). In the group over 60 years, the prevalence of *H pylori* infection was lower in CBP-patients (38/70, 54.2%) than in controls (22/38, 57.8%) ($P = 0.7$, OR 0.86, 95% CI 0.36-2.07) (Table 1).

Table 1 Seroprevalence of anti-*Helicobacter pylori* antibodies among patients with primary biliary cirrhosis [PBC] and controls

Age (yr)	Patients with PBC Hp (+)/tot (%)		Controls Hp (+)/tot (%)		*P*
<60	(50.6)	40/79	269/581	(46.2)	0.46
⩾60	(54.2)	38/70	22/38	(57.8)	0.7
Total	(52.3)	78/149	291/619	(47)	0.24

The anti-CagA antibodies were detected in 28.1% of patients with PBC (42/149) and in 44.8% of those with seropositivity for anti-*H pylori* (35/78). In our population, anti-CagA antibodies were present in 61.8% of a general population admitted to the Emergency Care Unit, as published elsewhere[13].

Out of the 10 patients with a past history of peptic ulcer, 7 had anti-*H pylori* antibodies in circulation. In 29 cases, the signs of portal hypertension [varices or congestive gastropathy] were shown by upper GI endoscopy while in 111 patients there were no abnormalities.

DISCUSSION

The prevalence of *H pylori* infection in patients with liver disease needed to be studied on the basis of clinical and experimental considerations.

From a clinical point of view, the medical history of cirrhotic patients was punctuated by frequent and recurrent hospitalisations due to high rate of complications. Among the most relevant of them, peptic ulcer and upper GI hemorrhage were of peculiar relevance, being life-threatening for the patient and of high cost for Health Care Services, requiring both emergency care and subsequent long hospital stay[14]. By a multivariate analysis, Calvet *et al*. found that male sex and *H pylori* seropositivity (OR 1.7, 95% CI 1.02-2.81) were variables independently related to peptic ulcer in cirrhotics with different etiologies[15]. Moreover, in the case of hemorrhage from peptic ulcer, the presence of cirrhosis was independently associated with increased mortality ($P<0.001$)[16]. Little information is available on the prevalence of peptic ulcer in subjects suffering from PBC or primary sclerosing cholangitis (PSC). The prevalence of duodenal ulcer (DU) in male cirrhotics was investigated by Rabinovitz *et al*. in 216 subjects. Occurrence of DU amounted to 7.8% in patients and 2.2 % in controls ($P<0.005$). When the patients were subdivided according to etiology, DU prevalence was observed in 9.4% of HBV-relate chronic hepatitis patients, 12.2% of alcohol-relate chronic hepatitis patients, 3.5% of cryptogenic, 6.6% of autoimmune cirrhosis, 9.5% of PSC and none of the patients with PBC. However, in the latter case only 9 patients were included[17].

Since peptic ulcer is related to the presence of *H pylori* infection in non-cirrhotic patients, it is logical to suppose a similar role for the bacterium also in subjects with cirrhosis.

A high prevalence of anti-*H pylori* antibodies in HCV-infected cirrhotic patients has been reported in several North Italian towns[18,19]. On the contrary, there was no increased seroprevalence in patients suffering from autoimmune hepatitis[20]. Fan *et al.* demonstrated a higher seroprevalence of *H pylori* in Chinese patients with HBV-related chronic hepatitis than in controls matched for age and socio-economic status[21]. In Taiwan, Chen *et al*. found no association between peptic ulcer and *H pylori* infection in cirrhotic patients[22]. Selection biases and methods of diagnosis were possible sources of the heterogeneity of the studies. Contrasting results might arise from the choice of tests used for the diagnosis of *H pylori* infection. Indeed, when the diagnosis relies solely on histological examination of gastric biopsies, sampling error is the source of severe misdiagnosis. The European *H pylori* Study Group has recommended to search for IgG anti-*H pylori* when performing an epidemiological investigation[23].

Regarding populations of subjects suffering from PBC, Floreani *et al*. showed that *H pylori* colonization was significantly more frequent in controls than in patients but IgG anti-*H pylori* were detected in the same percentage in the two groups[24]. Thus, the latter finding is in agreement with those of our study. Dohmen and coworkers in Japan, have found that *H pylori* is a possible pathogenic factor in atrophic corpus gastritis in PBC-patients. Furthermore, a positive correlation between the titers of anti-pyruvate dehydrogenase antibody and anti-*H pylori* was confirmed[25]. However, in this investigation,

no comparison with a control population has been made.

From an experimental point of view, infection of healthy A/JCr male mice with *H hepaticus* could result in chronic hepatitis and liver cancer in a short time[26]. Since this report, several other *H. species* have been subsequently found in the liver and biliary tract of cats and dogs suffering from hepatitis and hepatocellular carcinoma. *H. species* have been demonstrated both in the bile and in the gallbladder mucosa of Chilean patients with chronic gallbladder inflammation, raising the question as to whether the frequent finding of gallbladder cancer in Chile might arise from such an infection[6]. By polymerase chain reaction, hybridisation and partial DNA sequencing in human liver of patients with PBC or PSC, Nilsson *et al*. found the positivity for *Helicobacter* genus-specific primers in 11 out of 12 samples of PBC-subjects and in 9 out of 12 samples of individuals suffering from PSC[27].

In conclusion, we found that the seroprevalence of *H pylori* in subjects suffering from primary biliary cirrhosis was not more frequent than in controls, suggesting that the putative role of *H pylori* in triggering organ-specific autoimmunity does not hold true for PBC.

On the other hand, although these data do not provide proof for the association between *H pylori* infection and PBC, a type II statistical error, i.e. the probability of accepting the *null hypothesis* when it is false, cannot be ruled out.

REFERENCES

1 **Bulent K**, Murat A, Esin A, Fatih K, MMMurat H, Hakan H, Melih K, Mehmet A, Bulent Y, Fatih H. Association of *CagA* and *VacA* presence with ulcer and non-ulcer dyspepsia in a Turkish population. *World J Gastroenterol* 2003; **9**: 1580-1583

2 **Testino G**, Cornaggia M, De Iaco F. *Helicobacter pylori* influence on gastric acid secretion in duodenal ulcer patients diagnosed for the first time. *Panminerva Med* 2002; **44**: 19-22

3 **Mladenova I**, Pellicano R. Infectious agents and gastric tumours. An increasing role for Epstein-Barr virus. *Panminerva Med* 2003; **45**: 183-188

4 **Wotherspoon AC,** Doglioni C, Diss TC, Pan L, Moschini A, de Boni M, Isaacson PG. Regression of primary low-grade B-cell gastric lymphoma of mucosa-associated lymphoid tissue type after eradication of *Helicobacter pylori*. *Lancet* 1993; **342**: 575-577

5 **Roussos A**, Philippou N, Gourgoulianis KI. *Helicobacter pylori* infection and respiratory diseases: a review. *World J Gastroenterol* 2003; **9**: 5-8

6 **Fox JG**, Dewhirst FE, Shen Z, Feng Y, Taylor NS, Paster BJ, Ericson RL, Lau CN, Correa P, Araya JC, Roa I. Hepatic *Helicobacter* species identified in bile and gallbladder tissue from Chileans with chronic cholecystitis. *Gastroenterology* 1998; **114**: 755-763

7 **Bogdanos DP**, Baum H, Grasso A, Okamoto M, Butler P, Ma Y, Rigopoulou E, Montalto P, Davies ET, Burroughs AK, Vergani D. Microbial mimics are major targets of crossreactivity with human pyruvate dehydrogenase in primary biliary cirrhosis. *J Hepatol* 2004; **40**: 31-39

8 **Tanaka A**, Prindiville TP, Gish R, Solnick JV, Coppel RL, Keffe EB, Ansari A, Gershwin ME. Are infectious agents involved in primary biliary cirrhosis? A PCR approach. *J Hepatol* 1999; **31**: 664-671

9 **Vergara M**, Calvet X, Roque M. *Helicobacter pylori* is a risk factor for peptic ulcer disease in cirrhotic patients. A meta-analysis. *Eur J Gastroenterol Hepatol* 2002; **14**: 717-722

10 **Heathcote EJ**. Management of primary biliary cirrhosis. The American Association for the Study of Liver Diseases practice guidelines. *Hepatology* 2000; **31**: 1005-1013

11 **Ponzetto A,** Pellicano R, Morgando A, Cirillo D, Marchiaro G, Curti F, Rizzetto M. Seroprevalence of *Helicobacter pylori* infection among blood donors in Torino, Italy. *Minerva Gastroenterol Dietol* 2001; **47**: 3-7

12 **Palli D,** Vaira D, Menegatti M, Saieva C. A serologic survey of *Helicobacter pylori* infection in 3281 Italian patients endoscoped for upper gastroitestinal symptoms. The Italian *Helicobacter Pylori* Study Group. *Aliment Pharmacol Ther* 1997; **11**: 719-728

13 **Pellicano R**, Parravicini PP, Bigi R, Gandolfo N, Aruta E, Gai V, Figura N, Angelino P, Rizzetto M, Ponzetto A. Infection by *Helicobacter pylori* and acute myocardial infarction. Do cytotoxic strains make a difference? *New Microbiol* 2002; **25**: 315-321

14 **Rosina F,** Alaria P, Castelli S, Dirindin N, Rocca G, Actis GC, Borelli R, Ciancio AL, De Bernardi W, Fornasiero S, Lavezzo B, Lagget M, Martinotti R, Marzano A, Ottobrelli A, Sostegni R, Rizzetto M, Verme G. Effect of patient characteristics on hospital costs for cirrhosis: implications for the disease-related group [DRG] reimbursement system. *Ital J Gastroenterol* 1996; **28**: 401-405

15 **Calvet X,** Navarro M, Gil M, Lafont A, Sanfeliu I, Brullet E, Campo R, Dalmau B, Rivero E, Mas P. Epidemiology of peptic ulcer disease in cirrhotic patients: role of *Helicobacter pylori* infection. *Am J Gastroenterol* 1998; **93**: 2501-2507

16 **Dousset B,** Suc B, Boudet MJ, Cherqui D, Rotman N, Julien M, Fagniez PL. Surgical treatment of severe ulcerous hemorrhages: predictive factors of operative mortality. *Gastroenterol Clin Biol* 1995; **19**: 259-265

17 **Rabinovitz M,** Schade RR, Dindzans V, Van Thiel DH, Gavaler JS. Prevalence of duodenal ulcer in cirrhotic males referred for liver transplantation. Does the etiology of cirrhosis make a difference? *Dig Dis Sci* 1990; **35**: 321-326

18 **Ponzetto A,** Pellicano R, Redaelli A, Rizzetto M, Roffi L. *Helicobacter pylori* infection in patients with Hepatitis C Virus positive chronic liver diseases. *New Microbiol* 2003; **26**: 321-328

19 **Leone N,** Pellicano R, Brunello F, Cutufia MA, Berrutti M, Fagoonee S, Rizzetto M, Ponzetto A. *Helicobacter pylori* seroprevalence in patients with cirrhosis of the liver and hepatocellular carcinoma. *Cancer Detect Prev* 2003; **27**: 494-497

20 **Durazzo M,** Pellicano R, Premoli A, Berrutti M, Leone N, Ponzetto A, Rizzetto M. *Helicobacter pylori* seroprevalence in patients with autoimmune hepatitis. *Dig Dis Sci* 2002; **47**: 380-383

21 **Fan XG,** Zou YY, Wu AH, Li TG, Hu GL, Zhang Z. Seroprevalence of *Helicobacter pylori* infection in patients with hepatitis B. *Br J Biomed Sci* 1998 ; **55** : 176-178

22 **Chen JJ**, Changchien CS, Tai DI, Chiou SS, Lee CM, Kuo CH. Role of *Helicobacter pylori* in cirrhotic patients with peptic ulcer. *Dig Dis Sci* 1994; **39**: 1565-1568

23 Guidelines for clinical trials in *Helicobacter pylori* infection. Working Party of the European *Helicobacter pylori* Study Group. *Gut* 1997; **41**(Suppl 2): S1-S9

24 **Floreani A**, Biagini MR, Zappala F, Farinati F, Plebani M, Rugge M, Surrenti C, Naccarato R. Chronic atrophic gastritis and *Helicobacter pylori* infection in primary biliary cirrhosis: a cross-sectional study with matching. *Ital J Gastroenterol Hepatol* 1997; **29**: 13-17

25 **Dohmen K**, Shigematsu H, Miyamoto Y, Yamasaki F, Irie K, Ishibashi H. Atrophic corpus gastritis and *Helicobacter pylori* infection in primary biliary cirrhosis. *Dig Dis Sci* 2002; **47**: 162-169

26 **Ward JM**, Fox JG, Anver MR, Haines DC, George CV, Collins MJ, Gorelick PL, Nagashima K, Gonda MA, Gilden RV, Tully JG, Russell RJ, Benveniste RE, Paster BJ, Dewhirst FE, Donovan JC, Anderson LM, Rice JM. Chronic active hepatitis and associated liver tumors in mice caused by a persistent bacterial infection with a novel *Helicobacter species*. *J Natl Cancer Inst* 1994; **86**: 1222-1227

27 **Nilsson H**, Taneera J, Castedal M, Glatz E, Olsson R, Wadstrom T. Identification of *Helicobacter pylori* and *Helicobacter* species by PCR, hybridization and partial DNA sequencing in human liver samples from patients with primary sclerosing cholangitis or primary biliary cirrhosis. *J Clin Microbiol* 2000; **38**: 1072-1076

Edited by Wang XL and Xia HHX **Proofread by** Xu FM

PO Box 2345, Beijing 100023, China
Fax: +86-10-85381893
E-mail: wjg@wjgnet.com www.wjgnet.com

World J Gastroenterol 2004;10(21):3182-3184
World Journal of Gastroenterology
 ISSN 1007-9327

• BRIEF REPORTS •

Pathological characteristics of gastric leiomyoblastoma

Xiao-Feng Huang, Chun-Mei Wang, Bo-Rong Pan, Xiao-Wen Dai, Li Fang, Jia-Ji Yang, Hua Yu, Jun Ren

Xiao-Feng Huang, Chun-Mei Wang, Jia-Ji Yang, Hua Yu, Electron Microscope Center, Fourth Military Medical University, Xi'an 710032, Shaanxi Province, China
Bo-Rong Pan, Jun Ren, Department of Oncology, Xijing Hospital, Fourth Military Medical University, Xi'an 710032, Shaanxi Province, China
Xiao-Wen Dai, Li Fang, Department of Pathology, Chinese PLA 117 Hospital, Hangzhou 310013, Zhejiang Province, China
Supported by the Foundation of 117 Hospital, No.99008
Correspondence to: Chun-Mei Wang, Electron Microscope Center, Fourth Military Medical University, Xi'an 710032, Shaanxi Province, China. fmmuem@fmmu.edu.cn
Telephone: +86-29-83374572
Received: 2004-02-02 **Accepted:** 2004-03-24

Abstract

AIM: To determine the pathological characteristics of gastric leiomyoblastoma.

METHODS: All tissues were obtained during surgery or gastroscopy. Tissue specimens for examination by light microscope were 1 cm×1 cm×1 cm in size, fixed in 40 g/L neutral buffered formaldehyde, embedded in paraffin, and stained with hematoxylin and eosin. The fresh tissues obtained for electron microscopy were 1 mm×1 mm×1 mm in size, and fixed in phosphate buffered 30 g/L glutaraldehyde, postfixed in 10 g/L osmium tetroxide and dehydrated in graded alcohol, embebbed in Epon 812. Ultrathin sections of 50 nm were stained with uranyl acetate and lead citrate and examined under a JEM-2000 EX transmission electron microscope.

RESULTS: The most important histopathological feature of leiomyoblastoma was the predominance of large, rounded or polygonal cells with characteristic perinuclear clear zone in cytoplasms. The tumor cells arranged in patch, cell junction or junctional complex could be found occasionally between cells under electron microscope. Most of the neoplastic cytoplasms were filled with myofilaments, dense bodies, and dense patches. Rough endoplasmic reticulum dilatated as lakes, and large quantities of protein secretions of intermediate electron density were found in the dilated cisternae. Intracisternal segregation could also be found. The nuclei were round or oval, and anomalous nuclei were found in part of cells.

CONCLUSION: The diagnosis of gastric leiomyoblastoma can be confirmed by electron microscopy. The clear appearance of tumor cells is due to the dilation of rough endoplasmic reticulum, not fat droplets, glycogens or mucus in cytoplasm.

Huang XF, Wang CM, Pan BR, Dai XW, Fang L, Yang JJ, Yu H, Ren J. Pathological characteristics of gastric leiomyoblastoma. *World J Gastroenterol* 2004; 10(21): 3182-3184
http://www.wjgnet.com/1007-9327/10/3182.asp

INTRODUCTION

Gastric neoplasms are common in the world, specially in China[1-8]. Gastrointestinal stromal tumor (GIST) is the most common mesenchymal tumor of gastrointestinal tract[9], although GIST may arise from any portion of the foregut to hindgut, two thirds of stromal tumors originate from the stomach[10]. Leiomyoblastoma, also called bizarre leiomyoma or epithelioid leiomyoma, is a rare smooth muscle tumor characterized by epithelioid cells with clear cytoplasms and an unknown biological behaviour. It is an unusual type of smooth muscle tumor which is biologically benign in most cases, but on rare occasions may behave in a malignant manner and metastasize[11-15]. It is most frequently seen in the gastric wall but may occasionally be encountered in the uterus[16,17], tongue[18], round ligament[19], omentum[12], vulva[20], urethra[21], intestines, mesentery, retroperitoneum, mediastinum, and deep superficial soft tissues[22,23]. Gastric leiomyoblastoma is a benign neoplasia, extremely uncommon and potentially malignant, arising from the muscular layer of the stomach[24-26]. These neoplasms form solitary, well-defined, but not encapsulated, rounded or lobulated masses which, when small, tend to be localized intramurally. Multiple tumors are rare[27-30]. The growth may take place towards the lumen, resulting in a polypoid mass and is covered by an attenuated mucosa.

MATERIALS AND METHODS

All the cases were obtained from the Chinese PLA 117 Hospital. Information of these cases is shown in Table 1. The patient population consisted of two men and three women. Their mean age was 51.4 years, ranging from 48 to 58 years at the time of diagnosis (Table 1). No relevant information of family history was found.

Table 1 Principal manifestations of gastric leiomyoblastoma

No	Sex	Age (yr)	Manifestations
1	Male	48	Abdominal dull pain, gasterorrhagia, dyspepsia
2	Male	56	Abdominal pain, abdominal mass, hemafecia
3	Female	42	Abdominal pain, nausea, vomiting
4	Female	53	Abdominal pain, vomiting, black stool
5	Female	58	Interrupted hematemesis, cupressus defecation

The cytologic samples were negative in all cases. The patients were explored surgically and neoplasms of stomach resected. All tissue specimens for examination by light microscope were 1 cm×1 cm×1 cm in size, fixed in 40 g/L neutral buffered formaldehyde, embedded in paraffin, and stained with hematoxylin and eosin. The fresh tissues obtained for electron microscopy were 1 mm×1 mm×1 mm in size, and fixed in phosphate buffered 30 g/L glutaraldehyde, postfixed in 10 g/L osmium tetroxide and dehydrated in graded alcohol, embebbed in Epon 812. Ultrathin sections of 50 nm were stained with uranyl acetate and lead citrate and examined under a JEM-2000 EX transmission electron microscope.

RESULTS

Gross anatomy and gastroscopy

All resected tumors were well-circumscribed, and three tumors were located at the antro-pyloric region (cases 1, 3 and 4), one

at the body (case 2) and one at the gastric antrum (case 5). The size was measured between 2.5 cm and 13 cm, averaging 6.8 cm. The type of tumor growth was intraluminal (1/5) or extraluminal (2/5) or mixed (2/5). An ulcerated nodular tumor, located in the anterior wall and minor curvature of the gastric antrum (case 1), was found by gastroscopy.

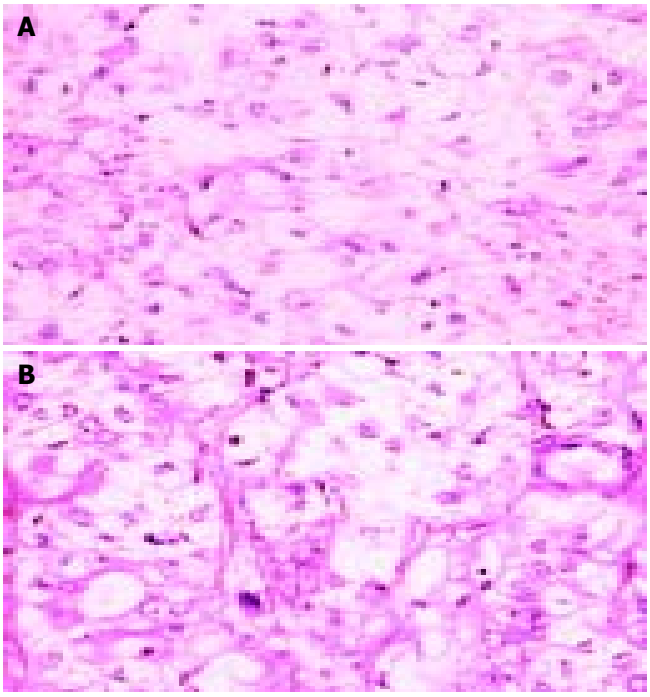

Figure 1 Round tumor cells, with clear cytoplasm, vary greatly in size and shape.

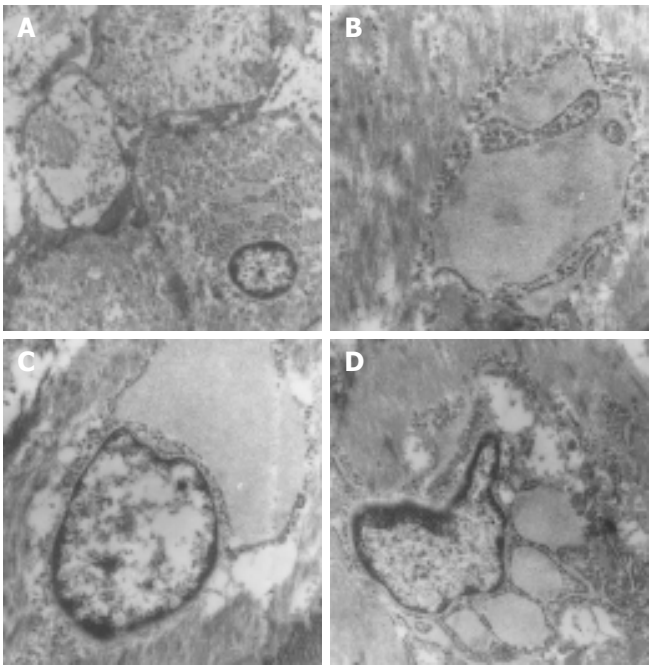

Figure 2 Ultrastructure of gastric leiomyoblastoma. A: Tumor cells with many microfilaments, B: Intracisternal segregation could also be found, C: Rough endoplasmic reticulum dilatated as lakes, and protein secretion of intermediate electron density was found in the dilated cisternae, D: Distorted nuclei were found in tumor cells.

Histopathological appearances

Round tumor cells with clear cytoplasm, varied greatly in size and shape in different parts of the same tumor (Figure 1). The cellular morphology of the muscle neoplasm was all homogenous and the frequency of mitosis was 2 mitoses in case 1 and 4 in case 5 in 10 HPFs, and some areas of fibrosis and degeneration were found in case 3. The most important feature of leiomyoblastoma was the predominance of large, round or polygonal cells with characteristic perinuclear clear zone in cytoplasm (Figure 1). The nuclei might be pleomorphic with prominent nucleoli.

Ultrastructural characteristics

Ultrastructural studies confirmed that the origin of these tumors was smooth-muscle cells, and they were fusiform and round with many microfilaments. Tumor cells arranged in patch, and the cell junction or junctional complex could be found occasionally between cells. Most of the neoplastic cytoplasms were filled with myofilaments, dense bodies, and dense patches (Figure 2 A, B). Rough endoplasmic reticulum dilatated as lakes, and large quantities of protein secretions of intermediate electron density were found in the dilated cisternae (Figure 2C). Intracisternal segregation could also be found (Figure 2B). The nuclei were round or oval, and distorted nuclei were found in part of cells (Figure 2D).

DISCUSSION

The most important ultrastructural features of leiomyoblastoma were myofilaments, dense bodies and dense patches present in most of the tumor cells. The perinuclear clear zone in cytoplasm was caused by dilation of rough endoplasmic reticulum. These characteristics proved that gastric leiomyoblastoma arised from smooth muscle cells of the gastrointestinal (GI) tract. Leiomyoblastoma was often previously diagnosed as GIST. Although the term GIST was first used in 1983 (by Mazur and Clark), the 1998 discovery by Hirota that GIST tumors could contain mutations in the c-kit gene and marked the beginning of a new understanding and reclassification of sarcomas of the GI tract. Prior to the year 2000, GISTs were classified as one of the types of soft tissue sarcoma (STS), including tumors of smooth-muscle origin (most commonly leiomyosarcoma, and also leiomyoma or leiomyoblastoma) and of neural-crest origin (eg, Schwannoma, or nerve sheath tumour).

Most tumors previously diagnosed as gastrointestinal autonomic nerve tumors (GANTs) are also now classified as GISTs and contain essentially the identical KIT mutations as GIST. What establishes GIST as a separate diagnosis from these other soft tissue sarcomas is not just the description of where the tumor is located, but also the additional factor that it is KIT (CD117) positive. Most GIST patients are also CD34 positive and desmin negative. Well, one of the best ways to identify the cancer cell type (aside from just looking at the cells under a microscope) is to determine the proteins that the cells make. Specialized tests allow the pathologist to do this, usually by determining whether the cells will bind to antibodies against the protein of interest. So, “kit-positive” means that the cells make the protein “kit”, desmin-negative means that the cells do not make the protein “desmin”.

With the development of new effective therapies for GIST, it is vitally important that patients with soft tissue sarcomas of the GI tract have their tumor slides tested for KIT (CD117) by a pathologist experienced with GIST and KIT. Some (perhaps many) patients with pathology reports that were done prior to 2001 may think they have leiomyosarcoma, leiomyoma, leiomyoblastoma, or GANT when in fact their pathology slides were never tested for KIT and they might have GIST. Once more, misdiagnosis can be a disaster. Pathology is critical. Fortunately, the pathology of GIST is now (2003) much better understood than it was in five years ago.

Another question is the origin of GIST. GISTs were previously thought to arise from smooth muscle cells of the GI tract. The discovery that GISTs could express KIT protein helps establish that GISTs do not originate from smooth muscles. The current thinking is that GIST tumors arise either from stem cells that differentiate towards interstitial cells of Cajal or directly from interstitial cells of Cajal (ICCs). The interstitial cells of Cajal are the pacemaker cells of the GI tract (they are named after a great Spanish biologist and microscopist named Cajal), they stimulate the movement (contractions) of the GI tract. These movements ("peristalsis") are the waves of contraction which force the digested food through the gut. GIST often spreads from the original (primary) site to distant locations. If this happens, these tumors are called metastases (or simply, "mets"). If GIST tumors metastasize they usually travel to the liver, or the peritoneum. Metastases to lymph-nodes and lungs are rare, but do occur. Metastasis is usually even worse than the growth of the primary one. Metastases can cripple a vital organ such as the liver. They are usually harder to treat than primary tumors. Metastases are the terrorist network of cancer, stealthily spreading to distant sites, where they can grow and do damage.

The results showed that gastric leiomyoblastoma cells did not differentiate to interstitial cells of Cajal, but differentiated to smooth muscle cells. Therefore, we think if definite smooth myocytes are found in this tumor, it should be diagnosed as leiomyoblastoma but not as GIST.

In summary, gastric leiomyoblastomas have a characteristic ultrastructure, electron microscopy may play a crucial role in diagnosis of gastric leiomyoblastoma.

REFERENCES

1 **Lu JB**, Sun XB, Dai DX, Zhu SK, Chang QL, Liu SZ, Duan WJ. Epidemiology of gastroenterologic cancer in Henan Province, China. *World J Gastroenterol* 2003; **9**: 2400-2403

2 **Zhang JH**, Li Y, Wang R, Geddert H, Guo W, Wen DG, Chen ZF, Wei LZ, Kuang G, He M, Zhang LW, Wu ML, Wang SJ. NQO1 C609T polymorphism associated with esophageal cancer and gastric cardiac carcinoma in North China. *World J Gastroenterol* 2003; **9**: 1390-1393

3 **Wang KJ**, Wang RT. Meta-analysis on the epidemiology of *Helicobacter pylori* infection in China. *Zhonghua Liuxingbingxue Zazhi* 2003; **24**: 443-446

4 **Roder DM**. The epidemiology of gastric cancer. *Gastric Cancer* 2002; **5**(Suppl 1): 5-11

5 **Wu K**, Crusius JB, Fan D, Pena AS. The immunogenetics and pathogenesis of gastric cancer. Highlights of the first Sino-European workshop on the immunogenetics and pathogenesis of gastric cancer. *Drugs Today* 2002; **38**: 391-417

6 **Kasakura Y**, Phan A, Ajani J. Adjuvant therapy for resected gastric carcinoma. *Surg Oncol Clin N Am* 2002; **11**: 431-444

7 **Wang G**, Hao C, Lai S. Endoscopic study on cancer of gastric cardia in the high incidence areas of China. *Zhonghua Zhongliu Zazhi* 2002; **24**: 381-383

8 **Gao CM**, Takezaki T, Wu JZ, Li ZY, Liu YT, Li SP, Ding JH, Su P, Hu X, Xu TL, Sugimura H, Tajima K. Glutathione-S-transferases M1 (GSTM1) and GSTT1 genotype, smoking, consumption of alcohol and tea and risk of esophageal and stomach cancers: a case-control study of a high-incidence area in Jiangsu Province, China. *Cancer Lett* 2002; **188**: 95-102

9 **Trupiano JK**, Stewart RE, Misick C, Appelman HD, Goldblum JR. Gastric stromal tumors: a clinicopathologic study of 77 cases with correlation of features with nonaggressive and aggressive clinical behaviors. *Am J Surg Pathol* 2002; **26**: 705-714

10 **House MG**, Guo M, Efron DT, Lillemoe KD, Cameron JL, Syphard JE, Hooker CM, Abraham SC, Montgomery EA, Herman JG, Brock MV. Tumor suppressor gene hypermethylation as a predictor of gastric stromal tumor behavior. *J Gastrointest Surg* 2003; **7**: 1004-1014

11 **Shi HY**, Yang XC, Zhang GZ. Malignant gastric leiomyoblastoma accompanied by metastasis in many sites: report of a case. *Xin Xiaohuabingxue Zazhi* 1994; **2**(Suppl 2): 39

12 **Sun XL**. The multiple leiomyoblastoma of omentum accompanied by metastasis of liver, spleen and colon transversum: report of a case. *Huaren Xiaohua Zazhi* 1998; **6**: 518

13 **Diaz Plasencia J**, Tantalean E, Guzman R, Pomatanta Plasencia J, Grados Mendez J, Vilela C. Malignant gastric leiomyoblastoma: case report. *Rev Gastroenterol Peru* 1997; **17**: 170-176

14 **Kamiga M**, Kimura W, Takasu N, Takeshita A, Ozawa K, Fuse A, Usuba O, Nagashima R. Successful resection of a liver metastasis from gastric leiomyoblastoma: report of a case. *Surg Today* 2000; **30**: 932-936

15 **Ballarini C**, Intra M, Ceretti AP, Prestipino F, Bianchi FM, Sparacio F, Berti E, Perrone S, Silva F. Gastrointestinal stromal tumors: a "benign" tumor with hepatic metastasis after 11 years. *Tumori* 1998; **84**: 78-81

16 **Watanabe K**, Ogura G, Suzuki T. Leiomyoblastoma of the uterus: an immunohistochemical and electron microscopic study of distinctive tumours with immature smooth muscle cell differentiation mimicking fetal uterine myocytes. *Histopathology* 2003; **42**: 379-386

17 **Modafferi F**. Epithelioid cell's uterine leiomyoma uteri. A case report with immunohistochemical study. *J Exp Clin Cancer Res* 2002; **21**: 295-298

18 **Sancho Alvarez A**, Poncela Blanco M, Morais Perez D, Martin Siguenza G, Peral Martinez JI. Leiomyoblastoma of the tongue. *Acta Otorrinolaringol Esp* 2001; **52**: 70-73

19 **Bakotic BW**, Cabello-Inchausti B, Willis IH, Suster S. Clear-cell epithelioid leiomyoma of the round ligament. *Mod Pathol* 1999; **12**: 912-918

20 **Hopkins-Luna AM**, Chambers DC, Goodman MD. Epithelioid leiomyoma of the vulva. *J Natl Med Assoc* 1999; **91**: 171-173

21 **Sakai Y**, Yamada T, Fukuda H, Ichiyanagi N, Kamata S, Nagahama K, Tanizawa A, Watanabe T, Saitoh H, Itoyama S. A case of epithelioid leiomyoma (leiomyoblastoma) of the urethra. *Hinyokika Kiyo* 2000; **46**: 41-43

22 **Hou YY**, Sun MH, Wei YK, Tan YS, Lu XY, Wang J, Zhu XZ, Zheng AH. Clinicopathological, immunohistochemical and molecular genetic study of intra-abdomen extra-gastrointestinal stromal tumors. *Zhonghua Binglixue Zazhi* 2003; **32**: 422-426

23 **Abdulkader I**, Cameselle-Teijeiro J, Gude F, Fraga M, Varela-Duran J, Barreiro F, Forteza J. Predictors of malignant behaviour in gastrointestinal stromal tumours: a clinicopathological study of 34 cases. *Eur J Surg* 2002; **168**: 288-296

24 **Simeth C**, Dellach C, Guarino G, Balani A. Gastric leiomyoblastoma. (Review of the literature in the light of a case). *Ann Ital Chir* 1999; **70**: 57-60

25 **Mazzocconi G**, Mantella F, Anselmi D, Nigita G, Terenzi A, Rossi Lemeni A, Sbaffi E. Gastric leiomyoblastomas: a clinical case report. *G Chir* 2000; **21**: 167-171

26 **Barrier A**, Huguier M, Levard H, Montariol T, Fagniez PL, Sauvanet A. Gastric stromal tumors. Results of a multicenter study. French Associations of Surgery Research. *Chirurgie* 1999; **124**: 494-502

27 **Simeth C**, Dellach C, Guarino G, Balani A. Gastric leiomyoblastoma. (Review of the literature in the light of a case). *Ann Ital Chir* 1999; **70**: 57-60

28 **Medina Perez M**, Reyes Lopez A, Garcia Ferris G. Epithelioid gastric leiomyosarcoma (malignant leiomyoblastoma) with intense expression of smooth muscle desmin and actin). *Rev Esp Enferm Dig* 1998; **90**: 595-596

29 **Sofka CM**, Semelka RC, Marcos HB, Calvo BF, Woosley JT. Metastatic gastric leiomyoblastoma: a case report. *Magn Reson Imaging* 1998; **16**: 343-346

30 **Nozoe T**, Nagamatsu A, Funahashi S, Kitamura M, Suehiro T, Matsumata T, Sugimachi K. Partial resection for leiomyoblastoma of stomach. *Hepatogastroenterology* 2001; **48**: 1806-1807

Edited by Zhu LH and Wang XL **Proofread by** Xu FM

PO Box 2345, Beijing 100023, China
Fax: +86-10-85381893
E-mail: wjg@wjgnet.com www.wjgnet.com

World J Gastroenterol 2004;10(21):3185-3187
World Journal of Gastroenterology
 ISSN 1007-9327

• BRIEF REPORTS •

Changes of cytosolic [Ca^{2+}]i in neutrophils in pancreatic microcirculation of rats with caerulein-induced acute pancreatitis under fluid shear stress

Zong-Guang Zhou, You-Qin Chen, Xu-Bao Liu, Wei-Ming Hu, Bo-Le Tian, Huai-Qing Chen

Zong-Guang Zhou, You-Qin Chen, Xu-Bao Liu, Wei-Ming Hu, Bo-Le Tian, Department of General Surgery & Institute of Gastroenteric Surgery, West China Hospital, Sichuan University, Chengdu 610041, Sichuan Province, China
Huai-Qing Chen, Institute of Biomedical Engineering, West China Center of Medical Sciences, Sichuan University, Chengdu 610041, Sichuan Province, China
Supported by the National Natural Science Foundation of China, No. 39770722 and the Key Project of National Outstanding Youth Foundation of China, No. 39925032
Correspondence to: Professor Zong-Guang Zhou, Department of General Surgery & Institute of Gastroenteric Surgery, West China Hospital, Sichuan University, Chengdu 610041, Sichuan Province, China. zhou767@21cn.com
Telephone: +86-28-85422484 **Fax:** +86-28-85422484
Received: 2004-03-27 **Accepted:** 2004-04-05

Abstract

AIM: To investigate the fluid shear stress induced changes of [Ca^{2+}]i in neutrophils in pancreatic microcirculation of experimental acute pancreatitis (AP).

METHODS: Wistar rats (n = 36) were randomized into three groups. A model of AP was established by subcutaneous injection of caerulein. Low-shear 30 viscometer was used to provide steady fluid shear stress on separated neutrophils. The mean fluorescent intensity tested by flow cytometry was used as the indication of [Ca2+]i quantity.

RESULTS: Under steady shear, cytosolic [Ca^{2+}]i showed biphasic changes. The shear rate changed from low to high, [Ca^{2+}]i in different groups decreased slightly and then increased gradually to a high level (P<0.05). A close correlation was observed between the cytosolic [Ca^{2+}]i level and the alteration of fluid shear stress in regional microcirculation of AP.

CONCLUSION: The increase of [Ca^{2+}]i is highly related to the activation of neutrophils, which contributes to neutrophil adhesion to endothelium in the early phase of AP. The effect of fluid shear stress on [Ca^{2+}]i may play a crucial role in pancreatic microcirculatory failure of AP.

Zhou ZG, Chen YQ, Liu XB, Hu WM, Tian BL, Chen HQ. Changes of cytosolic [Ca^{2+}]i in neutrophils in pancreatic microcirculation of rats with caerulein-induced acute pancreatitis under fluid shear stress. *World J Gastroenterol* 2004; 10(21): 3185-3187
http://www.wjgnet.com/1007-9327/10/3185.asp

INTRODUCTION

Studies have confirmed the hypothesis that microcirculatory derangements play a pivotal role in the pathogenesis of acute pancreatitis (AP), including the process of conversion from edematous to necrotizing injury[1-3]. Although several pathophysiological sequences, such as protease activation, free radical generation, and inflammatory mediator release, have been described in acute pancreatitis, the precise mechanism by which acute pancreatitis is initiated is unknown[4-7]. Cellular calcium, a key physiological signaling element in cell function and also a crucial pathological intracellular messenger in cell injury, appears to be involved in the initiation and development of acute pancreatitis[8-12]. Previous studies have suggested that AP is frequently associated with sequestration of inflammatory cells, particularly neutrophils, within pancreas, and it is generally believed to be an early and important event in the evolution of pancreatitis[13,14]. Recently, considerable attention has been directed at identifying the chemoattractant substances responsible for leukocyte sequestration within these tissues and the factors released from these inflammatory cells that contribute to progression of AP[15-21]. Cytosolic free Ca^{2+}, a well-known second messenger, takes part in many cellular reaction processes and regulates the activity of many enzymes[8]. Caerulein-induced AP has been shown to cause cytosolic free Ca^{2+} transient increase[9-12]. Increase in leukocyte cytosolic [Ca^{2+}]i might be involved in intercellular adhesion by regulating the affinity of surface adhesion molecules or by facilitating transendothelial leukocyte migration, which might lead to increased leukocytic infiltration and tissue damage during AP[9-12].

Previous studies mainly concentrated on the peripheral blood neutrophils during AP under static state due to limitation of experimental methodology. However, to the authors' knowledge, no reports are available about local pancreatic microcirculatory neutrophils during AP under flow state. Although the number of neutrophils in circulation is much less compared with the total mature neutrophils in the body, these circulating cells move with blood in the whole body, and execute disinfectant functions. The stored neutrophils replenish at a certain rate into the blood to maintain a dynamic balance between circulation pool and bone marrow storage pool[22,23]. When it is necessary, bone marrow can release more neutrophils to enhance the defense efficacy. So blood flow is an important physiological environment for neutrophils[22,23]. We first undertook to investigate the change of [Ca^{2+}]i in local pancreatic microcirculatory neutrophils during AP under fluid sheer stress. The results of this study might provide a new insight into the pathogenesis of AP.

MATERIALS AND METHODS

Animals

Adult male Wistar rats weighting 250-350 g were purchased from Center of Experimental Animals, Sichuan University, Chengdu, China. All animals were starved for 24 h prior to experimentation. All animal experiments were conducted according to the guidelines of the Local Animal Use and Care Committees and the National Animal Welfare Law.

Induction of acute pancreatitis

All rats of the experimental groups were injected with 5.5 μg/kg and 7.5 μg/kg of acaerulein (Sigma Co., USA) subcutaneously

at 0 and 1 h after the beginning of experiment respectively, while the rats of the control group were subcutaneously injected with normal saline solution.

Experimental protocol

Experimental animals were divided into three groups, with 12 rats each group. Group 1: normal control, group 2 (AP- I): rats at 2 h after the induction of AP , and group 3 (AP- II): rats at 4 h after the induction of AP. Rats in each experimental group were killed to obtain blood by splenic vein puncture at 2 and 4 h after first caerulein injection.

Preparation of neutrophils

Rat polymorphonuclear cells (PMNs) were isolated according to the technique described by Hjorth *et al*.[24] for human PMNs. Blood was immediately mixed with heparin (50 U/mL) and centrifuged in a discontinuous Percoll gradient to yield a fraction of approximately 97% purity. Cell viability, as assessed by trypan blue exclusion, was above 96% under all experimental conditions.

Shear stress action on neutrophil suspension

Low-shear 30 viscometer (Switzerland) was used to provide low shear rate (5.96/s, 14.98/s, 51.2/s, 94.5/s and 128.5/s), then 37 g/L formaldehyde was added to fix neutrophils after sheared for 1 min.

Measurement of [Ca^{2+}]i

Cells were loaded (5×10^6/mL) with the Ca^{2+}-sensitive fluorescent dye fluo-3/AM (2 μmol/L; Molecular probes, Eugene OR) at 37 ℃ for 30 min in 145 mmol/L NaCl, 5 mmol/L KCl, 1 mmol/L $MgCl_2$, 10 mmol/L glucose, 4 mmol/L probenecid, 10 mmol/L HEPES, pH 7.4. Fluorescence intensity was then measured with flow cytometry. The intensity of fluorescence correlated with the concentration of [Ca^{2+}]i. Therefore, the mean fluorescence intensity (MFI) indicated the level of [Ca^{2+}]i.

Statistical analysis

The results were expressed as mean±SD. The mean of MRI between groups was compared by a two-tailed Student's *t* tests. $P\leqslant0.05$ was considered statistically significant.

RESULTS

Under steady shear, cytosolic [Ca^{2+}]i had biphasic changes. When the shear rate was very low, [Ca^{2+}]i decreased slightly. With the increase of shear rate, [Ca^{2+}]i increased gradually. When the shear rate was increased higher than 50/s, [Ca^{2+}]i in the experimental group was higher than that in the control group. With the shear rate changed from low to high, cytosolic [Ca^{2+}]i gradually increased to a significantly high level compared with the stationary control ($P<0.05$). After treated with a shear rate of 128.5/s, the cytosolic [Ca^{2+}]i of AP-II group was significantly induced compared with AP-I group ($P<0.05$) (Figure 1).

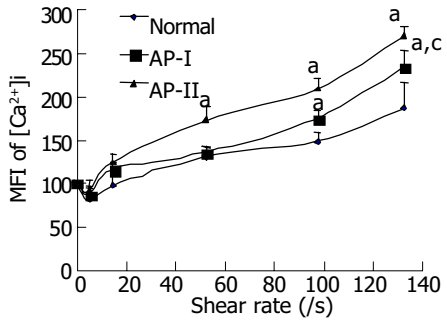

Figure 1 Effects of fluid shear stress on cytosolic [Ca^{2+}]i in neutrophils in pancreatic microcirculation of rats with AP. $^aP<0.05$ *vs* normal; $^cP<0.05$ *vs* AP- II.

DISCUSSION

Acute pancreatitis remains a clinical challenge because it is difficult to predict whether the disease is mild or runs a severe course with a possibly fatal outcome in a given patient[25]. In recent years, researches on the morphology of pancreatic microcirculation have revealed that the blood supply of pancreatic lobules in most cases is provided by a single intralobular arteriole[26]. This arteriole sends forth the tree-like branches when entering pancreatic lobule, and has no anastomosis with adjacent intralobular arterioles and their branches, and could be considered as an end-artery[26]. This characteristic suggested pancreatic lobules were susceptible to ischemic injury due to spasm of intralobular arterioles, embolization of arterioles, formation of microthrombi or compression by interstitial edema [1-3]. However, causative factors of early-stage ischemia and the precise triggering factors of local microcirculatory disturbance remain obscure[3].

Cellular calcium, a key physiological signaling element in cell function and also a crucial pathological intracellular messenger in cell injury, appears to be involved in the initiation and development of acute pancreatitis[7-12]. The present study provided several lines of evidence supporting this suggestion. We investigated whether calcium was involved in the priming response encountered during AP. We found that cytosolic [Ca^{2+}]i showed a biphasic changes when the neutrophil suspension was under a steady shear. When the shear rate changed from low to high, cytosolic [Ca^{2+}]i decreased slightly under a very low shear rate (5.96/s) and then increased gradually to a high level. From this study we could also infer that cytosolic [Ca^{2+}]i might be an identifying marker for AP.

Activation of neutrophils is one of the critical roles in pathologic process of AP, and cytosolic [Ca^{2+}]i has a close relation with neutrophil activation[27,28]. Our study demonstrated the fluid shear stress induced changes of cytosolic [Ca^{2+}]i in neutrophils in pancreatic microcirculation of rats with caerulein-induced AP. These lines of evidence indicate that altered intracellular calcium might play an important role in the initiation and development of AP. In conclusion, cellular calcium may be an important factor in the pathogenesis of cerulein-induced acute pancreatitis.

REFERENCES

1 **Vollmar B,** Menger MD. Microcirculatory dysfunction in acute pancreatitis. A new concept of pathogenesis involving vasomotion-associated arteriolar constriction and dilation. *Pancreatology* 2003; **3**: 181-190
2 **Chen HM,** Sunamura M, Shibuya K, Yamauchi JI, Sakai Y, Fukuyama S, Mikami Y, Takeda K, Matsuno S. Early microcirculatory derangement in mild and severe pancreatitis models in mice. *Surg Today* 2001; **31**: 634-642
3 **Menger MD,** Plusczyk T, Vollmar B. Microcirculatory derangements in acute pancreatitis. *J Hepatobiliary Pancreat Surg* 2001; **8**: 187-194
4 **Gomez-Cambronero LG,** Sabater L, Pereda J, Cassinello N, Camps B, Vina J, Sastre J. Role of cytokines and oxidative stress in the pathophysiology of acute pancreatitis: therapeutical implications. *Curr Drug Targets Inflamm Allergy* 2002; **1**: 393-403
5 **Frossard JL.** Pathophysiology of acute pancreatitis: a multistep disease. *Acta Gastroenterol Belg* 2003; **66**: 166-173
6 **Makhija R,** Kingsnorth AN. Cytokine storm in acute pancreatitis. *J Hepatobiliary Pancreat Surg* 2002; **9**: 401-410
7 **Weber CK,** Adler G. From acinar cell damage to systemic inflammatory response: current concepts in pancreatitis. *Pancreatology* 2001; **1**: 356-362
8 **Sutton R,** Criddle D, Raraty MG, Tepikin A, Neoptolemos JP, Petersen OH. Signal transduction, calcium and acute pancreatitis. *Pancreatology* 2003; **3**: 497-505
9 **Parekh AB.** Calcium signaling and acute pancreatitis: specific

response to a promiscuous messenger. *Proc Natl Acad Sci U S A* 2000; **97**: 12933-12934

10 **Raraty MG,** Petersen OH, Sutton R, Neoptolemos JP. Intracellular free ionized calcium in the pathogenesis of acute pancreatitis. *Baillieres Best Pract Res Clin Gastroenterol* 1999; **13**: 241-251

11 **Kruger B,** Albrecht E, Lerch MM. The role of intracellular calcium signaling in premature protease activation and the onset of pancreatitis. *Am J Pathol* 2000; **157**: 43-50

12 **Niederau C,** Luthen R, Klonowski-Stumpe H, Schreiber R, Soika I, Sata N, Bing H, Haussinger D. The role of calcium in pancreatitis. *Hepatogastroenterology* 1999; **46**: 2723-2730

13 **Acioli JM,** Isobe M, Kawasaki S. Early complement system activation and neutrophil priming in acute pancreatitis: participation of trypsin. *Surgery* 1997; **122**: 909-917

14 **Frossard JL,** Past CM. Experimental acute pancreatitis: new insights into the pathophysiology. *Front Biosci* 2002; **7**: d275-d287

15 **Bhatia M,** Moochhala S. Role of inflammatory mediators in the pathophysiology of acute respiratory distress syndrome. *J Pathol* 2004; **202**: 145-156

16 **de Dios I,** Perez M, de La Mano A, Sevillano S, Orfao A, Ramudo L, Manso MA. Contribution of circulating leukocytes to cytokine production in pancreatic duct obstruction-induced acute pancreatitis in rats. *Cytokine* 2002; **20**: 295-303

17 **Rau B,** Baumgart K, Kruger CM, Schilling M, Beger HG. CC-chemokine activation in acute pancreatitis: enhanced release of monocyte chemoattractant protein-1 in patients with local and systemic complications. *Intensive Care Med* 2003; **29**: 622-629

18 **Frossard JL,** Saluja AK, Mach N, Lee HS, Bhagat L, Hadenque A, Rubbia-Brandt L, Dranoff G, Steer ML. *In vivo* evidence for the role of GM-CSF as a mediator in acute pancreatitis-associated lung injury. *Am J Physiol Lung Cell Mol Physiol* 2002; **283**: L541-L548

19 **Bhatnagar A,** Wig JD, Majumdar S. Expression of activation, adhesion molecules and intracellular cytokines in acute pancreatitis. *Immunol Lett* 2001; **77**: 133-141

20 **Lundberg AH,** Granger N, Russell J, Callicutt S, Gaber LW, Kotb M, Sabek O, Gaber AO. Temporal correlation of tumor necrosis factor-alpha release, upregulation of pulmonary ICAM-1 and VCAM-1, neutrophil sequestration, and lung injury in diet-induced pancreatitis. *J Gastrointest Surg* 2000; **4**: 248-257

21 **Berney T,** Gasche Y, Robert J, Jenny A, Mensi N, Grau G, Vermeulen B, Morel P. Serum profiles of interleukin-6, interleukin-8, and interleukin-10 in patients with severe and mild acute pancreatitis. *Pancreas* 1999; **18**: 371-377

22 **Kantor AB,** Stall AM, Adams S, Watanabe K, Herzenberg LA. De novo development and self-replenishment of B cells. *Int Immunol* 1995; **7**: 55-68

23 **Suratt BT,** Young SK, Lieber J, Nick JA, Henson PM, Worthen GS. Neutrophil maturation and activation determine anatomic site of clearance from circulation. *Am J Physiol Lung Cell Mol Physiol* 2001; **281**: L913-L921

24 **Hjorth R,** Jonsson AK, Vretblad P. A rapid method for purification of human granulocytes using percoll. A comparison with dextran sedimentation. *J Immunol Methods* 1981; **43**: 95-101

25 **Beger HG,** Rau B, Isenmann R. Prevention of severe change in acute pancreatitis: prediction and prevention. *J Hepatobiliary Pancreat Surg* 2001; **8**: 140-147

26 **Zhou ZG,** Gao XH. Morphology of pancreatic microcirculation in the monkey: light and scanning electron microscopic study. *Clin Anat* 1995; **8**: 190-201

27 **Petty HR.** Neutrophil oscillations: temporal and spatiotemporal aspects of cell behavior. *Immunol Res* 2001; **23**: 85-94

28 **Davies EV,** Hallett MB. Cytosolic Ca2+ signalling in inflammatory neutrophils: implications for rheumatoid arthritis (Review). *Int J Mol Med* 1998; **1**: 485-490

Edited by Kumar M and Wang XL **Proofread by** Xu FM

PO Box 2345, Beijing 100023, China
Fax: +86-10-85381893
E-mail: wjg@wjgnet.com www.wjgnet.com

World J Gastroenterol 2004;10(21):3188-3190
World Journal of Gastroenterology
 ISSN 1007-9327

• BRIEF REPORTS •

Expression of human augmenter of liver regeneration in pichia pastoris yeast and its bioactivity *in vitro*

Qi Liu, Hui-Feng Yu, Hang Sun, Hua-Feng Ma

Qi Liu, Hui-Feng Yu, Hang Sun, Hua-Feng Ma, Institute for Viral Hepatitis, Chongqing University of Medical Sciences, Chongqing 400010, China
Supported by Excellent Youth Teacher Fund, Ministry of Education, No. 200065
Correspondence to: Professor Liu Qi, Institute for Viral Hepatitis, Chongqing University of Medical Science, Chongqing 400010, China. liuqiz@hotmail.com
Telephone: +86-23-63825854 Ext. 2225
Received: 2004-01-09 **Accepted:** 2004-02-26

Abstract

AIM: To construct a yeast expression system of human augmenter of liver regeneration (hALR) and to examine its bioactivity *in vitro*.

METHODS: With PCR and gene recombination techniques, cDNA of open reading frame of hALR was obtained from recombinant plasmid pcDNA3.1-hALR and inserted into plasmid pPIC9. The cDNA of hALR from recombinant plasmid pPIC9-hALR demonstrated by sequencing was subcloned into plasmid pPIC9K. The recombinant plasmid pPIC9K-hALR was transformed into GS115 with electroporation. hALR was expressed by GS115 under the induction of 5 mL/L methanol and purified with ultrafiltration after it was analyzed by 15% SDS-PAGE and Western blot. The effects of hALR on *in vitro* proliferation of QGY and $HepG_2$ cells were evaluated by ^{3}H-TdR methods.

RESULTS: The correctness and integrity of recombinant plasmids pPIC9-hALR and pPIC9K-hALR were identified by restriction digestion, PCR and sequencing methods, respectively. hALR as a secretive protein was successfully expressed by GS115. Its molecular weight was about 15 ku and the target protein was about 60% of the total protein in the supernatant from GS115 with plasmid pPIC9K-hALR. The results of Western blot of hALR showed the specific band. The high qualitative hALR was obtained through ultrafiltration. hALR could stimulate *in vitro* proliferation of QGY and $HepG_2$ cells in a dose-dependent manner, but there was a difference in reactivity to hALR between QGY and $HepG_2$.

CONCLUSION: The hALR as a secretive protein can be successfully expressed by GS115. It may stimulate *in vitro* proliferation of QGY and $HepG_2$ cells at a dose-dependent manner. But QGY and $HepG_2$ cells have different reactivities to hALR.

Liu Q, Yu HF, Sun H, Ma HF. Expression of human augmenter of liver regeneration in pichia pastoris yeast and its bioactivity *in vitro*. *World J Gastroenterol* 2004; 10(21): 3188-3190
http://www.wjgnet.com/1007-9327/10/3188.asp

INTRODUCTION

Augmenter of liver regeneration (ALR) is an important cytokine recently discovered and cloned from rat livers[1,2]. It could stimulate DNA synthesis of liver cancer cells *in vitro* and enhance liver regeneration in rats after partial hepatectomy, but there is a debate whether it could directly stimulate DNA synthesis of hepatocytes *in vitro*[1,3]. It has also been proved that ALR could partially reverse the liver fibrosis in experimental rats[4] and enhance the success rate of fetal pancreas transplantation in rats[5]. It seems to bring a bright future in the treatment of severe liver diseases. Although the recombinant human and rat ALR were successfully expressed in *E.coli* in our laboratory[6-8], there are some defects that the target protein as an inclusion body expressed in *E.coli* could not often be refolded and modified correctly and that the procedure to purify ALR is very complicated. Because the pichia pastoris expressing system could overcome all these defects, it was selected to express ALR, which could be secreted into supernatants so that it was easy to purify ALR. It is possible for us to carry out further study with purified ALR.

MATERIALS AND METHODS

Reagents, plasmid, bacteria and cell strain

Escherichia coli JM109 and TOP10F', plasmid pcDNA3.1-hALR, hepatocarcinoma HepG2 and QGY strains were preserved and monoclonal antibody against hALR was made in our laboratory[9]. *Pitch pastoris* GS115, plasmids pPIC9 and pPIC9K were from Invitrogen Corporation, USA. DNA ladder marker, restriction endonuclease, and T4 DNA ligase were from Shanghai Sango, China. Peptone and YNB were from Amresco Co. USA. Yeast power was from Oxoid. 8200 cell filter, 5 kD and 30 kD membranes were from Millipore Co. USA. Gene pulser-II was from Bio-Rad Co. Ltd., USA.

Preparation of hALR gene

According to the maps of plasmids pcDNA3.1-hALR, pPIC9 and pPIC9K, the sequences of primers were designed as follows: forward: $P_1$5'-CACTCGAGAAAAGACGGACCCAGCAGAAGC-3'. reverse: $P_2$5'-CTGCGGCCGCTTAGTCACAGGAGCCGTCCTTCC-3'. *Xho*I and *Not*I restriction sites were introduced and defined by the underline. Primers were synthesized by BoYa Co. Ltd. hALR sequence was amplified by polymerase chain reaction (PCR) for 30 cycles from pcDNA3.1-hALR containing the full-length open reading frame of hALR gene. Each cycle consisted of denaturation for 45 s at 94 ℃, annealing for 45 s at 62 ℃, and extension for 1 min at 72 ℃. The PCR products were analyzed on 15 g/L agarose gel electrophoresis as specific band examination.

pPIC9-hALR and pPIC9K-hALR construction and identification

The PCR products of hALR from the gel extraction and pPIC9 were digested with *Xho* I and *Not* I and then purified, respectively. pPIC9 and hALR fragments were mixed with 3:1 mol/L and ligated by T4 DNA ligase overnight at 16 ℃, then transformed into JM109 with $CaCl_2$ method. The positive clones were selected in LB plates with ampenicillin and identified by PCR, restriction enzyme digestion and sequencing, respectively. After the correction and integrity of recombinant pPIC9-hALR were

proved, pPIC9-hALR and pPIC9K were digested with *Sal*I and *Sac*I. A 3.4 kb fragment containing hALR was obtained from pPIC9-hALR and 6.3 kb fragment from pPIC9K. Both fragments were mixed with 2:1 mol/L, ligated by T4 DNA ligase and transformed into TOP10F' with $CaCl_2$ method. The positive clones were selected in LB plates with ampenicillin and karamycin and the plamids from them were identified by PCR and restriction enzyme digestion on the next day.

Transformation and expression

Recombinant plasmids pPIC9K-hALR (8 μL) and pPIC9K (8 μL) were linearized, respectively, by digestion with *Sal*I. Competent *pitch pastoris* GS115 was prepared according to the manual of Invitrogen Corporation. The linear palsmids pPIC9K (5-10 μg) and pPIC9K-hALR (5-10 μg) were mixed with competent GS115 (80 μL), respectively. Under the conditions of 1500V, 25 μF and 200 Ω, the competent GS115 was transformed by different mixtures using the Bio-Rad gene pulser, then planted and cultured in plates of minimal dextrose medium without histidine at 30 ℃ for 2 d for screening positive clones. The positive clones with pPIC9K-hALRp or PIC9K were respectively cultured in 3 mL buffered glycerol-complex medium (BMGY) overnight after identified by PCR. Then 15 μL of GS115 was planted into 5 mL BMGY medium and cultured at 28 ℃ until the optical density at 600 nm (A_{600}) reached four. The GS115 with pPIC9K-hALRp and PIC9K were collected by centrifugation, resuspended by buffered methanol-comlex medium to A_{600} reaching one and cultured continuously at 28 ℃ for 3 d. The 5 mL/L methanol in the medium was kept by methanol compensation at every 24 h. The expressed products at the different time points were analysed by 160 g/L SDS-PAGE and the expressed level was evaluated by computer scan.

Western blot analysis

Supernatants from GS115 with pPIC9K and pPIC9K-hALR were respectively loaded on 150 g/L SDS-PAGE for protein separation and transferred to polyvinylidene difluoride membrane by electrotransfer. After blocked with 50 mL/L milk in PBS, the membrane was incubated with monoclonal antibody (diluted 1:2 000) against hALR for 1 h at room temperature, washed three times with phosphate buffered saline, then mixed with goat anti-mouse IgG antibody coupled with horseradish peroxidase for 45 min, the bands were visualized by 3-3'-diaminobenzidine (DAB).

Purification and quantification

The ultrafiltration purification was selected according to the SDS-PAGE analysis of the supernatant from GS115 with pPIC9K-hALR there were no other bands except target one under 50 kD. The supernatant from GS115 induced by pPIC9K-hALR was centrifuged at 3 000 r/min for 10 min, and passed through 30 kD and 5 kD membranes and the filtrate between 30 kD and 5 kD was collected. As a control the supernatant from GS115 with pPIC9K was treated with same procedure as described above. The purified products were analyzed by 160 g/L SDS-PAGE and qualified by Lowary methods.

hALR bioactivity

Human hepatoma cell lines $HepG_2$ and QGY were planted at a concentration of 1×10^4cell/well in 96-well plates supplemented with 80 mL/L fetal bovine serum, 5×10^{-5} mol/L penicillin, 80 μg/mL streptomycin, and stimulated with different doses of hALR expressed by yeast and *E.coli* at 37 ℃, 50 mL/L CO_2 for 8-9 h. The supernatant from GS115 with pPIC9k as negative control was also added. Three parallel wells were stimulated by the same concentration of hALR. The cells were harvested after 12 h of culture by adding 1 μCi /well ^{3}H-TdR. The count per minute (cpm) value of cells from each well was measured by liquid scintillation counter.

Statistical analysis

The data were expressed as mean±SD. Comparison was carried out using analysis of variance. *P* value less than 0.05 was considered statistically significant.

RESULTS

PCR result and identification of recombinant plasmid

The specific 400 bp fragment of hALR amplified by PCR from plasmid pcDNA3.1-hALR was analysed by 15 g/L agarose gel electrophoresis. The correctness and integrity of hALR fragments in recombinant plasmid pPIC9-hALR were proved by *Xho*I+ *Not*I digestion and sequencing. The 3.4 kb fragment containing hALR was released from pPIC9K-hALR by digestion with *sal*I and *sac*I. The 400 bp fragment was also obtained from pPIC9K-hALR by PCR (Figure 1).

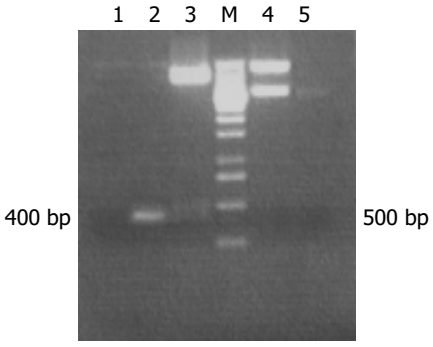

Figure 1 Identifications of recombination plasmid. Lane 1: amplified from pPIC9K; Lane 2: amplified from pPIC9K-hALR; Lane 3: pPIC9-hALR digested by *Xho*I+*Not*I; Lane M: 1 kb DNA ladder; Lane 4: pPIC9K-hALR digested by *Sac*I+*Sal*I (6.3 kb+3.4 kb); Lane 5: 3.4 kb fragment with hALR.

Expression and purification of hALR

Electrophoresis of supernatants from GS115 induced by pPIC9K-hALR showed that there was a specific band with 1.5×10^4 dalton molecular weight coinciding with the theoretical value and the target protein was about 60% of the total protein in the supernatant. There was no corresponding band in supernatant from GS115 transfected with pPIC9K. A single band of hALR was obtained through ultrafiltration purification (Figure 2).

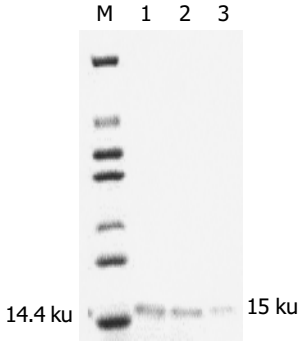

Figure 2 SDS-PAGE analysis of purified hALR. Lane M: protein marker; Lanes 1, 2, and 3: purified hALR.

Detection of protein exprcssion by Western blot

Western blot result showed that the supernatant from GS115 with pPIC9K-hALR could specially bind to monoclonal antibody against hALR in 15 kD site, but the supernatant from GS115 with pPIC9K could not bind (Figure 3).

Table 1 Effect of different dosages of hALR on $HepG_2$ and QGY proliferation (mean±SD)

Cells	Control		Concentrations of hALR from yeast and *E.coli*				
			0.1 ng	10 ng	1 μg	8 μg	16 μg
$HepG_2$	7 174±494	yeast	1 3779±1 431[a]	13 679±1 205[a]	15 279±1 802[a]	22 670±1 402[bc]	24 958±1 326[bc]
		E.coli	1 0754±2 756[a]	11 189±1 447[a]	12 997±1 683[a]	13 858±440[a]	14 411±1 452[a]
QGY	821±11	yeast	2 549±526[bc]	2 298±203[bc]	3 188±564[bc]	11 825±841[bc]	17 021±795[bc]
		E.coli	934±50[a]	883±106	1 222±168[a]	1 362±171[a]	6 209±225[b]

[a]$P<0.05$, [b]$P<0.01$ *vs* control; [c]$P<0.05$ *vs* hALR from *E.coli*.

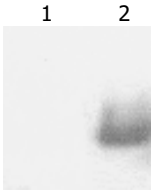

Figure 3 Western blot analysis of supernatants from GS115 treated with different plasmids. Lane 1: supernatant from GS115 with pPIC9K; Lane 2: supernatant from GS115 with pPIC9K- hALR.

Evaluation of hALR bioactivity

Results showed that hALR from GS115 with pPIC9K-hALR could stimulate the proliferation of $HepG_2$ and QGY on nanogram level in a dose-dependent manner. There was a marked difference in the reactivity to hALR between QGY and $HepG_2$ although both cells were from human liver cancer. In addition, hALR from yeast had stronger effect on the proliferation of $HepG_2$ and QGY than that from *E.coli* at same concentration (Table 1).

DISCUSSION

The Pichia pastoris system has been widely used in recent years due to its simple procedure, low expenditure and easy scaling up. It is more important that the foreign protein can be correctly refolded and modified, more than 200 proteins have been expressed by this system[10]. Our results showed that hALR with 1.5×10^4 dalton molecular weight as a secretive protein was successfully expressed by GS115 and about 60% of total protein was expressed in the supernatant. The ultrafiltration purification for hALR in the supernatant was applied because there were no other bands around the target protein, and a satisfactory purification effect was achieved. Our results demonstrated that not only the purification efficiency was greatly enhanced, but also the purification procedure was obviously simplified. Although it was reported that rat ALR could not directly stimulate liver cancer cells *in vitro*[1], our data demonstrated that hALR could stimulate QGY and $HepG_2$ proliferation in a dose-dependent manner. Previously, we and others also obtained the similar results in rat ALR researches[11,12]. These results suggested that ALR enhanced liver regeneration not only through indirect pathway i.e. immune regulation[1,13-16], but also through direct one. Our result showed that at the same concentration, hALR expressed in yeast had a stronger effect on the proliferation of $HepG_2$ and QGY than that expressed in *E.coli*, although it was reported that there was no N-glycosylation site in its amino acid sequence[1]. Our result suggests that there might exist some unknown modifications such as O-glycosylation site in hALR molecules expressed by yeast, and modification of protein after translation is very important for keeping higher bioactivity of target protein. Hence, the successful expression of ALR in pichia postoris and its purification may provide a good tool for further research in this field.

REFERENCES

1 **Hagiya M**, Francavilla A, Polimeno L, Ihara I, Sakai H, Seki T, Shimonishi M, Porter KA, Starzl TE. Cloning and sequence analysis of the rat augmenter of liver regeneration (ALR) gene: expression of biologically active recombinant ALR and demonstration of tissue distribution. *Proc Natl Acad Sci U S A* 1994; **91**: 8142-8146

2 **Hagiya M**, Francavilla A, Polimeno L, Ihara I, Sakai H, Seki T, Shimonishi M, Porter KA, Starzl TE. Cloning and sequence analysis of the rat augmenter of liver regeneration (ALR) gene: expression of biologically active recombinant ALR and demonstration of tissue distribution. *Proc Natl Acad Sci U S A* 1995; **92**: 3076

3 **Yang XM**, Xie L, Qiu ZH, Gong F, Wu ZZ, He FC. cDNA clone, expression and biological activity study of augmenter of liver regeneration. *Shengwu Huaxue Zazhi* 1997; **13**: 130-135

4 **Wang AM**, Yang XM, Guo RF, Zhang L, Li PJ, Wang QM, He FC. The recombinant agumenter of liver regeneration reverse fibrosis in experimental rat. *Zhonghua Ganzangbing Zazhi* 1999; **7**: 243

5 **Adams GA**, Maestri M, Squiers EC, Alfrey EJ, Starzl TE, Dafoe DC. Augmenter of liver regeneration enhances the success rate of fetal pancreas transplantation in rodents. *Transplantation* 1998; **65**: 32-36

6 **Liu Q,** Wang Z, Luo Y. The cDNA clone and sequence analysis of the coding region of human augmenter of liver regeneration (hALR) gene. *Zhonghua Ganzangbing Zazhi* 1999; **7**: 156-158

7 **Liu Q**, Shi XF, Luo Y, Zhang DF. Construction of prokaryotic expression vector of hALR and its expression in *E.coli. Zhonghua Ganzangbing Zazhi* 2000; **8**: 9-11

8 **Ma HF**, Liu Q. The cDNA clone of the coding region of rat augmenter of liver regeneration gene and its prokaryotic expression. *Chongqing Yikedaxue Xuebao* 2002; **27**: 9-11

9 **Ma HF**, Liu Q. Preparation of monoclonal antibody to human augmenter of liver regeneration: screening of hybridomas with unpurified antigen expressed by *E.coli. Zhongguo Mianyixue Zazhi* 2002; **18**: 671-673

10 **Cregg JM,** Cereghino JL, Shi J, Higgins DR. Recombinant protein expression in Pichia pastoris. *Mol Biotechnol* 2000; **16**: 23-53

11 **Yu HF**, Liu Q. Expression of rat augmenter of liver regeneration in pichia pastoris and evaluation of its bioactivity *in vitro*. *Zhonghua Ganzangbing Zazhi* 2003; **11**: 421-423

12 **Yang XM**, Hu ZY, Xie L, Wu ZZ, Wu CT, He FC. *In vitro* stimulation of HTC hepatoma cell growth by recombinant human augmenter of liver regeneration (ALR). *Shengli Xuebao* 1997; **49**: 557-561

13 **Francavilla A,** Vujanovic NL, Polimeno L, Azzarone A, Iacobellis A, Deleo A, Hagiya M, Whiteside TL, Starzl TE. The *in vivo* effect of hepatotrophic factors augmenter of liver regeneration, hepatocyte growth factor, and insulin-like growth factor-II on liver natural killer cell functions. *Hepatology* 1997; **25**: 411-415

14 **Gandhi CR**, Kuddus R, Subbotin VM, Prelich J, Murase N, Rao AS, Nalesnik MA, Watkins SC, DeLeo A, Trucco M, Starzl TE. A fresh look at augmenter of liver regeneration in rats. *Hepatology* 1999; **29**: 1435-1445

15 **Polimeno L**, Margiotta M, Marangi L, Lisowsky T, Azzarone A, Ierardi E, Frassanito MA, Francavilla R, Francavilla A. Molecular mechanisms of augmenter of liver regeneration as immunoregulator: its effect on interferon-gamma expression in rat liver. *Dig Liver Dis* 2000; **32**: 217-225

16 **Tanigawa K**, Sakaida I, Masuhara M, Hagiya M, Okita K. Augmenter of liver regeneration (ALR) may promote liver regeneration by reducing natural killer (NK) cell activity in human liver diseases. *J Gastroenterol* 2000; **35**: 112-119

Edited by Kumar M and Wang XL **Proofread by** Xu FM

PO Box 2345, Beijing 100023, China
Fax: +86-10-85381893
E-mail: wjg@wjgnet.com www.wjgnet.com

World J Gastroenterol 2004;10(21):3191-3193
World Journal of Gastroenterology
 ISSN 1007-9327

• BRIEF REPORTS •

Photocatalytic killing effect of TiO_2 nanoparticles on Ls-174-t human colon carcinoma cells

Ai-Ping Zhang, Yan-Ping Sun

Ai-Ping Zhang, Yan-Ping Sun, Chemical Engineering Department, Taiyuan University of Technology, Taiyuan 030024, Shanxi Province, China
Supported by the National Natural Science Foundation of China, No. 29776032 and the Natural Science Foundation of Shanxi Province, No.971013
Correspondence to: Yan-Ping Sun, Chemical Engineering Department, Taiyuan University of Technology, Taiyuan 030024, Shanxi Province, China. ypsun@tyut.edu.cn
Telephone: +86-351-6010070
Received: 2003-10-10 **Accepted:** 2003-12-29

Abstract

AIM: To investigate the photocatalytic killing effect of photoexcited TiO_2 nanoparticles on human colon carcinoma cell line (Ls-174-t) and to study the mechanism underlying the action of photoexcited TiO_2 nanoparticles on malignant cells.

METHODS: Ls-174-t human colon carcinoma cells were cultured in RPMI 1640 medium supplemented with 199 mL/L calf serum in a humidified incubator with an atmosphere of 50 mL/L CO_2 at 37 ℃. Viable cells in the samples were measured by using the MTT method. A GGZ-300 W high pressure Hg lamp with a maximum ultraviolet-A (UVA, 320-400 nm) irradiation peak at 365 nm was used as light source in the photocatalytic killing test.

RESULTS: The photocatalytic killing of Ls-174-t cells was carried out *in vitro* with TiO_2 nanoparticles. The killing effect was weak by using UVA irradiation without TiO_2 nanoparticles. In our studies, the photocatalytic killing effect was correlated with the concentration of TiO_2 and illumination time. Once TiO_2 was added, Ls-174-t cells were killed at a much higher rate. In the presence of 1 000 μg/mL TiO_2, 44% of cells were killed after 10 min of UVA irradiation, and 88% of cells were killed after 30 min of UVA irradiation.

CONCLUSION: When the concentration of TiO_2 is below 200 μg/mL, the photocatalytic killing effect on human colon carcinoma cells is almost the same as that of UVA irradiation alone. When the concentration of TiO_2 is above 200 μg/mL, the remarkable killing effect of photoexcited TiO_2 nanoparticles can be found.

Zhang AP, Sun YP. Photocatalytic killing effect of TiO_2 nanoparticles on Ls-174-t human colon carcinoma cells. *World J Gastroenterol* 2004; 10(21): 3191-3193
http://www.wjgnet.com/1007-9327/10/3191.asp

INTRODUCTION

The application of TiO_2 photocatalysis has received increasing attention since the first report of microbiocidal effects by Matsunaga *et al*. in 1985[1]. In recent years, in contrast to many studies using TiO_2 powder for photodecomposition of organic pollutants[2-9], few studies have investigated the application of TiO_2 in life science, especially in the field of cancer treatment[10-12]. The incidence of colon cancer is rising in China. Despite that surgical operation is used currently, people have recognized its limitation. The way to treat cancer usually includes radiation therapy and chemical therapy, which may generate severe side effects in human body. Therefore, this study tried to investigate a new therapy for cancer. Ls-174-t cells were used as experiment objects in this study. The photocatalytic killing effect of TiO_2 nanoparticles on malignant cells and its killing mechanism were investigated.

MATERIALS AND METHODS

Reagent preparation

TiO_2 colloid solutions were prepared[13,14] by hydrolysis of titanium isopropoxide, $Ti[OCH(CH_3)_2]_4$ (97%, Aldrich Chemical Co). In brief, 12.5 mL of $Ti[OCH(CH_3)_2]_4$ was added to 2 mL isopropanol, then the mixture was added to 150 mL of distilled deionized water containing 2 mL of 700 mL/L nitric acid and vigorously stirred for 6 h at 75 ℃. Approximately 150 mL of TiO_2 colloid solution being stable for several months at 4 ℃ was obtained after the organic layer was removed. The average diameter determined by Zetasizer $3000HS_A$ (USA) was 21.2 nm.

The pH value of TiO_2 colloid solutions used in the subsequent experiment had to be adjusted from 1.8 to 5.5-6.5 in order not to damage the normal growth of cells. Therefore, 1 mol/L NaOH aqueous solution and 1.5 mL/L polyvinyl alcohol were added to the colloid solutions before the pH adjustment to prevent the TiO_2 from precipitation. The final TiO_2 colloid solutions were sterilized by autoclaving and then diluted to the required concentration. Other chemical reagents used were all of analytical purity from commercial sources.

Cell culture and treatment

Human colon carcinoma cell lines Ls-174-t were purchased from Shanghai Institute of Cell Biology, Chinese Academy of Sciences, Shanghai, China. The cell lines were cultured in RPMI 1640 (Gibco) medium supplemented with calf serum 100 ml/L, penicillin (100×10^3 μ/L) and streptomycin (100 mg/L). pH was maintained at 7.2-7.4 by equilibration with 50 mL/L CO_2. Temperature was maintained at 37 ℃. Cells were sub-cultured with a mixture of ethylenedinitrile tetraacetic acid (EDTA) and trypsin. All experiments were performed using cells during the exponential growth phase. Cell concentration was determined by using a hemocytometer and the cell density was adjusted to the required final concentration.

Ls-174-t cells were treated with TiO_2 diluted in RPMI 1640 medium for 2 h at 37 ℃. Then the solutions were irradiated with a GGZ-300W high pressure Hg lamp (E_{max} = 365 nm) at room temperature. A UV pass filter was used to obtain a light wavelength between 300-400 nm. The light intensity at the liquid surface was measured by a VLX-3W radiometer-photometer (USA). The incident light intensity was 3.7 mW/cm^2. In our study, three groups of tests were carried out. One group was treated in the absence of TiO_2. Another group was treated in the absence of UVA. The third group was treated with different TiO_2 concentrations and irradiated by UVA.

Measurement of the viability of Ls-174-t cells

Viable cells in the samples were measured by using the MTT staining method[15]. MTT [3- (4, 5-dimethylthiazol-2-yl) -2, 5-diphenyl tetrazolium bromide] was dissolved in phosphate-buffered saline (PBS, pH 7.4) at 5 mg/mL and filtered to be sterilized. Twenty microliters of stock MTT solution were added to all wells for an assay, and plates were incubated at 37 ℃ for 4 h. One hundred and fifty microliters of DMSO were added to all wells and mixed thoroughly to dissolve the blue-violet crystals. After a few minutes at room temperature to ensure that all crystals were dissolved, the plates were read on a Bio-Rad Novapath^{tm} microplate reader (Japan), using a test wavelength of 595 nm, taking the solution without MTT as control. Then optical absorptions [A] were obtained. Plates were normally read within 1 h after DMSO was added. The survival rate could be calculated according to $[A]_t/[A]_i$, where $[A]_i$ is the optical absorption of untreated cells.

RESULTS

Determination of the average diameter of TiO_2 particles

Zetasizer 3000HSA (USA) was used to determine the average diameter of TiO_2 nanoparticles. The result is shown in Figure 1. The average volume size of TiO_2 nanoparticles was 21.2 nm.

Cytotoxicity of TiO_2 nanoparticles

The cytotoxicity of TiO_2 nanoparticles (without UVA irradiation) was determined by exposing cells to various concentrations of TiO_2 in RPMI 1640 (Gibco) medium for 24 h. The surviving fraction of the cells was greater than 90% when the concentration of TiO_2 was in the range of 1 000 μg/mL, as shown in Figure 2. The result confirmed that nonirradiated TiO_2 nanoparticles were not toxic to the Ls-174-t cells. It was consistent with those in literatures[16-17].

Effect of photoexcited TiO_2 nanoparticles on Ls-174-t cells

The fact that the surviving fraction was greater than 90% after 30 min as shown in Figure 3 (A) indicated that TiO_2 nanoparticles without UVA irradiation showed little toxicity to living cells. The killing effect of UVA without TiO_2 is shown in (B) with the surviving fraction of Ls-174-t cells given as a function of the UVA light irradiation time. About 20% cells were killed after 30 min exposure, whereas after 20 min exposure, more than 90% of the cells survived. Once TiO_2 was added, the Ls-174-t cells were killed at a much higher rate as shown in (C). For example, in the presence of 1 000 μg/mL of TiO_2, 44% of the cells were killed after 10 min of UVA irradiation, and after 30 min irradiation, 80 % of the cells were killed. Therefore it was concluded that photoexcited TiO_2 nanoparticles had an active killing effect on Ls-174-cells.

Effect of TiO_2 concentration on Ls-174-t cells activity

The effect of the TiO_2 concentration ranging from 200 to 1 000 μg/mL on the rate of cell killing by UVA light is shown in Figure 4. The light intensity was 3.7 mW/cm^2 and kept constant. The experimental results demonstrated that cell viability decreased monotonically as TiO_2 concentration increased and cell viability decreased with time.

Although a higher concentration of TiO_2 could achieve a higher reaction rate, the difficulties in separation and measurement had to be considered. So the effect of a higher TiO_2 concentration (C>1 029 μg/mL) on Ls-174-t cell activity was not investigated. The concentration of TiO_2 was set at <1 029 μg/mL with which the dark cytotoxicity was considered to be negligible. The range of TiO_2 concentrations was close to that used previously[18].

Morphological changes of Ls-174-t cells

Untreated and TiO_2-treated cells were collected by centrifugation and resuspended in RPMI 1640 medium. The samples were pipetted into a 24-well plate, which was directly observed with an inverted phase-contrast microscope. When treated by photoexcited TiO_2, the cellular shape was condensed and nuclei were dispersed in fragments.

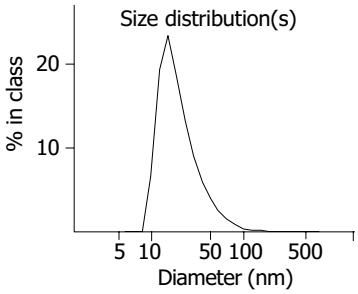

Figure 1 Volume size distribution of TiO_2.

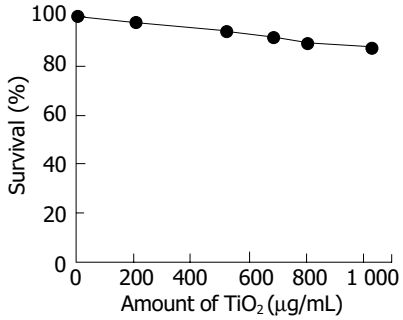

Figure 2 After Ls-174-t cells were incubated in RPMI 1640 medium for 24 h without irradiation, the survival of Ls-174-t cells was shown.

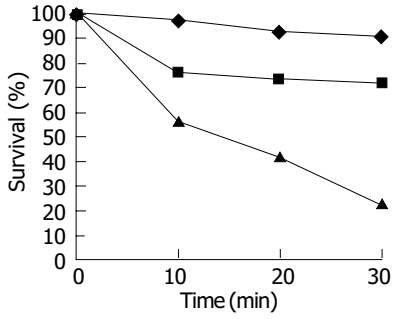

Figure 3 Effect of light and TiO_2 on viability of Ls-174-t cells. (A) TiO_2 (1 000 μg / mL) in the dark; (B) no TiO_2 in the light; (C) TiO_2 (1 000 μg / mL) in the light. Initial cell concentration: 5×10^5 cell / mL, light intensity: 3.7 mW / cm^2.

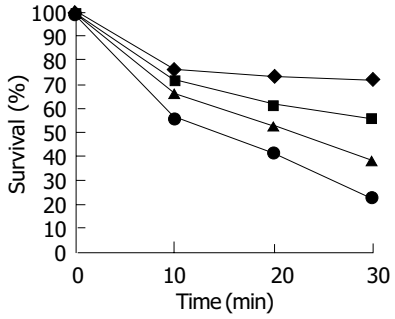

Figure 4 Influence of TiO_2 concentration on Ls-174-t cells activity. (A) 204 μg / mL, (B) 524 μg / mL, (C) 804 μg / mL, (D) 1 029 μg / mL.

DISCUSSION

In this experiment, the TiO_2 nanoparticle system was used, displaying its superiority. TiO_2 nanoparticles were easy to attach

to the cellular membranes and accumulate. They were also easy to enter into the cytoplasm via phagocytosis[19]. It could lead to accumulation of ROS on the surface of cell membranes and in the cytoplasm. Hence under light irradiation, TiO_2 nanoparticles had more significant cell killing effect *in vitro*.

Human colon carcinoma cells treated with photoexcited TiO_2 nanoparticles (C>200 μg/mL) were effectively damaged, with cells contracted and a lot of cell fragments simultaneously observed by an inverted phase-contrast microscope[18].According to these characteristics, we assumed that the mechanism of photoexcited TiO_2 in killing human colon carcinoma cells might be through a series of oxidized chain reactions and in inducing cell death by reactive oxygen species[20-25]. Human colon carcinoma cell damages occurred in two stages. The initial oxidative damage took place on the cell membranes, where the TiO_2 photocatalytic surface had its first contact with intact cells, the membranes became somewhat permeable. At this stage the cells did not lose their viability. Photocatalytic action made the cell membranes permeable, intracellular components began to leak from the cells and free TiO_2 nanoparticles might also diffuse into the damaged cells and directly attack intracellular components, eventually leading to cell death. It is different from the bactericidal effect of TiO_2 photocatalytic reaction. Bacteria are simple prokaryotic cells that do not contain the nucleus characteristics of eukaryotic cells. Whereas human colon carcinoma cells are eukaryotic cells and their structure is complex. Based on their structural differences, we assumed that killing cancer cells might be more difficult than killing bacteria by the photocatalytic reaction of TiO_2 nanoparticles.

In the present study, cultured human colon carcinoma cells were effectively killed by photoexcited TiO_2 nanoparticles *in virto*. The concentration of TiO_2 affected the photocatalytic killing effect. When the concentration of TiO_2 was below 200 μg/mL, there was only a slight decrease in survival ratio after UVA irradiation for more than 30 min. It was almost the same as that of UVA irradiation alone. It indicated that minor cell membrane leakage might occur and the cell viability was not lost. When the concentration of TiO_2 was above 200 μg/mL, the survival ratio decreased rapidly with increasing TiO_2 concentration. It indicated that major rupture of cell membranes and decomposition of essential intracellular components might take place, thus accelerating cell death. It verified the mechanism of TiO_2 nanoparticles in killing human colon carcinoma cells.

The photocatalytic killing effect of TiO_2 nanoparticles on human colon carcinoma cells suggested the idea of cancer treatment using TiO_2 nanoparticles and light irradiation. Under these conditions, it could be adapted to an anticancer modality by the local or regional treatment of the tumor with TiO_2 nanoparticles, followed by light irradiation focusing on the tumor. Although UVA light (320-400 nm) cannot penetrate the human body deeply, it may be possible that the modality will be applied to several human tumors in the future.

REFERENCES

1 **Matsunaga T,** Tomoda R, Nakajima T, Wake H. Photoelectrochemical sterilization of microbial cells by semiconductor powders. *FEMS Microbiol Lett* 1985; **29**: 211-214

2 **Byrne JA,** Eggins BR, Brown NMD, Mckinney B, Rouse M. Immobilisation of TiO_2 powder for the treatment of polluted water. *Appl Catal B Environ* 1998; **17**: 25-36

3 **Wang KH,** Hsieh YH, Ko RC, Chang CY. Photocatalytic degradation of wastewater from manufactured fiber by titanium dioxide suspensions in aqueous solution. *Environ Int* 1999; **25**: 671-676

4 **Byrne JA,** Eggins BR, Byers W, Brown NMD. Photoelectrochemical cell for the combined photocatalytic oxidation of organic pollutants and the recovery of metals from waste waters. *Appl Catal B Environ* 1999; **2**: L85-L89

5 **Horikoshi S,** Satou Y, Hidaka H, Serpone N. Enhanced photocurrent generation and photooxidation of benzene sulfonate in a continuous flow reactor using hybrid TiO_2 thin films immobilized on OTE electrodes. *J Photochem Photobiol A* 2001; **146**: 109-119

6 **Molinari R,** Grande C, Drioli E, Palmisano L, Schiavello M. Photocatalytic membrane reactors for degradation of organic pollutants in water. *Catal Today* 2001; **67**: 273-279

7 **Shephard GS,** Stockenstrom S, de Villiers D, Engelbrecht WJ, Wessels GE. Degradation of microcystin toxins in a falling film photocatalytic reactor with immobilized titanium dioxide catalyst. *Water Res* 2002; **36**: 140-146

8 **Muneer M,** Singh HK, Bahnemann D. Semiconductor-mediated photocatalysed degradation of two selected priority organic pollutants, benzidine and 1, 2-diphenylhydrazine, in aqueous suspension. *Chemosphere* 2002; **49**: 193-203

9 **Alhakimi G,** Studnicki LH, Al-Ghazali M. Photocatalytic destruction of potassium hydrogen phthalate using TiO_2 and sunlight: application for the treatment of industrial wastewater. *J Photochem Photobiol A* 2003; **154**: 219-228

10 **Fujishima A**, Cai RX, Otsuki J, Hashimoto K, Itoh K, Yamashita T, Kubota Y. Biochemical application of photoelectrochemistry: photokilling of malignant cells with TiO_2 powder. *Electrochim Acta* 1993; **38**: 153-157

11 **Mills A**, Hunte SL. An overview of semiconductor photocatalysis. *J Photochem Photobiol A* 1997; **108**: 1-35

12 **Fujishima A,** Rao TN, Tryk DA. Titanium dioxide photocatalysis. *J Photochem Photobiol C* 2000; **1**: 1-21

13 **Kormann C,** Bahnemann DW, Hoffmann MR. Preparation and characterization of quantum-size titanium dioxide. *J Phys Chem* 1988; **92**: 5196-5201

14 **O'Regan B,** Moser J, Anderson M, Gratzel M. Vectorial electron injection into transparent semiconductor membranes and electric field effects on the dynamics of light-induced charge separation. *J Phys Chem* 1990; **94**: 8720-8726

15 **Mosmann T.** Rapid colorimetric assay for cellular growth and survival: application to proliferation and cytotoxicity assays. *J Immunol Methods* 1983; **65**: 55-63

16 **Bernard BK,** Osheroff MR, Hofmann A, Mennear JH. Toxicology and carcinogenesis studies of dietary titanium dioxide-coated mica in male and female Fischer 344 rats. *J Toxicol Environ Health* 1990; **29**: 417-429

17 **Linnainmaa K,** Kivipensas P, Vainio H. Toxicity and cytogenetic studies of ultrafine titanium dioxide in cultured rat liver epithelial cells. *Toxicol In Vitro* 1997; **11**: 329-335

18 **Xu MH,** Huang NP, Xiao ZD, Lu ZH. Photoexcited TiO_2 nanoparticles through · OH- radicals induced malignant cells to necrosis. *Supramole Sci* 1998; **5**: 449-451

19 **Cai RX,** Hashimoto K, Itoh K, Kubota Y, Fujishima A. Photokilling of malignant cells with Ultrafine TiO_2 powder. *Bull Chem Soc Jpn* 1991; **64**: 1268-1273

20 **Jaeger CD,** Bard AJ. Spin trapping and electron spin resonance detection of radical intermediates in the photodecomposition of water at TiO_2 particulate systems. *J Phys Chem* 1979; **83**: 3146-3152

21 **Rao MV,** Rajeshwar K, Pal Verneker VR, DuBow J. Photosynthetic production of H_2 and H_2O_2 on semiconducting oxide grains in aqueous solutions. *J Phys Chem* 1980; **84**: 1987-1991

22 **Harbour JR,** Hair ML. Superoxide generation in the photolysis of aqueous cadmium sulfide dispersions. Detection by spin trapping. *J Phys Chem* 1977; **81**: 1791-1793

23 **Harbour JR,** Tromp J, Hair ML. Photogeneration of hydrogen peroxide in aqueous TiO_2 dispersions. *Can J Chem* 1985; **63**: 204-208

24 **Hong AP,** Bahnemann DW, Hoffmann MR. Cobalt (II) tetrasulfophthalocyanine on titanium dioxide: a new efficient electron relay for the photocatalytic formation and depletion of hydrogen peroxide in aqueous suspensions. *J Phys Chem* 1987; **91**: 2109-2117

25 **Hidaka H,** Horikoshi S, Serpone N, Knowland J. *In vitro* photochemical damage to DNA, RNA and their bases by an inorganic sunscreen agent on exposure to UVA and UVB radiation. *J Photochem Photobiol A* 1997; **111**: 205-213

Edited by Zhang JZ and Wang XL **Proofread by** Zhu LH and Xu FM

PO Box 2345, Beijing 100023, China
Fax: +86-10-85381893
E-mail: wjg@wjgnet.com www.wjgnet.com

World J Gastroenterol 2004;10(21):3194-3196
World Journal of Gastroenterology
 ISSN 1007-9327

• BRIEF REPORTS •

Gene expression profiling in Barrett's esophagus and cardia intestinal metaplasia: A comparative analysis using cDNA microarray

Ying Chang, Jun Gong, Bin Liu, Jun Zhang, Fei Dai

Ying Chang, Jun Gong, Jun Zhang, Fei Dai, Department of Digestion, Second Hospital of Xi'an Jiaotong University, Xi'an 710004, Shaanxi Province, China
Bin Liu, Department of Emergence Surgery, Shaanxi Provincial People's Hospital, Xi'an 710068, Shaanxi Province, China
Supported by the Clinical Principal Discipline Foundation of Public Health Ministry of China, No.20012130
Correspondence to: Professor Jun Gong, Department of Digestion, Second Hospital of Xi'an Jiaotong University, Xi'an 710004, Shaanxi Province, China. emulan@126.com
Telephone: +86-29-85212945 **Fax:** +86-29-87678758
Received: 2004-04-22 **Accepted:** 2004-04-29

Abstract

AIM: To study the difference of gene expression profile changes in Barrett's esophagus (BE) and cardia intestinal metaplasia (CIM) and to screen the novel genes in the early stage by cDNA microarray.

METHODS: cDNA retrotranscribed from an equal amount of mRNA from BE and CIM epithelial tissues was labeled with Cy3 and Cy5 fluorescence as probes. The mixed probe was hybridized with three pieces of BiostarH-40 s double dot human whole gene chip. The chips were scanned with a ScanArray 4000. The acquired images were analyzed using GenePix Pro 3.0 software.

RESULTS: A total of 141 genes were screened out that exhibited different expression in all three chips. There were 74 upregulated and 67 downregulated genes in gene expression profiles of BE which were two times of that in CIM.

CONCLUSION: There is a difference in gene expression level between BE and CIM epithelia. These 141 genes probably relate to the occurrence and development of BE and the progression to adenocarcinoma.

Chang Y, Gong J, Liu B, Zhang J, Dai F. Gene expression profiling in Barrett's esophagus and cardia intestinal metaplasia: A comparative analysis using cDNA microarray. *World J Gastroenterol* 2004; 10(21): 3194-3196
http://www.wjgnet.com/1007-9327/10/3194.asp

INTRODUCTION

The incidence of adenocarcinoma in the esophagus and gastroesophageal junction (GEJ) has been increasing over the last two decades in North America and Europe[1]. Barrett's esophagus (BE) is thought to be a premalignant condition for esophageal adenocarcinoma and most of adenocarcinomas at GEJ[2]. Recently the presence of cardia intestinal metaplasia (CIM) in some normal GEJ has been described[3]. The relation of this condition to BE has not yet been investigated.

Recently, cDNA microarray methods are applied to the study of gene expression. The differentially expressed genes in different specimens may be detected with parallel analysis by gene chips which has greatly improved the traditional experiments in that only a single or several gene expression can be observed for each test, thereby speeding up the identification of differentially expressed genes and the construction of differential expression profiles.

This study was conducted on three 4096-chips, to analyse the gene expression profiles between BE and CIM epithelia, and to screen novel genes by cDNA microarray, which is helpful to understand the molecular mechanism of cell transformation and provides molecular markers and target genes for clinical diagnosis, prevention and treatment of BE and esophageal adenocarcinoma and adenocarcinoma at GEJ.

MATERIALS AND METHODS

Tissue specimens

Tissue specimens in this study were provided by the Second Hospital of Xi'an Jiaotong University, with the approval of hospital and personnel authorities. BE and CIM tissues from 13 operated or biopsy specimens (7 BE and 6 CIM) were proved pathologically. For each sample, one part was cut and frozen in liquid nitrogen immediately after resection, and the other part was used for histopathological examination. Standardized endoscopy was performed by experienced endoscopists. The appearance of sternoclavicular joint (SCJ) was carefully studied from both prograde and retrograde views. BE was defined as any columnar-lined mucosa above the GEJ, which was further confirmed by Alcian blue staining. CIM was defined by the presence of barrel-shaped goblet cells in normal GEJ.

Chip preparation

4 086 of target cDNA clones used in cDNA chips were provided by United Gene Ltd. and cooperative fellows. These genes were amplified with PCR using universal primers and then purified with standard method. The quality of PCR was monitored by agarose gel electrophoresis. The obtained genes were dissolved in 3×SSC spotting solution and then spotted on silylated slides (Telechem. Inc) by Cartesian 7 500 Spotting Roboter (Cartesian, Inc). Each target gene was dotted twice. After spotting, the slides were hydrated for 2 h and dried for 0.5 h at room temperature. The samples were cross-linked with UV light and treated with 2 g/L SDS, H_2O and 2 g/L $NaNBH_4$ for 10 min respectively. Then the slides were dried in cold condition and ready for use.

Probe preparation

Total sample RNA was extracted by single step method. Briefly, after taken out from liquid nitrogen, specimens were ground into tiny powder while liquid nitrogen was added in ceramic mortar and then homogenized in D solution plus 10 mL/L mercaptoethanol. After centrifugation, the supernatant was extracted with phenol: chloroform (1:1), NaAc and acidic phenol: chloroform (5:1) respectively. The aqueous phase was precipitated by an equal volume of isopropanol and centrifuged. The precipitates were dissolved with purified H_2O. After further purification by LiCl precipitating method, the obtained RNA sample was analyzed.

mRNAs were isolated and purified with Oligotex mRNA Midi Kit (Quagen, Inc.). The fluorescence-labeled cDNA probe was prepared through retrotranscription, referring to the method of Schena. The probes from CIM tissue were labeled with Cy3-dUTP, while those from BE tissue with Cy5-dUTP respectively. The probes were mixed and precipitated by ethanol, and then resolved in 20 mL hybridization solution (5×SSC + 2 g/L SDS).

Hybridization and washing

Probes and chips were denatured respectively in 95 ℃ bath for 5 min, then the probes were added on the chip. They were hybridized in a sealed chamber at 60 ℃ for 15-17 h and washed in turn with solutions of 2×SSC + 2 g/L SDS, 0.1×SSC + 2 g/L SDS and 0.1% SSC for 10 min each, then dried at room temperature.

Fluorescent scanning and result analysis

The chips were read by Scan Array 4000 Scanner (General Scanning Inc). The overall intensities of Cy3 and Cy5 were normalized and corrected by a coefficient according to the ratios of the 40 located housekeeping genes. The acquired image was further analyzed by GenePix Pro 3.0 software with a digital computer to obtain the intensities of fluorescent signals and the Cy3/Cy5 ratio. The data were taken on an average of the two repeated spots. The differentially expressed genes were defined as follows: The absolute value of the Cy5/Cy3 natural logarithm was more than 0.69 (the variation of gene expression was more than 2-fold). Either Cy3 or Cy5 signal value was required for more than 800. The PCR results were satisfactory.

RESULTS

Scatter plot of hybridization signals on gene chip

The scatter plots that were plotted with Cy3 and Cy5 fluorescent signal values displayed a quite disperses pattern in distribution. Most of the spots gathered around a 45° line, in which red spots represented the area where the signal intensities varied between 0.5 to 2-fold compared with those of the control. Some yellow spots distributed beyond or far from 45° line indicated the existence of abnormal gene expressions in BE and CIM epithelia. Their signal intensities were 2 times more than that of the control (Figure 1).

Table 1 Gene function classification between BE and CIM epithelia

Gene function	*n*	Ratio>2.0	Ratio<0.5
Proto-oncogene and tumor suppression genes	9	6	3
Cell signals and transducing proteins	5	2	3
Cell cycle proteins	8	6	2
Extra-pressure reaction proteins	1	1	0
Cell regulatory proteins	4	4	0
Cell apoptosis related proteins	3	2	1
DNA synthesis, repair and recombinant proteins	3	2	1
DNA binding, transcription and its factor	4	3	1
Cell receptors	1	0	1
Cell surface antigen and adhesion proteins	10	4	6
Ion-channel and transporters	11	6	5
Metabolism-related proteins	16	7	9
Protein synthesis-related genes	11	6	5
Development-related genes	0	0	0
Other genes	38	17	21
New genes	17	8	9
Total	141	74	67

Results and gene expression pattern

As shown in Figure 2, 141 genes were screened out that exhibited different expressions in all three chips, there were 74 up-regulated and 67 down-regulated genes in the gene expression profiles of BE which was 2 times of that in CIM. These genes might be divided into 16 groups (Table 1) according to their functions.

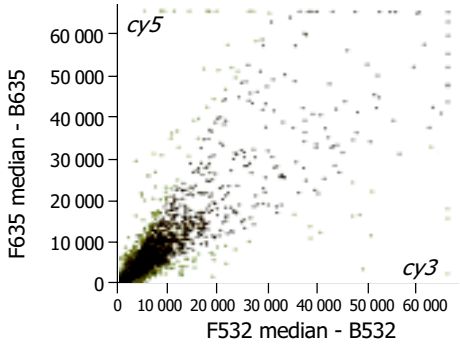

Figure 1 Scatter plot of hybridization signals on gene chip.

Figure 2 Fluorescence scanning of gene expressions on gene chip.

DISCUSSION

Over the last two decades, the incidence of adenocarcinoma of the esophagus and gastric cardia has been increasing rapidly. Barrett's metaplasia is recognized as a precancerous lesion of esophageal adenocarcinoma and most of the adenocarcinomas were found at the GEJ. Progression from metaplasia, dysplasia to adenocarcinoma has been well understood[4]. Traditionally Barrett's esophagus (BE) is defined as a circumferential segment of columnar lined epithelium of 2 or 3 cm in length in the lower esophagus. Recently this macroscopic definition has been questioned, as it excludes shorter segments and "tongues" of columnar lined epithelium, which are frequently found in the distal esophagus, and endoscopic measurements may be imprecise. It has therefore been proposed that the diagnosis of BE be reserved for patients with intestinal metaplasia detected in biopsy specimens from the distal esophagus. Recently the presence of cardia intestinal metaplasia (CIM) in some normal GEJ has been described[5-7]. Detection of intestinal metaplasia in the distal esophagus as well as within the gastric cardia was reported with increasing frequency[8]. The prevalence of BE was reported to vary from 2% to 12% and that of CIM from 5% to 23% in patients undergoing routine upper endoscopy[9]. The detection of intestinal metaplasia in the BE potentially committed patients to regular surveillance with biopsy. The incidence of adenocarcinoma in patients with BE was estimated to be 30-50 times that of the general population[10,11]. However, the exact incidence of cancer in patients with BE is unknown, and the role of CIM as a premalignant lesion is still unclear. The relation of this condition to BE has not yet been investigated. It is, however, not clear whether intestinal metaplasia of the

cardia and esophageal mucosa origins has a common pathogenesis and identical risk factors. Despite the frequent occurrence of cardia intestinal metaplasia and its association with *H pylori* gastritis and multifocal gastric intestinal metaplasia, there is still no evidence that this finding could indicate an increased risk of malignancy in the cardia. The well known association of traditional BE with symptoms and endoscopic features of gastroesophageal reflux disease (GERD) has, however, not been confirmed in CIM[12], Future studies should differentiate BE from CIM in order to enhance our understanding of the pathophysiology and the malignant potential of each clinical entity. It is therefore necessary to explore new and efficacious diagnostic methods to discriminate BE from CIM.

cDNA microarray methods have been applied in the study of gene expression, DNA sequence, novel genes and gene mutants, DNA polymorphism, and in screening drugs, diagnosing diseases and mapping gene library[13]. The differentially expressed genes in different specimens may be detected with parallel analysis by gene chips which has greatly improved the traditional experiments in that only a single or several gene expression can be observed for each test, thereby speeding up the identification of differentially expressed genes and the construction of different expression profiles. Profiling of differentially expressed genes of BE to each of the normal upper gastrointestinal (GI) mucosae, including gastric, duodenal, and squamous epithelia of the esophagus by cDNA expression array was also reported[14]. It has been shown that there was a clear distinction among the expression profiles of gastric, duodenal, and squamous epithelia whereas the BE profiles showed a considerable overlap with normal tissues. Furthermore, the clusters of genes that are specific to each of the tissues from BE, and a cluster of genes distinct from squamous and non-squamous epithelia, were identified. However, no investigation on the difference in gene expression profiles between BE and CIM epithelia by gene chip has been reported yet.

In the present study, we performed an analysis on three 4096 chips in order to acquire the difference in gene expression profiles between BE and CIM epithelia. The results showed that a total of 141 genes were screened out that exhibited different expressions in all three chips. In the gene expression profiles of BE there were 74 upregulated and 67 downregulated genes which were two times of those of CIM. A comparison between these two gene profiles showed that the gene expression levels were different between BE and CIM epithelia. These 141 genes probably relate to the occurrence and development of BE and the promotion or progression in adenocarcinoma, which might be helpful to understand the molecular mechanism of cell transformation and provides molecular markers and target genes for clinical diagnosis, prevention, treatment of BE and esophageal adenocarcinoma and most of adenocarcinomas at GEJ. The gene expression difference between BE and CIM detected by gene chip might provide a new direction for diagnosis, therapy and prevention of BE.

REFERENCES

1 **O'Connor JB,** Falk GW, Richter JE. The incidence of adenocarcinoma and dysplasia in Barrett's esophagus: report on the Cleveland Clinic Barrett's Esophagus Registry. *Am J Gastroenterol* 1999; **94**: 2037-2042

2 **Geboes K**. Barrett's esophagus: the metaplasia-dysplasia-carcinoma sequence: morphological aspects. *Acta Gastroenterol Belg* 2000; **63**: 13-17

3 **Morales TG**, Sampliner RE, Bhattacharyya A. Intestinal metaplasia of the cardia. *Am J Gastroenterol* 1997; **92**: 414-418

4 **Voutilainen M**, Farkkila M, Juhola M, Mecklin JP, Sipponen P. Complete and incomplete intestinal metaplasia at the oesophagogastric junction: prevalences and associations with endoscopic erosive oesophagitis and gastritis. *Gut* 1999; **45**: 644-648

5 **Spechler SJ**, Zeroogian JM, Antonioli DA, Wang HH, Goyal RK. Prevalence of metaplasia at the gastroesophageal junction. *Lancet* 1994; **344**: 1533-1536

6 **Goldstein NS**, Karim R. Gastric cardia inflammation and intestinal metaplasia: associations with reflux esophagitis and *Helicobacter pylori*. *Mod Pathol* 1999; **12**: 1017-1024

7 **Pereira AD**, Suspiro A, Chaves P, Saraiva A, Gloria L, de Almeida JC, Leitao CN, Soares J, Mira FC. Short segments of Barrett's epithelium and intestinal metaplasia in normal appearing oesophagogastric junctions: the same or two different entities? *Gut* 1998; **42**: 659-662

8 **Ruol A**, Parenti A, Zaninotto G, Merigliano S, Costantini M, Cagol M, Alfieri R, Bonavina L, Peracchia A, Ancona E. Intestinal metaplasia is the probable common precursor of adenocarcinoma in Barrett's esophagus and adenocarcinoma of the gastric cardia. *Cancer* 2000; **88**: 2520-2526

9 **Byrne JP**, Mathers JM, Parry JM, Attwood SE, Bancewicz J, Woodman CB. Site distribution of oesophagogastric cancer. *Clin Pathol* 2002; **55**: 191-194

10 **Hamilton SR**, Smith RL, Cameron JL. Prevalence and characters of Barrett's esophagus in patients with adenocarcinoma of the esophagugastric juncrion. *Hum Pathol* 1998; **19**: 942-948

11 **Dulai GS**, Guha S, Kahn KL, Gornbein J, Weinstein WM. Preoperative prevalence of Barrett's esophagus in esophageal adenocarcinoma: A systematic review. *Gastroenterology* 2002; **122**: 26-33

12 **Sharma P**, Weston AP, Morales T, Topalovski M, Mayo MS, Sampliner RE. Relative risk of dysplasia for patients with intestinal metaplasia in the distal esophagus and in the gastric cardia. *Gut* 2000; **46**: 9-13

13 **Xu SH,** Qian LJ, Mou HZ, Zhu CH, Zhou XM, Liu XL, Chen Y, Bao WY. Difference of gene expression profiles between esophageal carcinoma and its pericancerous epithelium by gene chip. *World J Gastroenterol* 2003; **9**: 417-422

14 **Barrett MT**, Yeung KY, Ruzzo WL, Hsu L, Blount PL, Sullivan R, Zarbl H, Delrow J, Rabinovitch PS, Reid BJ. Transcriptional analyses of Barrett's metaplasia and normal upper GI mucosea. *Neoplasia* 2002; **4**: 121-128

Edited by Wang XL and Chen WW **Proofread by** Xu FM

PO Box 2345, Beijing 100023, China
Fax: +86-10-85381893
E-mail: wjg@wjgnet.com www.wjgnet.com

World J Gastroenterol 2004;10(21):3197-3200
World Journal of Gastroenterology
 ISSN 1007-9327

• BRIEF REPORTS •

Antitumor immunity induced by DNA vaccine encoding alpha-fetoprotein/heat shock protein 70

Xiao-Ping Wang, Guo-Zhen Liu, Ai-Li Song, Hai-Yan Li, Yu Liu

Xiao-Ping Wang, Guo-Zhen Liu, Ai-Li Song, Hai-Yan Li, Yu Liu, Department of Pathology, Capital University of Medical Sciences, Beijing 100054, China
Supported by the Research Fund for Young Scholars of Beijing, No. 02120031
Correspondence to: Dr. Xiao-Ping Wang, Department of Pathology, Capital University of Medical Sciences, Beijing 100054, China. wxpphd@yahoo.com.cn
Telephone: +86-10-63051455
Received: 2004-03-18 **Accepted:** 2004-04-07

Abstract

AIM: To construct a DNA vaccine encoding human alpha-fetoprotein (hAFP)/heat shock protein 70 (HSP70), and to study its ability to induce specific CTL response and its protective effect against AFP-expressing tumor.

METHODS: A DNA vaccine was constructed by combining hAFP gene with HSP70 gene. SP2/0 cells were stably transfected with pBBS212-hAFP and pBBS212-hAFP/HSP70 eukaryotic expression vectors. Mice were primed and boosted with DNA vaccine hAFP/HSP70 by intramuscular injection, whereas plasmid with hAFP or HSP70 was used as controls. ELISPOT and ELISA were used to detect IFN-γ-producing splenocytes and the level of serum anti-AFP antibody from immunized mice respectively. *In vivo tumor challenge* was measured to assess the immune effect of the DNA vaccine.

RESULTS: By DNA vaccine immunization, the results of ELISPOT and ELISA showed that the number of IFN-γ-producing splenocytes and the level of serum anti-AFP antibody were significantly higher in rhAFP/HSP70 group than in hAFP and empty plasmid groups (95.50±10.90 IFN-γ spots/10^6 cells *vs* 23.60±11.80 IFN-γ spots/10^6 cells, 7.17±4.24 IFN-γ spots/10^6 cells, $P<0.01$; 126.50±8.22 μg/mL *vs* 51.72±3.40 μg/mL, 5.83±3.79 μg/mL, $P<0.01$). The tumor volume in rhAFP/HSP70 group was significantly smaller than that in pBBS212-hAFP and empty plasmid groups (37.41±7.34 mm^3 *vs* 381.13±15.48 mm^3, 817.51±16.25 mm^3, $P<0.01$).

CONCLUSION: Sequential immunization with a recombinant DNA vaccine encoding AFP and heat shock protein70 could generate effective AFP-specific T cell responses and induce definite antitumor effects on AFP-producing tumors, which may be suitable for some clinical testing as a vaccine for HCC.

Wang XP, Liu GZ, Song AL, Li HY, Liu Y. Antitumor immunity induced by DNA vaccine encoding alpha-fetoprotein/heat shock protein 70. *World J Gastroenterol* 2004; 10(21): 3197-3200
http://www.wjgnet.com/1007-9327/10/3197.asp

INTRODUCTION

The incidence of hepatocellular carcinoma (HCC) is increasing worldwide and accounts for as many as 1.2 million deaths annually. It is also rising rapidly in China because of hepatitis B and C infections[1,2]. Although surgery and liver transplantation are the effective therapy, most patients lost chance due to diagnosis at a late stage or underlying liver insufficiency in the setting of cirrhosis[3]. Novel therapies for HCC should be developed. A combined therapy is likely to prolong patients' life and living quality.

Much attention has been paid to the induction of host immunity to tumor cells. 80% of HCCs have a high expression of alpha-fetoprotein (AFP), which could serve as a target for immunotherapy[4-8]. AFP is an oncofetal protein during HCC development, which could generate weaker and less reproducible antitumor protection. A DNA-based vaccine may be a good method for enhancing host immunity[9-12]. A number of groups have shown that high levels of T-cell immunity could be generated using a heterogeneous prime-boost protocol, in which animals were primed and boosted with a plasmid vector encoding the stimulating molecules and targeted peptides[8-10]. In many of these vaccine models[11-15], heat shock protein 70 could combine with certain antigen prime enhanced immunogenicity, presumably through processing and presenting the antigen to host APCs. In the present study, we investigated whether the immunogenicity of AFP could be improved by presenting to APCs through HSP70 molecules. We constructed a eukaryotic expression vector containing the molecular chaperon-HSP70 and AFP fragments. Then priming mice with the genetic vaccine, we elicited robust strong protective immunity.

MATERIALS AND METHODS

Mice and cell line

Balb/c mice were provided by Department of Experimental Animal Center at Capital University of Medical Sciences. SP2/0 mice myeloma cells were maintained in RPMI 1640 (life Technologies, Inc.) supplemented with 100 mL/L fetal bovine serum (Hyclone Technologies, Inc.). The cells were transduced with pBBS212-hAFP or pBBS212-hAFP/HSP70 through calcium phosphorate precipitation (Promega Technologies, Inc.). Positive cell clones were screened by conditioned medium and supernatants were detected by AFP radioimmunoassay (Institute of Nuclear Sciences, Beijing) following the manufacturer's instructions.

Construction of recombinant expression vector

RT-PCR primers were designed to contain the partial hAFP coding region, including the signal sequence. The upper primers were5'-CCGCTCGAGATGAAGTGGGTGGAATCAA-3', while the down primers were 5'-CGCGGATCCTTATGGAGTGGGCTTTTTGTGTG-3'. RT-PCR template total RNA was isolated from HepG2 hepatocarcinoma cells by TRIzol (Life Technologies, Inc.) reagent. Then the 400-bp hAFP cDNA PCR products were cloned into the pBBS212 empty vector and pBBS212-HSP70 eukaryotic expression vector (provided by Dr. Ye L of Zhongshan Medical University, Guangzhou, China). pBBS212-hAFP/HSP70 and pBBS212-hAFP were constructed using the pBBS212 herpes simplex virus expressing vector, in which the backbone

contained the hygromycin resistance gene, being suitable for screening cell clones. The recombinant vectors were identified by restriction enzyme analysis and sequencing. Different plasmid and recombinant expressing vectors were stored at -80 ℃ for intramuscular immunization[16].

Mice immunized with recombinant expression vector

Forty female Balb/c mice were divided into rhAFP/HSP70 group, rhAFP group, HSP70 group and empty vector group, PBS group. Each group had 8 mice. Before injection, plasmid and recombinant expressing vectors were diluted in saline to 1 g/L. Various plasmids were injected into the left anterior tibialis muscle of mice. Priming and boosting with plasmid were performed with 100 μg rhAFP or rhAFP/HSP70 vector, whereas pBBS212-HSP70 and empty vectors were used as controls. A 25-gauge, 0.5-inch insulin syringe was used for intramuscular injection. Mice were intramuscularly boosted with above plasmids twice at intervals of two weeks after the first priming.

ELISPOT and ELISA assay

IFN-γ ELISPOT assay was used to measure the frequency of cells producing cytokine IFN-γ in splenocytes harvested from immunized mice. Two weeks after the last immunization, splenocytes were harvested and restimulated directly in anti-IFN-γ monoclonal antibody (PharMingen) coated ELISPOT plate wells *in vitro* with 5 μg/mL of AFP containing 100 mL/L fetal bovine serum, 10 U/mL of human interleukin-2. The plates were incubated at 37 ℃ for 24 h, then washed and incubated with a biotin-conjugated secondary antibody and developed. The color spots, representing cytokine producing cells, were counted under a dissecting microscope. To detect the level of anti-AFP antibody in mice, we examined the serum of mice tail vein after the last immunization by ELISA using AFP ELISA kits (Biotinge Biomedicine Co, LTD. Beijing) following the manufacturer's instructions.

In vivo tumor load

Another 40 female Balb/c mice were grouped and immunized as above. Tumor challenge was performed 2 wk after the last immunization with 1×10^5 AFP-transfected SP2/0 cells. SP2/0 AFP-transduced tumor cells for challenge were washed after enzymatic digestion and resuspended in 0.2 mL PBS per animal to be injected *s.c.* into the left flank, while empty plasmid and PBS were used as controls. The sizes of tumors were assessed 3 times a week using calipers. Tumor volume was approximated by the following calculation: $4/3\ \pi\ r^3$ (r = radius).

Statistical analysis

Results were expressed as mean±SD. The frequency of IFN-γ-producing splenic cells were valued using χ^2 test. The Student's t test was performed to analyze the significance of differences between the final tumor volumes of different groups. $P<0.05$ was considered statistically significant.

RESULTS

Prime-boost vaccines induced T-cell responses and anti-AFP antibody in Balb/c mice

Immunization of Balb/c mice with recombinant hAFP/HSP70 vector elicited much more strong T-cell responses than rhAFP group (95.50±10.90 IFN-γ spots/10^6 cells *vs* 23.60±11.80 IFN-γ spots/10^6 cells, $P<0.01$), whereas an intramuscular vaccination with plasmid-HSP70 and empty plasmid produced a weak response (95.50±10.90 IFN-γ spots/10^6 cells *vs* 9.25±5.44 IFN-γ spots/10^6 cells, 7.17±4.24 IFN-γ spots/10^6 cells, $P<0.01$). Recombinant hAFP/HSP70 immunized mice also produced a higher level of anti-AFP antibody than rhAFP group (126.50±8.22 μg/mL *vs* 51.72±3.40 μg/mL, $P<0.01$), while plasmid-HSP70 and empty plasmid produced a lower level (126.50±8.22 μg/mL *vs* 6.26±4.27 μg/mL, 5.83±3.79 μg/mL, $P<0.01$) (Table 1).

Boost immunization protected mice from in vivo tumor challenge

Balb/c mice were primed and boosted with rhAFP/HSP70, rhAFP, HSP70 and empty plasmid. The mice were challenged with SP2/0 cells, which were transduced with hAFP. Tumor sizes were significantly smaller in rhAFP/HSP70-immunized mice than in HSP70 and empty plasmid immunized mice (37.41±7.34 mm^3 *vs* 785.83±13.87 mm^3, 817.51±16.25 mm^3, $P<0.01$). Although rhAFP immunized group produced an obvious tumor, it was still significantly bigger than rhAFP/HSP70 group (37.41±7.34 mm^3 *vs* 381.13±15.48 mm^3, $P<0.01$) (Table 2).

DISCUSSION

Recent studies on the immunodominant epitopes of AFP have provided a solution to the obstacle of HCC immunotherapy. AFP is produced at low serum levels after birth throughout life[2-5]. The majority of human HCCs could overexpress the oncofetal antigen AFP, M_r 70 000 glycoprotein[4,5]. Despite being exposed to high plasma levels of this oncofetal protein during embryonic development, the body has a low immunity to it[3]. Butterfield *et al.*[17-19] recently found that four peptides of human AFP processed and presented in the context of HLA-A0201, could

Table 1 Spots of IFN-γ-producing splenic cells and level of anti-AFP antibody in mice (mean±SD)

Group	hAFP/HSP70	hAFP	HSP70	Empty	PBS
Spots (10^6 cells)	95.50±10.90[bd]	23.60±11.80[f]	9.25±5.44	7.17±4.24	5.54±2.16
Anti-AFP (μg/mL)	126.50±8.22[bd]	51.72±3.40[f]	6.26±4.27	5.83±3.79	3.42±2.35

[b]$P<0.01$, *vs* empty group; [d]$P<0.01$, *vs* HSP70 group; [f]$P<0.01$, *vs* empty group.

Table 2 Comparison of tumor growth in mice injected with hAFP-transduced SP2/0 tumor cells (mean±SD)

Group	No. of tumor-bearing/ No. of mice challenge	10 d after tumor challenge/ Size of tumor (mm^3)	20 d after tumor challenge/ Size of tumor (mm^3)
hAFP/HSP70	2/8	24.43±6.10[bd]	37.41±7.34[bd]
hAFP	5/8	73.64±8.53[f]	381.13±15.48[f]
HSP70	8/8	118.24±14.65	785.83±13.87
Empty	8/8	132.26±17.27	817.51±16.25
PBS	8/8	149.73±16.54	860.53±14.72

[b]$P<0.01$, *vs* empty group; [d]$P<0.01$, *vs* HSP70 group; [f]$P<0.01$, *vs* empty group.

be recognized by human T cell repertoire, and could be used to generate AFP-specific CTL in human T cell cultures. It was also found that murine immune system could generate T-cell responses to this oncofetal antigen[8]. Therefore, it may be a better target for immunotherapy. But AFP immunization alone still resulted in lower levels of specific response and poorly reproducible protective immunity[3-7].

How to enhance host's active immunity to AFP may be an interesting strategy for HCC therapy. Previous studies on AFP specific immunotherapy for HCC included AFP plasmid immunization, AFP-transduced DCs immunization and AFP plasmid prime-AFP adenovirus boost immunization[20-22]. AFP plasmid immunization produced detectable but low levels of AFP specific T cell responses and poorly reproducible protective immunity[7,20]. DCs engineered to express murine AFP demonstrated a powerful ability to generate tumor-specific immune responses[21]. However, the need for costly cell culture procedures limited their wide availability for clinical use, and the unstable culture technique might yield tolerating vaccines[8,21]. AFP plasmid prime-AFP adenovirus boost immunization could engender significant AFP specific T-cell responses and protective immunity in mice[22]. But the miscellaneous procedures precluded their use. In the present study, we tested a novel strategy to induce antitumor immunity by a DNA vaccine encoding both AFP and HSP70 in mice. We found that the vaccine could elicit strong AFP-specific T-cell responses and produce a distinctively protective effect on AFP-expressing tumors compared with other immunized groups. We should point out that the DNA vaccine hAFP also produced a definite antitumor immunity, but the effect was not sufficient and satisfactory in comparison with that of recombinant vaccine AFP/HSP70. It is of interest to note that recombinant DNA vaccines provoked not only the considerable stability of immunoprotection, but also a detectable level of anti-AFP antibody, although humoral immunity alone had a minor effect on antitumor activity[23,24].

In the study, we attributed the successful AFP specific T-cell responses in mice to the HSP70 molecules by mediating APCs to efficiently uptake and process of AFP. A number of investigations have shown that HSP70 itself has no antigenicity and its immunogenicity can be attributed to the peptide chaperones carried by itself[25-29]. It has been verified that HSP70 is a better molecular chaperone and adjuvant, which could process and present weak tumor antigens to MHC-I of host APCs, eliciting specific T-cell responses and CTL reactions[26-28]. Suzue *et al*.[29] using a recombinant heat shock fusion protein containing a large fragment of ovalbumin linked to HSP70 injected without adjuvants into Balb/c mice, CTLs were produced that recognized an ovalbumin-derived peptide and the mice were also protected against challenge with ovalbumin-expressing melanoma tumor cells. Several studies have shown that HSP70-associated peptides could anchor antigens on the cell membrane and directly present them to nature killer cells or γδ T cells as superantigens without dependence on the stimulation of MHC-I molecules[30-32]. In this experiment, tumor rejection assay demonstrated that recombinant vaccine AFP/HSP70 elicited strong specific antitumor immunity against AFP-producing SP2/0 cells than AFP DNA vaccine. The results indicated that AFP immunogenicity was greatly improved by HSP70 molecules and vaccination with DNA encoding HSP70 could increase both humoral and T-cell proliferation responses to AFP.

In summary, sequential immunization with a recombinant DNA vaccine encoding AFP and heat shock protein70 could generate effective AFP-specific T cell responses and induce definite antitumor effects on AFP-producing tumors, which may be suitable for some clinical testing as a vaccine for HCC.

REFERENCES

1 **Schafer DF,** Sorrell MF. Hepatocellular carcinoma. *Lancet* 1999; **353:** 1253-1257

2 **Qin LX,** Tang ZY. Hepatocellular carcinoma with obstructive jaundice: diagnosis, treatment and prognosis. *World J Gastroenterol* 2003; **9:** 385-391

3 **Tang ZY.** Hepatocellular carcinoma-Cause, treatment and metastasis. *World J Gastroenterol* 2001; **7:** 445-454

4 **Guo J,** Cai M, Wei D, Qin L, Huang J, Wang X. Immune responses of dendritic cells after loaded with cytotoxicity T lymphocyte epitope based peptide of human alpha-fetoprotein (hAFP). *Zhonghua Ganzangbing Zazhi* 2002; **10:** 178-180

5 **Grimm CF**, Ortmann D, Mohr L, Michalak S, Krohne TU, Meckel S, Eisele S, Encke J, Blum HE, Geissler M. Mouse alpha-fetoprotein-specific DNA-based immunotherapy of hepatocellular carcinoma leads to tumor regression in mice. *Gastroenterology* 2000; **119:** 1104-1112

6 **Hanke P**, Rabe C, Serwe M, Bohm S, Pagenstecher C, Sauerbruch T, Caselmann WH. Cirrhotic patients with or without hepatocellular carcinoma harbour AFP-specific T-lymphocytes that can be activated *in vitro* by human alpha-fetoprotein. *Scand J Gastroenterol* 2002; **37:** 949-955

7 **Hanke P**, Serwe M, Dombrowski F, Sauerbruch T, Caselmann WH. DNA vaccination with AFP-encoding plasmid DNA prevents growth of subcutaneous AFP-expressing tumors and does not interfere with liver regeneration in mice. *Cancer Gene Ther* 2002; **9:** 346-355

8 **Saeki A**, Nakao K, Nagayama Y, Yanagi K, Matsumoto K, Hayashi T, Ishikawa H, Hamasaki K, Ishii N, Eguchi K. Diverse efficacy of vaccination therapy using the alpha-fetoprotein gene against mouse hepatocellular carcinoma. *Int J Mol Med* 2004; **13:** 111-116

9 **Pancholi P,** Liu Q, Tricoche N, Zhang P, Perkus ME, Prince AM. DNA prime-canarypox boost with polycistronic hepatitis C virus (HCV) genes generates potent immune responses to HCV structural and nonstructural proteins. *J Infect Dis* 2000; **182:** 18-27

10 **Kumar V**, Sercarz E. Genetic vaccination: the advantages of going naked. *Nat Med* 1996; **2:** 857-859

11 **Leitner WW**, Ying H, Restifo NP. DNA and RNA-based vaccines: principles, progress and prospects. *Vaccine* 1999; **18:** 765-777

12 **Moelling K**. DNA for genetic vaccination and therapy. *Cytokines Cell Mol Ther* 1997; **3:** 127-135

13 **Srivastava PK**, Udono H. Heat shock protein-peptide complexes in cancer immunotherapy. *Curr Opin Immunol* 1994; **6:** 728-732

14 **Huang XF**, Ren W, Rollins L, Pittman P, Shah M, Shen L, Gu Q, Strube R, Hu F, Chen SY. A broadly applicable, personalized heat shock protein-mediated oncolytic tumor vaccine. *Cancer Res* 2003; **63:** 7321-7329

15 **Casey DG**, Lysaght J, James T, Bateman A, Melcher AA, Todryk SM. Heat shock protein derived from a non-autologous tumour can be used as an anti-tumour vaccine. *Immunology* 2003; **110:** 105-111

16 **Wang XP**, Chen RF, Song AL, Liu YF. Construction and identification of pBBS212-AFP / HSP70 eukaryotic expression vector. *Zhongliu Yanjiu Yu Linchuang* 2002; **14:** 363-365

17 **Butterfield LH**, Koh A, Meng W, Vollmer CM, Ribas A, Dissette V, Lee E, Glaspy JA, McBride WH, Economou JS. Generation of human T-cell responses to an HLA-A2.1-restricted peptide epitope derived from alpha-fetoprotein. *Cancer Res* 1999; **59:** 3134-3142

18 **Meng WS**, Butterfield LH, Ribas A, Heller JB, Dissette VB, Glaspy JA, McBride WH, Economou JS. Fine specificity analysis of an HLA-A2.1-restricted immunodominant T cell epitope derived from human alpha-fetoprotein. *Mol Immunol* 2000; **37:** 943-950

19 **Butterfield LH**, Meng WS, Koh A, Vollmer CM, Ribas A, Dissette VB, Faull K, Glaspy JA, McBride WH, Economou JS. T cell responses to HLA-A*0201-restricted peptides derived from human alpha fetoprotein. *J Immunol* 2001; **166:** 5300-5308

20 **Vollmer CM Jr**, Eilber FC, Butterfield LH, Ribas A, Dissette VB, Koh A, Montejo LD, Lee MC, Andrews KJ, McBride WH, Glaspy JA, Economou JS. Alpha-fetoprotein-specific genetic immunotherapy for hepatocellular carcinoma. *Cancer Res* 1999; **59:** 3064-3067

21 **Banchereau J**, Steinman RM. Dendritic cells and the control of immunity. *Nature* 1998; **392:** 245-252
22 **Meng WS**, Butterfield LH, Ribas A, Dissette VB, Heller JB, Miranda GA, Glaspy JA, McBride WH, Economou JS. alpha-Fetoprotein-specific tumor immunity induced by plasmid prime-adenovirus boost genetic vaccination. *Cancer Res* 2001; **61:** 8782-8786
23 **Le Poole IC,** Gerberi MA, Kast WM. Emerging strategies in tumor vaccines. *Curr Opin Oncol* 2002; **14:** 641-648
24 **Reilly RT,** Emens LA, Jaffee EM. Humoral and cellular immune responses: independent forces or collaborators in the fight against cancer? *Curr Opin Investig Drugs* 2001; **2:** 133-135
25 **Milani V,** Noessner E, Ghose S, Kuppner M, Ahrens B, Scharner A, Gastpar R, Issels RD. Heat shock protein 70: role in antigen presentation and immune stimulation. *Int J Hyperthermia* 2002; **18:** 563-575
26 **Harmala LA,** Ingulli EG, Curtsinger JM, Lucido MM, Schmidt CS, Weigel BJ, Blazar BR, Mescher MF, Pennell CA. The adjuvant effects of Mycobacterium tuberculosis heat shock protein 70 result from the rapid and prolonged activation of antigen-specific CD8+ T cells *in vivo*. *J Immunol* 2002; **169:** 5622-5629
27 **Noessner E,** Gastpar R, Milani V, Brandl A, Hutzler PJ, Kuppner MC, Roos M, Kremmer E, Asea A, Calderwood SK, Issels RD. Tumor-derived heat shock protein 70 peptide complexes are cross-presented by human dendritic cells. *J Immunol* 2002; **169:** 5424-5432
28 **Feng H,** Zeng Y, Graner MW, Likhacheva A, Katsanis E. Exogenous stress proteins enhance the immunogenicity of apoptotic tumor cells and stimulate antitumor immunity. *Blood* 2003; **101:** 245-252
29 **Suzue K,** Zhou X, Eisen HN, Young RA. Heat shock fusion proteins as vehicles for antigen delivery into the major histocompatibility complex class I presentation pathway. *Proc Natl Acad Sci U S A* 1997; **94:** 13146-13151
30 **Wei Y**, Zhao X, Kariya Y, Fukata H, Teshigawara K, Uchida A. Induction of autologous tumor killing by heat treatment of fresh human tumor cells: involvement of gamma delta T cells and heat shock protein 70. *Cancer Res* 1996; **56:** 1104-1110
31 **Dressel R**, Grzeszik C, Kreiss M, Lindemann D, Herrmann T, Walter L, Gunther E. Differential effect of acute and permanent heat shock protein 70 overexpression in tumor cells on lysability by cytotoxic T lymphocytes. *Cancer Res* 2003; **63:** 8212-8220
32 **Cheng WF**, Hung CF, Lin KY, Ling M, Juang J, He L, Lin CT, Wu TC. CD8+ T cells, NK cells and IFN-gamma are important for control of tumor with downregulated MHC class I expression by DNA vaccination. *Gene Ther* 2003; **10:** 1311-1320

Edited by Wang XL and Chen WW **Proofread by** Xu FM

PO Box 2345, Beijing 100023, China
Fax: +86-10-85381893
E-mail: wjg@wjgnet.com www.wjgnet.com

World J Gastroenterol 2004;10(21):3201-3204
World Journal of Gastroenterology
 ISSN 1007-9327

• BRIEF REPORTS •

Apoptosis pathway of liver cells in chronic hepatitis

Nai-Ling Chen, Ling Bai, Lin Li, Pei-Lan Chen, Chang Zhang, Chao-Ying Liu, Tao Deng, Hao Chen, Ke-Ming Jia, Zhen-Qiu Zhou

Nai-Ling Chen, Lin Li, Pei-Lan Chen, Chao-Ying Liu, Tao Deng, Ke-Ming Jia, Institute of Liver Disease, General Hospital of Beijing Military Command Beijing 100700, China
Ling Bai, Chang Zhang, Hao Chen, Department of Pathology, First People's Hospital of Lianyungang, Lianyungang 222002, Jiangsu Province, China
Zhen-Qiu Zhou, First People's Hospital of Lianyungang, Lianyungang 222002, Jiangsu Province, China
Supported by the National Natural Science Foundation of China, No. 39770660 and the Beijing Military Command Foundation, No. 95B008 and the Social Development Program of Lianyungang City, No. SH 0210
Correspondence to: Ling Bai, Department of Pathology, First People's Hospital of Lianyungang, Lianyungang 222002, Jiangsu Province, China. bailing1968@hotmail.com
Telephone: +86-518-5467012 **Fax:** +86-518-5462047
Received: 2004-01-10 **Accepted:** 2004-03-02

Abstract

AIM: To study the pathway of apoptosis in chronic liver disease and the role of mitochondria in programmed cell death.

METHODS: Liver biopsy specimens from 72 cases of chronic hepatitis and 29 cases of post hepatitis cirrhosis were studied. The pro-apoptotic protein Fas, FasL, Bax and the anti-apoptotic protein Bcl-2, Bcl-x_L, Bcl-2α were studied immunohistochemically by SP method. Specimens from 15 cases of chronic hepatitis and post hepatitis cirrhosis were examined for their ultramicrostructures with special attention to their mitochondrial changes. Specimens from 3 normal adults (demised in traffic accidents) were used as control.

RESULTS: The expression of proapoptotic proteins (Fas, FasL, Bax) in hepatocytes was significantly higher in the chronic hepatitis group than in the cirrhosis group ($P<0.001$). In the study of ultramicrostructure 364 hepatocytes were examined, from 12 cases of chronic hepatitis (including 10 mild cases, 1 moderate case and 1 severe case). Out of 364 hepatocytes 40 (11.0%) hepatocytes were found with various kinds of destruction in their mitochondria. Rupture of the outer membrane of mitochondria and the leakage of matrix from the intermembrane space were definitely demonstrated. The ultramicrostructural changes of mitochondria in the chronic hepatitis group were statistically higher than that in normal adults control group ($\chi^2=4.32$, $P<0.05$).

CONCLUSION: The result of the study was in support of the current view that the apoptotic process in chronic hepatitis patients were largely along the intrinsic pathway (mitochondrial pathway), given that the intrinsic and extrinsic pathways could interlinked (converged) at some point on their progression, also it is impossible at present to exclude the possibility that the two pathways could be chosen by hepatocytes in parallel simultaneously.

Chen NL, Bai L, Li L, Chen PL, Zhang C, Liu CY, Deng T, Chen H, Jia KM, Zhou ZQ. Apoptosis pathway of liver cells in chronic hepatitis. *World J Gastroenterol* 2004; 10(21): 3201-3204
http://www.wjgnet.com/1007-9327/10/3201.asp

INTRODUCTION

Fas receptor induced hepatocellular apoptosis has long been implicated in the pathogenesis of viral hepatitis and potentially other liver diseases. The apoptosis is initiated by binding of the Fas ligand expressed on the surface of lymphocytes to the Fas receptor on the hepatocytes[1-3]. After initiation the apoptotic process, the cascade reaction of caspases and eventually to the DNA fragmentation and cell death continued[4,5]. In addition to the above extrinsic pathway it was recognized recently that apoptosis can occur independent of cell surface receptors. Apoptosis can occur through the activation of p53 by DNA damage. Activation of p53 leads to translocation of proapoptotic protein Bax to the mitochondria and form pores at the outer mitochondrial membranes. The formation of pores induces the release of cytochrome c and other proteins from the intermembrane space. The released cytochrome c and other protein then activated other caspases and eventually lead to apoptosis (intrinsic pathway)[6-8]. In this study we tried to find out the apoptosis pathway in chronic hepatitis. We studied it by immunohistochemical method and ultramicrostructural examination of mitochondrial changes.

MATERIALS AND METHODS

Liver biopsy specimens from 72 cases of chronic hepatitis of more than one year and 29 cases of post-hepatitis cirrhosis were studied immunohistochemically, out of them 12 cases of chronic hepatitis, 3 cases post-hepatitis cirrhosis and 3 normal adults, were examined by electronmicroscopy for the ultramicrostructurs of apoptotic hepatocytes. Criteria of clinical and histological diagnoses were carried out in accordance with the consensus protocols published by the 10th Congress of Viral Hepatitis of China. The histological activity of hepatitis was assessed by the histological activity index (HAI) of Knodell *et al*.[9] The intensity of expression in immunohistochemical assay was divided into (-), (+), (++) and (+ + +) in this study[10,11].

Serum markers of HBV infection and anti-HCV antibody were detected by ELISA. Liver biopsy specimens were examined after hematoxylin and eosin staining. The immunohistochemical examination was carried out by streptoavidin peroxidase conjugation. Mouse anti-human Bcl-2, Bcl-X_L monoclonal antibody and rabbit anti-human Fas and rabbit anti-human FasL polyclonal antibodies were obtained from Santo Cruz (USA). Mouse anti-Bcl-2α monoclonal antibody was obtained from Maixin Bio company. Ultramicrostructure of mitochondria was studied by EM of Hitachi H-600 (Japan). The ultramicrostructure changes of mitochondria in specimens from 15 cases of chronic hepatitis and post hepatitis cirrhosis were examined with special attention to their mitochondrial changes. Specimens from 3 normal adults (demised in traffic accidents) were used as control. At least 15 hepatocytes in each section were observed.

The statistics was carried out by χ^2 with MINITAB software.

RESULTS

Immunohistochemical findings

Both the expressions of proapoptotic proteins (Fas, FasL, Bax) and antiapoptotic proteins (Bcl-2, Bcl-2α, Bcl-X_L) were found mainly in cytoplasm and membranes of hepatocytes. Some expressions could also be found in cytoplasma of epithelial cells of the biliary canaliculus. In 101 cases of chronic liver disease the proapoptotic protein expression was significant higher than the antiapoptotic protein expression. The proapoptotic proteins Fas, FasL, Bax were 87.5%, 94.4% and 91.7% respectively. the antiapoptotic proteins Bcl-2, Bcl-X_L, Bcl-2α were 56.9%, 61.1% and 38.9% (P<0.001) respectively in the chronic hepatitis group (Figures 1, 2, Tables 1-3).

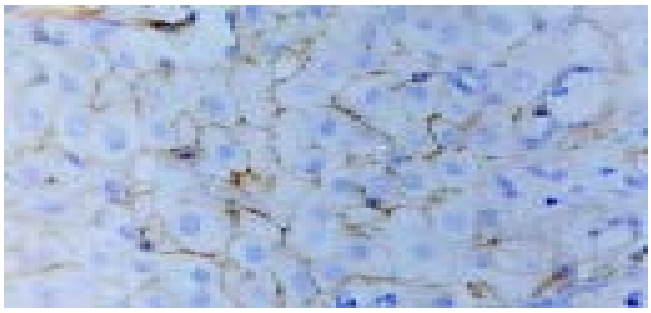

Figure 1 Expression of Fas in hepatocytes of chronic hepatitis (SP, original magnification: ×400).

Table 1 Positive expression of apoptotic proteins in the liver specimens of chronic liver disease (%)

	n	Fas	FasL	Bax	Bcl-2	Bcl-X_L	Bcl-2α
CH	72	63 (87.5)	68 (94.4)	66 (91.7)	41 (56.9)	44 (61.1)	28 (38.9)
LC	29	24 (82.8)	27 (93.1)	25 (86.2)	20 (69.0)	21 (72.4)	13 (44.8)

CH: Chronic hepatitis group. A: Fas: Bcl-2 χ^2 = 16.754, B: Fas: Bcl-X_L χ^2 = 13.131; C: Fas: Bcl-2α χ^2 = 36.575, D: FasL: Bcl-2 χ^2 = 27.517; E: FasL: Bcl-X_L χ^2 = 23.143, F: FasL: Bcl-2α χ^2 = 50.00; G: Bax: Bcl-2 χ^2 = 22.733, H: Bax: Bcl-X_L χ^2 = 18.635; I: Bax: Bcl-2α χ^2 = 44.242; I: P<0.001; J: Bcl-2: Bcl-2α χ^2 = 8.472, K: Bcl- X_L: Bcl-2α χ^2 = 7.111; J-K P<0.01. LC: Liver Cirrhosis group. L: FasL: Bcl-2α χ^2 = 15.789; M: Bax: Bcl-2α χ^2 = 10.898; I-M: P<0.001; N: Fas: Bcl-2α χ^2 = 9.032, P<0.01; O: FasL: Bcl-2 χ^2 = 5.497; P: FasL: Bcl- X_L χ^2 = 4.35; O-P: P<0.05.

Table 2 Degree of expression of proapoptotic proteins on the liver specimens of chronic liver disease (%)

	n	Fas			FasL			Bax		
		(+)	(++)	(+++)	(+)	(++)	(+++)	(+)	(++)	(+++)
CH	72	32 (44.4)	29 (40.3)	2 (2.8)	29 (40.3)	34 (47.2)	5 (6.9)	26 (36.1)	24 (33.3)	16 (22.2)
LC	29	13 (44.8)	9 (31.0)	2 (6.9)	8 (27.6)	15 (51.7)	4 (13.8)	11 (37.9)	14 (48.3)	0

Table 3 Degree of expression of anti-apoptotic proteins on the liver specimens of chronic liver disease (%)

	n	Bcl-2			Bcl-X_L			Bcl-2α		
		(+)	(++)	(+++)	(+)	(++)	(+++)	(+)	(++)	(+++)
CH	72	21 (29.2)	13 (18.1)	7 (2.8)	27 (37.5)	10 (13.9)	7 (9.2)	25 (34.7)	3 (4.2)	0
LC	29	12 (41.4)	6 (20.7)	2 (6.9)	12 (41.4)	7 (24.1)	2 (6.9)	8 (27.6)	9 (10.4)	2 (6.9)

Table 4 Apoptosis and mitochondria of the liver specimens of chronic liver disease

Code No.	HAI Score			Fas	Fasl	Bax	Bcl-2	Bcl-2α	Bcl-χ_l	A	B	A/B %
	G	S	HAI									
1	CH-mild	1	0	1	++	++	++	++	+	-	3	20	15.0
2	CH-mild	1	0	4	+	++	+++	+++	-	+	2	26	7.7
4	CH-mild	1	1	3	++	+	+	+	-	++	2	26	7.7
7	CH-mild	1	0	6	++	+++	++	++	-	++	4	36	11.2
9	CH-mild	1	0	2	+	+++	-	-	-	+++	6	25	24.0
10	CH-mild	1	0	1	++	+	-	-	-	++	5	41	12.2
11	CH-mild	2	0	3	+	++	-	-	+	-	2	37	5.4
13	CH-mild	1	0	2	-	+	-	-	-	+	1	31	3.2
14	CH-mild	1	0	1	++	-	-	-	-	-	1	15	6.7
15	CH-mild	1	0	3	++	+	-	-	-	+	4	31	12.9
3	CH-MOD	2	0	8	++	+	+	+	+	+	8	40	20.0
5	CH-SEV	4	15	15	++	+++	-	-	-	-	2	36	5.6
6	LC	3	12	12	+	+	+++	+++	-	++	0	15	
8	LC	4	15	15	-	-	+	+	-	+++	1	24	4.2
12	LC	4	8	8	+	+	-	-	-	++	5	34	14.7

MOD: Moderate; SEV: Severe; G: Grade; S: Stage. A: Number of hepatocytes with abnormal mitochondrial; B: Total number of hepatocytes examined by EM.

Figure 2 Bcl-2 expression on cell membranes and cytoplasma of hepatocytes of chronic hepatitis (SP, original magnification: ×400).

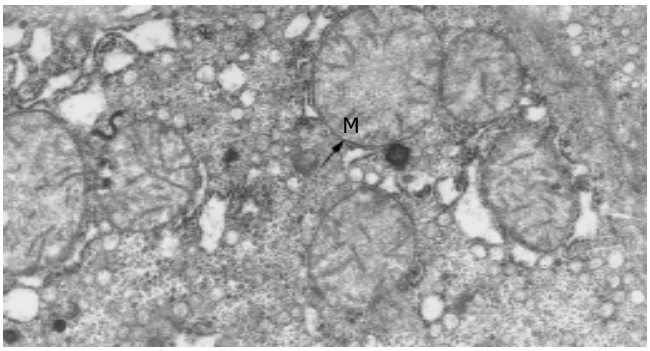

Figure 3 Normal mitochondria in normal adults (Trans-EM, original magnification: ×26 000).

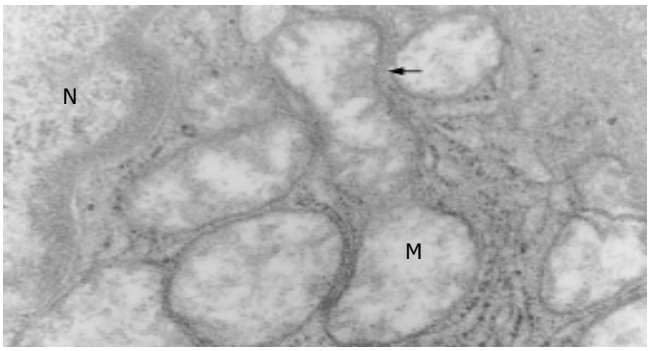

Figure 4 Membrane rupture, disappearance of crista due to apoptosis (Trans-EM, original magnification: ×25 000).

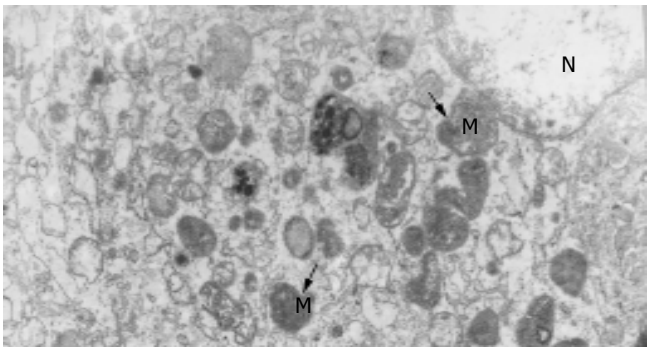

Figure 5 Herniation of matrix from ruptured membranes of apoptotic mitochondria (Trans-EM, original magnification: ×20 000).

Untramicrostructure findings

The ultramicrostructures of mitochondria in 12 cases of chronic hepatitis (including 10 mild cases, 1 moderate case and 1 severe case) were studied. Among the 364 hepatocytes examined, 40 hepatocytes (11.0%) were found with distinct abnormality in their mitochondria (Table 4). Changes of the mitochondria include disappearance of criastae, rupture of the outer membranes (Figures 3, 4), leakage of mitochondrial matrix,"herniation" of matrix from the ruptured membranes (Figures 5, 6).

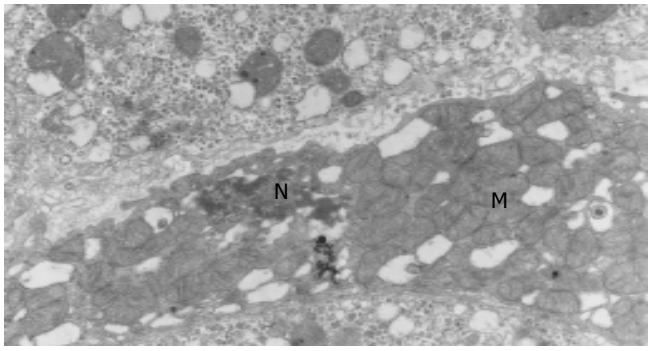

Figure 6 Degeneration and concentration of apoptotic mitochondria (Trans-EM, original magnification: ×15 000).

DISCUSSION

This study demonstrated that the proapoptotic proteins in chronic hepatitis were significantly higher than the antiapoptotic proteins. This was in strong contrast to many tumor cells whose antiapoptotic proteins were higher than proapoptotic proteins. It was also noted that in the 12 cases of chronic hepatitis patients of more than one year the outer mitochondrial membrane damages or ruptures were also in strong contrast to the normal adults control. Recent investigations inclined to support the view that the apoptosis of hepatocytes may be taken the intrinsic pathway (or mitochondrial pathway)[12-15]. In view of the prominent mitochondrial changes seen in this study the author was highly in favor of the current view that the apoptosis of hepatocytes in chronic hepatitis may begin from the injured DNA which activates the p53 protein to translocate the proapoptotic protein Bax to the mitochondrial and form pores at the outer mitochondrial membrane to release the cytochrome c to the cytosol. This begining lead to the complete death of the hepatocytes[16].

The result was considered consistent with the current view that the apoptosis in chronic hepatitis was a comparatively long persistent phenomenon which took place mainly along the intrinsic pathway (mitochondria pathway), although it was impossible at present to exclude the possibility that the intrinsic and extrinsic could take place in parallel simultaneously. Further study of the apoptotic pathway of chronic hepatitis would be helpful in finding out the effective methods of interrupting the progressive course of the disease.

ACKNOWLEDGEMENTS

We would like to express thanks to Professor Yao- Xuan Huang for directions.

REFERENCES

1 **Hengartner MO**. The biochemistry of apoptosis. *Nature* 2000; **407:** 770-776
2 **Ravi R,** Bedi A. Requirement of BAX for TRAIL/Apo2L-induced apoptosis of colorectal cancers: synergism with sulindac-mediated inhibition of Bcl-X_L. *Cancer Res* 2002; **62:** 1583-1587
3 **Zheng HC,** Sun JM, Wei ZL, Yang XF, Zhang YC, Xin Y. Expression of Fas ligand and Caspase-3 contributes to formation of immune escape in gastric cancer. *World J Gastroenterol* 2003;

9: 1415-1420

4 **Greenstein S,** Ghias K, Krett NL, Rosen ST. Mechanisms of glucocorticoid-mediated apoptosis in hematological malignancies. *Clin Cancer Res* 2002; **8:** 1684-1694

5 **Tsujimoto Y.** Bcl-2 family of proteins-Life-or-death. *Switch Clin Immunol* 2001; **36**: 266-273

6 **Adrain C,** Martin SJ. The mitochondrial apoptosome: a killer unleashed by the cytochrome seas. *Trends Biochem Sci* 2001; **26:** 390-397

7 **Capaldi RA.** The changing face of mitochondrial research. *Trends Biochem Sci* 2000; **25**: 212-214

8 **Feldmann G,** Haouzi D, Moreau A, Durand-Schneider AM, Bringuier A, Berson A, Mansouri A, Fau D, Pessayre D. Opening of the mitochondrial permeability transition pore causes matrix expansion and outer membrane rupture in Fas-mediated hepatic apoptosis in mice. *Hepatology* 2000; **31:** 674-683

9 **Knodell RG**, Ishak KG, Black WC, Chen TS, Craig R, Kaplowitz N, Kiernan TW, Wollman J. Formulation and application of a numerical scoring system for assessing histological activity in asymptomatic chronic active hepatitis. *Hepatology* 1981; **1**: 431-435

10 **Chen NL**, Bai L, Deng T, Zhang C, Chen H. Study on pathway of apoptosis in chronic liver disease. *Zhonghua Chuanranbing Zazhi* 2003; **21**: 122-124

11 **Chen NL**, Deng T, Chen PL, Li L. The regulation of apoptosis by Bcl-2, Bcl-χ_L, Bcl-2α and Bax in chronic liver disease. *Zhonghua Neike Zazhi* 2000; **39**: 808-810

12 **Jaeschke H,** Bajt ML. Regulation of apoptotic signaling pathways in hepatocytes *in vivo*. *Hepatology* 2003; **37**: 942-945

13 **Fang DC**. Genetic instability in the development of gastric cancer. *Shijie Huaren Xiaohua Zazhi* 2003; **11**: 1-5

14 **Newmeyer DD,** Ferguson-Miller S. Mitochondria: releasing power for life and unleashing the machineries of death. *Cell* 2003; **112**: 481-490

15 **Green DR**. Overview: apoptotic sina;ing pathways in the immune system. *Immunol Rev* 2003; **193**: 5-9

16 **Rathmell JC,** Thompson CB. Pathways of apoptosis in lymphocyte development, homeostasis, and disease. *Cell* 2002; **109**: S97-S107

Edited by Wang XL **Proofread by** Chen WW and Xu FM

PO Box 2345, Beijing 100023, China
Fax: +86-10-85381893
E-mail: wjg@wjgnet.com www.wjgnet.com

World J Gastroenterol 2004;10(21):3205-3207
World Journal of Gastroenterology
 ISSN 1007-9327

• BRIEF REPORTS •

Cloning and sequence analysis of gene oipA encoding an outer membrane protein of human *Helicobacter pylori*

Dao-Rong Chen, Ai-Long Huang, Xiao-Hong Tao, Pi-Long Wang, Zheng Jiang

Dao-Rong Chen, Xiao-Hong Tao, Pi-Long Wang, Zheng Jiang, Department of Gastroenterology, the First Affiliated Hospital, Chongqing University of Medical Sciences, Chongqing 400016, China
Ai-Long Huang, Institute of Viral Hepatitis, Chongqing University of Medical Sciences, Chongqing 400010, China
Supported by Fund of Chongqing Health Bureau, No. 001110438
Correspondence to: Dr. Dao-Rong Chen, Department of Gastroenterology, the First Affiliated Hospital, Chongqing University of Medical Sciences, Chongqing 400016, China. cdrcdr@mail.china.com
Telephone: +86-23-68122549
Received: 2004-02-14 **Accepted:** 20004-03-06

Abstract

AIM: To construct a recombinant *E. coli* strain that would highly express the proinflammatory outer membrane protein of human *Helicobacter pylori* (*H pylori*).

METHODS: The oipA DNA was amplified by PCR, inserted into pET-32a, and transformed into Top10 *E. coli* strain. This recombinant plasmid of Top10 was sent out for nucleotide sequence analysis. Finally this sequence AF479754 was compared with HP0638 and JHP0581.

RESULTS: The sequence of the aim gene was obtained. It had 924 base pairs. The identity was 95.32% against HP0638, 95.02% against JHP0581, which was higher than the identity between HP0638 and JHP0581.

CONCLUSION: Although the aim gene was obtained, but it was different from the published sequence of GenBank. It is not clear what makes this difference. Maybe it is because different strain was used or because there were some variations. So more researches are required to prove it.

Chen DR, Huang AL, Tao XH, Wang PL, Jiang Z. Cloning and sequence analysis of gene oipA encoding an outer membrane protein of human *Helicobacter pylori*. *World J Gastroenterol* 2004; 10(21): 3205-3207
http://www.wjgnet.com/1007-9327/10/3205.asp

INTRODUCTION

In order to find a good vaccine to end the coexistence of human and *Helicobacter pylori* (*H pylori*), some scientists have focused on exploring some outer membrane proteins in these 10 years. Yamaoka *et al*. found six bands of the outer membrane proteins in *H pylori* on gels by immunoblot assay kits, 116 ku (CagA), 89 ku (VacA), 35 ku, 30 ku, 26.5 ku and 19.5 ku (Lpp20)[1-5]. In which 35 ku band is broader than others. It always appears at 33-35 ku. Now a few scientists are studying the 35 ku protein including Yamaoka. They found that 33-35 ku protein was positive in 97.5% patients with peptic ulcer, 70% patients with chronic gastritis. The results showed that it was related to the presence of peptic ulcer. Yamaoka deduced that Hpo638 encoding outer membrane protein oipA had the most possibility, because it had great antigen characteristics, also could increase the serum level of IL-8. Later studies have shown that oipA is the only index that can differ duodenum ulcer from gastritis, respond to high location of *H pylori*, serious mucosal infiltration with neutrophils cells, and high level of IL-8.

As so far, there is no study on the oipA in our country. We used PCR techinology to amplify oipA gene, to construct the recombinant plasmid, and analyse the DNA sequence. We found that the target sequence AF479754 had some difference with HP0638 and JHP0581.

MATERIALS AND METHODS

Material

H pylori was afforded by the Department of Microbiology, Chongqing University of Medical Sciences. Top10 *E. coli* strain and pET32a(+) plasmid were presented by the Institute of Viral Hepatitis of Chongqing University of Medical Sciences. Endonucleases, T4 ligase and Pfu -Taq DNA polymerase were purchased from Promega. PCR marker was purchased from Shanghai Sangon. The kits for purification of plasmids and PCR products were obtained from Omega. Primers were synthesized in Shanghai Sangon.

Isolation and identification of H pylori

Each gastric biopsy specimen was inoculated on *H pylori* medium plates. The plates were incubated at 37 ℃ under microaerobic conditions (50 mL/L O_2, 100 mL/L CO_2 and 850 mL/L N_2) for 3 to 5 d. A bacterial isolate was identified as *H pylori* according to typical Gram staining morphology, biochemical tests positive for urease and oxidase, and agglutination with commercial rabbit antibody against whole cell of the microbe. All *H pylori* isolates were stored at -70 ℃.

Preparation of DNA template

Genomic DNA of *H pylori* were extracted by the conventional phenol-chloroform method and DNase-free RNase treatment. The obtained DNA was dissolved in TE buffer, and its concentration and purity were determined by ultraviolet spectrophotometry.

Polymerase chain reaction

Oligonucleotide primers were designed to amplify the whole sequence of oipA gene from *H pylori* strain 26 695 based on the published corresponding genomic sequences. The sequence of oipA sense primer with an endonuclease site of *Bam*H I was 5'-CCGGATCCATGAAAAAAGCTCTCTTACT-3'. The sequence of oipA antisense primer with an endonuclease site of *Xho*I was 5'-CGCGGCTCGAGTTAATGTTTGTTTTTAAAGTT -3'. The total volume per PCR was 100 L containing 2.5 mol/L each dNTP, 500 nmol/L each of the two primers, 15 mol/L $MgCl_2$, 3.0 U Pfu-Taq polymerase, 100 ng DNA template and 1×PCR buffer (pH8.8). The parameters for PCR were at 94 ℃ for 4 min, ×1; at 94 ℃ for 60 s, at 52 ℃ for 50 s, at 72 ℃ for 60 s, ×30; then at 72 ℃ for 7 min, ×1. The results of PCR were observed under UV light after electrophoresis in 10 g. l-1 agarose pre-stained with ethidium bromide.

Construction of H pylori oipA recombinant plasmid

PCR products were digested by endonucleases *Bam*H I and *Xho*I, meanwhile pET32a(+) plasmid was cut by *Bam*H I and *Xho*I. After purification by the kits for purification of PCR products, these two fragments were ligated with cohesive ends. Then the recombinant plasmid was transformed into *E. coli* line Top10. The *E. coli* Top10 containing the recombinant plasmid was amplified in LB medium containing AMP. Clones were picked out randomly through blue/white screening. Finally the plasmids were extracted with a plasmid extraction kit according to the manufacturer's instructions and identified by PCR and digestion endonucleases of *Bam*H I and *Xho*I.

Sequence analysis

Top10 *E.coli* strains containing recombinant plasmid were sent to Shanghai GeneCore Biotechnologies Co. for DNA sequence analysis.

RESULTS

PCR amplification of oipA encoding sequence

Target fragments of *oipA* genes with expected sizes amplified from DNA template of *H pylori* stains are shown in Figure 1.

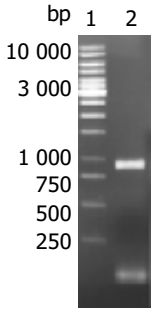

Figure 1 Amplification of human *H pylori oipA* gene by PCR. Lane 1: DNA markers (10 000, 8 000, 6 000, 5 000, 4 000, 3 500, 3 000, 2500, 2 000, 1 500, 1 000, 750, 500, 250 bp from top to bottom); Lane 2. *oipA* gene fragment (924 bp).

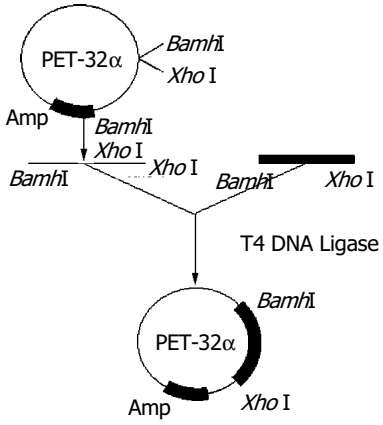

Figure 2 Construction technologic route of recombinant plasmids.

Construction and identification of recombinant plasmids

To construct the recombinant plasmid of *H pylori oipA*, purified PCR products were ligated with endonuclease-digested pET32a (+), and the recombinant was transformed into *E. coli* line Top10. White clones were picked out and confirmed by PCR and dual endonuclease digestion with *Bam*H I /*Xho*I. The technologic route is shown in Figure 2. Electrophoresis showed that a fragment of about 924 bp was released (Figure 3).

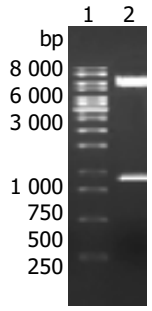

Figure 3 Dual endonuclease digestion identifications of recombinant plasmids. Lane 1: DNA markers (10 000, 8 000, 6 000, 5 000, 4 000, 3 500, 3 000, 2500, 2 000, 1500, 1 000, 750, 500, 250 bp from top to bottom). Lane 2: Digestion fragments of recombinant plasmids.

Sequence analysis

Samples were analyzed with an automatic sequence analyzer. Sequencing results are published in the GenBank. The accession number is AF479754. The identity was 95.32% against HP0638 and 95.02% against JHP0581, which was higher than the identity between HP0638 and JHP0581. HP0638 only was 918 bp while JHP0581 was 924 bp (6 bp TCTCTC at 37th site) and AF479754 also was 924 bp (6 bp CGAACA at 190th site).

DISCUSSION

How to prevent and eradicate *H pylori* infection is the core of the clinical therapy. The native immunity has little effect on it. Some experiments concluded that vaccine could decrease the infection, especial the incidence rate of piptic ulcer and gastric cancer. So an optimal vaccine can end the coexistence of human and *H pylori*. In recent 10 years, studies have gone deep in this wind of proteins, such as CagA, VacA, UreA, UreB, HSP, PldA, NAp.

Yamaoka deduced that Hp0638 encoding outer membrane protein oipA was the best candidate, because it had great antigen characteristics, and could increase the serum level of IL-8 also. Later studies showed that oipA was the only index that could differ duodenum ulcer from gastritis, respond to high location of *H pylori*, serious mucosal infiltration with neutrophil cells, and high level of IL-8. So far, there is no study on the oipA in our country. So we chose this subject. Our results showed that the identity was 95.32% against HP0638 and 95.02% against JHP0581, which was higher than the identity between HP0638 and JHP0581. The difference could be explained in two ways. One is that the strain we used was different from 26695 and J99. Different strains have different gene fragments, just as the difference between HP0638 and JHP0581. The other is that variation of the same strain induced the difference. Compared with JHP0581, AF479754 had the same base pairs. Only the insert site of 6 bp was different. It maybe one subtype of the same strain as 26695 or J99.

The value of the difference lay in three points. First, it contributes to the finding of new strains. Some surveys should be done in the whole country, to show the region characteristics of *H pylori*, and to confirm the main strains in our country. Second, it contributes to the analysis of the changes in pathogenicity and antigen activity, which are very important in elucidating the immune pathogeny. Third, it contributes to the development of new vaccines. The immunity study can provide some help to design the vaccine and optimal immune route. But a variety of strains would bring some difficulties to develop vaccines. So more work should be done to certify the pathogeny of *H pylori*, to develop effective vaccines for the eradication of *H pylori*.

ACKNOWLEDGEMENT

H pylori oipA sequence described in this paper was accepted by GenBank, GenBank accession number for it is AF479754.

REFERENCES

1 **Yamaoka Y**, Kodama T, Graham Y, Kashima K. Search for putative factors of Helicobacter pylori: the Low-Molecular-Weight (33-35K) antigen. *Dig Dis Sci* 1998; **43**: 1482-1487

2 **Shiesh SC**, Sheu BS, Yang HB, Tsao HJ, Lin XZ. Serologic response to lower-molecular-weight proteins of *H pylori* is related to clinical outcome of *H pylori* infection in Taiwan. *Dig Dis Sci* 2000; **45**: 781-788

3 **Yamaoka Y**, Kwon DH, Graham DY. A M(r) 34,000 proinflammatory outer membrane protein (oipA) of *Helicobacter pylori*. *Proc Natl Acad Sci U S A* 2000; **97**: 7533-7538

4 **Yamaoka Y**, Kikuchi S, el-Zimaity HM, Gutierrez O, Osato MS, Graham DY. Importance of *Helicobacter pylori* oipA in clinical presentation, gastric inflammation, and mucosal interleukin 8 production. *Gastroenterology* 2002; **123**: 414-424

5 **Ferrero RL**, Labigne A. *Helicobacter pylori* vaccine development in the post-genomic era: can in silico translate to *in vivo*. *Scand J Immunol* 2001; **53**: 443-448

Edited by Wang XL and Xu FM

PO Box 2345, Beijing 100023, China
Fax: +86-10-85381893
E-mail: wjg@wjgnet.com www.wjgnet.com

World J Gastroenterol 2004;10(21):3208-3211
World Journal of Gastroenterology
 ISSN 1007-9327

• BRIEF REPORTS •

Effect of hepatic glucose production on acute insulin resistance induced by lipid-infusion in awake rats

Ling Li, Gang-Yi Yang

Ling Li, Department of Clinical Biochemistry, Chongqing Medical University, Chongqing 400016, China
Gang-Yi Yang, Department of Endocrinology, The Second Affiliated Hospital, Chongqing Medical University, Chongqing 400010, China
Supported by the National Natural Science Foundation of China, No. 30270631, No. 30370671, Science Foundation of Chongqing Health Bureau, No. 99-3002 and Applied Basic Research Foundation of Chongqing Science and Technology Committee, No. 02-34 and Science Foundation of China Education Ministry, No. 2003-406
Correspondence to: Dr. Gang-Yi Yang, Department of Endocrinology, The Second Affiliated Hospital, Chongqing Medical University, Chongqing 400010, China. yanggangyi@hotmail.com
Telephone: +86-23-68486115 **Fax:** +86-23-68486115
Received: 2003-11-18 **Accepted:** 2003-12-08

Abstract

AIM: To explore the influence of hepatic glucose production on acute insulin resistance induced by a lipid infusion in awake rats.

METHODS: A hyperinsulinaemic-euglycaemic clamp was established in awake chronically catheterized rats. Two groups of rats were studied either with a 4-h intraarterial infusion of lipid/heparin or saline. Insulin-mediated peripheral and hepatic glucose metabolism was assessed by hyperinsulinaemic-euglycaemic clamp combined with [3-^{3}H]-glucose infusion.

RESULTS: During hyperinsulinaemic-euglycaemic clamp, there was a significant increase in plasma free fatty acid (FFA, from 741.9±50.6 to 2346.4±238.5 μmol/L, P<0.01) in lipid-infused group. The glucose infusion rates (GIR) in the lipid infusion rats, compared to control rats, were significantly reduced (200-240 min average: lipid infusion; 12.6±1.5 *vs* control; 34.0±1.6 mg/kg.min, P<0.01), declining to - 35% of the corresponding control values during the last time of the clamp (240 min: lipid infusion; 12.0±1.9 *vs* control; 34.7±1.7 mg/kg·min, P<0.0001). At the end of clamp study, the hepatic glucose production (HGP) in control rats was significantly suppressed (88%) from 19.0±4.5 (basal) to 2.3±0.9 mg/kg.min (P<0.01). The suppressive effect of insulin on HGP was significantly blunted in the lipid-infused rats (200-240 min: from 18.7±3.0 to 23.2±3.1 mg/kg·min (P<0.05). The rate of glucose disappearance (GRd) was a slight decrease in the lipid-infused rats compared with controls during the clamp.

CONCLUSION: These data suggest that lipid infusion could induces suppression of hepatic glucose production, impairs the abilities of insulin to suppress lipolysis and mediate glucose utilization in peripheral tissue. Therefore, we conclude that lipid-infusion induces an acute insulin resistance *in vivo*.

Li L, Yang GY. Effect of hepatic glucose production on acute insulin resistance induced by lipid-infusion in awake rats. *World J Gastroenterol* 2004; 10(21): 3208-3211
http://www.wjgnet.com/1007-9327/10/3208.asp

INTRODUCTION

Insulin resistance plays a primary role in the development of type 2 diabetes and is a feature of other disorders including obesity, dyslipidemias, hypertension, and cardiovascular disease[1]. The mechanism underlying the occurrence of insulin resistance is unknown but may be related to alterations in lipid metabolism[2]. More than 30 years ago, Randle and colleagues demonstrated that free fatty acids (FFA) competed with glucose for substrate oxidation in isolated rat heart and diaphragm muscle preparations and speculated that increased fat oxidation might cause insulin resistance associated with diabetes and obesity[3,4]. Subsequently, some studies have emphasized that, while an increase in circulating FFA during insulin clamp studies could promptly decrease the rate of carbohydrate oxidation, defective glucose uptake which could be detected 3-4 h after lipid infusion in humans[5,6]. Roden and Dresner have revealed that lipid/heparin infusions could increase plasma FFA levels, inhibit whole-body glucose disposal during hyper- and euglycemic-hyperinsulinemia and insulin-dependent glucose uptake by human forearm tissues *in vivo*, and also found that acute elevations in plasma fatty acids in humans resulted in decreased glucose transport activity, as reflected by decreased concentrations of intracellular glucose 6-phosphate and glucose[7,8]. Thus, it is possible that chronic elevation of endogenous FFAs contributes to insulin resistance in many pathophysiologic conditions in humans. Acute elevations in plasma FFA levels during a triglyceride emulsion infusion have also been shown to impaire insulin-mediated glucose uptake and to inhibit hepatic glucose production (HGP) in rats[9].

In the current study, we used a triglyceride and cholesterolester emulsion infusion in combination with hyperinsulinemic-euglycemic clamps to assess the impact of elevated FFA levels on HPG and overall insulin action.

MATERIALS AND METHODS

Preparation of animals

A total of 24 Male Sprague-Dawley rats weighing 250-300 g were housed in individual cages and subjected to an environmentally controlled room with a 12-h light/dark cycle, where they had free access to standard rat chow and water. Five to 7 d before the *in vivo* study, rats were anesthetized with an intraperitoneal injection of pentobarbital (50 mg/kg body mass). A silastic catheter (I.D. = 0.02 in) was inserted into the right internal jugular vein and extended to the level of the right atrium. The catheter for carotid artery was constructed with a short (25 mm) segment of polyethylene tubing (PE-10), connected to a 10-cm length of PE-50 by heating in a flame. The smaller end was advanced through the left carotid artery until its tip reached the aortic arch. The free ends of the catheters were attached to the long segments of steel tubing and tunneled subcutaneously around the side to the back of the neck where they were exteriorized through a skin incision and then securely anchored to the skin by a standard wounded clip. At the end of the procedure, catheters were flushed with 300 μL isotonic saline containing heparin (20 U/mL) and ampicillin (5 mg/mL) and then filled with a viscous solution of heparin (300 U) and 800 g/L polyvinylpyrollidone (PVP-10, Fisher, NJ) to prevent

refluxing of blood into the catheter lumen.

In vivo clamp studies

Animals were allowed at least five days to recover from the effects of surgery. All studies were conducted in the morning following a 12 to 14-h overnight fast. Throughout the study, the rats were allowed to move freely within the confines of a cage. One hour before clamping the venous and arterial lines were filled with a 9 g/L NaCl solution containing 10 IU/mL heparin. Three double lumen swivels, allowing separate fluid infusions, were connected to three peristaltic pumps. One arterial line was used for the infusion of a 250 g/L glucose solution at a variable rate and the other line was used for infusion of a mixture of (3-^{3}H)-glucose (Amersham Inc, USA), insulin and 150 mL/L lipid emulsion/heparin (20 U/mL). The venous blood sampling tube allowed frequent sampling and repletion of blood loss by means of fresh whole blood obtained from littermates.

At the start of euglycaemic clamp, continuous infusions of isotonic saline (control group, n = 12) and lipid emulsion with heparin (lipid group, n = 12) were maintained for 4 h at a rate 1.5 mL/h during prolonged euglycemic-hyperinsulinemic clamp studies. At t = 60 min, a bolus (6 μCi) and continuous infusion (0.2 μCi/min) of (3-^{3}H) glucose were initiated and continued throughout 3 h study. At t = 120 min, continuous infusions of insulin (4.8 mU/kg·min) and 250 g/L glucose were maintained for 2 h, 250 g/L glucose was adjusted every 5-10 min, maintaining basal plasma glucose concentrations (-5 mmol/L) during the insulin clamp studies. At t = 0, 120, 200, 220, 230 and 240 min, blood samples were collected for determination of plasma glucose, insulin, free fatty acid (FFA) and specific activity of tritiated glucose.

A separate set of 240 min lasting control clamp experiments without lipid infusion were performed to investigate the self-amplifying effect of long-term clamping on insulin-mediated glucose metabolism, since was glucose metabolism was not constant during a 240 min study[10]. The experimental procedure was identical to the lipid infusion clamps.

Analytical procedures

Plasma insulin was measured by radioimmunoassay (RIA) using rat insulin as standard (Linco Research, Inc. MO). Inter- and intra-assay variations of the insulin assay were 5.8% and 6.5%, respectively. Enzymatic colorimetric kits were used to determine plasma concentration of FFA (Wako Chemicals, Inc. VA). The inter- and intra-assay variations were 3.6% and 4.2%, respectively, during measurement of plasma FFA. Plasma for [3-^{3}H]-glucose radioactivity (150 μL) was deproteinized by barium hydroxide-zinc sulphate, the supernatant was evaporated to dryness at 60 ℃ to eliminate tritiated water and counted for 10 min in a beta scintillation counter.

Calculations

The rate of exogenous infused glucose to maintain euglycaemia during the steady-state period (from t = 180-240 min) was used for the assessment of insulin action. All calculations were carried out in this period when the total amount of glucose taken up by all tissues of the body was equal to the input of glucose into the body. During this steady-state, when the rate of glucose appearance (GRa) was equal to the rate of glucose disappearance (GRd), the glucose turnover rate, which equaled to GRa and GRd in mg/min, was calculated by dividing the [3-^{3}H]-glucose infusion rate (dpm/mg) by the steady-state value of glucose specific activity (dpm/mg). Under these conditions, the glucose turnover rate was equal to the sum of the rates of exogenous infused glucose and of hepatic glucose production (HGP). From this equation the rate of HGP was calculated. Since urinary glucose loss was not present, peripheral glucose uptake (PGU) was taken as glucose turnover rate which equaled to exogenous glucose infusion rate plus rate of HGP.

Statistical analysis

Data were presented with mean±SD. Comparisons between groups were made by the two-tailed Student's t test. All statistical analyses were performed using SPSS.

RESULTS

General characteristics of animals

There were no differences in the mean body mass between control and lipid-infusion rats. Basic plasma concentrations of glucose, insulin, and free fatty acids (FFA) were similar in the two groups (Table 1).

Table 1 General characteristics of control and lipid-infusion rats (n = 12, mean±SE)

Group	Control	Lipid-infusion
Body mass (g)	279±19	286±17
Fasting blood glucose (mmol/L)	5.2±0.1	5.1±0.2
Fasting plasma insulin (mU/L)	30.3±2.4	27.9±2.2
Fasting free fatty acids (μmol/L)	672.5±92.2	741.9±50.6

Effects of surgery

As expected, following surgery catheterized animals lost significant weight during the initial 24-h period, averaged 18±3 g. Following this catabolic stage they appeared well and normally active. Food intake was qualitatively normal, and average daily weight gain (-5g) closely resembled that of normal littermates that did not undergo surgery.

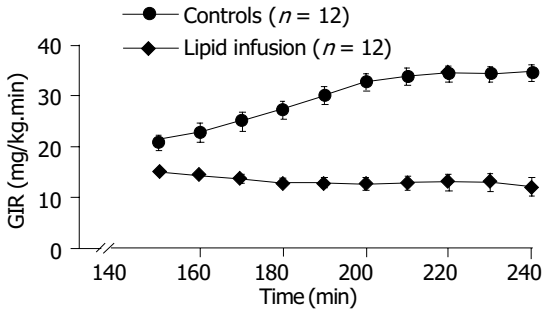

Figure 1 Time course of glucose infusion rate during hyperinsulinemic euglycemic clamping.

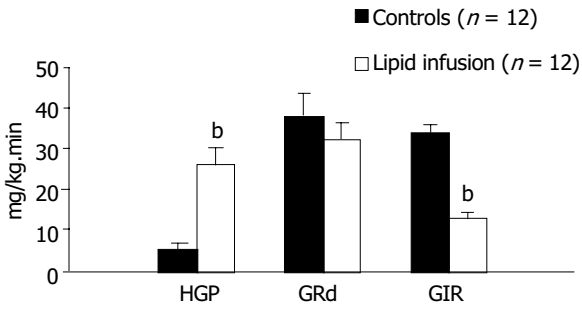

Figure 2 Steady-state hepatic glucose production, glucose disappearance rate, glucose infusion rate during hyperinsulinaemic-euglycaemic clamp studies in control and lipid-infused rats. ^bP<0.01, *vs* control.

Insulin clamp studies

A lipid infusion of 4 h at a rate of 1 mL/h was used to examine the effect on plasma insulin, FFA, peripheral glucose uptake

Table 2 Plasma parameters and glucose turnover data in control and lipid-infusion rats during euglycemic hyperinsulinemic claming (mean±SE)

Group	Basal	Clamping time (min)				
		120	200	220	230	240
			Glucose (mmol/L)			
Control (n = 12)	5.2±0.1	5.3±0.1	5.0±0.2	5.2±0.1	5.2±0.2	5.4±0.2
Lipid (n = 12)	5.1±0.2	5.3±0.2	5.2±0.2	5.3±0.2	5.5±0.2	5.5±0.2
			FFA (μmol/L)			
Control (n = 12)	672.5±92.2	642.3±104.8	240.6±20.9	221.3±27.4	201.8±29.8	183.1±21.4
Lipid (n = 12)	741.9±50.6	2807.2±348.8[bd]	3086.9±495.2[bd]	2518.8±416.7[bd]	2241.2±431.0[bd]	2346.4±238.5[bd]
			Insulin (mU/L)			
Control (n = 12)	30.3±2.4	34.7±6.4	89.5±7.9	90.7±7.4	88.3±5.9	101.3±6.3
Lipid (n = 12)	27.9±2.2	31.4±3.3	84.2±6.7	93.3±8.9	103.5±16.3	104.5±14.8
			GIR (mg/kg· min)			
Controls (n=12)	0		32.8±1.7	34.4±1.6	34.4±1.6	34.7±1.7
Lipid (n = 12)	0		12.7±1.3[b]	12.9±1.6[b]	12.9±1.8[b]	12.0±1.9[b]
			GRd (mg/kg·min)			
Controls (n = 12)		19.0±4.5	43.1±6.1[d]	40.1±6.7[d]	35.5±6.8[d]	33.2±3.2[d]
Lipid (n = 12)		18.7±3.0	36.3±3.1[d]	38.3±4.4[d]	32.4±4.5[d]	35.1±3.9[d]
			HGP (mg/kg·min)			
Controls (n = 12)		19.0±4.5	14.2±4.9[c]	10.2±4.4[d]	3.1±1.9[d]	2.3±0.9[d]
Lipid (n = 12)		18.7±3.0	23.4±4.3[bc]	25.3±3.7[bd]	21.5±3.5[b]	23.2±3.1[bd]

FFA: free fatty acids. GIR: glucose infusion rate. GRd: glucose disappearance rate. HGP: hepatic glucose production. [a]P<0.05; [b]P<0.01 *vs* control; [c]P<0.05; [d]P<0.01 *vs* Basal. The basal values of HGP were determined at 120 min.

and hepatic glucose production. During the euglycemic-hyperinsulinemic clamps blood glucose concentrations remained constant compared to the basal levels and were not different between control and lipid infusion studies. Plasma insulin concentrations increased similarly to ~100 mU/L in both studies (Table 2). The coefficients of variation in plasma glucose and insulin levels were 4.8 and 7.6 % , respectively, in all studies. In the control study the plasma concentration of FFAs dropped by ~65% once the euglycemic clamp was started, but it increased approximately fourfold (from 741.9±50.6 to 2346.4±238.5 μmol/L, P<0.01) within 120 min of hyperinsulinemic clamp in the lipid-infused group (Table 2). The time course of the glucose infusion rate (GIR) during insulin clamp is shown in Figure 1. The GIR in lipid infusion rats, compared to control rats, was significantly reduced (200-240 min average: lipid infusion; 12.6±1.5 *vs* control; 34.0±1.6 mg/kg·min, P<0.01, Table 2 and Figure 2), declining to ~35% of the corresponding control values during the last time of the clamp (240 min: lipid infusion; 12.0±1.9 *vs* control; 34.7±1.7 mg/kg·min, P<0.0001, Figure 1). After a 14-h fast there was no significant difference in HGP between the two groups (19.0±4.5 *vs* 18.7±3.0 mg/kg·min in control and lipid-infused rats, respectively). At the end of hyperinsulinemic-euglycemic clamp study, the HGP in control rats was significantly suppressed (88%) from 19.0±4.5 (basal) to 2.3±0.9 mg/kg·min (P<0.01, Table 2). The suppressive effect of insulin on HGP was significantly blunted in lipid-infused rats (180-240 min: lipid infusion; from 18.7±3.0 to 23.2±3.1 mg/kg·min P<0.05, Table 2). The time courses of HGP for controls and lipid-infused rats are shown in Table 2. During the clamp, the GRd was significant increased compared with basal values. Although the GRd had no significant difference between the two groups, there was a slight decrease in lipid-infused rats compared with controls (Table 2). Figure 2 shows the average values of HGP, GRd and GIR during the clamp in control and lipid-infused rats.

DISCUSSION

Obesity is associated with insulin resistance and hyperinsulinemia, two important cardiovascular risk factors[11]. What remains uncertain is how obesity produces insulin resistance and hyperinsulinemia. It has recently become clear, however, that FFA plays a pivotal role in this process. Although there are a number of studies on this subject, the precise mechanisms of FFA effect on insulin action are not completely understood. In the present study we examined the effect of a 4-h lipid infusion on *in vivo* insulin action in conscious rats, by the hyperinsulinaemic-euglycaemic clamp technique, in combination with a continuous infusion of [3-^{3}H]-glucose. This method is considered to be the most suitable for the measurement of *in vivo* insulin. In our hyperinsulinemic clamping, insulin infusion increased plasma insulin levels to an approximate three-fold over basal insulin level, whereas blood glucose was clamped at approximately 5.3 mmol/L in the control and lipid infusion groups. Plasma FFA concentrations were suppressed by approximately ~65% during clamps in the control group. But in lipid infusion rats, the FFA levels had a rapid increase more than 3.8-fold over basal levels and the increase was maintained to the end of hyperinsulinemic clamp, suggesting that lipid infusion impaired the antilipolytic action of insulin and promoted the release of fatty acids from adipocytes or infused lipid. It is widely known that elevated FFA levels could exert a deleterious effect on insulin's overall actions, and this has been demonstrated in both animals and humans[12]. The mechanisms underlying FFA-induced insulin resistance are not very clear, but elevated plasma levels of FFA produced at least two distinct biochemical defects: inhibition of insulin stimulated glucose transport and/or phosphorylation, and inhibition of muscle glycogen systhase activity[13].

In the attempt to better our understanding of the pathophysiology of lipid-induced insulin resistance, we examined the effect of lipid infusions on HGP. We found that HGP was suppressed by ~88% in the controls during hyperinsulinaemic-euglycaemic clamp, suggesting the impact of insulin on the suppression of endogenous glucose production. However, HGP was not significantly suppressed in lipid-infused rats. Thus, lipid infusion elevated the levels of circulating FFA and elevated FFA levels interfered with insulin's ability to inhibit hepatic glucose production. The increased hepatic glucose production in response to lipid infusion suggested that an experimental

elevation of circulating FFA levels could lead to hepatic insulin resistance. On the other hand, during insulin clamp glucose infusion rates (GIR), compared to control rats, were significantly reduced to -35% of the corresponding control values during the last time of the clamp. At clamping steady state, peripheral glucose uptake was equal to the sum of the rates of exogenous infused glucose (GIR) and hepatic glucose production (HGP). If HGP was completely suppressed, peripheral glucose uptake would equal to GIR (in controls). But, HGP was not significantly suppressed in lipid-infused rats, so peripheral glucose uptake was equal to GRa, which equaled to HGP plus GIR. Total glucose uptake is the sum of glucose removal by insulin-dependent as well as insulin-independent tissues. In the present study we found there was a slight decrease in GRa in lipid infusion groups, although the data did not reach statistical significance. Nonetheless, the trend is obvious since the brain and splanchnic tissues use glucose in an insulin-independent manner, roughly 750 g/L of total glucose utilization is considered to be insulin-independent in fasting condition. Thus, this might indicate that 4 h of lipid infusion induced a partial defect in insulin-stimulated peripheral glucose uptake, consistent with previous *in vivo* studies by Kim *et al*.[14]. Considering the absence of HGP-suppressing effect of insulin under lipid infusion condition, we concluded that an experimental elevation of circulating FFA levels by lipid/heparin infusions could lead to peripheral and hepatic insulin resistance. The mechanism of lipid-induced insulin resistance remains poorly understood and may involve different IRS-1-associated PI3-kinase activation[15], and the activity of IκB kinase-β (Ikk-β, a known serine kinase)[14,16].

In summary, the current studies showed that infusion of lipid emulsions with heparin to acutely raise plasma fatty acid concentrations could impaire the ability of insulin to stimulate overall body glucose disposal and also interfered with insulin's ability to inhibit hepatic glucose production. Thus, we propose that a sustained increase in circulating FFA causes a hepatic insulin resistance, and may lead to a partial defect in insulin-stimulated peripheral glucose uptake, which can be attributed to lipotoxic effect on insulin action.

REFERENCES

1 **Reaven GM.** Role of insulin resistance in human disease. *Diabetes* 1988; **37**: 1595-1607

2 **Boden G.** Role of fatty acids in the pathogenesis of insulin resistance and NIDDM. *Diabetes* 1997; **46**: 3-10

3 **Randle PJ,** Garland PB, Newsholme EA, Hales CN. The glucose fatty acid cycle in obesity and maturity onset diabetes mellitus. *Ann N Y Acad Sci* 1965; **131**: 324-333

4 **Randle PJ,** Garland PB, Hales CN, Newsholme EA.The glucose fatty-acid cycle: its role in insulin sensitivity and the metabolic disturbances of diabetes mellitus. *Lancet* 1963; **1**: 785-789

5 **Boden G,** Jadali F, White J, Liang Y, Mozzdi M, Chen X, Coleman E, Smith C. Effects of fat on insulin-stimulated carbohydrate metabolism in normal men. *J Clin Invest* 1991; **88**: 960-966

6 **Kelley DE,** Mokan M, Simoneau JA, Mandarino LJ. Interaction between glucose and free fatty acid metabolism in human skeletal muscle. *J Clin Invest* 1993; **92**: 91-98

7 **Roden M,** Price TB, Perseghin G, Petersen KF, Rothman DL, Cline GW, Shulman GI. Mechanism of free fatty acid-induced insulin resistance in humans. *J Clin Invest* 1996; **97**: 2859-2865

8 **Dresner A,** Laurent D, Marcucci M, Griffin ME, Dufour S, Cline GW, Slezak LA, Andersen DK, Hundal RS, Rothman DL, Petersen KF, Shulman GI. Effects of free fatty acids on glucose transport and IRS-1-associated phosphatidylinositol 3-kinase activity. *J Clin Invest* 1999; **103**: 253-259

9 **Griffin ME,** Marcucci MJ, Cline GW, Bell K, Barucci N, Lee D, Goodyear LJ, Kraegen EW, White MF, Shulman GI. Free fatty acid-induced insulin resistance is associated with activation of protein kinase C theta and alterations in the insulin signaling cascade. *Diabetes* 1999; **48**: 1270-1274

10 **Koopmans SJ,** van Mansfeld ADM, Jansz HS, Krans HMJ, Radder JK, Frolich M, de Boer SF, Kreutter DK, Andrews GC, Maassen JA. Amylin-induced *in vivo* insulin resistance in conscious rats: the liver is more sensitive to amylin than peripheral tissues. *Diabetologia* 1991; **34**: 218-224

11 **Fontbonne AM,** Eschwege EM. Insulin and cardiovascular disease. Paris prospective study. *Diabetes Care* 1991; **14**: 461-469

12 **Hevener AL,** Reichart D, Janez A, Olefsky J. Thiazolidinedione treatment prevents free fatty acid-induced insulin resistance in male wistar rats. *Diabetes* 2001; **50**: 2316-2322

13 **Boden G**. Free fatty acids (FFA), a link between obesity and insulin resistance. *Front Biosci* 1998; **15**: d169-175

14 **Kim JK,** Kim YJ, Fillmore JJ, Chen Y, Moore I, Lee J, Yuan M, Li ZW, Karin M, Perret P, Shoelson SE, Shulman GI. Prevention of fat-induced insulin resistance by salicylate. *J Clin Invest* 2001; **108**: 437-446

15 **Yu C,** Chen Y, Cline GW, Zhang DY, Zong HH, Wang YL, Bergeron R, Kim JK, Cushman SW, Cooney GJ, Atcheson B, White MF, Kraegen EW, Shulman GI. Mechanism by which fatty acids inhibit insulin activation of insulin receptor substrate-1 (IRS-1)-associated phosphatidylinositol 3-kinase activity in muscle. *J Biol Chem* 2002; **277**: 50230-50236

16 **Yin MJ,** Yamamoto Y, Gaynor RB. The anti-inflammatory agents aspirin and salicylate inhibit the activity of IκB kinase-β. *Nature* 1998; **396**: 77-80

Edited by Zhang JZ and Wang XL **Proofread by** Xu FM

PO Box 2345, Beijing 100023, China
Fax: +86-10-85381893
E-mail: wjg@wjgnet.com www.wjgnet.com

World J Gastroenterol 2004;10(21):3212-3214
World Journal of Gastroenterology
 ISSN 1007-9327

• BRIEF REPORTS •

Chronic gastritis rat model and role of inducing factors

Zun Xiang, Jian-Min Si, Huai-De Huang

Zun Xiang, Huai-De Huang, Department of Gastroenterology, First Affiliated Hospital, College of Medicine, Zhejiang University, Hangzhou 310003, Zhejiang Province, China
Jian-Min Si, Department of Gastroenterology, Sir Run Run Shaw Hospital, College of Medicine, Zhejiang University, Hangzhou 310016, Zhejiang Province, China
Correspondence to: Zun Xiang, Department of Gastroenterology, First Affiliated Hospital, College of Medicine, Zhejiang University, Hangzhou 310003, Zhejiang Province, China. xianghr@hotmail.com
Telephone: +86-571-87236863 **Fax:** +86-571-87236618
Received: 2003-12-28 **Accepted:** 2004-02-01

Abstract

AIM: To establish an experimental animal model of chronic gastritis in a short term and to investigate the effects of several potential inflammation-inducing factors on rat gastric mucosa.

METHODS: Twenty-four healthy, male SD rats were treated with intragastric administration of 600 mL/L alcohol, 20 mmol/L sodium deoxycholate and 0.5 g/L ammonia (factor A), forage containing low levels of vitamins (factor B), and/or indomethacin (factor C), according to an $L_8(2^7)$ orthogonal design. After 12 wk, gastric antral and body mucosae were pathologically examined.

RESULTS: Chronic gastritis model was successfully induced in rats treated with factor A for 12 wk. After the treatment of animals, the gastric mucosal inflammation was significantly different from that in controls, and the number of pyloric glands at antrum and parietal cells at body were obviously reduced ($P<0.01$). Indomethacin induced gastritis but without atrophy, and short-term vitamin deficiency failed to induce chronic gastritis and gastric atrophy. In addition, indomethacin and vitamin deficiency had no synergistic effect in inducing gastritis with the factor A. No atypical hyperplasia and intestinal metaplasia in the gastric antrum and body were observed in all rats studied.

CONCLUSION: Combined intragastric administration of 600 mL/L alcohol, 20 mmol/L sodium deoxycholate and 0.5 g/L ammonia induces chronic gastritis and gastric atrophy in rats. Indomethacin induces chronic gastritis only. The long-term roles of these factors in gastric inflammation and carcinogenesis need to be further elucidated.

Xiang Z, Si JM, Huang HD. Chronic gastritis rat model and role of inducing factors. *World J Gastroenterol* 2004; 10 (21): 3212-3214
http://www.wjgnet.com/1007-9327/10/3212.asp

INTRODUCTION

Chronic gastritis including chronic atrophic gastritis (CAG) is common and CAG is a precancer lesion. It is very important to study the etiology of chronic gastritis, especially CAG. We established an experimental animal model of chronic gastritis and investigated the effects of inducing factors on gastric mucosa of rats.

MATERIALS AND METHODS

Animals

Twenty-four healthy, male SD rats weighing 270-290 g were involved in this study. Animals were housed in a controlled environment with a 12/12 h light /dark cycle. The care and handling of the animals were in accordance with the National Institutes of Health Guidelines for the Care and Use of Laboratory Animals.

Chemicals and experimental design

Pure ammonia (Wujin Chemicals Factory,Jiangsu, China) was used to be diluted to a 0.5 g/L solution. Pure alcohol (Yixing Nanxin Chemicals Factory, Jiangsu, China) was diluted to a 60% solution and sodium deoxycholate (DOC-Na) (SERVA Company) was dissolved into sterilized water to make a 20 mmol/L solution. A mixture of carboxymethyl cellulose containing 0.5 mg/mL indomethacin was dispensed.

In this study, an $L_8(2^7)$ orthogonal test was used and comprised 8 testing members, 3 treatment factors (A,B and C) and 2 levels (with or without treatment). Triple tests were conducted and 24 rats were used. Factor A: 0.5 g/L ammonia solution was used as drinking water everyday, intragastric administration of 2 mL of 600 mL/L alcohol was given twice in fasting per week and intragastric administration of 2 mL of 20 mmol/L DOC-Na without fasting everyday but intragastric administration twice in fasting per week was also given. Factor B: forage containing less vitamin was given. Factor C: intragastric administration with 1mg indomethacin was given everyday. All above doses were used for each rat, the testing period was 12 wk. The control rats had free access to normal rat chow and water.

Histology study

All rats were sacrificed with luxation of cervical vertebra and their stomachs were removed after 12 wk. Gastric mucosa for histological examinations was cut along the lesser curvature from the lower esophagus to the upper duodenum. Samples were immersed in buffered 40 g/L formaldehyde and embedded in paraffin. Paraffin sections were sliced, mounted on glass slides and stained with hematoxylin and eosin (H&E) for histological study. Inflammation grades of gastric antrum and body were based on semi-quantity. Four inflammation grades were classified in accordance with pathological diagnosis of chronic gastritis set up on Huston symposium in 1994[1]. Four typical signs of inflammation grades were described: 0: no inflammation, the presence of few leukocytes infiltration in gastric mucosa; 1: mild inflammation, a few leukocytes infiltration in upper mucosa or at bottom of gastric glands; 2: moderate inflammation, a large number of leukocytes infiltration in total mucosa; 3: severe inflammation, leukocytes infiltration in heaps in total mucosa. Each inflammation grading result was based on an average of grades of 10 fields under microscope. Thickness of lamina propria mucosa of the stomach was measured at given points which was 150±10 μm away from the boundary of forestomach in body while 150±10 μm away from pyloric ring in antrum. Percentage ratio of pyloric gland area to total lamina propria area at gastric antrum was 100 μm to 200 μm away from pyloric ring. Also 10 intact oxyntic glands were observed at the above points in gastric body, parietal cell number in each gland and the median number were calculated.

Statistical analysis

All data were analyzed by using variance analysis of an $L_8(2^7)$ orthogonal test. $P<0.05$ was considered statistically significant.

RESULTS

Effect of inflammation grades on gastric mucosa

At antrum, inflammation grade of gastric mucosa induced by a single factor A was 1.50, 1.67 and 1.75 respectively on three repeated tests. It was significantly higher than that of the control. The grade induced by factor C also was higher than that of the control ($P<0.01$, Table1, Figure1). However, combined treatment of factors A+B+C, A+B, A+C had no effects on enhancing inflammation grades induced by a single factor A. In addition, a single factor B had no effect on inducing gastritis and inflammation grades induced by combined treatment of factors B+C had no difference from that induced by a single factor C (Table 1). The results were similar at gastric body (Table 1, Figure 2).

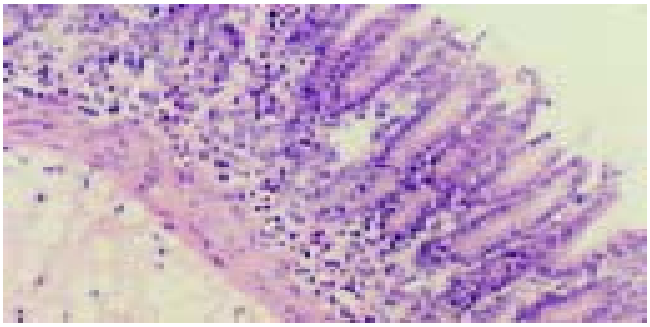

Figure 1 Severe infiltration of inflammatory cells, decreased thickness of lamina propria and lessened pyloric glands in gastric antrum of rats with gastritis induced by factor A. The results induced by factors A+B+C, A+C, A+B were similar. HE stain×100. Factor A: Combined intragastric treatments of 600 mL/L alcohol, 20 mmol/L sodium deoxycholate and 0.5 g/L ammonia;Factor B: Treatment of forage containing low levels of vitamins; Factor C: Treatment of indomethacin.

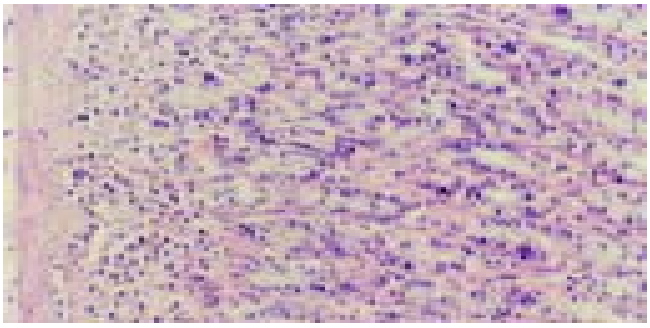

Figure 2 Severe infiltration of inflammatory cells, decreased parietal cells in oxyntic glands in gastric body of rats with gastritis induced by factor A with no changes in thickness of lamina propria. The results induced by factors A+B+C, A+C, A+B were similar. HE stain×100. Factor A: Combined intragastric treatments of 600 mL/L alcohol, 20 mmol/L sodium deoxycholate and 0.5 g/L ammonia; Factor B: Treatment of forage containing low levels of vitamins; Factor C: Treatment of indomethacin.

Effect of glandular atrophy on gastric mucosa

At antrum, the lamina propria mucosa of rats induced by single factor A was much thinner than that of the control ($P<0.01$, Table 2) while the lamina propria of rats induced by single factor B or C had no difference from that of the control and there was no statistical difference between that of rats induced by factors A+B+C, A+B, A+C and that of rats induced by single factor A (Table 2). By calculating the percentage ratio of pyloric gland area to total lamina propria area at antrum, we found the results were similar (Table 3, Figure 1). In addition, we found that although factors A, B or C had no effect on inducing the changes of lamina propria in gastric body, factor A induced a decrease of parietal cells in oxyntic glands. However, combined treatment of A+B+C, A+B, A+C had no synergistic effect with single factor A (Tables 2, 3 and Figure 2). Also no atypical hyperplasia and intestinal metaplasia in mucosa of gastric body and antrum in rats were observed in this study.

Table 1 $L_8(2^7)$ orthogonal test results of inflammation grades in stomachs of rats

Treatment factors	Triple orthogonal tests results					
	Antrum			Body		
A+B+C	2.10	1.83	2.00	1.67	1.60	1.64
A+B	1.67	1.50	1.63	1.30	1.40	1.38
A+C	2.10	2.10	1.83	1.67	1.64	1.67
A	1.50[b]	1.67[b]	1.75[b]	1.29[b]	1.25[b]	1.40[b]
B+C	1.17	1.25	1.00	1.00	1.08	0.90
B	0.75	0.75	0.83	0.60	0.67	0.63
C	1.25[d]	1.17[d]	1.00[d]	0.88[d]	1.00[d]	1.10[d]
Control	0.75	0.83	0.75	0.60	0.64	0.67

[b]$P<0.01$ *vs* the control, [d]$P<0.01$ *vs* the control. Factor A: Combined intragastric treatments of 60% alcohol, 20 mmol/L sodium deoxycholate and 0.5 g/L ammonia; Factor B: Treatment of forage containing low levels of vitamins; Factor C: Treatment of indomethacin.

Table 2 $L_8(2^7)$ orthogonal test results of thickness of lamina propria in stomachs of rats

Treatment factors	Triple orthogonal tests results (μm)					
	Antrum			Body		
A+B+C	40.0	38.5	36.5	310.0	290.0	305.0
A+B	43.5	41.5	45.0	383.5	283.5	338.5
A+C	46.5	36.5	36.5	311.5	313.5	325.0
A	43.5[b]	41.5[b]	45.0[b]	358.5	331.5	330.0
B+C	70.0	72.0	66.5	308.5	328.5	341.5
B	65.0	75.0	68.5	333.8	333.5	326.5
C	71.5	71.0	75.0	333.5	325.0	311.5
Control	66.5	71.5	75.0	300.0	310.0	313.5

[b]$P<0.01$ *vs* the control. Factor A: Combined intragastric treatments of 600 mL/L alcohol, 20 mmol/L sodium deoxycholate and 0.5 g/L ammonia; Factor B: Treatment of forage containing low levels of vitamins; Factor C: Treatment of indomethacin.

Table 3 $L_8(2^7)$ orthogonal test results of changes of glands in gastric lamina propria of rats

Treatment factors	Triple orthogonal tests results					
	Percentage ratio of pyloric gland area to total lamina propria at gastric antrum			Parietal cell number in observed oxyntic glands in gastric body		
A+B+C	0.2188	0.3750	0.3125	12	10	13
A+B	0.3750	0.3000	0.3750	14	12	14
A+C	0.3650	0.3125	0.3333	11	11	12
A	0.3438[b]	0.3750[b]	0.3230[b]	14[b]	12[b]	15[b]
B+C	0.5688	0.5150	0.5725	28	23	25
B	0.5385	0.5625	0.5313	25	26	23
C	0.5750	0.5840	0.6500	26	23	27
Control	0.5250	0.6050	0.5893	25	29	23

[b]$P<0.01$ *vs* the control. Factor A: Combined intragastric treatments of 600 mL/L alcohol, 20 mmol/L sodium deoxycholate and 0.5 g/L ammonia; Factor B: Treatment of forage containing low levels of vitamins; Factor C: Treatment of indomethacin.

DISCUSSION

CAG has been considered a precancerous disease[2], it is essential to establish a stable, economic and effective experimental animal model of chronic gastritis including CAG for further study on gastritis. Previous studies showed that three methods were practicable to establish experimental models. (1) Biologically induced animal models. Animals such as rats, cats were infected with *Helicobacter pylori* (*H pylori*) and an experimental model was induced. However, just some of these animals could be induced and models were unstable and it was time-consuming. (2) Animal models induced by physiochemical injury. Models of chronic gastritis were induced by single factors such as alcohol or sodium deoxycholate or ammonia or X-ray irradiation, but the models were unstable and atypical. (3) Immunologically induced animal models. Models of CAG were induced by hypodermic injection with homogeneic, xenogeneic or isogeneic stomach antigens,but the procedure was complicated and expensive, the effects were unstable[3-14].

The shortcomings of the above methods have limited further studies on etiology of CAG. However, according to previous studies, we concluded that factors such as infection of *H pylori*, excessive drinking, reflux of duodenal juice, long-term intake of nonsteroid drugs, malnutrition that could induce continuous gastritis, were considered to be the etiology of CAG[15-25]. In our study we tried to administer 600 mL/L alcohol to injure gastric mucosa, 20 mmol/L sodium deoxycholate (DOC-Na) as a simulator to reflux of duodenal juice, 0.5 g/L indomethacin to interfere with synthesis of prostaglandin (PG) that was proved to be effective for preventing gastric mucosa from injury and 0.5 g/L ammonia as a simulator to *H pylori* to induce continuous gastritis in rats. Finally we found that combined administration of 600 mL/L alcohol, 20 mmol/L DOC-Na and 0.5 g/L ammonia for 12 wk could induce an animal model of chronic gastritis with some features of early CAG especially in antrum. Furthermore, our study showed that atrophy of gastric mucosa in rats also developed from gastric antrum to body. It proved once again that excessive drinking, reflux of bile and infection of *H pylori* played a vital role in inducing chronic gastric mucosal inflammation. It also suggests that the above factors may probably induce CAG. However, we found that indomethacin induced only chronic gastritis but not atrophy of glands in mucosa and had no effect on enhancing glandular atrophy induced by alcohol, ammonia and DOC-Na. In addition, single treatment of forage containing few vitamins in our study could not induce chronic gastritis and glandular atrophy, it is perhaps because the testing duration was too short. The long-term roles of these factors in gastric inflammation and atrophy need to be further elucidated.

In conclusion, an animal model of chronic gastritis can be established by combined intragastric administration with 60% alcohol, 20 mmol/L sodium deoxycholate and 0.5 g/L ammonia. These factors play a vital role in etiology of chronic atrophic gastritis.

REFERENCES

1 **Dixon MF**, Genta RM, Yardley JH, Correa P. Classification and grading of gastritis. The updated sydney system. International workshop on the histopathology of gastritis, houstou 1994. *Am J Surg Pathol* 1996; **20**: 1161-1181

2 **Kapadia CR**. Gastric atrophy, metaplasia, and dysplasia: a clinical perspective. *J Clin Gastroenterol* 2003; **36**(5 Suppl): S29-36

3 **Hu PJ**, Zeng ZR, Lin HL, Chen MH, Chen W, Peng XZ. Effect of eradication of *Helicobacter pylori* on development and reversion of atrophic gastritis in animal study. *Zhonghua Xiaohua Zazhi* 2000; **20**: 155-158

4 **Oda T**, Marakami K, Nishizono A, Kodama M, Nasu M, Fujioka T. Long-term *Helicobacter pylori* infection in Japanese monkeys induces atrophic gastritis and accumulation of mutations in the p53 tumor suppressor gene. *Helicobacter* 2002; **7**: 143-151

5 **Kinoshita K**, Watanabe H, Ando Y, Katayama M, Yamamoto H, Hirano N, Yoshikuni S, Yamamoto T. Effects of subtotal resection of the fundus on development of intestinal metaplasia induced by X-ray irradiation in Donryu rats. *Pathol Int* 2000; **50**: 879-883

6 **Kawano S**, Tsujii M, Fusamoto H, Sato N, Kamada T. Chronic effect of intragastric ammonia on gastric mucosal structures in rats. *Dig Dis Sci* 1991; **36**: 33-38

7 **Watanabe H**, Hirose F, Takizawa S, Terada Y, Fujii I. Morphological and biochemical changes in the gastric mucosa of A/HEJ mice injected with a xenogeneic stomach antigen. *Acta Pathol Jpn* 1977; **27**: 869-876

8 **Watanabe H**, Uesaka T, Kido S, Ishimura Y, Shiraki K, Kuramoto K, Hirata S, Shoji S, Katoh O, Fujimoto N. Gastric tumor induction by 1, 2-dimethylhydrazine in Wistar rats with intestinal metaplasia caused by X-irradiation. *Jpn J Cancer Res* 1999; **90**: 1207-1211

9 **Eaton KA**, Radin MJ, Krakowka S. An animal model of gastric ulcer due to bacterial gastritis in mice. *Vet Pathol* 1995; **32:** 489-497

10 **Lee A**, Chen M, Coltro N, O'Rourke J, Hazell S, Hu P, Li Y. Long term infection of the gastric mucosa with *Helicobacter species* does induce atrophic gastritis in an animal model of *Helicobacter pylori* infection. *Zentralbl Bakteriol* 1993; **280**: 38-50

11 **Wang X**, Willen R, Svensson M, Ljungh A, Wadstrom T. Two – year follow-up of *Helicobacter pylori* infection in C57BL/6 and Balb/cA mice. *APMIS* 2003; **111**: 514-522

12 **Ikeno T**, Ota H, Sugiyama A, Ishida K, Katsuyama T, Genta RN, Kawasaki S. *Helicobacter pylori*-induced chronic active gastritis, intestinal metaplasia, and gastric ulcer in Mongolian gerbils. *Am J Pathol* 1999; **154**: 951-960

13 **Kim DH**, Kim SW, Song YJ, Oh TY, Han SU, Kim YB, Joo HJ, Cho YK, Kim DY, Cho SW, Kim MW, Kim JH, Hahm KB. Long-term evaluation of mice model infected with *Helicobacter pylori*: focus on gastric pathology including gastric cancer. *Aliment Pharmacol Ther* 2003; **18**(Suppl 1): 14-23

14 **Bergin IL**, Sheppard BJ, Fox JG. *Helicobacter pylori* infection and high dietary salt independently induce atrophic gastritis and intestinal metaplasia in commercially available outbred Mongolian gerbils. *Dig Dis Sci* 2003; **48**: 475-485

15 **Kamada T**, Haruma K, Hata J, Kusunoki H, Sasaki A, Ito M, Tanaka S, Yoshihara M. The long-term effect of *Helicobacter pylori* eradication therapy on symptoms in dyspeptic patients with fundic atrophic gastritis. *Aliment Pharmacol Ther* 2003; **18**: 245-252

16 **Kearney DJ**, Ritchie K, Peacock JS. Gastric-juice ammonia assay for diagnosis of *Helicobacter pylori* infection and the relationship of ammonia concentration to gastritis severity. *Am J Gastroenterol* 2000; **95**: 3399-3403

17 **Huizenga JR**, Vissink A, Kuipers EJ, Gips CH. *Helicobacter pylori* and ammonia concentrations of whole, parotid and submandibular/sublingual saliva. *Clin Oral Investig* 1999; **3**: 84-87

18 **Bujanda L**. The effects of alcohol consumption upon the gastrointestinal tract. *Am J Gastroenterol* 2000; **95**: 3374-3382

19 **Thuluvath P**, Wojno KJ, Yardley JH, Mezey E. Effects of *Helicobacter pylori* infection and gastritis on gastric alcohol dehydrogenase activity. *Alcohol Clin Exp Res* 1994; **18**: 795-798

20 **Brown AS**, Fiatarone JR, Wood P, Bennett MK, Kelly PJ, Rawlins MD, Day CP, James OF. The effect of gastritis on human gastric alcohol dehydrogenase activity and ethanol metabolism. *Aliment Pharmacol Ther* 1995; **9**: 57-61

21 **Bielecki K**, Zawadzki JJ. Observations on gastric histology, endoscopy appearance and *Helicobacter pylori* after corrective surgery for bile reflux gastritis. *Mater Med Pol* 1994; **26**: 9-12

22 **Dixon MF**, Mapstone NP, Neville PM, Moayyedi P, Axon AT. Bile reflux gastritis and intestinal metaplasia at the cardia. *Gut* 2002; **51**: 351-355

23 **Ito Y**, Suzuki K, Ichino N, Imai H, Sakaguchi H, Hokama M, Nishii M, Nakano H. The risk of *Helicobacter pylori* infection and atrophic gastritis from food and drink intake: a cross-sectional study in Hokkaido, Japan. *Asian Pac J Cancer Prev* 2000; **1**: 147-156

24 **Kitahara F**, Shimazaki R, Sato T, Kojima Y, Morozumi A, Fujino MA. Severe atrophic gastritis with *Helicobacter pylori* infection and gastric cancer. *Gastric Cancer* 1998; **1**: 118-124

25 **Ohkuma K**, Okada M, Murayama H, Seo M, Maeda K, Kanda M, Okabe N. Association of *Helicobacter pylori* infection with atrophic gastritis and intestinal metaplasia. *J Gastroenterol Hepatol* 2000; **15**: 1105-1112

Edited by Wang XL and Zhu LH **Proofread by** Xu FM

PO Box 2345, Beijing 100023, China
Fax: +86-10-85381893
E-mail: wjg@wjgnet.com www.wjgnet.com

World J Gastroenterol 2004;10(21):3215-3217
World Journal of Gastroenterology
 ISSN 1007-9327

• BRIEF REPORTS •

Effect of hepatitis B immunoglobulin on interruption of HBV intrauterine infection

Xiao-Mao Li, Min-Feng Shi, Yue-Bo Yang, Zhong-Jie Shi, Hong-Ying Hou, Hui-Min Shen, Ben-Qi Teng

Xiao-Mao Li, Yue-Bo Yang, Zhong-Jie Shi, Hong-Ying Hou, Hui-Min Shen, Ben-Qi Teng, Department of Obstetrics and Gynecology, Third Affiliated Hospital, Sun Yat-Sen University, Guangzhou 510630, Guangdong Province, China
Min-Feng Shi, Women's Hospital, School of Medicine, Zhejiang University, Hangzhou 310006, Zhejiang Province, China
Supported by the Science and Research Foundation of Guangzhou Science and Technology Committee, No.1999-J-005-01
Correspondence to: Professor Xiao-Mao Li, Department of Obstetrics and Gynecology, Third Affiliated Hospital, Sun Yat-Sen University, Guangzhou 510630, Guangdong Province, China. tigerlee777@163.net
Telephone: +86-20-85515609 **Fax:** +86-20-87565575
Received: 2004-02-06 **Accepted:** 2004-02-26

Abstract

AIM: To evaluate the efficacy of hepatitis B immunoglobulin (HBIG) in interrupting hepatitis B virus (HBV) intrauterine infection during late pregnancy.

METHODS: We allocated 112 HBsAg positive pregnant women into 2 groups randomly. Fifty seven cases in the HBIG group received 200 IU (unit) HBIG intramuscularly every 4 wk from the 28 wk of gestation to the time of delivery, while 55 cases in the control group received no special treatment. HBsAg, HBeAg, HBcAb, HBeAb, HBsAb and HBV DNA levels were tested in the peripheral blood specimens from all of the mothers at 28 wk of gestation, just before delivery, and in blood from their newborns within 24 h before administration of immune prophylaxis.

RESULTS: The intrauterine infection rate in HBIG group and control group were 10.5% and 27.3%, respectively, with significant difference ($P<0.05$). It showed ascendant trend as HBV DNA levels in the peripheral blood increased before delivery.

CONCLUSION: HBIG is potent to cut down HBV intrauterine infection rate significantly when administered to pregnant women regularly during late pregnancy. The possibility of HBV intrauterine infection increases if maternal blood HBV DNA $\geqslant 10^8$ copies/mL.

Li XM, Shi MF, Yang YB, Shi ZJ, Hou HY, Shen HM, Teng BQ. Effect of hepatitis B immunoglobulin on interruption of HBV intrauterine infection. *World J Gastroenterol* 2004; 10(21): 3215-3217
http://www.wjgnet.com/1007-9327/10/3215.asp

INTRODUCTION

China is a high incidence area of hepatitis B virus (HBV) infection, with a mean HBsAg positive rate of about 10%. Forty to fifty percent of chronic HBV carriers are caused by vertical transmission, which ranks it among the important modes of HBV infection and an important reason of so many HBV carriers in the crowd. Also, it has close correlations with chronic hepatitis, liver cirrhosis and liver cancer. Intrauterine transmission is one of the main resources of hepatitis B virus (HBV) vertical infection, but there is no definite prophylaxis up to now[1-6]. Through HBV DNA quantitation by fluorogenic quantitative polymerase chain reaction (FQ-PCR), we evaluated the efficacy of HBIG in interrupting HBV intrauterine infection during late pregnancy and analyzed the relation between maternal HBV DNA level and the rate of intrauterine transmission.

MATERIALS AND METHODS

Patients

The subjects were drawn from pregnant women who had undergone regular prenatal check-up, and had been admitted for labor and followed up at the Obstetric Department of the Third Affiliated Hospital of Sun Yat-Sen University from December 1999 to October 2001.

The following eligible criteria should all be met: (1) single pregnancy; (2) gestational age$\leqslant$28 wk; (3) HBsAg positive in serum; (4) normal liver and kidney functions; (5) serial tests were negative for HAV, HCV, HDV and HEV; (6) exclusion of fetal anomalies by B-ultrasonography; (7) no receipt of other agents that were under research, anti-virus, immunomodulating, cytotoxic or steroid hormones during pregnancy; (8) their husbands were not HBV carriers or hepatitis B patients; and (9) ability to give written informed consent.

Methods

A total of 112 pregnant women according to the criteria set above and their newborns of 112 cases were chosen. The pregnant women were randomly divided into a HBIG group (57 cases) and a control group (55 cases). Each case in the HBIG group received 200 IU of HBIG (produced by Sichuan Shuyang Pharmaceutical Ltd.) intramuscularly (im) every four weeks from 28 wk of gestation till delivery, while patients in the control group were given no special treatment. Blood specimens were tested for HBsAg, HBeAg, HBsAb, HBeAb, and HBcAb by enzyme linked immunosorbent assay (ELISA, assay kits produced by Zhongshan Biological Products Ltd.), and HBV DNA quantitation by FQ-PCR (assay kits produced by Da'an Genetic Diagnosis Center of Sun Yat-Sen University) in all the subjects at 28 wk and on the day of delivery, and their newborns (blood from femoral vein) 24 h after birth before the administration of immune prophylaxis. All the subjects followed-up regularly during pregnancy.

HBV intrauterine infection was defined as follows: HBsAg and/or HBV DNA positive in peripheral blood of newborns in 24 h after birth before the administration of active or passive immune prophylaxis.

Statistics

The quantity of HBV DNA was transformed to the form of $\log_{10}$ and then expressed as mean±SD. All data were analyzed as χ^2 (*chi*-square) test for positive difference and *t* test for comparisons of means between the 2 groups using SPSS 10.0 for windows. For all comparisons, $P<0.05$ was considered statistically significant.

RESULTS

Clinical characteristics of pregnant women

There were no significant differences between the two groups as for age, nation, gravidity, abortive parity, gestational weeks, way of delivery, or pregnant complications (P>0.1, Table 1).

Table 1 Clinical characteristics of pregnant women of each group

Characteristics	HBIG group (n = 57)	Control group (n = 55)
Age (yr)	26.9±1.8	27.8±2.8
Nationality of Han	57	55
Gravidity	1.5±0.9	1.9±1.2
Abortive parity	0.6±0.7	0.7±1.0
Gestational weeks	39.5±1.9	39±1.3
Rate of cesarean section	27 (47.4%)	25 (45.5%)
Threatened abortion	7	5
Threatened premature labour	2	2
Premature rupture of membrane	0	0
Pregnancy induced hypertension syndrome	1	1
Premature delivery	0	1
Postmature labour	0	0
Elderly primipara	0	0
Medical and surgical associated diseases	2	2
HBeAg positive rate	36 (63.2%)	28 (50.9%)
HBV DNA level (log_{10})	5.75±2.98	5.54±3.09

Intrauterine transmission of HBV

There were 6 cases of intrauterine infection in HBIG group. The counterpart in control group was 15. HBV intrauterine infection rate in HBIG group and control group were 10.5% and 27.3%, respectively, with significant difference (P<0.05, Table 2).

Intrauterine transmission and the level of HBV DNA in maternal serum

The levels of HBV DNA were divided into 7 grades according to the fluorescent signals set by the operation manual, with grade 0 (<10^5 copies/mL), grade 1 (<10^6 copies /mL), grade 2 (<10^7 copies/mL), grade 3 (<10^8 copies/mL), grade 4 (<10^9 copies/mL), grade 5 (<10^{10} copies/mL), and grade 6 (<10^{11} copies/mL). The intrauterine infection rate increased with the increase in HBV DNA level in maternal blood, with odds ratio (OR) increasing. The results of rank correlation and *chi*-square test indicated that although it showed an ascendant trend, there were no significant differences in intrauterine infection rate between grade 2 and grade 1, grade 3 and grade 2, grade 5 and grade 4. But there was significant difference between grade 3 and grade 4 (P<0.05, Table 3).

Table 3 HBV DNA levels in blood of mothers at delivery and HBV intrauterine infection

HBV DNA grade	Mothers (n)	Intrauterine infection		Value of OR
		n	Percentage (%)	
Grade 0 (<10^5copies / mL)	26	0	0	...
Grade 1 (<10^6copies / mL)	22	0	0	...
Grade 2 (<10^7copies / mL)	15	2	13.33	1.00
Grade 3 (<10^8copies / mL)	13	2	15.38	5.55
Grade 4 (<10^9copies / mL)	32	15	46.88	26.91
Grade 5(<10^{10}copies / mL)	4	2	50.00	30.50

Safety

No adverse events such as fever, rigor, skin rash, inflammation and scleroma at local injected area, or impairment of renal function as well as other discomforts were found during the medication of HBIG. As to Apgar score and development reference such as weight and height of the newborns at delivery, there were no significant difference between the 2 groups (P>0.1, Table 4).

Table 4 Development indices of neonates and Apgar score (mean±SD)

	Weight (kg)	Height (cm)	1-minute Apgar score
HBIG group	3.05±0.25	48.0±1.4	10±0.0
Control group	3.04±0.45	48.1±1.5	9.9±0.3

DISCUSSION

Several studies have proved that maternal infectivity is the most important factor in intrauterine transmission of HBV[7], in which HBV DNA shows directly the condition of replication and infectivity of the virus *in vivo*. The latter can be exactly reflected through HBV DNA quantitation by FQ-PCR test clinically[8,9]. With the prominent sensitivity and specificity of the FQ-PCR test, our study indicated that the intrauterine infection rate had significant correlation with the level of HBV DNA in the maternal serum before delivery, which showed an ascendant trend; the intrauterine infection rate significantly increased at the level of HBV DNA $\geqslant 10^8$ copies/mL, which was consistent with the findings by Ngui *et al.*[10]. Those findings suggest that the threshold of HBV DNA $\geqslant 10^8$ copies/mL is a potent index of HBV intrauterine infection. To those pregnant women whose serum levels of HBV DNA are high and have high infectivity, we propose to apply highly effective and safe anti-viral medicines to compress the replication of HBV and, therefore, rapidly and dramatically decrease HBV DNA level to interrupt intrauterine infection[11].

In this study, the intrauterine infection rate in the HBIG group and control group were 10.5% and 27.3%, respectively,

Table 2 Characters of neonatal HBV intrauterine infection

	Neonates n	HBsAg	HBeAg	HBcAb	HBeAb	HBsAb	HBV DNA	n	Intrauterine infection n (%)
Control group	55	+	-	+	+	-	-	2	15 (27.27)
		-	-	-	-	-	+	3	
		-	-	-	+	-	+	3	
		-	+	+	-	-	+	3	
		-	-	+	+	-	+	4	
HBIG group	57	+	-	+	+	-	-	1	6 (10.53)
		+	+	+	-	-	-	1	
		-	-	+	-	-	+	4	

which suggested that the intramuscular administration of HBIG regularly before delivery could effectively interrupt HBV intrauterine infection[12]. HBIG is a kind of passive antibody. One of its components, HBsAb, can combine with HBsAg, activate the complements, clear HBV, lower the level of virus in maternal blood, and thereby prevent and decrease the infection of normal cells. It was reported that the interruptive effect of HBV intrauterine infection by HBIG might correlate with the acquisition of neonatal passive immune, because placenta could transmit the antibody of IgG actively from mother to fetus during late pregnancy[13]. However, HBsAb was detected in none of the newborns in our study. The potential reason might be that the HBV level in maternal blood was so high (higher than the quantity that can be neutralized by the passive antibody) that the HBIG administrated to mother might not be enough to enter fetal body through placenta. So, we consider to increase the quantity of HBIG in our further studies of HBV intrauterine interruption.

We found that some newborns were HBsAg and HBV DNA negative but HBeAg positive in their blood drawn from femoral vein within 24 h after birth. Whether HBeAg can pass placenta is still under hot debate. It has been suggested that HBeAg can be more easily transmitted via placenta than HBsAg in that it is smaller than the latter and is free from agglutination[14]. HBeAg or the compound of HBeAg and α-HBeIgG can pass the barrier of placenta by means of active-transfer in human body[15]. One study also showed that some babies of HBV infected mothers were HBeAg positive and HBsAg negative in femoral blood at birth, and HBsAg titres of the mothers were significantly higher than HBeAg titres (200 times or more). So the positive HBeAg in neonatal serum could not be interpreted as contamination or leakage from the placenta, but can only be explained by that HBeAg can indeed cross placenta[16]. In our study, babies who were only HBeAg positive were born by mothers who were both HBsAg and HBeAg positive. Moreover, the sensitive and specific HBV-infection marker of HBV DNA quantitation were negative in neonatal peripheral blood, and HBeAg disappeared by 9-12 mo of age. So HBeAg in the neonatal peripheral blood is less likely to be an index of intrauterine infection, but transmitted passively from maternity.

REFERENCES

1 Hepatitis B vaccination-United States, 1982-2002. *Morb Mortal Wkly Rep* 2002; **51**: 549-552

2 **Kazim SN,** Wakil SM, Khan LA, Hasnain SE, Sarin SK. Vertical transmission of hepatitis B virus despite maternal lamivudine therapy. *Lancet* 2002; **359**: 1488-1489

3 **Gerdts V,** Babiuk LA, van Drunen Littel-van den Hurk, Griebel PJ. Fetal immunization by a DNA vaccine delivered into the oral cavity. *Nat Med* 2000; **6**: 929-932

4 **Chen DS.** Public health measures to control hepatitis B virus infection in the developing countries of the Asia-Pacific region. *J Gastroenterol Hepatol* 2000; **15**(Suppl): E7-10

5 **Mast EE,** Mahoney FJ, Alter MJ, Margolis HS. Progress toward elimination of hepatitis B virus transmission in the United States. *Vaccine* 1998; **16**(Suppl): S48-51

6 **Yu XL,** Chen CH, Zhong M. Reasons of failure in blocking mother-infant transmission of HBV by using vaccine and related strategies. *Zhonghua Huli Zazhi* 1997; **32**: 69-71

7 **Hamdani-Belghiti S,** Bouazzaou NL. Mother-child transmission of hepatitis B virus. State of the problem and prevention. *Arch Pediat*r 2000; **7**: 879-882

8 **Li XM,** Liu SL, Li X, Huang HJ, Lu JX, Gao ZL. The relative study of hepatitise B virus DNA in maternal blood, umbilical blood and breastmilk. *Acad J SUMS* 2000; **21**: 233-235

9 **Yang YB,** Teng BQ, Li XM, Lin CS, Hou HY, Shen HM. The application of PCR in the test of HBV DNA quantitation. *J Sun Yat Sen University* 2003; **24**: 20-23

10 **Ngui SL,** Andrews NJ, Underhill GS, Heptonstall J, Teo CG. Failed postnatal immunoprophylaxis for hepatitis B: characteristics of maternal hepatitis B virus as risk factors. *Clin Infect Dis* 1998; **27**: 100-106

11 **Li XM,** Yang YB, Hou HY, Shi ZJ, Shen HM, Teng BQ, Li AM, Shi MF, Zou L. Interruption of HBV intrauterine transmission: A clinical study. *World J Gastroenterol* 2003; **9**: 1501-1503

12 **Zhu Q,** Lu Q, Gu X, Xu H, Duan S. A preliminary study on interruption of HBV transmission in uterus. *Chin Med J* 1997; **110**: 145-147

13 **Yue YF,** Yang XJ, Zhang SL, Han XB. Clinical study on the prevention of HBV transmission from mother to infant by injection of HBIG in pregnant women with HBsAg. *Chin J Practical Gynecol Obstet* 1999; **15**: 547-548

14 **Rumi MA,** Begum K, Hassan MS, Hasan SM, Azam MG, Hasan KN, Shirin M, Khan AK. Detection of hepatitis B surface antigen in pregnant women attending a public hospital for delivery: implication for vaccination strategy in Bangladesh. *Am J Trop Med Hyg* 1998; **59**: 318-322

15 **Suga M,** Shibata K, Kodama T, Arima K, Yamada S, Yachi A. A case of HBs antigen negative fulminant hepatitis with IgM antibody to hepatitis B core antigen persisting more than seven years. *Gastroenterol Jpn* 1991; **26**: 661-665

16 **Wang JS,** Zhu QR. Infection of the fetus with hepatitis B e antigen via the placenta. *Lancet* 2000; **355**: 989

Edited by Kumar M **Proofread by** Xu FM

PO Box 2345, Beijing 100023, China
Fax: +86-10-85381893
E-mail: wjg@wjgnet.com www.wjgnet.com

World J Gastroenterol 2004;10(21):3218-3220
World Journal of Gastroenterology
 ISSN 1007-9327

• BRIEF REPORTS •

Mad2 and p27 expression profiles in colorectal cancer and its clinical significance

Gang-Qiang Li, Hong-Fu Zhang

Gang-Qiang Li, Department of Pathology, Chinese PLA 455 Hospital, Shanghai 200052, China
Hong-Fu Zhang, Department of Pathology, Anhui Medical University, Hefei 230032, Anhui Province, China
Correspondence to: Gang-Qiang Li, Department of Pathology, Chinese PLA 455 Hospital, Shanghai 200052, China. lgqfm@163.com
Telephone: +86-21-62800157-41168
Received: 2004-02-02 **Accepted:** 2004-03-12

Abstract

AIM: To investigate the expression of tumor suppressor gene *p27* and spindle checkpoint gene *Mad2* and to demonstrate their expression difference in colorectal cancer and normal mucosa and to evaluate its clinical significance.

METHODS: Immunohistochemical staining was used for detection of expression of Mad2 and *p27* in colorectal cancer and its corresponding normal mucosa.

RESULTS: *Mad2* was significantly overexpressed in colorectal cancer compared with corresponding normal mucosa ($P<0.01$, $\chi^2 = 7.5$), and it was related to the differentiation of adenocarcinoma, lymph node metastasis and survival period after excision ($P<0.05$, $\chi^2 = 7.72$, $\chi^2 = 4.302$, $\chi^2 = 6.234$). The rate of *p27* positive expression in adenocarcinomas and normal mucosa was 40% and 80% respectively. There was a significant difference in *p27* expression between adenocarcinomas and normal mucosa ($P<0.001$, $\chi^2 = 13.333$), which was related to the differentiation degree of adenoca rcinoma and lymph node metastasis ($P<0.05$, $\chi^2 = 8.901$ $\chi^2 = 4$). The positive expression of *p27* was not correlated with survival period after excision.

CONCLUSION: Defect of spindle checkpoint gene *Mad2* and mutation of *p27* gene are involved mainly in colorectal carcinogenesis and associated with prognosis of colorectal cancer.

Li GQ, Zhang HF. Mad2 and p27 expression profiles in colorectal cancer and its clinical significance. *World J Gastroenterol* 2004; 10(21): 3218-3220
http://www.wjgnet.com/1007-9327/10/3218.asp

INTRODUCTION

Genomic instability is a hallmark of malignant cells and occurs either in the form of microsatellite instability or in the form of chromosomal instability (CIN)[1]. Microsatellite instability is reflected by alteration in polymorphic, short, tandem repeats sequences and is associated with a small fraction of colorectal carcinomas with germ-line or somatic mutations of DNA mismatch repair genes[2]. On the other hand, CIN, characterized by an alteration in chromosome number and commonly detected as aneuploidy, is likely to occur in most human malignancies. The fact suggests that CIN may contribute to tumorigenesis[3-5]. In yeast, loss of mitotic checkpoint frequently leads to abnormal chromosome number, resulting in aneuploidy or polyploidy[6]. Two major groups of mitotic checkpoint genes, budding uninhibited by benomyl (BUB) 1-3 and mitotic arrest defect (MAD) 1-3, have been identified in budding yeast[7]. Mammalian homologues of the yeast mitotic checkpoint protein have also been characterized[8-10]. To date, little information is available in literature about the expression of *Mad2* in carcinoma tissue. In this study, we used immunohistochemical technique to examine the expression of *Mad2* and *p27* in colorectal cancer to elucidate the relation of *Mad2* and *p27* to carcinogenesis and clinical pathological factors.

MATERIALS AND METHODS

Specimens

Cancer tissues and corresponding normal tissues were obtained from Chinese PLA 455 Hospital from January 2001 to May 2003. No patient was treated with anti-neoplasm therapy before tumor removal. Fourty patients (22 males, 18 females, aged 25 to 79 years, median age 52.5 years) were as follows: 21 cases of well differentiated adenocarcinoma, 11 cases of moderately differentiated adenocarcinoma, 8 cases of poorly differentiated adenocarcinoma. Twelve cases survived less than 18 mo, 28 cases surivived more than 18 mo after excision. All the tissues were fixed in 40 g/L formaldehyde, embedded in paraffin, and cut into 4 μm thick serial sections.

Reagents

Mad2 polyclonal rabbit antibodies directed against humans were provided by China Science and Technology University. *P27* and immunohistochemical kit were purchased from Beijing Zhongshan Biological Technology Ltd.

Immunohistochemistry

Immunohistochemical staining was performed following the manufacturer's instructions. Anti-*Mad2* antibody was diluted to 1:120. Anti-*p27* was ready to use reagent. For the negative control, the primary antibody was substituted by animal serum. *Mad2* positive expression was stained as brown-yellow mainly in cell plasma. *P27* positive expression was also stained in cell plasma. A semi-quantitative evaluation was used to determine positively expressed cells by viewing 10 vision fields at ×400 magnification as follows[11]: negative (-), <10% cells were stained; mild positive (+), 11-25% cells were stained; moderately positive (++), 26-50% cells were stained ; strong positive (+++), >50% cells were stained. The last three grades were all regarded as positive.

Statistical analysis

The data were analyzed by SPSS version 10.0. χ^2 test was used for statistical analysis. $P<0.05$ was considered statistically significant.

RESULTS

Expression of Mad2 protein

The positive signals of *Mad2* protein were stained brown-yellow mainly in cell plasma and strength of color was directly proportional to positive percentage (Figure 1A). Positive

expression of *Mad2* protein was detected in 30 of 40 (75%) colorectal cancers, and 18 of 40 (45%) normal tissues. There was a significant difference in *Mad2* expression between colorectal cancer and normal tissue ($P<0.01$). Moreover, there were significant differences in *Mad2* expression among well, moderately, and poorly differentiated adenocarcinomas (Table 1). The expression of *Mad2* in colorectal cancer was related with lymph node metastasis and survival period after excision.

Table 1 Relationship between expression of *Mad2* protein and histological differentiation and lymph node metastasis

Groups	*n*	*Mad2*		Positive (%)	*P*
		+	-		
Normal tissue	40	18	22	45	
Adenocarcinoma	40	30	10	75	0.01
WD	21	12	9	61.9	
MD	11	10	1	99	
PD	8	8	0	100	0.041
Lymph node metastasis					
Absent	25	16	9	64	
Present	15	14	1	88	0.038
Survival period (months)					
<18	12	9	3	75	
⩾18	28	9	19	32	0.013

WD: well differentiated adenocarcinoma; MD: moderately differentiated adenocarcinoma; PD: poorly differentiated adenocarcinoma.

p27 protein expression in colorectal cancer and normal tissue

The positive signals of *p27* protein were stained brown-yellow mainly in cell plasma, weak nuclear staining was also observed. Immunoreactivity for *p27* was found in both normal and neoplastic tissues (Figure 1B). High expression of *p27* was observed in 32 normal tissues, and low expression was observed in remaining 8 normal tissues. Of 40 colorectal cancer samples, 16 (40%) had low expression of *p27*, and 24 (60%) had high expression. There was a significant difference in *p27* expression between colorectal cancer and normal tissue ($P<0.01$). Moreover, there were significant differences in *p27* expression among well, moderately, and poorly differentiated adenocarcinomas (Table 2). The expression of *p27* in colorectal cancer was related with lymph node metastasis. No relation of *p27* protein was found with survival period after excision.

Table 2 Relationship among expression of p27 protein and histological differentiation and lymph node metastasis

Groups	*n*	*p27*		Positive (%)	*P*
		+	-		
Normal tissue	40	32	8	80	
Adenocarcinoma	40	16	24	40	0.001
WD	21	13	8	61.9	
MD	11	2	9	18.2	
PD	8	1	7	12.5	0.012
Lymph node metastasis					
Absent	25	13	12	52	
Present	15	3	12	20	0.046
Survival period after excision					
<18	12	4	8	33.3	
⩾18	28	12	16	42.9	0.573

WD: well differentiated adenocarcinoma; MD: moderately differentiated adenocarcinoma; PD: poorly differentiated adenocarcinoma.

Correlation between Mad2 protein and p27

We analyzed the correlation between *Mad2* and *p27* protein expressions by χ^2 test. There was no significantly positive correlation between the expressions of *Mad2* and *p27*.

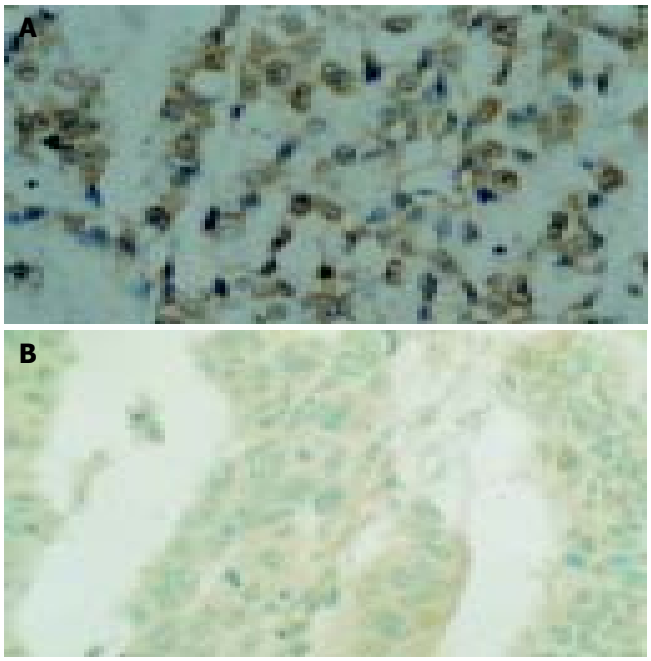

Figure 1 Strongly positive expression of *Mad2* and *p27* in poor differentiated and tubular adenocarcinomas. A: Strongly positive expression of *Mad2* in poor differentiated adenocarcinoma. B: Strongly positive expression of *p27* in tubular adenocarcinoma.

DISCUSSION

Mitotic checkpoints monitor the proper assembly of mitotic spindle and block the onset of anaphase unless all of the chromosomes are stably attached to a specialized region known as kinetochore[12]. It has been proposed that the mitotic checkpoint proteins, especially *Mad2*, may be crucial for generating the "wait" signal to prevent the onset of anaphase after microtubule disruption[13-15]. In the present study, the expressions of *Mad2* and *p27* proteins were examined in colorectal cancer and the corresponding normal tissue. *Mad2* expression in colorectal cancer was higher than that in the corresponding normal tissue. The expression of *Mad2* in colorectal cancer was related with histological differentiation, lymph node metastasis and survival period after excision. Our results regarding the expression of *Mad2* are not consistent with the finding that the reduced expression of *Mad2* in breast cancer cells reported by Li and Benezra[7], but it was similar to the study by Tanaka *et al*.[15]. The different expression might result from the surrounding in which cells lived. In an organ, cells could be influenced by nerves and endocrine hormones. Michel *et al.* showed that subtle differences in *Mad2* protein level markedly altered checkpoint function[16]. Therefore, inactivation of *Mad2* would be sufficient to lead to a haplo-insufficient effect and loss of mitotic checkpoint control. The most convincing evidence of the role of mitotic checkpoint defect in CIN in mammalian cells came from two recent studies in *Mad2*$^{-/-}$ mice, and in *Mad2*$^{-/-}$ human and mouse cells, showing that disruption of *Mad2* expression resulted in CIN[16,17]. It has been reported that CIN cells become aneuploidy, a hallmark of cancer that is associated with an aggressive tumor behavior and a poor prognosis[18]. Recent studies reported that the *Mad2* protein interacted with estrogen receptor β or the cytoplasmic domain of insulin receptors, which are thought to be regulators

of cellular growth[19-21]. Our study showed that *Mad2* protein overexpressed in cancer tissue was exclusively present in the cytoplasm of cancer cells. We speculate that cytoplasmic *Mad2* protein may enhance the positive regulatory action of estrogen receptor β and insulin receptor on cell proliferation.

P27 is a member of the Cip1/Kip1 family of cyclin-dependent kinase (CDK) inhibitors and a potential tumor suppressor gene[22]. Recent studies have demonstrated that targeted inactivation of *p27* could lead to development of multiple organ hyperplasia and malignancy *in vivo*[23,24]. In this study, we examined the expression of CDK inhibitor *p27* in colorectal adenocarcinomas and corresponding normal tissues. Low expression of *p27* was detected in cancer tissue compared with normal tissues. It was also related to histological differentiation and lymph node metastasis, but not related to survival period after excision. This evidence is similar to that previously reported in other tumors such as tumors of breast, stomach, prostate, lung, liver[25-32].

Orr-Weaver *et al*. thought that aneuploidy might increase the rate at which tumor suppressors are lost through the loss of heterozygosity. Our study showed that there was no significantly positive correlation between the expressions of *Mad2* and *p27*.

In conclusion, expressions of *Mad2* and *p27* are related to histological differentiation and lymph node metastasis of colorectal cancer. *Mad2* and *p27* proteins might be good markers for predicting histological differentiation and prognosis of colorectal cancer.

REFERENCES

1 **Rooney PH,** Murray GI, Stevenson DA, Haites NE, Cassidy J, Mcleod HL. Comparative genomic hybridization and chromosomal instability in solid tumours. *Br J Cancer* 1999; **80**: 862-873
2 **Lengauer C,** Kinzler KW, Vogelstein B. Genetic instabilities in human cancers. *Nature* 1998; **396**: 643-649
3 **Lengauer C,** Kinzler KW, Vogelstein B. Genetic instability in colorectal cancers. *Nature* 1997; **386**: 623-627
4 **Lengauer C,** Kinzler KW, Vogelstein B. DNA methylation and genetic instability in colorectal cancer cells. *Proc Natl Acad Sci U S A* 1997; **94**: 2545-2550
5 **Li R,** Murray AW. Feedback control of mitosis in budding yeast. *Cell* 1991; **66**: 519-531
6 **Hoyt MA,** Totis L, Roberts BT. S. cerevisiae genes required for cell cycle arrest in response to loss of microtubule function. *Cell* 1991; **66**: 507-517
7 **Li Y,** Benezra R. Identification of a human mitotic checkpoint gene: hsMAD2. *Science* 1996; **274**: 246-248
8 **Taylor SS,** Mckeon F. Kinetochore localization of murine Bub1 is required for normal mitotic timing and checkpoint response to spindle damage. *Cell* 1997; **89**: 727-735
9 **Jin DY,** Spencer F, Jeang KT. Human T cell leukemia virus type 1 oncoprotein Tax targets the human mitotic checkpoint protein MAD1. *Cell* 1998; **93**: 81-91
10 **Barnes DM,** Dublin EA, Fisher CJ, Levison DA, Millis RR. Immunohistochemical detection of p53 protein in mammary carcinoma: an important new independent indicator of prognosis? *Hum Pathol* 1993; **24**: 469-476
11 **Rudner AD,** Murray AW. The spindle assembly checkpoint. *Curr Opin Cell Biol* 1996; **8**: 773-780
12 **Amon A.** The spindle checkpoint. *Curr Opin Genet Dev* 1999; **9**: 69-75
13 **Waters JC,** Chen RH, Murray AW, Salmon ED. Localization of Mad2 to kinetochores depends on microtubule attachment, not tension. *J Cell Biol* 1998; **141**: 1181-1191
14 **Sharp-Baker H,** Chen RH. Spindle checkpoint protein Bub1 is required for kinetochore localization of Mad1, Mad2, Bub3, and CENP-E, independently of its kinase activity. *J Cell Biol* 2001; **153**: 1239-1250
15 **Tanaka K,** Nishioka J, Kato K, Nakamura A, Mouri T, Miki C, Kusunoki M, Nobori T. Mitotic checkpoint protein hsMAD2 as a marker predicting liver metastasis of human gastric cancer. *Jpn J Cancer Res* 2001; **92**: 952-958
16 **Michel LS,** Liberal V, Chatterjee A, Kirchwegger R, Pasche B, Gerald W, Dobles M, Sorger PK, Murty VV, Benezra R. MAD2 haplo-insufficiency causes premature anaphase and chromosome instability in mammalian cells. *Nature* 2001; **409**: 355-359
17 **Dobles M,** Liberal V, Scott ML, Benezra R, Sorger PK. Chromosome missegregation and apoptosis in mice lacking the mitotic checkpoint protein Mad2. *Cell* 2000; **101**: 635-645
18 **Pennisi E.** Cell division gatekeepers identified. *Science* 1998; **279**: 477-478
19 **Poelzl G,** Kasai Y, Mochizuki N, Shaul PW, Brown M, Mendelsohn ME. Specific association of estrogen receptor beta with the cell cycle spindle assembly checkpoint protein MAD2. *Proc Natl Acad Sci U S A* 2000; **97**: 2836-2839
20 **O'Neill TJ,** Zhu Y, Gustafson TA. Interaction of MAD2 with the carboxyl terminus of the insulin receptor but not with the IGFIR. Evidence for release from the insulin receptor after activation. *J Biol Chem* 1997; **272**: 10035-10040
21 **Gliozzo B,** Sung CK, Scalia P, Papa V, Frasca F, Sciacca L, Giorgino F, Milazzo G, Goldfine ID, Vigneri R, Pezzino V. Insulin-stimulated cell growth in insulin receptor substrate-1-deficient ZR-75-1 cells is mediated by a phosphatidylinositol-3-kinase-independent pathway. *J Cell Biochem* 1998; **70**: 268-280
22 **Masciullo V,** Sgambato A, Pacilio C, Pucci B, Ferrandina G, Palazzo J, Carbone A, Cittadini A, Mancuso S, Scambia G, Giordano A. Frequent loss of expression of the cyclin-dependent kinase inhibitor p27 in epithelial ovarian cancer. *Cancer Res* 1999; **59**: 3790-3794
23 **Kiyokawa H,** Kineman RD, Manova-Todorova KO, Soares VC, Hoffman ES, Ono M, Khanam D, Hayday AC, Frohman LA, Koff A. Enhanced growth of mice lacking the cyclin-dependent kinase inhibitor function of p27(kip1). *Cell* 1996; **85**: 721-732
24 **Fero ML,** Rivkin M, Tasch M, Porter P, Carow CE, Firpo E, Polyak K, Tsai LH, Broudy V, Perlmutter RM, Kaushansky K, Roberts JM. A syndrome of multi organ hyperplasia with features of gigantism, tumorigenesis, and female sterility in p27(kip1)-deficient mice. *Cell* 1996; **85**: 733-744
25 **Kawamata N,** Morosetti R, Miller CW, Park D, Spirin KS, Nakamaki T, Takeuchi S, Hatta Y, Simpson J, Wilcyznski S, Lee Y, Bartram C, Koeffler H. Molecular analysis of the cyclin-dependent kinase inhibitor gene p27/Kip1 in human malignancies. *Cancer Res* 1995; **55**: 2266-2269
26 **Tan P,** Cady B, Wanner M, Worland P, Cukor B, Magi-Galluzzi C, Lavin P, Draetta G, Pagano M, Loda M. The cell cycle inhibitor p27 is an independent prognostic marker in small (T1a, b) invasive breast carcinomas. *Cancer Res* 1997; **57**: 1259-1263
27 **Porter PL,** Malone KE, Heagerty PJ, Alexander GM, Gatti LA, Firpo EJ, Daling JR, Roberts JM. Expression of cell-cycle regulators p27Kip1 and cyclin E, alone and in combination, correlate with survival in young breast cancer patients. *Nat Med* 1997; **3**: 222-225
28 **Catzavelos C,** Bhattacharya N, Ung YC, Wilson JA, Roncari L, Sandhu C, Shaw P, Yeger H, Morava-Protzner I, Kapusta L, Franssen E, Pritchard KI, Slingerland JM. Decreased levels of the cell-cycle inhibitor p27Kip1 protein: prognostic implications in primary breast cancer. *Nat Med* 1997; **3**: 227-230
29 **Loda M,** Cukor B, Tam SW, Lavin P, Fiorentino M, Draetta GF, Jessup JM, Pagano M. Increased proteasome-dependent degradation of the cyclin-dependent kinase inhibitor p27 in aggressive colorectal carcinomas. *Nat Med* 1997; **3**: 231-234
30 **Thomas GV,** Szigeti K, Murphy M, Draetta G, Pagano M, Loda M. Down-regulation of p27 is associated with development of colorectal adenocarcinoma metastases. *Am J Pathol* 1998; **153**: 681-687
31 **Ciaparrone M,** Yamamoto H, Yao Y, Sgambato A, Cattoretti G, Tomita N, Monden T, Rotterdam H, Weinstein IB. Localization and expression of p27Kip1 in multistage colorectal carcinogenesis. *Cancer Res* 1998; **58**: 114-122
32 **Mori M,** Mimori K, Shiraishi T, Tanaka S, Ueo H, Sugimachi K, Akiyoshi T. p27 expression and gastric carcinoma. *Nat Med* 1997; **3**: 593-596

Edited by Kumar M and Wang XL **Proofread by** Xu FM

PO Box 2345, Beijing 100023, China
Fax: +86-10-85381893
E-mail: wjg@wjgnet.com www.wjgnet.com

World J Gastroenterol 2004;10(21):3221-3224
World Journal of Gastroenterology
 ISSN 1007-9327

• BRIEF REPORTS •

Effects of intestinal lymph on expression of neutrophil adhesion factors and lung injury after trauma-induced shock

Zuo-Bing Chen, Shu-Sen Zheng, Gao Yuan, Chen-Yan Ding, Yun Zhang, Xue-Hong Zhao, Lin-Mei Ni

Zuo-Bing Chen, Shu-Sen Zheng, Gao Yuan, Chen-Yan Ding, Yun Zhang, Xue-Hong Zhao, Lin-Mei Ni, Department of Emergency Surgery, First Affiliated Hospital, Zhejiang University School of Medicine, Hangzhou 310003, Zhejiang Province, China
Correspondence to: Zuo-Bing Chen, Department of Emergency Surgery, First Affiliated Hospital, Zhejiang University School of Medicine, 79 Qingchun Road, Hangzhou 310003, Zhejiang Province, China. chenzuobing@hotmail.com
Telephone: +86-571-87236303
Received: 2004-02-03 **Accepted:** 2004-02-24

Abstract

AIM: To study how intestinal lymph after trauma-induced shock (TIS) interferes with expression of neutrophil adhesion factors (CD11b and CD18) and causes lung injury.

METHODS: Thirty-two adult healthy Sprague-Dawley rats were randomly divided into four experimental groups. Groups 1 and 2 included rats with TIS caused by hitting the mid-upper part of both side femoral bones with a 2 500 kg raw-iron, and with or without ligation of mesenteric lymph duct. Groups 3 and 4 included rats with sham-TIS and with or without ligation of mesenteric lymph duct. Expression of neutrophil CD18 and CD11b in at 1 and 3 h after a 90-min TIS/sham-TIS was evaluated. These rats were killed at 3 h after TIS/sham-TIS, and lungs were taken immediately. The main lung injury indexes (the MPO activity and lung injury score) were measured.

RESULTS: The expressions of CD18 and CD11b at 1 and 3 h after a 90-min TIS and the main lung injury indexes were significantly increased compared with those in the sham-TIS groups ($P<0.05$). Moreover, at 1 and 3 h after TIS, the expressions of CD18 (32.12±1.25 and 33.46±0.98) and CD11b (29.56±1.35 and 30.56±1.85) were significantly decreased in rats with ligation of mesenteric lymph duct, compared with those (52.3±1.12 and 50.21±1.25, and 42.24±1.24 and 42.81±1.12, respectively) in those without the ligation (all $P<0.05$). The main lung injury indexes in rats with TIS with ligation of mesenteric lymph duct (0.96±0.12 and 6.54±0.35) were also significantly decreased, compared with those (1.56±0.21 and 9.56±0.23) in rats with TIS without the ligation (both $P<0.05$). However, there was no significant difference in expressions of CD18 and CD11b and the main lung injury indexes between the two sham-TIS groups.

CONCLUSION: Previous ligation of mesenteric lymph ducts prevents or alleviates the up-regulated expression of PMN CD18 and CD11b and the lung injury induced by TIS. Our findings also indicate that neutrophil adhesion molecule activation and lung injury during TIS appear to be caused by some factors that are released or produced by post-ischemic intestine through the mesenteric lymph pathway.

Chen ZB, Zheng SS, Yuan G, Ding CY, Zhang Y, Zhao XH, Ni LM. Effects of intestinal lymph on expression of neutrophil adhesion factors and lung injury after trauma-induced shock. *World J Gastroenterol* 2004; 10(21): 3221-3224
http://www.wjgnet.com/1007-9327/10/3221.asp

INTRODUCTION

Trauma-induced-shock (TIS) could lead to splanchnic ischemia-reperfusion and gut barrier failure[1]. These events could get the gut into an inflammatory cytokine-secreting organ, which contributes to the pathogenesis of shock-induced lung injury[2,3]. Lung injury generally occurs when mediators released by systemic inflammatory processes up-regulate polymorphonuclear neutrophil (PMN) interactions with endothelial cells (ECs), thus favoring PMN sequestration and attack on the lung. Shock and trauma-induced neutrophil activation has been implicated in the pathogenesis of adult respiratory distress syndrome (ARDS) and also as a contributory factor in the development of multiple organ dysfunction syndrome (MODS)[4,5]. Furthermore, enhanced endothelial-neutrophil interactions resulting in tissue injury appear to be the common pathways by which diverse initiating factors, such as bacterial infection, endotoxin, cytokines, shock, and ischemia can lead to organ injury and MODS[6]. These events have been implicated in the pathogenesis of pulmonary microvascular injury after intestinal ischemia-reperfusion injuries[7,8].

However, the exact mechanisms by which intestinal ischemia reperfusions subsequent to trauma and hemorrhage primes neutrophils remain uncertain. There are many discussions about this topic. Since Gonzalez *et al*. demonstrated that port vein blood did not contain such inflammatory mediators in patients with traumatic shock, such as endotoxin or bacteria, more and more people have attached importance to lymph pathway[9]. Some study in a rat model of trauma-hemorrhagic shock (T/HS) has shown that ligation of the main mesenteric lymph draining the intestine could prevent lung injury[10], and furthermore, it has been testified that mesenteric lymph from rats subjected to T/HS can prime neutrophils for an oxidative burst[11]. TIS mesenteric lymph can activate PMNs and increase their ability to injure ECs, and on the other hand, PMN exposure to mesenteric lymph is both necessary and sufficient for the activation of rat PMN respiratory burst by TIS. From a mechanical point of view, respiratory burst activation in response to G-protein-coupled agonists is characterized by enhanced cell calcium [Ca2+]i) flux response to GPC agonists tested[12,13]. In contrast, portal plasma from TIS rats lacks the potential to activate PMNs.

All these studies lead to the conclusion that lymph from the ischemic gut may be a crucial source of neutrophil priming factors after major hemorrhagic insults, such as lung injury, systemic inflammatory response syndrome (SIRS), MODS, and multiple system organ failure (MSOF). Therefore it has come to be accepted by more and more people that gut-induced lung injury is secondary to a shock-induced gut "inflammatory state", where gut-induced inflammatory factors enter the systemic circulation via mesenteric lymphatics rather than via portal bloodstream. To testify and further extend this concept that neutrophil priming activation was caused by release of factors

from gut into the mesenteric lymphatics, we performed this experiment to study whether TIS could up-regulate neutrophil adhesion molecule expression and cause lung injury, and whether such pathological changes could be prevented or alleviated by ligating mesenteric lymph ducts previously.

MATERIALS AND METHODS

Animals

Adult Sprague-Dawley rats (SD rats) weighing 300-350 g were used after a minimum acclimatization period of 7 d. The animals and their diet were provided by The Laboratory Animal Center, Zhejiang University, College of Medicine, China. The animals were had free access to food and water and were maintained in accordance with the guideline of the National Guide for the Care and Use of Laboratory Animals, and the experiment was approved by the Zhejiang University, College of Medicine.

Experimental design

The aim of this experiment was to assess how the lymph after TIS affected the expression of neutrophil adhesion molecules and caused lung injury in rats. Four groups were included. They were groups of rats subjected to TIS with or without mesenteric lymph duct ligation, and groups of rats subjected to sham TIS with or without mesenteric lymph duct ligation. Femoral artery blood samples were collected 1 and 3 h after a 90-min shock period for further evaluating the expression of PMN. Then these rats were killed immediately, lungs were removed for assessment of the severity of injuries, mainly by measuring myeloperoxidase (MPO) content and lung injury score.

TIS model

As previously described[14], rats were anesthetized intraperitoneally using sodium pentobarbital (50 mg/kg), and a femoral artery catheter was placed for measuring the artery pressure and an other side femoral artery catheter for taking blood. Then a midline laparotomy was performed to expose the mesenteric lymph duct, which was either ligated with 2-0 silk or just left intact according to the experimental need. The incision was closed. A 2 500 kg raw- iron was used to hit the rat's mid-upper part of both side femoral bones from 30 cm height to cause TIS, then the rat artery pressure was maintained at about 30 mmHg for 90 min, by blood withdrawal or normal saline infusion through one side of the femoral artery catheter, the other side of femoral artery catheter was used to measure the artery pressure. The rats were subjected to TIS for 90 min and then their traumatic legs were tied up closely. The animal body temperature during the experiment was maintained at about 37 ℃ by using a heating pad.

Sham-TIS model

Except trauma treatment and being subjected to shock state, the sham-TIS model accepted the nearly same treatment as TIS model.

Assay of blood CD11 b and CD18

Blood sample (1 mL) collected at 1 and 3 h after 90 min of TIS/sham-TIS state was collected and treated with anti-coagulant EDTANa2. A 100 μL blood sample was put into a 12 mm×75 mm tube and then 10 μL anti-rat CD11b or CD18 fluorescent labeled monoclonal antibody (BD Pharmingen) was added into the tube. The samples were gently vortexed for 10 min and then placed into a dark room for 40 min. Red blood cells of the sample were lysed and fixed with Coahem Q-PREP equipment (Couletr Company, USA) for 15 min on ice. After centrifuged and washed 3 times, PMN cells were analyzed for adhesion molecule expression using flow cytometer (ESPLL-XL, BECKMAN, USA) according to the recommendation of the manufacturer. The number of these neutrophils labelled with monoclonal antibody in 10 000 neutrophils was counted and the percentage was evaluated.

Assay of myeloperoxidase

Three hours later, rats were killed and the right lung was immediately taken and frozen. The frozen lung tissue was homogenized and processed for measuring myoloperoxidase (MPO) with the regent kit (Jiancheng Bio-Technology Company, Nanjing, China) according to the manufacturer's instructuons. One unit of MPO activity represented the amount of enzyme that reduced 1 μmol/L of peroxidase per minute.

Assay of lung injury sore

The lung tissue was fixed in 40 g/L formaldehyde, cut into 4 μm sections and stained with HE. The lung injury score (LIS)[15] was evaluated with OLMPUS optical microscope (Olympus, Japan). The severity of leukocyte sequestration in the lung tissue was classified as: 0 = 0%, 1 = 0-25%, 2 = 25-50%, 3 = 50-75%, 4 = 75-100%. The severity of leukocyte sequestration in lung alveoli was classified as: 0 = none, 1 = few, 2 = a lot, 3 = almost all, 4 = all. The severity of exudation (such as fibrin, transparent membrane and edema liquor) in lung alveoli was classified as: 0 = none, 1 = few, 2 = a lot, 3 = almost full, and 4 = absolute full.

Statistical analysis

Results were expressed as mean±SD. The data were analyzed with SPSS.11.0. The comparison among multiple groups was made with *t* test. Probabilities less than 0.05 were considered statistically significant.

RESULTS

The expressions of CD18 and CD11b in PMN were significantly increased after TIS with or without ligation of mesenteric lymph ducts compared with sham shock groups ($P<0.05$, Table 1). Both CD18 and CD11b expressions were up-regulated by the TIS pathological process. The expressions of CD18 and CD11b in sham shock with or without ligation of mesenteric lymph duct had no significant difference ($P>0.05$). It showed that ligation of mesenteric lymph duct itself had no effect on the expression of CD18 or CD11b. The results also showed that the expressions of CD18 and CD11b after TIS with ligation of mesenteric lymph duct were significantly decreased as compared with TIS without ligation of lymph duct ($P<0.05$). It was suggested that previous ligation of mesenteric lymph duct during TIS could down-regulate the expressions of CD18 and CD11b.

Table 1 Comparison of expressions of CD18 and CD11b in ratsof all groups at 1 and 3 h after 90 min of TIS/sham-TIS state(%)

Group	CD18		CD11b	
	1st h	3rd h	1st h	3rd h
TIS with ligation of mesenteric lymph duct (8)	32.12±1.25	33.46±0.98	29.56±1.35	30.56±1.85
TIS without ligation of mesenteric lymph duct (8)	52.3±1.12	50.21±1.25	42.24±1.24	42.81±1.12
Sham TIS with ligation of mesenteric lymph duct (8)	17.02±0.95	15.68±0.98	14.02±1.23	13.63±1.23
Sham TIS withtout ligation of mesenteric lymph duct (8)	16.23±1.20	16.25±0.53	13.61±1.25	13.51±1.65

The main lung injury indexes (MPO activity and lung injury score) of TIS group were significantly increased compared with sham shock group ($P<0.05$, Table 2). The results showed that the main lung injury indexes of sham shock groups with or without ligation of mesenteric lymph duct had no significant difference ($P>0.05$). It seemed that ligation of mesenteric lymph duct itself could not cause lung injury. The results also showed that the MPO activity and lung injury score of TIS with previous ligation of mesenteric lymph duct were significantly decreased as compared with TIS without ligation of lymph duct ($P<0.05$). It appeared that previous ligation of mesenteric lymph duct could alleviate lung injury effectively during TIS.

Table 2 Comparison of MPO activity and lung injury score in rats of all groups

Group (n = 8)	MPO activity (Ug^{-1} lung tissue)	LTS
TIS witht ligation of mesenteric lymph duct	0.96±0.12	6.54±0.35
TIS without ligation of mesenteric lymph duct	1.56±0.21	9.56±0.23
Sham TIS witht ligation of Mesenteric lymph duct	0.45±0.05	2.35±0.56
Sham TIS withtout ligation of Mesenteric lymph duct	0.50±0.08	2.53±0.41

DISCUSSION

It has been found that the phenomena of neutrophil activation is often companied by TIS, and that activated neutrophils may play a key role in the pathogenesis of lung injury or MODS, MSOF in TIS[16]. But the mechanism of neutrophil activation, lung injury or MODS is still uncertain. Therefore, the soluble factors in neutrophil activation subjected to TIS and the cellular mechanisms for neutrophil activation are the hot topics. A lot of evidence showed that ischemia-reperfusion gut was an important source of factors that might cause neutrophil activation, lung injury or MODS after TIS[17-19]. Post-ischemia gut has been shown to be a cytokine-generating organ, and the vascular bed of post-ischemia has been proven to be a priming bed for neutrophils by both clinical and experimental studies[20]. It is usually believed that the loss of gut barrier function in shock states leads to bacterial translocation. Then such a bacterial translocation might cause sepsis and organ dysfunction in TIS patients. However, studies about TIS showed that neither bacteria nor endotoxin was found in portal blood of severely injured trauma patients. These findings have made people to doubt the theory of bacterial translocation during TIS.

It has been shown that the TIS induced increase in pulmonary capillary permeability could be prevented by ligation of mesenteric lymph ducts[21], and mesenteric lymph from rats subjected to TIS, but not sham TIS could injure endothelial cells and increase their permeability[22]. Shock-induced up-regulation of pulmonary endothelial P-selection expression could also be alleviated by mesenteric lymph duct ligation.

Based on these clinical and experimental findings, people come to hypothesize that lymphatics might be the primary route by which intestinal factors leave the gut and cause subsequent injury of lung or other organs instead of portal route. Neutrophil-endothialial interaction is involved in endothelial cell injury and endothelial cell adhesion molecule up-regulation. In order to investigate this hypothesis, we designed these experiments. To explore how TIS lymph affected PMN activation and lung injury, we compared TIS rats with or without ligation of the mesenteric lymph ducts. CD18 and CD11b were chosen as the indicators of PMN activation, and MPO and lung injury score were chosen as the indicators of lung injury[23,24].

The results of our study showed that the expressions of PMN CD18 and CD11b and the main lung injury indexes (the MPO activity and lung injury score) of TIS at 1 and 3 h after 90 min of TIS state were significantly increased compared with those of sham shock group, but had no significant difference between two sham shock groups with or without ligation of mesenteric lymph ducts. The results also showed that previous ligation of mesenteric lymph ducts could down-regulate the expressions of CD18 and CD11b and alleviate lung injury in rats subjected to TIS. These results are consistent with the studies of Harkin *et al*.[25], who showed that mesenteric ligation prevented shock-induced CD11b up-regulation using a less severe shock model. The theory that the gut is a primary source of neutrophil-activating factors is consistent with our study and Adams *et al*.[26], who found that the ability of plasma from rats subjected to TIS to prime neutrophils for an augment respiratory burst was lost after lymph duct ligation.

Generally, it seems that factors contained in TIS intestinal lymph are both necessary and sufficient to account for neutrophil activation and priming after TIS. The intestine could produce a wide rage of inflammatory mediators, including cytokines, eicosanods, oxidants, platelet-activating factors, complement fragments, and endotoxin[27,28]. Many of these mediators can prime or activate neutrophils and endothelial cells directly or indirectly. It has been proven that primed and activated neutrophils are involved in the pathogenesis of posttraumatic inflammatory syndromes such as systemic inflammatory response syndrome (SIRS), adult respiratory distress syndrome (ARDS), MODS, and MSOF. It also has been testified that prevention of tissue neutrophil infiltration can reduce lung and other organ injury in the models of TIS[29]. The results of our experiment also showed that pathologic neutrophil activation by gut lymph was critical to the pathogenesis of TIS.

Since no bacteria or endotoxin was found in mesenteric lymph subjected to TIS, further work is needed to study on the characterization and identification the nertophil-activating factors in the TIS lymph. It has ever been thought that the lipid fraction of lymph was responsible for neutropil activation[30]. However, Daysl *et al*.[31] pointed out that the respiratory burst of rat neutrophils was stimulated by the aqueous but not lipid fraction of the lymph samples. The exact explanation for these conflicting results is not known, but it may suggest that TIS lymph contains several factors which are capable of activating neutrophils. So, further study may still be needed to define the factors in TIS gut lymph which could activate neutrophils and cause injury of lung or other important organs.

In conclusion, mesenteric lymph after TIS contains multiple biologically active agents. These agents have the potential to modify both PMN and EC behaviors, which are probably involved in the pathogenesis of lung injury after TIS. The results showed that up-regulated expressions of PMN CD18 and CD11b and the lung injury induced by TIS could be prevented or alleviated by previous ligation of mesenteric lymph ducts. These findings may indicate that lung injury during TIS is caused by PMN adhesion molecule activation induced by some factors released or produced by postischemic intestine through mesenteric lymph pathway rather than traditionally believed portal vein.

REFERENCES

1 **Deitch EA.** Role of the gut lymphatic system in multipale organ failure. *Curr Opin Crit Care* 2001; **7**: 92-98

2 **Farber A,** Connors JP, Friedlander RM, Wagner RJ, Powell RJ, Cronenwett JL. A specific inhibitor of apoptosis decreases tissue injury after intestinal ischemia-reperfusion in mice. *J Vasc Surg* 1999; **30**: 752-760

3 **Ariceta J,** Ferrer JV, Guerrero D, Tellechea E, Balen E, Lera JM. Metabolism of the intestine with intermediate ischemia after intestinal ischemia-reperfusion injury: therapeutic effects of somatostatin. *Transplant Proc* 1999; **31**: 2572

4 **Deitch EA,** Adams C, Lu Q, Xu DZ. A time course study of the protective effect of mesenteric lymph duct ligation on hemorrhagic shock-induced pulmonary injury and the toxic effects of lymph from shocked rats on endothelial cell monolayer permeability. *Surgery* 2001; **129**: 39-47

5 **Sambol JT,** Xu DZ, Adams CA, Magnotti LJ, Deitch EA. Mesenteric lymph duct ligation provides long term protection against hemorrhagic shock-induced lung injury. *Shock* 2000; **14**: 416-419

6 **Hammerman C,** Goldschmidt D, Caplan MS, Kaplan M, Schimmel MS, Eidelman AI, Branski D, Hochman A. Amelioration of ischemia-reperfusion injury in rat intestine by pentoxifylline-mediated inhibition of xanthine oxidase. *J Pediatr Gastroenterol Nutr* 1999; **29**: 69-74

7 **Fekete Z,** Hauser CJ, Adams JM, Adams CA Jr, Forsythe RM, Hasko G, Xu DZ, Livingston DH, Deitch EA. Injury-enhanced calcium mobilization in circulating rat neutrophils models human PMN responses. *Shock* 2001; **16**: 15-20

8 **Miner TJ,** Tavaf-Motamen H, Stojadinovic A, Shea-Donohue T. Ischemia-reperfusion protects the rat small intestine against subsequent injury. *J Surg Res* 1999; **82**: 1-10

9 **Gonzalez RJ,** Moore EE, Biffl WL, Ciesla DJ, Silliman CC. The lipid fraction of post-hemorrhagic shock mesenteric lymph (PHSML) inhibits neutrophil apoptosis and enhances cytotoxic potential. *Shock* 2000; **14**: 404-408

10 **Johnson JL,** More EE, Hiester AA, Tamura DY, Zallen G, Silliman CC. Disparities in the respiratory burst between human and rat neutrophils. *J Leukoc Biol* 1999; **65**: 211-216

11 **Adams CA Jr,** Sambol JT, Xu DZ, Lu Q, Granger DN, Deitch EA. Hemorrhagic shock induced up-regulation of P-selectin expression is mediated by factors in mesenteric lymph and blunted by mesenteric lymph duct interruption. *J Trauma* 2001; **51**: 625-632

12 **Adams JM,** Hauser CJ, Adams CA Jr, Xu DZ, Livingston DH, Deitch EA. Entry of gut lymph into the circulation primes rat neutrophil respiratory burst in hemorrhagic shock. *Crit Care Med* 2001; **29**: 2194-2198

13 **Koltuksuz U,** Ozen S, Uz E, Aydinc M, Karaman A, Gultek A, Akyol O, Gursoy MH, Aydin E. Caffeic acid phenethyl ester prevents intestinal reperfusion injury in rats. *J Pediatr Surg* 1999; **34**: 1458-1462

14 **Sun YG,** Huang ZH, Miao HF, Song HJ, Lei HY. Development of an experimental model of traumatic shock in rats. *Zhongguo Jiefangjun Yixue Zazhi* 2002: **12**; 1086-1087

15 **Holopainen R,** Aho H, Laine J, Halkola L, Kaapa P. Nitric oxide inhalation inhibits pulmonary apoptosis but not inflammatory injury in porcine meconium aspiration. *Acta Paediatr* 1999; **88**: 1147-1155

16 **Ustundag B,** Kazez A, Demirbag M, Canatan H, Halifeoglu I, Ozercan IH. Protective effect of melatonin on antioxidative system in experimental ischemia-reperfusion of rat small intestine. *Cell Physiol Biochem* 2000; **10**: 229-236

17 **Kazez A,** Demirbag M, Ustundag B, Ozercan IH, Saglam M. The role of melatonin in prevention of intestinal ischemia-reperfusion injury in rats. *J Pediatr Surg* 2000; **35**: 1444-1448

18 **Pockley AG,** Nakao M, Fairburn B, Wood RF. Effect of ischemia-reperfusion of the rat small bowel on peripheral blood neutrophil CD11b expression. *Transplant Proc* 2000; **32**: 1304

19 **Yoshida T,** Iwakiri R, Noda T, Okamoto K, Kojima M, Fukuyama K, Fujimoto K. Histaminergic effect on apoptosis of rat small intestinal mucosa after ischemia-reperfusion. *Dig Dis Sci* 2000; **45**: 1138-1144

20 **Vejchapipat P,** Williams SR, Spitz L, Pierro A. Intestinal metabolism after ischemia-reperfusion. *J Pediatr Surg* 2000; **35**: 759-764

21 **Dayal SD,** Hauser CJ, Feketeova E, Fekete Z, Adams JM, Lu Q, Xu DZ, Zaets S, Deitch EA. Shock mesenteric lymph -induced rat polymorphonuclear neutrophil activation and endothelial cell injury is mediated by aqueous factors *J Trauma* 2002; **52**: 1048-1055

22 **Yamamoto S,** Tanabe M, Wakabayashi G, Shimazu M, Matsumoto K, Kitajima M. The role of tumor necrosis factor-alpha and interleukin-1beta in ischemia-reperfusion injury of the rat small intestine. *J Surg Res* 2001; **99**: 134-141

23 **Kassirer M,** Zeltser D, Prochorov V, Schoenman G, Frimerman A, Keren G, Shapira I, Miller H, Roth A, Arber N, Eldor A, Berliner S. Increased expression of the CD11b/CD18 antigen on the surface of peripheral white blood cells in patients with ischemic heart disease: further evidence for smoldering inflammation in patients with atherosclerosis. *Am Heart J* 1999; **138**(3 Pt 1): 555-559

24 **Rizoli SB,** Kapus A, Parodo J, Rotstein OD. Hypertonicity prevents lipopolysaccharide-stimulated CD11b/CD18 expression in human neutrophils *in vitro*: role for p38 inhibition. *J Trauma* 1999; **46**: 794-798

25 **Harkin DW,** D'Sa AA, Yassin MM, Hoper M, Halliday MI. Gut mucosal injury is attenuated by recombinant bactericidal/permeability-increasing protein in hind limb ischemia-reperfusion injury. *Ann Vasc Surg* 2001; **15**: 326-331

26 **Adams CA Jr,** Xu DZ, Lu Q, Deitch EA. Factors larger than 100 kd in post-hemorrhagic shock mesenteric lymph are toxic for endothelial cells. *Surgery* 2001; **129**: 351-363

27 **Oberholzer A,** Oberholzer C, Moldawer LL. Sepsis syndromes: understanding the role of innate and acquired immunity. *Shock* 2001; **16**: 83-96

28 **Hauser CJ,** Fekete Z, Livingston DH, Adams J, Garced M, Deitch EA. Major trauma enhances store-operated calcium influx in human neutrophils. *J Trauma* 2000; **48**: 592-597

29 **Yaffe MB,** Xu J, Burke PA, Forse RA, Brown GE. Priming of the neutrophil respiratory burst is species-dependent and involves MAP kinase activation. *Surgery* 1999; **126**: 248-254

30 **Fukuyama K,** Iwakiri R, Noda T, Kojima M, Utsumi H, Tsunada S, Sakata H, Ootani A, Fujimoto K. Apoptosis induced by ischemia-reperfusion and fasting in gastric mucosa compared to small intestinal mucosa in rats. *Dig Dis Sci* 2001; **46**: 545-549

31 **Dayal** SD**,** Hasko G, Lu Q, Xu DZ, Caruso JM, Sambol JT, Deitch EA. Trauma/hemorrhagic shock mesenteric lymph upregulates adhesion molecule expression and IL-6 production in human umbilical vein endothelial cells. *Shock* 2002; **17**: 491-495

Edited by Wang XL and Zhang JZ **Proofread by** Xu FM

PO Box 2345, Beijing 100023, China
Fax: +86-10-85381893
E-mail: wjg@wjgnet.com www.wjgnet.com

World J Gastroenterol 2004;10(21):3225-3229
World Journal of Gastroenterology
 ISSN 1007-9327

• BRIEF REPORTS •

Inactivation of PTEN is associated with increased angiogenesis and VEGF overexpression in gastric cancer

Ye-Jiang Zhou, Yu-Xia Xiong, Xiao-Ting Wu, De Shi, Wei Fan, Tong Zhou, Yue-Chun Li, Xiong Huang

Ye-Jiang Zhou, Xiao-Ting Wu, Wei Fan, Tong Zhou, Yue-Chun Li, Xiong Huang, Department of General Surgery, West China Hospital, Sichuan University, Chengdu 610041, Sichuan Province, China
Yu-Xia Xiong, Department of Pharmacology, Luzhou Medical College, Luzhou 646000, Sichuan Province, China
De Shi, Department of General Surgery, the First Affiliated Hospital, Chongqing University of Medical Sciences, Chongqing 400016, China
Correspondence to: Xiao-Ting Wu, Department of General Surgery, West China Hospital, Sichuan University, Chengdu 610041, Sichuan Province, China. wxt1@medmail.com.cn
Telephone: +86-28-88036679
Received: 2004-02-02 **Accepted:** 2004-02-24

Abstract

AIM: To investigate the expression of PTEN/MMAC$_1$/TEP$_1$ and vascular endothelial growth factor (VEGF), their roles in biologic behavior and angiogenesis and their association in gastric cancer.

METHODS: Immunohistochemical staining was used to evaluate the expression of PTEN, VEGF and microvascular density (MVD) on paraffin-embedded sections in 70 patients with primary gastric cancer and 24 patients with chronic superficial gastritis (CSG). Expression of PTEN, VEGF and MVD were compared with clinicopathological features of gastric cancer. The relationship between expression of PTEN, VEGF and MVD as well as the relationship between PTEN and VEGF expression in caner cells were investigated.

RESULTS: PTEN expression significantly decreased (t = 3.98, P<0.01) whereas both VEGF expression and MVD significant increased (t = 4.29 and 4.41, respectively, both P<0.01) in gastric cancer group compared with CSG group. PTEN expression was significantly down-regulated (t = 1.95, P<0.05) whereas VEGF expression (t = 2.37, P<0.05) and MVD (t = 3.28, P<0.01) was significantly up-regulated in advanced gastric cancer compared with early-stage gastric cancer. PTEN expression in gastric cancer showed a negative association with lymph node metastasis (t = 3.91, P<0.01), invasion depth (t = 1.95, P<0.05) and age (t = 4.69, P <0.01). MVD in PTEN-negative gastric cancer was significantly higher than that in PTEN-positive gastric cancer (t = 3.69, P<0.01), and there was a negative correlation between PTEN expression and MVD (γ = -0.363, P<0.05). VEGF expression was positively associated with invasion depth (especially with serosa invasion, t = 4.69, P<0.01), lymph node metastasis (t = 2.31, P<0.05) and TNM stage (t = 3.04, P<0.01). MVD in VEGF-positive gastric cancer was significantly higher than that in VEGF-negative gastric cancer (t = 4.62, P<0.01), and there was a positive correlation between VEGF expression of and MVD (γ = 0.512, P<0.05). VEGF expression in PTEN-negative gastric cancer was significantly stronger than that in PTEN-positive gastric cancer (t = 2.61, P<0.05), and there was a significantly negative correlation between the expression of VEGF and PTEN (γ = -0.403, P<0.05).

CONCLUSION: Our results imply that inactivation of PTEN gene and over-expression of VEGF contribute to the neovascularization and progression of gastric cancer. PTEN-related angiogenesis might be attributed to its up-regulation of VEGF expression. PTEN and VEGF could be used as the markers reflecting the biologic behaviors of tumor and viable targets in therapeutic approaches to inhibit angiogenesis of gastric cancers.

Zhou YJ, Xiong YX, Wu XT, Shi D, Fan W, Zhou T, Li YC, Huang X. Inactivation of PTEN is associated with increased angiogenesis and VEGF overexpression in gastric cancer. *World J Gastroenterol* 2004; 10(21): 3225-3229
http://www.wjgnet.com/1007-9327/10/3225.asp

INTRODUCTION

Gastric cancer is one of the tumors with a relatively high incidence and mortality in the digestive system. Although many advanced measures have been taken to improve the outcome of patients suffering from gastric cancer, up to now, there has been no radical progress in reducing its incidence and mortality. This could be due to the fact that the underlying mechanism in tumorigenesis and progression of gastric cancer is still poorly understood. Many studies have demonstrated that tumor suppressor genes, such as *p*53, play an important role in oncogenesis and progression of various malignancies. Recently, many investigators have been interested in the role of PTEN/MMAC$_1$/TEP1, a novel tumor suppressor gene, located on chromosome band 10q 23.3. Accumulated evidence has suggested that inactivation of PTEN/MMAC$_1$/TEP1 gene was implicated in the carcinogenesis and progression of various tumors[1-10]. Loss of PTEN expression was dominantly attributed to the inactive alteration of PTEN gene, including mutations, deletions, loss of heterozygosity (LOH) and promoter methylation in various malignancies[11,12], meaning that the expressive intensity of PTEN could almost embody the status of *PTEN* gene.

Several studies have strongly implied that PTEN was associated with tumor-induced angiogenesis[13-16]. However, less information regarding the role of PTEN in gastric cancer, to our knowledge, was available. The present study was designed to investigate the role of PTEN in tumorigenesis and progression of gastric cancer and its association with angiogenesis and VEGF expression.

MATERIALS AND METHODS

Subjects

Surgical specimens of 70 patients with histologically confirmed primary gastric adenocarcinoma and 24 patients with chronic superficial gastritis and duodenal ulcer were obtained from Department of General Surgery, Affiliated Hospital, Luzhou Medical College and Department of General Surgery, West China Hospital, Sichuan University in 1996-2000. There were 56 male and 14 female patients in gastric cancer group with age range from 31 to 66 (mean 45) years while there were 21 male and three female patients in chronic superficial gastritis group with age

range from 28 to 43 (mean 35) years. All patients with gastric cancer had received radical resection or palliative surgical treatments, but no one had ever accepted chemotherapy and radiotherapy as well as biotherapy before operation.

Evaluation of clinicopathological features

In gastric cancer group, 18 tumors were categorized histologically as well-differentiation and 52 poor-differentiations. Eight tumors were categorized as early-stage gastric cancer and 62 advanced gastric cancer. Thrifty two patients had serosa invasion, and 46 had lymph node metastasis. According to the criteria set out by the Union of International Caner Commission (new TNM stage, UICC for gastric cancer, 1985), 20 tumors were categorized as stage I, 16 stage II , 30 stage III and four stage IV.

Antibodies and reagents

Rabbit anti-PTEN polyclonal antibody, rabbit ant-VEGF polyclonal antibody, mouse anti-CD34 monoclonal antibody and streptavidin-biotin-peroxidase (KIT-9710, UltraSensitive S-P for mouse or rabbit) as well as DAB reagents were all purchased from Maixin Corporation (Fuzhou, Fujian province, China).

Immunohistochemical staining

Five-micron paraffin-embedded sections were dewaxed in xylene, dehydrated in ethanol. Endogenous peroxidase activity was blocked by incubation of samples in a 3% solution of hydrogen peroxide in methanol and heated in pressure-cooker for 50 s to retrieve antigens. After washing with PBS, the samples were incubated for 60 min with primary antibody against CD34, PTEN or VEGF at 37 ℃, for 60 min with the biotin-conjugated second antibody and for 10 min with the third antibody streptavidin-peroxidase at room temperature, and then the immunoreactive products were stained with DAB and counter-stained with methyl green subsequently. PBS was used instead of the primary antibodies for negative controls.

Evaluation of PTEN and VEGF immunostaining

PTEN and VEGF protein expression in benign and malignant gastric epithelium cells was assessed according to the score graded as the percentage of positive immunoreactive cells and the score graded as positive immunoreactive intensity, and the sum of both was used to reflect the level of PTEN and VEGF protein expression. The score graded as percentage of positive immunoreactive cells was defined as follows: <10% as 0, 10-25% as 1, 25-50% as 2, and ⩾50% as 3. The score graded as positive immunoreactive intensity was defined as follows: negative stain (equal to background) as 0, weak positive stain (weak yellow) as 1, positive stain (yellow) as 2, and strong positive stain (brown) as 3. The sum of scores less than or equal to 2 (⩽2) was defined as negative PTEN ($PTEN^-$) or VEGF ($VEGF^-$) protein expression, and more than or equal to 3 (⩾3) as positive PTEN ($PTEN^+$) or VEGF ($VEGF^+$) expression.

Microvascular density counting

Microvascular density (MVD) was determined according to the criterion introduced by Weidner[17]: any separated single vascular endothelium cell or cluster of endothelium cells and microvascular tube with diameter less than 8 erythrocytes were counted. Briefly, the stained sections were screened at ×100 magnifications under a light microscope (Olympus) to identify four regions with the highest number of microvessels, which were then counted at ×200 magnifications, and the average was used to reflect MVD.

Statistical analysis

All results were expressed as mean±SD. Statistic software SPSS 11.5 for Windows was used to analyze the results using Student *t* test and Pearson correlation analysis. The accepted level of significance was $P<0.05$ (Two-tailed).

RESULTS

Characteristics and comparison of PTEN and VEGF expression and MVD in gastric cancer with those in chronic superficial gastritis

PTEN and VEGF expression were demonstrated to localize in cytoplasm of gastric glandular epithelium and tumor cells (Figures 1, 2). In gastric cancer, the positive immunoreactive signal in invasive front region was weaker for PTEN, but stronger for VEGF and microvessels (Figure 3) than that in the fundic region of tumor. There was a significant down-regulation of PTEN expression and a significant up-regulation of both VEGF and MVD in gastric cancer in comparison with those in chronic superficial gastritis (Table 1).

Table 1 Comparison in PTEN and VEGF expression and MVD between chronic superficial gastritis (CSG) group and gastric cancer (GC) group (mean±SD)

Groups	*n*	PTEN	VEGF	MVD
CSG	24	3.13±2.3	1.25±1.16	29.6±9.9
GC	70	1.34±1.75[b]	2.94±1.80[b]	48.3±19.9[b]

[b]$P<0.01$ *vs* CSG group.

Association of PTEN and VEGF expression and MVD with clinicopathological profiles in gastric cancer

As showed in Table 2, The down-regulation of PTEN expression was closely associated with the older patients (>35 years), invasion depth and lymphatic metastasis of tumor, and a downtrend of PTEN expression was observed with the increase of invasion depth of tumor, especially in advanced stage of gastric cancer (⩾T_2) (Table 2). The up-regulation of both VEGF expression and MVD were significantly associated with the invasion depth, lymphatic metastasis and TNM stage, but none of them was associated with the histological differentiation of gastric cancer (Table 2).

Table 2 Association of PTEN and VEGF expression and MVD with clinicopathologic profiles in gastric cancer (mean±SD)

Variables	*n*	PTEN	VEGF	MVD
Age (yr)				
⩽35	22	2.64±1.81	2.77±1.96	46.23±17.61
>35	48	0.83±1.33[b]	3.02±1.76	49.20±20.05
Gender				
Male	56	1.32±1.69	3.00±1.91	48.45±20.39
Female	14	1.71±1.82	2.71±1.73	47.54±12.72
Differentiation				
Well	18	1.56±1.82	3.33±1.88	45.94±17.08
Poor	52	1.35±1.69	2.81±1.86	49.07±20.72
Invasion depth				
T_1	8	2.50±1.73	1.5±1.91	27.94±12.1
⩾T_2	62	1.26±1.69[a]	3.13±1.82[a]	50.9±19.31[b]
<T_3	38	1.47±1.81	2.08±1.20	39.6±16.6
⩾T_3	32	1.31±1.66	3.97±1.15[a]	58.6±18.9[b]
LN metastasis				
Positive	46	0.87±1.36	3.57±1.77	53.9±18.2
Negative	24	2.42±1.93[b]	1.74±2.07[a]	37.5±19.3[b]
TNM Stage				
I+II	36	1.83±1.81	2.51±1.29	39.6±18.3
III+IV	34	0.97±1.55	3.41±1.18[b]	57.5±17.7[b]

[a]$P<0.05$, [b]$P<0.01$ *vs* different variables.

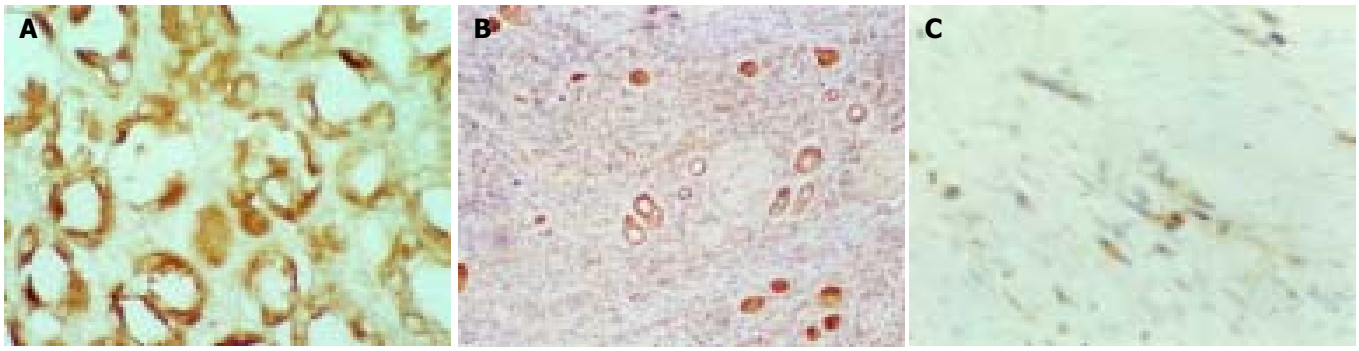

Figure 1 Expression of PTEN. A: Strongly positive expression in bening gastric glandular epithelium cells (Immunohistochemical staining, S-P×400). B: Positive expression in moderately differentiated cancer cells (Immunohistochemical staining, S-P×100). C: Weakly positive expression in poorly differentiated cancer cells. (Immunohistochemical staining, S-P×400).

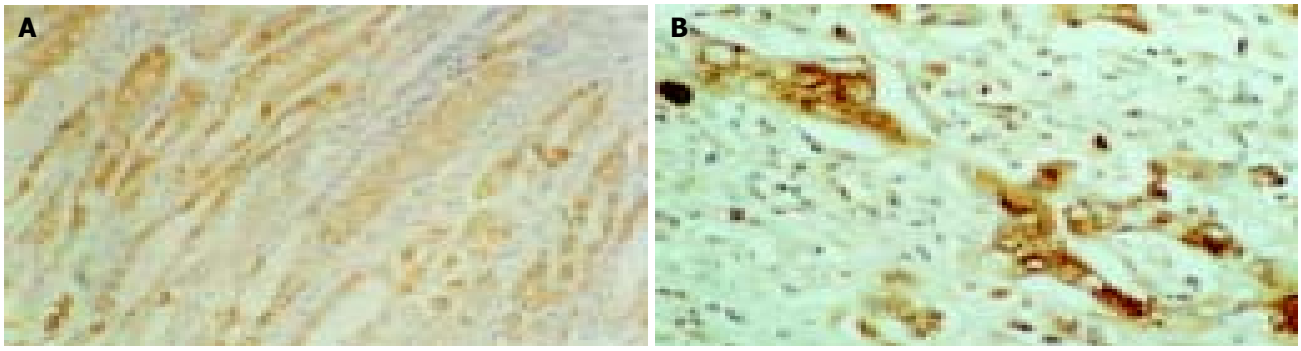

Figure 2 Expression of VEGF. A: Weakly positive expression in benign gastric glandular epithelium cells. B: Strongly positive expression in poorly differentiated cancer cells. (Immunohistochemical staining, S-P×400).

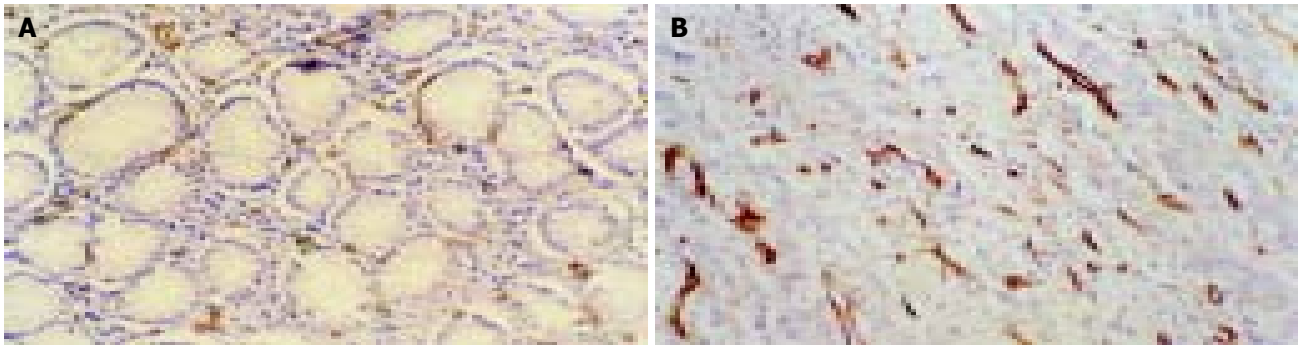

Figure 3 MVD in benign / malignant gastric tissues. A: Lessand weakly stained microvessel labeled by CD34 was regularly distributed among the benign gastric epithelium gland (Immunohistochemical staining, S-P×400). B: Increased and strongly stained microvessel labeled by CD34 was irregularly infiltrated in poorly differentiated adenocarcinoma (Immunohistochemical staining, S-P×200).

Correlation of PTEN and VEGF expression with MVD in gastric cancer

MVD was significantly higher in PTEN negative (n = 54) than in PTEN positive gastric cancer (n = 16) (52.7±19.6 *vs* 33.4±13.2, t = 3.69, P<0.01), and significantly higher in VEGF positive (n = 52) than in VEGF negative gastric cancer (n = 18) (52.71±19.59 *vs* 29.78±12.9, t = 4.62, P<0.001). There was a significantly negative correlation between MVD and the intensity of PTEN expression (γ = -0.363, P<0.05) and a positive correlation between MVD and the intensity of VEGF expression (γ = 0.512, P<0.01).

Correlation between VEGF and PTEN expression

The intensity of VEGF expression was significantly higher in PTEN negative than in PTEN positive gastric cancer (3.18±1.53 *vs* 2.15±2.19, t = 2.61, P<0.05). Furthermore, There was a significantly negative correlation between VEGF and PTEN expression (γ = -0.403, P<0.05).

DISCUSSION

PTEN/MMAC$_1$/TEP$_1$-encoding product, a dual-specificity protein-phospholipid phosphatase, which was involved in regulation of a variety of signal transduction pathways through dephosphorylation, including down-regulation of the activity of the focal adhesion kinase (FAK) to inhibit cell adhesion, invasion and metastasis[18-20], disabling of phosphatidylinositol 3-kinase (PI3'k)/Akt signal pathway to accelerate cell apoptosis and inhibit cell proliferation and inhibition of MAPK signal pathway to restrain cell differentiation[21-23]. Some studies[18-20,24-27] have demonstrated that anti-sense or deletion of PTEN gene significantly up-regulates the ability of cell proliferation, adhesion and migration, accompanied by increased activity of FAK and PI3'k/Akt, whereas over-expression of PTEN protein in wild-type PTEN transfected cells is detected, with a resultant cell cycle arrest, increased cell apoptosis, decreased potential in cell mitosis, proliferation, adhesion and migration, and the

concomitant decrease of FAK and PI3'k/Akt activities, suggesting that PTEN regulates negatively the growth, invasion and metastasis of tumors, and then the inactivation of PTEN greatly contributes to the tumorigenesis and progression of tumors.

So far, little information on the expression and role of *PTEN* gene in gastric cancer is available. Recently, Byun *et al.*[28] showed an abnormally low expression with only in 36% (20/55) gastric cancer tissues and 33% (5/15) cell lines while none of 71 cases with non-cancer tissues showed a decreased expression. The LOH of *PTEN* gene reached at 47% (14/30) and was closely linked to low expression of *PTEN m*RNA in gastric cancer. Furthermore, the rate of LOH was significantly higher in advanced gastric cancers (63%) than that in early-stage tumors (18%), and in poorly differentiated tumors (69%) than in well- or moderately differentiated tumors (29%). Fei *et al.*[29] compared PTEN expression in 26 gastric cancer, 21 first-degree relatives of gastric cancer patients and 12 healthy individuals by RT-PCR and immunohistochemistry, and found that PTEN expression was significantly decreased in gastric cancer group and the first-degree relatives group compared with those in matched non-malignant gastric tissues and healthy control group. Kang *et al.*[30] screened 310 cases with gastric carcinoma, and found that 62 cases lost PTEN expression, and the loss of PTEN expression was linked to the promoter methylation of *PTEN* gene, which was significantly associated with tumor depth and size, lymphatic invasion, advanced stage, pTNM stage, and patients' survival, implying that loss of PTEN expression is involved in the pathogenesis of gastric cancer. Nevertheless, there are some discrepant and conflict findings. One study from Japan did not find any mutation and promoter methylation of *PTEN* gene as well as the alteration of *m*RNA in gastric cancer cell lines and primary tumor tissues[31]. Another study showed that the mutation rate of *PTEN* gene was not significantly increased in human advanced gastric cancer[32], suggesting that PTEN does not participate in gastric carcinogenesis and progression as a tumor suppressor gene. In current study, PTEN expression was only slightly decreased in early gastric cancer cells but significantly decreased in advanced gastric cancer cells, compared with that in benign gastric epithelial cells. PTEN expression decreased as the invasion density increased, and lower PTEN expression was observed in gastric cancer with lymph node invasion and in TNM III/IV stage. Our results were very similar to those reported by Kang *et al.*[30], suggesting that loss of PTEN expression is a relatively later molecule event in the pathogenesis of gastric cancer, and thus plays more important role in the progression than in oncogenesis of gastric cancer. The malignant gastric epithelial cells with loss of PTEN expression may hold the characteristics with a high aggressive and metastatic potential, and thus PTEN can be considered as an objective and reliable marker reflecting the pathobiological behaviors of gastric cancer. Moreover, Lee *et al.*[33] showed that loss of PTEN expression was significantly associated with poor gastric carcinoma prognosis. In addition, we also observed a significantly decreased expression of PTEN protein in the older patients (>35 years) with gastric cancer compared with the younger patients, implying that PTEN may be more implicated in the gastric carcinogenesis in the elder. In other words, there might hold dissimilar tumorigenetic mechanisms between the older and younger patients with gastric cancer.

Angiogenesis is prerequisite for progressing tumor growth, invasion and metastasis. MVD in tumor tissue is unanimously considered as a better parameter to reflect the level of the neovascularization of tumor. VEGF, one of the most powerful pro-angiogenic factors, is dominantly involved in all the process including vascular endothelial cell mitosis, proliferation, adhesion and migration. VEGF expression is induced in a hypoxia-inducible factor alpha (HIF-1alpha)-dependent way through activation of the PI3 kinase signaling pathway[34]. VEGF and MVD are all involved in prognosis in various carcinomas[35-38]. Our results revealed a significantly increase in MVD and VEGF expression in gastric cancer cells, and both the VEGF expression and MVD were significantly associated with the invasion depth, lymphatic metastasis and pTNM stage. Furthermore, MVD was significantly correlated with the intensity of VEGF expression. These results suggest VEGF is dominantly involved in the neovascularization of gastric cancer, and thus facilitates the tumor's growth, invasion and metastasis.

Several studies[13-16] have suggested that PTEN is implicated in the regulation of tumor's angiogenesis, and loss of PTEN expression is closely associated with the increased neovascularization in various malignancies *in vitro* and *in vivo*. However, information on the relationship between PTEN protein expression and neovascularization in gastric cancer is scarce. Zheng *et al.* recently showed MVD was negatively related to PTEN expression in gastric cancer. In the present study, we also observed that MVD in PTEN negative gastric cancer was markedly higher than that in PTEN positive gastric cancer, and there was a significantly negative correlation between MVD and PTEN expression in gastric cancer tissue, implying that loss of PTEN expression is highly implicated in the neovascularization of tumor in gastric cancer.

The mechanism of PTEN-related angiogenesis is not well known. Recent *in vitro* studies[39-41] have suggested that loss of PTEN expression significantly up-regulates VEGF expression *via* modulation of HIF-1alpha expression and VEGF-mediated pro-angiogenic signaling through PI3'K/Akt-dependent signaling transduction pathway to enhance the anti-apoptotic, proliferative, and chemotactic activity of endothelial cells and the ability of tube formation. Jiang *et al.* screened the expression of *PTEN* and *HIF-1alpha* mRNA and VEGF protein in human colorectal tumor tissues, and observed a negative correlation of *PTEN* expression with *HIF-1alpha* (γ = -0.36, P< 0.05) and VEGF (γ = -0.48, P<0.05) and a positive correlation between VEGF and *HIF-1alpha* (γ = 0.71, P<0.01). In this study, we also found a significantly increase in VEGF expression in PTEN negative gastric cancer compared with PTEN positive gastric cancer, and that the intensity of VEGF expression was negatively associated with PTEN expression. Taking all these findings together, we postulate that VEGF is a key downstream molecule for PTEN function in carcinogenesis and progression in a wide range of human carcinomas including gastric cancer. Therefore, inactivation of *PTEN* gene could contribute to gastric tumor progression by directly functioning on tumor cells to enhance the ability of growth, anti-apoptotic, invasion and metastasis through up-regulation of PI3'K/Akt signaling transduction pathway, by up-regulating VEGF expression in tumor cells, which enhances the activity of tumor-derived angiogenesis and functions on vascular endothelial cells to increase angiogenesis in tumor tissues. Based on these data, it is concluded that PTEN and VEGF are reliable targets in the therapeutic approach for the inhibition of angiogenesis in gastric cancer.

REFERENCES

1 **Sato N**, Tsunoda H, Nishida M, Morishita Y, Takimoto Y, Kubo T, Noguchi M. Loss of heterozygosity on 10q23.3 and mutation of the tumor suppressor gene PTEN in benign endometrial cyst of the ovary: possible sequence progression from benign endometrial cyst to endometrioid carcinoma and clear cell carcinoma of the ovary. *Cancer Res* 2000; **60**: 7052-7056

2 **Kondo K**, Yao M, Kobayashi K, Ota S, Yoshida M, Kaneko S, Baba M, Sakai N, Kishida T, Kawakami S, Uemura H, Nagashima Y, Nakatani Y, Hosaka M. PTEN/MMAC1/TEP1mutations in human primary renal-cell carcinomas and renal carcinoma cell lines. *Int J Cancer* 2001; **91**: 219-224

3 **Mutter GL**, Lin MC, Fitzgerald JT, Kum JB, Baak JP, Lees JA, Weng LP, Eng C. Altered PTEN expression as a diagnostic

marker for the earliest endometrial precancers. *J Nat Cancer Inst* 2000; **92**: 924-930
4 **Davies MP**, Gibbs FE, Halliwell N, Joyce KA, Roebuck MM, Rossi ML, Salisbury J, Sibson DR, Tacconi L, Walker C. Mutation in the PTEN / MMAC1 gene in archival low grade and high grade gliomas. *Br J Cancer* 1999; **79**: 1542-1548
5 **Rubin MA**, Gerstein A, Reid K, Bostwick DG, Cheng L, Parsons R, Papadopoulos N. 10q23.3 Loss of heterozygosity is higher in lymph node-positive (PT2-3, N+) versus lymph node-negative (PT2-3, NO) prostate cancer. *Hum Pathol* 2000; **31**: 504-508
6 **Guanti G**, Resta N, Simone C, Cariola F, Demma I, Fiorente P, Gentile M. Involvement of PTEN mutations in the genetic pathways of colorectal cancerogenesis. *Hum Mol Genet* 2000; **9**: 283-287
7 **Kimura F**, Watanabe J, Hata H, Fujisawa T, Kamata Y, Nishimura Y, Jobo T, Kuramoto H. PTEN immunohistochemical expression is suppressed in G1 endometrioid adenocarcinoma of the uterine corpus. *J Cancer Res Clin Oncol* 2003: 20
8 **Chung MJ**, Jung SH, Lee BJ, Kang MJ, Lee DG. Inactivation of the PTEN gene protein product is associated with the invasiveness and metastasis, but not angiogenesis, of breast cancer. *Pathol Int* 2004; **54**: 10-15
9 **Kato H**, Fujimura M, Kumabe T, Ishioka C, Kanamaru R, Yoshimoto T. PTEN gene mutation and high MIB-1 labeling index may contribute to dissemination in patients with glioblastoma. *J Clin Neurosci* 2004; **11**: 37- 41
10 **Dicuonzo G**, Angeletti S, Garcia-Foncillas J, Brugarolas A, Okrouzhnov Y, Santini D, Tonini G, Lorino G, De Cesaris M, Baldi A. Colorectal carcinomas and PTEN / MMAC1 gene mutations. *Clin Cancer Res* 2001; **7**: 4049-4053
11 **Sano T**, Lin H, Chen X, Langford LA, Koul D, Bondy ML, Hess KR, Myers JN, Hong YK, Yung WK, Steck PA. Differential expression of MMAC / PTEN in glioblastoma multiforme: Relationship to localization and prognosis. *Cancer Res* 1999; **59**: 1820-1824
12 **Idoate MA**, Soria E, Lozano MD, Sola JJ, Panizo A, de Alava E, Manrique M, Pardo-Mindan FJ. PTEN protein expression correlates with PTEN gene molecular changes but not with VEGF expression in astrocytomas. *Diagn Mol Pathol* 2003; **12**: 160-165
13 **Hsu SC**, Volpert OV, Steck PA, Mikkelsen T, Polverini PJ, Rao S, Chou P, Bouck NP. Inhibition of angiogenesis in human glioblastomas by chromosome 10 induction of thrombospondin-1. *Cancer Res* 1996; **56**: 5684-5691
14 **Giri D**, Ittmann M. Inactivation of the PTEN tumor suppressor gene is associated with increased angiogenesis in clinically localized prostate carcinoma. *Hum Pathol* 1999; **30**: 419- 424
15 **Jiang BH**, Zheng JZ, Aoki M, Vogt PK. Phosphatidylinositol 3-kinase signaling mediates angiogenesis and expression of vascular endothelial growth factor in endothelial cells. *Proc Natl Acad Sci U S A* 2000; **97**: 1749-1753
16 **Wen S**, Stolarov J, Myers MP, Su JD, Wigler MH, Tonks NK, Durden DL. PTEN controls tumor-induced angiogenesis. *Proc Natl Acad Sci U S A* 2001; **98**: 4622-4627
17 **Weidner N**, Folkman J, Pozza F, Bevilacqua P, Allred EN, Moore DH, Meli S, Gasparini G. Tumor angiogenesis: a new significant and independent prognostic indicator in early-stage breast carcinoma. *J Natl Cancer Inst* 1992; **84**: 1875-1887
18 **Tamura M**, Gu J, Matsumoto K, Aota S, Parsons R, Yamada KM. Inhibition of cell migration, spreading, and focal adhesions by tumor suppressor PTEN. *Science* 1998; **280**: 1614-1617
19 **Cai T**, Lei QY, Wang LY, Zha XL. TGF-β_1 Modulated the expression of α 5 beta 1 integrin and integrin-mediated signaling in human hepatocarcinoma cells. *Biochem Biophys Res Commun* 2000; **274**: 519-525
20 **Zhang LN**, Yu Q, Wang LY, Jin JW, Zha XL. The effects of PTEN gene on migration and FAK phosphorylation of SMMC-7721 human hepatocarcinoma cell line. *Shengwu Huaxue Yu Shengwu Wuli Xuebao* 2003; **35**: 161-166
21 **Maehama T**, Dixon JE. The tumor suppressor, PTEN / MMAC, dephosphorylates the lipid second messenger, phosphatidylinositol 3,4,5-trisphosphate. *J Biol Chem* 1998; **273**: 13375-13378
22 **Besson A**, Robbins SM, Yong VW. PTEN / MMAC1 / TEP1 in signal transduction and tumorigenesis. *Eur J Biochem* 1999; **263**: 605-611
23 **Waite KA**, Eng C. Protean PTEN: form and function. *Am J Hum Genet* 2002; **70**: 829-844
24 **Persad S**, Attwell S, Gray V, Delcommenne M, Troussard A, Sanghera J, Dedhar S. Inhibition of integrin-linked kinase (ILK) suppresses activation of protein kinase B / Akt and induces cell cycle arrest and apoptosis of PTEN-mutant prostate cancer cells. *Proc Natl Acad Sci U S A* 2000; **97**: 3207-3212
25 **Sakurada A**, Hamada H, Fukushige S, Yokoyama T, Yoshinaga K, Furukawa T, Sato S, Yajima A, Sato M, Fujimura S, Horii A. Adenovirus-mediated delivery of the PTEN gene inhibits cell growth by induction of apoptosis in endometrial cancer. *Int J Oncol* 1999; **15**: 1069-1074
26 **Ghosh AK**, Grigorieva I, Steele R, Hoover RG, Ray RB. PTEN transcriptionally modulates c-myc gene expression in human breast carcinoma cells and is involved in cell growth regulation. *Gene* 1999; **235**: 85-91
27 **Saito Y**, Swanson X, Mhashilkar AM, Oida Y, Schrock R, Branch CD, Chada S, Zumstein L, Ramesh R. Adenovirus-mediated transfer of the PTEN gene inhibits human colorectal cancer growth *in vitro* and *in vivo*. *Gene Ther* 2003; **10**: 1961-1969
28 **Byun DS**, Cho K, Ryu BK, Lee MG, Park JI, Chae KS, Kim HJ, Chi SG. Frequent monoallelic deletion of PTEN and its reciprocal associatioin with PIK3CA amplification in gastric carcinoma. *Int J Cancer* 2003; **104**: 318-327
29 **Fei G**, Ebert MP, Mawrin C, Leodolter A, Schmidt N, Dietzmann K, Malfertheiner P. Reduced PTEN expression in gastric cancer and in the gastric mucosa of gastric cancer relatives. *Eur J Gastroenterol Hepatol* 2002; **14**: 297-303
30 **Kang YH**, Lee HS, Kim WH. Promoter methylation and silencing of PTEN in gastric carcinoma. *Lab Invest* 2002; **82**: 285-291
31 **Sato K**, Tamura G, Tsuchiya T, Endoh Y, Sakata K, Motoyama T, Usuba O, Kimura W, Terashima M, Nishizuka S, Zou T, Meltzer SJ. Analysis of genetic and epigenetic alterations of the PTEN gene in gastric cancer. *Virchows Arch* 2002; **440**: 160-165
32 **Wang JY**, Huang TJ, Chen FM, Hsieh MC, Lin SR, Hou MF, Hsieh JS. Mutation analysis of the putative tumor suppressor gene PTEN / MMAC1 in advanced gastric carcinomas. *Virchows Arch* 2003; **442**: 437- 443
33 **Lee HS**, Lee HK, Kim HS, Yang HK, Kim WH. Tumour suppressor gene expression correlates with gastric cancer prognosis. *J Pathol* 2003; **200**: 39-46
34 **Sodhi A**, Montaner S, Miyazaki H, Gutkind JS. MAPK and Akt act cooperatively but independently on hypoxia inducible factor-1alpha in rasV12 upregulation of VEGF. *Biochem Biophys Res Commun* 2001; **287**: 292-300
35 **Zheng S**, Han MY, Xiao ZX, Peng JP, Dong Q. Clinical significance of vascular endothelial growth factor expression and neovascularization in colorectal carcinoma. *World J Gastroenterol* 2003; **9**: 1227-1230
36 **Korkolopoulou P**, Konstantinidou AE, Kavantzas N, Patsouris E, Pavlopoulos PM, Christodoulou P, Thomas-Tsagli E, Davaris P. Morphometric microvascular characteristics predict prognosis in superficial and invasive bladder cancer. *Virchows Arch* 2001; **438**: 603-611
37 **Terlikowski S**, Lenczewski A, Sulkowska M, Famulski W, Sulkowski S, Kulikowski M. Tissue expression of VEGF as a prognostic factor in early cervical squamous cell carcinoma. *Folia Histochem Cytobiol* 2001; **39**(Suppl 2): 112-113
38 **Cianchi F**, Palomba A, Messerini L, Boddi V, Asirelli G, Perigli G, Bechi P, Taddei A, Pucciani F, Cortesini C. Tumor angiogenesis in lymph node-negative rectal cancer: correlation with clinicopathological parameters and prognosis. *Ann Surg Oncol* 2002; **9**: 20-26
39 **Gomez-Manzano C**, Fueyo J, Jiang H, Glass TL, Lee HY, Hu M, Liu JL, Jasti SL, Liu TJ, Conrad CA, Yung WK. Mechanisms underlying PTEN regulation of vascular endothelial growth factor and angiogenesis. *Ann Neurol* 2003; **53**: 109-117
40 **Koul D**, Shen R, Garyali A, Ke LD, Liu TJ, Yung WK. MMAC / PTEN tumor suppressor gene regulates vascular endothelial growth factor-mediated angiogenesis in prostate cancer. *Int J Oncol* 2002; **21**: 469-475
41 **Huang J**, Kontos CD. PTEN modulates vascular endothelial growth factor-mediated signaling and angiogenic effects. *J Biol Chem* 2002; **277**: 10760-10766

Edited by Xia HHX **Proofread by** Xu FM

PO Box 2345, Beijing 100023, China
Fax: +86-10-85381893
E-mail: wjg@wjgnet.com www.wjgnet.com

World J Gastroenterol 2004;10(21):3230-3233
World Journal of Gastroenterology
 ISSN 1007-9327

• BRIEF REPORTS •

Gallbladder motility in patients with hepatic cirrhosis before and after portal azygous disconnection

Hong-Xu Jin, Shuo-Dong Wu, Xue-Feng Zhang, Xian-Ying Chen, Guo-Xu Zhang

Hong-Xu Jin, Shuo-Dong Wu, Xue-Feng Zhang, Xian-Ying Chen, Guo-Xu Zhang, The Second Department of General Surgery, Second Hospital, China Medical University, Shenyang 110004, Liaoning Province, China
Xue-Feng Zhang, General Surgery, General Hospital of Shenyang Military Command, Shenyang 110016, Liaoning Province, China
Xian-Ying Chen, Guo-Xu Zhang, Department of Nuclear Medicine, General Hospital of Shenyang Military Command, Shenyang 110016, Liaoning Province, China
Correspondence to: Dr. Shuo-Dong Wu, The Second Department of General Surgery, Second Hospital, China Medical University, 36 Sanhao Street, Heping District, Shenyang 110004, Liaoning Province, China. hongxujin@tom.com
Telephone: +86-24-83955058
Received: 2004-02-06 **Accepted:** 2004-02-21

Abstract

AIM: To determine and compare the effect of vagus nerve on gallbladder motility in patients with hepatic cirrhosis before and after portal azygous disconnection (PAD).

METHODS: PAD operation (or Hassab's operation) was performed on 18 patients with portal hypertension, and anterior and posterior vagal trunks were cut. On d 3 before operation and d 10 after operation, ^{99m}Tc-EHIDA 185 MBq was administered intravenously to the patients, and scintigraphy was performed at 0.25 min/frame. A standard fat meal was administered 30 min after scintigraphy, and dynamic imaging was performed 60 min after the fat meal. Following appearance of the region of interest (ROI) in gallbladder, the time-activity curve of ROI was established. The following seven parameters were used: radioactivity at 30 min after injection of ^{99m}Tc-EHIDA (RC 30min), bile emptying fraction (EF), bile emptying period (EP), emptying rate (ER), latent period (LP), latent period radiocounting increment (LI), and latent period radiocounting increment rate (LR).

RESULTS: The RC 30 min decreased significantly after operation, compared with that before operation (2 693.6± 2 406.9 *vs* 5 606.8±2 625.4, $P<0.05$). The radiocounting of gallbladder increased gradually during LP. LP after operation was significantly longer than that before operation (13.36±5.92 *vs* 2.24±1.48, $P<0.01$). LI and LR after operation were significantly higher than those before operation (2 861.62±028.3 *vs* 331.21±421.02, and 113.42±49.52 *vs* 7.57±10.75, respectively, both $P<0.01$). EP after operation was significantly shorter than that before operation (18.5±6.3 *vs* 24.1±6.4, $P<0.05$). EF and ER after operation were significantly lower than those before operation (13.1±5.4 *vs* 32.3±16.3, and 0.7±0.3 *vs* 1.4±0.8, respectively, both $P<0.01$).

CONCLUSION: PAD operation is a good clinical model in studying the effect of vagus on gallbladder motility. The gallbladder tension after PAD operation decreases significantly during the interdigestive phase. The latent period of gallbladder contraction prolongs and the motility weakens apparently after a standard fat meal. Human vagus influences the gallbladder motility, and cutting of the nerve inhibits the gallbladder motility.

Jin HX, Wu SD, Zhang XF, Chen XY, Zhang GX. Gallbladder motility in patients with hepatic cirrhosis before and after portal azygous disconnection. *World J Gastroenterol* 2004; 10(21): 3230-3233
http://www.wjgnet.com/1007-9327/10/3230.asp

INTRODUCTION

Cholecystolithiasis results from multi-factors[1-5], of which gallbladder motor disfunction is an important factor[5,6]. Gallbladder motility is regulated by nerve system and body fluid[7], especially the vagus[8-10]. Because of the complicated interfering factor and its difficulty in control, there were few clinical studies on the gallbladder motility. In this study, vagus nerve effect on gallbladder motility was studied in patients with liver cirrhosis.

MATERIALS AND METHODS

Eighteen patients with portal hypertension (10 males and 8 females) with an average age of 50 years were included in this study. They had hypersplenotrophy and certain degree of hypersplenia. The esophagogastric varication was confirmed with gastroscope. No biliary abnormalities were found with ultrasonography. Hepatic function was classified as Child A level. Splenectomy (Hassab's operation) was performed, anterior and posterior trunks of vagus were cut off after inferior segment of esophagus was liberated. Aerofluxus was observed 48-96 h after operation. Hepatic function was recovered to Child A level 10 d postoperation.

With empty stomach on d 3 preoperation and d 10 postoperation, respectively, ^{99m}Tc-labeled diethyl acetyl acid anilide iminodiacetic acid scintigraphy (^{99m}Tc-EHIDA) 185 MBq was administered intravenously. American SPECT of GE Company was adopted to perform scintigraphy, 0.25 min/frame. Standard fat meals (ENSURE 250 mL standard solution containing caloric 1046.0 KJ, protein 14%, fattiness 31.5%, carbohydrate 54.5%) was provided for patients after 30 min of continuous displaying. The region of interest (ROI) in gallbladder and the time-activity curve of ROI were established (Figures 3A, B). Then, 7 parameters were used to analyze. the radiocounting of 99mTc-EHIDA injected 30 min later (RC 30 min), emptying fraction (EF, %), emptying period (EP min), emptying rate (ER, %/min): EF/EP, latent period (LP, min): the time from having fat meal to the initiation of contraction of gallbladder, latent period radiocounting increment (LI), latent period radiocounting increment rate (LR, %): the increased amount of radioactivity during LP/the initial radioactivity of LP×100. The results were expressed as mean±SD. SPSS11.0 software was used for analysis.

RESULTS

Each of the paired pre- and post-operative parameters was proved in normal distribution by normality test (Table 1).

Table 1 Comparison of gallbladder contractive function (mean±SD)

Parameters	Pre-surgery	Post-surgery
RC30 min	5 606.8±2 625.4	2 693.6±2 406.9[a]
LP (min)	2.24±1.48	13.36±5.92[b]
LI	331.21±421.02	2 861.6±2 028.3[b]
LR (%)	7.57±10.75	113.42±49.52[b]
EP (min)	24.1±6.4	18.5±6.3[a]
EF (%)	32.3±16.3	13.1±5.4[b]
ER (%/min)	1.4±0.8	0.7±0.3[b]

[a]$P<0.05$, [b]$P<0.01$, *vs* pre-operation.

Serum ^{99m}Tc-EHIDA in blood was rapidly taken by liver, egested to biliary system, stored and concentrated in gallbladder. Thirty min after injecting ^{99m}Tc-EHIDA, the radioactivity in gallbladder could reflect the bile quantity entered to gallbladder during interdigestive phase. The RC 30 min postoperation decreased obviously than that preoperation (2693.6±2406.9 *vs* 5606.8±2625.4, $P<0.05$) (Figure 1).

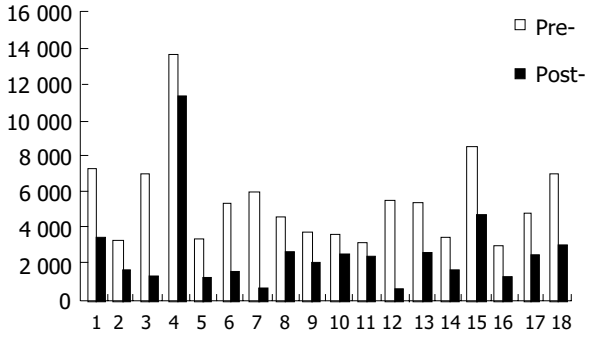

Figure 1 RC 30 min of gallbladder in pre-PAD and post-PAD.

LP in cirrhosis patients was very short preoperation, and LP prolonged significantly postoperation (13.36±5.92 *vs* 2.24±1.48, $P<0.01$). The radioactivity in gallbladder in LP increased gradually. LI and LR increased significantly postoperation (2861.6±2028.3 *vs* 331.21±421.02, 113.42±49.52 *vs* 7.57±10.75, $P<0.01$) (Figures 2A, B, C). EP in cirrhotic patients was shorter postoperation than that preoperation, EF and ER decreased significantly (13.1±5.4 *vs* 32.3±16.3, 0.7±0.3 *vs* 1.4±0.8, $P<0.01$) (Figures 2D, E, F).

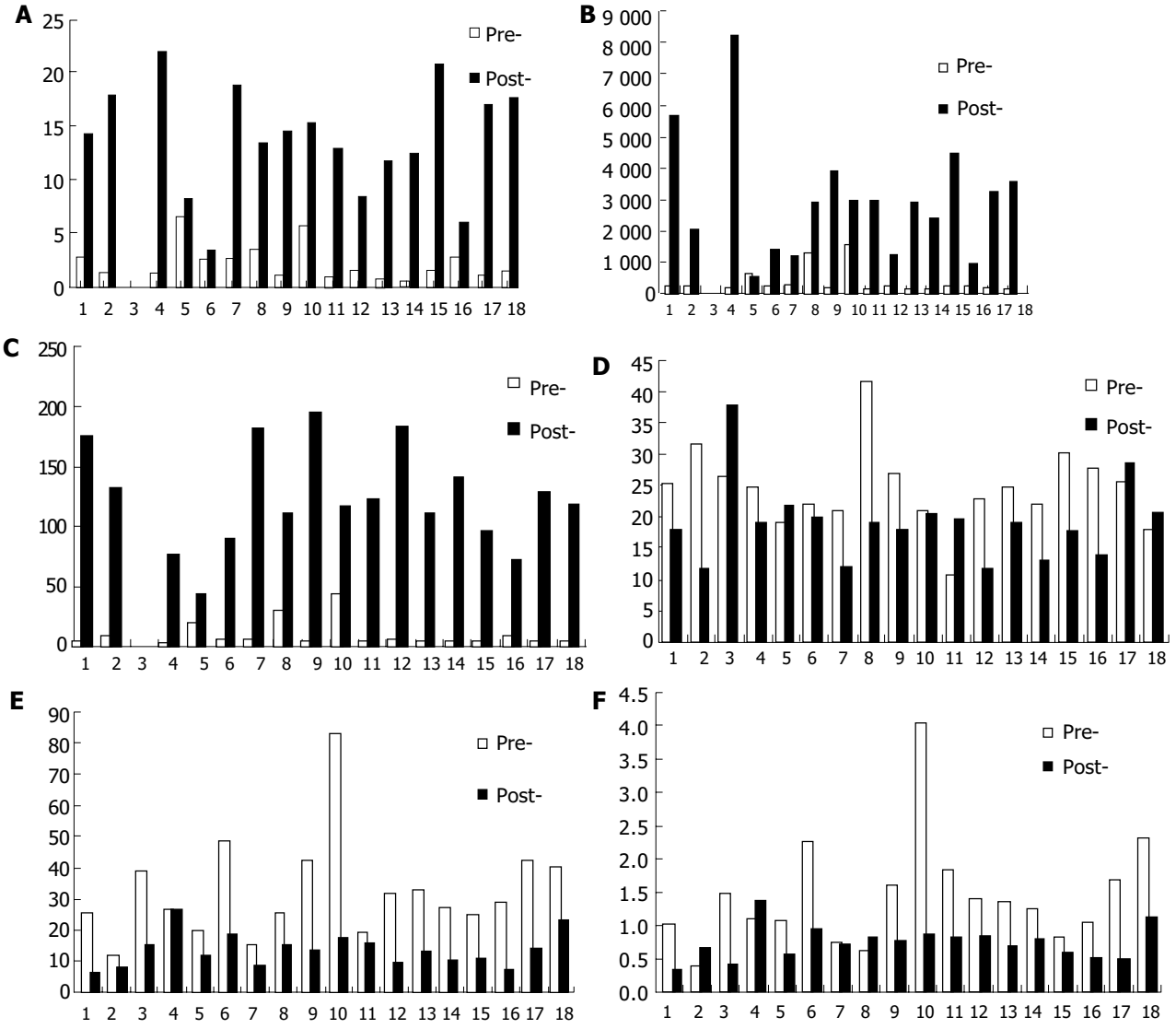

Figure 2 After administration of fat meal, changes in some parameters of gallbladder contraction. A: LP, B: LI, C: LR, D: EP, E: EF and F: ER.

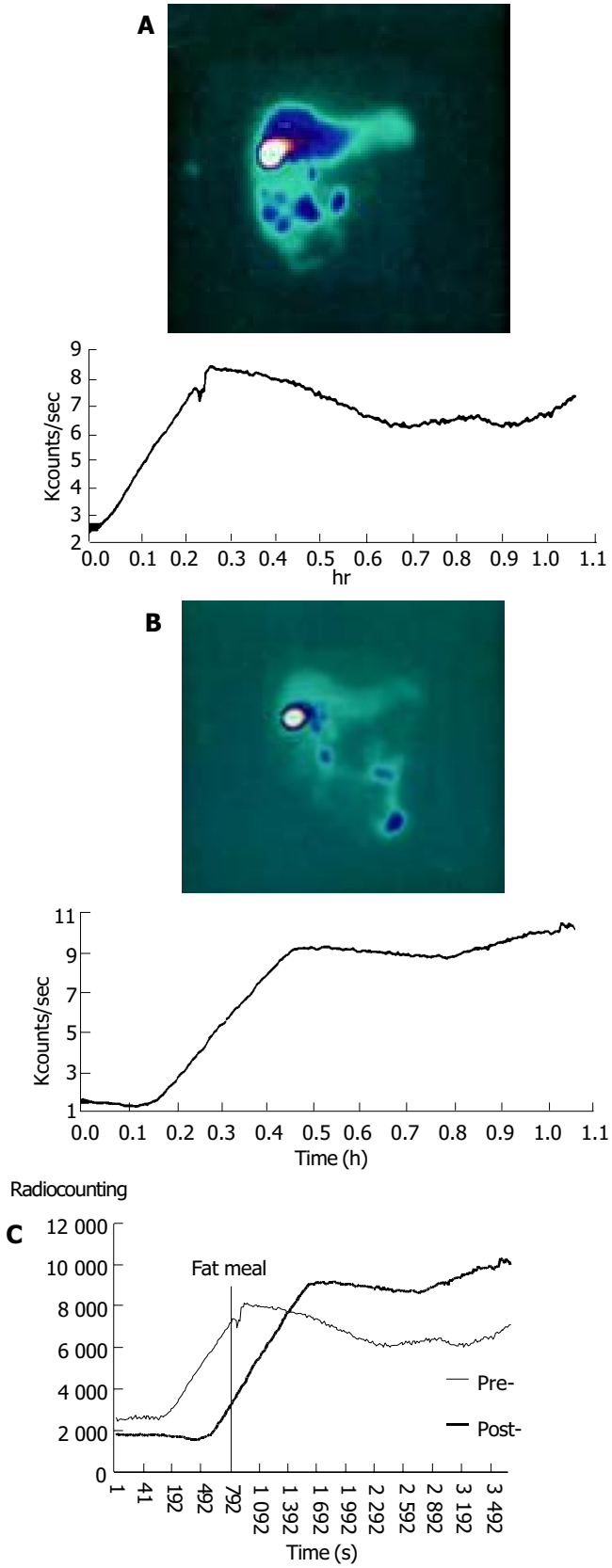

Figure 3 Time-activity curves of gallbladder in cirrhotic patients before (A) and after portal azygous disconnection (B) as well as their comparison (C).

DISCUSSION

The Portal azygous disconnection (PAD) is a clinical research model to study the function of human vagus. Most studies on vagus function in gallbladder motility were limited to animal experiments[9-13]. Some scholars studied the gallbladder motility after gastrectomy and speculated that human vagus had an important effect on gallbladder motility[14-16]. In PAD anterior and posterior trunks of vagus were cut, while the integrality of alimentary canal was maintained. Therefore, PAD could eliminate many disturbing factors. Although the basic liver function of patients could disturb the research, we reduced the disturbance to the lowest degree by adjusting liver function of every patient to Child A level, and auto-control method was used on same patient pre- and post-operation.

Radioactive nuclide ^{99m}Tc-EHIDA can be specifically taken by liver cells, then egested with bile and discharged through biliary system to intestinal tract. Dynamic flowing of bile can be displayed accurately by SPECT scintigraphy with a clear picture and a high resolution. It has little radiation damage to the patients, and is a good way to study the motility of gallbladder and biliary system[17-19].

Gallbladder motility is regulated by nerve system and body fluid factors. Gallbladder emptying after ingestion is affected by multiple factors. Vagus cholinergic fibers could cause gallbladder empty after ingestion, sham feeding could result in gallbladder emptying to 25-56%, and this function could be inhibited by cutting vagus or injection of atropine[8-11,20,21]. Acetylcholine and other parasympathomimetic drugs could enhance the gallbladder tension and motility. Stimulating the vagus of dogs with electric current caused contraction of gallbladder, and gallbladder contracted slowly after both sides of the vagus were completely cut[10]. In our study, vagus in patients with liver cirrhosis was cut off in PAD to study its effect on gallbladder motility. ^{99m}Tc-EHIDA scintigraphy was used. Gallbladder motility was compared between pre- and post-PAD. We found that EP was shortened post- PAD (P<0.05), EF and ER were significantly reduced, and the motility of gallbladder was obviously weak after meal. Our study showed that human vagus had an important regulatory effect on gallbladder motility after meal.

Vagus is an important factor for maintaining gallbladder tension during interdigestive phase[11,13,22], the gallbladder volume could increase two times if both sides of vagus were completely cut[10]. Gallbladder was a weak in situation during interdigestive phase, and appeared rhythmic contraction and relaxation[11]. Tenuity bile was continuously excreted by liver exchanges with condensed bile stored in gallbladder[23-25]. Our study showed that RC 30 min post-operation was significantly decreased when fasting. The reason might be that cutting the vagus reduced the gallbladder tension during interdigestive phase, and then affected the exchange of bile.

Cholecystolithiasis patients did not contract at once after meal, but had a long latent period[26]. In this study, LP post-operation after fat meal was prolonged (P<0.01). The gallbladder lost the contractive stimulation in cephalic phase after vagus was cut. The result in our study was similar to that previously described[27] (LI 2861.6±2028.3, LR 113.42±49.52%). We conclude that bile containing nuclides entering into gallbladder more rapidly results from the heightened pressure of biliary tract. The motility of Oddi's sphincter is adjusted by vagus[11], and the bile excreted by liver is mainly adjusted by body fluid[28-31]. Fat meal may increase the bile excreted by liver through humoral regulation, and amputation of the vagus can weaken the contraction of Oddi's sphincter cephalic phase, so the pressure of biliary tract increases. Further study is required for clarifying the mechanism in detail.

REFERENCES

1 **Vitek L**, Carey MC. Enterohepatic cycling of bilirubin as a cause of 'black' pigment gallstones in adult life. *Eur J Clin Invest* 2003; **33**: 799-810

2 **Wang DQ**, Carey MC. Susceptibility to murine cholesterol gallstone formation is not affected by partial disruption of the HDL receptor SR-BI. *Biochim Biophys Acta* 2002; **1583**: 141-150

3 **Chuang CZ**, Martin LF, LeGardeur BY, Lopez A. Physical activity, biliary lipids, and gallstones in obese subjects. *Am J Gastroenterol* 2001; **96**: 1860-1865
4 **Behar J**. Clinical aspects of gallbladder motor function and dysfunction. *Curr Gastroenterol Rep* 1999; **1**: 91-94
5 **Rubin M**, Pakula R, Konikoff FM. Microstructural analysis of bile: relevance to cholesterol gallstone pathogenesis. *Histol Histopathol* 2000; **15**: 761-770
6 **Shi JS**, Ma JY, Zhu LH, Pan BR, Wang ZR, Ma LS. Studies on gallstone in China. *World J Gastroenterol* 2001; **7**: 593-596
7 **Wang J**, Luo J, Yu X. Study on biliary motility in cirrhotic patients with portal hypertension. *Zhonghua Ganzangbing Zazhi* 2000; **8**: 35-36
8 **Shaffer EA**. Review article: control of gall-bladder motor function. *Aliment Pharmacol Ther* 2000; **14**(Suppl 2): 2-8
9 **Axelsson HG**. Effects of gallstone-promoting diet and vagotomy on the mouse gallbladder epithelium. *Hepatogastroenterology* 1999; **46**: 2149-2152
10 **Muramatsu S**, Sonobe K, Tohara K, Tanaka T, Mizumoto A, Ibuki R, Suzuki H, Itoh Z. Effect of truncal vagotomy on gallbladder bile kinetics in conscious dogs. *Neurogastroenterol Motil* 1999; **11**: 357-364
11 **Liu CY**, Liu JZ, Li ZY, Liu KJ. The vagus nerve coordinates the motion of gallbladder and sphincter of Oddi in the interdigestive period in rabbits. *Zhongguo Yingyong Shenglixue Zazhi* 2000; **16**: 347-349
12 **Tsukamoto M**, Enjoji A, Ura K, Kanematsu T. Preserved extrinsic neural connection between gallbladder and residual stomach is essential to prevent dysmotility of gallbladder after distal gastrectomy. *Neurogastroenterol Motil* 2000; **12**: 23-31
13 **Xie YF**, Liu CY, Liu JZ. Nucleus raphe obscurus participates in regulation of gallbladder motility through vagus and sympathetic nerves in rabbits. *Chin J Physiol* 2002; **45**: 101-107
14 **Kinoshita H**, Imayama H, Hashino K, Aoyagi S. Study of cholelithiasis after gastrectomy. *Kurume Med J* 2000; **47**: 105-108
15 **Hagiwara A**, Imanishi T, Sakakura C, Otsuji E, Kitamura K, Itoi H, Yamagishi H. Subtotal gastrectomy for cancer located in the greater curvature of the middle stomach with prevention of the left gastric artery. *Am J Surg* 2002; **183**: 692-696
16 **Vassilakis JS**, Pechlivanides G, Fountos A, Zoras OJ, Xynos E. Roux-en-Y gastroenterostomy severely disturbs emptying of the gallbladder. *J Am Coll Surg* 1994; **179**: 313-317
17 **Madacsy L**, Velosy B, Szepes A, Szilvassy Z, Pavics L, Csernay L, Lonovics J. Effect of nitric oxide on gallbladder motility in patients with acalculous biliary pain: a cholescintigraphic study. *Dig Dis Sci* 2002; **47**: 1975-1981
18 **Chen SD**, Tsai SC, Shiau YC, Ho YJ, Kao CH. Evidence of gallbladder function changes in hepatoma after transcatheter arterial embolization by quantitative Tc-99m DISIDA cholescintigraphy. *Hepatogastroenterology* 2001; **48**: 393-396
19 **Kao CH**, Hsieh JF, Tsai SC, Ho YJ, Chen SD. Evidence of impaired gallbladder function in patients with liver cirrhosis by quantitative radionuclide cholescintigraphy. *Am J Gastroenterol* 2000; **95**: 1301-1304
20 **Robertson MD**, Mason AO, Frayn KN. Timing of vagal stimulation affects postprandial lipid metabolism in humans. *Am J Clin Nutr* 2002; **76**: 71-77
21 **Fisher RS**, Rock E, Malmud LS. Gallbladder emptying response to sham feeding in humans. *Gastroenterology* 1986; **90**: 1854-1857
22 **Parkman HP**, Pagano AP, Ryan JP. Investigation of endogenous neurotransmitters of guinea pig gallbladder using nicotinic agonist stimulation. *Dig Dis Sci* 1998; **43**: 2237-2243
23 **Woods CM**, Mawe GM, Shaffer EA, Toouli J, T P Saccone G. Effects of bioactive agents on biliary motor function. *Curr Gastroenterol Rep* 2003; **5**: 154-159
24 **von Kiedrowski R**, Huijghebaert S, Raedsch R. Mechanisms of von cisapride affecting gallbladder motility. *Dig Dis Sci* 2001; **46**:939-944
25 **Luiking YC**, Akkermans LM, Peeters TL, Cnossen PJ, Nieuwenhuijs VB, Vanberge-Henegouwen GP. Effects of motilin on human interdigestive gastrointestinal and gallbladder motility, and involvement of 5HT3 receptors. *Neurogastroenterol Motil* 2002; **14**: 151-159
26 **Xynos E**, Pechlivanides G, Zoras OJ, Chrysos E, Tzovaras G, Fountos A, Vassilakis JS. Reproducibility of gallbladder emptying scintigraphic studies. *J Nucl Med* 1994; **35**: 835-839
27 **Pazzi P**, Petroni ML, Prandini N, Adam JA, Gullini S, Northfield TC, Jazrawi RP. Postprandial refilling and turnover: specific gallbladder motor function defects in patients with gallstone recurrence. *Eur J Gastroenterol Hepatol* 2000; **12**: 787-794
28 **Trauner M**, Boyer JL. Bile salt transporters: molecular characterization, function, and regulation. *Physiol Rev* 2003; **83**: 633-671
29 **Garcia F**, Kierbel A, Larocca MC, Gradilone SA, Splinter P, LaRusso NF, Marinelli RA. The water channel aquaporin-8 is mainly intracellular in rat hepatocytes, and its plasma membrane insertion is stimulated by cyclic AMP. *J Biol Chem* 2001; **276**: 12147-12152
30 **St-Pierre MV**, Kullak-Ublick GA, Hagenbuch B, Meier PJ. Transport of bile acids in hepatic and non-hepatic tissues. *J Exp Biol* 2001; **204**(Pt 10): 1673-1686
31 **Hooiveld GJ**, van Montfoort JE, Meijer DK, Muller M. Function and regulation of ATP-binding cassette transport proteins involved in hepatobiliary transport. *Eur J Pharm Sci* 2001; **12**: 525-543

Edited by Ren SY and Wang XL **Proofread by** Xu FM